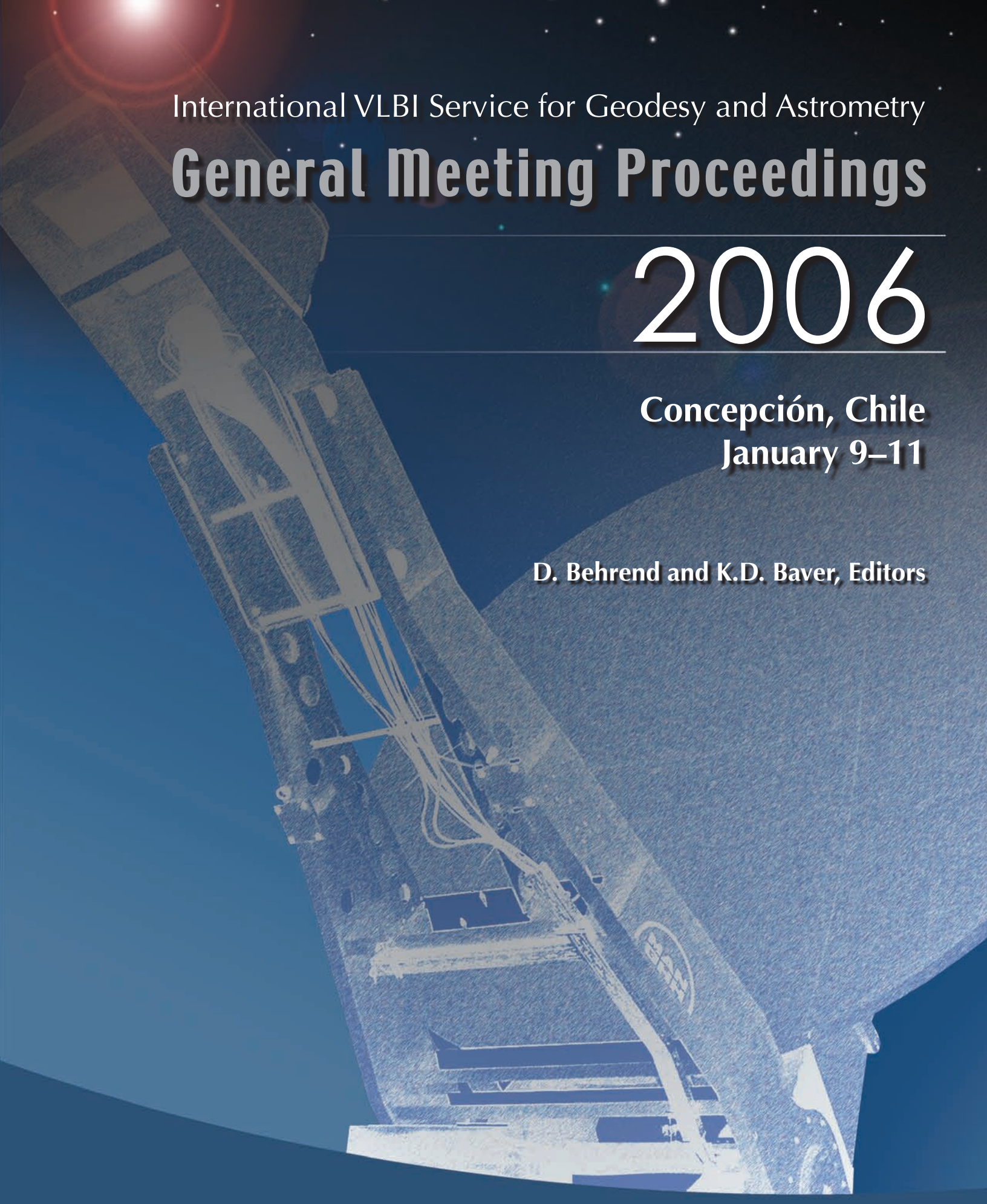

International VLBI Service for Geodesy and Astrometry

General Meeting Proceedings

2006

Concepción, Chile
January 9–11

D. Behrend and K.D. Baver, Editors

NASA/CP-2006-214140

Preface

This volume is the proceedings of the fourth General Meeting of the International VLBI Service for Geodesy and Astrometry (IVS), held in Concepción, Chile, January 9–11, 2006. The contents of this volume also appear on the IVS web site at

`http://ivscc.gsfc.nasa.gov/publications/gm2006`

The fourth General Meeting was held in Concepción, Chile, on the campus of the Universidad de Concepción. The meeting was hosted by the Chilean institutions of Universidad de Concepción, Universidad del Bío Bío, and Instituto Geográfico Militar, as well as the Bundesamt für Kartographie und Geodäsie, Germany—all institutions being IVS member organizations.

The keynote of the fourth General Meeting was the next generation VLBI system following the main theme of "Next Generation VLBI2010". A new geodetic VLBI instrument that will meet requirements for the coming decades is envisioned to have small, fast moving antennas, high-speed networks, new correlator systems, and a streamlined data analysis pipeline. Now is the time to initiate system studies and simulations as well as development projects and prototyping to help bring this vision into reality. The goal of the meeting was to provide an interesting and informative program for a wide cross-section of IVS members, including station operators, program managers, and analysts.

This volume contains the following:

- **Welcome addresses.** This section contains the welcome addresses from Universidad de Concepción and from the IVS Chair.
- **The papers presented at the meeting.** There are six major sections of this volume, each corresponding to a meeting session. Poster and oral papers are mixed. This volume includes 75 papers. The overheads of all oral presentations are available on the web at

  `http://ivscc.gsfc.nasa.gov/meetings/gm2006/GM2006_present.html`,

  including those papers for which no extended version was provided for publication. All papers were edited by the editors for usage of the English language, form, and minor content-related issues. Poster papers about IVS component status are not included in this volume; they have been published in the 2005 Annual Report, available on the web.
- **A splinter meeting report.** Included is a report about the seventh Analysis Workshop.
- **A list of registered participants.**
- **The meeting program.**
- **An author index.**

The April 2006 issue of the IVS Newsletter has a feature article about the meeting. The Newsletter is available at

`http://ivscc.gsfc.nasa.gov/newsletter/issue14.pdf`

Photographs taken during the meeting are available on the web at

`http://ivscc.gsfc.nasa.gov/meetings/gm2006/#Pictures`

This URL will display a section of the 2006 General Meeting web page with links to pages of photographs taken by several of the meeting's participants. The section also links to two movies taken during the Opening Ceremony.

Table of Contents

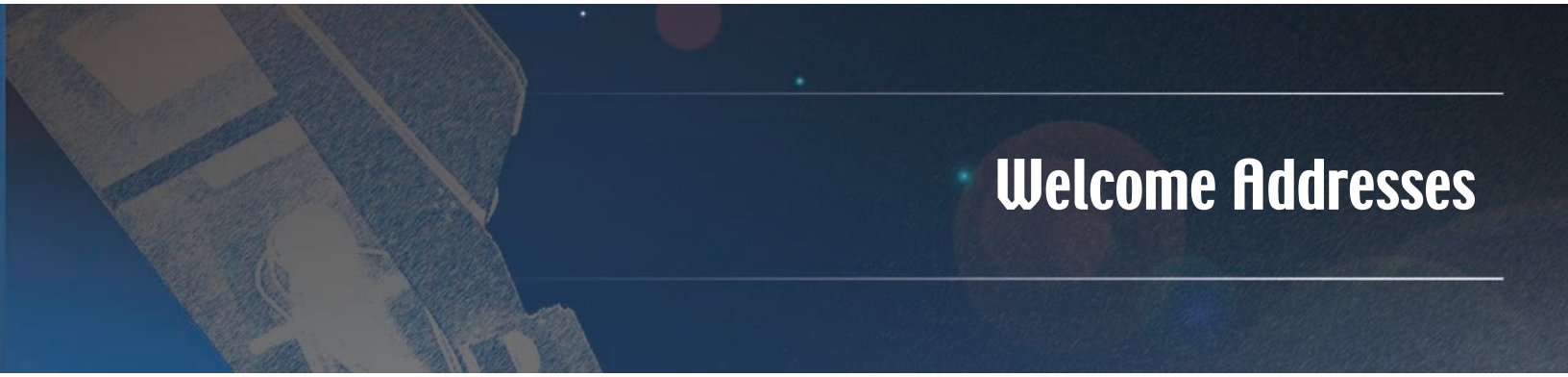
Welcome Addresses

Welcome Address of Universidad de Concepción, IVS 2006 General Meeting Proceedings, p.3–4
http://ivscc.gsfc.nasa.gov/publications/gm2006/welcome-lavanchy

Welcome Address of Universidad de Concepción

Professor Sergio Lavanchy

We are gathered here today for the inauguration of the 4th General Meeting of the International VLBI Service for Geodesy and Astrometry, which, as expressed in the announcement, brings together representatives from all IVS components to share information, hear peer reports, and plan future activities.

This meeting is organized by the Transportable Integrated Geodetic Observatory (TIGO), which came into being as a result of an agreement signed in Frankfurt, Germany on June 21st, 2000 giving Chile—and in particular the Region of Bío Bío—the first geodetic fundamental station in the southern hemisphere, integrating us into the global network of observatories.

The installations of TIGO have contributed data to the Global Reference System. It has also contributed with something that is very important: an important contribution to our academic work and research. The presence of TIGO at our university has motivated academics from various faculties, examples being the academic initiatives in geodesy, astronomy, and radioastronomy, which should be completed in March 2007.

The Universidad de Concepción, which cooperates together with the Universidad del Bío Bío and the Instituto Geográfico Militar in this initiative, is proud of the results obtained with the observatory that is located on this campus where today we gladly host this meeting. Indeed, we should note that the TIGO radio telescope ranks second in the international VLBI network in terms of quantity of observations, which enhances the importance of being located in the southern hemisphere.

We know that there are challenges ahead, such as the construction of a second telescope whose objective is to be able to perform the observations that are planned in the future. The ALMA project, which is being developed in northern Chile and which will house the largest radio telescope on Earth, has generated a very positive environment favorable to fulfilling this desire, and in general to the development of the various disciplines that are favored with initiatives such as the ones we have mentioned.

We believe that the construction of a second radio telescope in Chile provides a great opportunity to our country to transfer new technologies, generate new knowledge, and—something very important—contribute particularly to the training of engineers and physicists. Our university is committed to working towards the success of this initiative, and we hope to obtain the financing

required for this project at the national and/or international level.

Additionally, I would like to especially welcome the 75 experts from 17 countries who participate in this meeting, many visiting our country or South America for the first time. I know that you have an intense work program in the days ahead, but I hope that you will have the opportunity to see our region and especially our university.

Finally, I would like to thank all the people who have made this meeting possible, represented by the Organizing Committee presided by Dr. Wolfgang Schlüter from Germany, and Dr. Hayo Hase, Director of TIGO.

Professor D. Sergio Lavanchy Merino
Rector de la Universidad de Concepción

Welcome Address from IVS Chair, IVS 2006 General Meeting Proceedings, p.5–6
http://ivscc.gsfc.nasa.gov/publications/gm2006/welcome-schlueter

Welcome Address from IVS Chair

Honorable Authorities,
Rector Professor Lavanchy,
Dear VLBI Friends,
Dear Colleagues,

Dr. Wolfgang Schlüter, IVS Chair

I thank you, Rector Lavanchy for the warm welcome words. I would like to express my gratitude that the IVS General Meeting 2006 is held in Chile hosted by the University of Concepción. It is our fourth meeting. This is the first time we meet in the southern hemisphere. As the General Meeting is held every two years in the period January to March, we have been faced with real winter seasons so far. First, there was Kötzting/Wettzell, Germany, where we had snow; I remember the dinner evening. The second meeting was in Tsukuba; it was winter but not really cold. The third meeting took place in Ottawa; I remember the "Winterlude" with the ice sculptures in front of the hotel. Here in Concepción, it is summer and it is warm. Knowing the hospitality of the Chilean people, I am sure our meeting will be a very pleasant one.

It is with pleasure that I welcome you here in Concepción to our General Meeting 2006. As we have heard, we are about 75 participants from 17 countries. I regret that the number of participants is lower as compared to previous meetings. I think this is a result of travel costs and budget constraints, which are usually effective right at the beginning of the year. On the other hand, the number of local people was higher at the previous meetings. This might come from the fact that so far the number of geodetic VLBI experts per square kilometer in South America is lower than in the areas we had the previous meetings.

The Local Organizing Committee has done an outstanding job in preparing the meeting, and I would like to express my gratitude to Hayo Hase (chair of the LOC), Oscar Cifuentes and Jenny Neumann for their work, guaranteeing a pleasant stay in Concecpión.

The Program Committee has set up an excellent program—of course with contributions from the participants—with oral and poster presentations. I am looking forward to interesting discussions and expect a very fruitful and successful meeting. I thank the members of the Program Committee for their work, in particular Dirk Behrend, the new Director of the Coordinating Center, who coordinated the Program Committee.

We will enjoy the hospitality of Chile, and I thank the Rector Professor Lavanchy for the provision of the meeting facilities at the University of Concepción.

TIGO, the German Transportable Integrated Geodetic Observatory, is hosted by the University of Concepción. TIGO is operated by BKG in close collaboration with a Chilean Consortium led

by the University of Concepción. The other members of the Consortium are the University Bío Bío and the Military Geographic Institute (IGM) of Chile.

Concepción was elected out of 12 proposals, made by agencies in Argentina, Brazil, Chile, India, Indonesia and the Philippines in 1998. The University of Concepción, with the idea of the consortium, could offer and guarantee to take over responsibilities for the infrastructure and for the operation. Furthermore, the space geodetic network had a gap in this area, which needed to be filled. Today TIGO plays an important role in particular in the maintenance of the global reference frames and the determination of Earth rotation parameters. It contributes to IVS as well as to IGS and ILRS since April 2002. With the GGOS project of the International Association of Geodesy, which will result in a precise reference system, consistent for decades, the contribution from TIGO will become essential.

I mention this, as for more than five years we have had a very good collaboration, and I would like to remind you that observatories cost money and the load for TIGO is fairly shared. I would like to express my gratitude—as IVS Chair but also as representative of BKG—to the University of Concepción, the University Bío Bío and the IGM for the good collaboration and for the important contributions. Personally I would like to thank the Director for Research of the University of Concepción, Jaime Baeza, for his engagement.

The General Meeting will show results in VLBI at the state-of-the-art and will place emphasis on VLBI2010. The plans for future developments are of great importance and need coordination in order to make best use of the international resources. With the recently released report on VLBI2010 and the establishment of the VLBI2010 Committee, I think we have a good basis for developing our future. VLBI2010 will be a challenge not only in the next few years but for decades to come.

I am certain that the meeting will be very successful and will stimulate our work for the next two years. I wish all attendants to enjoy the conference and splinter meetings as well as the Chilean hospitality.

Thank you.

Dr. Wolfgang Schlüter
IVS Chair

Session 1

VLBI in Science and Application

Markus Rothacher: The Global Geodetic Observing System and the IVS Service, IVS 2006 General Meeting Proceedings, p.9–9
http://ivscc.gsfc.nasa.gov/publications/gm2006/rothacher

The Global Geodetic Observing System and the IVS Service

Markus Rothacher

GeoForschungsZentrum Potsdam
e-mail: rothacher@gfz-potsdam.de

No abstract available.

[Note from the Editors: The overheads of the oral presentation of this contribution can be downloaded from the IVS 2006 General Meeting web site. Please get the PowerPoint file of the presentation at the URL `ftp://ivscc.gsfc.nasa.gov/pub/general-meeting/2006/presentations/gm2006_1-03_rothacher.ppt`.]

Alexandre Humberto Andrei: GAIA and a New Optical Reference Frame, IVS 2006 General Meeting Proceedings, p.10–19
http://ivscc.gsfc.nasa.gov/publications/gm2006/andrei

GAIA and a New Optical Reference Frame

Alexandre Humberto Andrei

Observatório Nacional/MCT and Observatório do Valongo/UFRJ
e-mail: oat1@on.br

Abstract

The ESA mission GAIA, currently scheduled for launch in mid-2011 for a 5-year-mission, will repeatedly measure the position of nearly one billion stars to perform a statistically complete galactic census, carrying out astrometric, spectroscopic and multi-band photometric observations. The target position precision is 10μas at V=15 and 50μas at V=18. To translate such precision into astrometric accuracy, a primary frame formed by some 10,000 quasars will be used, recognized through the analysis of the satellite observation capabilities outputs themselves.

1. Overview

The ESA mission GAIA was initially named as an acronym for "Global Astrometry for Astrophysics". In this sense the astrometry performed, which will refer to a primary frame formed by quasars, is tailored towards the main astrophysics objective, namely a statistically complete census of the Galaxy. The astrometry, in turn, depends on the instrument and mission characteristics.

It is therefore instructive to list the mission's overall goals and scientific objectives. The most relevant among them include: (a) Mapping of the Milky Way; (b) Stellar physics (classification, masses, luminosities, temperatures, metalicities); (c) Kinematics and Dynamics of the Galaxy; (d) Distance scales (trigonometric parallaxes to 10 kpc, cepheids and RR Lyr calibration); (e) Age of the Universe (Cluster diagrams, distances, luminosity); (f) Dark matter (through potential tracers); (g) Reference frames (both primary defined by quasars and extended using stellar astrometry); (h) Extra-solar planets (Jupiter class, astrometric and photometric method); (i) Fundamental physics (PPN parameters, and constraints on the rate of change of the gravitational constant and on gravitational wave energy); (j) Solar system (Taxonomy, Masses, Orbits, and the discovery of new bodies).

The launch is scheduled for mid-2011, using a Soyuz launcher, for a mission of 5 years. The mission is an all sky survey at the end of which about 1 billion objects will be observed to obtain a statistically complete census of the Galaxy, and also of Solar System and extragalactic sources, up to the 20^{th} magnitude (Perryman, 2003a). For objects of the 15^{th} magnitude the astrometric precision can attain 10μas. Besides the astrometric ones, the observational capabilities include photometry (5 broad bands and 11 medium bands), radial velocity, and spectroscopy (low precision). Figure 1 shows the mission's timeline and orbital placement.

In the next two sections we present a review of the astrometric and, to a lesser extent, photometric capabilities that are going to be used to define the GAIA primary reference frame, followed by a discussion of the construction of the primary frame itself. In this sense this paper collects the efforts of several researchers connected to the mission, to whom our debt and appreciation are acknowledged from the start.

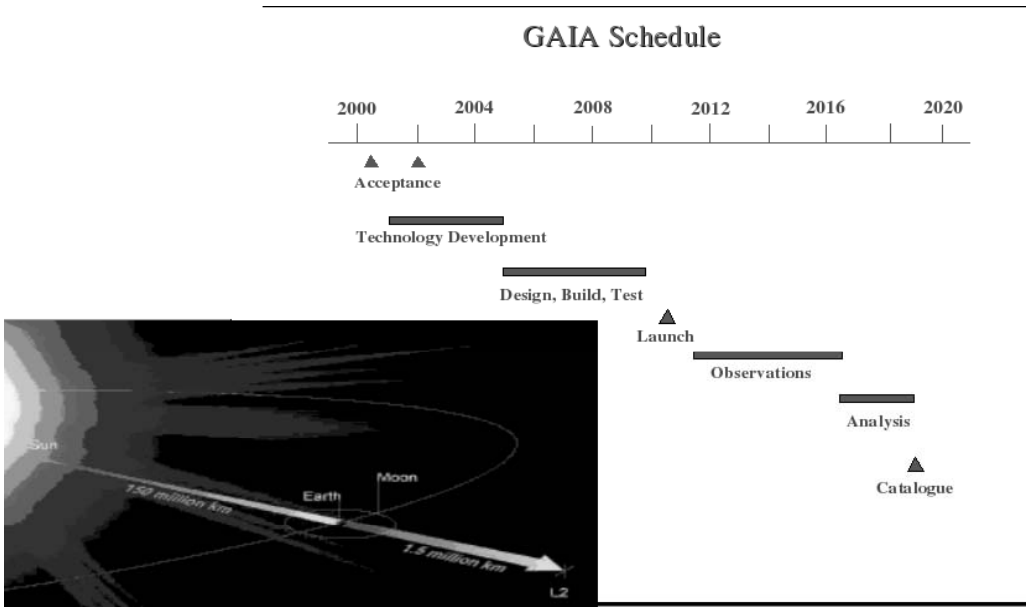

Figure 1. GAIA mission timeline. The detail shows an illustration of the L2 Lagrange point, around which the satellite Lissajous will orbit avoiding the Earth's shadow.

2. The ASTRO Instrument

The GAIA payload includes two astrometric ('Astro') telescopes separated by a basic angle of 106°, with a common focal plane, and radial velocity spectrometer and photometric instrument integrated in the 'Spectro' telescope, that precedes the Astro telescopes by 38° and 144°. Notice that the Astro telescopes also do broad band photometry. These primary instruments are supported by the opto-mechanical-thermal assembly consisting of (Perryman, 2003b): (i) a single structural torus supporting all mirrors and focal planes, employing silicon carbide for both mirrors and structure— there is a symmetrical configuration for the two astrometric viewing directions, with the Spectro system accommodated within the same structure; (ii) a deployable sunshield to avoid direct Sun illumination and rotating shadows on the payload module, combined with the solar array assembly; (iii) control of the heat injection from the service module into the payload module, and control of the focal plane assembly power dissipation in order to provide an ultra-stable internal thermal environment; (iv) an alignment mechanism on the secondary mirror for each astrometric instrument, with micron-level positional accuracy to correct for telescope aberration and mirror misalignment at the beginning of life; (v) a permanent monitoring of the basic angle, but without active control, on board. Figure 2 illustrates the payload assembly.

The integrated radial velocity spectrometer and photometric Spectro instrument comprises an all-reflective three-mirror telescope of aperture 0.5 × 0.5 m^2 and focal length 2.3m. The mirrors will be coated with Aluminum for enhanced performance in the near ultra-violet. The field of view is separated into a dedicated Sky Mapper, the radial velocity spectrometer, and an 11-medium-band-filters photometer (Katz, 2003).

The Spectro instruments share the Sky Mappers, that consists of two first columns of pixels (with another two columns duplication further up) to detect, confirm, and classify the entering

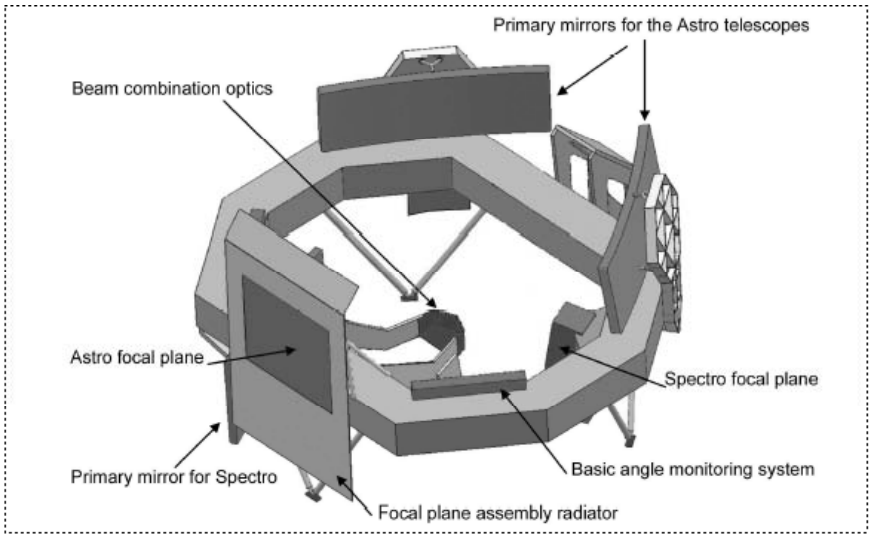

Figure 2. Schematic illustration of the GAIA payload. There is no deployable element (except for the sunshield, not shown in the figure). Note that the structure and mirrors are made of thermally stable SiC.

objects and to determine the operating windows to follow each transit, since not all pixels can be transmitted to ground due to telemetry demands. The Radial Velocity Spectrometer has as primary objective the acquisition of radial velocities to complement the proper motion measurements provided by Astro. The wavelength range is 848 to 874nm, with a resolving power of 1/11500 and a precision of 15 to 1km/s from the faint end to the bright end. It will provide the radial velocities of about 250 million stars up to the 18^{th} magnitude, collecting on average 100 spectra per star over the mission period (Katz, 2003, 2005). The medium band photometry instrument covers 11 medium bands using 8 blue-sensitive and 7 red-sensitive CCDs. The CCDs operate in time delay integration (TDI) mode, and the spatial resolution is 1×1.5 arcsec (i.e., $10 \times 15\mu$m pixels, along and across scan). Several bands measure the continuum while others are located on spectral features sensitive to luminosity, metallicity, element abundances, and H_α emission. Besides the stellar astrophysics results, the photometric measurements will play an all important part in the quasar recognition, particularly those that will form the primary reference frame (Jordi, 2003c).

All along the 5-year-mission the Astro instrument will obtain relative positions, from its two telescopes, for objects brighter than magnitude G=20 (which translates to Johnson V=21 for V-I=2.0, and V=20.5 for V-I=1.0). The overall optical path of each astrometric telescope is made of six anastigmatic, silver-coated reflectors, two of which are common for the two telescopes, to a focal length of 46.67m. The aperture is 1.4×0.5m^2. The two telescopes are separated by the 106° basic angle, and the two fields of view of $0.94° \times 0.74°$ are superimposed on the focal plane (Perryman, 2003c). Figure 3 brings details of the Astro focal plane.

The two first columns of the Astro focal plane contain the Sky Mappers (one for each telescope). They detect the objects entering the field of view, and communicate details of the transit to the subsequent astrometric and broad band photometric detectors. Real-time and telemetry bandwidth constraints impose a stern process of detection, confirmation, and selection of the sources that will actually be tracked. The scan is made within an observation window of 6×12 pixels or 12×12 pixels, respectively, for sources fainter or brighter than magnitude 16 (Lindegren, 2005). The

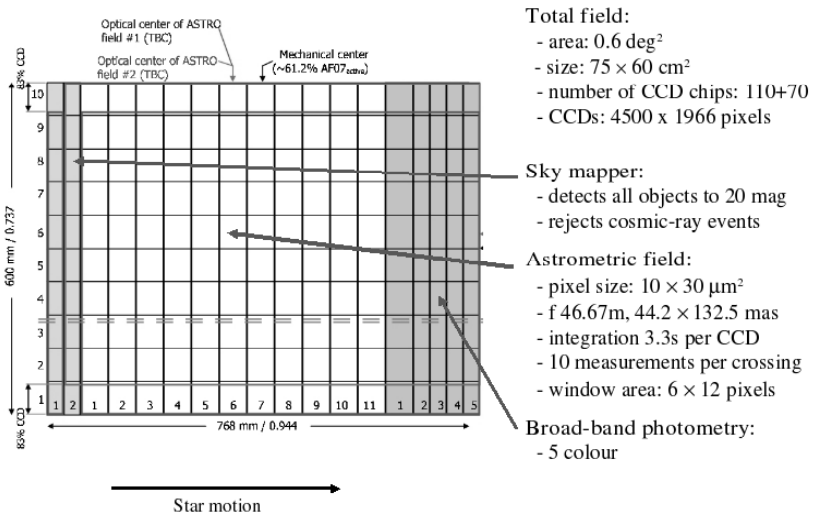

Figure 3. Schematics of the Astro focal plane. The points highlighted on the right are further developed in the text (Jordi, 2003a).

CCDs in the astrometric field sample the optical image (source brightness convolved with the point-spread function) in the along-scan direction by binning the charges across scan in a small read-out vector centered on the image detected in the Sky Mappers. Along scan, these vectors will be 6 or 12 samples wide and only these samples are transmitted to the ground. The astrometric field consists of 11 columns by 10 rows of CCDs (Arenou, 2003; Hog, 2003). Next is the broad band photometry field. In Figure 3 the so-called 2B system proposal is shown which has five bands covering the spectral region from 350 to 1050nm.

The resulting focal plane design consists of a mosaic of 180 CCDs with pixels of 10μm along scan $\times$ 30μm across scan size (44.2 mas $\times$ 132.6 mas). The sources are tracked in Time Delay Integration (TDI) mode. The same CCD design is used for the entire focal plane, with the only difference in the number of pixels along scan (2600 or 4500) and minor changes in the operating modes depending on the assigned functions. The size of the CCDs and the entire focal plane yields TDI and average end-of-mission integration times of 3.3 and 3175 seconds (supposing 82 transits), respectively (Jordi, 2003b).

The integration times naturally depend also on the satellite scanning law. GAIA will perform its observations from a controlled Lissajous-type orbit around the L2 Lagrange point of the Sun and Earth-Moon system (Mignard, 2005a). During its 5-year operational lifetime the satellite will continuously spin around its axis, with a constant speed of 60 arcsec/sec. As a result a great circle in the sky is swept in 6h, and a same field is seen by the two Astro telescopes with 106min of difference. GAIA's spin axis slowly precesses around the solar direction with a fixed angle of 50°, defined for thermal stability. The precession period is of 72 days, corresponding to 26 revolutions over the 5 years of the mission. As a result of the movements of spinning and revolution, on average, each object on the sky is observed 83 times (astrometric fields combined) (de Bruine, 2003a).

Just as was done for the Hipparcos mission, the measurements of the along scan distance between the mesh of objects enables to define instrumental corrections (e.g., satellite attitude and

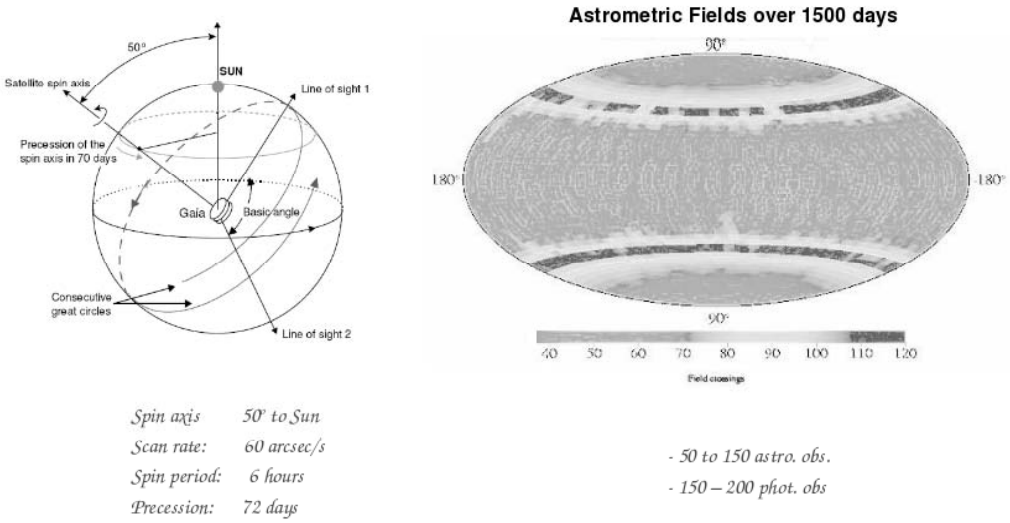

Figure 4. On the left, an illustration of the satellite attitude and varying orientation. On the right, a plot indicating in ecliptic coordinates the number of observations per region of the sky. Notice that the two darker strips of highest concentration of observations around 50° from the ecliptic plane are quite narrow, showing the evenness attained for the number of observations.

telescopes separation), to compute the objects' motion, and ultimately to establish a reference frame on the celestial sphere. Together with the properties of its optical and detector systems, the scanning law and mission lifetime determine GAIA's astrometric capabilities. The scanning law is chosen in such a way to maximize the uniformity of the end-of-mission sky coverage. In spite of this, the characteristics of the scanning law imply that the astrometric precision varies with direction on the sky. Moreover, for any given direction, there is a significant difference between attainable position, proper motion, and parallax accuracy. Generally, end-of-life position and proper motion (random) errors will be 20 per cent and 50 per cent smaller than end-of-life parallax (random) errors. The properties of GAIA's optical and detector systems are such that for stars brighter than V=12^{th} magnitude the photon noise is negligible. The end-of-mission astrometric accuracies for these stars will amount to a few μas, the so-called accuracy noise floor. For magnitudes between 12 and 20, photon noise determines that the expected end-of-life astrometric accuracies are about 10 to 20 μas at V=15 and a few hundred μas at V=20 mag. At a given magnitude (e.g. V=15 mag), the astrometric precision also depends on the apparent star color and on the quantum efficiency of the CCDs and the transmission of the optics. Figure 5 shows the varying precision relatively to magnitude and color (de Bruine, 2003b).

3. GAIA Primary Reference Frame

As seen, GAIA's mode of operation was chosen so that a highly coherent astrometric frame results from the combination of the more than 80 observations of each of the 1 billion objects in different subsets and orientation. The residual global rotation (w) of the frame can be removed by fitting the apparent proper motion of extragalactic sources. By restricting these objects only to QSOs and AGNs for the sake of pointlikeness, a quasi-inertial reference frame is built, in the sense

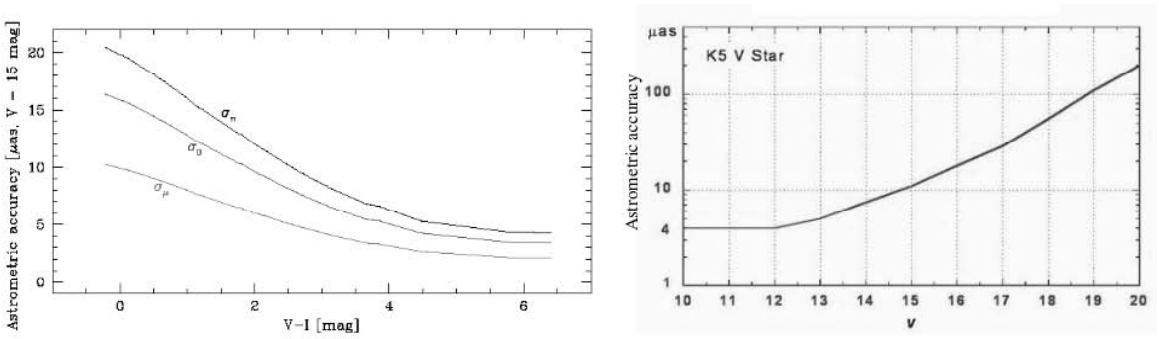

Figure 5. On the left, the variation of accuracy with color. For same conditions of magnitude, color and sky location, notice the increasing accuracy in the sense parallax to position and to proper motion. On the right, the variation of accuracy with magnitude, exemplified by a K5V star.

of the ICRF. Through this a direct realization of the ICRS is obtained in the optical domain, with an average individual astrometric accuracy of not worse than 100μas for hundreds of thousands of grid points. Figure 6 gives an account of the expected number of quasars. The components of w can be obtained from a selected sample, i.e. with no anomalous proper motion, simply by:

$$\mu_\alpha cos\delta \;=\; +\,w_x sin\delta cos\alpha \;+\; w_y sin\delta sin\alpha \;-\; w_z cos\delta; \qquad \mu_\delta \;=\; -\,w_x sin\alpha \;+\; w_y cos\alpha$$

A simulation presented by F. Mignard (2003), based on the Véron & Véron list of quasars (2001), shows that the non-rotation condition can be fulfilled to better than 1μas using a number of sources of the order of the ICRF (Figure 6). In the comparison, an additional noise of 20μas was included for source jitter. Notice that such noise would surpass the astrometric accuracy for sources brighter than the 15^{th} magnitude.

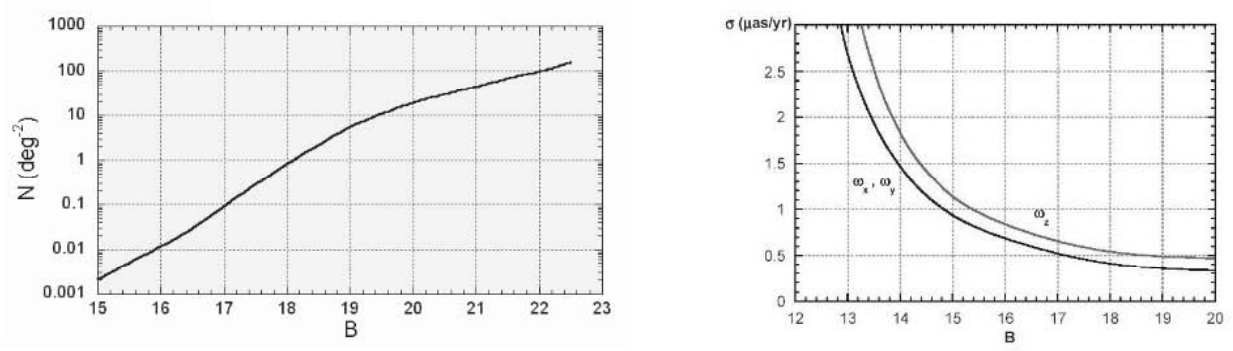

Figure 6. On the left, the quasars' surface density, from Hartwick and Schade (1990). On the right, the relation between the value of the GAIA primary frame global rotation (using galactic coordinates) and the magnitude of the quasars entering in its composition (from Mignard, 2003). The quasar distribution is from Véron & Véron (2001) and is reported as the cause for the worse result for w_z.

The small number of quasars required, if not to define, but certainly to consistently represent

the primary GAIA frame, prompts to verify the limits of the continuity for the relative orientation between the present realization of the ICRF and the one formed by the GAIA primary frame. It has been verified that the mean magnitude of the current ICRF's optical counterparts is about B=18. The typical position errors for the VLBI sources are about 0.4mas. Therefore taking the 212 defining ICRF sources and assuming that the error budget is dominated by the ICRF uncertainties, a value of about 50μas is found for the error in the origin offset between the VLBI and GAIA realizations of the ICRF.

A related question, naturally, refers to reasonable values for the "jitter"—spurious or systematic in nature—in the GAIA astrometric quasar measurements. Image centroiding problems can arise from different causes (e.g., underlying galaxy, imperfect instrumental chromaticity correction, even due to macrolensing), but would not result in long-term astrometric biases. On the other hand, random proper motions due to relativistic jets or more generally due to extra-core sub-milliarcsecond instabilities are not undisputedly understood yet. They could reach values of up to 500μas/year, thus posing an issue especially for the reconvening with the ICRF because of the limited number of sources. The main causes of non-erratic, non-globally systematic displacements can be expected to be:

- microlensing, due to galactic stars, typically smaller than 0.1μas/year;
- macrolensing, due to intervening galaxies, seldom larger than 10μas/year;
- systematic proper motions of 4μas/year, on average, due to the galactocentric acceleration of the Sun (Kovalevsky, 2005).

A non-negligible, systematic pattern for the quasars follows: a dual rotational field around the direction pointing towards the galactic center. That is, the maximum proper motion of 5μas/yr occurs at 90° away from the direction of the galactic center and vanishes at the galactic center direction, with no displacement at all.

For all its crucial importance for the basis of the GAIA astrometric frame, quasars represent only a fraction of around 0.0005% of the population of observed objects. Ways to detect the quasars in the population are: by the recognition of known quasars, by the absence of a parallax, by negligible proper motion (in the non-rotating frame), by short term variability, by the spectral signature (from the colors derived by the broad band and from the medium band photometers), by the radial velocity (for the few bright ones, directly by the radial velocity instrument, or as photometric redshift in the majority of cases). All criteria can be used, but there is a trade-off between completeness and efficiency. Completeness will be attained for the sake of the science objectives, in spite of a fraction of contaminants that can be spotted in a later analysis. Efficiency, in the sense of obtaining a very clean sample of quasars only, is however a prime demand for establishing the astrometric primary frame.

The efficiency rate to reach is equal or better than 99.95%. To this level, for example, parallaxes and proper motions should keep mainly a confirmatory role. The same is true for the radial velocity measurements, which mostly will be a part of the spectral energy distribution given by the photometric measurements. In particular, Mignard (2005b) discusses the power of parallax and proper motion tests, and conclude that their combination can be efficient to get rid of nearby stellar contaminants.

The recognition of known quasars finds its best exemplification in the ICRF (Ma et al., 1998; IERS, 1999; Fey et al., 2004), the 11^{th} edition of the V&V list (Véron-Cetty and Véron, 2003),

and the recently released SDSS DR4 quasar catalog (Adelman-McCarthy et al., 2006). For these databases, the apparent magnitudes and redshift limits are comparable to the ones within GAIA's reach, while other aspects must be considered more carefully, like the quantity of sources, their sky distribution, and the reliability of the identification. Figure 7 shows the sky distribution and lists the total numbers for the three databases. The ICRF sky distribution is the most even, but the sources quantity is the smallest. However, it is very likely to be used for the sake of continuity between the VLBI's and GAIA's realizations of the ICRS. Since the optical counterparts of the ICRF sources will provide adequate astrometric measurements for the most part, they could be used as a step to define GAIA's frame w residual rotation. The SDSS project covers about one quarter of the sky, permitting a useful test of GAIA's recognition scheme in these areas. The V&V list presents both adequate sky distribution and quantity of objects, though not homogeneity of coverage. It represents a compilation of results from more than a hundred of independent surveys, and a careful assessment of the individual points' reliability has to be envisaged for the degree of cleanness required to establish GAIA's primary frame.

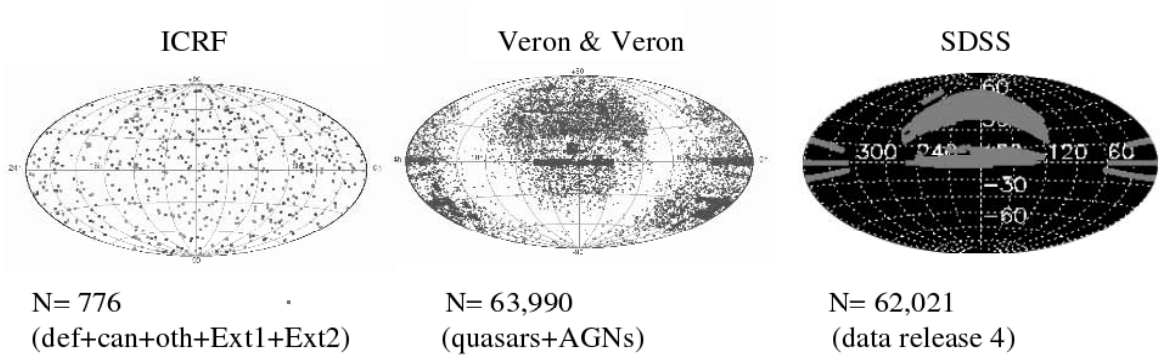

Figure 7. From left to right, the sky distribution of the most recent versions of the ICRF, of the Véron-Cetty & Véron list, and of the Sloan Sky Digitized Survey (SDSS). The plots include all sources that can potentially be used in GAIA's primary astrometric frame (e.g., the defining and candidate sources of the ICRF, quasars and AGNs for V&V). The total numbers are also given.

It becomes clear that in order to establish a large, well-distributed, and even set of quasars, GAIA will have to rely on internal strategies of quasar recognition. For G=20, the star/quasar ratio is about 1,500 in the galactic plane, but it decreases to a tenth at 60° galactic latitude. Besides the evident problems to observe quasars through the Milky Way, the added difficulty to distinguish them therein indicates a zone of avoidance within some 25° from the galactic plane. The most complete way of internal recognition of quasars by GAIA is through the photometric measurements carried out with the broad band and the medium band photometers. Claeskens and collaborators (2004) have generated a large library of synthetic spectra for the quasars, covering a wide range of redshifts, reddening and line strengths. Using in parallel spectral libraries for stars of every spectral class and type, binary stars and white dwarfs, they have correlated all these energy distributions with the different filters proposed for GAIA. Tests were conducted with templates to simulate the observations with realistic noise, and the quasars' locus in the colour space was well defined. By crossing the quasar's synthetic spectral energy distribution with GAIA's proposed photometric systems (Jordi, 2003d), Claeskens and collaborators (2006) have conclusively

shown that the combination of the broad band and medium band filters permits a photometric identification of quasars from virtually any type of stars, provided the bands overlap, that they are broad enough to cover the Lyα line and have good spectral coverage. Using only the broad band colors makes it quite difficult to distinguish quasars with z<2 from white dwarfs, a traditional contaminant in color-selected quasars. Another ambiguity comes from main sequence stars for quasars at 2.5<z<3.5. But this can be resolved with the medium band colors thanks to a better sensitivity to the Lyα line. A more difficult case appears with very reddened stars, but these will mainly be confined to the strong absorption region in the vicinity of the galactic plane, where quasars will not be collected for the primary astrometric frame. The photometric redshift can be retrieved as well, even if the actual spectral index differs significantly from that of the template used for the analysis.

GAIA will observe repeatedly each quasar and determine its location in the multi-dimensional color space. In this space, as discussed, they should occupy a different location from that of the stars, including white dwarfs. The GAIA internal, autonomous multi-color detection will be very efficient and will permit the selection of a 99.6% star-free sample of quasars. At G=19, 85% of the quasars are correctly identified with the level of stellar contaminants smaller than 0.01% (0.4% at G=20). Therefore, by reducing the level of completeness of the quasar sample it is possible to virtually eliminate any contaminants. Such a clean sample should contain about 15% of the quasar population, which still amounts to more than 50,000 sources. This is large enough to tie GAIA's astrometric solution to the non-rotating Universe.

4. Acknowledgements

GAIA is a project of the European Space Agency (ESA) with guidance from the scientific community organized into several working groups, coordination units and working packages, all under the auspices of the GAIA Science Team (GST). It is through the efforts of these people, ESA staff and the industrial partners that GAIA has reached its present advanced stage of development. Much of this article has drawn from the GAIA Concept and Technology Study Report (ESA 2000), complied by the former GAIA Science Advisory Group, and from the GAIA Information Sheets, which can be found at http://www.rssd.esa.int. More detailed information and references can also be obtained at that URL. I would like to acknowledge that a lot of information used in the presentation at the IVS General Meeting was gathered from recent presentations by F. Mignard (2005c).

References

[1] Adelman-McCarthy, J.K., Ageros, M.A., Allam, S.S., Anderson, K.S.J., Anderson, S.F., Annis, J., Bahcall, N.A., Baldry, I.K., Barentine, J.C., Berlind, A., and 131 coauthors, 2006, ApJS, 162, p38A.

[2] Arenou, F., 2003, "On-board Data Handling", in GAIA - Taking the Galactic Census.

[3] Bailer-Jones, C.A.L., 2005, Proc. of IAU Colloquium 196 (Cambridge University Press), ed. D.W. Kurtz, p.429.

[4] Bastian, U. and Hefele, H., 2005, Proc. of the Gaia Symposium "The Three-Dimensional Universe with Gaia" (ESA SP-576), ed. C. Turon, K.S. O'Flaherty, M.A.C. Perryman, p215.

[5] de Bruine, J., 2003a, "Scanning Law", in Gaia - Taking the Galactic Census.

[6] de Bruine, J., 2003b, "Astrometric Accuracy Assesment", in Gaia - Taking the Galactic Census.

[7] Claeskens, J.-F., Smette, A., and Surdej, J., 2005, Proc. of the Gaia Symposium "The Three-Dimensional Universe with Gaia" (ESA SP-576), ed. C. Turon, K.S. O'Flaherty, M.A.C. Perryman, p667.

[8] Claeskens, J.-F., Smette, A., Vandenbulcke, L. and Surdej, J., "Identification and redshift determination of QSOs with medium band photometry: application to GAIA", 2006, to appear in Mon.Not.Roy.Ast.Soc.

[9] ESA, 2000, "GAIA: Composition, formation and evolution of the Galaxy", ESA-SCI(2000)4.

[10] Fey, A.L., Ma, C., Arias, E.F., Charlot, P., Feissel-Vernier, M., Gontier, A.-M., Jacobs, C.S., Li, J. and MacMillan, D.S., 2004, Astron.Jour., 127, p3587.

[11] Hartwick, F.D.A. and Schade, D., 1999, Ann.Rev.Astron.Astrophys., vol28, p437.

[12] Hog, E.., 2003, "Sampling in the Astro Telescope", in Gaia - Taking the Galactic Census.

[13] IERS, 1999, "1998 IERS Annual Report", ed. D. Gambis, Observatoire de Paris, p. 87.

[14] Jordi, C., 2003a, "Astro Focal Plane", in Gaia - Taking the Galactic Census.

[15] Jordi, C., 2003b, "Astro Telescope", in Gaia - Taking the Galactic Census.

[16] Jordi, C., 2003c, "Photometric Objectives", in Gaia - Taking the Galactic Census.

[17] Jordi, C., 2003d, "Photometric Systems", in Gaia - Taking the Galactic Census.

[18] Katz, D., 2005, "Spectro Telescope", in Gaia - Taking the Galactic Census.

[19] Katz, D., 2003, "RVS Measurement Principle", in Gaia - Taking the Galactic Census.

[20] Kovalevsky, J., 2005, Proc. of the Gaia Symposium "The Three-Dimensional Universe with Gaia" (ESA SP-576), ed. C. Turon, K.S. O'Flaherty, M.A.C. Perryman, p675.

[21] Lindegren, L., 2005, Proc. of the Gaia Symposium "The Three-Dimensional Universe with Gaia" (ESA SP-576), ed. C. Turon, K.S. O'Flaherty, M.A.C. Perryman, p29.

[22] Ma, C., Arias, E.F., Eubanks, T.M., Fey, A.L., Gontier, A.-M., Jacobs, C.S., Sovers, O.J., Archinal, B.A., Charlot, P., 1998, Astron.Jour., 116, p516.

[23] Mignard, F., 2002, EAS Pub. Ser., vol. 2, Proc. of "GAIA: A European Space Project", ed. O. Bienaym and C. Turon, p327.

[24] Mignard, F., 2003, "The International Celestial Reference System: Maintenance and Future Realization", 25^{th} meeting of the IAU, Joint Discussion 16.

[25] Mignard, F., 2005a, "The L2 Orbit", in Gaia - Taking the Galactic Census.

[26] Mignard, F., 2005b, "Contribution of astrometry to QSO recognition with GAIA", 6^{th} meeting of the GAIA Reletivity and Reference Frame Working Group.

[27] Mignard, F., 2005c, Proc. of "Journes 2004 - systmes de rfrence spatio-temporels. Fundamental astronomy: new concepts and models for high accuracy observations", ed. N. Capitaine, p196.

[28] Perryman, M., 2003a, "Measurement Principle", in Gaia - Taking the Galactic Census.

[29] Perryman, M., 2003b, "Payload Overview", in Gaia - Taking the Galactic Census.

[30] Perryman, M., 2003sc, "Mission Timeline", in Gaia - Taking the Galactic Census.

[31] Véron-Cetty, M.-P.; Véron, P., 2001, Astron.Astrophys., 374, p92.

[32] Véron-Cetty, M.-P.; Véron, P., 2003, Astron.Astrophys., 412, p399.

Aleksander Brzeziński: Role of VLBI for Investigating Earth Rotation, IVS 2006 General Meeting Proceedings, p.20–29
http://ivscc.gsfc.nasa.gov/publications/gm2006/brzezinski

Role of VLBI for Investigating Earth Rotation

Aleksander Brzeziński

Space Research Centre, Polish Academy of Sciences
e-mail: alek@cbk.waw.pl

Abstract

Very long baseline interferometry is the only space-geodetic technique capable of independently determining all of the Earth orientation parameters: polar motion, spin (UT1, length of day) and precession-nutation (celestial pole offsets). Currently, it is the unique technique for monitoring the celestial pole offsets and the long-term variability of UT1. Regular determinations, for more than 20 years, of the parameters of Earth rotation by VLBI contributed considerably to the progress in the research concerning Earth rotation.

This paper gives an overview of the recent advances in selected topics of the theory of Earth rotation, achieved on the basis of the VLBI observations. We also report on our own investigations related to these topics.

1. Introduction

Regular determinations of the parameters of Earth rotation begun in 1899 with the establishment of the International Latitude Service. Up to the 1970s the estimates were based on the observations by optical astrometry and suffered from different systematic errors associated with this technique. In the late 1970s a number of new methods of monitoring changes in Earth rotation with unprecedented accuracy potential entered into use. These are the space-geodetic techniques: very long baseline interferometry (VLBI), satellite and lunar laser ranging (SLR, LLR), global positioning system (GPS) and doppler orbitography and radiopositioning integrated by satellites (DORIS). Noteworthy is the fact that improving the optical observations from the middle of 19th century to the 1970s led to the polar motion uncertainty being reduced by an order of magnitude, whereas the progress achieved during the next two decades resulted in a two-order improvement both in the angular accuracy and temporal resolution of the Earth rotation parameters.

Among the techniques of space geodesy, VLBI plays a particularly important role in monitoring variations in Earth rotation. The VLBI observations have been used to establish the extragalactic reference frame which is a primary materialization of the International Celestial Reference System (ICRS) (IERS, 2004, Chap. 2). The non-rotating celestial reference system in turn is necessary for parametrization of Earth rotation. VLBI is the only space-geodetic technique capable of independently determining all of the Earth orientation parameters (EOP): polar motion—terrestrial coordinates of the pole x, y—, spin—universal time UT1—, and precession-nutation—celestial pole offsets $\delta X, \delta Y$ (or, equivalently, $\delta\psi, \delta\epsilon$). Currently, it is the only technique enabling the determination of the celestial pole offsets and the observation of the long-term variability of UT1. VLBI has been used for monitoring time variations of the EOPs since 1979. However, the quality of the VLBI celestial pole offsets prior to 1984.0 was relatively low due to insufficient data coverage, baseline configurations, etc.; therefore it is better to reject the observations prior to this date when studying such fine effects as the irregular geophysical signals in nutation.

The high quality observations of Earth rotation by VLBI contributed considerably to the progress in the research concerning Earth rotation. We selected for this review the following three topics:

Sec. 2: Development of the high-precision precession-nutation model IAU 2000;

Sec. 3: Analysis of the free core nutation signal;

Sec. 4: Observational evidence of the high frequency polar motion (diurnal, semidiurnal).

We give a brief overview of the recent advances within each of the subjects, achieved on the basis of the VLBI observations. We also report on our own investigations related to these topics.

2. Precession-nutation Model IAU 2000

The International Astronomical Union (IAU) adopted in 1980 a new conventional model of nutation, the IAU 1980 theory of nutation (Seidelmann, 1982) which had to be used together with the IAU 1976 precession model. The new model was developed as a combination of two distinct parts, the rigid Earth precession-nutation series due to Kinoshita (1977) and the transfer function for an elastic, oceanless Earth with a liquid core, computed by Wahr (1981). The new model was expected to be adequate for accuracies reached by the space-geodetic techniques entering that time into routine use for the determination of the Earth orientation parameters.

Unfortunately, already in mid 1980s the VLBI observations revealed systematic differences with respect to the adopted model, which were much larger than the standard errors of observations (Herring *et al.*, 1986)—see Figure 1. An analysis of the observed celestial pole offsets with respect to the conventional model showed that the main components are the retrograde annual nutation and the long periodic trend. After extending the offset curves to more recent times (Figure 2a) the trend appeared to be composed of the polynomial part contributing to precession and the harmonic terms with main periods 18.6 and 9.3 years.

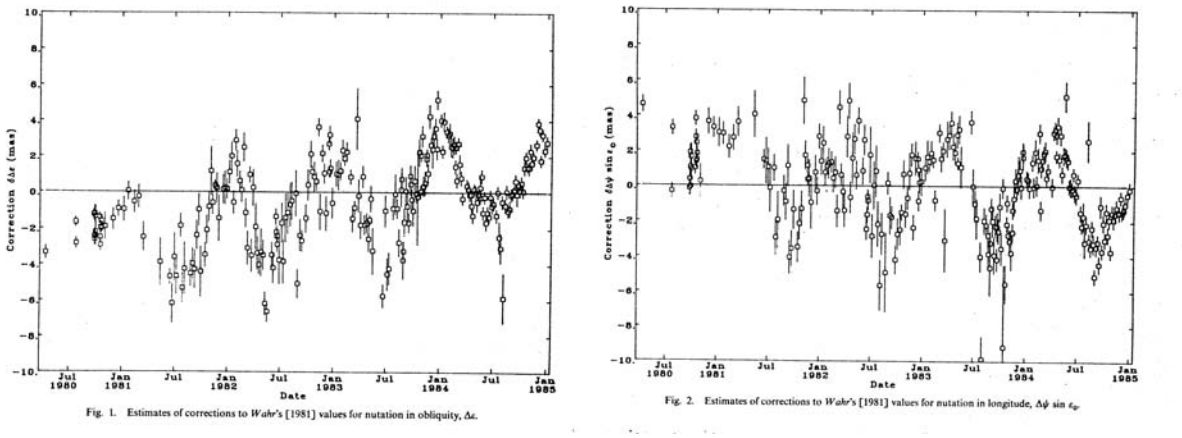

Fig. 1. Estimates of corrections to *Wahr*'s [1981] values for nutation in obliquity, $\Delta\varepsilon$.

Fig. 2. Estimates of corrections to *Wahr*'s [1981] values for nutation in longitude, $\Delta\psi \sin \varepsilon_0$.

Figure 1. Celestial pole offsets observed by VLBI with respect to the IAU 1976 precession model and the IAU 1980 theory of nutation (from Herring et al., 1985; 1986).

Gwinn *et al.* (1986) discussed the discrepancy between the IAU 1980 theory and the VLBI observations. They discovered that a large part of the discrepancies could be removed when changing the free core nutation (FCN) period in the resonance expression from its adopted hydrostatic value of 460 days to 430 days. This change of period in turn was interpreted as an increase of about

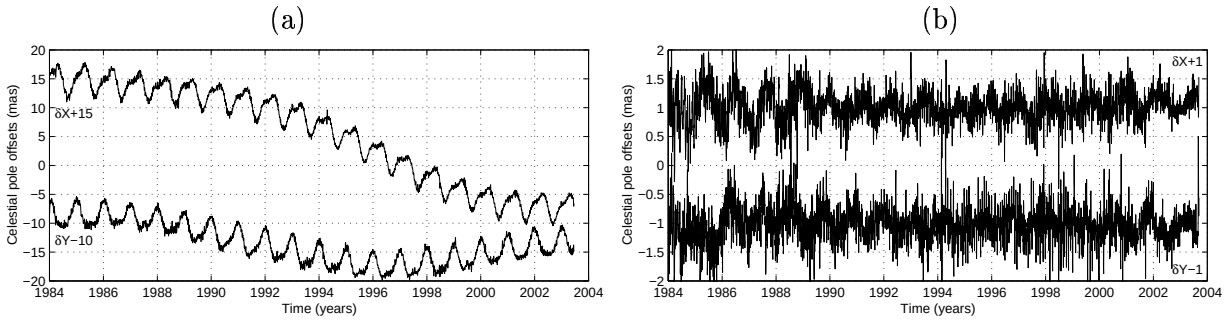

Figure 2. Celestial pole offsets observed by VLBI with respect to (a) the IAU 1976 precession model and the IAU 1980 theory of nutation and (b) the IAU 2000 precession-nutation model. The diagrams show the combination solution EOP(IERS)C04.

6% of the dynamical flattening of the liquid core corresponding to a change of the geometrical flattening of the core-mantle boundary by about 500 meters.

In 1994 the XXIInd General Assembly of the IAU (IAU GA) in the Hague established an inter-commission Working Group on the non-rigid Earth Nutation Theory under the leadership of Veronique Dehant (Resolution B8). At the same time the IAU GA asked the International Earth Rotation Service (IERS) to provide an empirical interim model of precession-nutation and to continue the observations of the celestial pole offsets with the most precise techniques available including the very long baseline interferometry (Resolution C1).

The Working Group continued its activity until 1999; see (Dehant *et al.*, 1999) for an extensive report. Finally, it came up with a proposal of a new precession-nutation model which was presented at the XXIVth IAU General Assembly in Manchester in 2000 and adopted by the IAU GA under the acronym IAU 2000 (Resolution B1.6). Implementation details of the model IAU 2000 were described in the IERS Conventions 2003 (IERS, 2004). In addition, the IERS Conventions Center provided the corresponding Fortran subroutines via the web (`http://www.iers.org/iers/ products/conv/`).

The new precession-nutation model is a combination of the rigid Earth nutation series REN 2000 (Souchay et al., 1999) and the nonrigid Earth transfer function MHB2000 (Mathews et al., 2002). The underlying structural model of the Earth, modified PREM, consists of the viscoelastic mantle, the liquid outer core and the solid inner core. It takes into account both the inertial and the electromagnetic coupling between the liquid core and the mantle. In addition, the MHB2000 transfer function includes contributions from the ocean tides and the influence of the atmospheric thermal tide S_1.

The accuracy of the full version of the new model, designated IAU 2000A, containing 678 lunisolar and 687 planetary terms, is at the 0.2 milliarcsecond (mas) level. Figure 2b shows the difference between the VLBI observations and the model IAU 2000. A short version of the model, designated IAU 2000B, has been developed for those who need a model only at the 1 mas level during the period 1995–2050. This simplified model contains less than 80 terms plus a bias correction to account for the effect of the planetary terms during the period of its validity.

A comparison of Figure 2a with Figure 2b shows that the IAU 2000 precession-nutation model agrees much better with the VLBI observations than the previous model IAU 1980. Nevertheless, this new model is not a perfect one; see, e.g., (Dehant *et al.*, 2003) for an extensive discussion. There

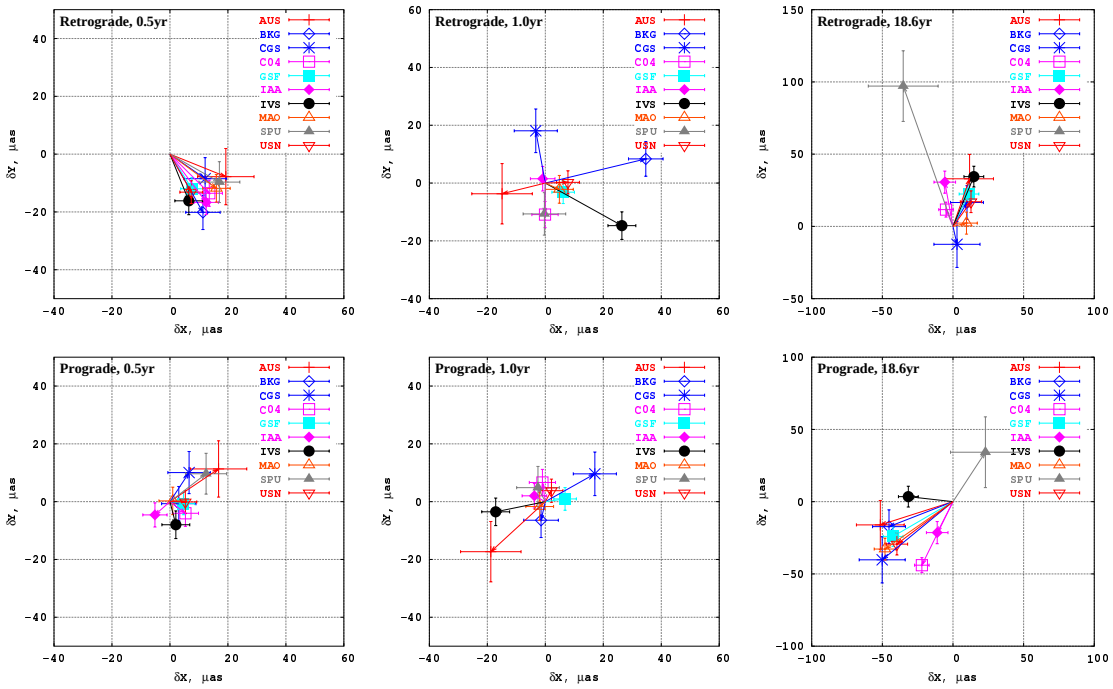

Figure 3. Corrections to the amplitudes of the IAU 2000 precession-nutation model derived from the time series of VLBI celestial pole offsets (from Bolotin and Brzeziński, 2005).

have been several attempts to improve its quality. An example is a new model of precession based upon the so-called P03 solution, which should replace the precession part of the IAU 2000 model (Capitaine *et al.*, 2005). Also the harmonic part of the IAU 2000 can contain imperfections. Bolotin and Brzeziński (2005) estimated corrections to the amplitudes of the conventional a priori model using different time series of the VLBI celestial pole offsets; see Figure 3. The corrections depend in general on the input solution with the following two exceptions. All the series yield similar results for the retrograde semiannual term (about 20 microarcseconds (μas)) and 6 of 10 series provide similar estimates of the prograde 18.6 year term (about 50 μas). Such common corrections indicate the difference between the a priori model and the observations at given frequencies.

But even with perfect coefficients of the model IAU 2000, it will be necessary that VLBI continue to monitor the celestial pole offsets. The reason is that the nutation contains components of geophysical origin which are partly unpredictable. These are the atmospheric and nontidal oceanic influences driven by the daily cycle in the solar heating. Such effects were estimated using the available subdiurnal estimates of the Atmospheric Angular Momentum (AAM) by Bizouard *et al.* (1998) and of the nontidal Oceanic Angular Momentum (OAM) by Brzeziński *et al.* (2004). They found non-negligible, up to 0.1 mas, contributions to the following nutation components: prograde annual, retrograde annual, prograde semiannual, and to the constant offset of the pole. [Note that in the IAU 2000 model the atmospheric and nontidal oceanic contributions are represented by the empirical "Sun-synchronous" correction to the amplitude of the prograde annual nutation (Mathews *et al.*, 2002, Tables 5 and 7).] But after removing the harmonic model, there still remains variability in AAM and OAM contributing to nutation at the level of several tenths of mas

(Brzeziński, *et al.*, 2004). The most important irregular effect of geophysical origin is the free core nutation, a pseudo-harmonic signal seen in time series of the celestial pole offsets (Fig. 2b), which will be considered in the following section.

3. Free Core Nutation

The free core nutation mode arises in the rotating body consisting of the spheroidal solid mantle filled by the liquid core. The mode is described by two parameters: the resonant period T_f and the dimensionless quality factor Q_f, which are usually combined into a single complex angular frequency $\sigma_f = 2\pi/T_f \cdot (1 + i/(2Q_f))$. The most up-to-date discussion of the FCN parameters is given by Mathews *et al.* (2002). They expressed the FCN angular frequency as

$$\sigma_f = -\Omega \left[1 + \frac{A}{A_m}(e_f - \tilde{\beta}) \right] \tag{1}$$

where Ω is the angular frequency of diurnal sidereal rotation, $e_f = (C_f - A_f)/A_f$ denotes dynamical ellipticity of the core, A and C are the mean equatorial and axial moments of inertia of the Earth with assumed axial symmetry ($A = B$), A_f, C_f, A_m, C_m are the corresponding moments of the core and of the mantle, respectively. The complex quantity $\tilde{\beta}$ is the compliance parameter characterizing the deformability of the fluid core under the centrifugal forcing associated with the wobble of the core relative to the mantle. This parameter includes also anelasticity and ocean tide effects.

The period of the FCN resonance depends primarily on e_f, which in turn is directly related to the geometrical flattening of the core-mantle boundary (CMB). If the flattening is computed under the assumption of hydrostatic equilibrium, the corresponding space-referred period of FCN is about 460 days (Wahr, 1981) which is almost 30 days longer than the period observed by VLBI. An agreement can be obtained by increasing of the core flattening corresponding to an extra difference between the equatorial and the polar radii of about 500 meters. When accounting for the electromagnetic torque at the CMB (Mathews *et al.*, 2002) this extra difference is reduced to about 380 meters.

The FCN quality factor Q_f arises primarily from the dissipative part of the electromagnetic torque at the CMB, contributing to $\tilde{\beta}$ (Mathews *et al.*, 2002).

The FCN resonance influences nutation in two different ways. The first one is a direct influence, that is free celestial motion of the pole excited by the angular momentum transfer from fluid layers (atmosphere, ocean, etc.). There is also an indirect influence consisting in the resonant enhancement of the amplitudes of those nutation terms that are close to the resonance. Particularly sensitive to the FCN resonance is the retrograde annual nutation.

An important part of research concerning the FCN resonance is the determination of the resonant parameters T_f and Q_f from the observations of Earth rotation. This estimation is much more efficient from the indirect effect. The most up-to-date values are these adopted in the MHB2000 transfer function (Mathews *et al.*, 2002) used to construct the IAU 2000 precession-nutation model: $T_f' = -430.20$ days $(429.93, 430.48)$, $Q_f = 20\,000$ $(18\,870, 21\,280)$, where the values in parentheses give the uncertainty limits, and the prime indicates that the period is expressed in the nonrotating celestial system. An alternative method of estimation, similar to that applied for the determination of the Chandler wobble parameters, consists in extracting the freely excited FCN signal from the time series of the VLBI celestial pole offsets (Figure 2b) and fitting the resonance parameters. This estimation is considerably less accurate than that based on the indirect effect, and significantly less

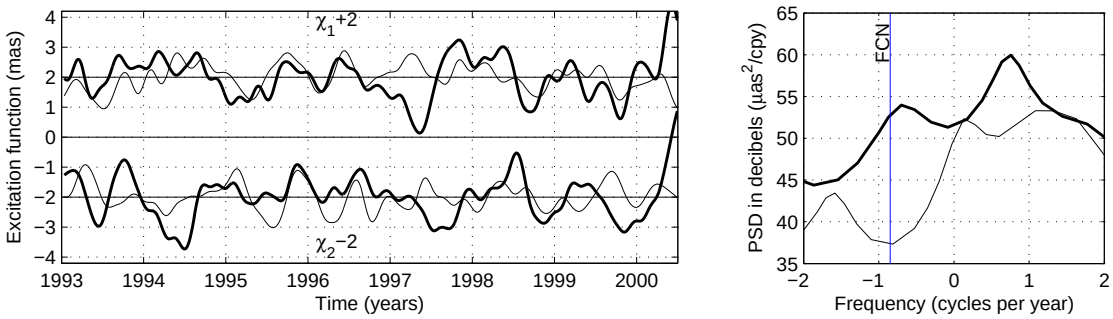

Figure 4. Comparison of the geodetic excitation of nutation (blue, thin) with geophysical excitation AAM+OAM (red, thick), in time domain (left) and in frequency domain (right) (from Brzeziński and Bolotin, 2006).

accurate than the corresponding procedure for the Chandler wobble (Brzeziński, 2005). Moreover, the result depends on the VLBI solution selected for the analysis and is sensitive to the initial reduction of the input series. Bolotin and Brzeziński (2005) analyzed eight individual solutions of the VLBI data analysis as well as two combined solutions, and estimated the FCN parameters from the maximum likelihood ARIMA modeling. The dispersion of estimates was quite large, between -435 and -418 days for the period and between 3000 and 14000 for Q. The best agreement with the indirect estimate was for the series `maotst01` (Bolotin, private communication): $T'_f = -431.0$ days $(418.8, 444.0)$, $Q_f = 7\,514$ $(3\,870, 130\,400)$. Note, however, the large uncertainty limits of the last estimate.

Another part of research concerning the FCN is a search for the process, or for the combination of processes, that excites the free oscillation and maintains it against the energy dissipation. This can only be done by tracking the free signal observed by VLBI and comparing it to the geophysical excitation data. A simple algorithm of comparison, similar to that applied routinely in the excitation studies of the Chandler wobble, was proposed by Brzeziński (1994, 2006). The first step consists in computing the corresponding "geodetic" excitation from the time series of the celestial pole offsets observed by VLBI. The estimate of the geophysical excitation, such as the atmospheric and nontidal oceanic angular momentum (AAM, OAM) functions, should be sampled more frequently than 2 times per day. Before the comparison, the retrograde diurnal component of the excitation which influences nutation should be extracted by the so-called complex demodulation at frequency -1 cycle per sidereal day.

Preliminary results of the FCN excitation study were reported by Brzeziński and Bolotin (2006). Figure 4 shows a comparison between the excitation inferred from the VLBI data and that representing the aggregated influence of the dynamically coupled system atmosphere-oceans. The time domain comparison shows a rough agreement in size. The overall correlation is small, at the level of 0.2. However, when performing the sliding-window correlation analysis we could detect periods with high correlation, up to 0.8, but also periods with significant negative correlation. A comparison of the power spectral densities shows that geophysical excitation functions contain more power at the FCN frequency than needed to explain the observed signal, by a factor of about 30. The integration of cross-power spectrum in the vicinity of the FCN frequency, yields a high coherence magnitude, over 0.7. But surprisingly, the estimated argument of coherence is close to 180°, that

is the geodetic and geophysical excitations are out of phase.

In conclusion we should say that the reported results concerning the atmospheric and oceanic excitation of the FCN, though promising in several aspects nevertheless have to be treated as preliminary. Such investigations should be continued using alternative subdiurnal estimates of the atmospheric and oceanic excitation of Earth rotation.

4. High Frequency Polar Motion

Polar motion contains high frequency signals which have been predicted from theory and, at least in some cases, confirmed by observations. The first group consists of the components associated with the atmospheric normal modes. These are the pseudoharmonic oscillations with the following standard codes, central periods and mean amplitudes:

ψ_3^1, retrograde period 10 days, amplitude up to 0.5 mas,

ψ_1^1, retrograde period 1.2 days, amplitude about 30 μas,

ξ_2^1, period about 0.6 days, amplitude of the order of 1 μas.

(Here by "mean amplitude" we understand square root of the total variance of oscillation). All those three components are clearly visible in the AAM data, but only ψ_3^1 could be detected so far in the space-geodetic observations of polar motion; see Brzeziński *et al.* (2002) for details.

The second group is a set of quasi diurnal and quasi semidiurnal harmonic terms with amplitudes up to 300 μas, excited by the ocean tides. The retrograde diurnal components of excitation contribute to nutation and have been taken into account in the conventional precession-nutation model IAU 2000 discussed in Sec.2. The remaining prograde diurnal and retrograde/prograde semidiurnal components contributing to polar motion are described by the model provided by the IERS Conventions 2003 (IERS, 2004; Tables 8.2a and 8.2b). In addition, there are also prograde diurnal terms in polar motion caused by the direct influence of the tidal gravitation on the triaxiality (that is inequality of the principal equatorial moments of inertia A and B) of the Earth; see Brzeziński and Mathews (2003) for an extensive discussion. This effect is considerably smaller than that due to the ocean tides—the maximum amplitudes are about 15 μas. Nevertheless the corresponding model is also included in the IERS Conventions 2003 (IERS, 2004; Table 5.1).

Finally, there are also high frequency variations in Earth rotation associated with the atmospheric thermal (radiational) tides S_1 and S_2. These are the diurnal and semidiurnal terms modified by the oceanic response to the atmospheric forcing. Among them only the effect of the Sun-synchronous S_1 term has been included in the IAU 2000 precession-nutation model in the form of a correction to the amplitude of prograde annual nutation. Our estimation of the atmospheric and nontidal oceanic contributions yielded the amplitudes of 9 μas for both diurnal prograde and semidiurnal polar motions (Brzeziński *et al.*, 2004).

Theoretical models of the ocean tide contributions to diurnal and semidiurnal polar motion could be constrained from VLBI observations by Sovers et al. (1993), Herring and Dong (1994), Gipson (1996). In addition, several special VLBI campaigns like CONT94, CONT02, CONT05, have been organized to estimate less regular high frequency geophysical signals in Earth rotation and compare them with the existing theoretical models.

But even from the routine VLBI observations with one session in 3 to 5 days, it is possible to determine quasi-periodical geophysical signals within diurnal and subdiurnal frequency bands. The method, proposed originally by Herring and Dong (1994) and further developed by Mathews and Herring (2000), Brzeziński (2000), relies upon the so-called frequency demodulation technique.

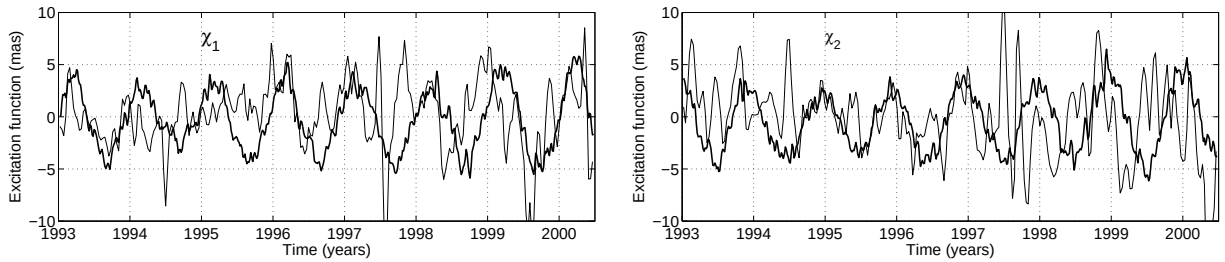

Figure 5. Excitation of the prograde diurnal polar motion by the dynamically coupled system atmosphere-ocean: geodetic excitation inferred from VLBI data (blue, thin) and AAM+OAM (red, thick). Data sets were taken from Kudryashova and Petrov (2006) and Brzeziński *et al.* (2004).

Kudryashova and Petrov (2006) applied this technique to estimate the prograde diurnal polar motion form 1989 to 2004. We converted this signal into the "geodetic" excitation function and compared it to the corresponding atmospheric and nontidal oceanic angular momentum data taken from Brzeziński *et al.* (2004); see Figure 5. Both signals are highly coherent which proves that the diurnal polar motion series estimated from the VLBI observations is a real physical signal. Our recent study (Bolotin and Brzeziński, 2006) described in detail the procedure of extracting the high-frequency (diurnal, semidiurnal, etc.) signals in polar motion and UT1 from the standard VLBI observations, which can be used for comparisons with the available geophysical excitation data.

5. Concluding Remarks

The VLBI observations provide important data sets for modeling changes in Earth rotation and for their geophysical interpretation. Currently, VLBI is the only technique for monitoring the motion of the celestial pole. The time series of the celestial pole offsets estimated from the VLBI observations are important for further improvements of the conventional precession-nutation model. This is also the only way of representing the irregular geophysical signals such as the free core nutation, which cannot be predicted perfectly. VLBI observations are also very useful for constraining the high frequency signals in Earth rotation, though not the whole potential of the technique has been utilized so far. It is extremely important for both practical reasons and the scientific studies concerning global dynamics of the Earth that VLBI continues its mission of monitoring the Earth orientation parameters on a regular basis. An optimal representation of the Earth rotation data would be achieved if the VLBI observing sessions could be conducted with daily spacing.

Acknowledgements. I thank Sergei Bolotin for valuable comments and suggestions concerning the manuscript. This research has been supported by the Polish Ministry of Scientific Research and Information Technology under grant No. 5 T12E 039 24. Participation in the Fourth IVS General Meeting was supported by grant No. 4 T12E 039 29.

References

[1] Bizouard Ch., A. Brzeziński, and S. D. Petrov, Diurnal atmospheric forcing and temporal variations of the nutation amplitudes, *Journal of Geodesy*, **72**, 561–577, 1998.

[2] Bolotin S. and A. Brzeziński, Investigation of the FCN signal from the available time series of VLBI nutation data, *Astron. Astrophys.*, submitted, 2005.

[3] Bolotin, S. and A. Brzeziński, A search for geophysical signals in diurnal and semidiurnal polar motion from analysis of the routine VLBI observations, *Geophysical Research Abstracts*, **8**, abstract EGU06-A-01665, 2006.

[4] Brzeziński, A., Polar motion excitation by variations of the effective angular momentum function, II: extended model, *manuscripta geodaetica*, **19**, 157–171, 1994.

[5] Brzeziński A., The CEP and geophysical interpretation of modern Earth rotation observations, *Proc. IAU Colloquium 178 "Polar Motion: Historical and Scientific Problems", eds. S. Dick, D. McCarthy and B. Luzum*, Astronomical Society of the Pacific, Conference Series Vol. 208, 585–594, 2000.

[6] Brzeziński A., Chandler wobble and free core nutation: observation, modeling and geophysical interpretation, *Artificial Satellites*, **40**, No. 1, 21–33, 2005.

[7] Brzeziński, A., A simple digital filter for the geophysical excitation of nutation, *Journal of Geodesy, Special VLBI issue*, submitted, 2006.

[8] Brzeziński, A. and S. Bolotin, Atmospheric and oceanic excitation of the free core nutation: observational evidence, *Proc. Journées Systèmes de Référence Spatio-Temporels 2005, eds. A. Brzeziński, N. Capitaine and B. Kołaczek*, Space Research Centre of the Polish Acad. of Sciences, Warsaw, in press, 2006.

[9] Brzeziński, A. and P. M. Mathews, Recent advances in modeling the lunisolar perturbation in polar motion corresponding to high frequency nutation: report on the discussion of the IAU Comm. 19 WG on Nutation, *Proceedings Journées Systèmes de Référence Spatio-Temporels 2002, eds. N. Capitaine and M. Stavinschi*, Ars Docendi, Paris, 101–108, 2003.

[10] Brzeziński A., Ch. Bizouard and S. Petrov, Influence of the atmosphere on Earth rotation: what new can be learned from the recent atmospheric angular momentum estimates? *Surveys in Geophysics*, **23**, 33–69, 2002.

[11] Brzeziński, A., R. M. Ponte and A. H. Ali, Non-tidal oceanic excitation of nutation and diurnal/semidiurnal polar motion revisited, *J. Geophys. Res.*, **109**, No. B11, doi: 10.1029/2004JB003054, 2004.

[12] Capitaine, N., P. T. Wallace, and J. Chapront, Improvement of the IAU 2000 precession model, *Astron. Astrophys.*, **432**, 355–367, 2005.

[13] Dehant V., et al., Considerations concerning the non-rigid earth nutation theory, *Cel. Mech. Dynamical Astr.*, **72**, 245–310, 1999.

[14] Dehant, V., M. Feissel-Vernier, O. de Viron, C. Ma, M. Yseboodt, and Ch. Bizouard, Remaining error sources in the nutation at the sub-milliarcsecond level, *J. Geophys. Res.*, **108**, doi: 10.1029/2002JB001763, 2003.

[15] Gipson, J. M., Very long baseline interferometry determination of neglected tidal terms in high-frequency Earth orientation variatons, *J. Geophys. Res.*, **101** (B12), 28,051–28,064, 1996.

[16] Gwinn, C. R., T. A. Herring, and I. I. Shapiro, Geodesy by radio interferometry: studies of the forced nutations of the Earth 2. Interpretation, *J. Geophys. Res.*, **91**, No. B5, 4755–4765, 1986.

[17] Herring, T. A., and D. Dong, Measurement of diurnal and semidiurnal rotational variations and tidal parameters of Earth, *J. Geophys. Res.*, **99** (B9), 18,051–18,071, 1994.

[18] Herring, T. A., C. R. Gwinn, and I. I. Shapiro, Geodesy by radio interferometry: studies of the forced nutations of the Earth 1. Data analysis, *J. Geophys. Res.*, **91**, No. B5, 4745–4754, 1986.

[19] IERS Conventions 2003, D. McCarthy and G. Petit (eds.), *IERS Technical Note No. 32*, Verlag des Bundesamts für Kartographie und Geodäsie, Frankfurt am Main, 2004, (electronic version is available from `http://www.iers.org/iers/products/conv/`).

[20] Kinoshita, H., Theory of rotation of the rigid Earth, *Celes. Mech.*, **15**, 277–326, 1977

[21] Kudryashova, M. V. and S. D. Petrov, Diurnal polar motion from VLBI observations, *Proc. Journées Systèmes de Référence Spatio-Temporels 2005, eds. A. Brzeziński, N. Capitaine and B. Kołaczek*, Space Research Centre of the Polish Acad. of Sciences, Warsaw, in press, 2006.

[22] Mathews, P. M. and T. A. Herring, On the reference pole for Earth orientation and UT1, *Proc. IAU Colloquium 180 "Towards Models and Constants for Sub-Microarcsecond Astrometry", eds. K. Johnston, D. McCarthy, B. Luzum and G. Kaplan*, U.S. Naval Observatory, Washington DC, USA, 164–170, 2000.

[23] Mathews, P. M., T. A. Herring, and B. A. Buffet, Modeling of nutation-precession: New nutation series for nonrigid Earth, and insights into the Earth's interior, *J. Geoph. Res.*, **107**, doi: 10.1029/2001JB000390, 2002.

[24] Seidelmann P. K., 1980 IAU theory of nutation: The final report of the IAU working group on nutation, *Celes. Mech.*, **27**, 79–106, 1982.

[25] Souchay, J., B. Loysel, H. Kinoshita, and M. Folgueira, Corrections and new developments in rigid Earth nutation theory: III. Final tables 'REN-2000' including crossed-nutation and spin-orbit coupling effects, *Astron. Astrophys.*, **318**, 639–652, 1999.

[26] Sovers, O. J., C. S. Jacobs, and R. S. Gross, Measuring rapid ocean tidal Earth orientation variations with very long baseline interferometry, *J. Geophys. Res.*, **96**, No. B11, 19,959–19,971, 1993.

[27] Wahr J. M., The forced nutations of an elliptical, rotating, elastic and oceanless Earth, *Geophys. J. R. astr. Soc.*, **64**, 705–727, 1981.

Massimo Tarenghi: The ALMA Project, IVS 2006 General Meeting Proceedings, p.30–30
http://ivscc.gsfc.nasa.gov/publications/gm2006/tarenghi

The ALMA Project

Massimo Tarenghi

ALMA Consortium
e-mail: mtarengh@eso.org

No abstract available.

[Note from the Editors: The overheads of the oral presentation of this contribution can be downloaded from the IVS 2006 General Meeting web site. Please get the PDF file of the presentation at the URL ftp://ivscc.gsfc.nasa.gov/pub/general-meeting/2006/presentations/gm2006_1-06_tarenghi.pdf.]

Markus Vennebusch et al.: IVS' Contribution to the IERS Combination Pilot Project and to the ITRF2005 - Status & Results, IVS 2006 General Meeting Proceedings, p.31–35
http://ivscc.gsfc.nasa.gov/publications/gm2006/vennebusch1

IVS' Contribution to the IERS Combination Pilot Project and to the ITRF2005 - Status & Results

Markus Vennebusch, Sarah Böckmann

Geodetic Institute of the University of Bonn
Contact author: Markus Vennebusch, e-mail: vennebusch@uni-bonn.de

Abstract

The VLBI group of the Geodetic Institute of the University of Bonn (GIUB), Germany combined the individual solutions of almost 3600 VLBI sessions on the level of datum free normal equation matrices. These combined sessions form an important basis for the new ITRF2005 and for the new combination strategy within the IERS Combination Pilot Project for the combination of all geodetic space techniques (VLBI, GPS, SLR and DORIS). In this paper the status and some results of this so-called VLBI intra-technique combination will be presented to show the quality of VLBI SINEX data. The results contain comparisons of EOP series derived from IVS SINEX data as well as Helmert parameters of the combined solutions with respect to ITRF2000.

1. IVS' Activities in the Combination Pilot Project

Since about 2002 large efforts have been made by the IVS Analysis Centers in order to contribute their solutions to the IERS CPP.

Most of the software packages used for routine data analysis have been modified to generate SINEX files containing datum-free normal equation matrices. Since CALC/SOLVE and OCCAM (LSM) perform the least squares adjustment by using normal equations, these software packages generate datum-free normal equations in its pure form as it should be provided to the IERS CPP by every technique. Special attention should be paid to SteelBreeze (developed at MAO, Main Astronomical Observatory, Kiev), a software based on Square Root Information Filter technique (SRIF) which is also able to generate SINEX files containing datum-free normal equation matrices.

Currently there are seven IVS Analysis Centers using four different software packages contributing their solutions to the VLBI-intra-technique-combination and to the IERS CPP. Table 1 shows the analysis centers and the software used for regular data analysis.

AC	Name	Software
AUS	Geoscience Australia, Canberra, Australia	OCCAM (Kalman)
BKG	Bundesamt für Kartographie und Geodäsie, Leipzig, Germany	CALC/SOLVE
DGFI	Deutsches Geodätisches Forschungsinstitut, Munich, Germany	OCCAM (LSM)
GSFC	Goddard Space Flight Center, Washington D.C., USA	CALC/SOLVE
MAO	Main Astronomical Observatory, Kiev, Ukraine	SteelBreeze
SHA	Shanghai Astronomical Observatory, China	CALC/SOLVE
USNO	U.S. Naval Observatory, Washington D.C., USA	CALC/SOLVE

Table 1. IVS analysis centers contributing to the CPP

The analysis centers mentioned in Table 1 reprocessed almost all available VLBI data in order to generate SINEX files. About 4100 VLBI sessions (starting in 1979 till 2005) have been analysed by (at most) seven analysis centers. A daily updated website, available at

http://vlbi.geod.uni-bonn.de/sinex_combination/SINEX_statistics.html

lists all sessions available and shows the current status of file submissions to the IVS Data Centers.

2. VLBI – Intra-technique Combination

For the VLBI-intra-technique combination a software called *dogs-cs* (developed at the German Geodetic Research Institute (DGFI), Munich) as well as PERL-scripts (developed at GIUB) are used to combine up to seven individual solutions to an official IVS solution for the IVS CPP.

The VLBI-intra-technique combination consists of the following steps:

2.1. Download of Individual Normal Equations (SINEX Files)

Up to seven SINEX files containing datum-free normal equation matrices of the individual contributions are being downloaded from one of the IVS Data Centers. This process is done automatically at GIUB. As soon as there are enough (usually four to five) individual contributions of a single VLBI session the combination process is started.

2.2. Conversion of SINEX Data into dogs-cs Format

A conversion tool called *snx2dogs* has been developed at GIUB in order to convert all data necessary for the combination into special binary format for *dogs-cs*. If necessary, another tool (from DGFI) generates datum-free normal equation matrices from covariance matrices (contained e.g. in AUS solutions).

2.3. Computation of EOP from the Individual Solutions

The next step consists of the reconstruction of the individual solutions after transformation to the same set of apriori values and to the same reference epoch. After reducing nutation parameters and imposing the same datum definition (usually by fixing all station positions) earth orientation parameters and their rates are estimated and are compared to the combined solution in a later step. These residuals are used to detect outlier solutions which will be excluded from the combination.

The steps are as follows:

- Since every IVS Analysis Center uses different sets of apriori values, the individual normal equations have to be transformed to a common set of apriori values for TRF and EOP. Usually the apriori values of the first contributing normal equations are used as the common set of apriori values.
- The epochs of the results of the individual contributions of one VLBI session may differ by up to 15 minutes. This is caused by the fact that the reference epoch of the parameters is computed as the weighted mean of the epochs of the delay observables. Excluding observations or even entire stations might lead to different mean epochs which have to be accounted for in the combination. This transformation is performed by a *dogs-cs* subroutine.

- Reduction of nutation parameters is necessary because of different nutation models used in the different software packages. Therefore the normal equation system and the vector of unknowns is being partitioned such that only the parameters of interest remain (see e.g. ANGERMANN ET AL., [3]).
- The datum definition is usually performed by fixing all station positions. This step is only necessary for outlier detection, it does not have any impact on the accumulation of datum-free normal equations described below.

2.4. Scaling of the Individual Normal Equation Matrices

In order to equalize the impact of the individual contributions **in the inter-technique combination** it is necessary to scale every matrix by the factor "1 / *number of contributions for the particular session* = 1 / *number of analysis centers used in the combination*".

2.5. Weighting of the Individual Normal Equation Matrices

In order to account for the different qualities of the individual contributions, some kind of quality criterium must be found. Using the statistical information from the SINEX file (as e.g. WEIGHTED SQUARE SUM OF O-C) the residuals of the individual solutions concerning the combined solution can be computed (see e.g. ANGERMANN ET AL., [3]) and can be used to estimate variance components (see e.g. KOCH, [1]). The reciprocal variance factors are then used as weights for the following step of accumulation.

This step is still under development. Investigations of different methods for variance component estimation are currently being carried out.

2.6. Accumulation and Combination

This part forms the actual combination step of the datum-free normal equation matrices. Based on the accumulation theorem for pre-reduced normal equation matrices (see e.g. MIKHAIL, [2]) the normal equations are added by a *dogs-cs* subroutine.

2.7. Imposing Datum Definition and Inversion of the Combined Normal Equation Matrix

Using the same datum definition as for the individual contributions for the accumulated normal equations, combined EOP and their rates are being estimated.

2.8. Analysis of Individual EOP and Their Rates w.r.t. Combined EOP (Residuals)

As a first quality check the EOP results of the individual contributions are being compared with the combined results. If the residuals exceed a certain threshold (usually $2 \cdot \sigma_{Combination}$) the solution containing the outlier will be excluded and the combination will be repeated without this particular solution.

2.9. Determination of Helmert Parameters w.r.t. to ITRF2000

In the next step an NNT/NNR condition is imposed on the combined datum-free normal equation matrix in order to generate an (undeformed) TRF solution. Then Helmert parameters of the resulting coordinates w.r.t. ITRF2000 are computed in order to check the quality of the polyhedron formed by the combined solution and to detect outlier stations or other station anomalies.

2.10. Generation of SINEX File Containing Accumulated Normal Equations

If there are no station anomalies, the accumulated datum-free normal equation matrix is being written into a new SINEX file containing all station components, polar motion, dUT as well as their rates.

2.11. Submission of Combined Normal Equations

At last, the combined SINEX file is send to one of the IVS Data Centers where it is automatically downloaded to the IERS CPP data center.

3. Current Investigations

Using the strategy described above, more than 3600 VLBI sessions have been combined sessionwise on the level of datum-free normal equation matrices (the remaining 500 sessions are either too small for reasonable parameter estimation or they were designed for special purposes and are therefore not suitable for the combination). Each combined session can be used as contribution to the IERS CPP as well as for internal VLBI investigations. The results of the internal investigations (e.g. determination of EOP or site positions) are also being used as quality checks and validation of the contributions to the IERS CPP.

3.1. Earth Orientation Parameters

VLBI SINEX data containing data of sessions from 1979 to 2005 have been used to generate EOP series. In order to obtain EOP usually all station positions have been fixed to their a priori positions and only EOP and their rates have been estimated.

EOP series resulting from this method have been compared to EOP series generated from other techniques (e.g. GPS, SLR, etc.) as well as to IERS C04.

3.2. Station Components

Each individual VLBI session can also be used to estimate site positions of each station participating in the particular session. Using all available data from 1984 till now, time series of site positions can be generated and can be compared to time series derived by other techniques.

A comparison of time series of the coordinates of about 40 VLBI stations with co-located GPS stations shows a good agreement in the particular trends. This shows the suitability of VLBI data for the ITRF2005.

3.3. Helmert Parameters

Another quality check is the computation of Helmert parameters for the individual combined solutions with respect to ITRF2000. The agreement of the combined site positions with the ITRF (in terms of scale and residuals) shows the quality of the individual VLBI polyhedron and its suitability for the ITRF2005 combination.

4. Outlook and Future Tasks

The generation of consistent VLBI time series of EOP and station coordinates requires independency from a single VLBI software package alone. Only the combination of the results of different VLBI software packages can produce a reliable basis for a further combination with other space geodetic techniques.

In addition, the VLBI-Intra-technique combined products not only serve as contribution to the inter-technique combination, but these time series can also be used as an independent validation of the inter-technique solution as well as for further VLBI investigations.

The VLBI time series generated in form of pre-reduced normal equation matrices show the capability of VLBI SINEX data as a promising contribution to the ITRF2005. So far, both the comparisons with station components of GPS and the Helmert parameters show good agreement. The final results will be presented in another paper soon.

Nevertheless, the following problems or tasks still have to be solved:

- Transformation of the reference epoch towards 12 UTC
- Introducing correlations between different analysis centers
- Transformation of nutation parameters based on different nutation models into one common set for a uniform modelling of the movement of the rotation axis in space.
- Investigations for a consistent estimation of atmosphere parameters at fixed epochs taking into account horizontal gradients.

References

[1] Koch, Karl-Rudolf: *Parameter Estimation and Hypothesis Testing in Linear Models*, Springer, New York, 1999.

[2] Mikhail, E., F. Ackermann: *Observations and Least Squares*, IEP, New York, 1976.

[3] Angermann et al.: *ITRS Combination Center at DGFI: A Terrestrial Reference Frame Realization*, Deutsche Geodätische Kommission, München, 2004.

Jinling Li et al.: Ionosphere Delay Corrections in Satellite VLBI Observations, IVS 2006 General Meeting Proceedings, p.36–40
http://ivscc.gsfc.nasa.gov/publications/gm2006/jl-li

Ionosphere Delay Corrections in Satellite VLBI Observations

Jinling Li, Li Guo, Bo Zhang

Shanghai Astronomical Observatory
Contact author: Jinling Li, e-mail: JLL@SHAO.AC.CN

Abstract

In this paper the ionosphere delay correction in satellite VLBI observations is discussed. The Total Electron Content (TEC) along the ray path measured by VLBI dual-band technique and predicted by GPS observations for Seshan25 — Urumqi baseline and baselines of CONT02 were compared, showing that the TEC from GPS observations could be applied to correct the satellite VLBI observations, but there sometimes exists a significant systematic bias in the VLBI observed TEC. This bias could vary between two VLBI trackings and so for each tracking of satellite the ERS observations are required to determine the bias regardless whether the S/X dual-band satellite observations are available or not.

1. Introduction

In astrometric/geodetic VLBI the S/X dual-band observations are ordinarily used to correct the ionosphere delay. However, in the Chinese lunar mission Chang'E-1, the S/X dual-band observations cannot always be guaranteed during the satellite positioning and trajectory determination by range, Doppler and VLBI. It is therefore necessary to make the ionosphere delay corrections by using other means besides the VLBI dual-band technique, for instance using GPS data. In addition, it needs to be decided whether the dual-band technique is still directly applicable to the ionosphere delay correction of satellite VLBI observations or not.

In the following sections firstly we review some basic methods in the determination of the ionosphere delay or the Total Electron Content (TEC) by VLBI dual-band technique and by GPS observations in Section 2. Then after processing the observations of VLBI and GPS the TEC deduced from the two techniques are compared. The observations we used are from the archives of the International GPS Service (IGS) and the International VLBI Service for Geodesy and Astrometry (IVS). Section 3 is about the Chinese Seshan25 — Urumqi baseline, while Section 4 is about the baselines of CONT02. Lastly in Section 5 we discuss the scheme of ionosphere delay correction in the satellite VLBI observations.

2. Some Basic Principles and Methods

The earth's ionosphere is defined as the part of the upper atmosphere above 100 km from the ground, where the free electron density reaches its peak value between the altitudes of 300 km and 500 km; the electrons are mainly centered in the F region. The retardation of the ionosphere to a radio signal is inversely proportional to the square of the signal frequency (Takahashi et al., 2000). Based on this, the TEC along the ray path can be estimated by using the dual-frequency observations. In astrometric/geodetic VLBI, the S/X dual bands are used; in GPS, the L band frequencies 1575.42MHz and 1227.60MHz are used, the IGS sites are equipped with dual-frequency receivers. The methods to obtain TEC from VLBI and GPS are briefly reviewed in the following.

2.1. TEC from VLBI

In the case of cold plasma approximation, the ionosphere correction, $\Delta\tau_{ion}$ (s), to radio signal at frequency f (Hz) is expressed as (Takahashi et al., 2000),

$$\Delta\tau_{ion} = 1.34 \times 10^{-7} f^{-2} TEC \tag{1}$$

where TEC is the total electron content in a volume with a cross section of $1m^2$ and along the ray path. In astrometric/geodetic VLBI, suppose the frequencies of the S/X dual bands are f_s and f_x, and the corresponding delays are τ_s and τ_x , then the X band ionosphere delay correction $\Delta\tau_{ion-x}$ is as follows ,

$$\Delta\tau_{ion-x} = \frac{f_s^2}{f_s^2 - f_x^2}(\tau_x - \tau_s) + const \tag{2}$$

The second term is included in the estimation of the quasi-clock offset in ordinary astrometric/geodetic VLBI data analysis of extragalactic radio sources (ERS). Thus, even if it is unknown, it should not result in any problem in the estimation of other parameters.

In the database of astrometric/geodetic VLBI, the observation directions and the ionosphere delay corrections at reference frequency are already exhibited. Based on this correction and $Eq.(1)$ the TEC difference at the two ends of a baseline in the lines of sight and at the observation epoch could be easily deduced. In the following we call this the TEC measured by VLBI.

2.2. TEC from GPS

From the pseudo range observations P_1 and P_2 by a GPS receiver, the following equation is easy to get (Liu et al., 1999).

$$TEC = 9.52437(P_2 - P_1) \tag{3}$$

where TEC is in $TECU$ (10^{16} electrons), P_1 and P_2 are in $meters$. That is, the TEC in the line of sight could be directly deduced from GPS dual-frequency pseudo ranges. Similarly, from the carrier phase data it is easy to get,

$$TEC = 9.52437(\lambda_2\varphi_2 - \lambda_1\varphi_1) + 9.52437(\lambda_2 N_2 - \lambda_1 N_1) \tag{4}$$

where λ and φ are the wavelength (m) and phase (fraction of a cycle) of the carrier signal respectively. N is the number of cycles. Let $L_g = \lambda_2\varphi_2 - \lambda_1\varphi_1$ and $D = \lambda_2 N_2 - \lambda_1 N_1$. L_g can be taken as pseudo observation and D is unknown or ambiguity. From $Eqs.(3)$ and (4) we have

$$\Delta P_2 P_1 = P_2 - P_1 = L_g + D \tag{5}$$

For ordinary hardware of GPS receiver, the precision of L_g is usually two to three orders higher than $\Delta P_2 P_1$. By estimating the ambiguity D in $Eq.(5)$ with a linear Kalman filter, the precision of $\Delta P_2 P_1$ can be improved and accordingly the TEC in the line of sight can be deduced with a higher precision than solely using pseudo ranges as in $Eq.(3)$.

Assuming a thin shell ionosphere model with an altitude of $h = 350km$ above ground, the TEC in $Eq.(3)$ to (5) is slant at the intersection point of the ray path with the shell $(STEC)$, it is converted into vertical TEC $(VTEC)$ in the form $VTEC = STEC * f(R, h, z)$,

$$f(R, h, z) = \left[1 - \left(\frac{R}{R+h} sinz\right)^2\right]^{-1/2} \tag{6}$$

where z is the elevation and R is the earth's radius.

After the data processing the TEC time series in the zenith direction of GPS receivers co-located with VLBI antennas could be deduced and mapped to the VLBI observation directions. In the following we refer to this as the TEC predicted by GPS.

3. About the Baseline Seshan25 — Urumqi

Seshan25 (Shanghai) and Nanshan (Urumqi) VLBI stations began astrometric/geodetic observations in 1989 and 1993, respectively, and by the end of 2004 there were 14 24-hour VLBI sessions accompanied by synchronous GPS observations. As an example Fig.1 and 2 demonstrate the TEC comparison on March 9 and April 13 of 2004, where the "TEC by VLBI" is converted (as shown by *Eq.*(1) and (2)) from the X band ionosphere delay correction which is directly extracted from the VLBI database, while the "TEC by GPS" is deduced from the co-located GPS observations in the way shown by *Eq.*(3) to (5). The slant line indicates a perfect linear relationship with the slope as one.

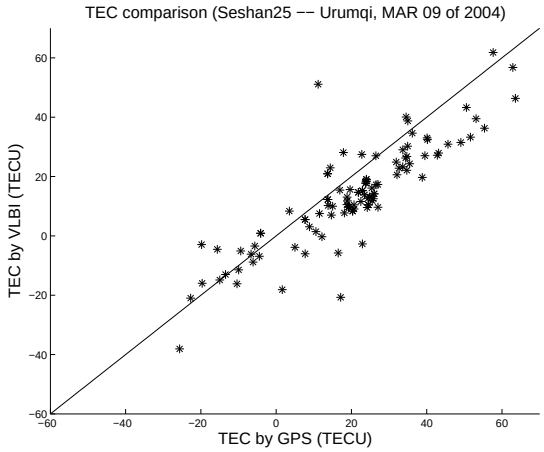

Figure 1. TEC comparison on March 9 of 2004.

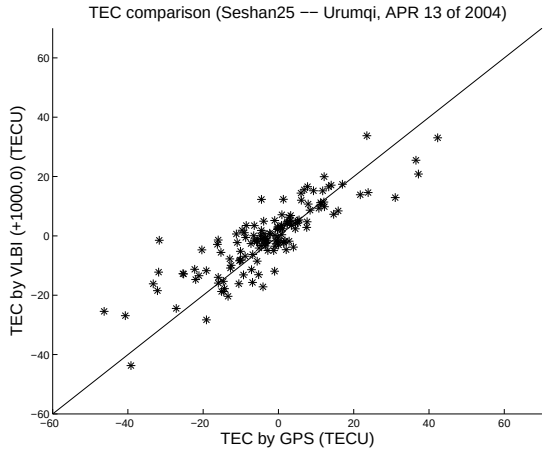

Figure 2. TEC comparison on April 13 of 2004.

In Fig.1 the TEC from the two techniques are correlated with each other very well with a correlation coefficient of 0.92 and there is no obvious systematic difference. The TEC difference is mostly within $[-10, +20]TECU$ with a *wrms* of $9.7TECU$, equivalent to delays in X-band of about $[-0.2, +0.4]ns$ and a *wrms* of $0.19ns$. In Fig.2 however, TEC by VLBI and GPS exhibits an obvious systematic difference of about $1000TECU$, equivalent to $20ns$ delay in X-band. The correlation coefficient is about 0.87. After the correction of the systematic difference the residual TEC difference by VLBI and GPS is between $[-15, +15]TECU$ with a *wrms* of $7.3TECU$, equivalent to delays in X-band of $[-0.3, +0.3]ns$ and a *wrms* of $0.15ns$.

For Fig. 2, the average TEC prediction by GPS is about $0TECU$, while VLBI gives a value of about $-1000TECU$. Even in the highest solar activity stage so great a TEC value is definitely impossible, which shows that there exists a systematic bias in the VLBI observed TEC and that this bias is varying with time being different for different observation sessions. This bias could originate from various aspects such as phase calibration, settings of *a priori* values in correlation, process of fringe searching and so on (Corey, 2006). In ordinary astrometric/geodetic VLBI data analysis of ERS, the sources of this bias and the relative weight of each factor are not necessarily

concerned, but are all parameterized as part of the quasi-clock offset and by doing so it should not affect the solutions of other parameters such as the station and radio source coordinates as well as the Earth Orientation Parameters. However, in the data analysis of satellite positioning and orbit determination by VLBI, the practice of real data reduction shows that it is impossible to simultaneously solve for this offset along with satellite parameters because of correlation. It is possible to determine this quasi-clock offset independently by using ERS observations. In order to check the time variation characteristics of the systematic bias in the VLBI observed TEC and to discuss the manners for the interpolated ERS observations, we analyze in the following the situation for the CONT02 campaign.

4. About the Baselines of CONT02

CONT02 is one of the continuous observation campaigns organized by IVS from October 16 to 31 of 2002, aimed at demonstrating the ability of VLBI to continuously observe the Earth Orientation Parameters and consists of 5 24-hour sessions. For each session the observation is from UTC18:00 to UTC17:50 of the next day. Generally the observation data flow of every baseline is interrupted about 30 minutes between every two neighboring 24-hour sessions and it is continuous during each session except for occasional failures. Observation antennas are Algopark, Gilcreek, Hartrao, Nyales20, Westford, Kokee, Onsala60 and Wettzell and all have co-located GPS receivers.

The TEC by VLBI observation and GPS prediction are compared for each baseline of CONT02 and a typical example is shown in Fig.3. Dots are TEC by VLBI observation, crosses are TEC by GPS prediction, asterisks and lines at the bottom of each plot indicate the interruptions of the data flow due to shift of sessions or occasional failures. Fig.3 shows that during the continuous observation period the trend of TEC by VLBI observation and by GPS prediction is consistent to each other; the correlation coefficient is larger than 0.80. However, there sometimes exist obvious systematic jumps at session shifts or periods of occasional failure. Jumps could be as high as several hundred $TECU$, which is equivalent to delays of several nanoseconds in X-band. It is not true that all the session shifts or occasional failures are accompanied by systematic jumps, but all the jumps take place at some of the shifts or failures.

5. Concluding Remarks

We conclude from the above that during the satellite positioning and orbit determination by VLBI it is feasible to make the ionosphere delay corrections by using GPS observations, but that the systematic bias in VLBI measured TEC needs to be properly handled. We make the following three points:

1. In the case of single band satellite VLBI observations, it is feasible to correct the ionosphere delay by GPS predictions, but the quasi-clock corrections should be determined by VLBI single band observations of ERS because the dual-band observation could contain systematic bias. The key issue is to sustain the TEC precision of GPS prediction and to be aware of the variation of the quasi-clock correction.
2. In the case of dual-band satellite VLBI observations, the ionosphere delay corrections in the determination of quasi-clock correction from ERS observations and in the satellite positioning and orbit determination should be made by single technique only, either by VLBI dual-band

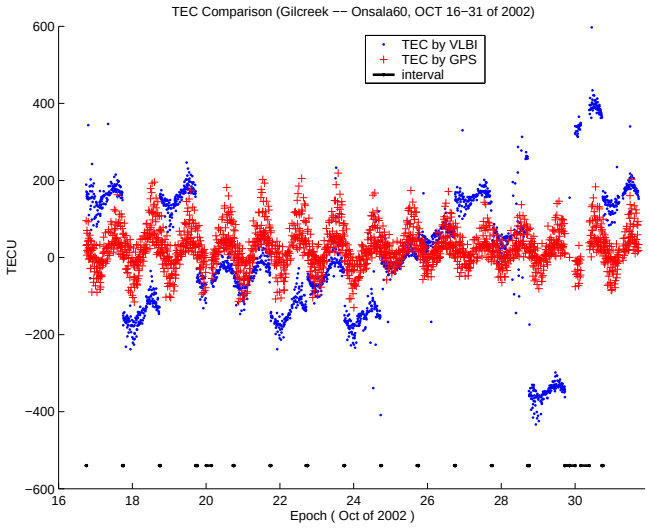

Figure 3. Gilcreek — Onsala60 baseline TEC comparison measured by VLBI and GPS during CONT02

technique or by GPS prediction, but not in a combined way.

3. The ambiguity in the VLBI observed delay is also a part of the quasi-clock offset, which could vary from time to time. In order to determine this offset and to be aware of its variation during the satellite VLBI observation, the ERS observation should be interpolated. It is good to observe more than one ERS within each interpolation for a precise determination of this offset and monitoring its variation.

Acknowledgements The authors show great thanks to Dr. B. Corey from MIT Haystack Observatory for his explanation about the jumps in the VLBI observed TEC. This work is partly supported by the Natural Science Foundation of China (10173019, 10473019), Chinese Academy of Sciences (KJCX2-SW-T1) and the Chinese lunar mission.

References

[1] Corey, B., private communication, 2006.

[2] Liu, J., J. Chen, Y. Zhang et al., Principle and Method of Wide Area Differential GPS. Beijing: Sino Maps Press, 95-102, 1999.

[3] Takahashi, F, T. Kondo, Y. Takahashi et al., Very Long Baseline Interferometer. TokyoOhmsha Press, 208-216, 2000.

A. Costa et al.: GPS Meteorology over Northeast Brazil: Perspectives, IVS 2006 General Meeting Proceedings, p.41–41
http://ivscc.gsfc.nasa.gov/publications/gm2006/costa

GPS Meteorology over Northeast Brazil: Perspectives

A. Costa [1], *A. M. Pereira de Lucena* [2], *P. Kaufmann* [3], *F. Sales Ávila Cavalcante* [4], *F. Geraldo de Melo Pinheiro* [4], *F. de Assis Tavares Ferreira da Silva* [2], *J. Bosco Verçosa Leal Jr.* [4], *V. de Paula Silva Filho* [5]

[1] *FUNCEME and UECE*
[2] *INPE*
[3] *Mackenzie University*
[4] *UECE*
[5] *FUNCEME and INPE*

Contact author: A. Costa, e-mail: alex@funceme.br

Abstract

FUNCEME, the Ceará State Foundation for Meteorology and Water Resources, UECE, the State University of Ceará, INPE, the Brazilian National Institute for Space Research and Mackenzie University are establishing a cooperative program in which the meteorological use of GPS information over Northeast Brazil is one of its components. It is well known that knowing accurately the GPS position, one may calculate the delay in the signal from the satellite to the receiver in order to estimate the integrated water vapor in the atmosphere. In fact, that information is already a by-product, available at the IGS site. In order to incorporate this information into the operational activities at FUNCEME, we proposed to calibrate and validate the GPS-based data by using surface and upper-air observations as well as satellite retrievals.

[Note from the Editors: The overheads of the oral presentation of this contribution can be downloaded from the IVS 2006 General Meeting web site. Please get the PowerPoint file of the presentation at the URL ftp://ivscc.gsfc.nasa.gov/pub/general-meeting/2006/presentations/gm2006_1-09_costa.ppt.]

Robert Heinkelmann et al.: Global VLBI Solution IGG05R01, IVS 2006 General Meeting Proceedings, p.42–46
http://ivscc.gsfc.nasa.gov/publications/gm2006/heinkelmann2

Global VLBI Solution IGG05R01

Robert Heinkelmann [1], *Johannes Boehm* [1], *Harald Schuh* [1], *Volker Tesmer* [2]

[1)] *Institute of Geodesy and Geophysics/University of Technology, Vienna*

[2)] *Deutsches Geodätisches Forschungsinstitut, Munich*

Contact author: Robert Heinkelmann, e-mail: rob@mars.hg.tuwien.ac.at

Abstract

The global solution IGG05R01 includes simultaneously estimated station position, velocity and source coordinate catalogues as well as time series of EOP. It is the first solution of global parameters at the IVS Special Analysis Center Institute of Geodesy and Geophysics (IGG), the first global VLBI solution in Austria, and the second solution using the OCCAM software package with the least-squares method (LSM) together with DOGS-CS. In this paper we introduce the technical details and present results, which show that this solution, in spite of some modelling deficiencies and neglected geophysical model corrections, is already of good quality.

1. Introduction

At the Special Analysis Center IGG, Vienna, a global VLBI solution has been obtained using the OCCAM 6.1 package with the least-squares method (LSM) to determine local parameters and the DOGS-CS software, developed at the DGFI, Munich, for the addition and solution of normal equations to solve for global parameters. With this effort the IGG aims to contribute to future realizations of IVS and IERS combined products, such as ICRF, ITRF, and EOP time series. Investigations are planned on the dependencies between troposphere parameters, meteorological data, station positions and velocities, in particular on the height component, and scale factor and scale rates. In recent studies (Heinkelmann et al., 2005a, [3]) it has been pointed out that deficiencies of the terrestrial reference frame (TRF) significantly influence the troposphere parameters and inherent long-term trends. It was demonstrated that this statement also holds the other way around, because mapping functions and troposphere parameters depend on the input of meteorological data. They also significantly influence the station positions and velocities. Therefore, a homogeneous meteorological data set is indispensable for the determination of a reliable TRF, and a reliable TRF is necessary to obtain consistent troposphere parameters. The meteorological data for IGG05R01 are from the European Center for Medium-Range Weather Forecasts (ECMWF) and from the surface meteorological data recorded at the IVS sites, which were carefully homogenized (Heinkelmann et al., 2005b, [4]).

2. General Characteristics of IGG05R01

To achieve an un-constrained TRF, quasar coordinates, EOP, and station positions and velocities have to be estimated simultaneously (Tesmer et al., 2004, [8]) in a free adjustment applying minimal constraints. The minimal constraints define the origins and axes of the reference frames by forcing the sum of rotations and the sum of translations to be zero. This is due to the fact that - by definition - all overall rotations and translations between the CRF and the TRF are to

be expressed by the EOP. In IGG05R01 station positions and linear velocities are modelled and given as coordinates with respect to a reference epoch. The reference epoch of IGG05R01 is the reference epoch of ITRF2000: 1997.0 (1997-01-01). In case of an episodic motion of the antenna two sets of coordinates are reported (before and after the change). While source coordinates are considered constant in time, the EOP are estimated locally session by session and handled as a time series.

2.1. Session Criteria

The global solution IGG05R01 consists of 3,414,325 observations and formal errors from 2702 dual-band sessions in NGS-format between 1984-01-04 and 2005-11-28 taken from the IVS Data Centers. Although Mark III VLBI observations are available from 1979 on, the sessions included in IGG05R01 begin in 1984 with the start of the regular type of session IRIS-A (International Radio Interferometric Surveying, Atlantic), to achieve temporal homogeneity. The total number of geodetic VLBI sessions[1] for almost 22 years of observation is 4490. Although the solution includes only about 60% of the total number of sessions, it nevertheless represents a high amount of significant information. Among the excluded sessions are the intensive sessions and all other sessions which were performed on a single baseline, sessions carried out by small national or regional networks, e.g. JADE (JApanese Dynamic Earth observation by VLBI), and other sessions which are not suitable to determine reliable EOP[2], sessions where the RMS of the postfit residuals exceeds 2 cm, sessions where the fraction of outliers exceeds 3.5%, sessions where the number of parameters exceeds the number of observations[3].

2.2. Station Criteria

The total number of VLBI sites within the ITRF2000 is 136. However, only a small subset (37%) of non-mobile stations takes part in almost all of the geodetic VLBI observations. Thus, the IGG05R01 solution includes only the 50 most frequently used VLBI antennas. The 59 mobile antennas of ITRF2000, except TIGO at Wettzell, and 27 non-mobile antennas which participated in a small number of sessions are excluded. Stations from outside of the ITRF2000 are SVETLOE as well as TIGO at Concepcion. 15 out of the 50 stations were selected for the datum definition (see Table 1). This small subset of stations provides a long observational history, a global temporal and spatial coverage, and it is free of earthquake, rail repairing, and other episodic station motions.

Table 1. The 15 stations used for the TRF datum definition of IGG05R01

ALGOPARK	FORTLEZA	HARTRAO	HOBART26	KASHIMA
KAUAI	KOKEE	MATERA	NRAO20	NYALES20
ONSALA60	RICHMOND	SESHAN25	WESTFORD	WETTZELL

[1] Sessions available in NGS-format from IVS Data Centers on January 6, 2006.

[2] As suggested by the IVS Analysis Coordinator (http://vlbi.geod.uni-bonn.de/IVS-AC/data/exclude.html).

[3] The number of parameters is not constant, it depends on the parameterization, i.e. on the type and resolution of the auxiliary parameters.

2.3. Source Criteria

At least three observations to a source are necessary per session in order to estimate the two source coordinates with minimal redundancy. To ensure reliability the position of a source is only estimated globally, if it participates in at least three sessions. These criteria are fulfilled by 552 radio sources out of the total number of 667 within ICRF-Ext.1 in our solution. For the CRF datum definition no-net-rotation (NNR) with regard to the 199 stable sources defined by Feissel-Vernier (2003, [2]) were applied.

3. Results

3.1. IGG05R01-CRF

The estimated source coordinates do not show systematic differences with regard to the a priori coordinates taken from the ICRF-Ext.1. Considering the reported source position errors of the ICRF-Ext.1 the deviations between the solutions are negligible.

3.2. IGG05R01-TRF

The horizontal and vertical velocities of the stations included in IGG05R01 are compared to the VTRF2005 (Nothnagel, 2005, [6]), a combined TRF obtained from five VLBI solutions. In general, horizontal and vertical velocities agree very well. Small differences in horizontal components occur at KWAJAL26 and SYOWA stations due to the small number of observations. At the VLBA (Very Long Baseline Array) telescopes differences in the vertical components are significant. The sessions of the types VLBA and RDV (Research and Development - VLBA) contain most of the observations of these telescopes. These sessions are currently not included in our solution. The differences in the vertical component of the 15 datum sites are displayed in Figure 1. The interaction of position and velocity becomes more evident by the application of datum transformations of the coordinates from the reference epoch 1997.0 to the beginning (1984.0) and the end (2005.0) of the time span. Then, the vertical components of the TRFs deviate less than 4 cm w.r.t. ITRF2000 and up to 1 cm w.r.t. each other during the whole time span. To get an overall measure of the agreement between the two TRFs the coordinates of the twelve regularly used stations (IVS (2005), [5]) were transformed from IGG05R01 to ITRF2000 for the two epochs 2000 and 2010. The Helmert parameters are given in Table 2.

3.3. IGG05R01-EOP

The IGG05R01 includes time series of nutation offsets, polar motion and $\Delta UT1$ offsets and rates, estimated locally for each single session. The nutation model used is MHB2000, without the free core nutation (FCN) terms. A priori EOP are taken from the IERS-C04 series. Figure 2 shows nutation estimates in longitude $\Delta\psi$ and in obliquity $\Delta\epsilon$ w.r.t. the MHB2000 model.

4. Conclusions and Outlook

The global solution IGG05R01 is already of good quality. It can be improved by extending the number of stations, the number of sources, and the included session types, modelling non-linear post-seismic and other station motions, acounting for thermal telescope deformation and

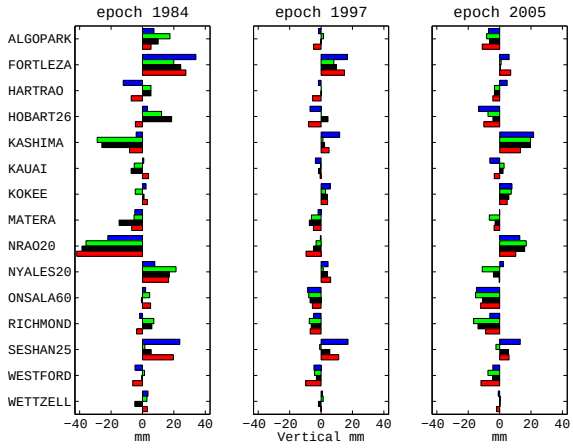

Figure 1. Comparison of the vertical components of the 15 datum stations at three epochs w.r.t. ITRF2000. Compared solutions from top to bottom: IGG05R01-TRF in blue (grey 80%), VTRF2003 (Nothnagel, 2003, [7]) in green (grey 30%), VTRF2005 in black, and the current VLBI solution of DGFI, 05R02 in red (grey 50%).

Table 2. Parameters of a Helmert transformation of twelve regularly used stations (IVS 2005, [5]) from IGG05R01-TRF to ITRF2000. * at Earth radius

epoch		**2000**		**2010**	
α	$[\mu as]$	**-37.4**	± 151	**112**	± 240
β	$[\mu as]$	**-66.6**	± 155	**-238**	± 247
γ	$[\mu as]$	**-51.4**	± 148	**-82.4**	± 236
ΔX	$[mm]$	**1.5**	± 4.0	**-2.1**	± 6.3
ΔY	$[mm]$	**-2.6**	± 3.9	**-1.5**	± 6.2
ΔZ	$[mm]$	**1.0**	± 3.8	**-0.9**	± 6.0
scale	$[ppb]$	**0.81**	± 0.59	**0.84**	± 0.94
scale	$[mm^*]$	**5.2**		**5.4**	

atmospheric loading corrections, applying the new Vienna mapping functions VMF1 (Boehm et al., 2006, [1]) and a priori non-zero atmospheric gradients, and optimizing inherent soft and hard constraints.

References

[1] Boehm J., B. Werl, H. Schuh: Troposphere mapping functions for GPS and VLBI from ECMWF operational analysis data, J. Geophys. Res., in press, 2006

[2] Feissel-Vernier M.: Selecting stable extragalactic compact radio sources from the permanent astro-geodetic VLBI program. Astronomy and Astrophysics, 403, 105-110, 2003

[3] Heinkelmann R., J. Boehm, H. Schuh: IVS long-term series of Tropospheric Parameters. In: Vennebusch M., Nothnagel A. (Eds.): Proceedings of the 17^{th} Working Meeting on European VLBI for Geodesy and Astrometry, Noto, Italy, 69-73, 2005

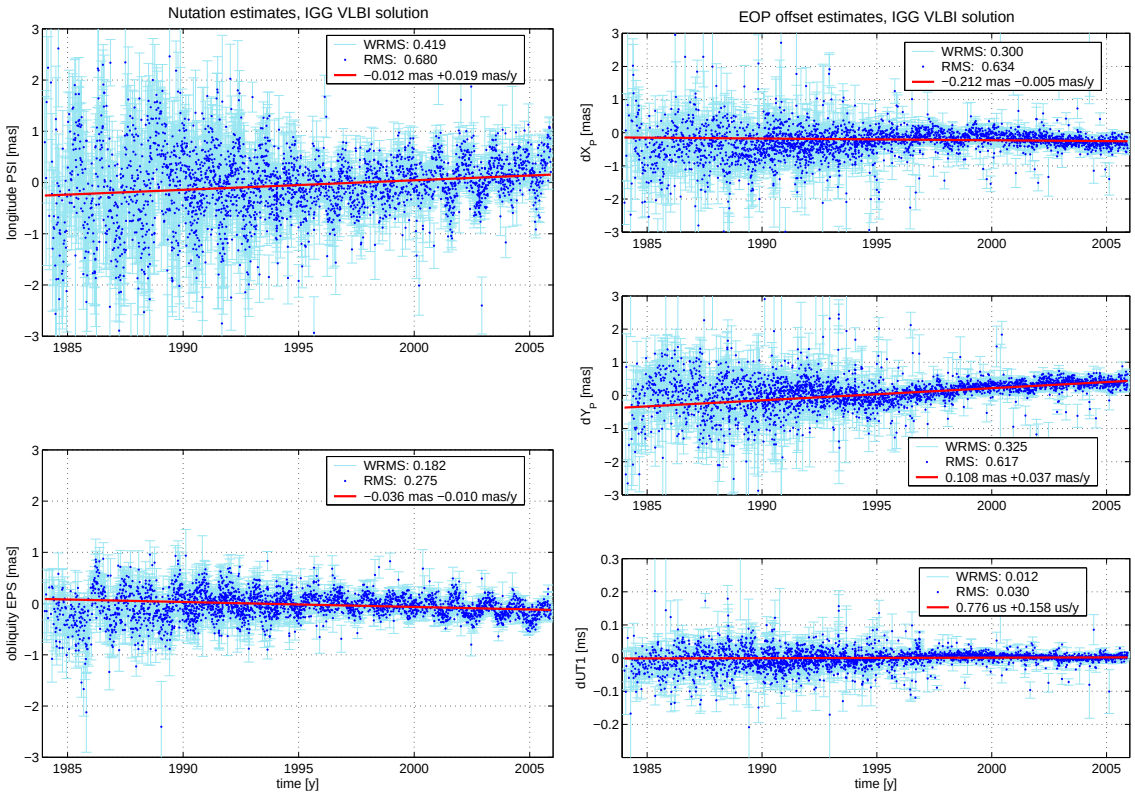

Figure 2. IGG05R01 nutation series w.r.t. MHB2000 model without FCN (left) and IGG05R01 Earth rotation parameters w.r.t. IERS-C04 (right). The nutation series are dominated by a quasi-harmonic signal with a period of about 430 days (FCN). The small trend in the Y-Pole component is probably due to a small inconsistency in the IERS-C04 series stemming from a constrained determination independently of the TRF and CRF solutions.

[4] Heinkelmann R., J. Boehm, H. Schuh: Homogenization of surface pressure recordings and its impact on long-term series of VLBI tropospheric parameters. In: Vennebusch M., Nothnagel A. (Eds.): Proceedings of the 17^{th} Working Meeting on European VLBI for Geodesy and Astrometry, Noto, Italy, 74-78, 2005

[5] IVS (2005): International VLBI Service for Geodesy and Astrometry: Annual Report 2004, D. Behrend, K. Baver (Eds.), NASA/TP-2005-212772, 2005

[6] Nothnagel A.: VTRF2005 - A combined VLBI Terrestrial Reference Frame. In: Vennebusch M., Nothnagel A. (Eds.): Proceedings of the 17^{th} Working Meeting on European VLBI for Geodesy and Astrometry, Noto, Italy, 118-124, 2005

[7] Nothnagel A.: VTRF2003: A Conventional VLBI Terrestrial Reference Frame. In: Schwegmann W., Thorandt V. (Eds.): Proceedings of the 16^{th} Working Meeting on European VLBI for Geodesy and Astrometry, Leipzig, Germany, 195-205, 2003

[8] Tesmer V., H. Kutterer, H. Drewes: Simultaneous Estimation of a TRF, the EOP and a CRF. In: Vandenberg, N., K. Baver (Eds.): IVS 2004 General Meeting Proceedings, NASA/CP-2004-212255, 311-314, 2004

Nobuyuki Kawano et al.: International VLBI Tracking of SELENE, IVS 2006 General Meeting Proceedings, p.47–51
http://ivscc.gsfc.nasa.gov/publications/gm2006/kawano

International VLBI Tracking of SELENE

Nobuyuki Kawano, Hideo Hanada, Koji Matsumoto

National Astronomical Observatory of Japan
Contact author: Nobuyuki Kawano, e-mail: kawano@miz.nao.ac.jp

Abstract

The Japanese lunar explorer SELENE will be launched in 2007. Two sub-satellites, Relay satellite and VLBI satellite, will transmit S and X band carrier signals for precisely measuring the lunar gravity field. It is expected that Wettzell, Shanghai, Urumqi, Hobart and the VERA stations take part in intensive international VLBI observations. The observation period will be 8 hours, 3 days a week in two separate months.

1. Outline of Geodetic Observations in SELENE

The Japanese lunar explorer SELENE will be launched in summer of 2007. SELENE consists of 3 satellites: a main satellite and two sub-satellites, the latter being a VLBI satellite and a relay satellite. They will be entered into different polar orbits of 2,400 km, 800 km and 100 km of apolune, respectively. However, all three satellites have the same perilune of 100 km. Differential VLBI observations will be conducted between the two sub-satellites in order to determine the low degree coefficients of the lunar gravity field. Fig. 1 shows the concept of SELENE.

The Moon is the nearest celestial body from the Earth. However the Moon's origin and evolution remain vague, but are closely related to those of the Earth. We have been trying to extend geodetic measurements to the Moon in order to understand them better, in a similar fashion to studies on the Earth. One of the main problems remaining about the origin and evolution is the existence of a core. The momentum of inertia gives constraints about the size and density of the core, and it can be derived from the dynamical flatness and low degree coefficients of the spherical harmonics of the lunar gravity field. The Moon has been measured by some geodetic methods such as LLR and VLBI observations to radio sources placed on the Moon. The flatness has been precisely determined from LLR. However, the low degree coefficients are not known well enough to determine the momentum of inertia with high accuracy. For this reason, we aim at the precise determination of the low degree coefficients in SELENE project. The key technology to accomplish this purpose is VLBI. We decided to propose an international VLBI observation campaign with an IVS network, with Wettzell playing an important part.

Fig.2 shows the outline of the observations for the geodetic mission of SELENE. Three kinds of observations will be carried out. The first one is a 2-way Doppler measurement. It will be carried out when the satellites make their closest approach. The second is 4-way Doppler: a stable frequency signal is sent to the main orbiter via Rstar and sent back the same way, when the main orbiter is farthest away. This measurement fills the gap in the gravity field at the far-side left by the 2-way Doppler measurements. The last one is a VLBI observation. VLBI observations are essential for the determination of the lunar gravity field around the rim area and for the orbit determination of the relay satellite. The lunar gravity field has been measured by Doppler frequency so far. It is not sensitive to the motion perpendicular to the line of sight, but VLBI is sensitive to this

direction. Hence, VLBI observations combined with Doppler frequency observations can greatly improve the lunar gravity field. VLBI observations are frequently carried out when the orbit is in face-on.

Fig.3 shows the estimation error (Matsumoto et al. 2002) of the spherical harmonics as a function of the degree of the expansion, compared with the results of the Lunar Prospector obtained by Doppler frequency measurements. VLBI observations decrease the error to one-tenth for the lower degrees. In addition to this improvement in low degree coefficients, the relay satellite enables us to directly measure the gravity field in the far-side through the variation of orbital motion of the main satellite. It also decreases the error in higher degrees, by one or two orders of magnitude.

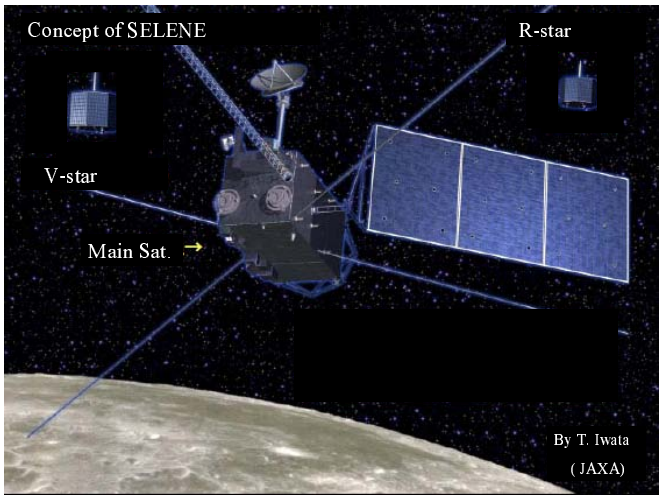

Figure 1. Concept of SELENE.

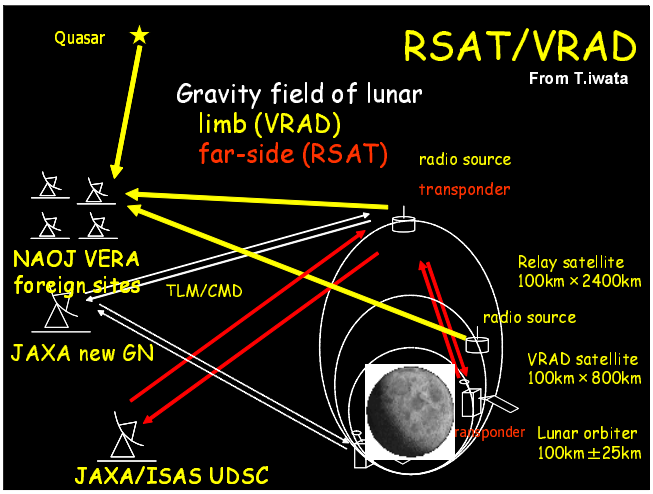

Figure 2. Geodetic observation of SELENE.

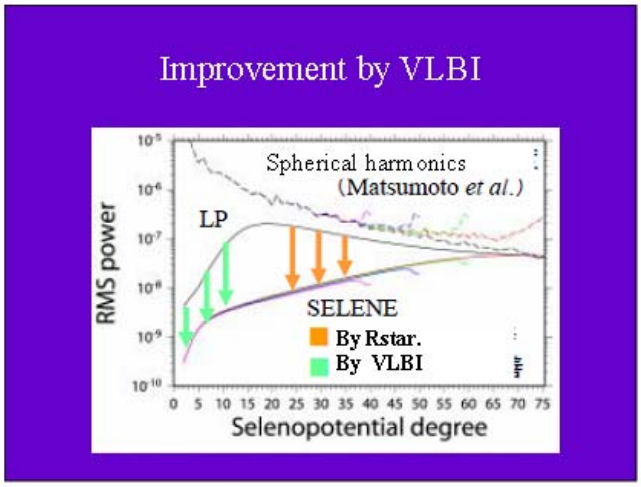

Figure 3. Error estimation of the spherical harmonics for the lunar gravity field.

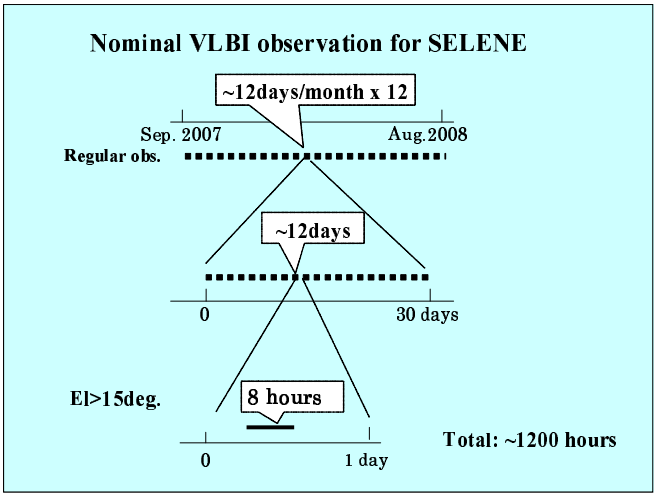

Figure 4. Nominal VLBI observations by VERA.

2. VLBI Observations

VLBI observations are classified in two categories. One consists of regular observations with the VERA network, which is the Japanese domestic VLBI network with about 2000 km baseline lengths. Regular observations will be done 3 days per week over a one year observation window. An observation day requires about 8 hours of observing, when the elevation angle exceeds 15 degrees at all stations. The total observation period amounts to 1,200 hours.

The other important observations are intensive VLBI observations. We propose that three stations (Shanghai and Urumqi, both China and Hobart, Australia) join these observations. Unfortunately, this network has a shape of a long triangle in the North-South direction as shown in Fig. 5. If Wettzell is added, this network broadens both in North-East and East-West direc-

tion, creating an optimal configuration. Therefore we submitted a proposal to the IVS Observing Program Committee.

The International VLBI observation campaign will be run twice for a period of 1 month each during the 1 year nominal observation window of SELENE. The campaigns are divided into two parts: a core observation during face-on and an extended observation. The core observation will be held twice a month while the orbit is in face-on, and the face-on continues for four days. Each daily observation session is carried out for four hours which is the duration of the common view. In the extended observation, 4 hours will be shared regularly for a daily observation. The total amount of core observations reaches 64 hours and that of extended observations are about 100 hours.

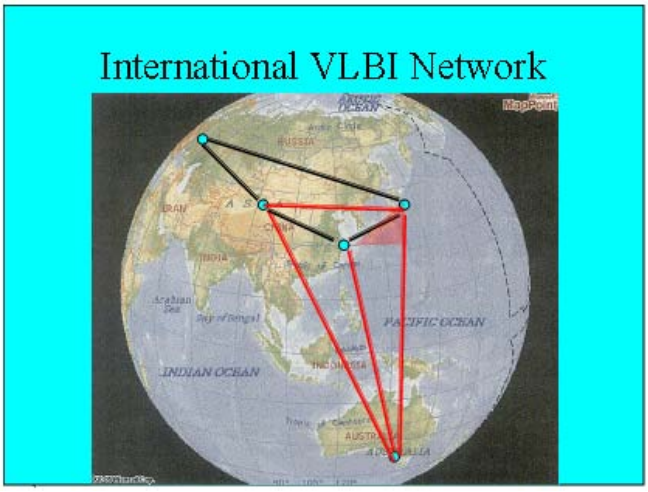

Figure 5. Expected International VLBI network.

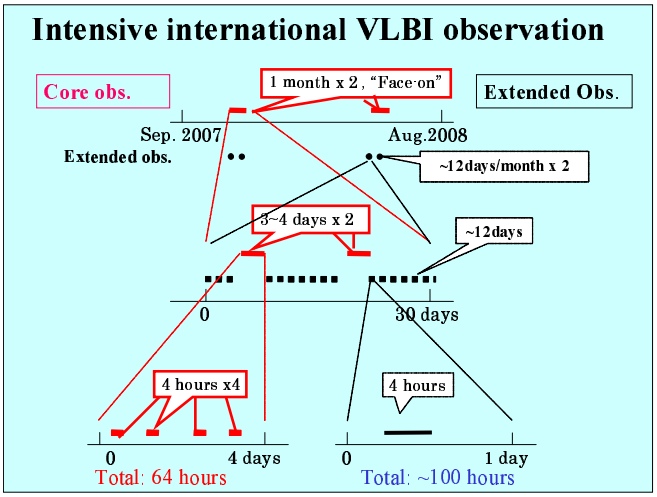

Figure 6. International VLBI Observation.

3. Transmitted Signal and Orbits

Finally the characteristics of the transmitter onboard SELENE are shown in Table 1 and Table 2. Three frequencies are distributed from 2.2 GHz to 2.3 GHz, and one frequency is on X-band. The received signals are sampled with a very narrow VLBI terminal named SRTP. Polarization is RHCP for all signals. Three satellites are brought into different orbits, although the inclination and perilunes are all 90° and 100 km respectively, and they fly in the same orbital plane.

Table 1. Characteristics of the transmitters onboard SELENE.

Center frequency	2212 MHz	2218MHz	2287 MHz	8456 MHz
Band width	CW	CW	CW	CW
Sampling rate	200 ksps	200 ksps	200 ksps	200 ksps
Recording	Hard disc drive			
EIRP	24 mW	24 mW	24 mW	250 mW (Rstar) 38 mW (Vstar)
Polarization	RHCP	RHCP	RHCP	RHCP

Table 2. Orbit characteristics of three spacecraft.

	Perilune	Apolune	Inclination	Period
Main orbiter	100 km	100 km	90°	-120 min.
Vstar	100 km	800 km	90°	-153 min.
Rstar	100 km	2400 km	90°	-240 min.

References

[1] Matsumoto, K., K. Heki, and H. Hanada, Global Lunar Gravity Field Recovery from SELENE, IVS2002 General Meeting Proceedings, 381–385,2002.

Xiuzhong Zhang et al.: Spacecraft Tracking with the Chinese VLBI Network, IVS 2006 General Meeting Proceedings, p.52–55
http://ivscc.gsfc.nasa.gov/publications/gm2006/zhang

Spacecraft Tracking with the Chinese VLBI Network

Xiuzhong Zhang, Team of Chinese VLBI Network

Shanghai Astronomical Observatory, Chinese Academy of Sciences
Contact author: Xiuzhong Zhang, e-mail: xzhang@shao.ac.cn

Abstract

VLBI system with highest resolution is used by astronomers to study the most distant objects in detail. e-VLBI has got rapid progress in the past several years. With these characteristics, the VLBI systems are more and more used for spacecraft orbiting application. We briefly introduce the system configuration of the Chinese VLBI network and the orbiting experiment done with the Chinese VLBI network.

1. Introduction

Spacecraft tracking technologies used range and range rate as a basic method for target orbiting. There are some advantages to do spacecraft orbiting with range and range rate system. For example, only one station could complete spacecraft orbiting task. But only using range and range rate systems makes it difficult to determine spacecraft position in deep space. Angle information should be used to make high precision position determination of spacecraft.

VLBI system with highest angle resolution technique (less than 1 mas) is used by astronomers in the radio wave domain; e-VLBI rapidly progressed in recent years; more computing power is available in a single IC chip. With these technique characteristics, the VLBI systems are more and more used for spacecraft orbiting applications. Some events are shown in following:

1. 1980s: VLA as a supersensitive deep space "downlink" station
2. 1980s: NASA DSN stations (Goldstone, Robledo, Tidbinbilla) begin their VLBI duties
3. 1990s: phase-referencing "satellite-3C279" demo (Asaki, Sasao et al.)
4. Activities of spacecraft tracking with VLBI in Japan [1]
5. 2005: Radio Astronomy segment of the Huygens mission [2]

In China, we started spacecraft tracking with the Chinese VLBI network in 2001. Different orbiting spacecraft have been observed with Chinese VLBI network, e.g., GEO, TC-1, TC-2, SMART-1 and the deep space probe. Now we prepare to do the orbit determination of CE-1.

2. Spacecraft Tracking with the Chinese VLBI Network

The spacecraft signal is different from the signal of a radio source. Table 1 shows the differences of the spacecraft and radio source signals.

Some modifications of the VLBI station and VLBI correlator are necessary to adapt for the signal characteristics of a spacecraft. The antenna servo system and the dynamic range of the correlator should be improved for spacecraft tracking and signal correlation. The software correlator and hardware correlator have been used for data correlation. Our hardware correlator is specially designed for spacecraft tracking. There are 16 bits word length processor in hardware correlator to process the spacecraft range and range rate signal, which has more than 40dB dynamic range.

Table 1. Signal characteristic of spacecraft and radio source

	Bandwidth	Signal to noise rate	Spectrum	Signal dynamic range	Range rate
Spacecraft	Narrow	strong	special	large	large
Radio source	Wide	weak	continual	small	small

The automatically fringe finder function is specifically designed for spacecraft signal processing. Normally, the predicted orbit is not accurate enough for the correlator. The real time correlation function is also specially designed for spacecraft tracking. At the station, the Mark 5 system records the data and sends them to the correlation center via network. The data rate is limited to smaller than 10Mbps. The real time interface of the correlator reads the data stream from the Internet and writes to FIFO to smooth the data stream. There is 1 GB DDR RAM in the FIFO. For 10Mbps data rate stream, this FIFO can buffer more than 13 minutes.

2.1. Test Observation and Results

Since 2001 we have done several spacecraft tracking observations using the Chinese VLBI network. The target orbit of these observations were different: they were GEO, ellipse orbit, lunar probe and the deep space probe.

Smart-1 orbiting observation with Chinese VLBI network has been done in last March. Smart-1 is an ESA lunar project. It was launched in 2003. Some information about the observations are shown in the following:

Observing time (UT):	March 20, 2005; 10h30m–16h50m.
Orbit of Smart-1:	polar orbit, 2833 km apolune, 498 km perilune, 4.95-hr period.
Stations:	Seshan (25 m), Nanshan (25 m), Kunming (3 m).
Frequency of carrier wave:	2235.10 MHz.
Observation frequency:	2230.99–2238.99 MHz.
Bandwidth:	8.0 MHz.
Radio sources:	3C84, 4C39.25, 3C279.
Recording system:	Mark 5A, 16 Mbps.
Data processing:	Shanghai VLBI data processing center.
Integration time:	4 s.

Fig. 1 shows the structure of SMART-1 range and range rate signal in wide band mode and narrow band mode.

Fig. 2 shows the comparison results of delay and delay rate between VLBI observation and ESA Smart-1 reconstruction orbit. The best standard error of delay in SH-UR baseline is less than 1ns.

3. Future Plan

The Chinese lunar probe, CE-1, will be launched in 2007. The Chinese VLBI Network will do some tracking observations for orbiting of CE-1. Chinese VLBI network will be extended to 4

stations and will include a data processing center.

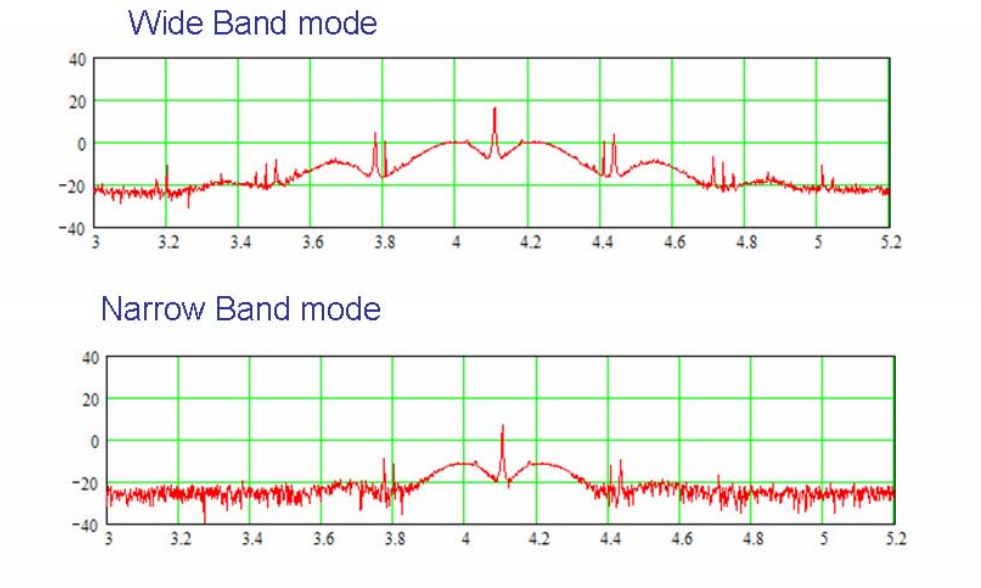

Figure 1. Smart-1 S-Band (2.2GHz) downlink signal.

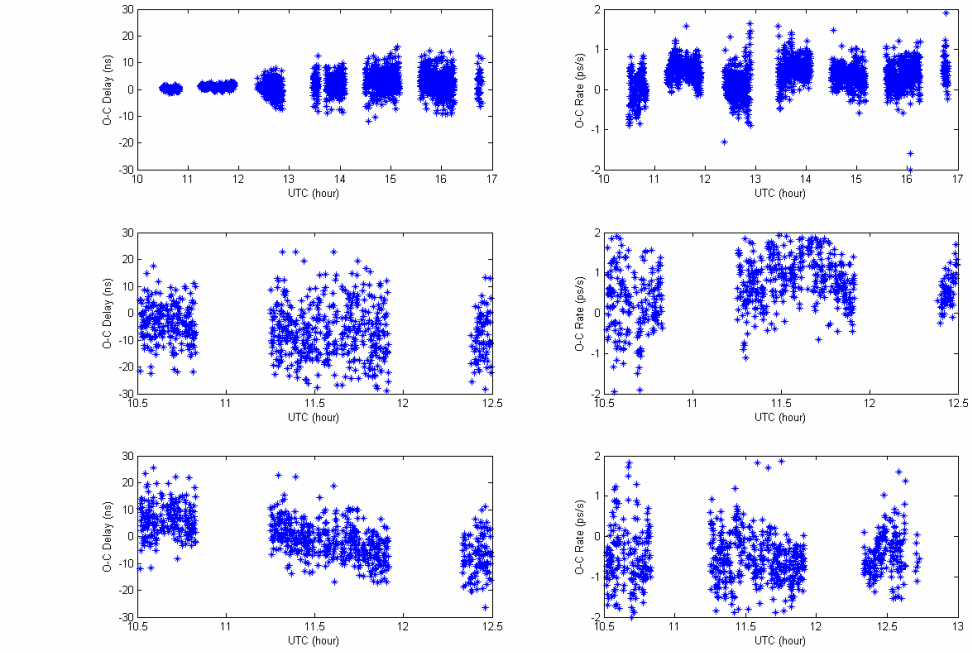

Figure 2. Comparison of VLBI observation and ESA Smart-1 reconstruction orbit delays and delay rates.

References

[1] N.Kawano, H.Hanada and K.Matsumoto , "International VLBI tracking of SELENE", this volume.

[2] J. Lebreton, O.Witasse, "An overview of the descent and landing of the Huygens probe on Titan", Nature, Vol. 438/8 December 2005, P.758-764.

Takaaki Jike et al.: The First Year of VERA Geodetic Experiments, IVS 2006 General Meeting Proceedings, p.56–57
http://ivscc.gsfc.nasa.gov/publications/gm2006/jike

The First Year of VERA Geodetic Experiments

Takaaki Jike [1], *Yoshiaki Tamura* [2], *Seiji Manabe* [2], *NAOJ VERA Group* [1]

[1)] *VERA Observatory, National Astronomical Observatory of Japan*
[2)] *Mizusawa Observatory, National Astronomical Observatory of Japan*
Contact author: Takaaki Jike, e-mail: jike@miz.nao.ac.jp

Extended Abstract

VERA (VLBI Exploration of Radio Astrometry) aims at the revelation of the structure and dynamics of our galaxy by measuring 3-D positions and motions of galactic compact radio objects with 10 micro-arc-seconds level accuracy. To achieve such highly accurate measurements, geodetic VLBI observations are crucial for the VERA project.

Four antennas, Mizusawa, Iriki, Ogasawara and Ishigaki, constitute the VERA network on the Japanese islands. The longest baseline is Mizusawa-Ishigaki (about 2270km) and the shortest baseline is Iriki-Ishigaki (about 1016km). Monitoring of these baseline-vectors and their stability with 1-2mm accuracy is the main purpose of the VERA geodetic VLBI observations.

For this objective, we hold VERA internal geodetic VLBI experiments on a semi-regular basis. Also, besides these experiments, VERA participates in the Japanese Dynamic Earth Observation (JADE) by GSI for connecting the VERA network to the international VLBI network and carries out continuous GPS observations at the VERA sites for interpolating geodetic VLBI solutions and for confirming rapid variations.

The semi-regular VERA internal geodetic VLBI experiments started in November 2004, and are continued twice a month in 2006, excluding periods of antenna maintenance. The experiments in the graph of Figure 1 have been analyzed by December 2005. The special notes of this experiment are regular use of high-speed sampler, digital filter unit and 1-Gbit recording system, adopting of the Mitaka FX Correlator for correlation processing, and geodetic analysis by CALC3/MSOLV software package.

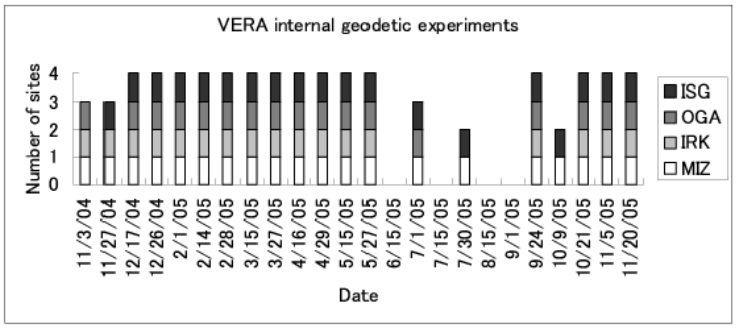

Figure 1. Result of VERA internal geodetic VLBI experiments.

We obtained long-term averaged coordinates and rates of VERA antenna reference points from the solutions of 20 experiments with about 2mm and 0.4mm/y errors. A typical error ellipsoid

obtained from 1 experiment is shown in Figure 2. The size of the ellipsoid is about ± 2mm in the East-West and North-South directions, and about ± 7mm in the vertical direction.

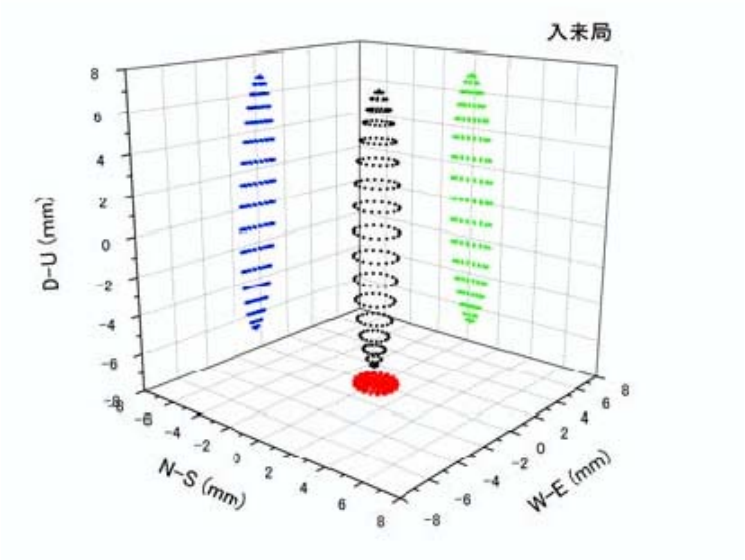

Figure 2. Typical error ellipsoid obatined from geodetic analysis of 1 experiment.

Baseline lengths of the VERA network as measured by VLBI and GPS are compared. We detected similar changes in most of the VLBI and GPS results. Motions of some baselines have a non-linear signature like the seasonal variation shown in Figure 3. It is a future task to reveal the reason of these variations. Differences of baseline length between VLBI and GPS are about 2cm in maximum. It might be due to insufficient accuracy of local tie vector between VLBI and GPS points.

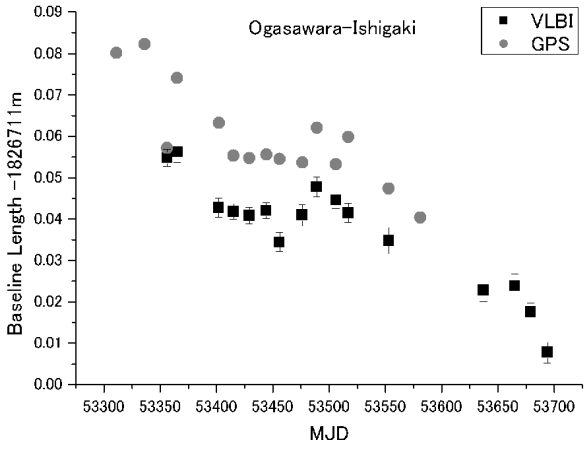

Figure 3. Time variations of Ogasawara-Ishigaki baseline length.

H. Kobayashi et al.: VERA System and Recent Results, IVS 2006 General Meeting Proceedings, p.58–58
http://ivscc.gsfc.nasa.gov/publications/gm2006/kobayashi

VERA System and Recent Results

H. Kobayashi [1], *S. Manabe* [1], *N. Kawaguchi* [1], *K.-M. Shibata* [1], *Y. Tamura* [1], *O. Kameya* [1], *M. Honma* [1], *T. Hirota* [1], *H. Imai* [2], *T. Omodaka* [2]

[1)] *VERA Observatory, National Astronomical Observatory of Japan*

[2)] *Department of Science, Kagoshima University*

Contact author: H. Kobayashi, e-mail: hideyuki.kobayashi@nao.ac.jp

Abstract

VERA is the first VLBI array, which is designed to be free from atmosphere phase fluctuations. It has four VLBI stations with 2,300 km maximum baseline length within the Japan archipelago. The observing frequencies are 2, 8, 22, and 43 GHz. 22 and 43 GHz frequencies are mainly used for H2O and SiO maser object observations, respectively. And 2 and 8 GHz bands are mainly used for geodetic observations. VERA uses a 1 Gbps recording system with cassette magnetic tapes. They are correlated by the VSOP correlator at Mitaka. VERA performs astrometry observations with 10 micro-arc-second accuracy to detect annual parallaxes around the galaxy. In order to achieve such high accuracy, the VLBI technique has to be used with phase referencing techniques. To compensate for phase fluctuations of interferometer visibilities, which are mainly caused by the atmospheric turbulences and phase drifts of local oscillators, VERA antennas have a two-receiver system which makes simultaneous observations of two objects. By comparing the visibility phase between these two objects, simultaneous phase referencing VLBI is achieved. Usually a galactic maser object is selected as a target and an extra galactic object is selected as a reference source. The talk presents the status of VERA and some results.

[Note from the Editors: The overheads of the oral presentation of this contribution can be downloaded from the IVS 2006 General Meeting web site. Please get the PDF file of the presentation at the URL ftp://ivscc.gsfc.nasa.gov/pub/general-meeting/2006/presentations/gm2006_1-14_kobayashi.pdf.]

Mamoru Sekido et al.: VLBI Delay Model for a Radio Source at Finite Distance, IVS 2006 General Meeting Proceedings, p.59–63
http://ivscc.gsfc.nasa.gov/publications/gm2006/sekido

VLBI Delay Model for a Radio Source at Finite Distance

Mamoru Sekido [1], *Toshio Fukushima* [2]

[1)] *Kashima Space Research Center/National Institute of Information and Communications Technology*
[2)] *National Astronomical Observatory Japan*
Contact author: Mamoru Sekido, e-mail: sekido@nict.go.jp

Abstract

A new VLBI Delay model for radio source at finite distance is presented. The geometrical effect of curved wavefront is fully considered with pseudo source vector defined by $\vec{K} = (\vec{R}_{01} + \vec{R}_{02})/(R_{01} + R_{02})$. Our VLBI delay model gives delay in the scale of terrestrial time (TT) with the baseline vector on the TT-scale. Since the new delay model is in a similar form as the current standard VLBI delay model (consensus model), implementation into a current VLBI analysis software, such as CALC/SOLVE and OCCAM, will be relatively easy. Our VLBI delay model is regarded as expansion of the consensus model from infinite to finite region in terms of distance to radio source. Accuracy of the new delay model is better than 1 ps in ground based VLBI observations of radio sources. The applicable range is from radio sources at altitude of 100 km or more. Analytical correction terms to adapt the consensus model to finite-distance radio sources is also given under the condition that the distance to the radio source is farther than 10 pc. This may be useful for analysis of parallax for galactic radio sources.

1. Introduction

The standard VLBI delay model, the so-called consensus model [1, 2], is designed to compute accurately the time differences of signal arrival between two stations on the earth for a radio source at infinite distance. However the effect of curved wave fronts has to be taken into account for radio sources at finite distance. For radio sources closer than 200 kpc, the effect of a curved wavefront will exceed 1 ps on VLBI observations with 12000 km baseline [7]. Pulsars, maser sources, and all radio sources in our galaxy are included. Radio sources in the solar system ,such as planets and space probes, are important targets from VLBI observation; however intolerable errors will be caused if the effect of curved wavefront is not considered. Moyer [3] provides a delay model by computing the difference of light time for two legs from a spacecraft to observation stations. This is a straight forward approach and it has been used in deep space missions by JPL/NASA in practice. As this model is fairly different from the current VLBI delay model, an implementation into VLBI analysis software is not so simple. VLBI-like approaches, in which the difference of light time is computed analytically, were proposed by several authors [4, 5, 6]. Fukushima proposed an iterative scheme to determine VLBI delay in the lunar project[5]. Klioner gives analytical formulas for radio sources in the solar system [4]. These models, however, do not give a relation between the baseline and the time delay observable in the TT-frame, in which the practical delay measurements are performed, but in the TDB-frame or Barycentric Celestial Reference System (BCRS), which are not directly accessible. BCRS is defined in Resolution B1.3 of IAU General Assembly in 2000 (see appendix of reference [2]). TDB-frame is a kind of the barycentric celestial reference system that differs from BCRS only by a scaling factor L_B. Its time coordinates is regarded as Barycentric Dynamical Time (TDB). TT-frame is a non-rotation celestial reference system differing from Geocentric Celestial Reference System (GCRS) by a constant scale L_G. The GCRS is also defined in IAU Resolution

B1.3 as a non-rotation local flat coordinate system near the earth, in which the spatial scale is defined as consistent with Geocentric Coordinate Time (TCG). The spatial scale of the TT-frame is consistent with Terrestrial time (TT). Current major VLBI analysis software packages, such as CALC/SOLVE and OCCAM, deal with delay data and station coordinates in the TT-frame. The International Terrestrial Reference System (ITRS) is defined in the GCRS, although realizations of the ITRS, such as ITRF2000, are actually given in the TT-frame. Due to these reasons, our new VLBI delay model is intended to give the relation between baseline vector and delay observable in the TT-frame. This paper presents formulas from our new VLBI delay model. See paper [7] for detail of the derivation of the formulas and comparison with other models.

2. The New VLBI Delay Model

The basic formula of the new VLBI delay model is given as

$$(TT_2 - TT_1)_{\mathrm{Finite}} = \left\{ -\left[1 - 2\frac{W_\mathrm{E}}{c^2} - \frac{\vec{V}_\mathrm{E}^2 + 2\vec{V}_\mathrm{E}\cdot\vec{v}_2}{2c^2}\right]\frac{\vec{K}\cdot\vec{b}}{c} - \frac{\vec{V}_\mathrm{E}\cdot\vec{b}}{c^2}\left[1 + \widehat{\vec{R}}_2\cdot\frac{\vec{V}_2}{c} - \frac{(\vec{V}_\mathrm{E}+2\vec{V}_2)\cdot\vec{K}}{2c}\right] + \Delta T_{g,21}\right\} / \left[(1+\widehat{\vec{R}}_2\cdot\frac{\vec{V}_2}{c})(1+H)\right], \quad (1)$$

where suffices 0,1,2, and E indicate radio source, observation station 1, 2, and geocenter, respectively. W_E is the gravitational potential given by $W_E = \sum_{J\neq E} GM_J/|\vec{X}_E - \vec{X}_J|$. $\vec{X}_i$ is the position vector of $i = (0,1,2,E)$ in the TDB-frame. The TDB-frame is chosen as barycentric celestial reference system in our derivation, because the position and velocity of objects in the solar system are given by planetary ephemeris such as JPL ephemeris DE405. $\vec{V}_i$, $(i = 2, E)$ is the coordinate velocity of i with respect to the solar system barycenter (SSB). $\vec{v}_2$ is the geocentric station vector of station 2. $\vec{b}$ is a baseline vector given by the transformation of the coordinates in ITRF2000 into the celestial reference frame (see chapter 5 of [2]).$\vec{K}$ is a pseudo source vector introduced by Fukushima [5], by which the geometrical effect of the curved wavefront is expressed. It is given by

$$\vec{K} \stackrel{\mathrm{def}}{=} \frac{\vec{R}_1 + \vec{R}_2}{R_1 + R_2}, \text{ where } \vec{R}_i = \vec{X}_i(T_1) - \vec{X}_0(T_0), \text{ and } R_i = |\vec{R}_i|, \quad (2)$$

where i=1,2. The position vectors $\vec{X}_0(T)$ should be given by a predicted orbit as function of time in the TDB-frame. The position vector in TDB-frame $\vec{X}_i$ (i=1,2) are given with geocentric station coordinates in the TT-frame $(\vec{\xi}_i, TT_1)$ as

$$\vec{X}_i(T_1) = \vec{X}_\mathrm{E}(T_1) + \left(1 - \frac{W_\mathrm{E}}{c^2} - L_C\right)\vec{\xi}_i(TT_1) - \left(\frac{\vec{V}_\mathrm{E}\cdot\vec{\xi}_i(TT_1)}{2c^2}\right)\vec{V}_\mathrm{E}, \quad (3)$$

where $\vec{X}_E, \vec{X}_J, \vec{V}_2$, and W_E are given by planetary ephemeris. Scaling factor $L_C = 1.48082686741\times 10^{-8} \pm 2\times 10^{-17}$ [8]. $\widehat{\vec{R}}_2$ is a unit vector given by $\widehat{\vec{R}}_2 = \vec{R}_2/R_2$. The epoch, when the signal departed from radio source 0, is denoted T_0 in TDB and the arrival time at station 1 is T_1. Observed delay data are time tagged with UTC. Here the arrival time at station 1 is denoted as UTC_1. Then the

corresponding TT_1 is computed from UTC_1 by

$$TT_1 = (\mathrm{TT} - \mathrm{TAI}) + (\mathrm{TAI} - \mathrm{UTC}) + UTC_1, \tag{4}$$

where (TT-TAI) is 32.184 for historical reason. (TAI-UTC) is 32 sec in 2005 and is 33 sec from 0h UTC on 1st January 2006. Then T_1 in TDB is computed by using time ephemeris $\Delta T_\oplus(T_{eph})$ [8] as

$$T_1 = TT_1 + \Delta T_\oplus(TT_1) - \Delta T_\oplus(TT_0) + \frac{V_E \cdot \vec{\xi_1}}{c^2}, \tag{5}$$

where TT_0 corresponds to 0h UT on January 1st, 1977. $\vec{\xi_1}$ is the geocentric vector of station 1 in TT-frame. The epoch of the signal emission from the radio source in TDB (T_0) is obtained by solving the light time equation

$$T_0 = T_1 - \frac{\left|\vec{X}_0(T_0) - \vec{X}_1(T_1)\right|}{c} - 2\sum_J \frac{GM_J}{c^2} \ln \frac{R_{1J} + R_{0J} + R_{01}}{R_{1J} + R_{0J} - R_{01}}, \Delta T_{g,01}. \tag{6}$$

The last term is the gravitational effect in the ray path from radio source 0 to observation station 1. In this term, the position of the gravitating body J must be evaluated at the epoch of closest approach of the photon to the gravitating body. The light time equation (6) may be solved by numerical iteration such as the Newton-Raphson method and the solution converges very rapidly. The term H in the denominator of equation (1) is the correction term with Halley's method [7].

$$H = \left|\frac{\vec{V}_2}{c} \times \hat{\vec{R}}_2\right|^2 \frac{\vec{K} \cdot \vec{b}}{2R_2}. \tag{7}$$

The gravitational effect $\Delta T_{g,21}$ is composed from several terms as discussed by Klioner [4]: Post-Newtonian ΔT_{pN}, effect in the field of moving body ΔT_M, influence of quadruple field ΔT_Q, rotation of the bodies ΔT_R, and the post-post-Newtonian effects ΔT_{ppN}.

$$\Delta T_{g,21} = \Delta T_{pN} + \Delta T_M + \Delta T_R + \Delta T_Q + \Delta T_{ppN}. \tag{8}$$

The Post-Newtonian term (ΔT_{pN}) is the most significant and it must be included at least for the sun, moon and major planets (Jupiter, Saturn, Venus, Mars, and the Earth). This term is given by

$$\Delta T_{pN} = 2\sum_J \frac{GM_J}{c^3} \ln\left(\frac{R_{2J} + R_{0J} + R_{20}}{R_{2J} + R_{0J} - R_{20}}\right)\left(\frac{R_{1J} + R_{0J} - R_{10}}{R_{1J} + R_{0J} + R_{10}}\right). \tag{9}$$

According to Klioner [4], the post-post-Newtonian term of the Sun becomes a few hundreds of a ps in case of grazing rays and several ps when the source direction is 1 deg. away from the Sun. The term ΔT_Q reaches a few tens of a ps when the ray passes through the rim of Jupiter or Saturn. The term ΔT_M of Jupiter and ΔT_R of the sun reaches 0.5 ps when the ray passes the rim of these gravitating bodies. Refer to literature [9, 4] for formulas of each gravitational effect.

3. Adapting the Consensus Model for Finite-Distance Radio Source

For source distances up to 200 kpc and an Earth-diameter baseline the curved wavefront causes delay effects of larger than 1 ps. A full consideration of this effect is indispensable for observing radio source in the solar system. However, when the distance to the radio source from the earth is larger than 10 pc, the effect of the curved wavefront can be approximated with a few correction terms with parallax vectors $\vec{p}_M$ and $\vec{p}_2$ as

$$\Delta\tau_{\mathrm{Finite}} - \Delta\tau_{\mathrm{IERS}} = (\Delta T_{g,12} - \Delta t_g) + \frac{\vec{b}\cdot\vec{p}_M}{c}\left(1 - \vec{k}\cdot\frac{\vec{V}_2}{c}\right) - \frac{\vec{k}\cdot\vec{b}}{c}\left(\vec{p}_2\cdot\frac{\vec{V}_2}{c} - H\right) + O(b\varepsilon^2), \tag{10}$$

where $\vec{p}_M = \vec{\varepsilon}_M - (\vec{\varepsilon}_M\cdot\vec{k})\vec{k}$, $\vec{p}_2 = \vec{\varepsilon}_2 - (\vec{\varepsilon}_2\cdot\vec{k})\vec{k}$. $\vec{\varepsilon}_i = \vec{X}_i/R$ (i=1,2), and $\vec{\varepsilon}_M = (\vec{\varepsilon}_1 + \vec{\varepsilon}_2)/2$. See paper [7] for details of the derivation of the approximation. The right hand side of equation (10) can be used as correction terms to the consensus model adapting it to finite distance radio sources. Galactic radio sources such as pulsars and maser sources are candidates for such targets. Parallax measurements have been traditionally made by mapping source positions on the celestial sphere with data observed in multiple seasons. Then, the parallax parameter is estimated by fitting their apparent motion with a model. This technique has been used used since the era of classical optical measurement. And the same technique is still used in modern VLBI, in which the delay observable is directly available. Equation (10) suggests the possibility of parallax parameter estimation by the least squares technique, directly using the delay data-set from multiple seasons. See paper [7] for the partial derivative of the delay with respect to the parallax parameter. Equation (10) gives the daily variation with 40 ps amplitude in the case of PSR1937+21 (3.6kpc), for example. This approach may enhance the precision of parallax measurement. Possible difficulty in this approach may be delay resolution to detect the variation and clock discontinuity among VLBI sessions at different epochs.

References

[1] Eubanks, T. M. A Consensus Model for Relativistic Effects in Geodetic VLBI. Proc. of the USNO workshop on Relativistic Models for Use in Space Geodesy: 60–82, 1991

[2] McCarthy, D. D. and Petit, G. IERS Conventions, IERS Technical Report No.32, 2003.

[3] Moyer, T. D. Formulation for Observed and Computed Values of Deep Space Network Data Types for Navigation, JPL Monograph 2 (JPL Publication 00-7) 2000. JPL Deep Space Communications and Navigation Series, John Wiley & Sons. Inc., Hoboken New Jersey ISBN 0-471-44535-5

[4] Klioner, S, "General relativistic model of VLBI observables", in Proc. AGU Chapman Conf. on Geodetic VLBI: Monitoring of Global Change, Cartger, W. E.(ed.) NOAA Technical Report NOS 137 NGS 49, American Geophysical Union, Washington D.C, 188–202, 1991.

[5] Fukushima, T. Lunar VLBI observation model. Astron. Astrophys. 291: 320–323, 1994.

[6] Sovers, O. J., J. L. Fanselow, and C. S. Jacobs, Astrometry and Geodesy with radio interferometry: experiments, models, results, Reviews of Modern Physics, 70: No.4: 1393–1454, 1998.

[7] Sekido, M and T. Fukushima, A VLBI delay model for a finite distance radio source. J. Geodesy, 2006, in print.

[8] Irwin A. W. and Fukushima T. A numerical time ephemeris of the Earth. Astron. Astrophys. 348: 642–652,1999.

[9] Brumberg V. A., Post-post-Newtonian propagation of light in the Schwarzschild field. Kinematica Fizika Neb. 3(1): 8–13,1987

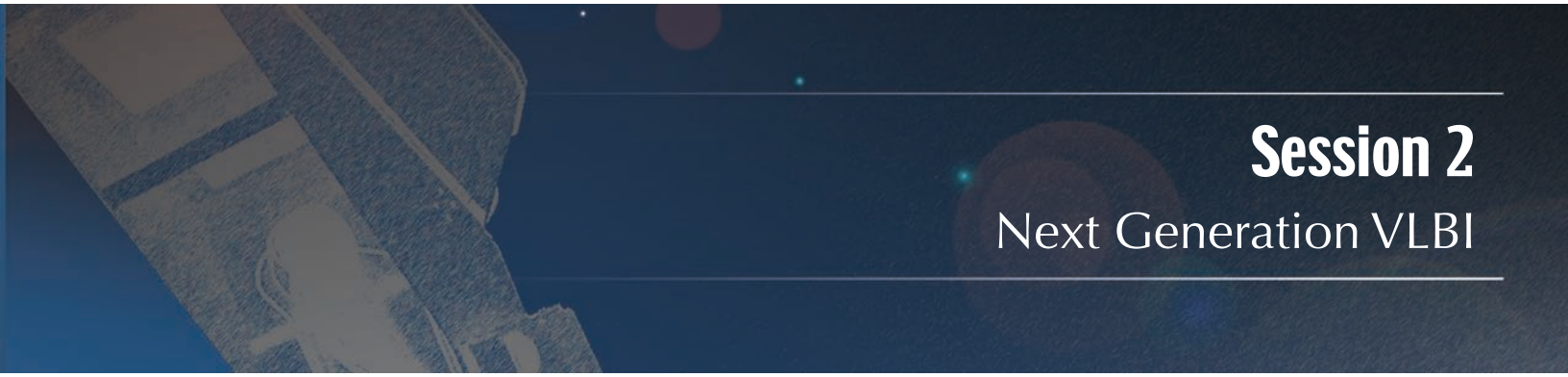

Session 2

Next Generation VLBI

Bill Petrachenko: Achieving a Quantum Leap in Observation Density, IVS 2006 General Meeting Proceedings, p.67–71
http://ivscc.gsfc.nasa.gov/publications/gm2006/petrachenko

Achieving a Quantum Leap in Observation Density

Bill Petrachenko

Natural Resources Canada

e-mail: Bill.Petrachenko@nrc-cnrc.gc.ca

Abstract

It is a general rule of thumb in geodetic VLBI that performance improves as the observation density (number of scans per day) increases. An acquisition system and observing strategy will be described for increasing the number of scans per day by roughly an order of magnitude. This will be achieved at a sensitivity that allows nearly all ICRF sources to be observed each day. Resulting benefits will be discussed.

1. Introduction

The purpose of this study is to investigate if it will be technically feasible by 2010 to increase the number of observations per day at each station by roughly an order of magnitude. Today, each site typically makes 200 to 450 observations per day. The goal here is to achieve one observation every 30 s, or 2880 observations per day. Two factors are needed to increase the observation density: shorter integration times, and shorter switching times between sources. Both factors will be addressed in more detail in the following sections, along with a discussion of related risks and benefits.

In order to maximize the advantage of increasing the observation density, additional performance-related targets need to be considered, e.g.:

- The system (antenna, electronics, etc) should be capable of achieving the VLBI2010 delay precision target of 4 ps for most observations.
- The system should have enough sensitivity to detect most ICRF sources at a level where the VLBI2010 delay precision target can be met.
- The system should have low enough capital and operating costs to encourage the establishment of 20-40 globally distributed stations of uniform design.
- The system should have high enough performance in other aspects to ensure that the benefits of the new VLBI2010 delay precision target will not be masked. For example, it must have high enough electrical, mechanical and geological stability, and it must have the ability to model and calibrate the troposphere at a high level.

2. Benefits of Increased Observation Density

Increasing observation density has the potential to improve performance in the following ways:

- The troposphere can be sampled more uniformly.
- The troposphere can be modeled with more temporal and spatial structure.

- The reference oscillators can be modeled with more temporal structure.
- The number of degrees of freedom can be increased, leading to *improved robustness of solutions and increased precision due to averaging.*
- A monolithic observing strategy can be developed to fulfill all IVS goals simultaneously, leading to *Increased internal consistency of products.*
- More sources can be observed each day, leading to *Improved connection to the ICRF.*
- More scans per day can be acquired per source, leading to *An improved ability to use internally acquired geodetic VLBI data to map sources and make source structure corrections.*
- Sensitivity to sub-daily geophysical processes would be enhanced.

3. Phase Delay

As stated in Section 1, one of the two factors required to increase observation density is the use of short integration times. Unfortunately, in the current geodetic VLBI mode of operation (which uses group delays at S and X-band), short integrations are difficult to achieve while still maintaining a capability for both high delay precision and access to most sources in the ICRF—in particular, if a lower cost antenna system is desired. As the phase delay is very precise, relative to the group delay, using it might provide the key to resolving this dilemma. Unfortunately, the phase delay is corrupted by an integer cycle ambiguity. With present systems, the phase ambiguity can, in fact, be resolved, but only at high signal-to-noise ratio (SNR). This defeats the purpose, because a high SNR is not compatible with either a lower-cost antenna system or the use of weaker sources. In this section, a system will be proposed where phase ambiguities can be resolved, even at low SNR. This innovation is key to achieving the targets laid out in Section 1.

Unlike the two-band S/X systems currently in use, the system proposed here uses a much larger number of IF bands. Technologically, this is enabled by the use of broadband feeds like the ones being developed at Chalmers University [1] for the SKA. Analytically, the process for combining the data to resolve RF phase involves three steps. First, the group delays are determined. Next, those group delays are used to resolve (in sequence from easiest-to-resolve pair to hardest-to-resolve pair) the phase differences between all pairs of adjacent bands. Finally, using the group delays from the first step and the phase differences from the second, an attempt can be made to resolve the RF phase ambiguities.

An analysis was made to determine the number of IF bands which make it possible to resolve RF phase at the lowest SNR. In the considered examples, the number of bands ranged from two to eleven, and, in each case, the broadband frequency range was 2-13 GHz. It was assumed that the IF bands had a uniformly filled 1 GHz bandwidth and that there was equal signal strength in each band. Phase resolution was achieved at a 5-sigma confidence level. For each system, the band frequencies were varied in 0.25 GHz steps across the full 2-13 GHz range, taking care to ensure that the bands did not overlap.

The results are summarized in Table 1. As can be seen, the system that exhibited the best performance (with respect to minimum overall SNR required to resolve RF phase) was the one that used five bands. Although not shown in the table, each of the systems was capable of achieving a delay of better than 2.5 ps at the minimum useable SNR, i.e. they were all capable of achieving the VLBI2010 delay precision target.

Table 1. Number of IF bands (NoB) vs. the minimum overall SNR required for phase resolution.

No. of IF Bands	2	3	4	5	6	7	8	9	10	11
Overall SNR	35.84	17.01	12.72	11.61	11.83	12.20	12.50	13.11	13.76	14.39

4. Sensitivity Considerations

As stated in Section 1, one of the secondary goals of this study is to be able to detect most of the ICRF sources with sufficient sensitivity to achieve the VLBI2010 delay precision target.

In a survey performed by Fey and Charlot in 2000 [2], the VLBA observed 225 ICRF sources. As part of the analysis, Gaussian component models were fitted to the uv data. The percentile distributions of the S and X-band principle component fluxes from the survey are displayed in Table 2. To the extent that the 225 sources of the survey are representative of the ICRF, these numbers provide a good estimate of the flux limits required to use the majority of ICRF sources—although, for the poorer ICRF sources, correlated flux degrades quickly as baseline length increases.

Table 2. Percentile distribution of the S/X-band principle component fluxes for 225 ICRF sources [2].

Percentile (sources)	0	5	10	20	30	40	50	60	70	80	90
S-band flux (mJy)	170	260	310	400	480	570	670	850	990	1190	1730
X-band flux (mJy)	110	160	190	230	290	350	440	510	610	760	1250

Next, consider the performance of an interferometer with the following characteristics: antenna diameter, 12 m; antenna efficiency, 50%; Tsys, 50 deg K; and, VLBI processing factor, 0.7. The system will have six optimally positioned IF bands, each with a completely filled 1 GHz bandwidth, two polarizations and 2-bit sampling. An integration time of 5 s will be assumed. Using the minimum SNR required to resolve phase when using six bands (see Table 1), it can be shown that the above system can resolve phase using a source as weak as 120 mJy. Given that the minimum principle component flux of the above survey was 110 mJy, it should be possible (in the absence of complications due to RFI, source structure, or dispersive electronics) to use that system to achieve the VLBI2010 delay precision target for nearly all sources of the ICRF.

5. Data Rate Considerations

With the exception of data rate, the system described above is very conservative with respect to cost and feasibility. However, it does produce a total data rate of 48 Gbits/s. Fortunately, with the low and decreasing cost of RAM, it is no longer necessary to record the entire bandwidth in real time. For example, 5 s of data acquired at 48 Gbits/s could be stored temporarily in a 30 Gbyte RAM buffer and then written to disk at 8 Gbits/s over a 30 s period. An extrapolation performed in 2004 [3] (along with current trends) indicates that disk capacity and rate will advance to the point that, by 2010, it will be possible, using a single pack of 16 disks, to sustain an 8 Gbits/s data rate for 24 hours.

6. Slew Rate Considerations

Thus far, a practical system has been described that, under perfect conditions, has the capability of achieving the VLBI2010 delay precision target of 4 ps for virtually all sources in the ICRF. A source dwell time of no longer than 5 s is required, along with a 25 s period to write the remaining data to disk and simultaneously to slew. In order to achieve the goal of acquiring one source every 30s, it only remains to define the antenna slew parameters required to perform a full end-to-end slew within 25 s. In the calculation, the time needed for the antenna to accelerate/decelerate between stationary and full speed isassumed to be 5 s. Two variations of an alt-az drive will be considered, both being capable of full sky coverage. One uses 360 degrees of azimuth motion and 90 degrees of elevation motion (i.e. the elevation motion is from horizon to zenith), and the other uses 180 degrees of azimuth motion and 180 degrees of elevation motion (i.e. the elevation motion is from horizon to horizon). For the first option, a speed and acceleration of 18 deg/s and 3.6 deg/s^2 respectively are required for the azimuth drive and 4.5 deg/s and 0.9 deg/s^2 for the elevation drive. For the second option, a speed and acceleration of 9 deg/s and 1.8 deg/s/s respectively are required for both axes.

The calculation of the above speeds is based on the assumption that each source change will require a full end-to-end slew. This allows complete flexibility in sheduling. However, depending on the optimization criteria, real schedules may, in fact, require significantly shorter average slew distances and hence tolerate slower slew rates while still achieving an average of one observation every 30 s.

7. Observing Scenarios

When an order-of-magnitude increase in observing density (proposed in this paper) is coupled with the VLBI2010 recommendation for a 20 to 40-station network observing continuously, it is possible to envision very powerful observing scenarios. In a straightforward example, a global network could be used to observe all 717 sources of the ICRF at least eight times each day. Although very powerful and unified by today's standards, this scenario might not be optimum, due to the uniform weighting of sources. Other scenarios might begin by selecting a number (perhaps 200) of the best ICRF sources. A large fraction of a session could then be dedicated to observing those sources with the remainder of the session dedicated to monitoring, on a rotating basis, other candidate sources, either from the ICRF or astronomical calibrator lists.

Regardless of the details, any of these scenarios will be very powerful for source structure corrections. If maps for the primary (e.g. 200 best) sources are generated once per week, and a 20 to 40-station network operates daily, thousands of uv points will be available for each map. With this amount of data, it should be possible to make effective structure corrections relative to the stable AGN cores, making it possible to define the ICRF axes very precisely relative to that frame. This will have obvious benefits for the ICRF, ITRF and EOP.

8. Risks

Known risks are discussed below:

- **Source Structure.** It has been assumed that sources have no structure. In the real world, this is not true. The degree to which source structure affects both sensitivity requirements

and the ability to resolve phase ambiguities needs to be studied. The feasability of mapping (or modeling) sources and then correcting for the structure also needs to be considered.

- **Dispersive Electronics.** Electronics have been assumed to be perfectly linear. In the real world, this is not true. An attempt should be made to reduce the problem through careful design, but some self-calibration will almost certainly still be required. Temporal stability of the electronics will then become a larger issue.
- **RFI.** It has been assumed here that there is no RFI. In reality, RFI is a growing problem. Electronics need to be designed to be (at least) RFI tolerant, and further investigation is required to determine the degree to which the sensitivity conclusions of this paper need to be scaled to account for the presence of RFI.
- **Data rate.** It has been assumed that a practical sustained data rate of 8 Gbits/s can be achieved by the year 2010. State-of-the-art disk and data transmission performance needs to be monitored on a regular basis to verify the validity of that prediction.
- **Slew rate.** Currently, the fastest antenna involved in regular IVS observations (TIGO) has a slew rate of 6 degrees per second. The mechanical and cost implications of using faster slew rates need to be investigated.
- **Sensitivity.** Increased sensitivity could help reduce a number of the above risk factors. To anticipate that possibility, antennas larger than 12m could be considered, cooled feeds could be used to reduce Tsys, or larger existing antennas could be used in conjunction with the 12 m atennas to produce baselines with enhanced sensitivity.

9. Conclusion

It has been shown that, in the absence of known risk factors, it should be feasible by 2010 to build practical systems that will allow observation density to increase by an order of magnitude. Potential benefits have been discussed. To proceed beyond this point, a thorough theoretical examination of all known risks needs to be carried out. After that, if warranted, performance tests should begin using a prototype system.

References

[1] Olsson, R., P.-S. Kildal, S. Weinreb, The Eleven Antenna: A Compact Low-Profile Decade Bandwidth Dual Polarized Feed for Reflector Antennas, In: IEEE Transactions on Antennas and Propagation, Vol. 54, No. 2, Feb. 2006, p. 368-375.

[2] Fey, A.L., P. Charlot, VLBA Observations of Radio Reference Frame Sources. III. Astrometric Suitability of an Additional 225 Sources, In: ApJ Sup. Series, 128:17-83, 2000.

[3] Mujunen, A., J. Ritikari, VLBI2010: Commercial-off-the-Shelf Technology Perspecives in 1996, 2003, and 2010, In: International VLBI Service for Geodesy and Astrometry 2004 General Meeting Proceedings, Ottawa, Canada, Feb. 9-11, NASA/CP-2004-212255, p. 56-59.

Alan R. Whitney et al.: A Wide-Band VLBI Digital Backend System, IVS 2006 General Meeting Proceedings, p.72–76
http://ivscc.gsfc.nasa.gov/publications/gm2006/Whitney2

A Wide-Band VLBI Digital Backend System

Alan R. Whitney, Shep S. Doeleman, Brian Fanous, Hans F. Hinteregger, Alan E.E. Rogers

MIT Haystack Observatory

Contact author: Alan R. Whitney, e-mail: arw@haystack.mit.edu

Abstract

Virtually all next-generation radio astronomy applications, including VLBI, will be enhanced by inexpensive new Digital Back-End (DBE) processors. Haystack Observatory is collaborating with the UC Berkeley Space Sciences Laboratory to develop a powerful and low-cost replacement for the current analog BBCs for both geodesy and astronomy VLBI applications. Based on a general-purpose FPGA-based signal-processing board developed at UC Berkeley, each board will accept two analog 500MHz BW IF signals, and process each into 2^n channels (for example, sixteen 32MHz BW channels or thirty-two 16 MHz channels) with a total aggregate output rate of 4 Gbps to two VSI output connectors. We report on the status of this DBE system and possibilities for utilizing it for both geodetic and astronomy applications.

1. Introduction

The work described in this paper couples modern high speed A/D converters and FPGA based architectures to develop a versatile new VLBI digital backend (DBE) system that will bring dramatic improvements to the practice of both geodetic and astronomical VLBI. In particular, the development of a small module based on this modern technology will:

- Replace nearly a rack full of currently used analog backend equipment
- Interface easily to the receiver system of almost any radio telescope in the world
- Extend the output data rate by a factor of four to 4Gbps; use of multiple parallel DBE's will allow data rates to easily and economically extend to 8 or 16 Gbps
- Interface directly with the new generation of high-data-rate VLBI data systems, including the Mark 5B/5B+ developed at Haystack Observatory
- Cost ∼5% of that of the current backend system

From an historical perspective, this development is very timely. In 1980, the Mark III VLBI system was introduced with a maximum data recording rate of 224Mb/s [1]. This rate was achieved at great expense using a ∼$200K special-purpose Mark III recorder using magnetic tapes costing nearly $1000 each and was reserved for only the most demanding scientific observations. Today, 22 years later, these tape-based systems are being rapidly replaced by disk-based systems, such as the Mark 5A and Mark 5B [2], that cost less than $20K and record at 1 Gbps with media costs less than 25% that of magnetic tape. However, just as importantly, the VLBI backend systems in use today are still based on the same basic analog technology as the Mark III system with only modest improvements. Furthermore, though each backend system originally cost on the order of $100-200K, they are irreplaceable (and almost unmaintainable) due to obsolescence of critical parts. The DBE described here will replace these old backend systems at a fraction of the cost of the original, offer much expanded capability, and become a welcome complement to the new generation of disk-based VLBI data systems.

2. Current Generation of VLBI Backend Systems

The current generation of VLBI backend systems had their origins largely in the 1970's and early 1980's, resulting in the systems that are still in use for the majority of the world's VLBI observatories. A typical current-generation VLBI backend system is shown in Figure 1. An IF signal in a fixed range of 500-1000 MHz is processed through a suite of (up to) 14 analog baseband-converter (BBC) modules; each BBC module selects a small slice, typically up to 16 MHz wide, of the IF and translates it to a pair of adjacent USB/LSB channels. Each of the output channels from up to ∼14 BBC modules is then digitally sampled at the Nyquist rate, formatted and time-tagged by an accompanying 'formatter'; the formatter is typically limited to an aggregate data rate of 1024 Mbps (Mark IV). The data are then recorded onto magnetic tape or disks.

Though this backend system, or small variants, has been the mainstay of VLBI observations, it suffers from several serious drawbacks:

- Fixed IF-frequency input range: Even current Mark IV and VLBA systems use different IF ranges, while many modern RF-IF systems, particularly those at shorter wavelengths, employ IF frequencies ranges that extend as high as 10-12 GHz; this requires custom electronics at each such VLBI site in order to move the IF to the proper range for the current VLBI backends.
- High cost: Each of the BBC modules costs ∼$10K-$25K to procure, and several parts are obsolete and nearly impossible to obtain. Similarly, the accompanying formatter module cost is ∼$10K-$50K and also contains obsolete parts.
- Non-uniformity of channel bandpasses: Due to the analog nature of the BBC electronics, channel-to-channel differences may be significant. Analog-filter variations of up to ∼2.5% can produce phase errors up to several degrees.
- Lack of expandability: Expanding data rates beyond 1024 Mbps is a practical impossibility due the high cost and non-availability of the needed components.
- Physical bulk: The current system of IF distribution, analog BBCs and formatters requires nearly a rack full of equipment, which is very expensive and fragile to ship.

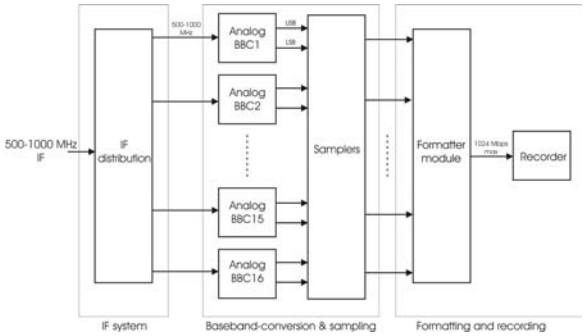

Figure 1. Simplified diagram of current VLBI backend system

2.1. Goals of the DBE

The development of the DBE system seeks to address all the aforementioned drawbacks of current systems and aims for a dramatic increase in capability. Figure 2 outlines the new backend system. The primary features of this new system are:

- Flexible IF-frequency input range: An arbitrary 500 MHz slice can be selected from each of two input IFs whose frequency range may be anywhere from 100MHz to 12GHz; this IF frequency range is designed to be compatible with both current and expected future systems. The same 500 MHz slice is selected from each of the two input IFs to support dual-polarization observations, for example.
- Uniformity of channel bandpasses: The conversion to baseband is accomplished fully digitally using a polyphase filter bank (PFB), ensuring absolute channel-to-channel uniformity.
- Dual VSI output interfaces: Dual VLBI Standard Interface [3] outputs clocked at rates to 64 MHz can support an aggregate data rate of up to 4 Gbps from 1000 MHz of aggregate bandwidth (Nyquist sampling, 2 bits/sample). Recording can be done on any VSI-compliant device.
- Low cost: The projected cost of the new sampling and baseband conversion module is $\leq$\$10K, at least a factor of ten lower than the current system. Furthermore, the need for a separate formatter is eliminated since the Mark 5B recording system formats all data internally.
- Easy expandability: The low-cost and small physical volume of the backend units will allow easy expansion to as much as $\sim$16 Gbps with multiple Mark 5B+ (2 Gbps) recorders.
- Easy transportability: A full 4 Gbps backend system, including two Mark 5B+ units, will occupy $\sim$21 inches of standard rack space. A complete 16 Gbps system with 4 IF/PFB units and 8 Mark 5B+ units will occupy two modest-size racks; this is considerably smaller than the current tape-based system with 1 Gbps capability!

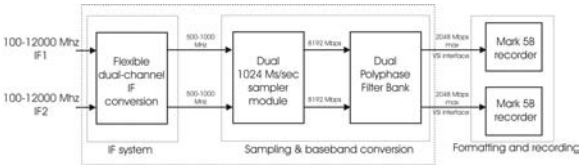

Figure 2. Simplified block diagram of new VLBI backend system including flexible IF-conversion

2.2. Flexible IF-Conversion Module

In order to convert the output from the telescope or array receiver we plan to design and build flexible IF conversion electronics that will select an arbitrary 500 MHz segment of an IF spanning the range 0.1-12 GHz and translate it to a 500 MHz wide frequency band centered at 750 MHz. The center frequency of 750 MHz is convenient since the 1024 Ms/sec sample rate for the A/D converter will be alias-sampled to cover a baseband from 8 to 508 MHz. The sample rate of 1024 MHz, rather than an even 1000 MHz, is needed for the PFB in order to provide the standard 16 MHz (32 Ms/sec) and 32 MHz (64 Ms/sec) VLBI channels. The filter sharpness

will allow 14 channels of 32 MHz bandwidth with full flatness, plus two outer-edge channels with somewhat reduced flatness (i.e. a total of 2048 Mbps output from *each* PFB for each wideband input channel). Figure 3 shows a block diagram of the proposed converter module. The converter will process two IF channels which share both LO1 and LO2. Estimated replication cost for a dual channel IF converter is ~5K$.

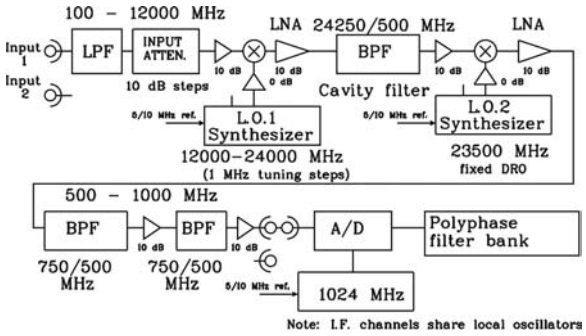

Figure 3. Block diagram of proposed IF-to-baseband converter module

2.3. Sampling and Baseband Conversion Module

The sampling and baseband-conversion modules are adapted from similar designs originally developed at the Berkeley Space Sciences Laboratory in support of the CARMA project. Figure 4 shows a simplified block diagram.

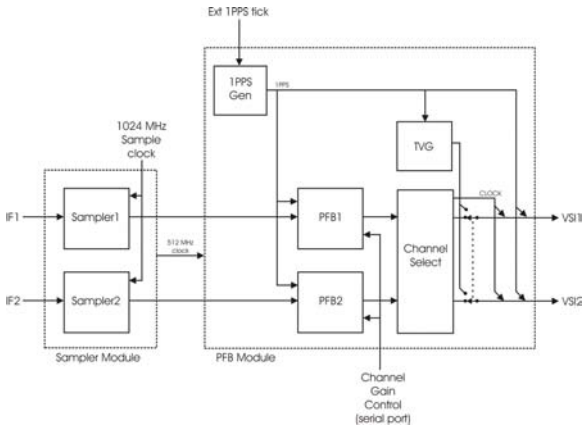

Figure 4. DBE implementation on the Berkeley prototype FPGA-based board

The data from the two IFs are sampled at 1024 Ms/sec 8 bits/sample by dual samplers in a single chip; the sample clock is supplied externally and is phase-locked to the station hydrogen-maser frequency standard. The sample data are processed by two independent FPGA-based PFBs to segment each 500 MHz IF into 2^n adjacent frequency channels spanning the 500 MHz IF bandwidth. The selection of the value of n is done by downloading the FPGA with a design particular to the value of n; depending on the requirements of the user, the value of n can be adjusted from 0 (single 512 MHz channel) to about 8 (256 channels of 2 MHz each). This flexibility

in choosing baseband-channel bandwidth guarantees backward compatibility with all channel-bandwidth modes of the current backend analog equipment, as well as support for future modes requiring channel bandwidths up to a single 512 MHz channel.

Analysis carried out on the PFB algorithms [4] indicates that out-of-band response for each channel exceeds 50 dB, far better than can be done with analog filtering in the current analog BBCs. The channels to be recorded are selected in the Channel-Select sub-section of the FPGA and output to two independent VSI output buses at a maximum aggregate data rate of 4096 Mbps. An externally-generated station 1PPS signal provides a one-time reference tick to initiate a module-based 1pps generator. An on-board Test Vector Generator (TVG) provides test signals for verification of the VSI interfaces to the recording system. An externally generated channel-gain control will act to keep the channel signal gains optimal for 2-bit sampling normally used in VLBI. A photo of a prototype DBE board under test at Haystack Observatory is shown in Figure 5.

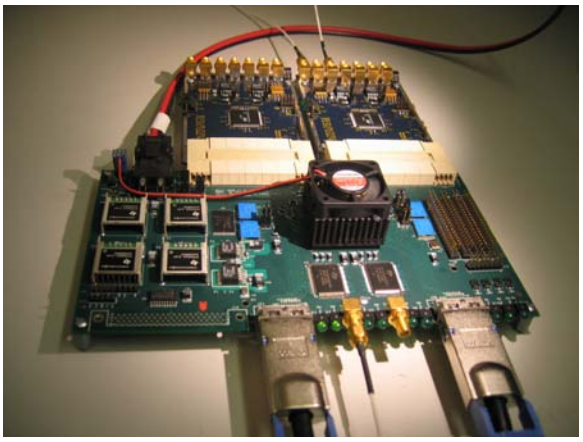

Figure 5. Prototype DBE board undergoing testing

3. Summary

Once the DBE units are commercially available, it is expected that their use will quickly become widespread. Their low cost and high performance will have a dramatic and lasting impact on the VLBI research infrastructure.

References

[1] Rogers, A.E.E. et al, *Science*, 219, 51, 1983.

[2] The Mark 5 web site at *http://web.haystack.mit.edu/mark5/Mark5.htm* contains much additional information about the Mark 5 system.

[3] "VLBI Standard Hardware Interface Specification - VSI-H", Revision 1.0, 7 August 2000, available at *http://dopey.haystack.edu/vsi/index.html.*

[4] Rogers, A.E.E., Hinteregger, H.F., Mark 5 Memo Series, #018, *ftp://web.haystack.edu/pub/mark5/018.pdf*, 2004.

Peter Shield et al.: A New Lower Cost 12m Full Motion Antenna, IVS 2006 General Meeting Proceedings, p.77–82
http://ivscc.gsfc.nasa.gov/publications/gm2006/shield

A New Lower Cost 12m Full Motion Antenna

Peter Shield, Mark Godwin

InterTronic Solutions, Patriot Antenna Systems Inc.
Contact author: Peter Shield, e-mail: pshield@intertronicsolutions.com

Abstract

A new lower cost 12m Ka band antenna and pedestal together with a novel high accuracy control system has been designed and delivered to NASA JPL for the DSN array. This new antenna was designed and manufactured by Patriot Antenna Systems to suit their higher volume manufacturing techniques and has taken advantage of the latest mechanical structures and control loop components available to achieve cost targets for larger Ka band antennas never seen before. The surface accuracy of this new design is 0.012 inches RMS including temperature and wind effects and its control system is capable of less than 0.005 degree RMS absolute pointing accuracy (spatial coordinates) using fast response position and speed control loops. The control system uses only economical, standard commercial modules and provides a wide speed range - repositioning to anywhere on sky within 2 minutes and with tracking at speeds down to much less than 1 millidegree/sec. Corrections for axes misalignments are built into the controller and a choice of interfaces allows antennas in an array to be nodes on a LAN such that a controlling computer can broadcast common instructions to all antennas. Each antenna can store track data to execute at scheduled times and has facilities for initial pointing calibration and calibration monitoring. This antenna is suitable for deep space communications, radio astronomy, conventional GEO and even LEO satellite communications. Several options are available for the drive system mechanics including conventional gear drives in both axes as well as more economical precision jack screw elevation drives.

1. Introduction to Patriot

Patriot has a 300,000 sq. ft. factory in Albion, Michigan, USA. Patriot's advanced mechanical design & analysis tools and capabilities include the

- principal design tools
  - AutoCAD and
  - Solid Works.
- Mechanical analysis is available for
  - wind load and forces software (MIT Lincoln Lab Report 71G-5),
  - Von Mises stress/deflection calculations,
  - thermal effects,
  - natural resonant frequency, and
  - FEA using Ansys.
- Laser photogrammetry rounds out the mechanical design and analysis tools.

Patriot is also very well equipped with all the latest high volume antenna manufacturing tools needed. These include

- a new large Taurus mill for tooling,
- a new laser cutter and welder,
- CNC mills and CNC lathes,
- 22 presses ranging from 50–1250 tons,
- press brakes, shears, and saws

providing complete manufacturing capabilities.

Figure 1. Patriot facilities at Albion, Michigan, USA.

Powder coating is used as a finish treatment instead of regular paint, as powder is much more durable and environmentally friendly. Patriot has two powder coating lines together with huge warehouses. Proven stretch-formed antenna panels are used that provide superior, accurate surfaces and repeatability; in-house tooling and machinery is used to stretch the panels.

2. 12m Cassegrain Antenna Key Specifications

The key specifications and features of the 12m Cassegrain antenna are:

- Surface accuracy: 0.3 mm (0.012 inches) overall RMS. Contributing causes: 0.008″ manufacturing, 0.005″ wind, 0.005″ temperature, and 0.005″ gravity. Easily suitable for use at up to 32 GHz.
- Dual shaped, F/D 0.375.
- Pointing accuracy: 0.005°.
- No on site panel alignments required.
- Factory assembled mount reduces installation time.
- Designed for lower cost volume manufacture in a wide range of sizes and configurations.
- Operating temperature range: -15°C to +55°C.

- Specifications apply in winds of up to 35 mph.
- 100 mph survival in stow.
- Antenna mounts on a typical 24-ft square, 4-ft thick concrete pad.
- Included with antenna are a template and bolts for setting into the pad.
- $+5^\circ$ to 90° elevation travel.
- $\pm 270^\circ$ azimuth travel.
- Antenna weight: 34,500 lbs.
- Entire antenna ships on two trucks or in two standard 40 ft shipping containers.

Figure 2. 12 meter antenna installed at JPL.

3. 12m Antenna Detailed Mechanical Features

The main antenna components are the pedestal (made of welded steel), the turning head assembly, and the reflector and hub (made of aluminum).

3.1. Turning Head

The turning head assembly is attached to the azimuth bearing and provides the azimuth and elevation motion of the antenna system. The base plate of the turning head is machined concurrently for the bearing and gearbox interfaces. This approach provides very accurate meshing of the drive pinions to the azimuth gear with minimal field alignment.

Figure 3. Constructing the 12m antenna.

3.2. Azimuth Drive

The azimuth drive is a typical dual pinion anti-backlash design which includes integral pinions, fail-safe brakes, drive motors and gearboxes. The azimuth drive components are bolted together into an assembly that bolts vertically onto the turning head.

3.3. Elevation Drive

The elevation drive assembly consists of an oversized 100 ton ball screw actuator, gearbox, motor, brake and encoder bolted together in a horizontal assembly. Due to the geometry of the antenna the elevation actuator is always loaded in compression under operational conditions. This eliminates the effects of backlash in the system.

3.4. Reflector Assembly

The reflector assembly consists of the hub, radial trusses, bracing, panels, rear closeouts, sub-reflector and subreflector supports. The hub is a drum structure with machined interfaces for the pedestal and radial ribs. The front face of the hub also is the interface plane for the feed system and support structure. The ribs are attached to the hub at machined interface points and supported by back support struts and bracing that rigidly tie the reflector system together. There are 24 main ribs with 24 intermediate ribs to help support the outer tier of panels. The

subreflector struts are pin-connected to the reflector and arranged in a quad configuration and provide mounting and adjustment for the lightweight composite subreflector. The rear closeouts provide added stiffness and means of thermal protection for the structure. This reflector system has been chosen for its rigidity, ease of manufacture and ease of installation. The design is cost effective and easily transported. Installation time is minimized by the use of highly accurate parts and minimal alignment requirements.

4. Maintenance Features

The maintenance features can be summarized as follows:

- Azimuth motors and gearboxes are changeable without major work.
- The elevation jack is replaceable without cranes etc.
- In-pedestal electronics permits easy access to the drives.
- Only simple routine maintenance procedures are required.

5. 12m Antenna Detailed Electrical Features

The philosophy adopted in the design of the pointing control system was to use COTS equipment and to minimize or even eliminate ad hoc equipment. This approach has resulted in a configuration in which the position control loops are closed within inverter drives, rather than in an external computer as is often the case in antenna pointing systems

The inverters used supply variable frequency, three phase power to the motors to control speed. Motor speed feedback is supplied by 4096 line/revolution incremental encoders. On both axes a feed-forward speed control loop and a precision position loop are used. A 4 msec update rate is used for the position control loop.

Brushless AC servo motors are used as they provide the high torque required for accurate servo position control. The motors also include brakes and speed encoders. On the azimuth axis two 2.5-kWatt motors and gearboxes are used in a torque biased configuration. In the elevation axis one 3.25-kWatt motor is used.

A control equipment cabinet is used for the drive electronics. This is housed in the pedestal eliminating the need for a separate building.

The antenna can be supplied with various software interfaces that enable the complete elimination of a separate ACU.

Go-to commands, program track and several coordinate systems can be accommodated. Exceptionally versatile and accurate motion is accomplished with the control system. A very wide speed control range can be achieved with no overshoot when arriving on target.

26 bit Heidenhain optical absolute encoders are used that can provide a resolution of 0.0000054 degrees. The smallest increment actually used is 0.0001 degrees.

Antenna repositioning to anywhere on the sky within 2 minutes and tracking at speeds down to much less than 1 millidegree/sec are achieved. Corrections for axes misalignments are built into the controller and a choice of interfaces allows antennas in an array to be nodes on a LAN such that a controlling computer can broadcast common instructions to all antennas. Each antenna can store track data to execute at scheduled times and has facilities for initial pointing calibration and calibration monitoring

6. 12m Antenna Measured Performance

The maximum slew and scan rates are:

- up to 3–6 deg/sec in azimuth.
- up to 0.7–3 deg/sec in elevation.
- Speed range changes can be accomplished by using modified gearbox ratios.
- Accurate pointing down into the 1–2 millidegree range has been reported from measurements made so far.

7. 12m Antenna Applications and Configurations

The 12m antenna supports the follwing applications and configurations:

- fixed pointing;
- limited motion;
- full motion: ±270 degrees;
- GEO communications;
- LEO communications;
- DSN tracking;
- TT&C applications;
- radio astronomy;
- 2-port or 4-port feed configurations;
- high wind and other custom designs;
- CP/LP switchable, monopulse feeds;
- antenna drive and control system pptions;
- 6 to 18 meter for S, C, Ku, Ka, and X-band;
- 3rd tilt axis for keyhole elimination.

Contact Information

For further details please contact:

Peter Shield
InterTronic Solutions Inc
452 Aime-Vincent
Vaudreuil-Dorion
Quebec, Canada, J7V 5V5
Tel: +1-450-424-5666
Fax: +1-450-424-6611
Email: pshield@intertronicsolutions.com

Gordon Lacy et al.: A Preliminary Design Study for an Affordable 12 Metre Carbon Composite Radio Telescope, IVS 2006 General Meeting Proceedings, p.83–83
http://ivscc.gsfc.nasa.gov/publications/gm2006/lacy

A Preliminary Design Study for an Affordable 12 Metre Carbon Composite Radio Telescope

Gordon Lacy [1], *Peter Dewdney* [1], *Bill Petrachenko* [2]

[1)] *National Research Council Canada*

[2)] *Natural Resources Canada*

Contact author: Gordon Lacy, e-mail: gordon.lacy@nrc-cnrc.gc.ca

Abstract

Carbon composites are ideal materials for geodetic VLBI antennas. They allow structures to be fabricated that are simultaneously light and stiff. In terms of antenna design, this translates into a reflector surface that exhibits minimal gravitational (or wind) deflection. If the back support structure, the yoke, and the pedestal are also fabricated from carbon composites, the low coefficient of thermal expansion minimizes annual (and diurnal) thermal height signatures along with tilts due to differential solar irradiation.

A preliminary design study has been undertaken to determine the feasibility of constructing an affordable 36 GHz carbon composite radio telescope, which also has high thermal stability and high slew rates. The conclusion is that such a telescope can be produced. Material and labour costs for a prototype telescope come in at values less than fabricated metal telescopes; and, although economies of scale are important, the numbers at which the process becomes feasible are much smaller than for other processes such as hydroforming.

The telescope has a very lightweight all carbon composite structure. The dish, together with its supporting beams is molded as a single unit using a new composite manufacturing process. Using this process, together with an optimized composite structural design, both the labour and material costs can be kept low. Such a structure can be designed to be wind dominated rather than gravity dominated. In this way a very lightweight structure can be produced that performs well at 36 GHz under some lesser wind condition, with the requirement for stronger winds being survival alone. Alternatively the telescope can be designed to perform in full wind (say 30 mph) at 36 GHz or higher. The limitation is strictly weight and cost.

Since the antenna structure will weigh about 15% of a typical all-metal design, achieving high slew rates will be considerably easier. An innovative option for achieving very high slew rates is to use brushless linear motors. This type of drive system exhibits zero wear because it has no contacting parts. It also has very low inertia and zero backlash. With this type of drive system, full sky slewing times on the order of 20 to 30 seconds are easily obtained. The cost increase for linear drives over conventional geared drives is not large when compared to the total cost of the telescope.

Chopo Ma: Uses of the ICRF and Implications for Future VLBI, IVS 2006 General Meeting Proceedings, p.84–88
http://ivscc.gsfc.nasa.gov/publications/gm2006/ma

Uses of the ICRF and Implications for Future VLBI

Chopo Ma

Goddard Space Flight Center

e-mail: cma@gemini.gsfc.nasa.gov

Abstract

Since its inception on 1 Jan 1998, the fundamental ICRF has been set by the VLBI positions of 212 "defining" extragalactic radio sources. In all, there are $\sim$ 3000 sources with usefully accurate ($<$ few mas) positions consistent with the ICRF. The uses of the ICRF include fundamental astrometry, monitoring of Earth orientation, and spacecraft navigation. For fundamental astrometry, stability and accuracy are most important, and realizations at different frequencies must be in proper registration. However, there is no preferred frequency, and the GAIA mission has the potential for an optical ICRF with 500,000 objects at the 50 microarcsec level some time after the planned 2011 launch. The radio ICRF should be properly prepared for a transition to assure long term stability and consistency. Earth orientation monitoring requires objects attached to the solid Earth, and VLBI will continue to be the fundamental technique. For this purpose it is essential that the new VLBI stations contemplated in the VLBI2010 report be capable of observing a sufficiently large and well-distributed set of stable sources, and identifying these sources is an on-going effort. Spacecraft navigation by differential VLBI is planned using the Ka-band telemetry signal, and work has begun towards an ICRF realization suitable for this purpose. The balancing of different needs related to the VLBI ICRF is discussed.

1. Introduction

Since 1 January 1998 the fundamental ICRF (International Celestial Reference Frame) has been set by VLBI positions of extragalactic radio sources, formally the 212 defining sources. The $\sim$ 3000 radio sources with accurate positions in the ICRS (International Celestial Reference System) have uses in fundamental astrometry, geodesy, spacecraft navigation, and astrophysical observing. Consequently, the observations and analysis for continued strengthening, refinement, and densification of the VLBI source catalogue as well as the development of advanced VLBI instrumentation such as VLBI2010 must balance the various needs. In addition, the transition to an optical extragalactic celestial reference frame with many more objects and significantly improved precision must be prepared.

2. Fundamental Astrometry

The ICRF-Ext.2 (Fey et al., [2]) shown in Figure 1 is the latest refinement of the original ICRF (Ma et al., [4]). It retains the positions of the 212 defining sources unchanged as well as the overall error characteristics of the ICRF while improving the positions of the remaining sources and adding $\sim$15% more. For fundamental astrometry accuracy and stability of positions and distribution over the sky are of greatest importance. The data used for the original ICRF spanned 1979.7 - 1995.6. However, Gontier et al. [3] showed that data after $\sim$1990 are considerably better for astrometry than the older data in the ICRF analysis, and Feissel-Vernier [1] showed that some of the 212 ICRF defining sources are less than ideal when considering the currently available VLBI data. The overall data distribution is deficient in the southern hemisphere, and many of the ICRF defining sources

have been poorly observed since 1995. Consequently the IVS began a celestial reference frame (CRF) monitoring program in 2004 to improve the data set for high quality astrometric sources and for ICRF defining sources, which is described below.

3. Geodesy

VLBI geodesy encompasses two main areas, regular monitoring of EOP (Earth orientation parameters), for which VLBI has unique capabilities, and maintaining the ITRF (International Terrestrial Reference Frame), to which VLBI contributes scale and long term data. These observing sessions use a subset of the VLBI sources often called the geodetic catalogue. The current geodetic catalogue has ∼100 sources and is shown in Figure 2. The geodetic catalogue has evolved over the years following development of VLBI instrumentation and networks, and the small number of geodetic sources constitute well over 90% of all VLBI geodetic/astrometric observations. Ideally geodetic sources should be strong, point-like and stable in position, but very few sources meet all the criteria all the time. In particular, as shown in Figure 2, there has been a trade-off between stability and source strength in some cases, and sources that are usually quite good occasionally drop in flux density or evolve structure for some period. MacMillan (this volume) shows some effects in the geodetic results caused by source instability. Maintaining and updating the geodetic catalogue has been a sporadic effort, hampered by the absence of objective criteria and sufficient data for regularly adding or removing sources. As with fundamental astrometry, the geodetic catalogue should be improved in the future by data from the CRF monitoring program.

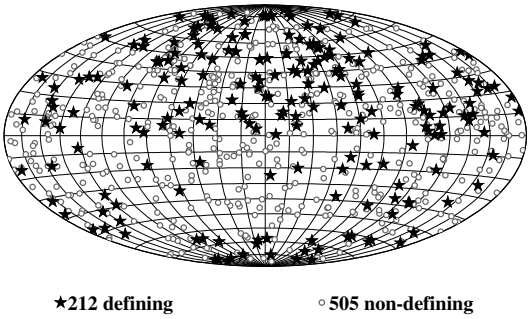

Figure 1. ICRF Ext.2 sources.

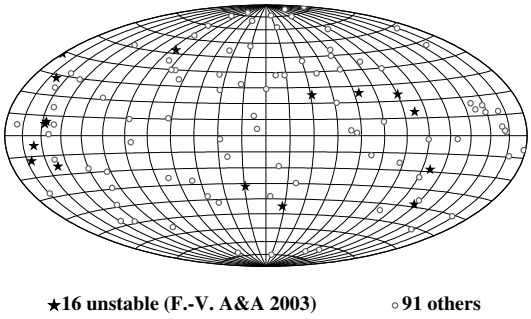

Figure 2. Geodetic sources.

4. Celestial Reference Frame Monitoring Program

The CRF monitoring program was started by the IVS in the spring of 2004 to remedy serious gaps in the astrometric observing profile, primarily the paucity of data for most of the stable sources identified in Feissel-Vernier [1] and subsequent analysis (Feissel-Vernier, personal communication). See Figure 3. Potentially stable sources, i.e., those with insufficient data to determine stability but no obvious deficiencies (Figure 4) as well as poorly observed ICRF defining sources are also included. Some stable sources and some ICRF defining sources are in the geodetic catalogue and are not included in the CRF monitoring list since they have more than sufficient observations. The

current set of CRF monitoring sources is shown in Figure 5.

The CRF monitoring program uses ∼10% of the observations of certain geodetic sessions (currently R1 and RDV) to systematically observe sources in the CRF monitoring list. The goal is to have at least one session per target source every six months. Figure 6 shows that this goal is being met. These data will allow the extension of the Feissel-Vernier [1] time series analysis and improvement of the positions of the ICRF defining sources. In addition, the RDV sessions, which use the VLBA and up to ten other stations, provide data for structure maps. The CRF monitoring data will be essential to properly select defining sources for the next radio-frequency ICRF realization. To increase the data in the southern hemisphere, the IVS has focused its astrometric observing program on mid and far southern sources.

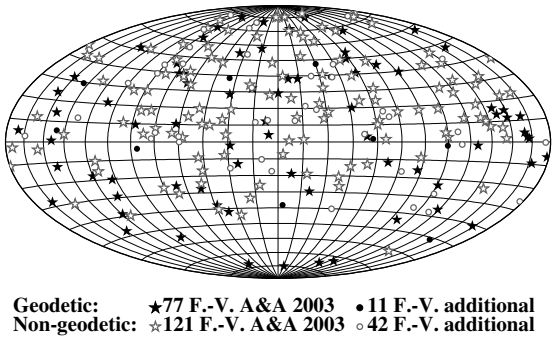

Figure 3. Total stable sources.

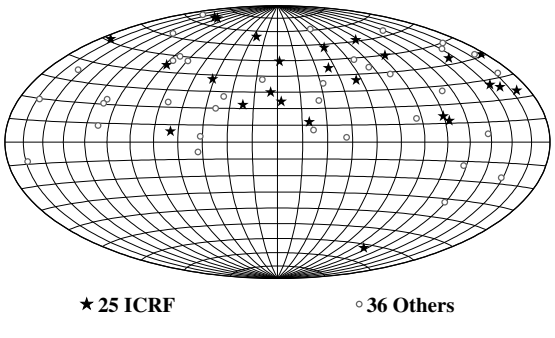

Figure 4. Potentially stable sources from M. Feissel-Vernier (personal communication).

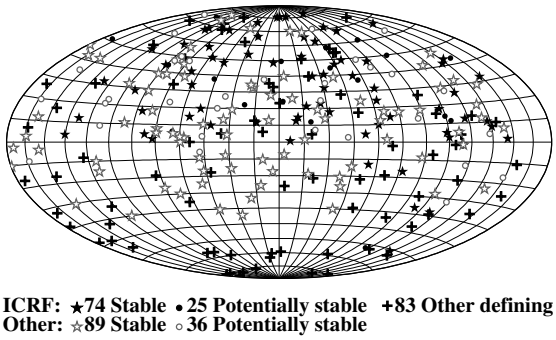

Figure 5. Total CRF monitoring sources.

5. Spacecraft Navigation

Spacecraft navigation using differential VLBI has become a standard technique for NASA spacecraft equipped with delta-DOR (Differential One-way Range) at X-band and has been tested at Ka-band. The Cassini-Huygens probe was tracked while descending to Titan in January 2005 by a global array of astronomical VLBI stations using phase referencing at S-band. Such spacecraft navigation requires a high density of sources near the ecliptic with positions at the telemetry frequency. As the telemetry frequency has evolved from S-band (2 GHz) to X-band (8 GHz) to Ka-band (30 GHz) to provide greater signal bandwidth, the source catalogues must also evolve.

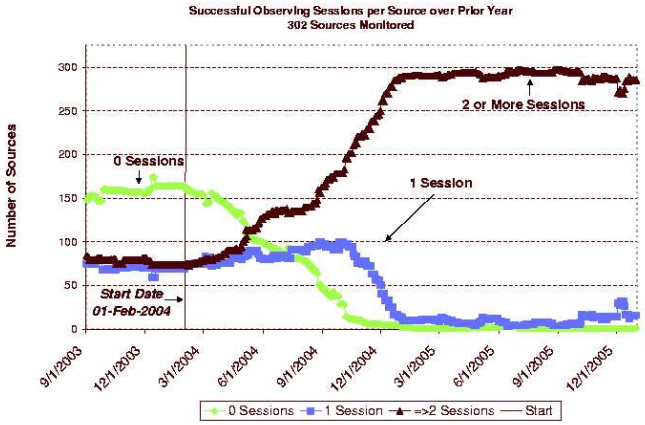

Figure 6. Source monitoring.

Since there is not yet sufficient observing capability to build a true Ka-band catalogue, K-band (22 GHz) and Q-band (43 GHz) observations have been used as proxies. See Jacobs et al. (this volume). These higher frequency observations have shown that sources are generally more compact but weaker than at S/X-band.

6. Astrophysical Observing

A standard technique for observing weak radio sources with VLBI is phase referencing, i.e., integrating the differential VLBI signal between a weak target source and a nearby calibrator. Many sources of error are cancelled or sharply reduced in this mode. For this purpose the spatial density and distribution of the calibrator catalogue are most important, and the requirements for absolute position accuracy are somewhat relaxed. Figure 7 shows the VLBA Calibrator Survey (VCS) sources up through the third VCS densification. These positions at the ∼1 mas error level are the result of a series of VLBA sessions begun in 1994 (Petrov et al., [5]). The finished catalogue should be essentially complete at the 200 milliJansky level for S/X-band sources above -30 deg.

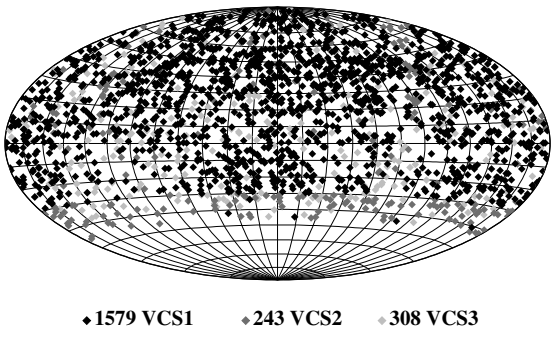

Figure 7. VCS sources.

7. Future Fundamental ICRF at Optical Wavelengths

The GAIA mission is scheduled for launch at the end of 2011 and has the potential for an optical ICRF with 500 000 extragalactic objects at the 50 microarcsec level. See Andrei (this volume). Transferring the orientation of the radio ICRF precisely and accurately to such an optical ICRF will not be trivial since most of the radio ICRF objects are at the faint end of the sensitivity planned for GAIA. In addition, nonregistration of the radio and optical emission points and source structure in the radio (and possibly in the optical at the planned GAIA precision) will add noise to the orientation transfer. It may be desirable to focus some VLBI observing over the coming years on a small set of quasars where the balance of radio and optical strength and position precision make them the best candidates for the tie. However, it is possible that the best tie will come from using the largest number of objects although the radio and/or optical positions are not the best.

8. Considerations for Future Observing and Technical Developments

Since there is not an infinite amount of VLBI observing at all relevant radio frequencies with global networks of large antennas, it is impossible to improve all aspects of ICRF use equally. In the abstract, a better radio ICRF would use higher frequencies than S/X-band for source compactness (and probably source position stability) and large, geographically well distributed antennas to cover the full sky more densely by observing weaker sources. In practice, it is likely that the past and future S/X-band data will continue to be the basis for the best radio ICRF, and the existing large antennas will be needed for catalogue maintenance and source monitoring. For EOP monitoring, which can never be done using the optical GAIA ICRF, a limited but well distributed set of strong, stable sources observable by the smaller, faster antennas envisioned by VLBI2010 is required. For spacecraft navigation sources along the ecliptic must be found and accurate positions at the telemetry frequencies must be determined. Observations for this purpose may become a separate effort from the general astrometric program. Phase reference observations will continue to be well served by the VCS catalogue. This set of sources may also provide the link to the GAIA optical frame if a larger number of tie objects with larger uncertainties is better than a severely limited set of sources optimized at both the radio and the optical wavelengths.

References

[1] M. Feissel-Vernier, Selecting stable extragalactic compact radio sources from the permanent astro-geodetic VLBI program, A&A 403, 105, 2003.

[2] A. Fey, C. Ma, F. Arias, P. Charlot, M. Feissel-Vernier, A-M. Gontier, C. Jacobs, and D. MacMillan, The second extension of the ICRF, Astron. J 127, 3587, 2004.

[3] A.-M. Gontier, K. Le Bail, M. Feissel and T. Eubanks, Stability of the extragalactic VLBI reference frame, A&A 375, 661, 2001.

[4] C. Ma, F. Arias, T. Eubanks, A. Fey, A.-M. Gontier, C. Jacobs, O. Sovers, B. Archinal, and P Charlot, The International Celestial Reference Frame as realized by very-long-baseline-interferomtry, Astron. J. 116, 516, 1998.

[5] L. Petrov, Y. Kovalev, E. Fomalont, and D. Gordon, Third VLBA Calibrator Survey, AJ, 129, 1163, 2005.

Zhijun Xu et al.: Real Time Correlator in FPGA, IVS 2006 General Meeting Proceedings, p.89–92
http://ivscc.gsfc.nasa.gov/publications/gm2006/zhijun

Real Time Correlator in FPGA

Zhijun Xu, Xiuzhong Zhang, Renjie Zhu, Chunmei Lu, Zhong Chen, Fengchun Shu, Weiming Zheng

Shanghai Astronomical Observatory, China

Contact author: Zhijun Xu, e-mail: xuthus@shao.ac.cn

Abstract

Real time correlator is very important for the Chinese e-VLBI development and the China Luna project. Taking advantage of the Field Programmable Gate Array (FPGA) technique, we developed a three stations real time hardware correlator at Shanghai Astronomical Observatory (SHAO). This paper briefly describes the architecture of the real time correlator and presents some results from real observation data.

1. Introduction

The Field Programmable Gate Array (FPGA) technique developed very fast in recent years. It can realize very complex algorithms and control logic now. The real time hardware correlator developed at Shanghai Astronomical Observatory also takes advantage of the FPGA technique. At present, the FPGA chip used is an XC4VSX35 which is Virtex-4 SX Platform FPGA series chip produced by Xilinx Company. Later we will upgrade the correlator to five stations using the same chip or the higher version XC4VSX55. In this paper, the main characteristics and the details of the overall architecture are described. Then the correlator results are presented.

2. Real Time Correlator

2.1. Characteristics

The correlator we developed is a three stations FX correlator with one IF, which will later be upgraded to 5 stations with eight IFs. The data rate is up to 32 mega samples per second with 1 or 2 bits per sample. The integration time can be 32.768 milliseconds to 1 hour, typically it is 5 seconds. The input data format can be Mark IV or Mark 5, the VSI interface is also under development. The data sources are from disk array or via network. Outputs of the correlator are via net or saving to disk files. The fringe searcher and Phase Cal are still software version and later will also be implemented in hardware.

2.2. System Architecture

As shown in Figure 1, each station (in three cities, Shanghai, Urumchi and Kunming) has a Mark 5 recorder. During observation, the data from Mark 5 recorder are transfered via network to the Play Back Device (PBD) computer. Each PBD has 1G DDR RAM as FIFO, the data stored in the RAM is sent to each Play Back Interface (PBI) via a 7300A high speed digital I/O card. The PBI decodes Mark IV or Mark 5 data and sends outputs to the FFT&MAC board. One FFT&MAC board can process one IF data; 8 IFs shall have 8 boards. The FFT&MAC

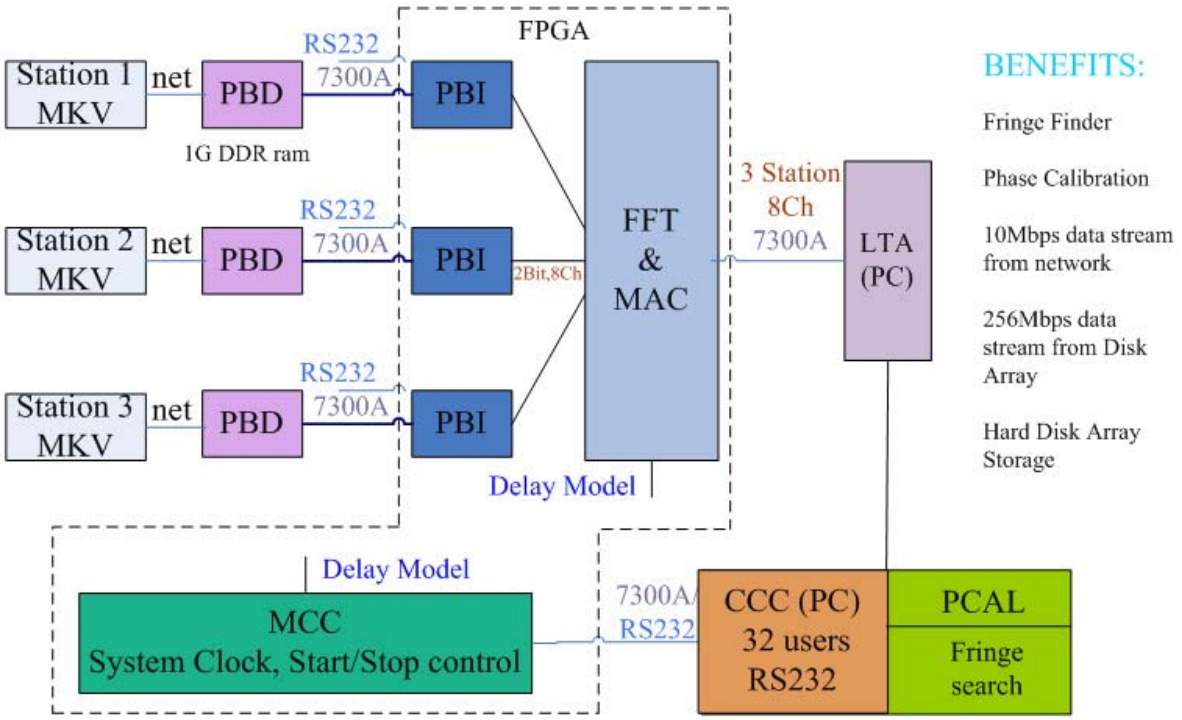

Figure 1. Architecture of the Correlator.

board has integer bit delay, fringe stopping, Fast Fourier Transform (FFT), Fractional Sample Time Correction (FSTC), multiple and accumulate (MAC) functions. The delay models needed for integer bit delay, fringe stopping and FSTC process on the FFT&MAC board are sent from the Master Control Card (MCC). Also, the MCC sends the system clock, start/reset control signal to the each PBI and FFT&MAC board. The output data from the FFT&MAC board are sent to the Long Term Accumulator (LTA) computer via 7300A high speed digital I/O card. The final results are displayed in real time on the monitor. The result data are saved in FITS format or sent to the Control Card Computer (CCC). The CCC will process fringe searcher and Phase Cal. Also, it generates the delay models and control commands to the MCC controlling the overall correlator.

The entire three stations correlator system consists of five computers and five FPGA boards. The five computers are three for Play Back Device (PBD), one for Long Term Accumulator (LTA) and one for Control Card Computer (CCC). The five FPGA boards are three for Play Back Interface (PBI), one for FFT&MAC board and one for Master Control Card (MCC). Both PBI and MCC boards are using FPGA chip XC3000 which belongs to the Virtex-II product series of Xilinx Company. The FFT&MAC board is using the XC4VSX35 chip and the speed grade is 10.

3. Results

Figure 2 and Figure 3 are the results from real observation data. Figure 2 shows the fringe result of the Shanghai—Urumchi baseline of TC-1 satellite observations with integration time of

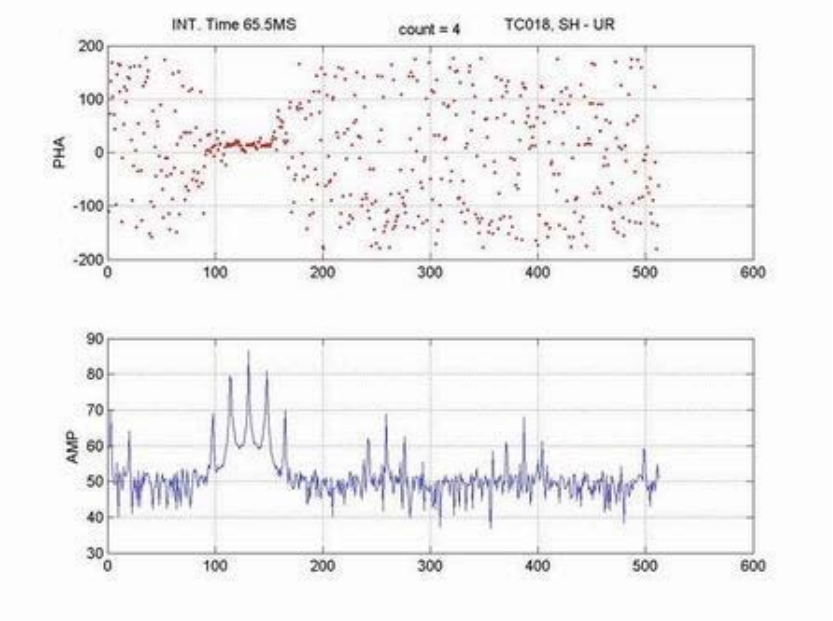

Figure 2. TC-1 results with integration time of 62.5 ms.

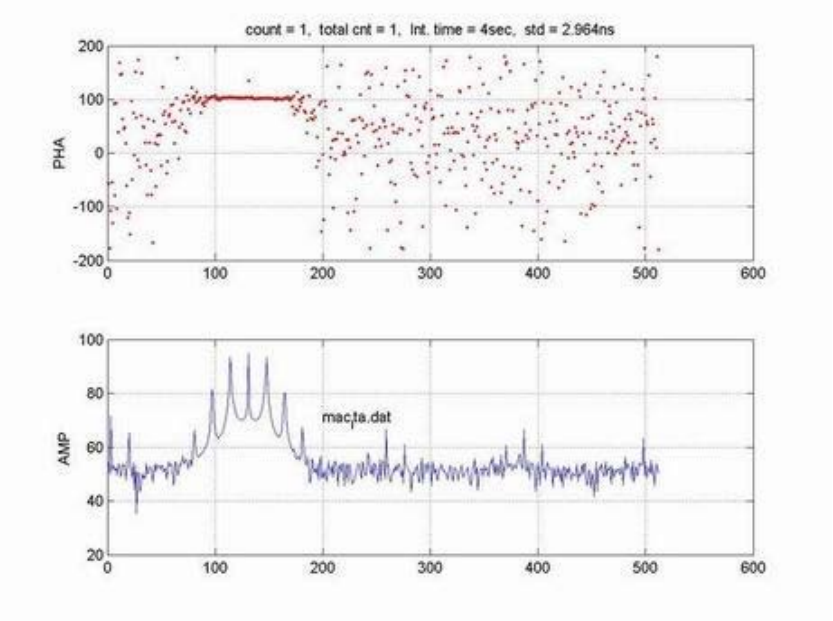

Figure 3. TC-1 results with integration time of 4 second.

62.5 ms, Figure 3 is the result of the same observation with integration time of 4 second.

References

[1] Zhang, XZ,. Zheng, WM,. Shu, FC,. Hang, ZY,. Xiang, Y., CVN Correlator and its Future, New Technologies in VLBI, Astronomical Society of the Pacific Conference Series Volumes, Vol.306, 287-300, 2003

Joerg Wresnik et al.: Simulations for VLBI2010, IVS 2006 General Meeting Proceedings, p.93–97
http://ivscc.gsfc.nasa.gov/publications/gm2006/wresnik1

Simulations for VLBI2010

Joerg Wresnik, Johannes Boehm, Harald Schuh

Institute of Geodesy and Geophysics (IGG), Vienna University of Technology, Austria
Contact author: Joerg Wresnik, e-mail: wresnik@mars.hg.tuwien.ac.at

Abstract

In October 2003 the International VLBI Service for Geodesy and Astrometry (IVS) installed Working Group 3 (WG3) 'VLBI2010' to examine current and future requirements for geodetic VLBI systems. A clear demand was stated by WG3 that thorough and systematic simulation studies should be done. At the Institute of Geodesy and Geophysics of the Vienna University of Technology different simulations are carried out to propose new observing strategies and schedules, to improve troposphere and clock modeling, to find the best antenna configuration and to optimize the network geometry. The software packages used for the simulations are described and first results are presented.

1. Introduction

There has been a lot of discussion in recent years how VLBI could exploit its present resources more efficiently and how future VLBI networks should look like. In October 2003 the International VLBI Service for Geodesy and Astrometry (IVS) installed Working Group 3 (WG3) 'VLBI2010' to examine current and future requirements for geodetic VLBI systems. Based on its report (Niell et al., 2005 [2]) the VLBI2010 Committee was set up to promote and guide research into the improvement of the 'technique' of geodetic VLBI. The Institute of Geodesy and Geophysics (IGG) of the Vienna University of Technology will support these activities by carrying out thorough simulation studies.

2. Simulation Studies at IGG Vienna

The simulation studies are realized by a sequence of three software programs. After scheduling the observations with SKED (Vandenberg, 1999 [3]), the artificial observations are transformed to databases in NGS format which are input for the VLBI analysis software package OCCAM (Titov et al., 2001 [4]). The covariance and correlation matrices in SINEX format are then entered into a Matlab program called VV-SIM (Vienna VLBI-Simulation), which allows the interpretation of the results with distinct numbers and illustrative figures to deliver objective criteria for comparing the various options.

Figure 1. Flow diagram of the software packages. It is very important to define interfaces (NGS and SINEX) which can be used by other groups, too.

2.1. Program SKED

Simulated schedules are created with the software package SKED (Vandenberg, 1999 [3]). This program is based on catalogue files for observed frequencies, radio sources and stations with certain specifications like diameter and slewing rate. For the simulation studies, the catalogue files need to be extended by virtual stations at different locations and of different quality. The schedule can be optimized in different ways (sky coverage, maximum numbers of observations, etc.), and the output of SKED is transformed to NGS format which can be used as input for OCCAM.

2.2. Program OCCAM

The analysis program OCCAM is using the classical Gauss-Markov model for the least-squares analysis:

Table 1. Gauss-Markov Model.

$v = Ax - l$	observation equations	(1)
$Nx - A^T Pl = A^T PAx - A^T Pl = 0$	normal equations	(2)
$x = N^{-1} A^T Pl$	solution for the unknowns	(3)
$Q_{xx} = \sigma_0^2 N^{-1}$	variance-covariance matrix	(4)
$\sigma_0^2 = \frac{v^T Pv}{n-u}$	a posteriori variance factor	(5)
$k_{ij} = \frac{q_{ii}}{\sqrt{q_{ii}^2 + q_{jj}^2}}$	correlations between the unknowns	(6)

v is the vector of the residuals to the observations, A the design matrix, l the difference between observed and computed values (o-c), P the weight matrix.

For the simulation studies two different approaches for the l-Vector (observed minus computed) are used.

2.2.1. No Observations

The l-vector (o-c) is disregarded. Supposing that realistic standard deviations are used to set up the weight matrix P for the observations, the a posteriori variance factor σ_0^2 is set to unity, the covariance matrix can be determined with equation (4) and the correlation matrix with equation (6). This has been already realized at IGG, and first results are shown below.

2.2.2. Monte-Carlo Simulation

The l-vector (o-c) is subject to both random errors and systematic errors. Troposphere and clock parameters are subject to stochastic variations (Treuhaft and Lanyi, 1987 [5] and Herring et al., 1990 [1]), i.e., they will be simulated as stochastic processes with realistic variances. On the other hand, extreme weather conditions will be taken from numerical weather models to add systematic variations of the l-vectors. The information of the l-vectors will also be transformed backwards to the databases (NGS format), and thus can be used by other software packages, too.

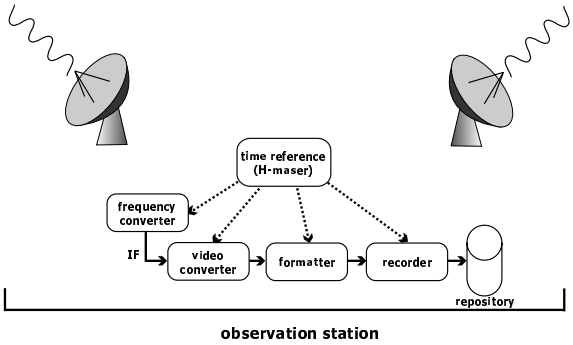

Figure 2. Two antennas at one site.

Additionally, certain modifications will be made with OCCAM, e.g. the introduction of condition equations to account for two co-located VLBI antennas using the same clock (Figure 2). Careful Monte-Carlo simulations have to be carried out to assess the real benefit of this approach.

2.3. VV-SIM

The third program used for the simulations is VV-SIM (Vienna VLBI-Simulation).It is written in Matlab. Its main task is to convey the results of the VLBI analysis in a clear and illustrative form that certain parameters can be extracted easily, e.g. the standard deviations of the unknown parameters or the correlations between the unknowns. The first results and illustrations of VV-SIM are shown below. This software package is based on input data in SINEX format and can be used by other groups, too.

3. First Results of the Simulations

The following network configurations are purely theoretical and only for test purposes. The unusual configuration should help to understand the influence of network configurations and baseline lengths on the cofactors of the Earth orientation parameters (EOP). For all simulations described below the VLBI analysis with the software package OCCAM was realized by setting o-c to zero (Section 2.2.1).

3.1. NET1: Greenwich Network

In the first example, the stations are located on the Greenwich meridian, starting with a latitude of 0° up to 90° North and on the longitude of 180° with a latitude of 0° up to 90° North using a spacing of 30°. The results of the simulation with this 7 station network can be seen in Table 2.

3.2. NET2: Equator Network

The stations are located on the equator, with a spacing of 45°. We get a network with 8 stations. The results of the simulation can be seen in Table 2.

3.3. NET3: CONT05 4^{th} Day

The next simulation was done for the 4^{th} day of CONT05. The o-c vector was set to zero, and realistic relations between the cofactors are expected. The correlations between the parameters give information about the quality of the network. The results of the simulation can be seen in Table 2.

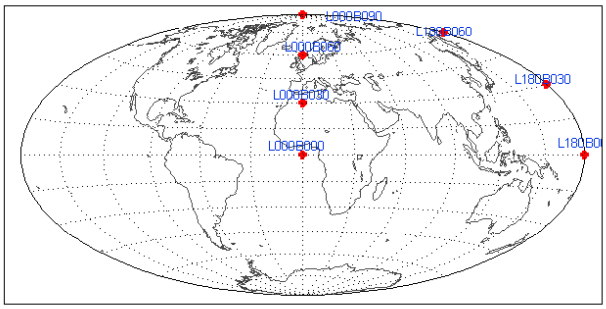

Figure 3. Station distribution Greenwich meridian (NET1).

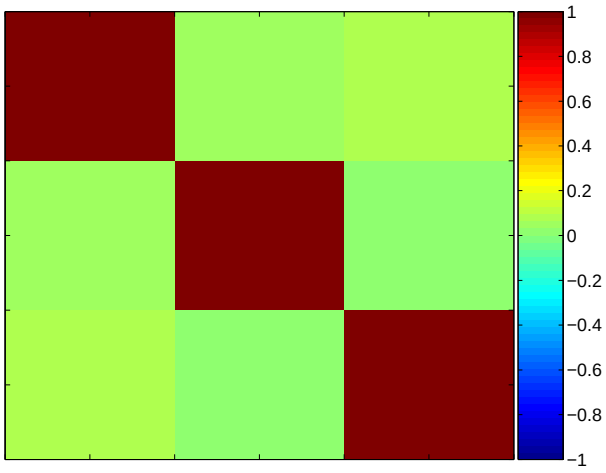

Figure 4. Correlations between xp, yp and dut1 for the station destribution described in Figure 3.

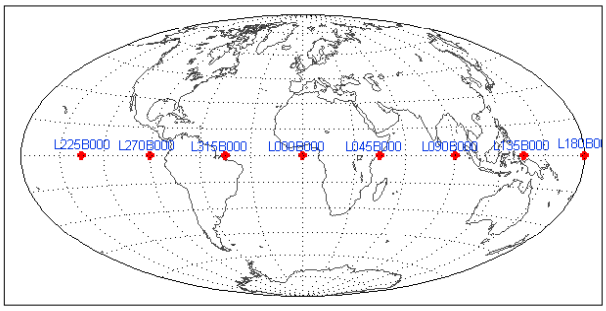

Figure 5. Station distribution equatorial (NET2).

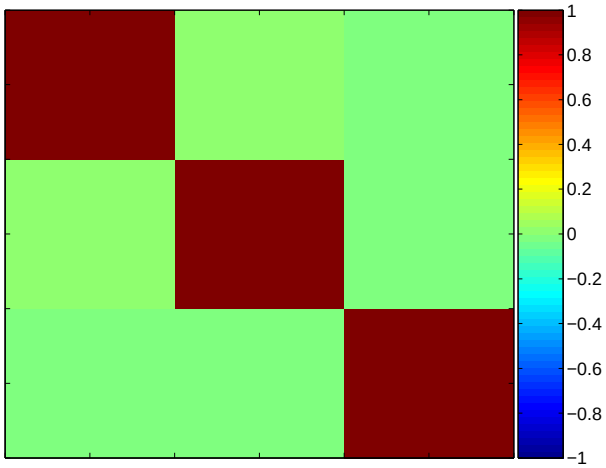

Figure 6. Correlations between xp, yp and dut1 for the station destribution described in Figure 5.

Table 2. Cofactors and Correlations of the EOP (xp, yp and dut1) for the different station distributions NET1, NET2 and NET3.

	Cofactors			*Correlations*		
	xp $[\mu as]$	yp $[\mu as]$	dut1 $[\mu s]$	xp-dut1	yp-dut1	xp-yp
NET 1	33.4	17.3	0.7	0.069	0.024	0.054
NET 2	11.1	10.8	0.3	-0.022	-0.029	0.025
NET 3	12.8	16.0	0.6	-0.369	0.323	0.187

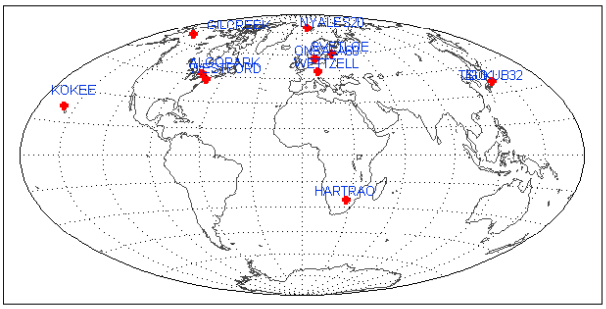

Figure 7. Station distribution CONT05 (NET3).

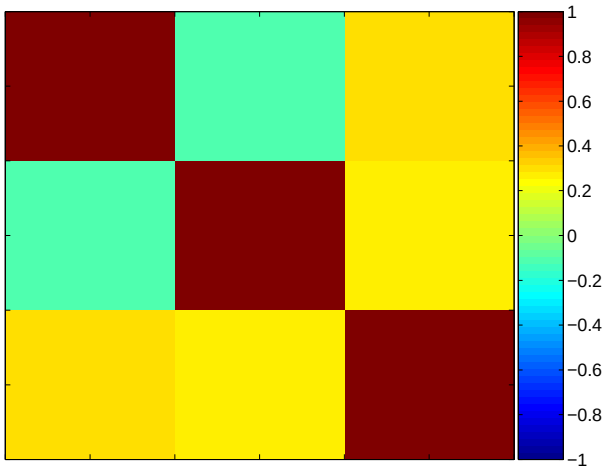

Figure 8. Correlations between xp, yp and dut1 for the station destribution described in Figure 7.

4. Conclusions

Simulation studies play a critical role for the development of a future geodetic VLBI system. Thus, it is important to carry out these studies as realistic as possible, i.e. with the most accurate specifications of future VLBI antennas or sophisticated models for clock and troposphere parameters. Furthermore, it is absolutely necessary to provide as many interfaces to other software packages as possible (SINEX, NGS) to be able to cross-check the results.

5. Acknowledgements

The authors would like to thank the Austrian Science Fund for supporting this work (P18404-N10).

References

[1] Herring, T.A., J.L. Davis, and I.I. Shapiro, Geodesy by Radio Interferometry: The Application of Kalman Filtering to the Analysis of Very Long Baseline Interferometry Data, Journal of Geophysical Research, Volume 95, No. B8, pp 12561-12581, 1990.

[2] Niell, A.E., A. Whitney, B. Petrachenko, W. Schlueter, N. Vandenberg, H. Hase, Y. Koyama, C. Ma, H. Schuh and G. Tuccari, VLBI2010: Current and Future Requirements for Geodetic VLBI Systems, 2005.

[3] Vandenberg, N., NVI, Inc.: Interactive/Automatic Scheduling Program, Program Reference Manual, NASA/Goddard Space Flight Center, 1999.

[4] Titov, O., V. Tesmer and J. Boehm, Occam Version 5.0 Software User Guide, AUSLIG Technical Report 7, 2001.

[5] Treuhaft, R.N., and G.E. Lanyi, The effect of the dynamic wet troposphere on radio interferometric measurements, Radio Science, Volume 22, No. 2, pp 251-265, 1987.

Markus Vennebusch: Singular Value Decomposition - A Tool for VLBI Simulations, IVS 2006 General Meeting Proceedings, p.98–102
http://ivscc.gsfc.nasa.gov/publications/gm2006/vennebusch2

Singular Value Decomposition - A Tool for VLBI Simulations

Markus Vennebusch

Geodetic Institute of the University of Bonn
e-mail: vennebusch@uni-bonn.de

Abstract

Usually VLBI observations are adjusted by least-squares approaches like the Gauss-Markoff model with the use of normal equations. It is well known that parameter estimation methods based on this strategy show some numerical disadvantages. To overcome these problems a new approach makes use of a more stable least-squares algorithm, called singular value decomposition (SVD) and provides interesting insight into the composition of the estimated parameters and shows the impact of particular observations on the parameters.

For an example VLBI session the results of the new method will be presented and the suitability of the SVD approach for simulations and for the improvement of VLBI schedules will be shown.

1. Introduction

In many scientific analyses or engineering problems it is necessary to determine parameters of a linear (or linearized) model after performing (many) more measurements than necessary for a unique solution. This leads to an overdetermined system of linear equations which is commonly solved in a least-squares sense by e.g. using the Gauss-Markoff-Model (see e.g. Koch, [2]). Many VLBI data analysis software packages use this approach for the determination of e.g. earth orientation parameters, site positions, etc. One of the most common (and simple) methods for the estimation of the parameters in the model

$$A\mathbf{x} = \mathbf{b} \quad \text{with} \quad \Sigma_{bb} = \sigma_0^2 \cdot P^{-1} \tag{1}$$

is based on solving a system of normal equations, i.e. by using the well-known formula

$$\hat{\mathbf{x}} = (\mathbf{A'PA})^{-1}\mathbf{A'P}\ \mathbf{b} \quad \text{and} \quad \Sigma_{\hat{\mathbf{x}}\hat{\mathbf{x}}} = \hat{\sigma}_0^2 \cdot (\mathbf{A'PA})^{-1}, \tag{2}$$

with

$\mathbf{A}$	the design matrix (or Jacobi matrix) containing the partial derivatives of the observations equation with respect to the parameters to be determined (= functional model). $\mathbf{A'}$ means the transpose of this matrix,
$\mathbf{P}$	the weight matrix as the inverse of the variance/covariance matrix (= stochastical model),
$\mathbf{b}$, Σ_{bb}	the vector of observations (also known as O-C-vector) and its variance-covariance matrix and
$\hat{\mathbf{x}}$, $\Sigma_{\hat{\mathbf{x}}\hat{\mathbf{x}}}$	the (estimated) vector of unknowns and its variance/covariance matrix.

Equation (2) yields a least-squares solution, i.e. it determines $\hat{\mathbf{x}}$ while minimizing the square sum of the residuals: $\| A\mathbf{x} - \mathbf{b} \|^2$.

In the language of linear algebra the least squares principle can be visualized geometrically by vector spaces and projections on the so-called column space of $\mathbf{A}$, i.e. the vector sub-space formed by the columns of the design matrix $\mathbf{A}$ (see e.g. ADAM, [1] or STRANG/BORRE, [6]).

In the following a quite unknown (at least in geodesy) approach for a least-squares solution of the system (1) is used which avoids normal equations and which reveals a lot more of geometrical information about the adjustment problem. This approach is based on the direct analysis of the design matrix by **Singular Value Decomposition (SVD)** which both preserves the numerical stability of the system to be solved and yields important information about the impact of certain observations on particular parameters.

The goal of these investigations is the application of an uncommon algebraic parameter estimation method in order to get deeper insight into the adjustment process and to give a 'geometrical' interpretation of the adjustment process. Furthermore, interesting auxiliary means for the assessment of the functional model can be derived from SVD and can be applied to the adjustment of VLBI sessions. This approach can be regarded as further development of existing simulation strategies. The information gained from these analyses will support the improvement of VLBI schedules.

2. Basics of Linear Algebra

2.1. Least-squares Solutions of Overdetermined Systems of Linear Equations

For the solution of an (usually) inconsistent system of linear equations like (1) Linear Algebra provides different approaches which are more or less numerically stable (see e.g. STRANG/BORRE, [6]). As mentioned above in geodetic applications the most common approach is the computation and solution of the associated system of normal equations. Other –so-called direct–methods as e.g. QR-decomposition are directly applied to the design matrix and preserve the lengths of the vectors associated with the system to be solved.

One of these length preserving, direct approaches is the singular value decomposition which decomposes an arbitrary matrix of dimension $m \times n$ into

$$\mathbf{A} = \mathbf{U} \cdot \mathbf{S} \cdot \mathbf{V}' = \mathbf{U} \begin{pmatrix} \mathbf{D} & \mathbf{0} \\ \mathbf{0} & \mathbf{0} \end{pmatrix} \mathbf{V}' \qquad \text{with } \sigma_1 \geq \sigma_2 \geq \ldots \geq \sigma_r > 0. \tag{3}$$

$\mathbf{U}$ is an orthogonal matrix of dimension $m \times m$ whose columns form the so-called left singular vectors $\mathbf{u}_i$. $\mathbf{S}$ is an $m \times n$-matrix only containing the so-called singular values σ_i on its main diagonal and $\mathbf{V}$ is an orthogonal $n \times n$-matrix whose columns $\mathbf{v}_i$ form the so-called right singular vectors. By definition, the singular values σ_i are ordered in decreasing order.

Although $\mathbf{A}$ might be of arbitrary dimension for the following only the overdetermined case ($m > n$) is considered.

Decomposition (3) can be understood as a generalization of an eigenvalue decomposition of a rectangular matrix. MEYER, [4] shows that the singular values are just the square roots of the eigenvalues of $\mathbf{A}' \cdot \mathbf{A}$ and the right singular vectors correspond to the eigenvectors of $\mathbf{A}' \cdot \mathbf{A}$. The left singular vectors correspond to the eigenvectors of $\mathbf{A} \cdot \mathbf{A}'$.

Especially in geophysical and geological applications the algebraic terms 'row and column space' are replaced by the more descriptive terms 'model space' and 'data space', respectively, since they depict the most important vector spaces associated with the adjustment process (see

e.g. STRANG/BORRE, [6], MENKE, [3]).

After transforming the column space and the row space of **A** to the new bases formed by the left and the right singular vectors respectively the system is called to be transformed to its canonical form in which the least squares problem becomes simpler and thus more lucid (see e.g. STRANG/BORRE, [6]).

2.2. Geometrical Interpretations

Instead of using equation (2) the decomposition of the design matrix (formula (3)) can be used to solve (1) in a least-squares sense by:

$$\hat{\mathbf{x}} = \mathbf{V}_r \cdot \mathbf{S}_r^{-1} \cdot \mathbf{U}_r' \cdot \mathbf{b} = \sum_{n=1}^{r} \frac{\mathbf{u}_i \cdot \mathbf{b}}{\sigma_i} \cdot \mathbf{v}_i \tag{4}$$

where

r	denotes the rank of the system,
$\mathbf{V}_r$	is an $n \times r$ matrix formed by the first r columns of $\mathbf{V}$,
$\mathbf{U}_r$	is an $m \times r$ matrix formed by the first r columns of $\mathbf{U}$ and
$\mathbf{S}_r$	is an $r \times r$ matrix formed by the first r rows and columns of $\mathbf{S}$.

Equation (4) shows that the least-squares solution is formed by superimposing r 'slices' $\mathbf{v}_i$ i.e., the i^{th} 'slice' of the solution vector consists of the respective $\mathbf{u}_i, \mathbf{v}_i, \sigma_i$ and the vector of observations $\mathbf{b}$.

According to STRANG/BORRE, [6] the first r left singular vectors $\mathbf{u}_i$ $(i = 1, \ldots, r)$ are called canonical vectors and "reveal observations which should have been performed with larger weight" since they have a large impact on the adjustment results. This can also be seen in the so-called "Data resolution matrix" described below. The first r right singular vectors $\mathbf{v}_i$ $(i = 1, \ldots, r)$ depict those parameters (or linear combinations of parameters) which are best determined. Right singular vectors $\mathbf{v}_i$ belonging to zero- (or very small) singular values show parameters which are totally undetermined.

2.3. Resolution Matrices

One of the analysis tools derived from SVD are so-called *resolution matrices* (see e.g. MENKE, [3]): For example,

$$DRM = U_r \cdot U_r' \tag{5}$$

is called **Data Resolution Matrix (DRM)** and serves as a projection operator onto the column space/data space of the design matrix. This matrix (also known as 'hat-matrix' in statistics) deserves a closer look since it provides a lot of information of the adjustment problem. The main diagonal of this matrix reveals the *importances* of the observations and thus the sensitivity of certain observations. Errors in observations with large importance values strongly impact the estimation results.

Furthermore

$$MRM = V_r \cdot V_r' \tag{6}$$

represents the so-called **Model resolution Matrix (MRM)** and serves as a projection operator onto the row space/model space of the design matrix. The MRM can be used for better investi-

gation of separability of the parameters compared to the well-known correlation matrix (see e.g. KOCH, [2]).

3. Application Example

The methods described above have been applied to the analysis of the baseline Kokee - Wettzell within the Multi-Intensive session RD0404 (04JUN16XA). During 24 hours 415 observations have been performed on this baseline which have been used to estimate four parameters: (1) clock offset for Kokee, (2) tropospheric zenith path delay for Kokee (3) and for Wettzell, and (4) $dUT1$.

The design matrix for this (quite unusual but appropriate) parametrisation has been generated by using OCCAM 6.1 and the singular value decomposition has been performed with additional software written in Fortran 95.

Figure 1 shows a part of the components of the singular value decomposition of the design matrix of this session: the four right singular vectors $\mathbf{v}_1$ through $\mathbf{v}_4$ together with their respective singular values reveal the estimability and separability of the four estimated parameters (or some linear combinations of them). These components can be used for so-called model space investigations.

The first right singular vector $\mathbf{v}_1$ (together with the corresponding singular value σ_1 and the left singular vector $\mathbf{u}_1$, which is not shown here) mostly affects the second and the third parameter: the tropospheric zenith path delay for both Kokee and Wettzell. The second component ($\mathbf{v}_2$, σ_2 and $\mathbf{u}_2$) mostly affects the fourth parameter, which is the earth rotation $dUT1$[1]. In the same way $\mathbf{v}_3$, σ_3 and $\mathbf{u}_3$ as well as $\mathbf{v}_4$, σ_4 and $\mathbf{u}_4$ offer some insight into the generation of parts of the solution vector concerning the remaining parameters. $\mathbf{v}_4$ and σ_4 depict the least precisely determined parameter which is the clock offset at Kokee station.

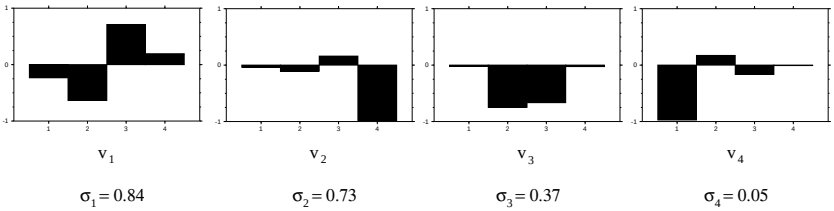

Figure 1. Right singular vectors v_1 through v_4 and singular values σ_1 through σ_4 (order of parameters: clock offset Kokee, zenith path delay Kokee and Wettzell, $dUT1$).

Figure 2 shows the main diagonal of the data resolution matrix (see equation (5)). Large values reveal observations which are (due to their geometry) of special importance for the parameter estimation process in general and thus need further considerations. Comparing Figure 2 with a list of all observations performed on this baseline, for this parametrisation (i.e. for this set of parameters to be estimated) especially observations to sources with low declinations are important. Assuming the rule of thumb that baselines with a long equatorial extension are mostly suitable for

[1] Analysis of the corresponding left singular vector $\mathbf{u}_2$ would reveal observations which are mostly important for earth rotation determination (since -in this case- the so-called 'importances' shown below almost give the same information $\mathbf{u}_2$ is not explicitly shown here).

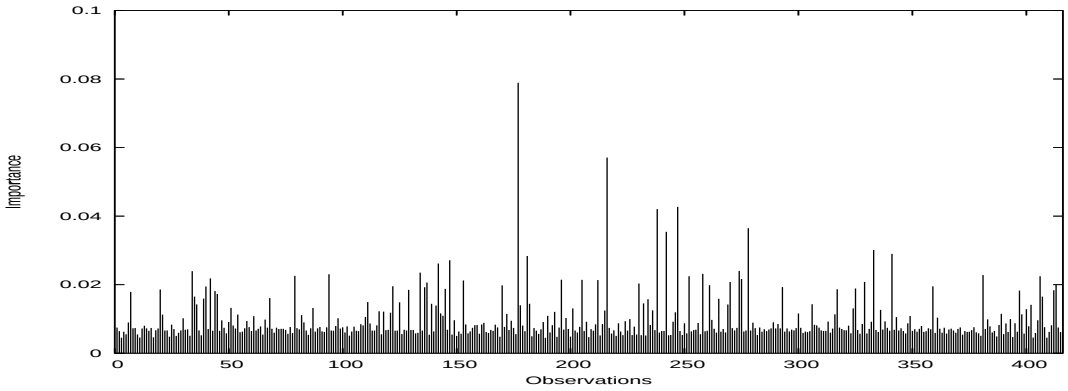

Figure 2. "Importances" of observations for R0404-baseline Kokee - Wettzell

the determination of earth rotation this result agrees with the theoretical results e.g. described by SCHUH, [5] and other authors.

4. Conclusions & Outlook

Investigations have shown that least-squares solutions of overdetermined systems of linear equations computed by singular value decomposition can be used as a tool for simulations in VLBI data analysis. SVD yields 'geometrical' insight into the adjustment problem and gives important information which can be used to improve VLBI observation schedules. Disadvantages of this approach might be larger memory requirements and longer computation times compared to the normal equation approach.

This method and the analysis tools derived from SVD will be applied to larger adjustment problems / larger observation networks in order to better understand the analysis of VLBI observations and to improve scheduling in general. A user-friendly software tool (for any type of adjustment problem) based on the graphical user interface-toolkit QT is being developed at GIUB and will be applied to the analysis of other VLBI sessions. The results will be presented in the future.

References

[1] Adam, J.: A detailed study of the duality relation for the least squares adjustment in euclidean spaces, Bull. Geod. 56, pp. 180-195, 1982.

[2] Koch, K. R.: Parameter Estimation and Hypothesis Testing in Linear Models, Second, Updated and Enlarged Edition, Springer, 1999.

[3] Menke, W.: Geophysical Data Analysis: Discrete Inverse Theory, Academic Press Inc., 1984.

[4] Meyer, C. D.: Matrix Analysis and Applied Linear Algebra, Society for Industrial and Applied Mathematics (siam), 2000.

[5] Schuh, H.: Die Radiointerferometrie auf langen Basen zur Bestimmung von Punktverschiebungen und Erdrotationsparametern, Ph.D. thesis, Rheinische Friedrich-Wilhelms-Universität zu Bonn, 1987.

[6] Strang, G., K. Borre: Linear Algebra, Geodesy and GPS, Wellesley-Cambridge Press, 1997.

Anthony Searle: Network Size Simulations, IVS 2006 General Meeting Proceedings, p.103–103
http://ivscc.gsfc.nasa.gov/publications/gm2006/searle2

Network Size Simulations

Anthony Searle

Geodetic Survey Division/Natural Resources Canada

e-mail: asearle@nrcan.gc.ca

Abstract

A series of SKED/SOLVE simulations investigates the potential size and configuration of a fictitious network of identical stations characteristic of the recommendations of the VLBI2010 report. Standard observing strategies and bandwidths are applied.

1. VLBI2010 Simulations

In the VLBI2010 report, the authors suggest a VLBI network of 20-40 globally distributed small antennas. Unfortunately, at the time of writing, software used to insert simulated schedules into SOLVE was able to handle only 16 stations. Due to this restriction, fictitious networks of 6, 8, 12, and 16 stations were created and scheduled, and simulated results were put through SOLVE to determine Earth orientation uncertainties. Station positions were chosen to be globally distributed and placed without regard to landmass. A recording speed of 1 Gbps was used and data was recorded in X and S bands.

Table 1. Simulation results

Stations	No. Obs	σ X-pole (uas)	σ Y-pole (uas)	σ UT1 (us)
6	2406	43.42	29.81	2.02
8	4512	7.18	7.53	0.97
12	8474	6.38	6.38	0.91
16	15966	4.60	4.52	0.60

2. Comments

As the number of observations grows large, the limits of the CALC/SOLVE analysis become apparent; eventually the improvements to the uncertainties become very small and unrealistic. Similarly, if we reduce the parameterization of the nuisance parameters in "traditional" simulations, the uncertainties of the desired parameters improve—in reality this is not the case. For further investigations of VLBI2010 strategies a more complete simulation tool will have to be designed. Similarly, VLBI2010 may represent a fundamental shift in the quantity of data produced by VLBI; many of the processing tools, from scheduling to solving, will have to be re-thought and possibly rebuilt.

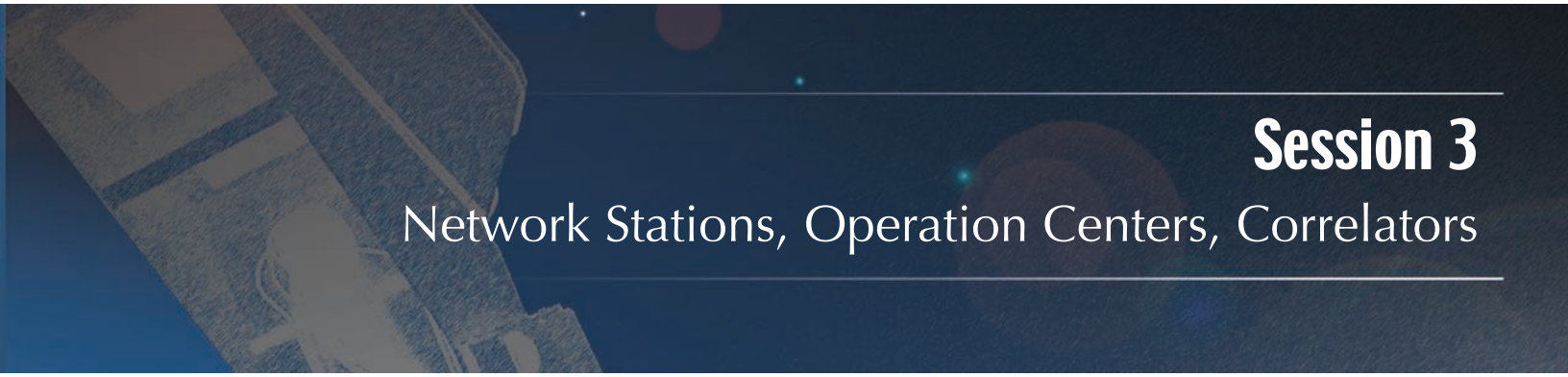

Session 3

Network Stations, Operation Centers, Correlators

Jesús Gómez-González et al.: A New 40 Meter Radiotelescope at Yebes (Spain) for Geodetic VLBI Studies, IVS 2006 General Meeting Proceedings, p.107–116
http://ivscc.gsfc.nasa.gov/publications/gm2006/gomez

A New 40 Meter Radiotelescope at Yebes (Spain) for Geodetic VLBI Studies

Jesús Gómez-González [1], *Francisco Colomer* [2], *Alberto Barcia* [3], *José Antonio López-Fernández* [3]

[1)] *Instituto Geográfico Nacional*

[2)] *Observatorio Astronómico Nacional*

[3)] *Observatorio Astronómico Nacional (CAY)*

Contact author: Francisco Colomer, e-mail: f.colomer@oan.es

Abstract

The construction of a new 40-m parabolic radiotelescope at Yebes, near Madrid (Spain), is being finalized. The instrument, built by the Spanish Instituto Geográfico Nacional (Ministerio de Fomento) will soon operate at frequencies between 2 and 115 GHz, and will become a key partner for both the astronomical (in European and global projects) and the geodetic VLBI communities (through IVS), with an estimated participation in observations of 50 days/year for the latter.

During the last decade, IGN has collaborated in the EUROPE and CORE campaigns with the 14-m radiotelescope. The staff is acquainted with the concepts, observing procedures and instrumentation involved. New infrastructures are being constructed in Yebes, such as a high speed fiber optic link to GEANT, and a new building to hold a gravimeter system, in order to enable the station to become a geodetic fundamental station soon. Scientific projects in Geodesy and Astrometry are also being conducted by IGN scientists.

1. Introduction

The Observatorio Astronómico Nacional (OAN) of Spain, which is a department of the Instituto Geográfico Nacional (IGN, Ministerio de Fomento), operates a 14 meter radiotelescope at Yebes (Guadalajara, Spain). This facility has been a network station of the IVS until 2003, and has participated regularly in the geodetic VLBI campaigns to study the tectonic plate motions in Europe, Earth rotation, and pole motion. The main contribution of OAN to IVS is the realization of geodetic VLBI observations. Table 1 shows the observing campaigns in which Yebes (14-m) has participated in the period 1995-2003.

The construction of a new 40 meter radiotelescope is nearly completed in Yebes (see Fig. 1). A new S/X receiver will be installed in 2006, in order to resume geodetic VLBI observations. The VLBI equipment has been constantly upgraded (including Mark 5A) and is fully operational.

Table 1. Number of geodetic VLBI sessions Yebes has observed (1995-2003).

Experiment type	CORE-B	EUROPE	IVS-T2
Number of Sessions	13	21	5

Figure 1. The new 40-m radiotelescope of OAN at Yebes, for geodetic and astronomical VLBI.

2. Description of the 40 Meter Radiotelescope

The 40-m radiotelescope is of turning-head type on an azimuth-elevation mount. The optical configuration is a Nasmyth-Cassegrain system: parabolic reflector, hyperbolic subreflector, and a 45° flat mirror to reflect the beam laterally. The Nasmyth focus is at 11 meters from the vertex of the paraboloid, therefore the instrument has a large receiver cabin for optimal frequency flexibility.

Moreover, the telescope subreflector can be placed in two positions: one for primary focus operation (exposing the primary focus receiver horn through a hole in the subreflector center), the other for the Nasmyth-Cassegrain focus. In this second case, the subreflector can be moved with high precision (30 μm) on six axes to correct the gravity deformation of the telescope backstructure (see Fig. 2). The telescope is designed following the homology principle (when deformations change the paraboloid, the focus change is corrected for by moving the subreflector). The surface panel precision is better than 60 μm, with a total surface rms of 150 μm. This allows a maximum observing frequency of 120 GHz, with an aperture efficiency of 50%. The minimum frequency of operation is set by the size of the beams inside the receiver cabin, and is around 2 GHz. Pointing is better than 5″ (winds below 10 m/s). The telescope is designed to survive winds up to 50 m/s.

The final design and control of the works has been made by the German company MAN Tech-

Figure 2. Left: sketch of the subreflector (M2) support structure. Right: actual subreflector cabin.

Table 2. RMS error budget of the 40-m radiotelescope surface.

	RMS
Panels	65 μm
Panels deformation	25 μm
Deformation steel structure (15 m/s wind)	95 μm
Mechanical alignment	80 μm
Total	150 μm

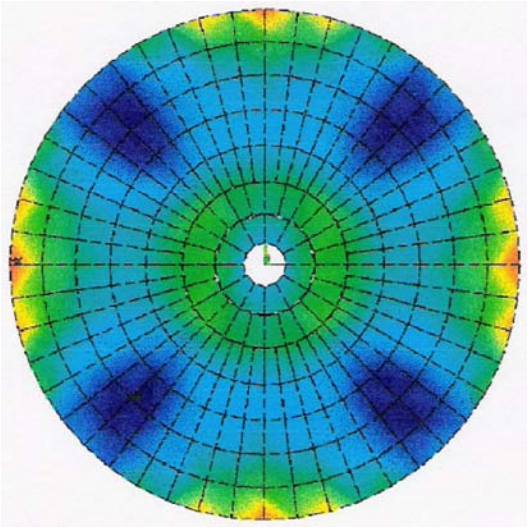

Figure 3. Expected gravity deformations of the 40 meter radiotelescope.

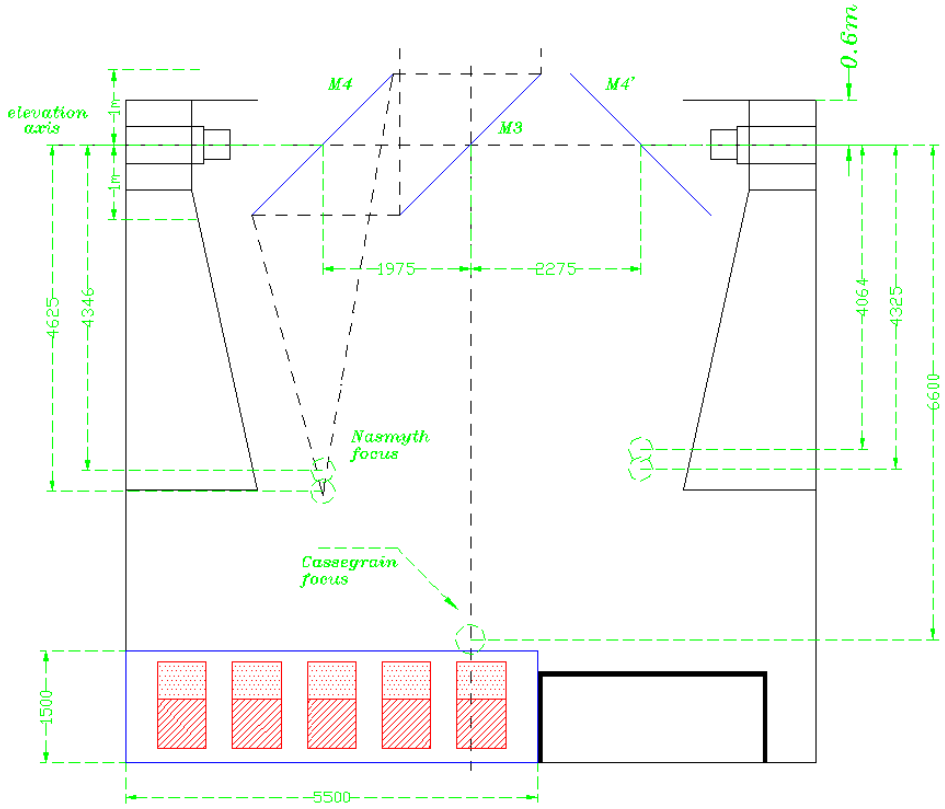

Figure 4. Sketch of the 40-m radiotelescope receiver cabin.

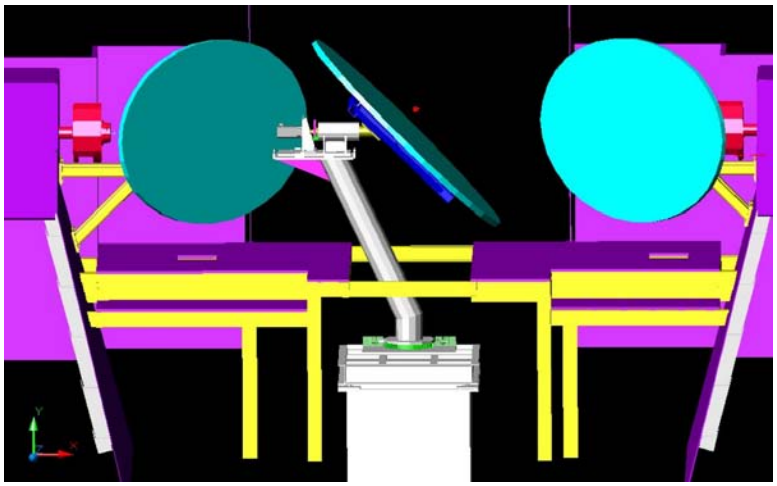

Figure 5. Nasmyth mirror (center) and two M4/M4' mirrors.

Figure 6. M5 mirror support of the low frequency branch M4'.

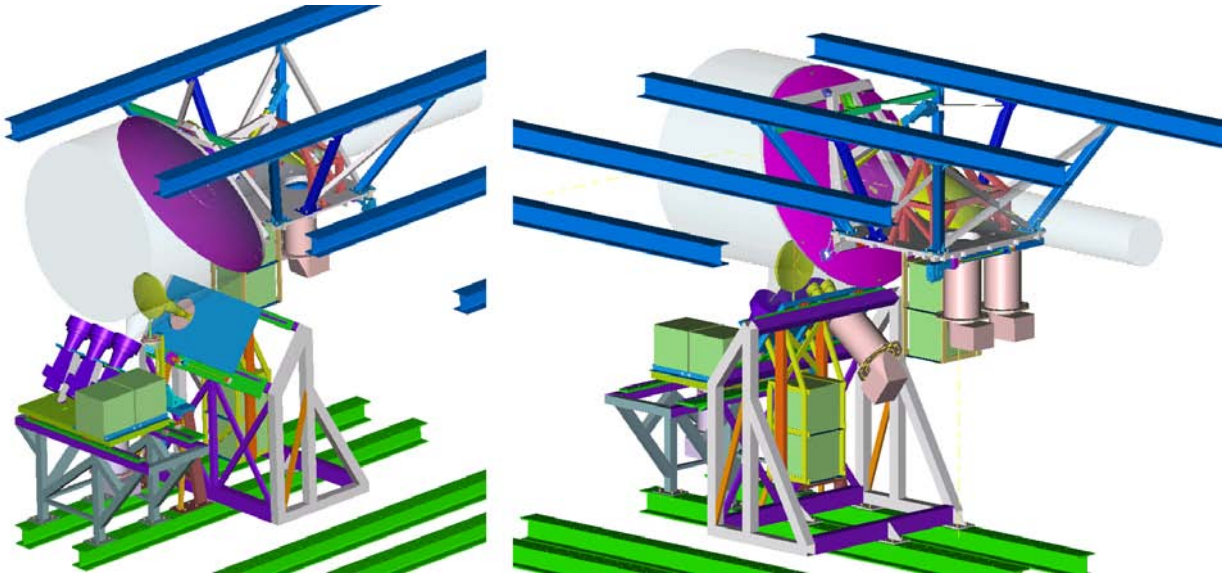

Figure 7. Configuration of the S/C/Ch (purple horns in the left image) and X/Ku (small yellow horns in the right image) receivers on the M4' branch.

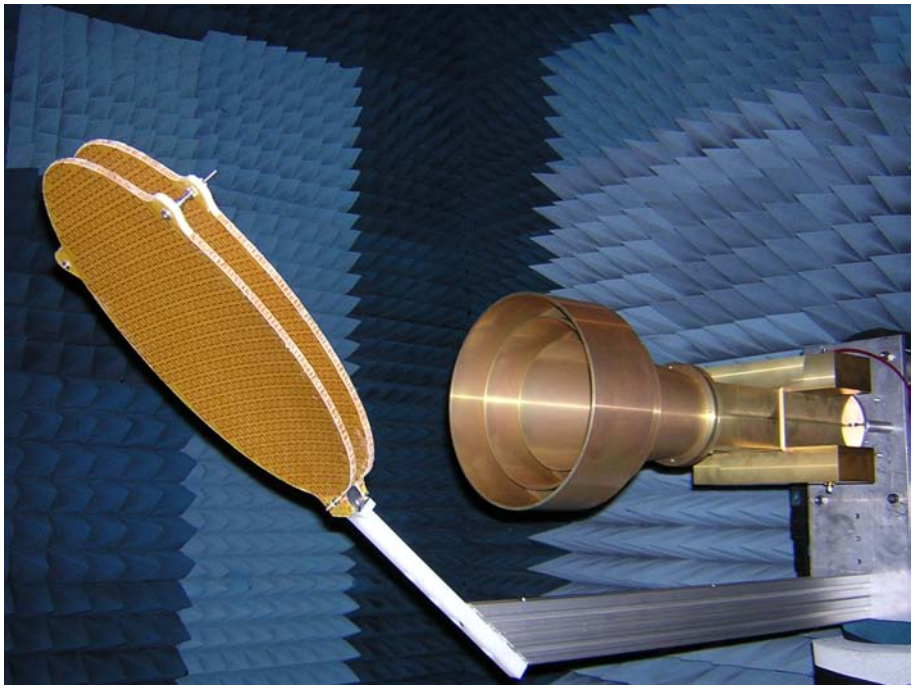

Figure 8. S-band horn with polarizer and dychroic mirror.

Figure 9. Cryostat of the 22 GHz receiver.

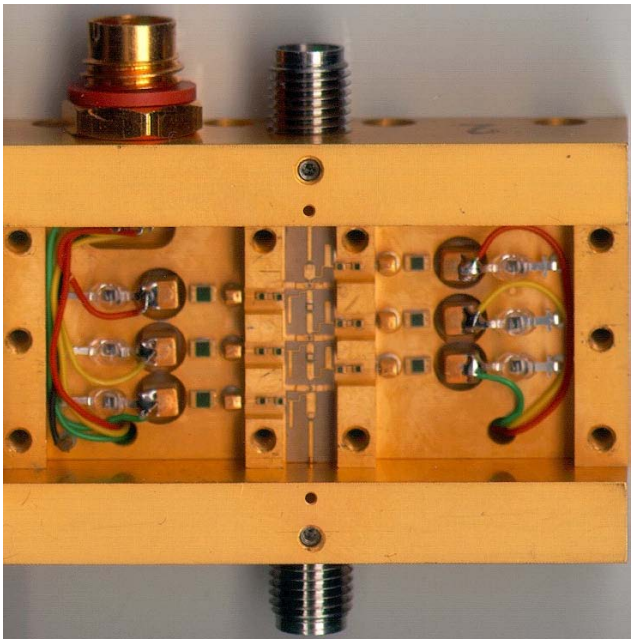

Figure 10. Details of a HEMT amplifier of the 22 GHz receiver, designed and built at OAN-Yebes.

nologie AG (now MT Aerospace AG). The concrete tower was built in 1999 by ACS (Spain), and the rest of the instrument by Schwartz-Hautmont Construcciones Metálicas (Tarragona, Spain). The elevation rotating structure weighs 500 tons, where 200 tons are for the trusswork and 100 tons are for the 420 panels. The backstructure is covered by a protective cladding, which is ventilated inside to avoid asymmetric warming of the structure.

The receiver cabin is very large: $8 \times 9 \times 3.5$ meters. It is divided into two independent branches, selected by moving the Nasmyth mirror (M3) towards two other mirrors, called M4 and M4'. This defines two different foci, located at about 4.5 meters from the M4 mirrors. The M4 branch will hold the high frequency receivers (above 22 GHz), while the M4' branch will hold the low frequency ones. Up to seven frequency bands can be supported on the M4' branch: S, X, C, Ku, 22 GHz and 30 GHz. This configuration allows simultaneous observations with at least two receivers. Note that the 30 GHz receiver may be installed in any of the two branches, allowing simultaneous observations with the current geodetic VLBI S/X receivers.

All receivers are designed for double circular polarization (LCP and RCP), and will be operated by remote control. The first to be installed will be those of the 20.75 – 24.45 GHz band, the new S/X (early in 2007) and C (5–6 GHz) bands, followed later by the millimeter receivers (76–116 GHz, and 40–50 GHz). Other receivers (3.3 GHz and 30 GHz) are under study. An additional receiver on the Ku band (12 GHz), uncooled, will be installed on the primary focus cabin to perform holographic measurements of the main reflector, in order to adjust the paraboloid surface with high precision.

The telescope will move in the range of -90^{o} to $+430^{o}$ in azimuth and 0^{o} to 90^{o} in elevation, at a maximum slew speed of $3^{o}/s$ in azimuth and $1^{o}/s$ in elevation. The minimum slew velocity is $0.0001^{o}/s$, for a pointing accuracy better than $5''$ with winds up to 10 m/s (normal operation).

3. Other Instrumentation at OAN–Yebes

3.1. The 14-m Radiotelescope

The Observatorio Astronómico Nacional (OAN) operates a 14 meter radiotelescope at Yebes (Guadalajara, Spain). This facility has been a network station of the IVS until 2003, and has participated regularly in the geodetic VLBI campaigns to study the tectonic plate motions in Europe, Earth rotation, and pole motion. This instrument is however not operational nowadays, therefore VLBI observations will be resumed after the completion of the new 40 meter radiotelescope described above.

3.2. GPS

The GPS station at Yebes (Fig. 11), established in 1999 and run by IGN, is the reference point of the Spanish fiducial network since 2002. In 2004, it became an IGS station with code 'YEBE'. It uses the station H-maser as reference.

In 2001, a new analysis center for EUREF was set up by IGN in Madrid ('IGE'). It processes 30 stations from Spain, Portugal, Morocco, France, and UK, among others. It is one of 15 EUREF LACs (local analysis centers).

3.3. Gravimetry

Measurements of absolute gravity at the 14-m telescope building have been performed. A project of constructing a building is being finalized, which will allow the installation of permanent equipment for constant gravity monitoring (see Fig. 12).

4. Research

The OAN group performs high precision astrophysical VLBI studies of maser emission towards late-type stars, which will not be discussed here. However we point out that we have modified the Astronomical Image Processing System (*AIPS*) to allow the processing of full polarization data on antennas with Nasmyth optics. Similar developments will be needed if full polarization is to be used in geodetic VLBI, following the VLBI2010 project.

The OAN group is working on a new method, *Source/Frequency phase referencing*, to measure frequency-dependent position shifts of source cores with high accuracy. The first successful application to measure the core shift of the quasar 1038+528 A at S and X-bands has been reported, and the results have been validated by comparison with those from standard phase referencing techniques (Rioja et al., 2005). The method is an extension of the technique developed and demonstrated by Middelberg et al. (2005), which uses fast frequency switching observations and relies on the transfer of calibration from the lower to the higher frequency. Our new proposed method endows it with astrometric applications by adding a strategy to calibrate the ionospheric contribution. We forsee it holds a big potential at high frequencies, in particular when applied to observations of molecular line emission. In geodesy unaccounted source core shifts introduce errors in the estimated ionospheric-free observables, and hence in the astrometric/geodetic products from the analysis.

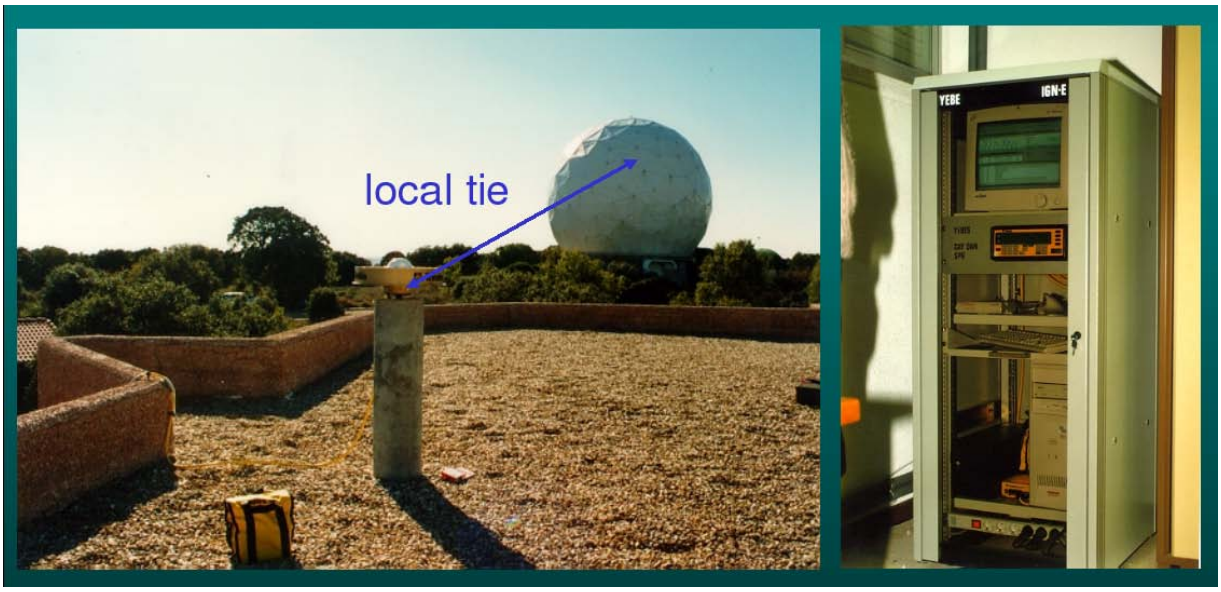

Figure 11. The IGS station "YEBE".

Figure 12. Artistic impression of the gravimeter building in Yebes (center), with sketch of the possible location (right) of the gravimeters (left).

5. Future Plans

We expect first-light on the new 40 meter radiotelescope at Yebes in 2006, after the construction and commissioning are finished. The telescope is expected to be operational at S/X bands by the end of 2006 or early 2007. Other frequencies of operation will be 4-7 GHz, 10-15 GHz, 21-24 GHz (first light receiver), 30-32 GHz, 40-50 GHz, and 72-116 GHz. Connection of this telescope to GEANT (1 Gbps fiber optics link) is progressing within the frame of the EXPReS EU project. The measurement of the 40-m phase-center and local-tie to the 14-m telescope and the GPS antenna will also be performed in 2006.

Collocation of geodetic techniques (40-m VLBI radiotelescope, GPS receiver in IGS station, and gravimeters) will allow Yebes to become a Geodetic Fundamental Station in the coming years.

References

[1] Gómez–González, J., "The New 40-m Radiotelescope of the National Astronomical Observatory Spain at Yebes". 2nd millimeter-VLBI science workshop. IRAM, Granada, Spain, 27-29 May 1999. Edited by A. Greve and T.P. Krichbaum. St. Martin d'Heres, France; IRAM, 1999, p. 85.

[2] López–Fernández, J.A., Alcolea, J., Barcia, A., Tercero, F., "Configuración óptica del radiotelescopio de 40m del CAY". Informe Técnico OAN 2001-7. (see `http://www1.oan.es/informes/archivos/IT-OAN-2001-7.pdf`).

[3] Garrigues, A., de Vicente, P., Almendros, C., Fernández, J., Abad, J.A., "Montaje del Mark 5 en rack". Informe Técnico OAN 2005-7. (see `http://www1.oan.es/informes/archivos/IT-OAN-2005-7.pdf`).

[4] Barcia, A., de Vicente, P., "Caracterización del máser de hidrógeno del CAY". Informe Técnico OAN 2005-8. (see `http://www1.oan.es/informes/archivos/IT-OAN-2005-8.pdf`).

[5] de Vicente, P., "Nuevo emplazamiento de la antena GPS en el CAY". Informe Técnico OAN 2005-9. (see `http://www1.oan.es/informes/archivos/IT-OAN-2005-9.pdf`).

[6] López–Fernández, J.A., Malo, I., Tercero, F., Abad, J.A., Almendros, C., Fernández, J., Yagüe, J.M., "Criostato del receptor de 22GHz del CAY". Informe Técnico OAN 2005-12. (see `http://www1.oan.es/informes/archivos/IT-OAN-2005-12.pdf`).

[7] Rioja, M.J., Dodson, R., Porcas, R.W., Suda, H., Colomer, F., "Measurement of core shifts with astrometric multi-frequency calibration". Proceedings of the 17th Working Meeting on European VLBI for Geodesy and Astrometry, Noto (Sicily, Italy), p. 125-130 (2005)

M. Machida et al.: K5/VSSP Data Processing System of Small Cluster Computing at Tsukuba VLBI Correlator, IVS 2006 General Meeting Proceedings, p.117–126
http://ivscc.gsfc.nasa.gov/publications/gm2006/machida

K5/VSSP Data Processing System of Small Cluster Computing at Tsukuba VLBI Correlator

M. Machida [1], *M. Ishimoto* [1], *K. Takashima* [1], *T. Kondo* [2], *Y. Koyama* [2]

[1)] *Geographical Survey Institute, Japan*
[2)] *National Institute of Information and Communications Technology, Japan*
Contact author: M. Machida, e-mail: machida@gsi.go.jp

Abstract

A software correlation system at Tsukuba VLBI Correlator of Geographical Survey Institute (GSI) is in process of upgrading its architecture with using the K5/VSSP which is a PC-based software correlator package for geodetic VLBI developed by National Institute of Information and Communications Technology (NICT). Performing software correlation is based on a set of NICT's K5/VSSP kernel programs which cover calculating a priori delay and rate, correlation processing and bandwidth synthesis. As an initial step, we introduced one management computer, 24 data servers and eight rack mount correlation servers. The second step of upgrading K5/VSSP correlation system was building aid application "PARNASSUS" with graphical user interface to aid operating K5/VSSP kernel programs. K5/VSSP enables a distributed computing for software correlation since it provides data storage in Unix files for every four channels per scan. "PARNASSUS" serves to optimize operator's input into kernel program and to handle distributed correlation comprehensively.

As for GSI, there has been an increase in demand for intensive and domestic sessions in the last few years. For the Tsukuba VLBI Correlator it means that a larger amount of data had to be processed. However routine run of K5/VSSP correlator, which was operated in the distributed computing, did not take extra operational time for data processing so far in spite of the increased number of sessions. A hot debate, involving new-fasioned VLBI technology, has developed in the IVS community. For stations and correlators, a development of some kind of active system has been proposed by laboratories around the world. GSI opts for K5/VSSP.

1. Introduction

The topic of this presentation is involved in software correlation system for processing VLBI data using K5/VSSP. Firstly, general architecture and current form of K5/VSSP both at station and correlator sides are provided as background information. The process of distributed computing for treating a large amount of data in the software correlation system is demonstrated. Finally,future plans for the K5/VSSP software correlation system are presented.

2. System Upgrade at Tsukuba VLBI Correlator

Our recent work at the Tsukuba VLBI Correlator was shifting the correlation system toward K5/VSSP. Figure 1 is a photo of the K5/VSSP software correlation system which currently consists of 24 Linux computers as data servers, each of which can share a couple of disk cartridges at once through a drive unit with 16 drive slots, eight rackmount Linux computers with 3GHz Intel Xeon dual CPUs as correlation servers and one Linux computer for file handling and management.

The installation of the K5/VSSP recording system into the network stations of GSI was finished in early 2004. Station and Correlator should fit together in data format and data storing media.

Efforts to shift from the K4 to the K5/VSSP software correlation system had been made at the Tsukuba VLBI Correlator since autumn, 2004. The Tsukuba VLBI Correlator fully switched to K5/VSSP software correlation processing in April 2005. It became more efficient at processing data with distributed computing in K5/VSSP software correlation system. We have operated K5/VSSP in this fashion as a software correlator for IVS.

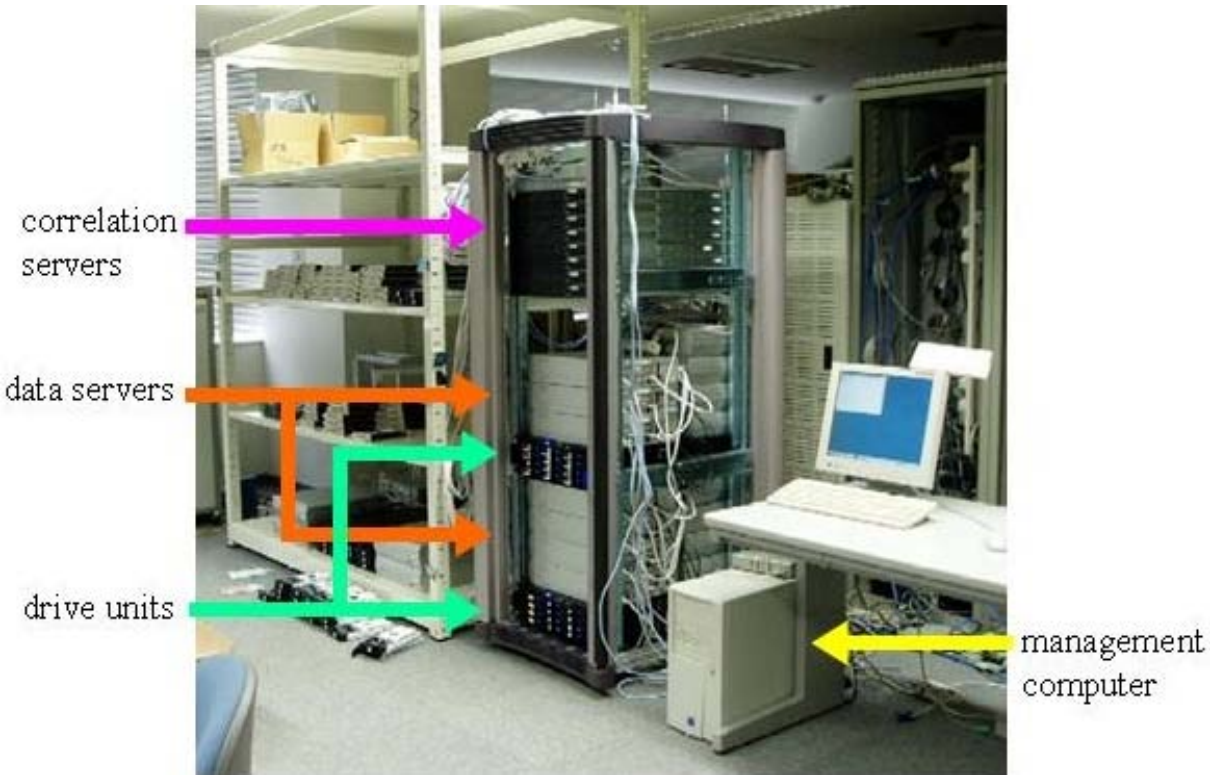

Figure 1. View of the K5/VSSP software correlation system at Tsukuba VLBI Correlator

2.1. K5/VSSP at a Station

Figure 2 is a simplified diagram of acquiring and recording data on K5/VSSP at GSI's network station. The left half of the figure shows the traditional block diagram of data acquisition. Emphasis in the figure is on the right half with the K5/VSSP recording system. The K5 acquisition system puts raw data from every four channels per scan into Linux files that are stored on removable disk cartridges (Figure 3) as formatted binary file.

K5/VSSP has eVLBI capability. In Intensive sessions (IVS-INT02) on the TSUKUB32-WETTZELL single baseline for monitoring UT1, data is recorded on K5/VSSP at TSUKUB32 and on Mark 5 at WETTZELL. Shortly after observation, recorded data at WETTZELL is transferred to Tsukuba VLBI Correlator through the Internet.

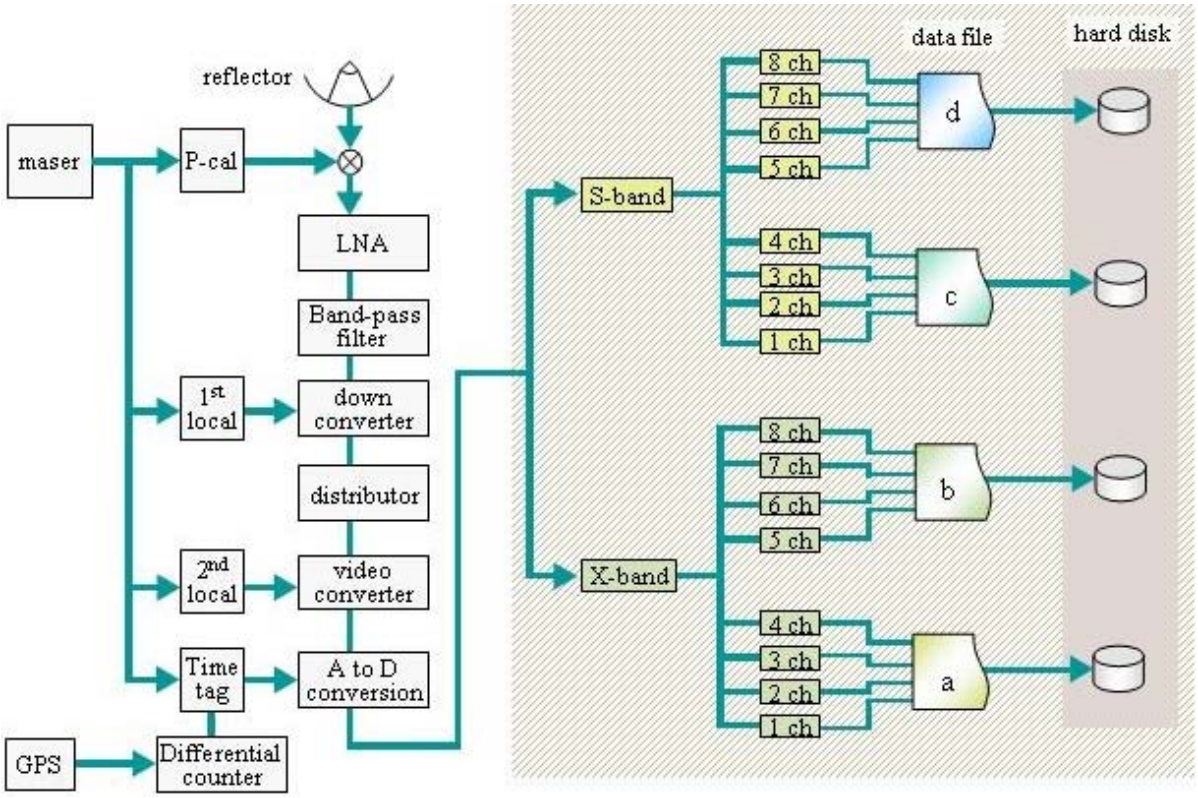

Figure 2. Simplified diagram of K5/VSSP at a station

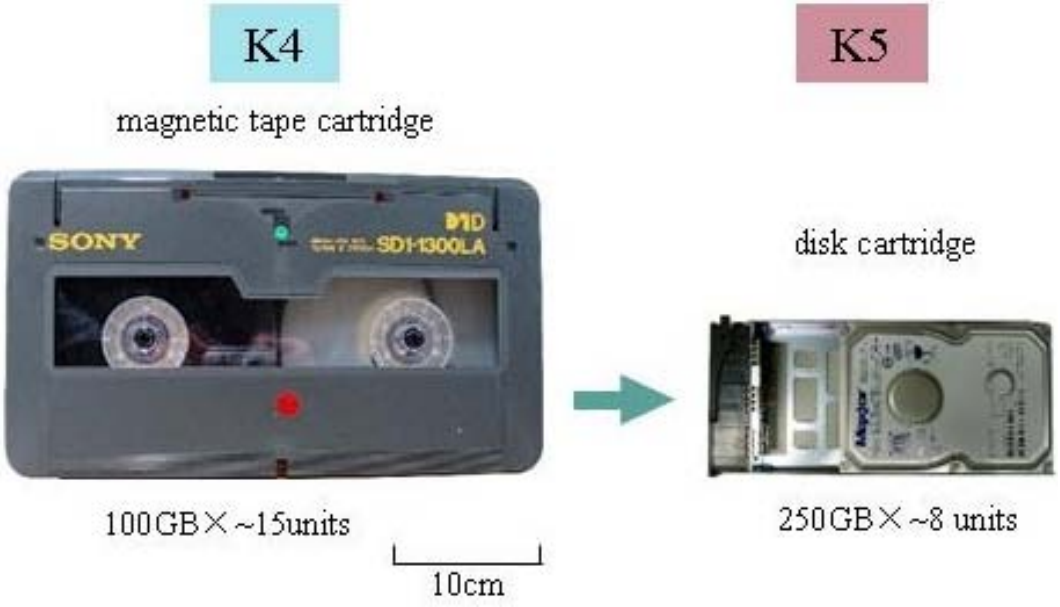

Figure 3. Media for storing data: from MT (magnetic tape) to disk

2.2. K5/VSSP at the Correlator

As described, K5/VSSP enables data file handling on Linux computers, which leads to processing data on software correlator. Figure 4 shows the components of the K5/VSSP software correlation system in its current form. Each data server can share a couple of disk cartridges at once through a drive unit with 16 drive slots where disk cartridges from stations are put into for use. We prepare three drive units for 24 data servers. The brief procedure for mounting data files on the system is to insert the disk cartridge into the drive slot (Figure 6) and to execute the mount command. Directories are shared among computers by Network File System (Figure 7). Once the operator enters in a management computer, raw data and auxiliary files such as schedule, session log and a priori are accessible since they are transparent to the operator by NFS. Accessing a data disk on a data server is distributed, as is the processing of the data.

When we started with the K5/VSSP software correlation system, it was operated in a preliminary form (Table 1). Figure 8 gives a simplified flow chart of the data processing with the K5/VSSP software correlation system. Four kernel programs, "apri_calc", "cor", "sdelay" and "komb" are the most essential elements to make software correlation from raw data within the equipment. "apri_calc" calculates a priori delay and rate for each scan per single baseline. "cor" executes software correlation. "sdelay" makes rough fringe directly from correlator output. "komb" is a bandwidth synthesis program to obtain multi-band delay. These programs come from NICT's K5/VSSP software correlator package, which was originally developed by T. Kondo, Y. Koyama and their co-workers at NICT. Based on an agreement of research cooperation between GSI and NICT, the Tsukuba VLBI Correlator is allowed to take advantage of these products which are licensed under NICT.

Table 1. Improvement of K5/VSSP software correlation system

.

preliminary form	current form
single task control manually input	multi-task control graphical user interface
kernel program ——	kernel program aid application "PARNASSUS"

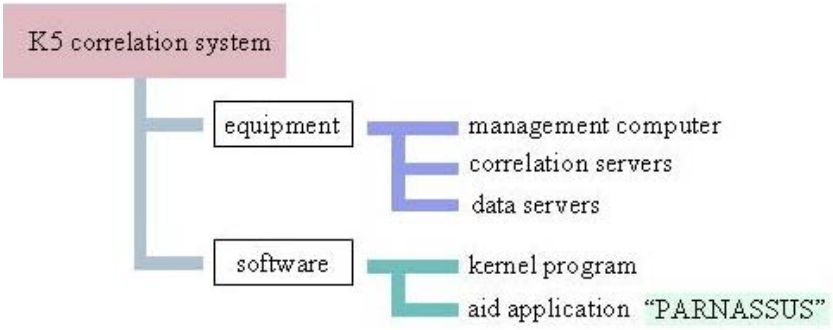

Figure 4. Components of K5/VSSP software correlation system

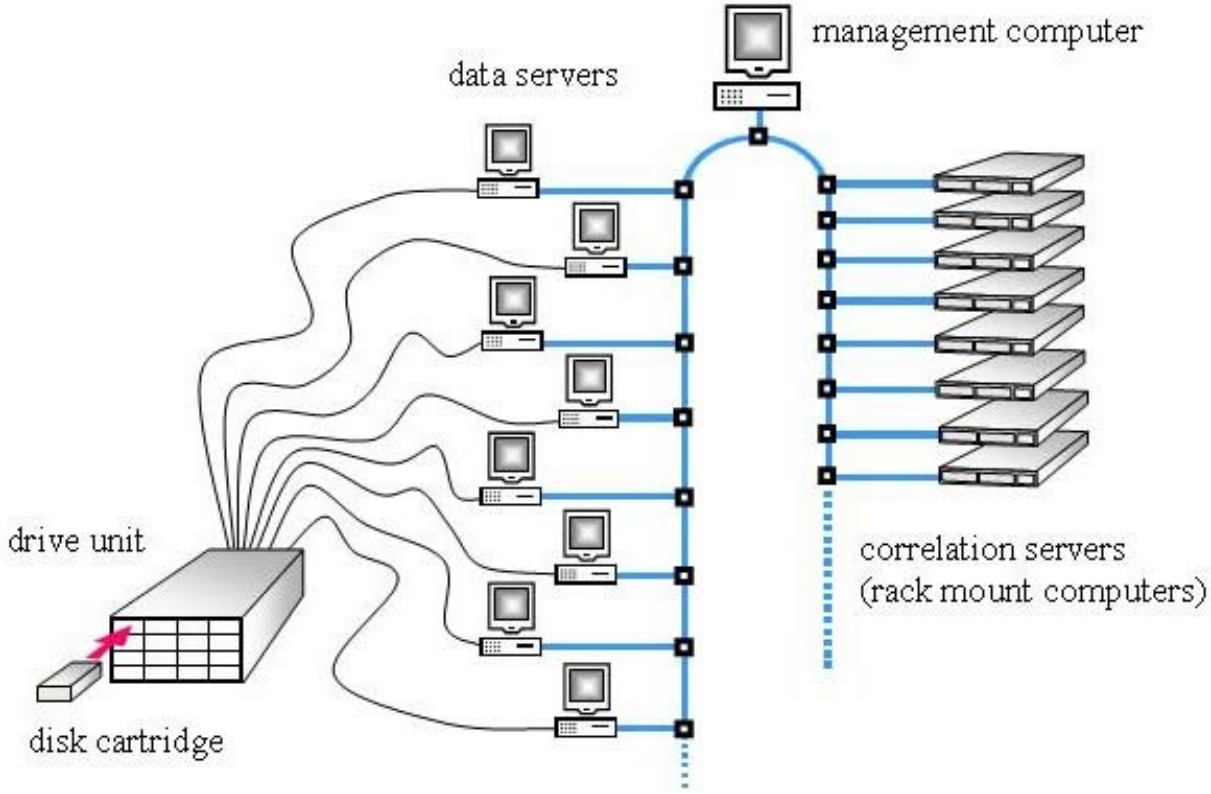

Figure 5. Equipment level of K5/VSSP software correlation system

Figure 6. Disk cartridge and drive unit

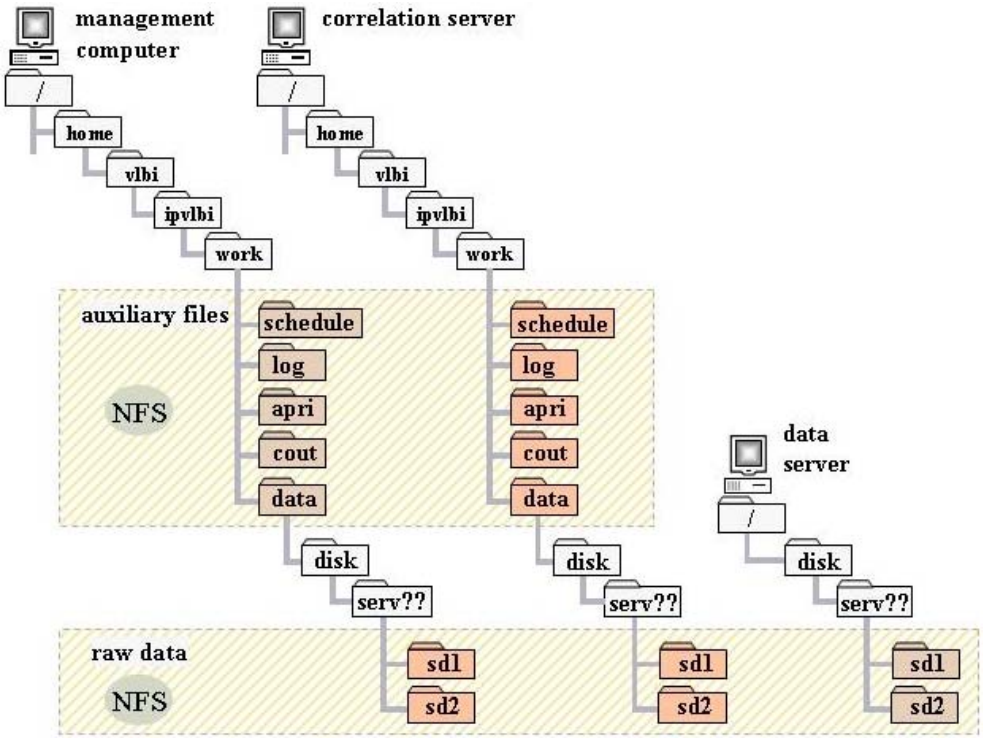

Figure 7. File sharing logic

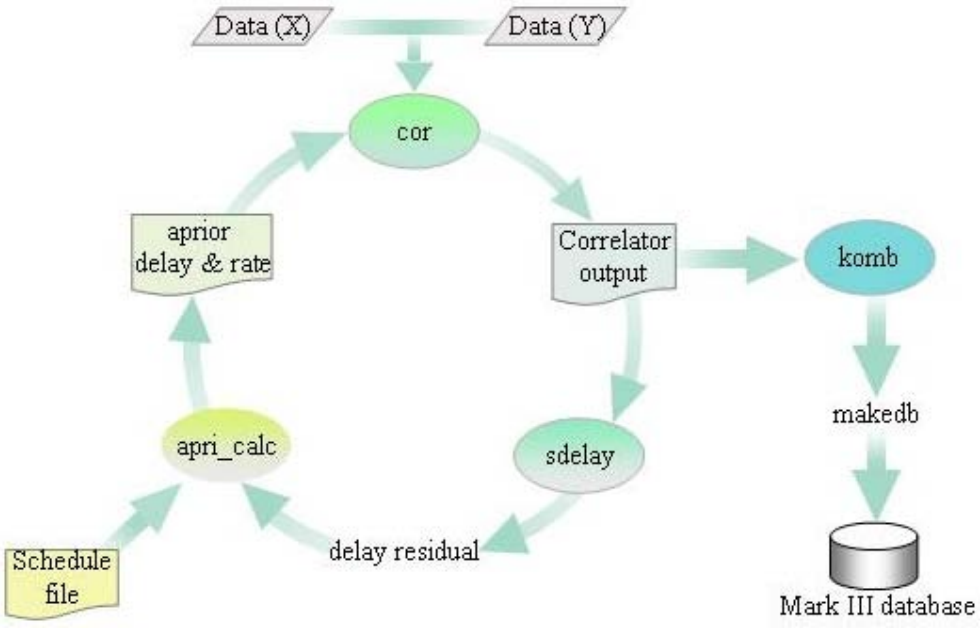

Figure 8. Data processing flow

2.3. Aid Application "PARNASSUS"

The kernel programs have the ability to process only one scan of a single baseline. There was an increase in the number of sessions to be processed at the Tsukuba VLBI Correlator(Figure 9). The only use of four kernel programs in the software correlation was too simple to meet the demands for processing many scans for multi-baselines. As a solution, we have developed an aid application software, "PARNASSUS" (Processing Application in Reference to NICT's Advanced Set of Softwares Usuable for Synchronization), to handle with sessions of multi-baselines, creating the operator's workbench by providing a graphical user interface and facilitating multi-task control. The application succeeds in optimizing operator's input into kernel program and comprehensively handling distributed correlation.

There were some steps toward a full combination of "PARNASSUS". The idea of developing an application to aid the operator's input occurred to us in autumn, 2004. As a private advisory group, K. Takashima, M. Ishimoto and M. Machida were in charge of planning, primary design, requirements definition and functional specification to the application. K. Takano (Advanced Engineering Services Co., Ltd) mainly took control of structual design, coding, programming, testing and installation as a developer.

- March 2005, PARNASSUS 1.0 covered calculating apriori delay&rate
- September 2005, PARNASSUS 1.1 covered executing correlation
- December 2005, PARNASSUS 1.2 covered bandwidth synthesis

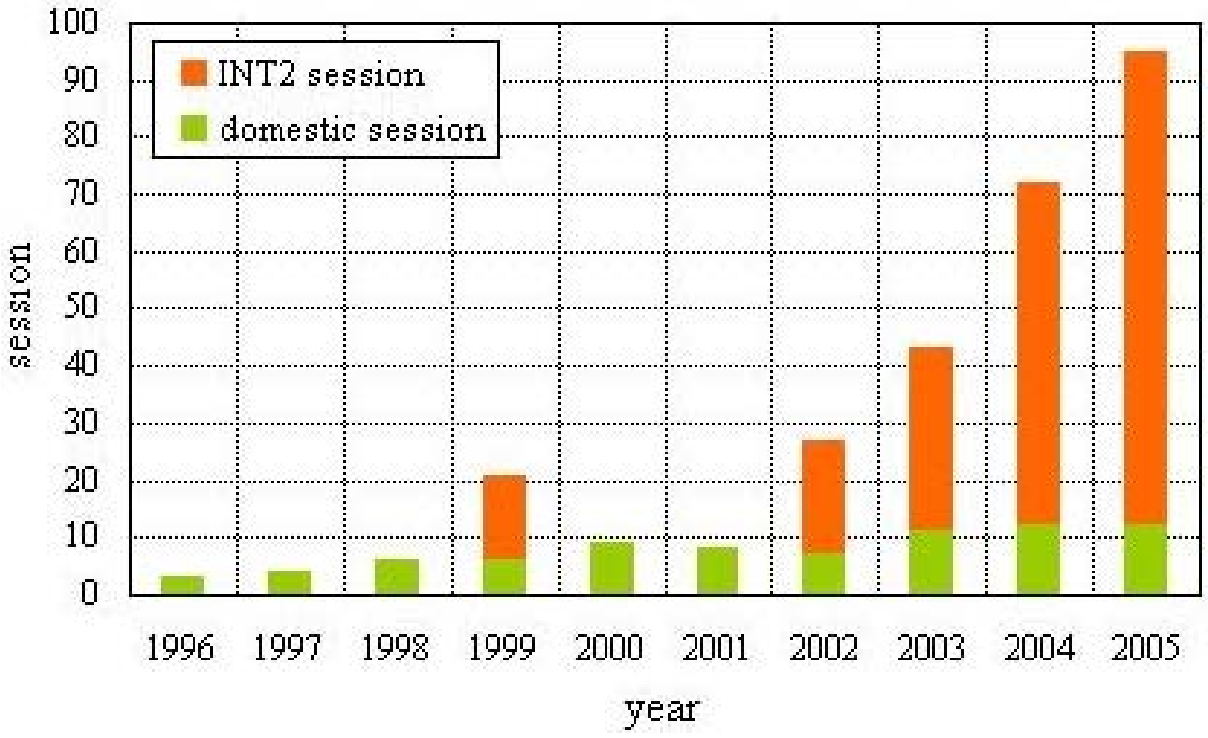

Figure 9. Demand for intensive and domestic sessions at Tsukuba VLBI Correlator

2.4. Distributed Computing

The difference between preliminary and current forms is explained here. Figure 10 is a simplified explanation of distributed computing in a preliminary form. Each image of horses and carrots represents correlator servers and data set, respectively. Correlator servers keep watching a task information. Once there is an uncorrelated data set, the task is accessible from any correlator server that is not occupied by processing another task. Sometimes the correlation system in the preliminary form did not work properly. There might be a conflict between correlator servers to get a task because of lacking access control to tasks in this form.

In current form (Figure 11), aid application "PARNASSUS" on a management computer keeps watch on the tasks. Once there is a uncorrelated data set, the task is distributed to any of the vacant correlator servers under control of "PARNASSUS".

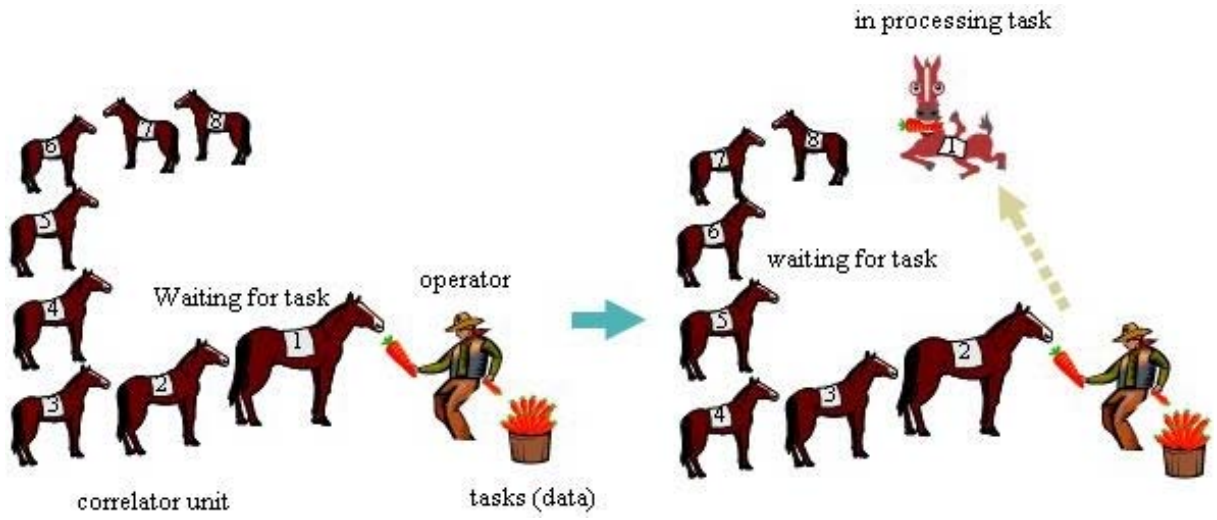

Figure 10. Data handling in preliminary form

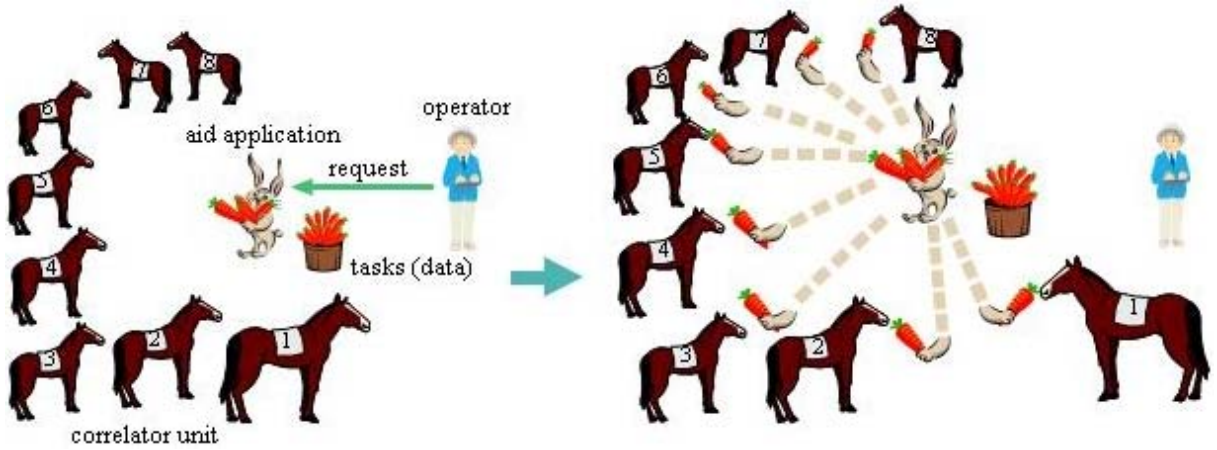

Figure 11. Data handling in current form

2.5. Fringe Search in Distributed Computing

Another issue for the K5/VSSP software correlation system is the fringe search in distributed computing. Ordinarly, a fringe is found within a few microseconds. But in the case of a gross clock offset of the time tag, it takes a lot of time to detect a fringe. K5/VSSP software correlation system can give a solution to that problem. Firstly, we have a wide range divided into some subsiduary range (Figure 12:left). W denotes the lag window size in the subsiduary range. A and B are end points in a whole search range. Then "PARNASSUS" starts the fringe search in each subsiduary range by distributed computing (Figure 12:right).

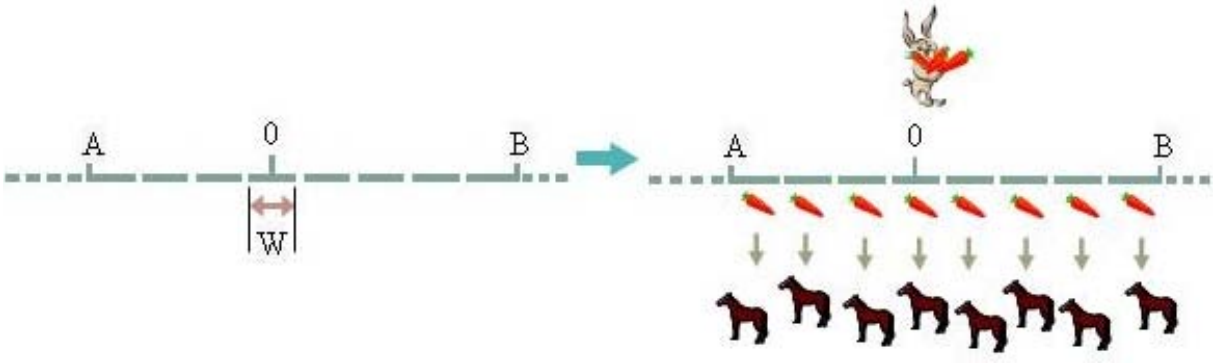

Figure 12. Fringe search in distributed computing

2.6. Performance

Figure 13 shows an efficiency comparsion between K4 and K5/VSSP correlation systems using the processing factor (PF). Black points come from PF of IVS-INT02 sessions which were processed on K4. White points are PF of IVS-INT02 sessions which were processed on K5/VSSP software correlation system. The average PF in the depicted period is 1.82 for K4 and 0.83 for K5/VSSP. There is a decrease of PF from KT to K5/VSSP. As mentioned earlier, we upgraded from K4 to K5/VSSP in April 2005. The improvement of PF in processing the intensive sessions results from introducing K5/VSSP. We did not have to extend our duty time for processing data despite of increased number of intensive and domestic sessions. It was efficient to process data with K5/VSSP software correlation system.

3. Future Plans

One of our goals in order to speed up processing is to work on the expansion of our K5 software correlation system. We will add eight correlation servers and eight data servers to the existing K5/VSSP correlation system.

The developement and testing of interactive "PARNASSUS 1.3", covering the range from calculating a priori to creating a database, is one of the priorities in the first half of 2006. Implementation plans for "PARNASSUS 2" running in batch mode will be discussed in the advisory group of the VLBI team of GSI.

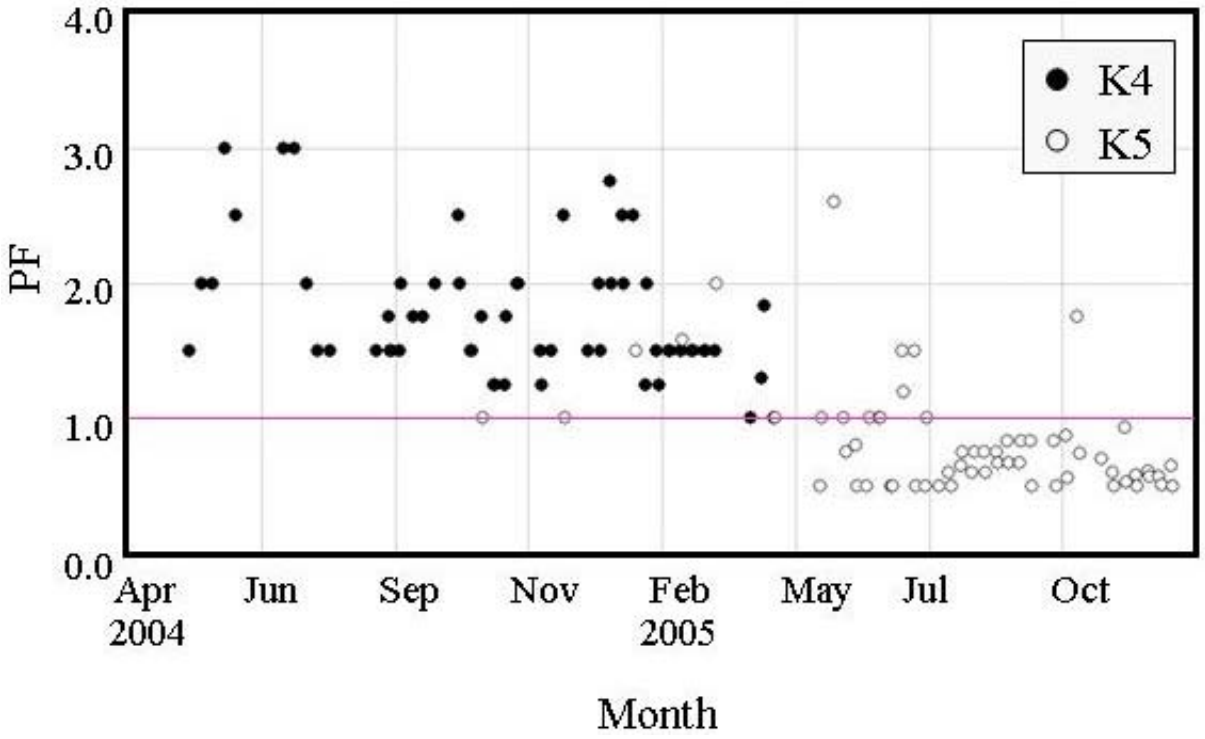

Figure 13. Efficiency comparsion with PF from Intensive session

Gonzalo Remedi et al.: Remote Control of VLBI Operations, IVS 2006 General Meeting Proceedings, p.127–131
http://ivscc.gsfc.nasa.gov/publications/gm2006/remedi

Remote Control of VLBI Operations

Gonzalo Remedi [1], *Sergio Sobarzo* [2], *Hayo Hase* [3]

[1)] *Universidad del Bío Bío - TIGO*
[2)] *Universidad de Concepción - TIGO*
[3)] *Bundesamt für Kartographie und Geodäsie - TIGO*

Contact author: Gonzalo Remedi, e-mail: gonzalo.remedi@tigo.cl

Abstract

The Geodetic Observatory TIGO developed an easy-to-use software which enables remote control and monitoring of VLBI operations. This software is a Java-applet and can be executed from any web browser. Several tests have been successful. The remote control operation of VLBI opens new observation strategies involving more observation without additional staff by making use of operators in different time zones operating more than one radiotelescope.

1. Introduction

The VLBI network consists of many geographically distant stations. Remote control of a VLBI station can provide a distributed operation supporting other stations in different time zones. Having a system that is able to automatically check the general status of the ongoing experiment can be helpful to respond to warnings or errors quicker than using only the log file. Remote trouble shooting is also considered to a certain extent. In the present document a remote control VLBI software with all its implementation issues is explained. The developments are described in detail in Remedi [1].

2. Objectives

The main idea of a VLBI remote control software is to give the ability to control a radiotelescope station from anywhere and from any platform without the need of installation of any kind of software on the client computer.

The location of some remote VLBI stations implies that the Internet connection has a limited bandwidth. In addition computers are not always fast enough to run heavy programs. These conditions suggest a second objective which is the use of minimal network and computer resources.

The third objective is the development of a program of easy and very intuitive use in order to facilitate the manipulation by people with less experience and to have a fast diagnosis of the current experiment with just one look at the main client screen.

3. Implementation

3.1. Servers

At VLBI stations, the so-called VLBI Field System Software (FS) is widely used for VLBI operations. Our software is based on additional servers, which interact with FS variables. These

servers retrieve actual values from the shared memory area, before they pack and send them through the network as it is shown in Figure 1.

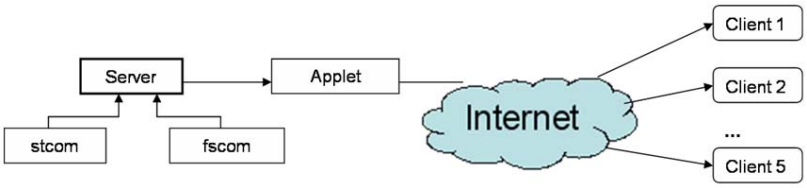

Figure 1. Communication flow diagram between servers and clients on the Internet [2].

Currently there are 4 servers. Each of these starts together with the FS and waits for incoming connections from the remote clients. The value of the maximum simultaneous connection can be modified according to the processor and network capabilities (see also [3]).

3.1.1. Monitoring Server

The monitoring server takes a selection of FS parameters containing the most relevant status information from the FS and station shared memory and put them into a formatted TCP frame which is sent to the client computer. A frame of formatted data is sent to the connected clients each second. This guarantees that the network link utilization is efficient, and as minimal as possible, and that the remote client receives permanently 1 second samples of the status.

3.1.2. Log Server

The log server only sends the changes of the log file every second. It continuously scans for changes in the size of the log file and then transmits the most recent changes to the client using minimum network resources.

3.1.3. Control Server

The control server is always waiting for incoming frames sent from the client with FS commands inside. This program receives the command and then sends it to the FS main program where the command is processed and executed.

3.1.4. Chat Server

The chat server resides in the web page server and is written in Java. It takes incoming messages from the chat applets connected and distributes them to the other connected clients. This allows for discussions between remote (and local) operators. It is needed to pass the control from one client-operator to the other.

3.2. Clients

The clients were implemented in Java as an applet. A screen shot is shown in Figure 2. Each server corresponds to one client, which means we have actually also four clients: monitoring,

control, log and chat.

The main advantage of Java is that you can execute the application on any platform, regardless whether it is Windows, Linux, Mac or any other OS (Figure 3). A typical Java applet works in the following way:

1. A web server offers a Java code. (the Java codes have the extension *.class).
2. Somebody on the Internet, with a Java compatible web browser, makes a connection to the server.
3. The server sends the HTML document and the Java code (*.class).
4. Both (the HTML document and the Java code) arrive at the remote computer of the user that made the connection, and then the Java Virtual Machine inside the browser transforms the Java code into a code that is understood by the operating system of the local machine and executes the program inside the web page.
5. If the user makes a connection to another URL or quits the browser, the client program terminates its execution at the remote computer.

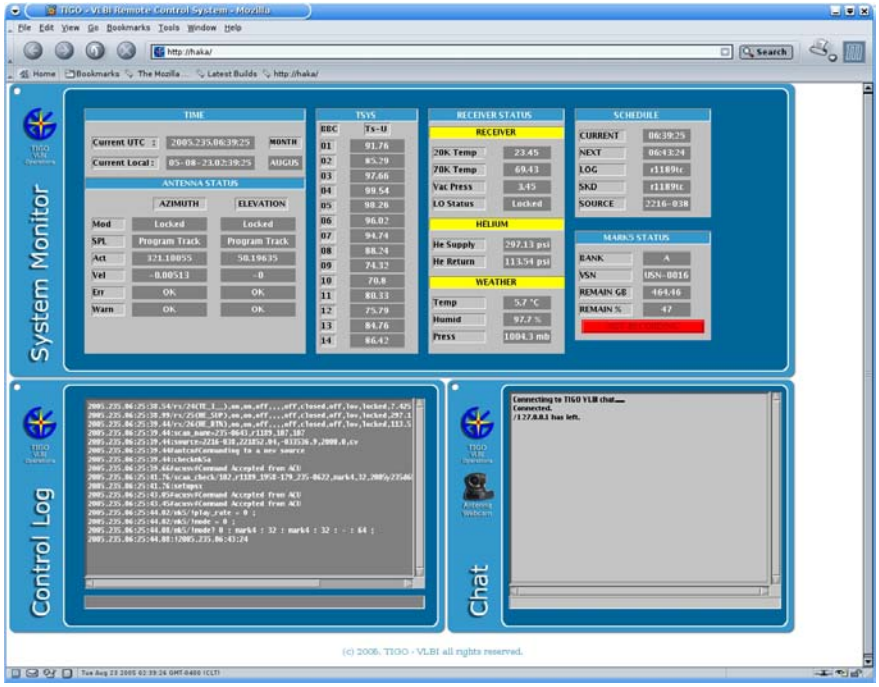

Figure 2. View of the Remote Control applet in a browser.

3.2.1. Monitoring Client

The function of this client is to show the received data of the Monitoring Server. It is an applet. It consists of four panels, each one with specific data of the shared memory.

The first panel is used to monitor the antenna status, UTC and local time.

The second panel shows the system temperatures derived from the SQL-detectors of all base-band converters.

The third panel shows the receiver status with temperatures of the cold stages, helium pressure, LO-status and the meteorological parameters temperature, pressure and humidity.

The fourth panel shows the status of the running experiment with schedule and source name, current and next scan.

The last panel shows the status of the Mark 5 recording system.

3.2.2. Log Client

The log client is in charge of receiving data sent by the log server. In fact, what it does is receive a package of data sent by the server and then display it in a text area. Hence it displays all the log entries, as they are seen on the local screen of the FS computer. The given information is useful to identify errors in the execution of commands.

3.2.3. Control Client

The control client is in charge of sending the commands entered by the remote operator to the control server.

The server accepts commands in SNAP language. The main process in the FS determines the validity of a SNAP command. The remote operator is informed about the response of the FS, by the usual log-entry wich can be seen in the log client panel.

3.2.4. Chat Client

The chat client allows the communication between the users who are connected to the application (applet).

For security reasons the web page and the applets must reside on another computer than the FS computer. But Java doesn't allow the execution of an applet if this tries to connect to another machine which is different to the applet host machine. This problem was solved by a redirection from the client via the applet host computer to the FS-computer by using IP tables.

It implies also a modification to Java security policy. The configuration file in the web page host machine needs to enable all the network permissions: accept, connect, listen and resolve for each of the ports used by the remote connection, for example:

```
permission java.net.SocketPermission "IP_of_the_remote_machine:port1", "accept, connect, listen, resolve";
permission java.net.SocketPermission "IP_of_the_remote_machine:port2", "accept, connect, listen, resolve";
permission java.net.SocketPermission "IP_of_the_remote_machine:port3", "accept, connect, listen, resolve";
permission java.net.SocketPermission "IP_of_the_remote_machine:port4", "accept, connect, listen, resolve";
```

These modifications are only possible if we have the necessary safety measures to avoid an undesired access. In this case the main filter is the firewall where the connections to the application are authorized only to specified IP addresses. A further access restriction can be realized by username and password.

4. Future Work

It is possible to implement the servers in the FS official distribution. The first step is to define a standard set of variables for monitoring and include them into the FS shared memory area, as

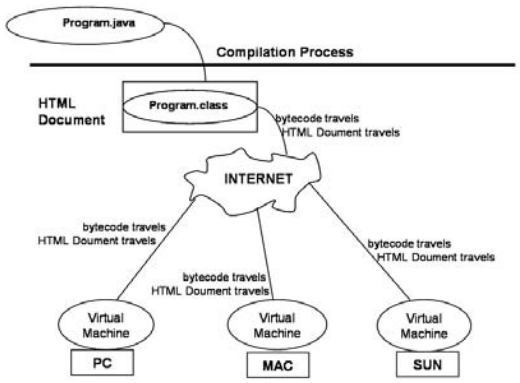

Figure 3. Each platform has its own virtual machine that allows the execution of a program in Java. The program is executed locally on each computer.

it can be done following our example. The second step is that every station must fill the correct values in the shared memory modifying the station software.

Other improvements that can be added are the addition of new key variables to the monitoring scheme and the use of sound alerts in the applets. Also automatic log comment generation can be implemented.

Since the monitoring can not handle all the possible errors of a station, it is possible to extract the last error from the log file and show it permanently.

Visual and acustic guidance of the remote operator can be provided by adding webcam or videoconferencing capabilities, which are currently under development.

4.1. Conclusions

With this application it is possible to share the operators load between co-observing VLBI stations and to avoid night shifts when control can be passed to an operator in a daylight time zone.

The advantages of the open source software tools were used for the development of this application. This avoided costly development tools like Microsoft technologies.

The appliaction is fully functional now. It is possible to integrate other features depending on the specific needs of the VLBI station and the operator's experiences.

References

[1] Remedi, G. A., Sistema de Control Remoto para el Monitoreo de un Radiotelescopio, Computer Engineer Thesis, 2005.

[2] Stevens, W. R., UNIX Network Programming, Volume 1, Second Edition: Networking APIs: Sockets and XTI, Prentice Hall, 1998.

[3] Stevens, W. R., UNIX Network Programming, Volume 2, Second Edition: Interprocess Communications, Prentice Hall, 1999.

Tuhwan Kim et al.: National Geodetic VLBI Plan in Korea, IVS 2006 General Meeting Proceedings, p.132–136
http://ivscc.gsfc.nasa.gov/publications/gm2006/kim

National Geodetic VLBI Plan in Korea

Tuhwan Kim [1], *Tetsuo Sasao* [2], *Younghee Kwak* [2], *Taekyoung Jung* [3], *Minsoo Bae* [4], *Wonkuk Lee* [3], *Jongwan Kim* [3]

[1)] *Ajou University*

[2)] *Ajou University and Korea Astronomy and Space Science Institute*

[3)] *National Geographic Information Institute*

[4)] *High Gain Co., Ltd.*

Contact author: Tuhwan Kim, e-mail: thkim@ajou.ac.kr

Abstract

A project of constructing the first geodetic VLBI system in Korea is in progress at the National Geographic Information Institute (NGII). The primary purpose for this antenna will be to participate in the IVS international geodetic VLBI observations, and to maintain the Korean geodetic origin precisely defined in the world geodetic frame, the ITRF. However, since there was no former research or project about geodetic VLBI in Korea, a new R&D is necessary on the fundamental design of the VLBI system. In this presentation, a preliminary study on the necessity of geodetic VLBI in Korea and basic specifications for a core station of geodetic VLBI will be presented together with the possibility of constructing a VLBI antenna in Korea.

1. Geodetic VLBI in Korea

1.1. Korea - Japan VLBI Observation

In 1995, Korea - Japan Collaborative VLBI observations were performed by the National Geographic Information Institute (NGII), Korea, and the Geographical Survey Institute (GSI), Japan, for an accurate connection of the geodetic networks of the two countries, accurate determination of the standard datum of Korea in the ITRF, and understanding tectonic activities in East Asia [2].

The observations were carried out during October and November with a 5m transportable VLBI antenna in Suwon, which was temporarily provided by GSI, and a 26m antenna in Kashima (Figure 1). Three out of four 24-hour sessions yielded satisfactory results which allowed to connect the geodetic networks with mm-level accuracy and to determine ITRF coordinates of the standard datum of Korea.

1.2. Construction Plan for Suwon and KVN Antennas

In 2001, the Korea Astronomy and Space Science Institute (KASI) started the construction of the Korean VLBI Network (KVN). The KVN will be composed of three new-generation 21m radio telescopes to be installed in Seoul, Ulsan, and Jeju. Though the KVN will be mainly used for mm-wave VLBI astronomy, partial use for geodesy is also officially planned. Completion of the Network is expected at the end of 2007 [5].

The NGII is planning to construct a dedicated geodetic VLBI antenna of 26m or 30m diameter in Suwon in order to accurately maintain the national standard datum and eventually establish a

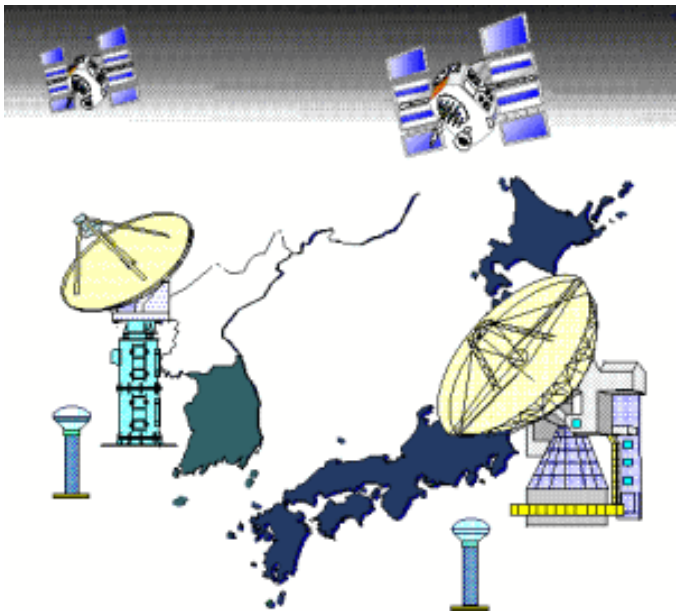

Figure 1. Korea-Japan VLBI&GPS Experiments [2].

Figure 2. Site locations of the Suwon and KVN antennas in Korea

highly accurate new national geodetic system consistent with the ITRF. The planned locations of the KVN and Suwon antennas are shown in Figure 2.

2. Roles of the Dedicated Geodetic VLBI Antenna in Korea

The Suwon antenna will contribute to better define the ITRF in Eastern Eurasia, where no observing site has been selected as sufficiently stable for the ITRF datum definition [1]. According to GPS observations carried out by Yonsei University and KASI [6], the Korean Peninsula is tectonically more stationary than other areas in East Asia. Therefore, we expect that the new dedicated geodetic VLBI antenna in the middle of the Korean Peninsula will be an important stable site for the ITRF.

Also the Suwon antenna will be a stable fiducial point for precise monitoring of crustal deformations, by means of mobile VLBI antennas, in tectonically active areas in Eastern Eurasia. Such a monitoring is indispensable for clarifying mechanisms of disasters, such as the huge tsunami earthquake in 2004, and eventually prevent them.

The Suwon and the KVN antennas will form a powerful domestic VLBI network for geodynamical studies.

First, the domestic network will determine the Euler parameters of the assumed Amurian plate (AM), where a large area of East Asia, including the Korean Peninsula, is likely to reside. Results of previous studies based on seismic and GPS data have not been sufficiently consistent about the plate parameters. We expect that another independent space geodetic technology, with VLBI known to be highly stable and accurate, will finally solve the problem [3][4].

Second, collaborative VLBI and GPS observations will enable us to better examine the internal deformation of the Korean Peninsula. The results of the GPS analysis by Park et al. (2001) suggested possible effects of the northwestward tectonic stress due to the AM - PH (Philippine Sea plate) convergence on the southeastern part of the Korean Peninsula. In particular, the characteristic bend of the Peninsula could be a result of the stress acting on internal faults, striking nearly perpendicularly to the stress trend. New domestic VLBI observations will give us further insight into the tectonics of this region.

3. Considered Specifications for the Suwon VLBI System

Detailed designing of the new geodetic VLBI antenna in Suwon is now starting. Preliminary specifications are shown in the following table, which are subject to change after further discussions, especially in view of valuable comments given at the General Meeting.

Table 1. Preliminary specifications of Suwon geodetic VLBI system

Aperture Diameter	26m or 30m
Slew Rate	$>$ 2 - 3 deg/s in Az and El
Surface Accuracy	$\sim$ 0.37 mm rms($<$10m/s wind)
Pointing Accuracy	$\sim$0.002 rms($<$10m/s wind)
Receiving Bands	2/8/(32), 22/43GHz
Data Acquisition	K-5 Backend System
Recording System	K-5 HD Array
Correlator	4-station class software correlator for geodetic VLBI

We believe that the domestic industry in Korea is capable of producing geodetic VLBI antennas.

For example, a domestic antenna manufacturer, which has provided a number of large aperture satellite communication antennas, is now constructing three KVN antennas under a contract with a US company.

To avoid severe human-made interferences at lower frequencies in geodetic VLBI observations, we need to shift observation frequencies to higher ones. Fortunately, the KVN will have multi-channel receivers including K/Q bands, and for the Suwon antenna it is also considered to install K/Q receivers. Hence we can have a good chance to make a real experiment of the higher frequency simultaneous DUAL-BAND VLBI. The first thing that we have to confirm is if the higher frequency geodetic VLBI is as fruitful as, or better than, S/X.

Not only for geodetic VLBI observations, the Suwon antenna can also support astrophysical observations of the KVN and the VERA (VLBI Exploration of Radio Astrometry, Japan) using K/Q bands. Moreover, from a practical point of view, having 22 GHz and 43 GHz receivers will be useful for achieving high pointing accuracy of our antenna, since we will be able to use many bright water and SiO maser sources for pointing measurements.

4. Construction Schedule

The following table shows a tentative construction schedule of the Suwon geodetic VLBI system.

Table 2. A tentative construction schedule of the Suwon geodetic VLBI system

	2006		2007		2008	
Antenna	Design	Foundation	Manufacture			Test
Receiver			Design	Manufacture		Test
Cable Transmission system			Module purchase	Install		Test
Backend system			Design	Manufacture		Test
Clock, Frequency system					Purchase	Test
Delay, Phase calibration system					Purchase	Test
Correlator		Design & Manufacture				Test
Observatory	Design	Foundation	Construction			

References

[1] Altamimi, Z., P. Sillard, and C. Boucher, "ITRF2000: A new release of the International Terrestrial Reference Frame for earth science applications," *J. Geophys. Res.*, **107**(B10), ETG 2-1 - ETG 2-19, 2002.

[2] Ishihara, M., Y. Fukuzaki, A. Yoshimura, M. Tobita, H. Amemiya, T. Kawahara, M. Nemoto, O. Otaki, M. Yazawa, A. Itabashi, T. Saito, M. Sasaki, Y. Iimura, and S. Miyazaki, "Japan-Korea VLBI and GPS observation," *J. GSI*, **86**, 1996.

[3] Kwak, Younghee, Study for Plate Motion in Korean Peninsula by Geodetic VLBI, Master's Thesis, Ajou University, 2005.

[4] Kwak, Younghee, T. Sasao, and T. Kim, Preliminary study on plate motion measurements in Korean Peninsula by new Korean VLBI, this volume, 2006.

[5] Minh Y. C., Roh, D. G., Han, S. T., and Kim, H. G., "Construction of the Korean VLBI Network(KVN)," *ASP Conference Series*, **306**, 2003.

[6] Park,Pil-Ho, U. Chwae, Y. Ahn, and K. Choi, "Preliminary GPS results and a possible neotectonic interpretation for South Korea," *Earth Planets and Space*, **53**, 937-941, 2001.

Pierre Kaufmann: Radio Astronomy and VLBI in Brazil, IVS 2006 General Meeting Proceedings, p.137–141
http://ivscc.gsfc.nasa.gov/publications/gm2006/kaufmann

Radio Astronomy and VLBI in Brazil

Pierre Kaufmann

CRAAM, Escola de Engenharia da Universidade Presbiteriana Mackenzie & ROEN, NE Space Radio Observatory (Fortaleza Station)

e-mail: kaufmann@craam.mackenzie.br

Abstract

The first VLBI experiments in Brazil were carried out in the 70's using the Itapetinga 13.7-m radio telescope, near São Paulo, southeast Brazil, by the Mackenzie group, who had pioneered radio astronomy in the country more than a decade earlier. The world wide interest in geodetic VLBI resulted in the installation of the Eusébio facilities, State of Ceará (Fortaleza Station), northeast Brazil, in the early 90's. We summarize the major steps to attain these accomplishments and discuss the supporting needs and requirements to foster academic cooperation.

1. Brief Historical Introduction

Radio astronomy activities in Brazil have been carried on by the Mackenzie group since 1960 at sites located in São Paulo State. Permanent facilities were built at Mackenzie's Itapetinga Radio Observatory, Atibaia, in 1970, where a 13.7-m radome-enclosed radio telescope was built in 1971 (Figure 1, [1,2]). Several international cooperative programs were carried out since then in various research areas including solar physics, ionosphere radio propagation, solar-terrestrial physics, radio astrophysics and instrumentation.

An intensive collaboration was established with MIT Haystack Observatory in the early 70's with the aim of obtaining the first north-south VLBI observations. Two sensitive K-band maser receivers were developed under the leadership of S. H. Zisk and installed at Haystack's 37-m radio telescope and at the Itapetinga radio telescope. Several new water vapor celestial masers were discovered with Itapetinga single dish observations [3]. The first successful VLBI tests were obtained on celestial water vapor line sources with Haystack Observatory in 1978 in one of the last runs using the Mark I system [4]. The Itapetinga VLBI facility was upgraded with a Mark II terminal and was successfully used in the 1974 Venus flyby Vega balloon tracking experiment at 1.7 GHz [5]. The first quasar imaging results adding a long north-south baseline with Itapetinga were obtained at 11 GHz in 1984 [6], showing the dramatic improvement in the resolution of the celestial object (Figure 2).

2. Cooperation for Exploring Geodetic VLBI

The interest of the global geodetic VLBI community to have a complete station in Brazil was discussed during the 1988 XXth Baltimore IAU General Assembly by several international groups, in particular NOAA's NGS, NASA, U.S. Naval Observatory and Germany's IfAG (now BKG). An agreement was made in 1989 between NOAA and the Brazilian institutes of São Paulo University (USP), National Space Research Institute (INPE), Campinas State University (Unicamp), and Mackenzie Presbyterian University (CRAAM). The first site considered was Mackenzie's Itapetinga

Figure 1. The Itapetinga Radio Observatory, Atibaia, near São Paulo city, with the 13.7-m radome-enclosed antenna built in 1971.

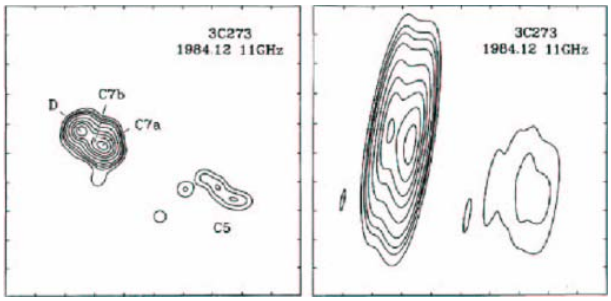

Figure 2. 3C273 images at 11 GHz obtained using Effelsberg (100-m), Haystack (37-m), Green Bank (43-m), Ft. Davis (26-m) and Owens Valley (40-m) with Itapetinga (13.7-m) at left, and without at right [6].

Radio Observatory, near São Paulo, with an existing local infrastructure; but the notion was discarded due to visibility limitations (at low elevation angles) for the existing 13.7-m antenna. Then the USP site at Pirassununga, São Paulo State, was taken into consideration. However, in view of the international community's preference for having a VLBI site as far east and equatorial as possible, the attention was directed to coastal northeastern Brazil despite known difficulties with limitations in local infrastructure. The site named Barreira do Inferno, Natal, Rio Grande do Norte, a former launching site for sounding missiles, had good infrastructure available; but its selection had to be dropped because of difficulties to get the necessary government clearance for using it as a site for a VLBI station. The next and ultimately selected site was located at INPE facilities near the town of Eusébio, in the metropolitan area of Fortaleza, State of Ceará.

3. The North-East Space Radio Observatory at Eusébio (Fortaleza Station)

NOAA arranged for the relocation of a TIW 14.2-m radio telescope antenna from NRAO at Green Bank to Eusébio (Figure 3). Other subsystems (Mark III terminal, H-maser, cryogenic radiometers for X- and S- bands) were made available by NOAA, USNO and NASA. A continuously tracking GPS receiver was added to the site by NOAA. Brazil has contributed with substantial human, material and cash resources. The Ministry of Science and Technology has provided US$250K for erecting the radiotelescope. Other contributions came from the four initially involved institutes, the local Ceará Foundation for Meteorology and Water Resources (FUNCEME), and the Brazilian Institute of Geography and Statistics (IBGE, the national geodetic institute): for the site adaptation, the antenna final assembly with instrumentation, the first complete geodetic survey, training of local people, fixing and renewing of the buildings, the stand-by generator, communications, etc. The Eusébio (Fortaleza) station was named the North-East Space Radio Observatory (ROEN).

ROEN started operations in 1992 and was officially dedicated in 1993. Since then regular VLBI observations were carried out with a relatively small number of shut down periods for major maintenance. Important mechanical repairs were done in the first years, e.g. to fix pedestal drives misalignments and gear box damages, which were done by local people and mechanical workshops. The station's operational costs were shared between NOAA and the Brazilian partners involved.

In 1999 the International Association of Geodesy (IAG) gave a recognition award to the Fortaleza team for the quality of their geodetic VLBI observations.

Figure 3. The 14.2-m radio-telescope antenna being installed at Eusébio (Fortaleza area), Ceará State, in 1992, part of the supporting team, from left: Edmilson (INPE), Joaquim (CRAAM), J.D. (NOAA), João Batista (Funceme), Macilio (INPE), Wellington (Funceme) and Avicena (INPE).

In addition to the geodesy services of the international and Brazilian (IBGE) communities, the principal justification of the geodetic VLBI operations in Brazil were the prospects of academic cooperation in astrophysics, geophysics, geodesy and related fields. Several studies on time variations of quasars and BL Lac spatial structures were done using data processed at the Washington correlator [7]. Other proposed collaborative efforts, however, did not materialize as expected.

4. Brazilian Space Geodesy Program Support

In view of NOAA's decision to discontinue their activities in geodetic VLBI in 1997, the program was reviewed by all parties involved at a visit to Eusébio (Fortaleza station) site, and a meeting at Mackenzie Presbyterian University. All Brazilian partners were present at the meeting as well as international participants from NASA, USNO and IfAG (now BKG). It was agreed that there would be a regular international contribution to the annual program cost, comparable to the Brazilian share. Major instrumentation additions, replacements or repairs would be sponsored by

NASA, while the Brazilian partners should raise funds for complementary improvements at the observatory. Since time was needed for a new formal agreement between NASA and the Brazilian Space Agency (AEB), the existing agreement with NOAA was used to transfer necessary funds in the meantime. The NASA-AEB Agreement was signed in 2002, and the NASA—Mackenzie contract was signed in 2004. The ROEN operations in the intermediate five years were difficult, due to poor and irregular funding because of NOAA administrative difficulties. However, despite these difficulties, ROEN never interrupted operations in any scheduled geodetic VLBI experiment or GPS data recording and transmission, thanks to the professional dedication and responsibility of the observatory team, led by A. Macilio Pereira de Lucena. Mackenzie Presbyterian Institute many times advanced their own resources in order to keep the observatory running.

The support conditions for the ROEN operations have improved in 2004 as a consequence of the NASA-Mackenzie Contract. However the necessary resources from the international partners dropped below the needs because of two major reasons: a) the U.S. dollar lost a substantial part of its value with respect to the Brazilian Real: from May 2004 to January 2006 the devaluation was on the order of 50%, and even more compared to previous years, when the original agreement was established; b) the contribution of the international partners to the maintenance remains considerably under-dimensioned even without taking into account the foreign currency devaluation, and no additional funds are available to complement and upgrade the instruments as planned.

5. Recent Developments and Prospects

A Mark 5 recording system has been recently received and installed. New funds are now necessary to build the Mark IV video converters, to add auxiliary and test instruments needed for developments and maintenance, and to replace defective units. NOAA has recently replaced the GPS receiver and antenna (Figure 5).

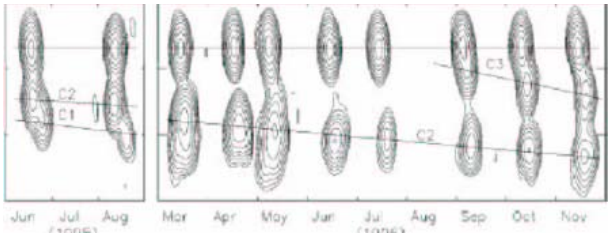

Figure 4. Superluminal BL Lac source expansion as observed at 8.8 GHz [7].

Figure 5. The new NOAA GPS antenna installed on the roof of the main ROEN building.

A new high data rate optical fiber connection is now under construction and will link ROEN at an initial rate of 2.5 Gbps in the first semester of 2006 enabling e-VLBI capabilities in the course of the year. This new connection is part of the GigaFor network [8] sponsored by the Brazilian

Ministry of Science and Technology and the Ministry of Education, corresponding to an investment of US$1.5M for ROEN. The maintenance cost of about US$75K/year will be shared among five academic institutions in the Fortaleza area.

The Ceará State University (UECE) and Mackenzie Presbyterian University signed a cooperation agreement in 2005 intended to support the UECE research program on atmospheric physics, in collaboration with ROEN, exploring the meteorology parameters inferred from GPS and VLBI measurements [9].

In addition to the dramatic international funding deficit indicated above, the fostering of academic cooperation with international institutions on research subjects related to the VLBI and GPS geodetic observations carried out at ROEN, is another requirement to be fully implemented in order to justify the Brazilian institutes' involvement and their investments in the program.

References

[1] Kaufmann, P., D'Amato, R., A Brazilian radio telescope for millimeter wavelengths, Sky and Telescope, 45, 144, 1973.

[2] Kaufmann, P., R.E. Schaal, J.C. Raffaelli, The effect of slowly varying surface errors in large millimeter wave antennas - A practical verification in the Itapetinga 45-ft reflector, IEEE Trans. Ant. Propagat., AP-26, 854, 1978.

[3] Kaufmann, P. et al., New H2O celestial sources associated with H II regions in the Southern Hemisphere, Nature, 260, 306, 1976.

[4] Kaufmann, P. et al., The Itapetinga contribution on north-south high resolution VLBI experiments, in The Impact of VLBI on Astrophysics and Geophysics (M.J. Reid and J.M. Moran, editors), Proc. 129th IAU Symposium, Kluwer, 495, 1988.

[5] Preston, R.A. et al., Solar system VLBI astrometry: the Venus ballon experiment, in The Impact of VLBI on Astrophysics and Geophysics (M.J. Reid and J.M. Moran, editors), Proc. 129th IAU Symposium, Kluwer, 319, 1988.

[6] Biretta, J.A. et al., Observations of 3C273 with high North-South resolution, Astrophys. J., 292, L5, 1985.

[7] Tateyama, C.E. et al., Observations of BL Lacertae from the geodetic VLBI archive of the Washington correlator, Astrophys. J., 500, 810, 1998.

[8] http://www.rnp.br/wrnp/2005/

[9] Costa, A. et al., GPS meteorology over northeast Brazil, this volume.

Wolfgang Schlüter et al.: Footprint Observations at the Fundamental Station Wettzell, IVS 2006 General Meeting Proceedings, p.142–146
http://ivscc.gsfc.nasa.gov/publications/gm2006/schlueter1

Footprint Observations at the Fundamental Station Wettzell

Wolfgang Schlüter, Thomas Klügel, Christian Schade

Bundesamt für Kartographie und Geodäsie, Fundamentalstation Wettzell
Contact author: Wolfgang Schlüter, e-mail: wolfgang.schlueter@bkg.bund.de

Abstract

Footprint observations are performed in order to document the geological stability of a geodetic observatory. Beside a local survey network, which usually covers the observatory area of some 100 meters, some geodetic footprint markers, forming a footprint network, should be established at about 10 to 50 km apart from the observatory. The markers had to be included in the geodetic survey to monitor regional movements.

7-20 km apart from the Fundamental Station Wettzell, four footprint points were established, permanently observed with GPS. Observations were available for a period of more than two years from the four sites. The data was analysed together with the GPS observations taken from those GPS-receivers which are integrated in the international networks, such as IGS and EUREF and in the national network GREF. With respect to a selected geodetic reference marker in Wettzell, for which motion is observed with a tilt meter, the observations are evaluated and day to day coordinates are generated by employing the GPS Bernese Software Processing Engine. The time series show a precision in the order of a few millimeters. Moreover systematic and seasonal effects can be seen.

1. The Footprint Network, Local Survey Network, and GPS Array

The footprint network (Figure 1) of the Fundamental Station Wettzell consists of four geodetic markers in the area of the observatory, spread out to 8 km in north-south and up to 20 km in east-west. The site selection was dependent on the geological structure of the area and on logistical aspects for the operation of permanent GPS receivers. Continuous geodetic observations, done with the highest accuracy, allowed the demonstration of the local, geological stability of the observatory site. This information is important in ensuring that the plate motion is represented by the observed station motion derived from VLBI, SLR and GPS techniques. The footprint network is required in addition to the local survey network (Figure 2), which allows the determination of local ties between the VLBI, SLR and GPS reference points.

On top of the observation platform of the main building, five GPS antennas were set up and combined to form a GPS array (Figure 3). The array includes the IGS, EUREF and GREF GPS receivers, which are named WTZR, WTZA, WTZZ , WTZT and WTZJ. An official description can be found in the site sheets of the respective GPS Services. In addition, a webcam was installed, in order to monitor the weather conditions day-by-day.

Pillar 21 (Figure 4) of the local survey network was equipped with an ASHTECH GPS antenna. Inside the pillar, an AGI 722 borehole tilt meter was installed, providing information about the pillar motion with a resolution of 0.1 microradian. For a period of five years, it could be stated that the overall motion is less than 0.4 mm.

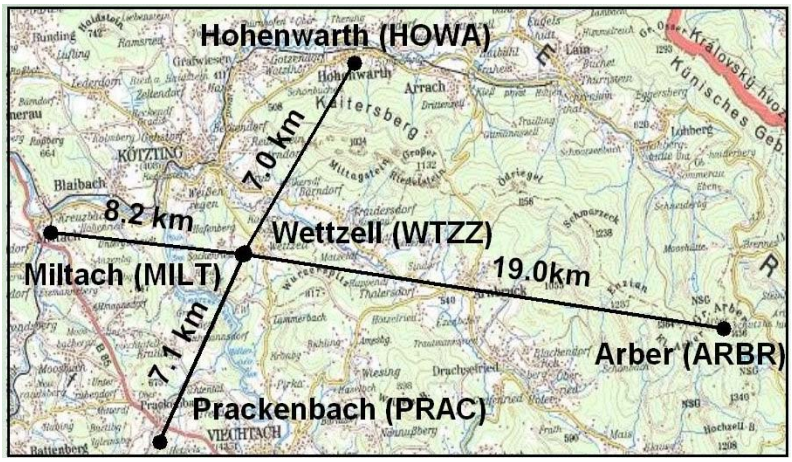

Figure 1. Footprint network of the Fundamental Station Wettzell.

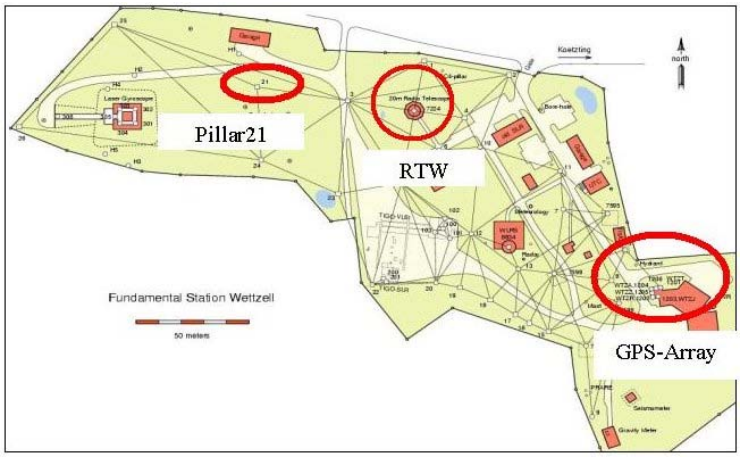

Figure 2. Local Survey Network of the Fundamental Station Wettzell.

2. Data Analysis

Employing the Bernese Software Processing Engine, Version 5, GPS observations covering a period of more than two years were analysed. Pillar 21, which shows a stability of better than 0.4 mm, was fixed. The residuals in the north, east, and height components, derived from the L3 phase solutions, are shown in Figure 5 for two selected points, WTZA and WTZR of the GPS array. Seasonal influences of the order of 1 mm could be seen in the east component and of the order of 0.5 mm in the north component. There was no significant variation in the height component. More scatter could be seen in the winter periods, when snow covered the antennas.

Figures 6, 7, and 8 show the residuals of the footprint markers ARBR, HOWA, MILT and PRAC. Compared to the residuals of the GPS array results, the scatter of the residuals for the footprint markers is larger. At short baselines, common systematic errors like tropospheric or ionospheric delays or orbit errors are cancelled out, which result in more precise coordinates for

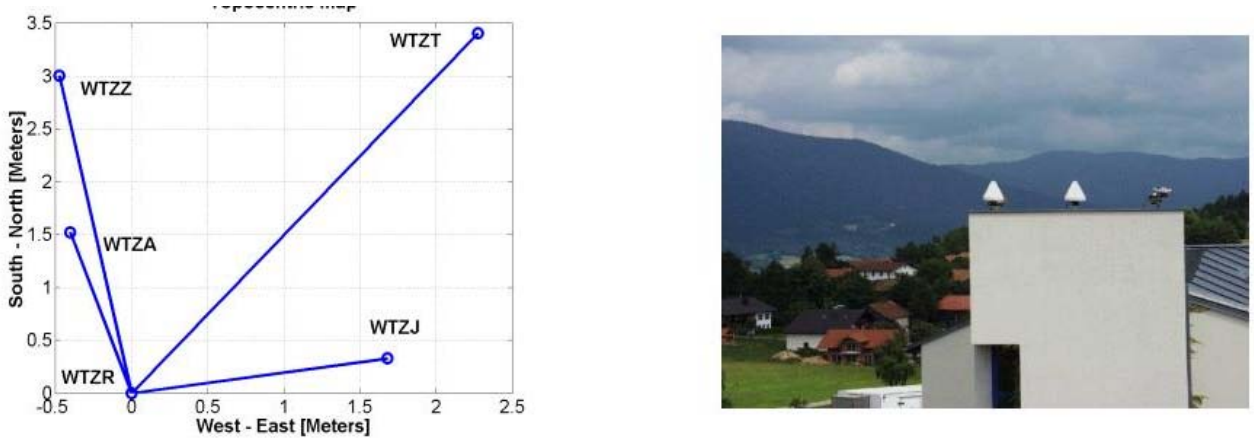

Figure 3. Map (left) and platform view (right) of the GPS array.

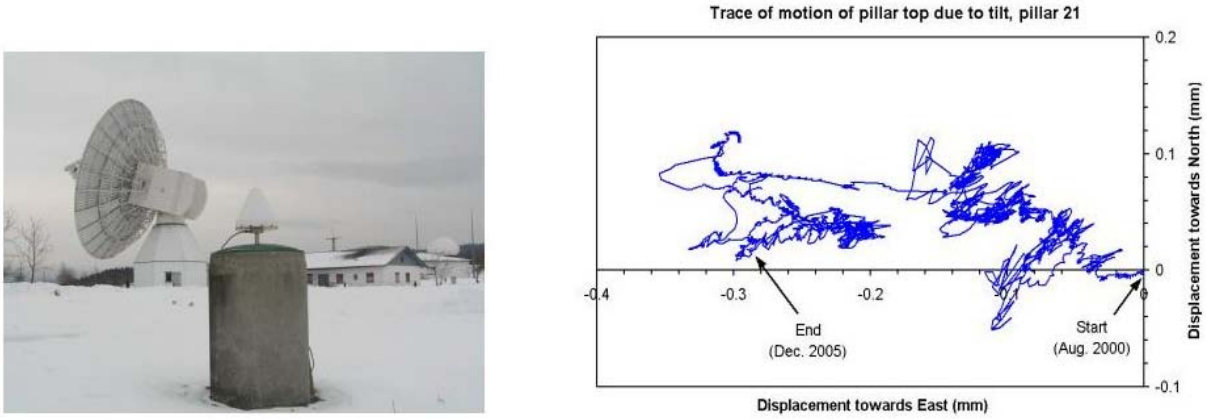

Figure 4. (left) Pillar 21 with the tilt meter. (right) Motion of the pillar from August 2000 to Dec 2005.

the GPS array than for the footprint network with baselines of several km. Seasonal variations can be seen in the residuals of the footprint markers, but the variations are not as significant as those for the GPS array stations. No changes in the height could be seen.

3. Conclusions

The monitoring of the site stability was performed with a precision better than 1 mm. This indicates that the area around the Fundamental Station Wettzell is stable. Seasonal effects of the order of less than 2 mm, particularly in the east component, were detected. No significant height changes occurred.

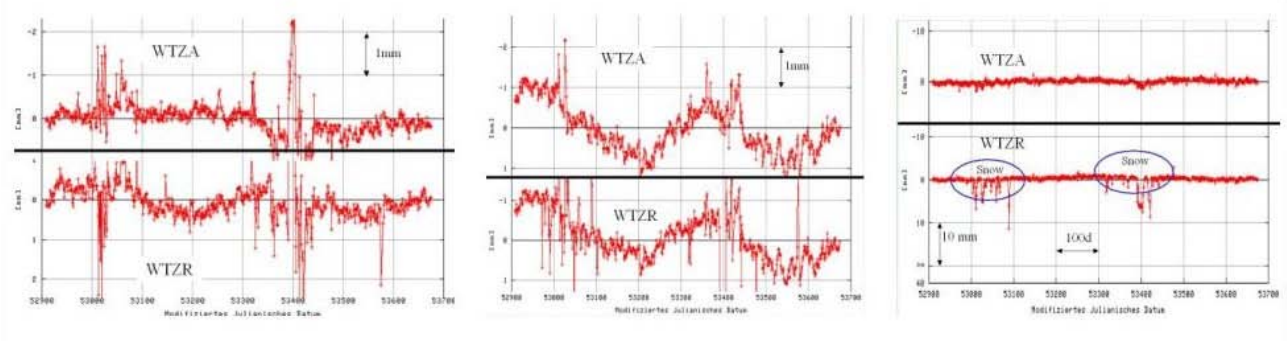

Figure 5. Residuals in the north, east, and height component of WTZA and WTZR.

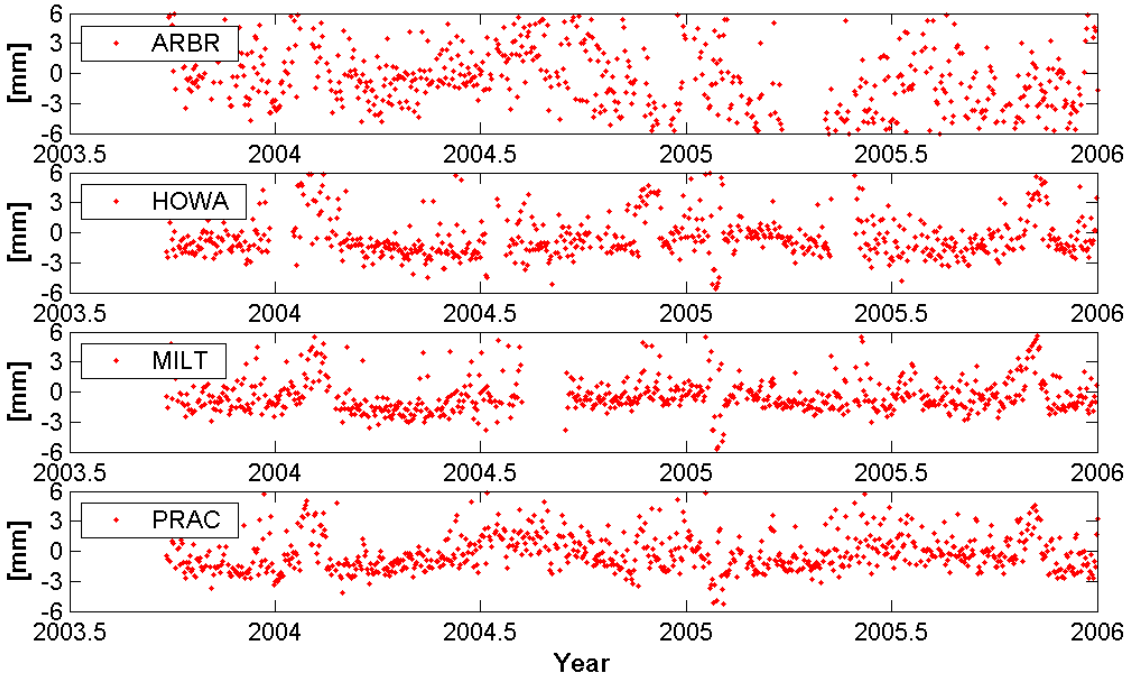

Figure 6. Residiuals in north of the footprint points.

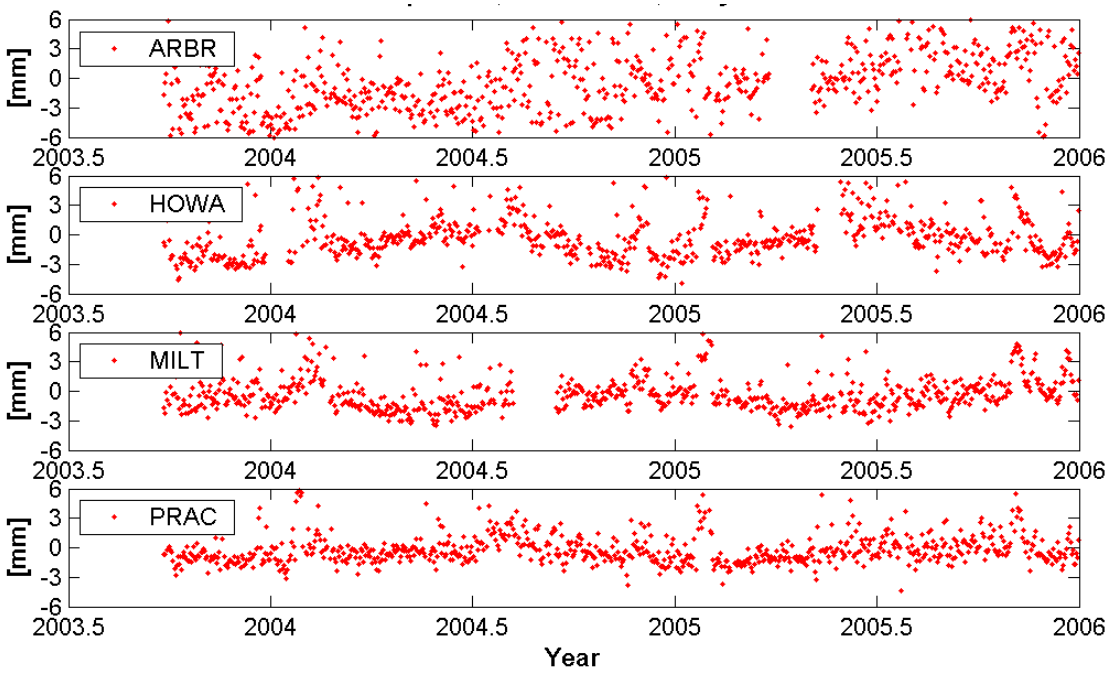

Figure 7. Residuals in east of the footprint points.

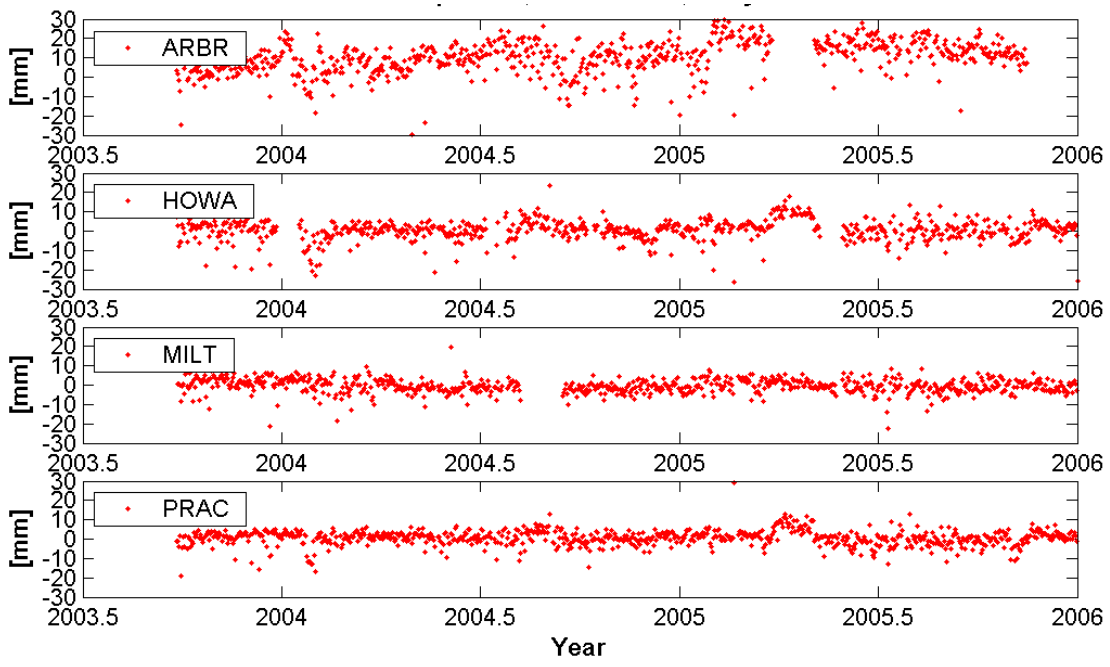

Figure 8. Residuals in height of the footprint points.

Arno Müskens et al.: Bonn Correlator Report for Astronomy and Geodesy , IVS 2006 General Meeting Proceedings, p.147–151
http://ivscc.gsfc.nasa.gov/publications/gm2006/mueskens

Bonn Correlator Report for Astronomy and Geodesy

Arno Müskens [1], *Walter Alef* [2], *Dave Graham* [2], *Alessandra Bertarini* [1]

[1)] *Geodätisches Institut der Universität Bonn*

[2)] *Max-Planck-Institute für Radioastronomy, Bonn*

Contact author: Arno Müskens, e-mail: mueskens@mpifr-bonn.mpg.de

Abstract

We report on the present status, capabilities and usage of the correlator, the processing efficiency for both astronomy and geodesy experiments, and on the planned upgrade to 12 stations. A short overview of the e-vlbi status and recent developments is given as well as a summary of the CONT05 sessions.

1. Introduction

The Bonn Mark IV correlator is hosted at the Max-Planck-Institut für Radioastronomie (MPIfR) Bonn, Germany. It is funded and operated by the MPIfR and by the (BKG) in cooperation with the Geodetic Institut of the Universität Bonn (GIUB)

The Mark IV processor system consists of the standard Mark IV 16-station-capable correlator unit installed by Haystack Observatory in December 1999. It is used for MPIfR-based astronomical observations with an emphasis on mm-wavelengths, astrometry and special VLBI experiments, and for geodetic observations under the auspices of the GIUB and in cooperation with the International VLBI Service (IVS).

For geodesy, VLBI can accurately measure the geodetic parameters associated with the shape of the Earth and its orientation in inertial space. This includes the positions and velocities of the sites occupied by VLBI antennas, UT1-UTC, polar motion and nutation.

The interaction of the astronomical and geodetic VLBI communities as realized at the Bonn correlator is a very good example in the world of VLBI for interdisciplinary synergies and cross-fertilisation of ideas, methods and efforts.

2. Present Status and Upgrades

2.1. Present Status

The Bonn correlator (Fig 1) is one of four Mark IV VLBI data processors worldwide and has been operational since 2000.

Nine of the 16 possible station inputs of the correlator are presently used. The station units handle the station-related operations and interface the nine tape playback units to the correlator. Eight Mark 5A disk playback units are operational and are connected to the station units in parallel with the tape drives. The operators can easily configure the correlator to accept Mark 5 disks or tapes. The total disk space for storing raw correlator data has grown in response to user demand to more than 1 TB.

Figure 1. Left: Part of the Mark IV data processor: correlator rack with two Mark 5 playback units and two station units as well as one playback tape drive. Right: one of the three new racks equipped with three Mark 5B units and space for the correlator interface boards (CIB).

Tape recordings with 32 tracks and Mark 5 recordings with 64 tracks can be correlated in one pass. This corresponds to maximum data-rates of 256 and 1024 Mbits/s respectively. Currently the correlator supports Mark IIIA, Mark IV, VLBA and Mark 5A formats, 1- or 2-bit sampling, with fanout up to 1:4.

The Mark IV correlator is intensively used. It has been possible to meet the increasing demand for correlation both from astronomy and geodesy by improving correlator software and firmware, the performance of the tape playback units, and by further streamlining operations. A leap in correlation efficiency has resulted from the use of Mark 5A disc-based systems, which offer substantially more robust recording characteristics, virtually error-free data, and random positioning within the recorded data. For Mark 5A-only experiments (e.g. IVS-R1) the correlator can run unattended for many hours.

2.2. Upgrading and Expansion

MPIfR and BKG decided in 2004 to upgrade the correlator to 12 Mark 5B disk playback systems. Similar projects are underway at MIT Haystack Observatory and USNO in Washington.

The expansion from 9 to 12 stations is only possible by using the Mark 5B system, as this system includes a newly designed station unit for the Mark IV correlator. As part of the Mark 5B development mostly done by MIT Haystack, MPIfR has developed and manufactured so-called high-speed serial links in sufficient numbers that also the Haystack and USNO correlators can be upgraded. MPIfR and MIT Haystack have further agreed on a joint project for upgrading the correlator software to allow the correlation of 12 stations simultaneously, on implementing the correlation of 2 Gbits/s recordings which will be correlated at a rate of 1 Gbits/s, and on replacing

the present HP-UX based workstation with a more powerful and cheaper solution based on the Linux operating system.

At present three new cabinets have been built up each to be populated with four Mark 5s initially either of A and B-type as well as correlator interface boards required for Mark 5B units (Fig 1). Towards the end of 2006 we expect to be able to remove the remaining tape units.

3. e-VLBI

Media shipment is presently the most time-consuming operation. This will be changed by global high-speed networks. When the Mark 5 system was introduced for VLBI data recording, its potential for the direct transmission of data to the correlator via internet was realized. The development of e-VLBI capabilities has been undertaken in the USA, mostly by MIT Haystack Observatory, in Japan, and in Europe. The involvement of the MPIfR has been hindered considerably by the prohibitive costs of network connections and traffic in Germany as provided by the German academic research network (DFN) and the German Telekom.

Several futile attempts were made to find other ways to connect the Bonn Correlator to the internet at a bit rate of initially 1 Gbits/s, which seems to be the minimum rate to achieve at least VLBI data-rates of 512 Mbits/s. For the present maximum data-rate of the Mark IV data acquisition systems of 1024 Mbits/s, two 1 Gbit connections would be required.

As the planning now stands the MPIfR will install private fibres between MPIfRs 100m-antenna at Effelsberg and the institute at Bonn. A few fibres to connect the institute to the University of Bonn are already in the building. To connect e-VLBI from the University to the European academic network Géant the optical testbed VIOLA[1] might be used. The MPIfR has submitted a proposal to become an associated member of the VIOLA activities. Data transfer via VIOLA would be free of charge.

E-VLBI will use separate fibres to the normal Internet traffic to avoid problems with Internet security. It is planned to drive the e-VLBI fibres at 10 Gbits/s if possible. The VIOLA connection to Géant is limited to only 2.5 Gbits/s. Gbit connectivity to the correlator can be expected in summer 2006, and to the telescope at Effelsberg possibly in 2007.

4. Geodetic Correlation

4.1. Overview

The total correlation time from the beginning of January to the end of November 2005 was 7026 hours, of which about 40% were dedicated to astronomy experiments and 60% to geodesy experiments (Fig 2). Most of the time the correlation was performed by either one of the two day-time operators or one of the five students who cover night shifts and weekends. Unattended correlation was possible for the sessions that involved a maximum of eight Mark 5-equipped stations, no tapes and which needed only one module per station, like the geodetic IVS-R1 series. However in some cases a recorrelation was then needed due to Mark 5 software and station unit failures.

The processing factor (PF), defined as the ratio between the hours spent correlating to the hours spent recording the data, decreased with respect to 2004 as more stations upgraded to

[1] http://www.viola-testbed.de/

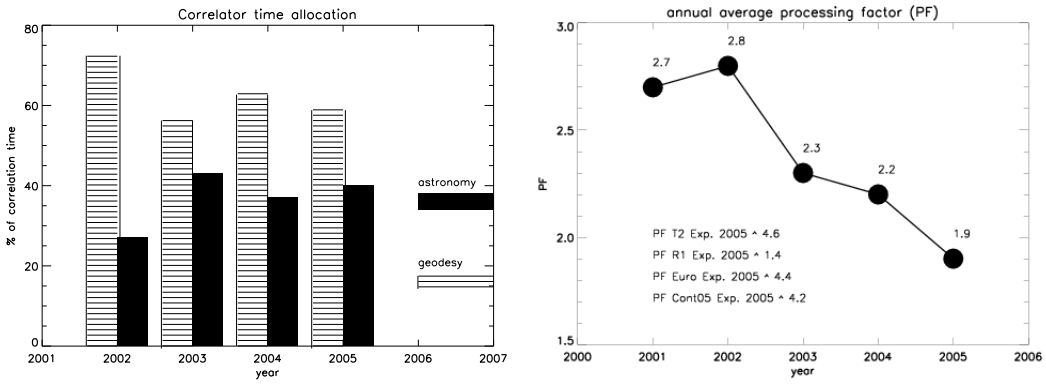

Figure 2. Left: Correlator time allocation for the last years in percentage. Right: Annual averaged processing factor (PF) plotted against the year.

Mark 5 recorders (Fig 2).

In 2005 the geodetic Bonn Correlator group correlated and released about 50 experiments, including IVS-R1, IVS-T2, EUROPE, five CONT05 sessions and one test with the Zelenchuckskaya station. IVS-Ohig 2004 experiments were correlated in December 2005 due to delays in transferring the Syowa data to Mark 5 modules.

Astronomers and geodesists have an agreement concerning correlator usage. The IVS-R1 series always have priority since they must be processed and analysed within 14 days of the observation. Other, non-urgent experiments are processed sequentially according to the requirements of the two groups.

Ftp-VLBI was successfully used to verify the operation of the Ohiggins station. A 60 second scan at a recording bitrate of 128 Mbits/s was transferred via ftp to Bonn in a few hours and fringes were found with the Mark IV correlator.

4.2. CONT2005

The involvement of the Bonn correlator in the CONT05 sessions started early in 2005, when IVS asked for the first time whether Bonn could support the correlation of part of the campaign. In late summer the three correlators involved (Haystack, Washington, Bonn) started to plan how to manage the CONT05 campaign. Based on correlator availability and an estimated processing factor (PF = obs. time / corr. time) it was decided how many sessions would be correlated where.

Bonn correlated the sessions C0501, C0507, C0508, C0514 and C0515. A processing factor of four could be achieved. The correlator control file preparation turned out to be a bit more elaborate than normal, partly due to the multiple passes required — three — and partly due to software problems caused by the unusually large observing logs and control files. Four out of five sessions ran smoothly. Unfortunately about 70% of the C0507 data needed recorrelation due to station-unit problems which led to an increased processing factor. During the campaign it became clear that the correlation and processing at the three correlators had to be standardised to minimise sytematic differences between the sessions of the CONT05 campaign. This successful

approach will be retained for future experiments [2] .

5. Astronomy Correlation

The astronomical group correlated several projects observed in the European VLBI network, chiefly for local PIs but also for densification of position catalogues of compact sources and station position measurements of EVN antennas at 22 GHz. The Bonn correlator is used for analysis in the global 3 mm array, presently this uses 8 VLBA antennas and 5 antennas in Europe. All stations record with Mark 5A units at 512 Mbits/s in a 64-track mode. Subsections of the network also record at 1 Gbit/s. Multiple passes are necessary, particularly for spectral line correlation using 512 lags. Bonn technical and astronomical staff are also involved in optimising data acquisition at several stations and in water vapour radiometer (WVR) development.

6. Shipment and Logistic

The shipping time from the stations to the correlator was less then six days for almost all the stations, with some exceptional delays caused by the transport companies. In the case of Tsukuba the shipping lasted a couple of days longer than normal, since the data were transfered via e-VLBI from the station to Haystack. In Haystack the data were copied on a Mark 5 disk that was then shipped to Bonn. We are currently trying to improve the shipment from the correlator to the network stations by searching for better logistics providers.

7. Summary

All Mark IV data processors consist of a 16-station correlator, but they have been equipped with only seven to nine playback and station units. With the introduction of the lower-cost Mark 5B to replace both the MarkİV playback and station units, the correlators can be extended to up to 16 stations with moderate resources.

In the next step forward, MPIfR and BKG will upgrade the correlator to 12 stations by adding four Mark 5B units. This will include new Linux-based computers and a software upgrade to be developed in collaboration with Haystack observatory.

The reduced number of tape drives and station units will still be maintained until all IVS stations have upgraded to Mark 5.

In summer we expect to have Gbit/s connectivity from the correlator into Géant (European Academic Network) via dedicated fibres and shared lines of the 10 Gbit/s optically-switched test network VIOLA.

[2] for more details see http://ivscc.gsfc.nasa.gov/program/cont05/diary_bonn_corr.txt

Sergei Gulyaev et al.: The IVS in the Southern Hemisphere: New Zealand Perspectives, IVS 2006 General Meeting Proceedings, p.152–156
http://ivscc.gsfc.nasa.gov/publications/gm2006/gulyaev

The IVS in the Southern Hemisphere: New Zealand Perspectives

Sergei Gulyaev [1], *Tim Natusch* [1], *Brent Addis* [1], *Steven Tingay* [2], *Adam Deller* [2]

[1)] *Auckland University of Technology*
[2)] *Swinburne University of Technology*
Contact author: Sergei Gulyaev, e-mail: sergei.gulyaev@aut.ac.nz

Abstract

Efforts to build a radio astronomy capability in New Zealand took a big step forward with the first successful VLBI experiment between New Zealand and Australia. The 1.6 GHz observation of PKS 1921-293 took place in late July, between a 6 m telescope in New Zealand and the Australia Telescope Compact Array (ATCA), with the data being correlated on the Swinburne University of Technology's supercomputer. This result follows 6 months of intense development and testing of the systems with the support of a number of institutions. Plans for the future development of New Zealand VLBI, as well as the reasons for New Zealand involvement in the IVS are discussed.

1. Introduction

In 2005 Auckland University of Technology (AUT) became a new affiliated member organization of the IVS.

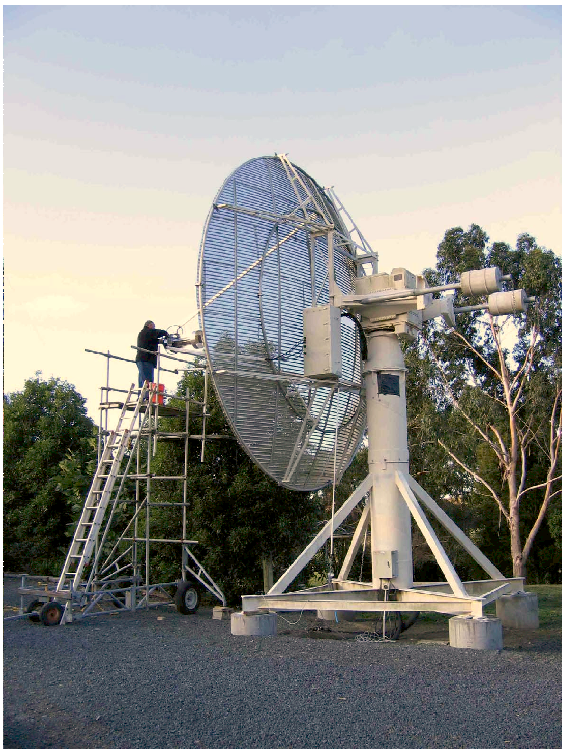

Figure 1. 6m radio telescope near Auckland (New Zealand).

The IVS has set itself the goal of achieving 1mm positional and 1mm/year velocity precision for the ITRF [1]. It is generally agreed that attaining as homogeneous a distribution of IVS sites on the Earth's surface as possible must form a vital part of the strategy to realise this goal. The current map of sites indicates a very heavy weighting in favour of the Northern Hemisphere [2]. A New Zealand site would be ideally placed to redress this imbalance (figure 2). It would provide an opportunity for extended and more continuous observation of sources and ionospheric effects. "Gaps" in coverage that currently limit achievable precision of the ITRF and EOP measurements would be reduced.

Recently New Zealand changed from Geodetic Datum 1949 (NZGD1949) to NZGD2000 [3]. The NZGD1949, which served the cadastral system of New Zealand for the last 50 years, had internal distortions of up to 7 m due to the limitations of the survey technology used to define it and the effects of earth deformation. The new datum NZGD2000 closely matches the ITRF, and the ellipsoid chosen is the Geodetic Reference System 1980 (GRS80).

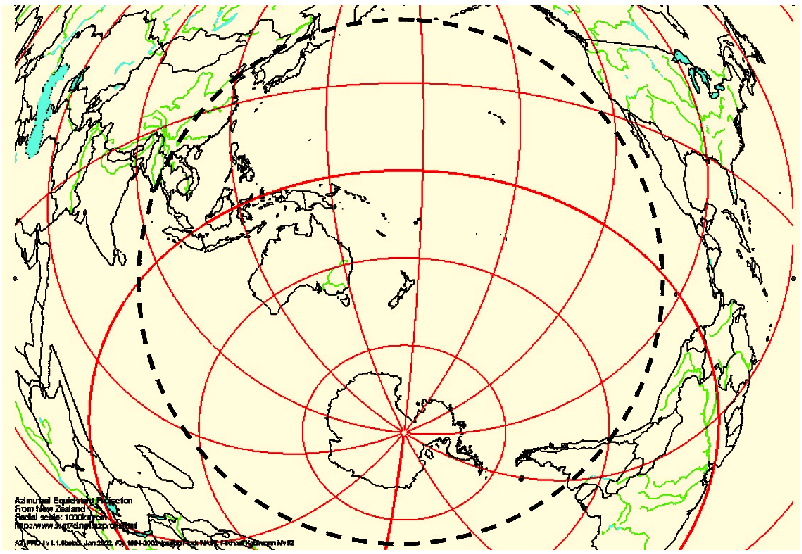

Figure 2. New Zealand's strategic location in the Southern Hemisphere. New Zealand is in the centre of the map. Radius of the dashed circle is 10,000 km along a great circle, which corresponds to a 9,000 km baseline. (Projection: Azimuthal equidistant.)

The new datum definition is frozen at the specified epoch (2000.0) and does not include time dependencies, such as station velocities, rates of change for transformation parameters, etc. In reality, such changes will occur in the future: e.g. large coordinate jumps may be required in geologically dynamic New Zealand as a result of earthquakes or localised mark movement. Therefore, monitoring of changes between the datum as a whole and the global reference frame (ITRF) is essential. While a GPS station network allows building a relative local velocity model, only VLBI is able to directly link this (local) model to the ITRF. Development of a New Zealand VLBI service for geodesy is one of the central tasks in sustaining the New Zealand Geodetic Datum 2000 in the future and maintaining its link to the ITRF.

There is also a need to consider the continuing effects of ground deformation and the requirements of New Zealand's national height datum for the foreseeable future. VLBI is required for vertical datum development in New Zealand.

2. Current Work

Current work in Radio Astronomy is centred on the newly formed Centre for Radiophysics and Space Research (CRSR) located at AUT (Auckland University of Technology). AUT has undertaken the task of developing VLBI facilities in New Zealand. This work is being conducted in collaboration with Swinburne University of Technology (Melbourne) and with the support of the Australia National Telescope Facility and the University of Tasmania at Hobart in Australia.

A grant of NZ$300,000 was obtained from the New Zealand Ministry of Economic Development (MED) to support this work. The MED sees VLBI activity as a potential user of the Advanced Network, which in turn forms a vital component of the government's Digital Strategy.

A self contained radio astronomy receiving and recording system for VLBI was constructed (see details in [4]). The major items of equipment include:

- Receiver operating at 1.658 GHz centre frequency, 16 MHz bandwidth.
- An 8 bit sampler / digitiser based on a Maxim 1448 ADC.
- Disk based recording system constructed from a Dell Poweredge 1600SC fitted with a Metsahovi VSIB interface card.
- Stanford Research Systems FS725 Rubidium Frequency Standard.
- Trimble Thunderbolt precision GPS oscillator.

Feed and downconversion system are locked to the Rubidium frequency standard. A 2.5 hour loop time constant was used to discipline the FS725 to the 1 PPS signal produced by the GPS unit. This combination provided sufficient control of the long term drift of the Rubidium without being too detrimental to its short term stability. The Rubidium was calibrated with the use of Hydrogen masers (in Hobart and Parkes). It proved to be stable to $\approx 10^{-12}$.

Signals from the prime focus of the telescope were collected by a circular waveguide with simple scalar choke ring and a single linear polarisation pickup.

The whole package was designed as a portable system for use on different radio telescopes, since the one thing that New Zealand lacks at the moment is ready access to a large collecting area, fully steerable antenna.

We are exploring possibilities arising from collaboration with Australia. A number of Trans-Tasman tests have been conducted in 2005 between the AUT system installed on a 6 metre dish located at Karaka, South Auckland, and the Australia Telescope Compact Array in Narrabri, Australia. This work has been successful, with fringes located from the recorded data and high resolution image of the quasar PKS1921-293 obtained for the first time (figure 3).

These measurements form the beginning of monitoring geographic location of the New Zealand RT with respect to the LBA (Australia) antennas. The geographic location of the 6m RT is:

$\phi = -37^o05'53.4183$"
$\lambda = 174^o49'43.6518$"E
Ellipsoid height= 58.492 m
Geoid height= 32.935 m

The geocentric coordinates of the 6m RT are:

$X = -5072744.194$ m
$Y = 459085.7453$ m
$Z = -3826123.922$ m

The distance between the ATCA at Narrabri and New Zealand 6m dish was found from the first VLBI test to be 2398483.72 ± 0.01 m.

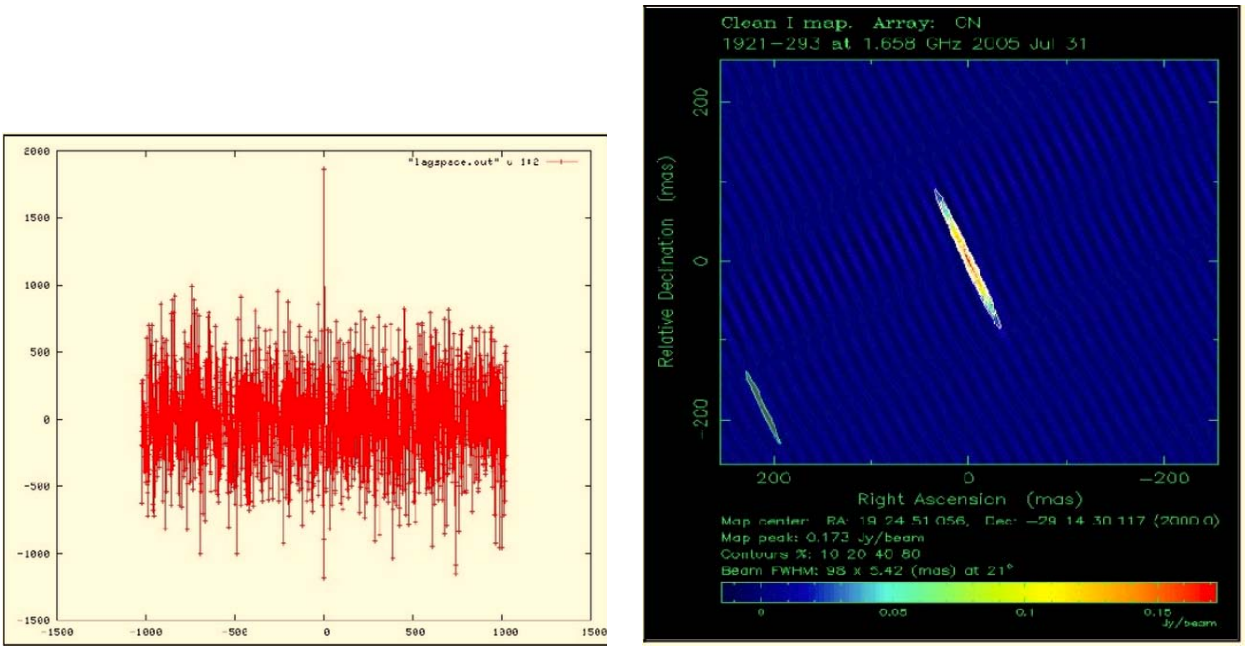

Figure 3. The first fringe and image of PSK1921-293 obtained from Australia–New Zealand VLBI. (From [4].)

3. Future Plans

The central task for New Zealand radio astronomy is to acquire a radio telescope with bigger collecting area and parameters determined in the IVS WG3 Report [1]. This development will most likely be conducted in the framework of the ongoing development with Geoscience Australia.

Venture Southland, a regional development group, has acquired an 11m dish for its site in Awarua and is working with AUT to prepare it for radio astronomy. A high-speed network linking New Zealand research institutions is expected to be up and running in the second half of 2006, and will facilitate an eVLBI system.

We plan to conduct further VLBI tests with Australia, to study the opportunity for establishing Trans-Tasman eVLBI, and as a medium-term goal to explore possibilities to work with other VLBI stations (e.g. with Japan).

We plan to further strengthen collaboration between the Centre for Radiophysics and Space Research (AUT) and leading New Zealand geoscience/geodesy institutions, such as Land Infor-

mation NZ, and the Institute of Geological and Nuclear Sciences with the aim of sustaining the NZGD2000 and monitoring tectonic deformations.

A search for radio quiet sites for a New Zealand radio telescope facility is underway. New Zealand's geographic location makes it a natural place for possible extension of the planned Australian SKA from 3000 km to almost 6000 km baseline, increasing the spatial resolution of the SKA telescope. Four trial sites with favourable natural conditions, and well developed infrastructure and communications have been pre-selected as potential SKA sites. The level of RFI at the potential sites will be monitored in 2006. The New Zealand Ministry of Economic Development has granted $60,000 scholarship to an AUT postgraduate student to conduct this investigation.

4. Acknowledgements

We are very grateful to our colleagues from ATNF and the University of Tasmania who made our development possible.

References

[1] Arthur Niell, et al. VLBI2010: Current and Future Requirements for Geodetic VLBI Systems. IVS WG3 Report. IVS-NASA, September 16, 2005.

[2] IVS Annual Report 2004. Eds.: D.Behrend and K.D.Baver. Pp.4-5.

[3] Don Grant and Graeme Blick. The development and implementation of New Zealand Geodetic Datum 2000, presented at IUGG 99 General Assembly, Birmingham UK, July 1999.

[4] Sergei Gulyaev, Tim Natusch, et al. Development of New Zealand Radio Astronomy and Trans-Tasman Long-Baseline Array. Southern Stars, 44, 4, pp. 2-18, 2005.

Brian Corey et al.: Antenna Cross-Polarization Characteristics at Geodetic VLBI Stations, IVS 2006 General Meeting Proceedings, p.157–161
http://ivscc.gsfc.nasa.gov/publications/gm2006/corey

Antenna Cross-Polarization Characteristics at Geodetic VLBI Stations

Brian Corey, Michael Titus

MIT Haystack Observatory

Contact author: Brian Corey, e-mail: bec@haystack.mit.edu

Abstract

We describe the design, analysis, and preliminary results of observations carried out in July 1996 to measure the S/X-band cross-polarization response of the nominally right-circularly-polarized (RCP) feeds at geodetic antennas. At VLBA sites the left-circular (LCP) response is typically –22 to –28 dB relative to RCP, and always <–20 dB. Cross-polarization is significantly higher at some non-VLBA sites, with values of –20 to –15 dB at X-band. Corresponding errors in the X-band multiband delays due to the cross-polarization are of order 5–10 ps over 360 MHz on baselines to non-VLBA sites.

1. Introduction

A major source of instrumental error in geodetic VLBI is cross-polarization in the nominally right-circularly-polarized (RCP) antenna feeds [4]. For two antennas observing with imperfect RCP feeds, the interferometric signal on an unpolarized source, normalized relative to the response to a purely RCP source, is [1, 3]:

$$\frac{R_1 R_2^* \text{ (unpol source)}}{R_1 R_2^* \text{ (pure RCP source)}} \;=\; 1 \;+\; D_{1R}\, D_{2R}^*\, e^{2i(\phi_1 - \phi_2)} \qquad (1)$$

where D_{iR} is the LCP leakage term for the station i RCP feed given by the L/R complex ratio between the feed voltage responses to the two E-field polarization senses, and ϕ_i is the feed rotation angle (which, in the case of an alt-az antenna mount, is the parallactic angle). The group delay error τ_L caused by the LCP contamination is the partial derivative with respect to frequency of the argument of equation (1). For weak cross-polarization ($|D_{1R} D_{2R}^*| \ll 1$), τ_L reduces to the frequency derivative of the imaginary component and can be expressed as the sum of two terms:

$$\tau_L = A\, \cos 2(\phi_1 - \phi_2) \;+\; B\, \sin 2(\phi_1 - \phi_2) \qquad (2)$$

Because τ_L depends on feed rotation angle, it varies with pointing direction for all but equatorial-mount antennas, and hence is correlated with geometry. In general, the delay errors do not close around a triangle of stations.

The level of LCP contamination at some geodetic stations has been determined previously by two methods: (1) τ_L has been estimated from the geodetic group delays by fitting for the A and B coefficients in the equation above (D. MacMillan, 1993, unpublished); and (2) upper bounds on $|D_R|$, and therefore on τ_L, have been calculated from RL/RR fringe amplitude ratios measured in special experiments with dual-polarization stations (R. Potash, 1994, unpublished). Here, we describe the design, analysis, and preliminary results of observations carried out to determine the complex D terms, not just upper limits on their magnitude, for a large number of geodetic stations.

Table 1. Stations and frequency sequences for July 1996 polarization sessions

	RDPLR1	**NAPS2**	**GTRF11**	
Stations	FD-VLBA(Fd) HN-VLBA(Hn) KP-VLBA(Kp) LA-VLBA(La) OV-VLBA(Ov) PIETOWN(Pt)	ALGOPARK(Ap) GILCREEK(Gc) NL-VLBA(Nl) WESTFORD(Wf) YLOW7296(Yk)	BR-VLBA(Br) FORTLEZA(Ft) HOBART26(Ho) MK-VLBA(Mk) SC-VLBA(Sc)	DSS65(65) HARTRAO(Hh) KASHIMA(Ka) NYALES20(Ny)
Freq. sequence	6 special	CDP-SX	DSNVLBA	
# S/X freqs.	2 / 2 per seq.	6 / 8	6 / 8	
S/X total span	128 / 722 MHz	85 / 360 MHz	100 / 360 MHz	
Polarization	RCP & LCP	RCP only	RCP only	

2. The 1996 Polarization Experiments

On 22-23 July 1996, a special R&D experiment, RDPLR1, ran concurrently with two regular geodetic sessions, NAPS2 and GTRF11 — see Table 1 for some particulars. During each RDPLR1 scan, the six participating VLBA antennas recorded both polarizations at two S-band and two X-band frequencies. The RDPLR1 schedule had two distinct parts:

1. During the first eight hours, 3C84, OQ208, and 1308+326 were observed, with scans cycling through four different, dual-polarization, four-frequency sequences. The eight S- and eight X-band frequencies observed at the VLBA sites were selected to sample well the frequencies observed in the two geodetic sessions, and to include a few higher frequencies in each band.
2. During the remaining 16 hours, two of the RDPLR1 stations (Kp and La) were tagged along on NAPS2, and the other four (Fd, Hn, Ov, and Pt) were tagged along on GTRF11. In each session, the RDPLR1 stations alternated between two dual-polarization frequency sequences, for a total of four frequencies per band.

The observations with the RDPLR1 stations from all three sessions were processed at the MIT Haystack correlator. For most geodetic scans the SNR was expected to be too low to yield fringes for the cross-hands (RL) correlation; therefore only nine NAPS2 scans and 32 GTRF11 scans with high SNR were correlated.

3. Analysis

The analysis proceeded in two steps. First we estimated the VLBA D terms from the data from part 1 of RDPLR1, and then we applied the results to the data from the geodetic sessions.

The method used to estimate the D terms follows the procedure described in Section 4 of Roberts *et al.* [3] (see also [2]). We summarize the essential points here. For a radio source with no net circular polarization, the ratios between the cross-hands and parallel-hands (RR) visibilities may be written, to first order in the source fractional linear polarization and D terms, as

$$\frac{R_1 L_2^*}{R_1 R_2^*} \;=\; G_2^* \, (\tilde{M}_{12} \, e^{-2i\phi_2} \;+\; D_{1R} \, e^{+2i(\phi_1 - \phi_2)} \;+\; D_{2L}^*) \qquad (3)$$

$$\frac{L_1 R_2^*}{R_1 R_2^*} \;=\; G_1 \; (\tilde{M}_{21}^* \; e^{+2i\phi_1} \;+\; D_{1L} \;+\; D_{2R}^* \; e^{+2i(\phi_1 - \phi_2)}) \qquad (4)$$

where G_i is the L/R ratio between the complex voltage gains for station i, $\tilde{M}$ is the complex fractional linear polarization of the source, and D_{iL} is the RCP leakage term for the LCP feed. G_i can be estimated from the parallel-hands visibility ratios $L_1 L_2^* / R_1 R_2^*$, provided there are three or more stations in a scan. (The G_i phases cannot be determined unambiguously but must be referred to a reference station, which we chose to be Fd.) For 3C84 and OQ208, $|\tilde{M}|$ at centimeter wavelengths is $< 0.1\%$ [3], and the $\tilde{M}$ terms may consequently be ignored. The equations simplified in this manner are the basis for a linear least-squares solution for the unknown real and imaginary components of the D terms. It is essential that the feed angle difference $\phi_1 - \phi_2$ vary in the data set, in order to break the degeneracies among the D-term components that would otherwise occur.

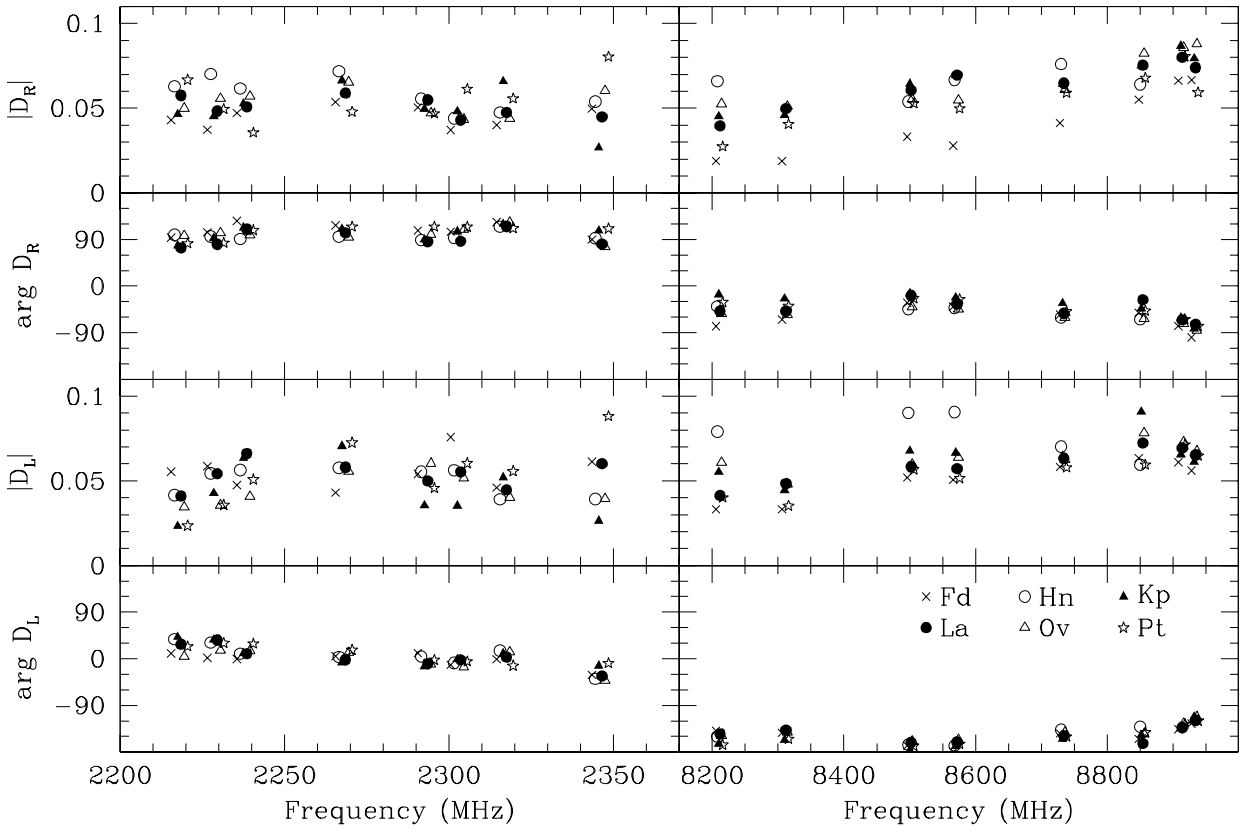

Figure 1. Frequency dependence of D terms for RDPLR1 VLBA stations. In descending order from top: D_R magnitude, D_R phase (in degrees), D_L magnitude, and D_L phase. In each plot, the magnitude or phase is plotted for 6 stations at 8 frequencies; in order to reduce overlap, the plot symbols for different stations are offset slightly in frequency. Based on the repeatability of the results of the LSQ solutions with different data sets and methods of weighting, the standard error σ in the real and imaginary components of D is estimated to be 0.005-0.010; the corresponding errors in the magnitudes and phases are σ and $\sigma/|D|$ radian, respectively. The uncertainties would have been signficantly lower but for a VLBA set-up problem that caused the loss of the first 100 minutes, during which the feed rotation angles were changing most rapidly.

Once the D terms for the six dual-polarization stations are known, they can be applied to the results of the geodetic observations to estimate the D terms for the NAPS2 and GTRF11 stations. During correlation, the "remote" station on each baseline (*i.e.*, station 2) was always a dual-polarization station. Using equation (3), one may then estimate the D_{1R} term for the geodetic station by dividing the observed RL/RR visibility ratio by the known (except for the reference $R-L$ phase at Fd) G_2^* station gain ratio, subtracting the known quantity D_{2L}^*, and then counter-rotating by $2(\phi_1 - \phi_2)$. $\tilde{M}$ is assumed to be zero. Because some of the geodetic sources have fractional linear polarizations up to a few percent on VLBI scales, the results may be corrupted at this level. The hope is that, by averaging the D terms over multiple sources and (u, v) spacings, the error introduced by neglecting $\tilde{M}$ will be ∼1% or less. Observations on the highly polarized quasar 1921-293 were excluded from the analysis.

4. Results

Figure 1 presents the D terms estimated from the dual-polarization data acquired by the VLBA antennas on 3C84 and OQ208, during the first part of RDPLR1. In no case does the magnitude exceed 0.1 in voltage, or –20 dB in power. While the magnitudes often differ by a factor of 2-3 among the six stations, the phases are tightly clustered. The multiband error τ_L estimated from the D_R terms has a maximum magnitude of 1.0±0.1 ps at X and 2.2±0.5 ps at S over all feed angles $\phi_1 - \phi_2$ and over all 15 VLBA-VLBA baselines.

The D_R terms estimated for the non-RDPLR1 VLBA stations in NAPS2 and GTRF11 (*viz.*, Nl, Br, Mk, and Sc) in the second stage of the analysis are consistent with those in Figure 1.

The D_R terms deduced for the non-VLBA geodetic antennas in NAPS2 and GTRF11 are generally larger than for the VLBA antennas, as shown in Figure 2. The S-band cross-polarization at Yk is particularly strong. The X-band cross-polarization at the four NAPS2 stations is generally $>$ –20 dB. The fact that the X-band characteristics – especially the frequency dependence of the phase – at these four stations are similar is to be expected, as they use the same type of feed.

Table 2. S-band / X-band τ_L^{max} (ps) for baselines among four NAPS2 stations and for Kp-NAPS2 baselines

	Ap	**Gc**	**Wf**	**Yk**
Ap		14 ± 4 / 5 ± 2	8 ± 2 / 9 ± 1	43 ± 7 / 8 ± 2
Gc			8 ± 3 / 4 ± 2	45 ± 12 / 2 ± 3
Wf				24 ± 6 / 6 ± 2
Kp	4 ± 2 / 6 ± 1	8 ± 2 / 5 ± 1	3 ± 1 / 7 ± 1	14 ± 4 / 9 ± 1

Table 2 lists the maximum magnitude of τ_L calculated over all $\phi_1 - \phi_2$ for the baselines among the four NAPS2 stations in Figure 2, and for the baselines between a representative VLBA station, Kp, and the NAPS2 stations. (For weak cross-polarization, τ_L^{max} is simply the root-sum-square of the A and B coefficients in equation (2).) The similarity in the frequency dependence of the X-band D_R phases among the NAPS2 stations is largely responsible for the relatively small values of τ_L^{max} on the NAPS2 baselines: because the argument of $D_{1R}D_{2R}^*$ is small, the frequency dependence of the argument of equation (1) is reduced from what it otherwise might be. Indeed, it is the difference in the X-band D_R phase characteristics between Kp and the NAPS2 stations that causes τ_L^{max} on the Kp baselines to have values in the same range as those on the internal NAPS2 baselines

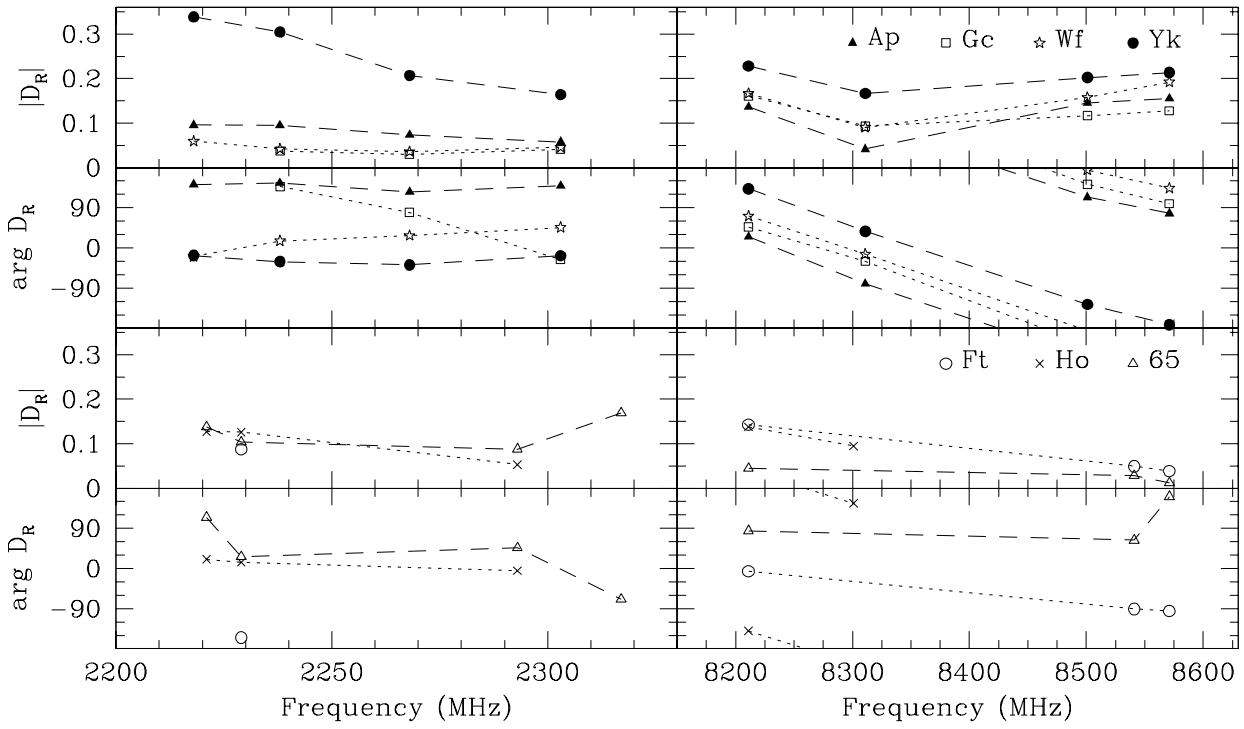

Figure 2. Frequency dependence of D_R for selected geodetic stations. Top plots show the magnitude and phase (in degrees) for four NAPS2 stations, and the lower plots do the same for three GTRF11 stations. Each point represents the mean of $\geq$2 D_R estimates ($\geq$5 in most cases) from different scans or different baselines. Based on the rms scatter of $\leq$0.03 in the real and imaginary components, the standard errors σ in these components are estimated to be 0.01-0.02; the corresponding errors in the magnitude and phase are σ and $\sigma/|D_R|$ radian, respectively.

despite the much smaller $|D_R|$ magnitudes for Kp.

Because the NAPS2 D terms are available at only four frequencies, the values in Table 2 should be considered only illustrative of what τ_L^{max} would be in a geodetic session with more, or different, frequency channels, especially if the new frequency sequence spans a wider RF bandwidth.

References

[1] Herring, T.A., Precision and Accuracy of Intercontinental Distance Determinations Using Radio Interferometry, Ph.D. thesis, MIT, 1983.

[2] Massi, M., G. Comoretto, M. Rioja, G. Tofani, Baseline Errors on European VLBI Network Measurements: II. Instrumental Polarization, Astron. Astrophys. Suppl., **116**, 167-176, 1996.

[3] Roberts, D.H., J.F.C. Wardle, L.F. Brown, Linear Polarization Radio Imaging at Milliarcsecond Resolution, Astrophys. J., **427**, 718-744, 1994.

[4] Rogers, A.E.E., Instrumentation Improvements to Achieve Millimeter Accuracy, in Proceedings of the AGU Chapman Conference on Geodetic VLBI: Monitoring Global Changes, NOAA Technical Report NOS 137 NGS 49, 1-6, 1991.

Claudio Abbondanza et al.: An Investigation on a GPS-based Approach to Local Tie Computation, IVS 2006 General Meeting Proceedings, p.162–166
http://ivscc.gsfc.nasa.gov/publications/gm2006/abbondanza

An Investigation on a GPS-based Approach to Local Tie Computation

Claudio Abbondanza [1], *Monia Negusini* [2], *Pierguido Sarti* [2], *Luca Vittuari* [1]

[1)] *DISTART, Università di Bologna, Italy*
[2)] *IRA, Istituto Nazionale di Astrofisica, Italy*
Contact author: Claudio Abbondanza, e-mail: claudio.abbondanza@mail.ing.unibo.it

Abstract

The estimation of eccentricity vectors at co-location sites represents a crucial aspect in order to combine reference frames stemming from different space-geodetic techniques. We investigate the possibility to pursue a thorough eccentricity vector estimation via a GPS Survey. Unlike terrestrially estimated eccentricities, the GPS derived ties have the following qualities: they are easy to perform—not requiring very highly specialized manpower and fatiguing surveys—and save time, thus allowing to speed up the whole process (from survey to computation). Here we examine the local tie derived from a GPS Survey that was conducted at the Astronomical Observatory of Medicina (Italy) in 2002, the proper geometrical modelling of the tie computation and the correct fitting into an ITRF frame. In the case at hand, the GPS derived tie is checked through a comparison with the terrestrial local tie performed at the same co-located site of Medicina.

1. Introduction

This investigation elaborates on the possibility of determining the local tie through a **purely GPS-based survey** performed at the ITRF co-located site of Medicina (Italy). Each local tie is characterized by an intrinsic precision not only related to the way it has been surveyed but also to the proper geometrical modelling and, consequently, to the conditions applied during the least-squares estimation in a rigorous, statistically-based procedure. Furthermore, if a terrestrial survey is executed, the eccentricity vector components, finally aligned to ITRF, seem to depend on the transformation performed in order to carry out the transition from the local topocentric reference frame, where the tie was classically surveyed, and the final realization of ITRF [1]. Processing and obtaining local eccentricities vectors via GPS-based surveys could allow to overcome the difficulties related to the aforementioned RF transition. In fact, since GPS directly operates in a geocentric reference frame, the transition to ITRF is automatically achieved avoiding the difficulties related to measuring the deflections of the vertical. The local ties computation has been done so far using CLEMeNT (Co-Location Estimation Model et Network Transformation), a in-house software, which showed satisfactory results in least-squares estimations both for highly precise terrestrial datasets [2] and for simulated and intrinsically noisy ones [3]. The accuracies reached in processing noisy datasets have inspired the possibility to perform GPS based local ties by means of a new release—**GPS-CLEM**— modified *ad hoc* in its structure in order to include a brand new ensemble of constraints which are going to strengthen the definition of the tracking points of the local tie.

2. GPS Datasets Used in the Analysis

The datasets here analyzed were acquired in September 2002 using 5 GPS receivers, in a survey context usually defined as *rapid-static*. Three out of five GPS antennae were fixed on three ground reference pillars, while two roving receivers were installed on the external part of the VLBI dish, thus describing circular arcs during the rotations of the radiotelescope. The GPS data processing has been executed by means of the Bernese GPS software V4.2 [5]. The data collected during the aforementioned campaign have been processed along with data acquired by the permanent IGS station installed at the same co-located site. Unfortunately, a failure in the power supply due to a thunderstorm brought about an interruption of the planned schedule. The VLBI antenna was moved in elevation and azimuth in such a way that the two mobile GPS antennae acquired observations at a given position for 15 minutes. The data were processed using a rapid static approach [4], utilizing two different phase center variation models: the IGS and NGS relative PCV (elevation-dependent models). As shown later, the choice of a PCV model considerably impacts the eccentricity vectors estimation.

3. The GPS Based Local Ties Estimation Procedure

The eccentricity vectors represent the geometrical connections between the reference points, each of them belonging to a specific space-geodetic technique. Regarding the case of Medicina, the *local tie* can be reckoned as the vector bridging the VLBI tracking point and the GPS *ARP* (Antenna Reference Point). A rigorous, statistically based estimation of the local ties has been performed so far using CLEMeNT, an in-house software implemented in Matlab environment and developed by a French-Italian Joint Research Group. It provides a **LSE** (Least-Squares Estimation) of the eccentricity vectors of co-located techniques performing, at the same time, a Network Transformation in order to align the local tie into a specific ITRS realization; for more details the interested reader is referred to [2]. The set of condition and observation equations, translated into a LSE context, creates the stochastic kernel of **CLEMeNT**; in fact, it executes an estimation process based on an approach performing a Mixed Model Least-Squares Adjustment (see e.g. [6]). The GPS points' coordinates, resulting from the Bernese v.4.2 GPS processing, are treated as new unknowns in the estimation process and, at the same time, they play the role of observations, each of them provided with an *a priori* statistical information (the complete variance-covariance matrix). Furthermore geometrical constraints which define the tracking points of the involved space-geodetic techniques are properly translated and included into the same estimation context, playing the role of condition equations that the cloud of points must strictly comply with.

4. The New Software Release: GPS-CLEM

The core of **GPS-CLEM**, in the stochastic structure itself, has remained unchanged, but unlike the former release it is a GPS focused one. New features have been introduced, extending the software's capabilities: an additional module has been added, which performs statistical testing focusing on the standardized observational residuals (Data Snooping) and allows to identify and localize potential blunders affecting the observations. The introduction of new geometric conditions on the surveyed set of points entails the possibility to extract further geometric parameters strictly related to the space-geodetic technique involved in the tie computation (for instance, the axis offset

of the VLBI antenna).

5. A Deeper Look into GPS-CLEM: The New Ensemble of Implemented Conditions

Here we summarize the conditions applied:

1. **Intra-group parallelism of elevation and azimuthal surfaces** As the VLBI radiotelescope moves, the mobile GPS receivers register the points' positions occupied in the rapid static survey so that they theoretically describe canonical planar curves. During the rotation in elevation, the mobile GPS receivers describe a group of elevation circles: they are simultaneously surveyed and have to be parallel to each other. Similarly during the rotational motion in azimuth, the GPS receivers describe horizontal circles; the circles pertaining to this group must be parallel to each other.
2. **Inter-axial orthogonality** The condition refers to the two principal axes involved in the radiotelescope rotations imposing the two representative VLBI axes to be mutually orthogonal.
3. **Equivalence of elevation circles' radius** The elevation circle arcs traced out by the same GPS antenna and belonging to different elevation axis realizations must have the same radius.
4. **Axis offset estimate** This condition leads to define the VLBI axis offset valid for a radiotelescope, e.g. as in the Medicina case. Since the axis offset can be regarded as the Euclidean distance between one of the moving axis and the fixed axis, we can compute an offset from each realization of the elevation axis. As the axis offset is an intrinsic geometrical feature for the radiotelescope, it has to be univocally defined; hence we can set the axis offsets computed from different realizations to a unique value in the estimation procedure.

6. Running GPS-CLEM

The procedures involved in a typical GPS-CLEM run are as follows: 1. Reading input data coming from the **BERNESE 4.2** GPS postprocessing software; 2. Application of **Geometrical Conditions** to the sets of points described by the GPS antennae; 3. Building of the **Normal Conditioned Linear System** implied by the **MMLSA** (Mixed Model Least-Squares adjustment); 4. Estimation in a least-squares sense of the VLBI radiotelescope Invariant Point; 5. Recursive **Data Snooping** procedure in order to erase the points' coordinates burdened with blunders; 6. Insertion of additional points involved in the local tie computation; 7. Extraction of the SINEX file which contains the local tie estimate including its variance-covariance (vcv) matrix.

7. Performing the Solutions through GPS-CLEM

The Medicina eccentricity vector has been measured within a local ground control network during four different terrestrial surveys (2001, 2002, 2003 and 2005). In this investigation we compare the results obtained during the 2002 terrestrial campaign and the purely GPS-based survey carried out in the same period. The solution criterion we have adopted provides different tie estimations gradually increasing the applied constraints from a low degree of conditions to a high one, so displaying the effects of the conditions over the eccentricity vectors. Here the performed

solution types are reported, in association with the name tags used during the processing: **(cum1)** applies the *Loosely Constrained Solution* provided with the former release of CLEMeNT; **(cum4)** adds to the previous approach the intra-group parallelism condition; **(cum5)** applies the conditions of intra-group parallelism and interaxial orthogonality; **(cum2)** adds the univocal estimate of the axis offset; **(cum3)** furnishes the further condition of radius' equivalence.

8. Analysis of GPS Derived Tie Solutions

The analysis of the performed solutions relies on two different aspects: first, a comparison between the terrestrial-classical tie and the GPS tie, both aligned to ITRF aimed at evaluating the agreement of the GPS tie to the classical one. Because of the effects of the alignment procedure of the classical tie from the topocentric system to the ITRF, great attention must be paid to the Euclidean norm of the eccentricity vector, which is invariant for the reference system changes. Secondly, an evaluation of the accuracy reached in the tie computation in the terms of vcv components. It has to be emphasized that the 2002 Medicina terrestrial tie has been determined by means of a loosely conditioned solution. This is the reason why, as shown in Figure 1, an excellent agreement between the **(cum1)** GPS based local tie and the terrestrial one in the terms of modulus has been achieved. Furthermore the solutions display a relevant dependence on the chosen PCV antenna model, both in the eccentricity vector moduli and in their accuracy. Best results have been obtained with the NGS PCV model performing a Data Snooping. Figure 2 points out the differences coming from the PCV model choice for solution **(cum2)**.

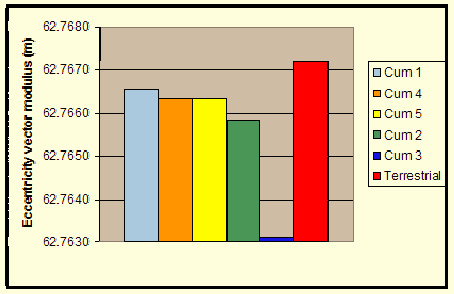

Figure 1. Local tie modulus variation (NGS PCV)

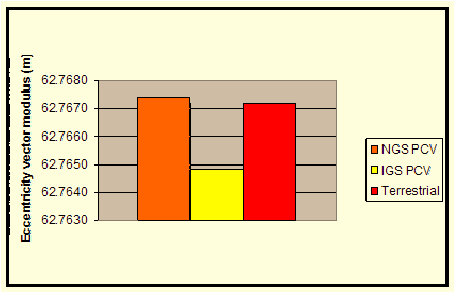

Figure 2. Influence of PCV over local tie modulus (**cum2**)

It has to be pointed out that, as the number of applied conditions increases, the tie accuracy generally improves, with the exception for the **(cum3)** case (Figure 3). Best agreement and accuracies have been achieved in the case of NGS PVC model with a (cum2) solution. Figure 4 shows the differences of the geocentric components between the terrestrial local tie and the GPS derived one.

9. Conclusions and Future Developments

The GPS local tie survey has great advantages if compared with the terrestrial survey: it is time-saving and easy to perform, there is no need of high precision topographic survey skills and, in principle, local ties could be performed regularly at all VLBI co-location sites. At the same time,

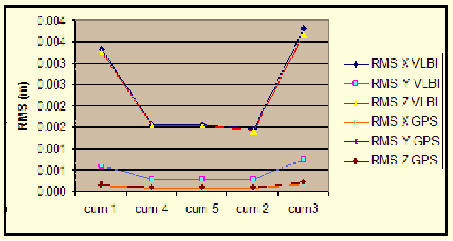

Figure 3. RMS of geocentric components of the tie

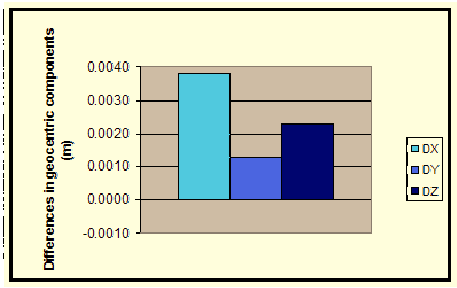

Figure 4. GPS based minus classical tie

this approach to computation provides encouraging results, which suggest further investigations. The ensemble of computed solutions displays a relevant dependence on the Phase Centre Variation modelling. This is the reason why an absolute PCV model will be tried out in the forthcoming future. Furthermore the differences in the geocentric components between the terrestrial local tie and the GPS derived one have to be carefully investigated, for the terrestrial local ties, in the attempt of isolating the effect of reference system transformation. The accuracies achieved with this approach, regarding that the analyzed datasets are quite critical from the geometrical point of view. As a matter-of-fact, beyond the shortcomings strictly related to the GPS technique which strongly affect the solution—multipath effects, satellite constellation not uniformly accessible as the radiotelescope moves—the employed datasets show a geometrical weakness as a consequence of a black-out that occurred at the observatory during the survey. Considering the scarcity in the number of involved surfaces, it could be of interest to strengthen the geometrical robustness by adding surveyed points, which results in an increased overall redundancy in the estimation process.

References

[1] Ray, J., Z. Altamimi, Evaluation of co-location ties relating the VLBI and GPS reference frames Journal of Geodesy (2005) 79: 189-195.

[2] Sarti, P., P. Sillard, L. Vittuari, Surveying co-located space geodetic instruments for ITRF computation Journal of Geodesy (2004) 78:210-222.

[3] Dawson, J., G. Johnston, P. Sarti, L. Vittuari, Indirect approach to invariant point determination for terrestrial frame reference computation In: IAG Symposium Proceedings, Cairns, 2005.

[4] Tomasi, P., P. Sarti, L. Vittuari, M. Negusini, 2002 local geodetic survey of VLBI and GPS reference points and ex-centre at Medicina, Proceedings of Working Meeting on European VLBI for Geodesy and Astrometry, Leipzig, (2003).

[5] Hugentobler, U., S. Schaer, P. Fridez, Bernese GPS Software Version 4.2. (Eds. 2001) Astronomical Institute, University of Berne, pp. 515.

[6] Sillard, P., Estimation par moindres carrès, Collection IGN, Éditeur Lavoisier, 2001.

Daniel Hernandez et al.: GPS on the VLBI Telescopes at Onsala and Ny-Ålesund, IVS 2006 General Meeting Proceedings, p.167–171
http://ivscc.gsfc.nasa.gov/publications/gm2006/hernandez-haas

GPS on the VLBI Telescopes at Onsala and Ny-Ålesund

Daniel Hernandez, Rüdiger Haas

Onsala Space Observatory, Department of Radio and Space Science, Chalmers University of Technology
Contact author: Rüdiger Haas, e-mail: haas@oso.chalmers.se

Abstract

In the years 1999 and 2000 the VLBI stations at Onsala and Ny-Ålesund were equipped with GPS antennas mounted on top of the radio telescopes. Since then several GPS measurement campaigns were carried out to check the stability of the telescopes and to monitor the local tie between the reference monuments for the International VLBI Service for Geodesy and Astrometry (IVS) and the International GPS Service (IGS). In this paper we present the results of the analysis of the GPS observations recorded since the antennas were installed.

1. Introduction

The Onsala Space Observatory has a long record in geodetic VLBI observations, going back to the late 60ies of the last century [1]. Today it is an active network station in the International VLBI Service (IVS). Since the late 1980ies, the observatory is also active in using the Global Positioning System (GPS), and contributes today as network station to the International GNSS Service (IGS). The Ny-Ålesund Geodetic Observatory is active in both IVS and IGS since the 1990ies [2].

Both space geodetic stations play an important role for the International Terrestrial Reference Frame (ITRF) due to their northern location and the availability of co-located geodetic techniques. The precise knowledge of the local geodetic tie between the reference points of the co-located techniques and the monitoring of its stability over time is fundamental for the maintenance of the ITRF. Furthermore it is a crucial prerequisite for a combined use and interpretation of VLBI and GPS data for geophysical and geodynamical investigations.

2. GPS Antennas on the Radio Telescopes at Onsala and Ny-Ålesund

In the summer of 1999 two choke ring GPS antennas were installed on the 20 m radio telescope at Onsala [3]. One of the antennas was permanently mounted on the top of the sub-reflector structure close to its Apex position, therefore this antenna is referred as APEX in the following. The other antenna was sporadically mounted close to the Vertex position of the telescope and is therefore referred as VTEX in the following.

The 20 m radio telescope at Ny-Ålesund is different from the one at Onsala. The most important differences are that this telescope is of prime-focus type, thus does not have a sub-reflector, and that it is not enclosed by a radome. The ideal position to install a GPS antenna was the Vertex position where an antenna was mounted in the summer of 2000 [4], called NVTX in the following. The installation project was supported as an LSF-project of the EC and by the Norwegian Mapping Authority (Statens Kartverk). Unfortunately, the GPS antenna had to be dismounted in the summer of 2004.

3. GPS Data and Analysis

GPS observations were performed with APEX, VTEX and NVTX on campaign basis. The campaign could only be observed when the radio telescopes were not occupied with other observing activities, e.g. geodetic VLBI measurements. Thus, no continuous observation campaigns for longer than a week were available, and there are large gaps between different campaigns.

During the observation campaigns GPS data were recorded every 30 seconds while the telescopes were pointing close to zenith for at least 24 hours. The data were analyzed using the two software packages GIPSY-Oasis II [5] and Bernese GPS Software Version 5.0 [6].

For the first analysis step we used GIPSY-Oasis II with the Precise Point Positioning strategy (PPP) [7]. This analysis approach allows a quick first check of the data quality and reveals epochs with obvious problems that have to be excluded from the further data analysis. The left picture in Fig. 1 shows an example of postfit phase residuals from a PPP-solution for the APEX antenna at Onsala. The residuals are roughly within ±3 cm and indicate that the data are useful for a more detailed analysis.

The next analysis step was performed with the Bernese GPS software. Here we used the double difference approach on the short baselines between the local IGS monuments and the GPS antennas on the radio telescopes. The main advantage is that this strategy completely eliminates the satellite and receiver clock errors. We estimated relative tropospheric parameters for one of the stations on the short baselines, applying standard mapping functions [8]. A quasi-ionosphere-free analysis approach was used since the distance between the telescopes and the reference stations are very short, i.e. less than 100 m. The data of the IGS reference stations were downloaded from SOPAC GPS data archive [9]. The right picture in Fig. 1 shows an example of residuals for an L1-only solution on the baseline ONSA–APEX. The residuals are roughly within ±1 cm, indicating that the double difference approach is more accurate than the PPP-solution.

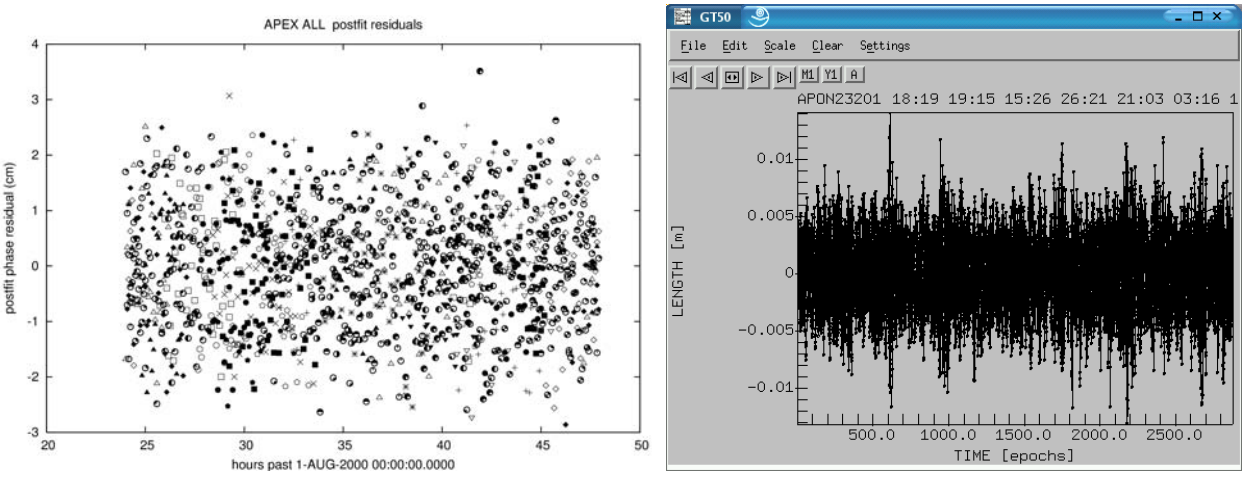

Figure 1. Left: Postfit phase residuals in (cm) from a GIPSY PPP-solution. Right: L1-residuals in (m) from a Bernese double-difference analysis for the baseline APEX-ONSA.

4. Results for North, East and Up Components

Data from both stations were analyzed in detail with Bernese using the double differencing strategy. We performed L1-only, L2-only, and ionospheric-free L3-solutions. The L1- and L2-only solutions gave clearly better results. The results are baseline components relative to the local IGS reference stations. Unfortunately, the telescopes at both stations were not positioned exactly into the zenith position during the GPS campaigns, but deviated by up to 1.5° in elevation. We tried to correct for this mis-positioning by applying a correction for it whenever we had exact information about the telescope position. We used an average elevation for those epochs where we did not have the exact information about the telescope elevation. Mean positions were subtracted from the coordinates, resulting in time series of relative north, east and up components. Obviously outliers were removed from the time series. For Ny-Ålesund we also analyzed data from the second IGS site NYA1 as a reference in order to be able to check the reliability of the NVTX analysis. We picked the same epochs for which data for NVTX were available.

Fig. 2 shows time series of North, East and Up components relative to a mean value for APEX in the left and VTEX in the right picture. The results for NVTX and NYA1 at Ny-Ålesund are shown in Fig. 3 in the left and right picture, respectively. The formal errors of the individual data points are on the order of 0.2-0.3 mm for the North and East components, and 1.0-1.3 mm for the Up component. The corresponding repeatabilities for APEX, VTEX, NVTX and NYA1 expressed as root-mean-square (RMS) values are shown in Table 1.

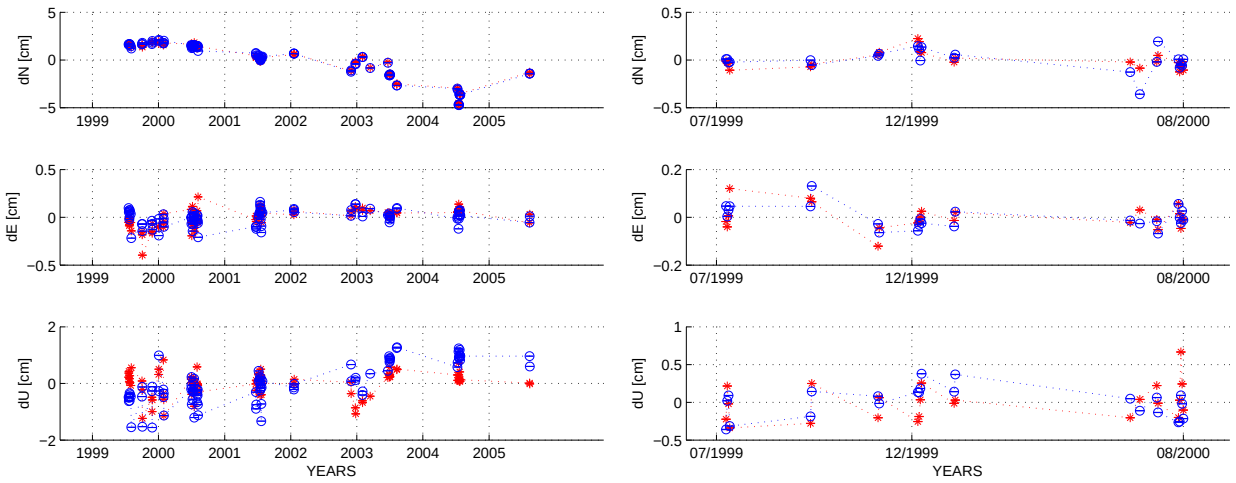

Figure 2. Time series of daily solutions for APEX (left) and VTEX (right). Shown are delta North (dN), delta East (dE) and delta Up (dU) in centimeters with respect to a mean value. Stars (red) correspond to L1-solutions, circles (blue) to L2-solutions.

5. Discussion and Conclusions

The results show that the repeated GPS campaigns on the radio telescopes at Onsala and Ny-Ålesund do give RMS repeatabilities on the order of a couple of mm to cm. The two different solutions, L1 and L2, mainly follow each other quite well, however with biases.

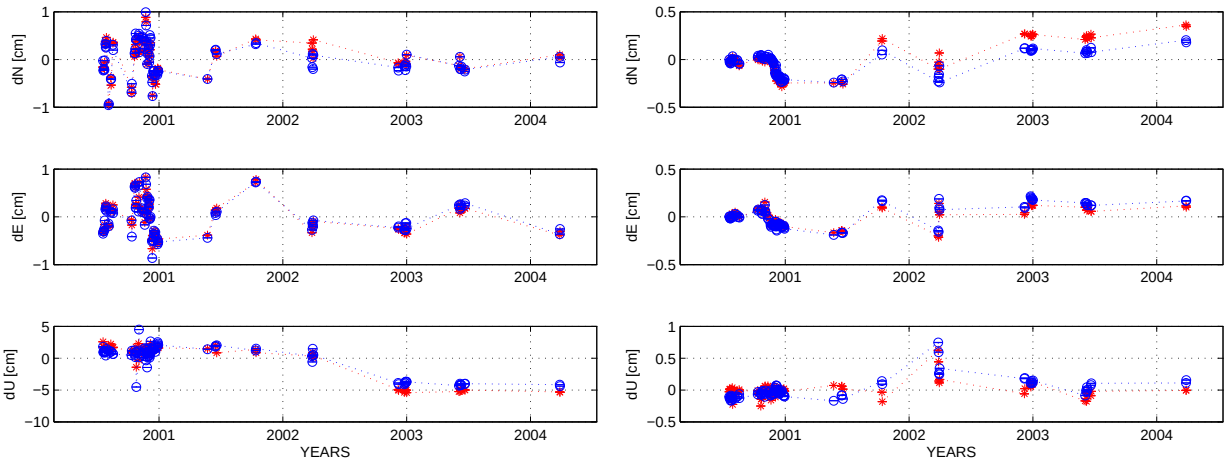

Figure 3. Time series of daily solutions for NVTX (left) and NYA1 (right). Shown are delta North (dN), delta East (dE) and delta Up (dU) in centimeters with respect to a mean value. Stars (red) correspond to L1-solutions, circles (blue) to L2-solutions.

Table 1. North, East and Up repeatabilities in mm for APEX, VTEX, NVTX and NYA1 for L1 and L2 solutions. The footnotes for NVTX mean: (1) all NVTX data, (2) only NVTX data until July 2002, (3) only NVTX data after July 2002.

	APEX		VTEX		NVTX[1]		NVTX[2]		NVTX[3]		NYA1	
component	L1	L2	L1	L2	L1	L2	L1	L2	L1	L2	L1	L2
North	20.0	20.0	0.8	1.0	3.5	3.5	4.1	3.9	0.9	1.0	1.6	1.1
East	0.8	0.7	0.4	0.4	3.3	3.3	2.8	2.8	2.4	2.4	0.9	1.0
Up	3.0	6.6	2.2	2.0	28.8	23.1	4.4	4.8	1.5	2.0	1.1	1.4

The APEX North component appears to show some drift over time that also reflects in the large RMS value of about 20 mm. The values in 1999 and 2000 lie close together, however the later values differ from these first data points. We do not have an explanation for this, but suspect that there was a difference between the different observation campaigns concerning whether a pointing model was used or not. The use of a pointing model does slightly change the telescope elevation and azimuth. Unfortunately, we do not have information about the telescope elevation for all observation epochs, and thus could not correct for the deviation from the zenith for all epochs with appropriate corrections. Also the Up component of APEX seems to show some drift. However, a mis-pointing of the telescope does influence the North and East components much more than the Up component. Therefore, we hesitate to explain the variation in the Up-component by whether a pointing model was used or not. The APEX East component gives an RMS repeatability below 1 mm.

For VTEX we have unfortunately only few data points. Due to modifications in the telescope receiver cabin it was not possible to keep the mounting equipment for the VTEX antenna in place after 2000. The RMS repeatability values are on the order of roughly 3 mm.

We suspect that both APEX and VTEX did suffer from increased multipath effects due to the

metal structure of the radome enclosing the Onsala 20 m radio telescope.

The time series for NVTX show better results for the North and East components than for the Up component. The Up component appears to be affected by a bias in the summer of 2002, which reflects in the large RMS values of 29 and 23 mm for the L1 and L2 solutions. The exact reason for this bias is unknown to us, but may be due to dismounting and re-mounting of the antenna during an LSF-project in the summer of 2002 [10]. If we use only data before or after July 2002 the RMS repeatability for the Up component reduces considerably, see Table 1. Compared to NYA1, the NVTX results are worse by a factor of about 3. This might partly be explained by a higher level of multipath at the vertex position of the radio telescope compared to the NYA1 GPS monument.

In general, the current level of accuracy of the performed measurements does not allow to monitor local-ties with sub-mm accuracy. This appears only to be possible with classical geodetic methods that have been performed at Ny-Ålesund and Onsala previously [10], [11]. For the GPS measurements on the VLBI telescopes the knowledge of the exact position of the radio telescope in terms of elevation and azimuth is of crucial importance. Thus, in future measurement campaigns we need to monitor the antenna position more precisely.

References

[1] Scherneck, H.-G., Elgered, G., Johansson, J.M., Rönnäng, B.O.: Space geodetic activities at the Onsala Space Observatory: 25 years in the service of plate tectonics. *Phys. Chem. Earth*, **23**, 811–824, 1998.

[2] Digre, H. G., Rekkedal, S., Holland, D. C., Hanssen, R. I., Plag, H.-P.: NYAL Ny-Åelsund 20-metre Antenna. *IVS Annual Report 1999*, ed. N. R. Vandenberg, NASA/TP-1999-209243, 80–84, 1999.

[3] Bergstrand, S., Haas, R., Johansson, J.: An Independet Stability Check of the Onsala 20m Radio Telescope Using the Global Positioning System. *14th Working Meeting on European VLBI for Geodesy and Astrometry*, ed. P. Tomasi, F. Mantovani, M. Perez Torres, 83–88, 2000.

[4] Haas, R., Bergstrand, S., Johansson, J.: Establishing a New GPS-VLBI tie at NyÅlesund. *14th Working Meeting on European VLBI for Geodesy and Astrometry*, ed. P. Tomasi, F. Mantovani, M. Perez Torres, 73–78, 2000.

[5] Webb, F. H., Zumberge, J. F.: An introduction to GIPSY/OASIS-II. *JPL Publication D-11088*, Jet Propulsion Laboratory, Pasadena, 1993.

[6] Hugentobler, U., Dach, R., Pierre, F.: Bernese GPS Software Version 5.0. *Printing Office of the University of Bern*, 2004.

[7] Zumberge, J. F., Hefflin, M.B., Jefferson, D.C., Watkins, M.M., Webb, F.H.: Precise point positioning for the efficient and robust analysis of GPS data from large networks. *J. Geophys. Res.*, **102(B3)**, 5005–5018, doi:10.1029/96JB03860, 1997.

[8] A.E. Niell, "Global mapping functions for the atmosphere delay at radio wavelength", *J. Geophys. Res.*, **101(B2)**, 3227–3246, doi:10.1029/95JB03048, 1996.

[9] `ftp://garner.ucsd.edu/pub/rinex`

[10] Steinforth, C., Haas, R., Lidberg, M., Nothnagel, A.: Determination of Local Ties at Ny-Ålesund. *Proc. IERS Workshop on site co-location*, ed. B. Richter, W. Schwegmann, and W. R. Dick, **IERS TN-33**, Verlag des Bundesamtes für Kartographie und Geodäsie, 84–92, 2005.

[11] Haas, R., Eschelbach, C.: The 2002 Local Tie at the Onsala Space Observatory. *Proc. IERS Workshop on site co-location*, ed. B. Richter, W. Schwegmann, and W. R. Dick, **IERS TN-33**, Verlag des Bundesamtes für Kartographie und Geodäsie, 55–63, 2005.

P. Bolli et al.: Photogrammetry, Laser Scanning, Holography and Terrestrial Surveying of the Noto VLBI Dish, IVS 2006 General Meeting Proceedings, p.172–176
http://ivscc.gsfc.nasa.gov/publications/gm2006/bolli

Photogrammetry, Laser Scanning, Holography and Terrestrial Surveying of the Noto VLBI Dish

P. Bolli [1], *S. Montaguti* [1], *M. Negusini* [1], *P. Sarti* [1], *L. Vittuari* [2], *G.L. Deiana* [3]

[1)] *IRA-INAF, Bologna, Italy*
[2)] *DISTART, Università di Bologna, Italy*
[3)] *OAC-INAF, Cagliari, Italy*

Contact author: P. Sarti, e-mail: p.sarti@ira.inaf.it

Abstract

Since the late 90's, different surveying approaches have been independently applied to the Noto VLBI antenna. In particular, holography, photogrammetry, triangulation, trilateration, GPS and laser scanning have been used for determining the shape, the deformation and the position of the radiotelescope, its dish and its components. These datasets represent an interesting source of independent information that must be compared, combined, processed and used for validation with a comprehensive approach. We briefly summarize the experiments carried out at the antenna by different groups that are active within the Institute of Radioastronomy, explicitly referring to their work and highlighting the potentials of a combination of these methods and their results.

1. Introduction

In 2001 an active surface system was implemented on the Noto antenna [1]. It has been realized through 244 electromechanical actuators under computer control. They ensure that the paraboloid is maintained at each elevation. The actuators were mounted underneath each convergence panel forming the primary mirror (Figure 1). The main goal of the active surface is to recover the misalignment of panels induced by gravitational effects. If the active surface is properly working, a flattening of the antenna gain curve over elevation is expected.

Figure 1. Actuators of the active surface installed in Noto.

Figure 2 shows a comparison between measurements made at 43 GHz (Cassegrain focus) with and without enabling the active surface. Other antenna efficiency measurements performed at different frequencies can be found at: http://www.ira.inaf.it/actsurface/index.html.

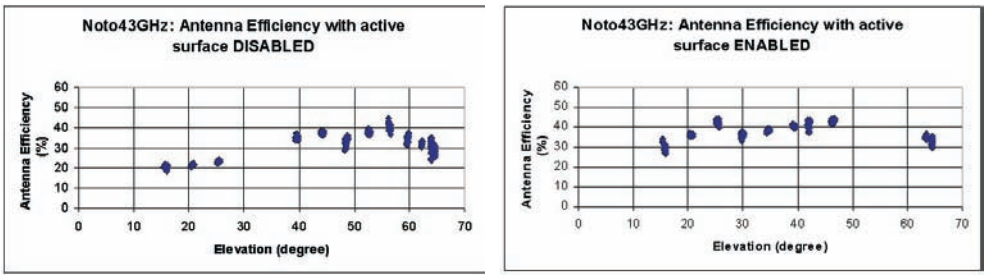

Figure 2. Antenna efficiency at 43 GHz not using (left) and using (right) the active surface.

Photogrammetry, terrestrial measurements, holography, and laser scanning, among other techniques, can be applied in a comprehensive investigation of the shape of the dish, thus improving the antenna's performance and the accuracy of the technique itself.

2. Photogrammetry

Photogrammetry is a three-dimensional coordinate measuring technique that is based on processing of images, its main products being Digital Surface Models (DSMs), orthoimages and 3-D reconstruction of the objects. Processing is usually made by an analytical plotter or a Digital Photogrammetric System (DPS). By taking photographs of an object from at least two different locations, the overlapping part of each stereopair can be mapped in 3-D. Photogrammeric surveys of Noto's antenna surface were performed in December 2000 and April 2002 [2] using a large format (230mm x 230mm) terrestrial metric camera CRC1 (Geodetic System Inc.). Figure 3 shows the differences between the theoretical shape of the VLBI parabola and the real shape as determined in 2000.

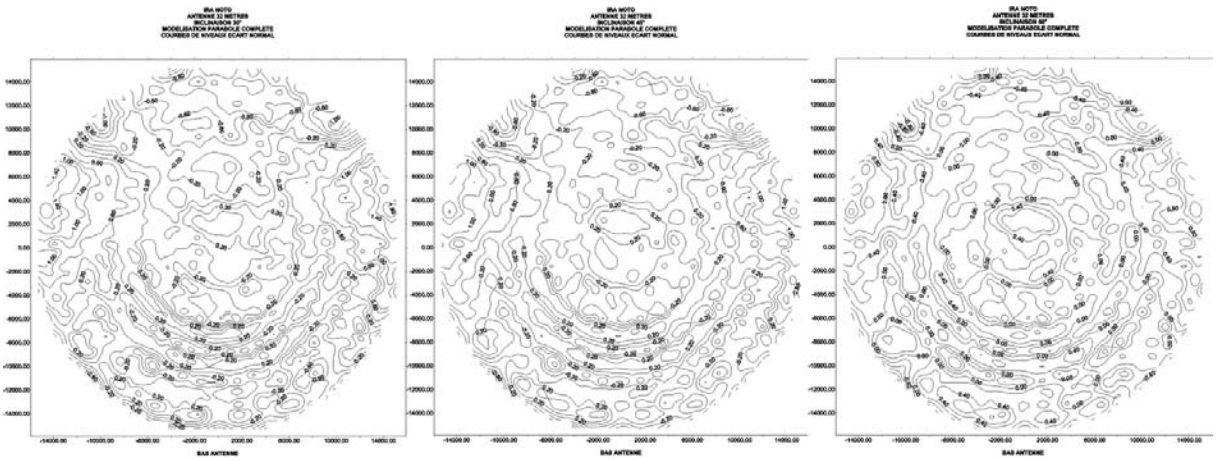

Figure 3. Difference with respect to the theoretical shape of the parabola (mm), at 30, 45, 60 of elevation (focal lengths: 10256.21mm, 10257.23mm and 10257.74mm respectively).

3. Holography

Holography is a very promising technique to evaluate the real profile of the radiotelescope mirrors. System requirements for performing holographic surveys can be easily satisfied at a well-equipped radio astronomical observatory. A holographic survey of the Noto antenna has been performed [3] and results obtained using this approach can be compared to the other surveying approaches here described. The holography technique is based on the Fourier transformation between the antenna beam pattern, $P(u,\nu)$, and the field distribution over the aperture plane, $E_{ap}(x,y)$: $E_{ap}(x,y) = \mathrm{FT}\ [P(u,\nu)]$ as shown in Figure 4. In particular, the factor of interest is the phase distribution on the surface map, which gives the surface alignment errors.

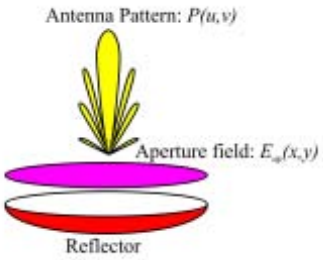

Figure 4. Scheme of antenna beam pattern $P(u,\nu)$, and field distribution over the aperture plane $E_{ap}(x,y)$.

A numerical result obtained by an antenna simulator is plotted in Figure 5. An antenna pattern produced by a parabolic reflector with several deformations corresponds to a phase of the aperture field not constant, as expected for an ideal parabolic profile. Hence, the holography technique consists of measuring the antenna far-field pattern. This step can be done by observing a source with a stable and well-known position in the sky. Several alternatives are available: geo-stationary satellites, strong astronomical sources (like masers) and, finally, local transmitters. In order to map the antenna pattern in a $u\nu$-plane, several measurements need to be performed around the source position: the wider the $u\nu$-plane, the higher the deformations space resolution.

Since both amplitude and phase of the antenna pattern are necessary, a coherent receiver is requested. There are two main methods to determine the phase pattern: one, called phase retrieval method, based on recovering it through power measurements performed with two receiver placed close to each other. The other, the interferometric method, consists of having two coherent measurement systems: the target antenna, usually the radio telescope, and the reference reflector antenna, usually a small satellite dish. The advantages of the interferometric method are its high accuracy and fast computation; on the other hand it needs an additional receiver for the reference antenna. Then, to obtain the phase difference, the two antenna signals are processed by a cross-correlator. Restricting the measurement to N beamwidths, the profile shape is determined with a spatial resolution of approximately D/N, D being the antenna diameter. Moreover, a good accuracy is assured when the signal is characterized by a high signal to noise ratio. Holography receiver and data acquisition system must have a large dynamic: the power level for on-source can be 105 times stronger than that of N beamwidths off-axis.

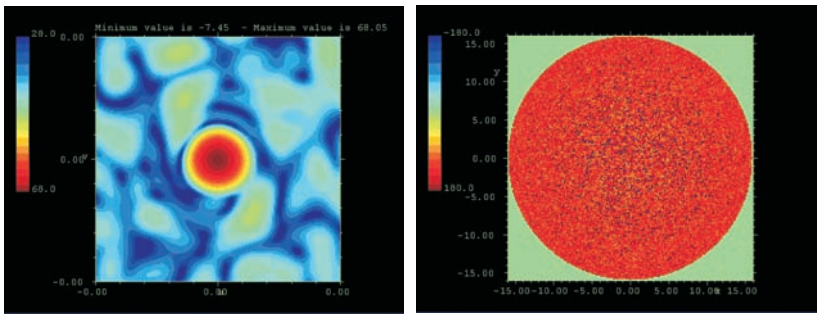

Figure 5. Antenna pattern produced by a parabolic reflector with deformations (on the left) corresponds to a phase of the aperture field not constant (on the right), as expected for an ideal parabolic profile.

4. Topographical Local Survey

In September 2005 high accuracy topographical surveys were realized at Noto and Medicina observatories in order to monitor the stability of ground control networks and to perform a rigorous estimate of the VLBI-GPS eccentricity vectors. For a detailed and comprehensive description of the survey method adopted in the field operations, see [4]. In addition, triangulation has also been used to locate, within the topocentric frame, the positions of the spheres used as targets during the laser scanning survey, thus realizing common points in the two surveying approaches.

5. Laser Scanning

In September 2005, the two INAF VLBI antennas (Noto and Medicina) were surveyed for the first time with the laser scanning technique. Our aim was to realize a 3-D model of the dish and to position it with respect to the local ground control network. The instrument used in this experiment was a TRIMBLE-MENSI GS200 which can store the position of about 5000 points per second with a resolution in range of about 1.5 mm @ 50m. The GS200 uses a laser pulse, which can determine the distance between the scanned points and the instrument itself by recovering the double-way travel time of the signal. The acquisition of the three-dimensional coordinates of the points belonging to the VLBI antenna is performed using an auto-focus laser with a spot size of 3 mm @ 50 meters. The grid step is fixed by the user taking into account the resolution and the amount of data; Figure 6a shows an example of surveyed points clouds. Both Noto's and Medicina's antenna surfaces have been scanned at different elevation angles of the radiotelescopes. In order to use the instrument within the inner dish surface, ad hoc supports were realized and fixed to the primary mirror (Figure 6b and 6d). The raw data acquired with laser scanning systems intrinsically define a cloud of points expressed with respect to an instrumental reference system; the different parts of the surface (clouds) are connected in a common reference system by means of common points (these points have been observed with total stations, too). In this survey, the connecting points have been physically materialized through appropriate spheres placed on the external border of the VLBI antenna dish (Figure 6c): their centers can be recognized by the laser system. Through an ad hoc terrestrial survey, the positions of the spheres' centers have been determined with respect to the topocentric reference system.

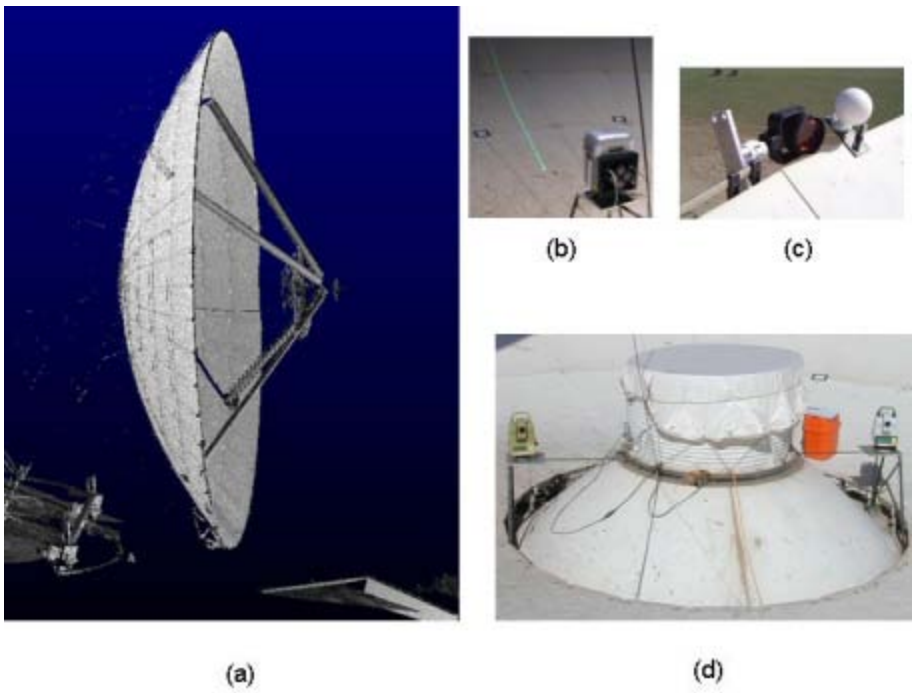

Figure 6. (a) Example of laser scanning derived cloud of points, (b) laser scanner during the acquisition of the inner part of the VLBI dish, (c) sphere used to align the laser scanner acquisition in a topographical local frame, (d) high accuracy total stations occupying the same points as the laser scanner in order to connect the spheres' centers positions to the local topographical network.

6. Outlook

The measurements collected applying these different approaches now form a comprehensive set of information that must be carefully handled and comprehensively combined for recovering and validating relative and absolute gravitational deformations of the antenna. Both geodetical and astronomical applications of VLBI will greatly benefit from this information.

References

[1] Orfei, A., M. Morsiani, G. Zacchiroli, G. Maccaferri, J. Roda, F. Fiocchi, An Active Surface for Large Reflector Antennas", IEEE Antennas and Propagation Magazine (2004), 46, 4, pp. 11-19.

[2] Bolli, P., G. Grueff, Correcting secondary mirror surface errors in Noto 32 m radiotelescope using the 'active' primary mirror, Electronics Letters (2003), 39 5, pp. 416-417.

[3] Tuccari, G., S. Buttaccio, G. Nicotra, Phase reference holography of the Noto 32 m VLBI antenna, Elecmn. Len. (2001), 37, (17), pp. 1060-1062.

[4] Vittuari, L., P. Sarti, P. Sillard, P. Tomasi, M. Negusini, Surveying the GPS-VLBI Eccentricity at Medicina: Methodological Aspects and Practicalities - Proc. of the IERS Workshop on site co-location. Matera, Italy, 23 - 24 October 2003. IERS Technical Note; 33 (2005). 148 pp.

Yoshihiro Fukuzaki et al.: Status and Results of JARE Syowa Station, Antarctica, IVS 2006 General Meeting Proceedings, p.177–181
http://ivscc.gsfc.nasa.gov/publications/gm2006/fukuzaki

Status and Results of JARE Syowa Station, Antarctica

Yoshihiro Fukuzaki [1], *Kazuo Shibuya* [2], *Koichiro Doi* [2]

[1)] *Geographical Survey Institute, Japan*
[2)] *National Institute of Polar Research, Japan*
Contact author: Yoshihiro Fukuzaki, e-mail: fukuzaki@gsi.go.jp

Abstract

The Japanese Antarctic Research Expedition (JARE) has started regular VLBI experiments at Syowa Station (69.0° S and 39.6° E) on East Ongul Island, Antarctica in 1998. This series of experiments was called 'Syowa VLBI session' or 'SYW session.' Three stations in the Southern Hemisphere, Syowa, Hobart (Australia) and HartRAO (South Africa), have participated in this session. Since 1999, Syowa Station has also participated in 'OHIG session'. SYW session ended in December 2004 and Syowa Station started to participate in CRF deep-south (CRD) session in addition to OHIG in 2005. The K5 recording system was partly introduced in 2004 and fully replaced K4 in 2005 at Syowa Station. Until the end of 2005, Syowa Station has performed 65 experiments, 42 experiments of which were carried out from May 1999 to December 2004 have been reduced and analyzed using CALC/SOLVE. The results show that the length of the Syowa-Hobart baseline is increasing linearly with a rate of 54.4 ± 0.9 mm/yr. The Syowa-HartRAO baseline is also increasing, but at the lower rate of 11.1 ± 0.7 mm/yr. These results approximately agree with those of GPS and the NNR-NUVEL-1A plate motion model. On the other hand, we cannot find a significant change with the Syowa-O'Higgins baseline. The current status of Syowa Station and the results of the analysis are briefly reported.

1. Status of the Station

Syowa Station is located at 69.0° S and 39.6° E on East Ongul Island, Antarctica, which is the southernmost VLBI station. It has grown to be one of the key stations for global geodynamics in the Southern Hemisphere. There are an IGS GPS station, a DORIS beacon, a superconducting gravimeter, a seismometer and a tide gauge in addition to VLBI, as reported in [1].

Regular experiments started in February 1998 with Hobart and HartRAO. This series of experiments was named 'SYW session.' Syowa Station has also participated in 'OHIG session' since 1999. The 1999 experiment was the first VLBI observation on an intra-Antarctic plate baseline. SYW session ended in December 2004 and Syowa Station started to participate in CRF deep-south (CRD) session in addition to OHIG in 2005. Until the end of 2005, 65 experiments were performed.

The K4 recording system was used until 2004. The K5 recording system was partly introduced in 2004 and fully replaced K4 in 2005. The data obtained by K5 system in 2005 were brought back from Syowa Station to Japan and ftp-transferred to Haystack Observatory via NiCT server to be converted into the Mark 5 format.

2. Analysis Results

2.1. Variation of Baseline Length

We used the CALC/SOLVE analysis software developed by GSFC. The versions of CALC and SOLVE that were used are 9.12 and 2003.05.16, respectively. We chose Hobart, HartRAO,

Fortaleza and Kokee as stations with fixed station coordinates and velocities in ITRF2000, and solved for the station coordinates and velocities of Syowa, O'Higgins and TIGO-Concepción for each epoch. The models for Earth orientation parameters, ocean tide loading and atmospheric effects used in our analysis are listed in Table 1.

Table 1. List of the models used in our analysis

	VLBI	**GPS**
Earth Orientation Parameter	NASA Goddard Space Flight Center VLBI group	IERS EOP Product Center
Ocean Tide Loading	Scherneck model	Scherneck model
Atmosphere		
Dry and Wet	Niell's mapping function	Niell's mapping function
Gradient	Not applied	Not applied
Pressure Loading	Not applied	Not applied

The 42 baseline solutions for the sessions from 1999 through 2004 are estimated by using the SOLVE interactive mode. Solid diamonds with error bars in Figure 1 show the results for the baseline lengths for Syowa-Hobart (top), Syowa-HartRAO (middle), and Syowa-O'Higgins (bottom), respectively. Applying a simple linear model for baseline evolution, secular changes in baseline lengths are detectable. The length of the Syowa-Hobart baseline is increasing with a rate of 54.4 ± 0.9 mm/yr. The Syowa-HartRAO baseline shows a smaller but still significant increase of 11.1 ± 0.7 mm/yr. The Syowa-O'Higgins baseline gives a small (-1.9 ± 3.2 mm/yr) apparent shrink.

On the other hand, the GPS baseline length results are estimated by using the GIPSY OASIS II software package in precise point positioning (PPP) mode. The point positioning results of both ends of a baseline from the corresponding daily files are used to calculate the baseline lengths and plot the daily solutions. In the analysis, default models of different Earth orientation parameters that are not used for the VLBI analysis were applied as summarized in Table 1. The results from VLBI and GPS are summarized in Table 2.

Table 2. Summary of the baseline change rates from VLBI and GPS

	VLBI (mm/yr)	**GPS** (mm/yr)
Syowa - Hobart	54.4 ± 0.9	56.0 ± 0.3
Syowa - HartRAO	11.1 ± 0.7	13.0 ± 0.2
Syowa - O'Higgins	-1.9 ± 3.2	0.6 ± 0.7

2.2. Coordinates

By using the SOLVE batch mode, the VLBI coordinates and velocities of the antenna reference point were obtained in the ITRF2000 frame at the epoch of 1997.0 as given in column 1 (VLBI estimate) of Table 3. For comparison, the ITRF2000 website gives the corresponding coordinates from GPS at the epoch of 1997.0 as given in column 4 (GPS from ITRF2000).

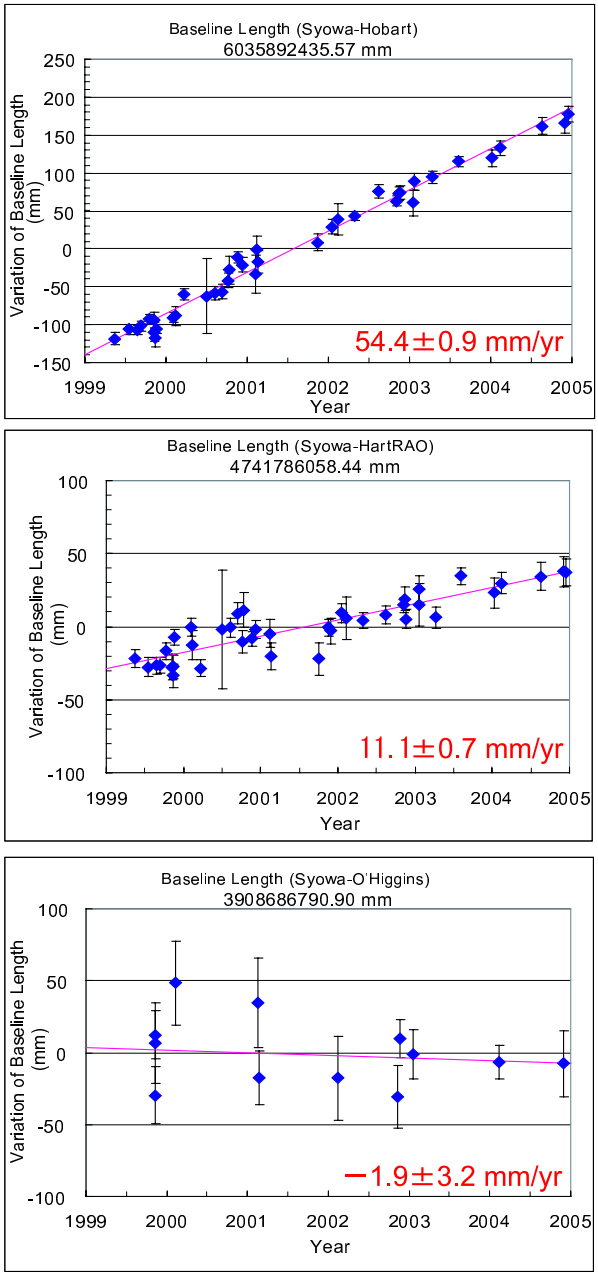

Figure 1. Time-series of 3D baseline lengths for Syowa-Hobart (top), Syowa-HartRAO (middle) and Syowa-O'Higgins (bottom).

The current best estimate of the local tie vector is obtained as -13.714 m for X component, 120.574 m for Y component, and 24.362 m for Z component, respectively. The maximum uncertainties are on the order of 1-2 cm for each component.

A summary of VLBI and GPS coordinates is given in Table 3. We note that subtracting the local tie (column 2) from the estimated VLBI coordinates (column 1) results in offset-corrected

VLBI coordinates at the IGS GPS marker; these values are tabulated in column 3 (offset-corrected VLBI).

Subtracting the GPS from ITRF2000 coordinates (column 4) results in the differences shown in column 5 (difference). They are less than 2 cm, constituting the current degree of consistency between the VLBI system and the GPS system at Syowa Station.

Table 3. Summary of VLBI and GPS coordinates

	VLBI estimate, this paper (m)	local tie (m)	offset-corrected VLBI (m)	GPS from ITRF2000 (m)	difference (cm)
X	1766194.111 ± 0.002	-13.714 ± 0.01	1766207.825	1766207.841 ± 0.003	-1.6
Y	1460410.924 ± 0.002	120.574 ± 0.01	1460290.350	1460290.350 ± 0.002	0.0
Z	-5932273.308 ± 0.005	24.362 ± 0.02	-5932297.670	-5932297.680 ± 0.007	1.0

2.3. Topocentric Position Change

When we convert the geocentric coordinates of Syowa Station into topocentric coordinates and plot the measured height versus time after each observation epoch, the vertical change rate amounts to 1.5 ± 1.2 mm/yr from VLBI and 2.3 ± 0.3 mm/yr from GPS. The topocentric velocities of the Syowa reference points are summarized in Table 4.

In a similar fashion, the crustal uplift rates for O'Higgins Station can be estimated to 4.4 ± 0.7 mm/yr from VLBI and 5.9 ± 0.5 mm/yr from GPS.

Table 4. Topocentric velocities of the Syowa reference points

Up (mm/yr)	**East (mm/yr)**	**North (mm/yr)**	**reference**
1.5 ± 1.2	-4.3 ± 0.3	2.8 ± 0.4	VLBI (1999-2004), this paper
2.3 ± 0.3	-4.4 ± 0.2	-0.2 ± 0.2	GPS (1999-2003), this paper
2.5 ± 0.3	-5.4 ± 0.1	0.8 ± 0.1	GPS (1999-2004), JPL website
3.6 ± 0.2	-6.5 ± 0.8	3.2 ± 0.9	DORIS (1999-2004) from P. Willis

2.4. Comparison with Plate Motion Model

Since the vertical uplift trend at Syowa and O'Higgins Stations will cause some change in the horizontal baseline, we correct for this by assuming the uplift rates of 2 mm/yr (Syowa) and 5 mm/yr (O'Higgins), respectively. Thus the estimated opening rates are 53.5 ± 0.9 mm/yr (VLBI) and 55.1 ± 0.3 mm/yr (GPS) for Syowa-Hobart, 10.4 ± 0.7 mm/yr (VLBI) and 12.3 ± 0.2 mm/yr (GPS) for Syowa-HartRAO, and -2.9 ± 3.2 mm/yr (VLBI) and -1.6 ± 0.7 mm/yr (GPS) for Syowa-O'Higgins, respectively.

The predicted rates of the baseline length change by the NNR-NUVEL-1A model are 52.73 mm/yr (Syowa-Hobart) and 11.46 mm/yr (Syowa-HartRAO), respectively. Since the NNR-NUVEL-1A model adopts one rigid Antarctic-plate, the model postulates zero change for the Syowa-O'Higgins baseline length. The horizontal baseline change rates are summarized in Table

5.

Table 5. Summary of the horizontal baseline change rates from VLBI, GPS and NNR-NUVEL-1A

	VLBI (mm/yr)	**GPS** (mm/yr)	**NNR-NUVEL-1A** (mm/yr)
Syowa - Hobart	53.5 ± 0.9	55.1 ± 0.3	52.73
Syowa - HartRAO	10.4 ± 0.7	12.3 ± 0.2	11.46
Syowa - O'Higgins	-2.9 ± 3.2	-1.6 ± 0.7	—

3. Summary

- Routine geodetic VLBI observations at Syowa Station have been made since 1998 among the Southern Hemisphere network including O'Higgins, Hobart, HartRAO, Fortaleza and TIGO-Concepción.
- SYW session ended in December 2004 and Syowa Station started to participate in CRF deep-south (CRD) session in addition to OHIG in 2005.
- K5 recording system was partly introduced in 2004 and fully replaced K4 in 2005.
- The data of 42 experiments carried out from May 1999 to December 2004 have been reduced and analyzed using CALC/SOLVE. The rates of change of baseline length as measured with VLBI are consistent with those determined by GPS and NNR-NUVEL-1A within 3 sigma. The results do not yet have a high level of significance of the change in the baseline length between Syowa (East Antarctica) and O'Higgins (West Antarctica).
- The estimated vertical change rates with VLBI indicate 2 and 4 mm/yr uplift rates at Syowa and O'Higgins Stations, respectively.
- The offset-corrected VLBI coordinates at Syowa Station have inconsistencies of less than 2 cm against the independently estimated GPS coordinates, where the accuracy of local tie is estimated as 1-2 cm for each component.

References

[1] Shibuya, K., Doi, K. and Aoki, S. (2003): Ten years' progress of Syowa Station, Antarctica, as a global geodesy network site. Polar Geoscience, 16, 29-52.

[2] Shibuya, K. and Doi, K. (2005): JARE Syowa Station 11-m Antenna, Antarctica, in International VLBI Service for Geodesy and Astrometry 2004 Annual Report, 107-110, NASA/TP-2005-212772, ed. by D. Behrend and K.D. Baver.

[3] Fukuzaki, Y., Shibuya, K., Doi, K., Ozawa, T., Nothnagel, A., Jike, T., Iwano, S., Jauncey, D.L., Nicolson, G.D. and McCulloch, P.M. (2005): Results of the VLBI experiments conducted with Syowa Station, Antarctica. J. Geod., 79, 379-388.

Session 4

New Technology Developments in VLBI

Gino Tuccari et al.: DBBC – A Flexible Platform for VLBI Data Processing, IVS 2006 General Meeting Proceedings, p.185–189
http://ivscc.gsfc.nasa.gov/publications/gm2006/tuccari1

DBBC – A Flexible Platform for VLBI Data Processing

Gino Tuccari [1], *Salvatore Buttaccio* [1], *Gaetano Nicotra* [1], *Ying Xiang* [2], *Michael Wunderlich* [3]

[1)] *INAF, Istituto di Radioastronomia*
[2)] *Shanghai Observatory, Chinese Academy of Science*
[3)] *Max-Planck Institut für Radioastronomie*
Contact author: Gino Tuccari, e-mail: g.tuccari@ira.inaf.it

Abstract

The development of the first version of DBBC is complete and an extended testing phase is planned for 2006. The instrument is a flexible tool that realizes a complete analog VLBI pre-recording terminal in digital technology, with the additional capacity to process data in a different fashion for multiple narrow or fewer very wide band channels without changing any hardware part. We show a description of this instrument, report on the performance with the present implementation, and point out the potentiality for a different implementation using the same hardware. Moreover a description of the second version is given with some details on new hardware parts for additional functionalities, such as RFI mitigation, and AD sampling at the receiver site.

1. Introduction and General Description

The main idea behind the 'DBBC' project is to replace the existing VLBI terminal with a complete and compact system to be used with any VSI compliant recorder or data transport. Moreover the cost has to be limited by making use of commercially available components.

Hardware programmability is a fundamental feature in order to optimize the architecture for a particular, requested functionality the instrument, because different performance involves a different number of gates necessary to perform the required functionality. Under these assumptions, maximum input and output data rates are the limitation and they have to be set so that they satisfy the present and possible future requirements.

The new development needs to be fully compatible with the existing terminals and correlators in order to minimize the efforts to introduce them at the stations and to eliminate any modification at the correlator side, still maintaining the possibility to upgrade to a new class of correlators. The possible upgrades have to be mostly software in order to avoid modifying any hardware part, to save cost and to simplify the operations, so that programmable hardware is the main component. However, a hardware upgrade will still be possible, because a standard in the connection of the different elements is defined.

The entire project is based on a flexible architecture, composed of one or more FPGA boards as computation elements, placed in a mixed cascading/parallel structure, so as to guarantee a parallel usage of data input and a shared parallel output data flow.

In a DBBC a single system unit is composed of four RF/IF Input in the ranges 0.01-512 MHz, 512-1024 MHz, 1024-1536 MHz, 1536-2048 MHz, and 2048-2100 MHz with each of them feeding a 1.074 GHz clock sampler. Then four polarizations or bands are available for a single group of output channels. A group of 64 channels is able to handle a shared combination of channels coming from the four bands, supporting two VSI output connectors as output.

Multiple architecture can be used to take advantage of adopting fully re-configurable FPGA Core Modules, where one of such modules is an autonomous board populated with an appropriate number of gates, fed by any of the four IFs, and sharing the output data bus. Narrow or wide bandwidth channels per module can be assigned, maintaining the maximum number of gates provided by the Core Module. Modular realization for a stack processing is provided, which implies the use of one or more Core Modules for achieving a higher number of gates and then more processing capability. The input bus is cascaded, with very low skew, between modules.

An analog monitor, produced by DA conversion, has been added for testing purposes, in order to be able to evaluate with a common spectrum analyzer the contents of the different channels and their performance. This has been proved particularly useful in order to adopt standard equipment normally in use at a radio-telescope. Field System support is required to configure the different modules and allow standard settings, while still getting total power measurements of the converted channel. A limited effort should be assured on the FS side to include the support for the DBBC due to the implicit FS-like structure of the commands the DBBC is able to recognize.

Different configurations can be supported to obtain similar, but not identical, functionalities, such as SSB down converter, wide band parallel FIR, and poly-phase FIR/FFT, to mention a few. The possibility to independently tune different channels, and to have them filtered at different bandwidth, though an obvious feature in the analog implementation, is not so obvious a solution for the digital implementation, as different solutions could appear to be more appropriate. For this reason the project allows implementation of different architectures and the ability to change them at convenience.

A Core Module can handle a maximum input bandwidth of more than 34 Gbit/s, and a maximum output bandwidth of 8.192 Gbit/s. Two high rate buses are present, named HSI and HSO, respectively, with the addition of a further Control/Configuration/Monitor bus, named CCM.

2. System Components

In Figure 1 the DBBC is shown, while a schematic view of the instrument is visible in Figure 2. Signals coming from the receivers trough the Conditioning Module are kept at the proper level before the sampling process.

The ADBoard (Figure 3) performs the analog-to-digital conversion at a rate of 2^{30} Hz. Four of these units are able to feed four IFs with 8-bit representation in the processing units, the Core Module boards (Figure 4). The maximum number of such FPGA boards is 16 in a stack configuration. The FiLa (First/Last) board (figure 5) opens and closes the chain. This board is indeed used in the initial and final part of the stack to perform more functions: 2 VSI interfaces, DA monitor, Timing synchronization and Clock Synthesizer, Communication, JTAG channel.

The FPGAs Core Configuration represent the firmware to perform the desired functionality, such as the SSB base band conversion. Different architectures can be used because of the full programmability of the module.

The Power Distributor board generates the supply voltages for each board of the chain. The software, able to manage the entire functionality of the DBBC, is run on a compact PC board with the help of two PCI commercial interfaces. System Management Software is Field System oriented, so that standard commands to set and use the instrument are Field System-like, requiring a minimum effort to integrate the DBBC into that environment.

Figure 1. DBBC Back-end System.

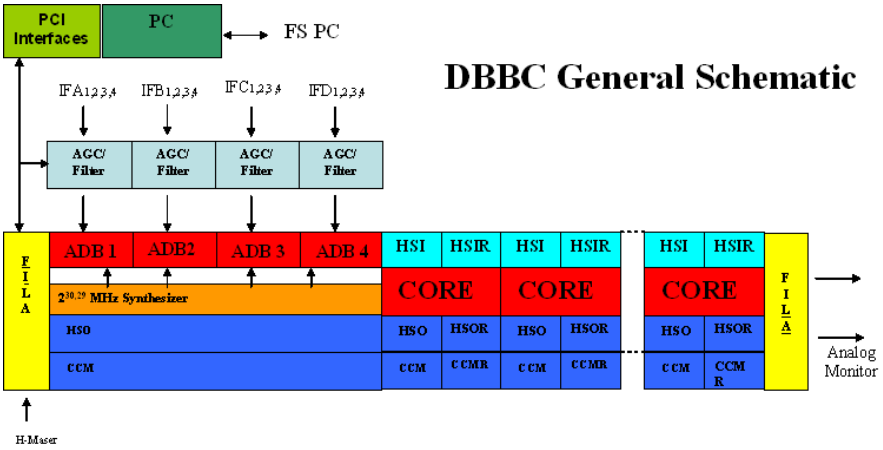

Figure 2. DBBC schematic functional representation.

3. Configuration

Different architectures can be used in the Core Modules, having different performance and behaviors. One possible configuration is the DDC digital down converter in the sense of the classical implementation. In such a solution a direct SSB conversion is typically performed between a high data rate sampled IF band and a lower data rate base band. One or two channels are generated for each converter, as in the analog implementation. Important differences, greatly improving the performance are present: the local oscillator is a Numerically Controlled Oscillator (NCO), the mixer is complex as Look Up Table multiplier, the low-pass band filters are Finite Impulse Response (FIR). Decimation circuitry is adopted because of the high ratio between IF and output data rate and is performed with multirate/multistage FIR. Digital Total Power (DTP) measurement at base band level is adopted; Rescaling/Gain Control (RGC) is adopted for dynamic range control and final data representation. The tuning step is 1 Hz, giving the possibility to finely tune the receiver

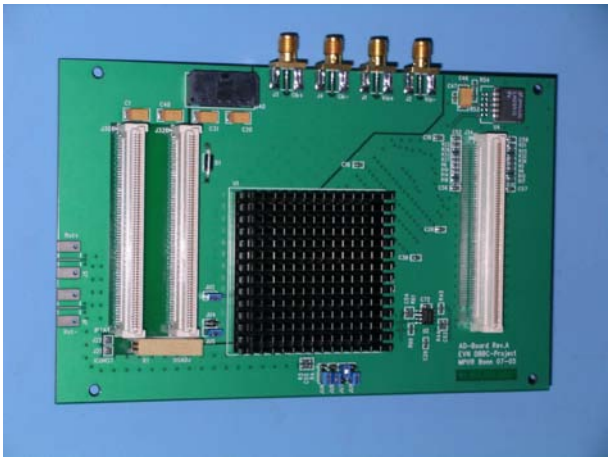

Figure 3. ADBoard - Sampler board 8-bit at 2^{30} Hz clock frequency.

Figure 4. Core Module Board is the processing element, with three high data rate I/O bus.

for spectroscopy or any other precise frequency settings. Narrow bandwidth typically adopted is defined for this project in the range: 16, 8, 4, 2, 1, 0.5, 0.25 MHz. Output data rate is 32 or 64 MHz at present in order to be able and fit with the standard, now adopted VSI-H data rate. A 128 MHz clock rate is the maximum supported.

4. Upgrade

Testing with real observations started with mDBBC (IRA-SHAO agreement): fringes have been detected on both analog-digital and digital-digital baselines. First analog-digital fringes have been detected on the Seshan-Urumuqi baseline on Nov 23, 2004, while first digital fringes were detected on the Noto-Seshan baseline on Feb 2, 2005.

2006 will be dedicated to an observation–optimization process. Moreover, an update program for improving performance is under way. It includes FPGA Virtex4 device testing for double

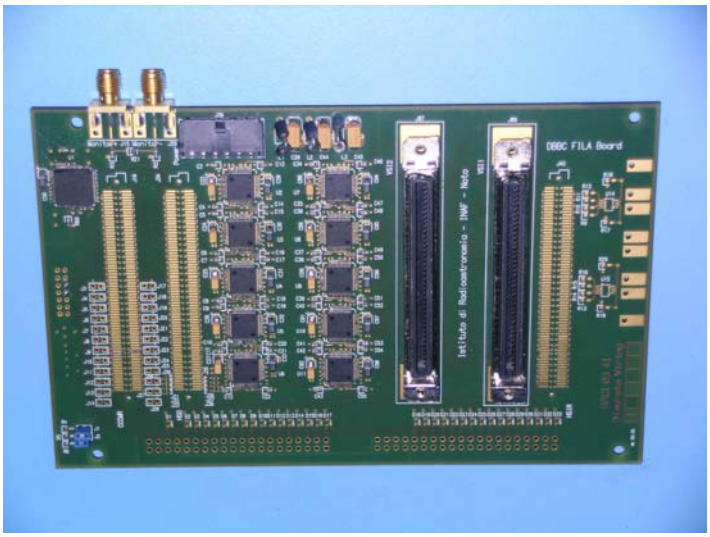

Figure 5. FiLa Board - Support two VSI interfaces, DA converter, PC communication, JTAG programming.

processing clock and price reduction; Faster AD sampler for increasing the input bandwidth; AD sampler placed inside the receiver and sampled data sent through an optical fiber; RFI Mitigation Board; and the first Core Module (same hardware) acts as RFI processor in transferring the pure sampled data with proper configuration.

5. Conclusions

The DBBC system is a highly flexible instrument because it is able to produce independent tunable channels for full compatibility with the existing acquisition system and correlators. One Core Module board replaces a BBC module. Combination of up to 4/16 IFs in a single module is possible. The DBBC system is also able to handle an equi-spaced multichannel configuration for producing contiguous non-tunable channels. A Core Module board is able to produce multiple channels. More solutions are possible within the same system using software selection. A minimal architecture is composed of 1 ADBoard, 1 Core Module (multichannel configuration, or any other), 1 FiLa board (VSI interface, DA converter, etc). A maximal architecture in one system is composed of 4 Conditioning Modules, 1 FiLa board, 4 ADBoards, 16 CoreModules, 1 FiLa board, PC and PCI interfaces. Such wide range of hardware and software conditions allow one to assemble a low cost system with the needed performance.

References

[1] G. Tuccari, Development of a Digital Base Band Converter (DBBC): Basic Elements and Preliminary Results In: New Technologies in VLBI, Astronomical Society of the Pacific Conference Series, Vol. 306, p.177-192, 2004.

Ying Xiang et al.: FPGA Implementation in DBBC, IVS 2006 General Meeting Proceedings, p.190–194
http://ivscc.gsfc.nasa.gov/publications/gm2006/xiang

FPGA Implementation in DBBC

Ying Xiang [1], *Gino Tuccari* [2], *Wenren Wei* [1]

[1)] *SHAO-CAS, Shanghai Astronomical Observatory, China*

[2)] *INAF-IRA, National Astrophysical Institute-RadioAstronomy Institute, Italy*

Contact author: Ying Xiang, e-mail: yxiang@shao.ac.cn

Abstract

As one of the main equipments for VLBI stations, the VLBI data acquisition rack takes on the tasks of frequency selection, data collection, data encoding, data recording and etc. As the main part of this equipment, Analog Base-band Converter (Analog BBC) has very complex analog circuits which is obsolete and very expensive. This paper mainly describes the use of digital integrated circuits (FPGAs: Field Programmable Gate Array circuits) to realize the corresponding algorithm called Digital Base-band Converter (DBBC) to take the place of the analog BBC. A simplified version of the DBBC named miniDBBC and achieved in a collaboration between China and Italy, produced some experimental results in real VLBI observations.

1. Introduction

The speed of circuits and resource capacity in Field Programmable Gate Array circuits (FPGAs) has had a rapid development in recent years. In DBBC, we also take advantage of FPGAs to realize our algorithm and make it a very flexible platform for VLBI data processing. At present, the type of FPGA we use in digital BBC is XC3000 which is the product of Virtex-II series of Xilinx company and the speed grade is 6. Later we will upgrade to Virtex-4 series, the newest product for Xilinx. There are two kinds of possible configurations considered in FPGAs. One is called the digital down converter, the other is equally spaced multi-channel configuration. With the first configuration, we could fulfill all the functions of the existing analog BBC. In the paper, the digital BBC is analyzed first in the overall architecture and then in detail (sections 2 and 4). The experimental results are presented in section 3.

2. Algorithm of Digital Down Converter Configuration in FPGA

The BBC is required to band selection in wide band signal and suppress the undesired sideband to generate single sideband signal. The digital down converter configuration is shown in Figure 1. The analog signal is digitized by an A/D sampler and then input to FPGAs. Figure 1 shows a channel of DBBC to implement in FPGA. Prior to digital filtering, the digital signal is down-converted by multiplying it with the Direct Digital Frequency Synthesizer (DDS). Here the DDS is used to generate the local oscillation signal. The transformation generates two signals in quadrature. The I and Q signals are filtered separately, differentially phase-delayed by 90 degrees by means of a Hilbert filter, and then combined together. Finally the combined signal is passed through the digital shape filter determining the band-pass shape. Several channels can be in existence in one device at the same time depending on how much resource in FPGA. These channels can work independently.

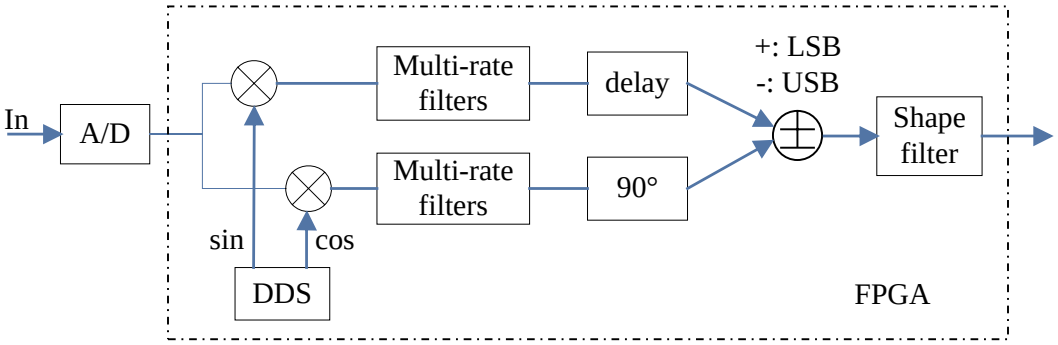

Figure 1: the digital down converter configuration

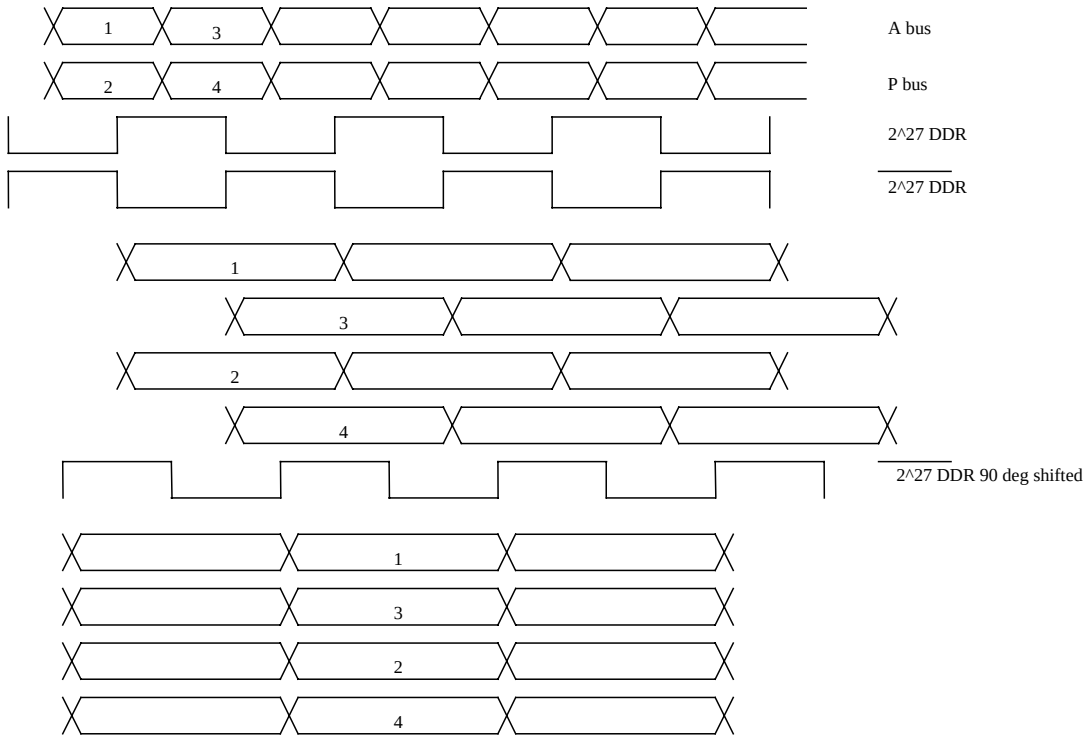

Figure 2: DDR mode and processing with 4-bus parallel in FPGA

At present, the speed of input/output port in FPGA could reach very high while in the double data rate (DDR) mode, the performance of high-speed data transfer will be double. In FPGA the input signals are serial-to-parallel immediately, and then they are processed at relative low speed to ensure the circuits' reliability. In Figure 2, 2-bus data (time division) from A/D sampler are clocked by rising and falling edges—producing 4-bus data in parallel while adopting a clock with 90-degree shift. With the multi-bus data in FPGA, the digital filters and down-converter also

need to be implemented in parallel. A poly-phase filter is adopted to realize digital filtering while parallel DDS with different initial phase are used. The algorithm of parallel DDS implementation is as follows.

$$F_{cir} = \frac{f_{out} \cdot 2^{B_{\theta(n)}}}{f_{clk}} mod(2^{B_{\theta(n)}}) \tag{1}$$

$$\Delta\phi = 2\pi f_{out} \cdot \frac{1}{f_s} = \frac{2\pi}{M}\frac{f_{out}}{f_{clk}} \tag{2}$$

Where F_{cir} : Phase increment

$\Delta\phi$: Initial phase difference between two branches

f_{clk} : Clock frequency in FPGA

f_{out} : Digital local oscillator frequency needed to generate

$B_{\theta(n)}$: Bit-width in phase accumulator

f_s : Sampling frequency

M : Number of the parallel branches

3. Experimental Results of MiniDBBC

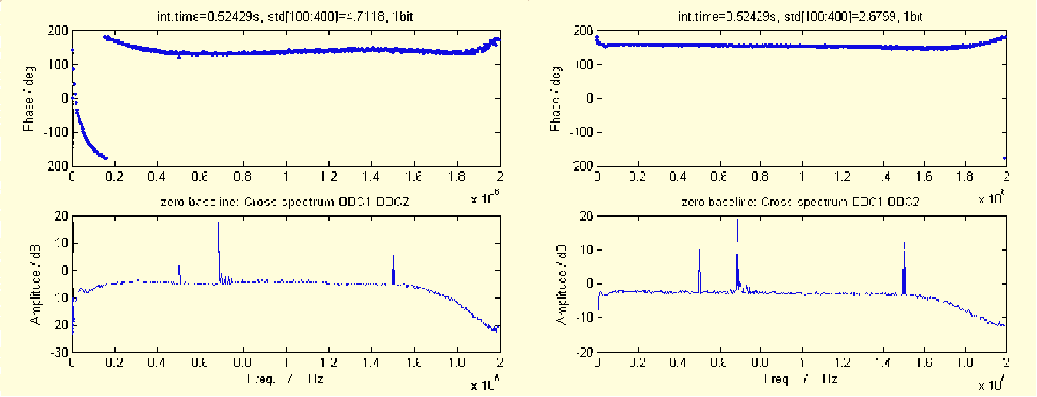

Figure 3: The zero baseline fringe

The DBBC has the simplified version, called miniDBBC and being the result of a collaboration between China and Italy which produced some experimental results in real VLBI observations (Fig 3, Fig 4). Figure 3 shows the fringes of the zero baseline observed in Sheshan. The left picture is the fringe correlated with miniDBBC and analog BBC. The right one is produced by correlation with two analog BBC. From the left picture, we can see an obvious nonlinearity in phase near the area of zero frequency (the big jump is a 360 degree wrap). To determine the reason, we measured the analog BBC and miniDBBC's phase characteristic using PCAL method. We found that the miniDBBC's phase is linear, but that there is a nonlinearity in the analog BBC's phase whose shape is similar to the left drawing. The different channels' performances of analog BBCs are almost identical, so the fringe of two analog BBCs is almost flat. Figure 4 is the fringe of 3C454 radio source correlated with data by Sheshan using miniDBBC and Urumqi using analog BBC.

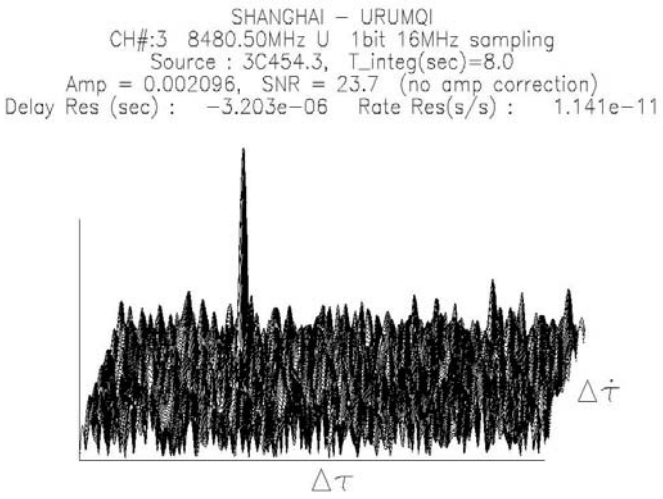

Figure 4: The fringe of radio source 3C454.3

4. Other Possible Configuration Algorithm

Using FPGA makes DBBC hardware become a highly flexible platform. We can download different configurations to implement different functions or upgrade. There are other configurations for DBBC, such as poly-phase filter + FFT (Fig 5). The advantage of this configuration is that many channels could be realized at the same time and saving the resources in FPGA. The disadvantage is that these channels are not independent; the band space between two neighboring channels is equal and cannot be tuned separately.

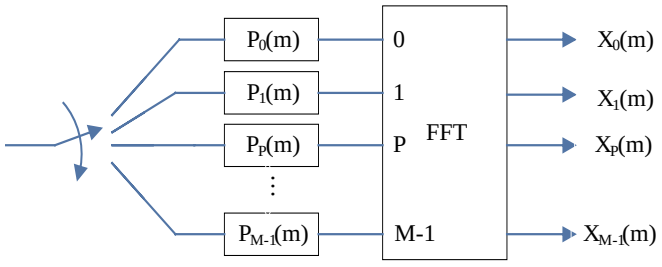

Figure 5: The poly-phase filter + FFT configuration

Acknowledgements

This work is supported by the National Natural Science Foundation of China General Program (10503009). We thank Zhang Xiuzhong, Shu Fengchun, Zhu Renjie, Tu Ruimin and other colleagues of the Chinese VLBI Network for their help.

References

[1] Comoretto G. A Digital BBC for the ALMA Interferometer, ALMA Memo 305, 2000

[2] Tuccari G. Development of a Digital base Band Converter (DBBC): Basic Elements and Preliminary Results. "New Technologies in VLBI", ASP Conference Series, Vol. 306, 2003, ed. Y. C. Minh (San Francisco: ASP), pp. 177-192

[3] Crochiere R., Rabiner L. Multirate Digital Signal Processing, New Jersey Prentice-Hall Inc., 1983

Tetsuro Kondo et al.: Development of a New VLBI Sampler Unit (K5/VSSP32) Equipped with a USB 2.0 Interface, IVS 2006 General Meeting Proceedings, p.195–199
http://ivscc.gsfc.nasa.gov/publications/gm2006/kondo

Development of a New VLBI Sampler Unit (K5/VSSP32) Equipped with a USB 2.0 Interface

Tetsuro Kondo, Yasuhiro Koyama, Hiroshi Takeuchi, Moritaka Kimura

Kashima Space Research Center, National Institute of Information and Communications Technology
Contact author: Tetsuro Kondo, e-mail: kondo@nict.go.jp

Abstract

The National Institute of Information and Communications Technology (NICT) has developed a new VLBI sampler unit named K5/VSSP32 dedicated to e-VLBI which is a successor to the K5/VSSP. The maximum sampling frequency per channel of the K5/VSSP32 is 64 MHz, which is four times as fast as that of K5/VSSP. In addition to the maximum sampling frequency, there is a difference in the interface to a host PC. A USB 2.0 (Universal Serial Bus specification revision 2.0) interface is used to connect the sampler with a host PC in the K5/VSSP32, while a PCI-bus interface is in the K5/VSSP. It is hence possible to use even a notebook PC for VLBI observations with the K5/VSSP32.

1. Introduction

The National Institute of Information and Communications Technology (NICT) has developed a new sampler dedicated to geodetic VLBI system named K5/VSSP32 that is equipped with a USB 2.0 (Universal Serial Bus specification revision 2.0) interface. Recent samplers developed by NICT are categorized into two types: One is K5/VSI series equipped with a VSI (VLBI Standard Interface) interface and the other is K5/VSSP series aiming at direct connection with a PC. K5/VSSP32 belongs to the latter category. K5/VSSP is the name of the sampler developed first in this category in order to reduce network-cost and to improve interconnectivity with other sites in a real-time VLBI system. K5/VSSP sampler is a PCI bus board mountable on a motherboard of a standard PC and has a maximum sampling frequency of 16 MHz per channel. It has contributed to broaden the base for VLBI users, i.e., any PC equipped with a K5/VSSP PCI-bus board can be a VLBI recorder, and the data transfer through the Internet is easily realized. K5/VSSP has also progressed greatly the development of the software correlator. K5/VSSP32 is a successor to the K5/VSSP, but a USB 2.0 is newly adopted as an interface with a host PC. Maximum sampling frequency per channel is increased up to 64 MHz. As a K5/VSSP32 unit has 4 channel analog inputs, 4 units can cover 16 channels which is a sufficient number of channels in case of geodetic VLBI. In the meantime, K5/VSSP32 can connect to a notebook PC or a laptop PC through USB 2.0 interface. It is hence possible to use a notebook PC as a recorder not only for a VLBI observation but also for a general purpose observation such as acquiring geophysical data. We carried out a VLBI fringe test using both a desktop PC and a notebook PC, and we successfully got fringes.

2. K5/VSSP32 Sampler

Figure 1 shows a block diagram of the K5/VSSP32 sampler unit. There are 4 analog input channels in a unit. Each channel signal is fed to an operational amplifier (AD8061) that has the

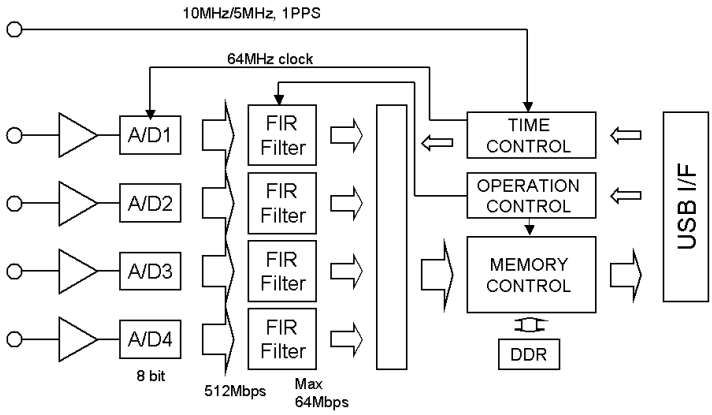

Figure 1. A block diagram of the K5/VSSP32 sampler.

bandwidth of 300 MHz, then it is sampled by using an 8-bit analog-to-digital (A/D) converter (AD9283) with the sampling frequency of 64 MHz. The AD9283 has an input bandwidth of 475 MHz that is wider than that of the AD8061, thus signals up to 300 MHz, which is limited by the input operational amplifier AD8061, can be handled by the K5/VSSP32 sampler. Each digitized signal is fed to a digital filter section equipped by using an FPGA. Low-pass-filters (LPFs) with cut-off frequencies of 2, 4, 8, 16, and 32 MHz are implemented in the digital filter section. Insertion of LPFs or bypassing the filter is selectable from a host PC. Each filtered signal is re-sampled with sampling parameters given from a host PC and is formatted into 1-second frame data that has a format compatible with the K5/VSSP, but has an expanded header. Clock signals to operate the K5/VSSP32 sampler are generated from a reference signal. Either 10 MHz or 5 MHz signals can be used as a reference signal. The FPGA (Altera EP2S30) that is the same one where digital filters are implemented carries out the signal processing. A USB 2.0 is used as an interface with a host PC. Figure 2 shows a picture of the K5/VSSP32 unit and the 16-ch module consisting of 4 units. Table 1 summarizes the specifications of K5/VSSP32 compared with the K5/VSSP.

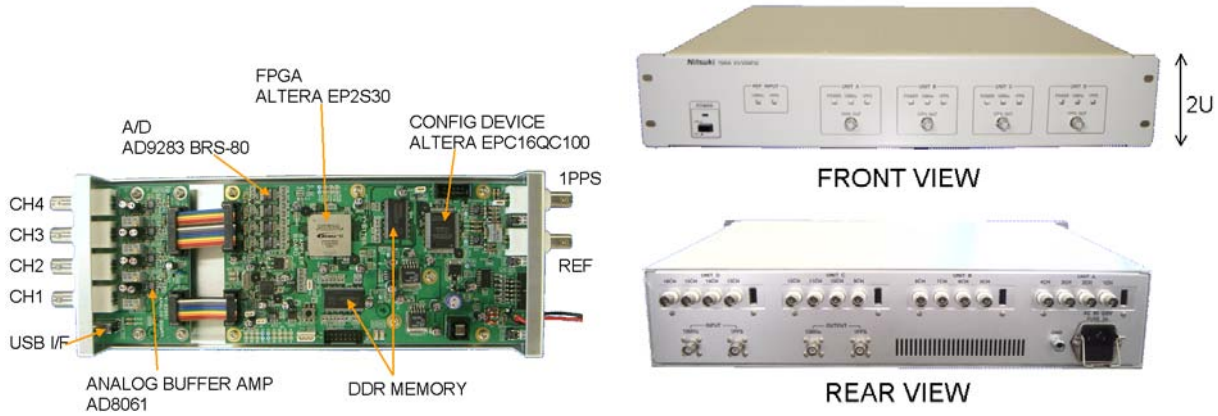

Figure 2. A picture of the K5/VSSP32 unit (left) and the 16-ch K5/VSSP32 module (right).

Table 1. Specifications of K5/VSSP and K5/VSSP32

	K5/VSSP	K5/VSSP32
Sampling frequency (MHz)	0.04, 0.1, 0.2, 0.5, 1, 2, 4, 8, 16	0.04, 0.1, 0.2, 0.5, 1, 2, 4, 8, 16, 32, 64
LPF (digital filter)(MHz)	–	2, 4, 8, 16, through
Analog bandwidth	100 MHz	300 MHz
AD bits	1, 2, 4, 8	1, 2, 4, 8
# of ch/unit	4	4
Maximum data rate	64 Mbps/ch 64 Mbps/unit 256 Mbps/4units	64 Mbps/ch 256 Mbps/unit 1024 Mbps/4units
DC offset	not adjustable	adjustable from a host PC
Reference signals	1 PPS, 10 MHz	1 PPS, 10 MHz / 5 MHz
Header size	64 bits	256 bits (typical) *
Interface with PC	PCI-bus	USB2.0

* 96 bits (fixed) + variable auxiliary field (160 bits typical)

2.1. Fringe Test

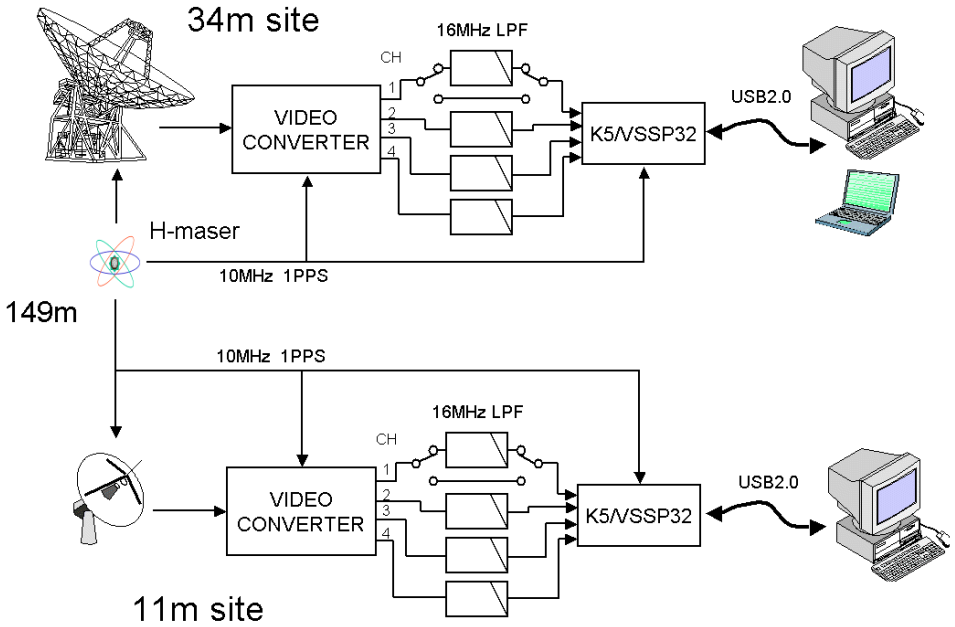

Figure 3. A block diagram of test observation.

A test observation using the K5/VSSP32 sampler was carried out on Nov.10, 2005 using a 34-m antenna and an 11-m antenna at Kashima (baseline length is about 149 m). Figure 3 shows

a block diagram of the test observation. A prototype model of K5/VSSP32 was used at the test observation, and no digital filter was implemented at that time. Therefore we used an analog low-pass-filter to reduce aliasing. A desktop PC was used as a host PC at both the 34-m and 11-m antenna sites. A notebook PC (Dell INSPIRON 700m) was also used as a host PC at the 34-m antenna site. Table 2 summarizes scan information and sampling parameters at the test observation.

Table 2. Summary of test observation on Nov.10, 2005

RF frequency	CH1: 8210.99 MHz CH2: 8220.99 MHz CH3: 8250.99 MHz CH4: 8310.99 MHz
PCAL signals	34-m antenna : 1 MHz step 11-m antenna : 5 MHz step
Sampling parametrs	32 MHz × 1 bit × 4 ch 32 MHz × 1 bit × 1 ch 64 MHz × 1 bit × 1 ch
Sources	3C345, 3C84
Scan information	Scan #1 07:11:00–07:11:10 3C345 32MHz×1bit×4ch Scan #2 07:13:30–07:13:40 3C345 64MHz×1bit×1ch Scan #3 07:18:00–07:18:10 3C84 64MHz×1bit×1ch Scan #4 07:19:30–07:19:40 3C84 32MHz×1bit×4ch Scan #5 07:24:00–07:24:10 3C84 32MHz×1bit×1ch *

* A notebook PC was used at 34-m antenna

The observed data was processed by using the K5 software correlator [1] immediately after observation finished. Correlation results are shown in Figure 4 for CH 1. The periodic component with a period of 0.2 μsec seen in the delay direction (seen clearly in Scan #1) is due to the phase calibration (PCAL) signals injected to both antennas. Correlations between PCAL signals appear as periodic signals with the period being inverse to the least common multiple of each PCAL signal's frequency step, i.e., 0.2 μsec(=1/5MHz). Baseline length is short ($\sim$149 m) and expected fringe rate is only 0.1 Hz or less. Moreover the integration period is only 5$\sim$6 seconds, so that correlations between PCAL signals are not well-separated from those derived from the radio source on the fringe rate domain. Although correlations of PCAL signals are overlapped with fringes from the radio source, we can see a clear peak at the center of the delay and fringe-rate space for all scans. As the center position corresponds to the a-priori delay and fringe rate calculated from the antenna position and radio-source position, we can conclude that we could get a good fringe for all scans. In particular, the fringe obtained for scan #5 is memorable as it was the first one observed by a notebook PC.

3. Conclusion

We have developed a new sampler named K5/VSSP32, which is a successor to the K5/VSSP and is equipped with a USB 2.0 interface. The maximum sampling frequency is increased up to 64

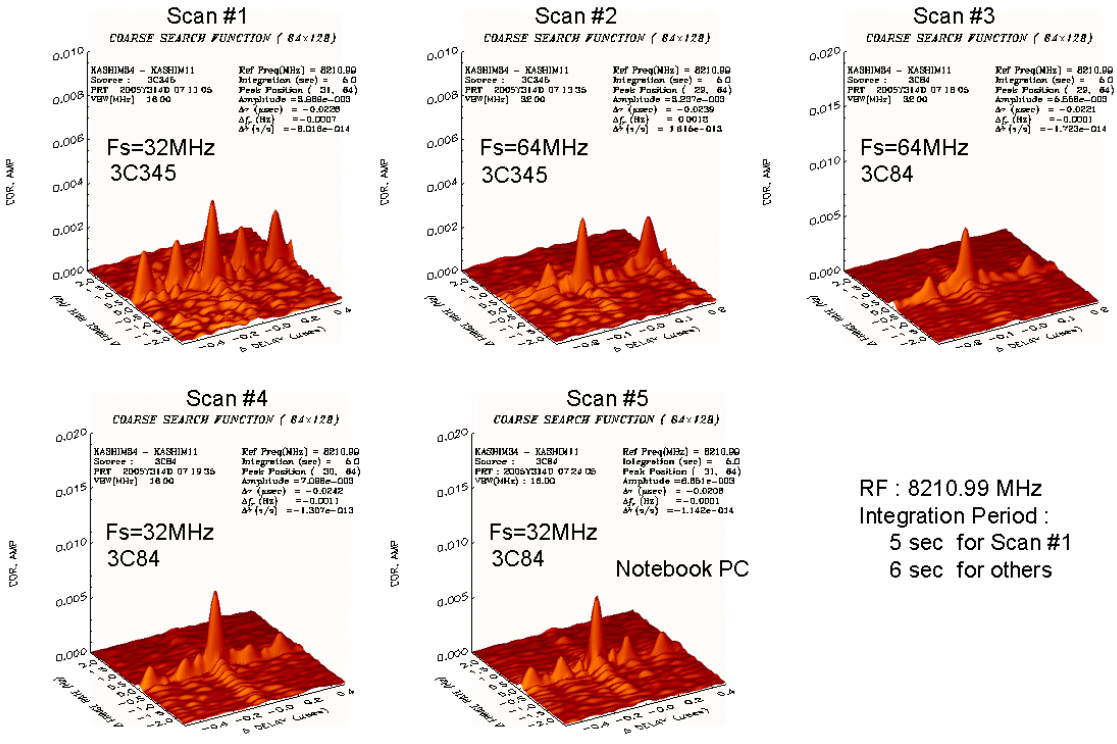

Figure 4. Correlation results for CH 1.

MHz and the maximum data rate per unit is also increased up to 256 Mbps. The adoption of the USB2.0 interface enables us to use a notebook or laptop PC as a host PC of the sampler. Thus K5/VSSP32 can be used not only for VLBI observations but also for general-purpose geophysical observations which require precise time tags. A fringe test using K5/VSSP32 demonstrated that the new sampler has a good performance in terms of system coherence. We also got the first fringe successfully as an observation using a notebook PC. We will carry out a 24-hour experiment using the K5/VSSP32 to verify the performance as a geodetic VLBI sampler.

References

[1] Kondo,T., M. Kimura, Y. Koyama, and H. Osaki, Current status of software correlators developed at Kashima Space Research Center, *IVS 2004 General Meeting Proceedings, edited by N. R. Vandenberg and K. D. Baver, NASA/CP-2004-212255*, 186–190, 2004.

Alan R. Whitney: The Mark 5B VLBI Data System, IVS 2006 General Meeting Proceedings, p.200–204
http://ivscc.gsfc.nasa.gov/publications/gm2006/Whitney1

The Mark 5B VLBI Data System

Alan R. Whitney

MIT Haystack Observatory
e-mail: arw@haystack.mit.edu

Abstract

The Mark 5B VLBI data system is designed to support the VSI-H international specification. It is based on the same physical platform and uses the same disk-modules as the Mark 5A; it also supports the same maximum data rate of 1024 Mbps. Data formatting and time-tagging is done internally within the Mark 5B. This allows, for example, existing VLBA systems to bypass the VLBA formatter, which is limited to 512 Mbps, and connect directly to the output of VLBA samplers (through a simple interface) at a maximum data rate of 1024 Mbps. For existing 14-BBC Mark IV systems, the Mark 5B allows connection of all 14 BBC's to two Mark 5B's for a total aggregate data rate of 1792 Mbps. In addition, the Mark 5B is designed to support all critical functionality of the Mark IV Station Unit, so that the Mark 5B may play back directly to the Mark IV correlator through a simple interface. The Mark 5B system is expected to be available to the VLBI community in early/mid 2006.

1. Mark 5B VLBI System Goals

Incorporating primarily low-cost PC-based components, the Mark 5B system [1] supports data rates up to 1024 Mbps, recording to an array of inexpensive removable IDE/ATA disks (see Figure 1). The general goals of the Mark 5B system are low cost, robust operation, 1 Gbps data rate, conformance to VSI-H specification, easy transportability, and 24-hour unattended operation at 1 Gbps.

All but the last goal have now been achieved; the last goal, 24-hour unattended operation at 1 Gbps, is expected to be attained by the end of 2006 with continued development in high-capacity disk technology.

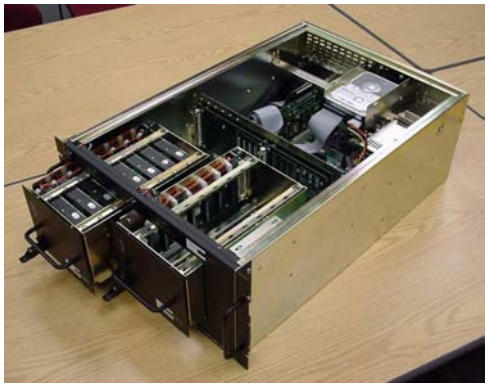

Figure 1. Mark 5 VLBI data system

2. Characteristics of the Mark 5B Data System

The Mark 5B system has the following characteristics:

- Uses the same chassis and disk packs as the Mark 5A (see Figure 1)
- Implements the VLBI Interface Standard
- Maximum record/playback data-rate is 1024 Mbps (same as Mark 5A)
- Requires new Mark 5B I/O card, currently under design
- Eliminates the need for an external formatter (but requires mating VSI interfaces)
- With a 14-BBC Mark IV DAS, up to 1792 Mbps can be recorded with two parallel Mark 5B systems
- Mark IV Station Unit capabilities are designed into the Mark 5B so that Mark 5B systems can be connected to Mark IV correlators without the use of a Mark IV Station Unit.
- Built-in phase-cal extraction and state-counting during recording and playback
- Xilinx FPGA design is updateable via software download from PC (Mark 5A FPGA requires programming from a separate external source)
- Upgrade from Mark 5A to Mark 5B requires only replacement of Mark 5A I/O interface card with a Mark 5B I/O interface card

3. Mark 5B Design

The Mark 5B can be configured as either a DIM (Data Input Module) or DOM (Data Output Module) via software control, which loads the selected personality into the on-board FPGA. We will describe the DIM and DOM separately.

3.1. Data Input Module (DIM)

The DIM is responsible for accepting the data on the VSI input connector, properly time-tagging it, and sending it to the Mark 5 disk module. A simplified block diagram of the DIM is shown in Figure 2.

DIM functionality is a straightforward implementation of the VSI-H specification [4]. 32 data bit-streams (BSn) accompanied by corresponding CLOCK, 1PPS and PVALID signals arrive on an MDR-80 connector carrying LVDS signals. The 1PPS signal is used just once (on command) to synchronize the internal Data Observe Time (DOT) clock, which thereafter keeps time only by counting CLOCK cycles. Two alternate external 1pps inputs are also available for synchronization, labeled ALT1PPS and ALT2PPS. ALT1PPS is carried on a VSI-specified MDR-14 connector with LVDS levels; ALT2PPS is available as a TTL-level SMB connector on the board. Only one of these 1pps signals may be selected to initialize the DOT clock. After DOT clock initialization, the external 1pps signal is not used by the DIM.

The number of active bit streams to be recorded may be 1, 2, 4, 8, 16 or 32, as per the VSI-H specification. The selected bit streams are multiplexed, as necessary, before writing to the 32-bit wide FPDP bus which drives the writing of the disks. The disk data are divided into sequential 10,000-byte Disk Frames (DF), each of which is preceded by a 32-byte non-data-replacement Disk

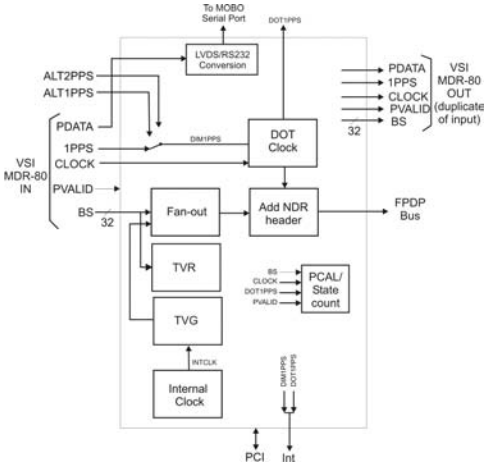

Figure 2. Simplified block diagram of Mark 5B DIM

Frame Header (DFH) and includes a sync-word, a DF number (modulo one second), and time encoded in the same format as a VLBA tape frame header, including the accompanying 16-bit CRCC code. The DF frame number is always reset to 0 at every second tick.

Also included in the DIM is a standard VSI test-vector generator (TVG) and test-vector receiver (TVR). The TVG data can be written to disk for analysis either by software, or may be played back to a TVR in a DOM.

An on-board phase-cal processor can extract 16 tones from each of 16 channels of data, as well as state counts for each channel [5]. Both the phase-cal and state-count information may be read every second; the state-count information may be used to dynamically adjust signal levels coming into the data-acquisition system in order to optimize the signal-to-noise ratio of 2 bit/sample data.

The PDATA signal is converted to RS-232 and sent to an on-board RS-232 connector, where it may be interfaced to a serial input port on the host PC for processing.

A 'cascade' mode of operation of the Mark 5B is supported so that the signals received on the VSI MDR-80 connector are replicated on a VSI MDR-80 output connector. This feature may be used to 'daisy-chain' Mark 5B systems together to extend the total unattended observing time.

3.2. Data Output Module (DOM)

The DOM is responsible for accepting data that has previously been recorded on disk, then reconstructing replicas of the original data streams and timing signals on the VSI MDR-80 output connector. A simplified block diagram of the DOM is shown in Figure 3.

When operating as a VSI DOM, operation is quite straightforward. External timing reference signals DPS1PPS and DPSCLOCK, normally generated by the correlator to which the DOM is interfaced, assure that the data output of the DOM is correct in epoch and rate. The data arriving from the disks via the FPDP bus are stripped of Disc Frame Headers, de-multiplexed as necessary, and a crossbar is used to restore the bit-streams to their original positions in the bit-stream mask. The data are then regenerated with a delay (w.r.t. the DPS1PPS and ROT1PPS ticks) according to user specification. The signals emerging from the VSI output MDR-80 connector are a mirror of the signals which were input into the DIM at the time of the recording. An on-board phase-cal

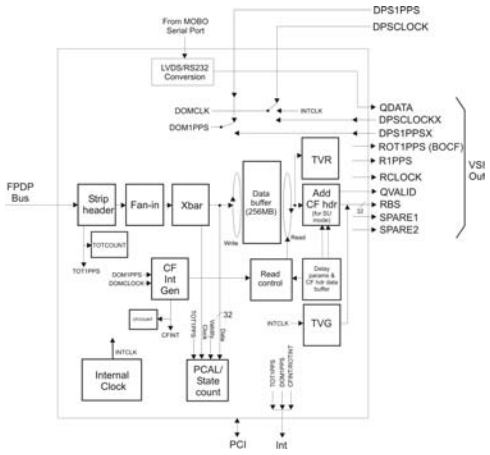

Figure 3. Simplified block diagram of Mark 5B DOM

processor can extract 16 tones from each of 16 channels of data, as well as state counts for each channel; the processing results are read periodically and transmitted to the correlator.

The DOM also includes both a TVG and a TVR for testing purposes.

4. Station Unit Emulation Capability

Configured as a DOM, the Mark 5B can also act as a replacement for the Mark IV Station Unit so that the Mark 5B can interface directly to a Mark IV correlator. Operating in DOM station-unit mode, the Mark 5B has several functions:

- Delays the data according to a fifth-order spline polynomial supplied to the Station Unit before presentation to the correlator proper
- Inserts headers into the data stream with model information to be used by the correlator proper
- Extracts up to 16 phase-calibration signals from each channel
- Counts state statistics to properly normalize correlation coefficients

The implementation of these functions is aided by an on-board 256 MB memory module which allows rapid dynamic changes in the data-delay at intervals specified by the controlling delay model.

5. Mark 5B I/O Interface Board

An annotated photo of the Mark 5B I/O board [6] is shown in Figure 4. Note that there are separate MDR-80 connectors for VSI-H input and output. Also note the 256MB memory module that is piggybacked onto the board to support operation of the Mark 5B in 'station unit' mode.

6. Playback Compatibility with Mark 5A

The Mark 5B data format is designed so that disk modules recorded on a Mark 5B in several commonly-used modes can be played back on an enhanced Mark 5A unit, dubbed 'Mark 5A+'.

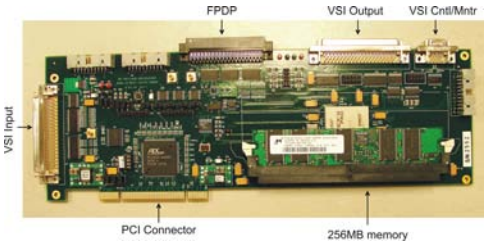

Figure 4. Mark 5B I/O Interface Board

The Mark 5A+ requires that additional capability be added to the Mark 5A; the engineering work to add this capability is now in progress and will require only a reconfiguration of the FPGA on the Mark 5A I/O interface board. The playback format of the Mark 5A+ unit when reading Mark 5B disks will be VLBA track format. This 'compatibility' mode will allow data recorded on Mark 5B systems to be correlated on existing Mark 5A correlators during the transition period to Mark 5B.

7. Summary

The Mark 5B system is the second in the line of Mark 5 VLBI data systems and the first to implement the VSI-H standard. Built on the same platform as the Mark 5A, the Mark 5B offers both a simple migration path for existing Mark 5A users and an inexpensive VSI-compatible VLBI data system for new installations. In addition, a Mark 5B/Mark 5A compatibility path has been established to ease in the transition from Mark 5A to Mark 5B. The Mark 5 systems are being developed with support from BKG, JPL, KVN, MPI, NASA, JIVE, NRAO and USNO. When development is completed, the Mark 5B system design will be transferred to Conduant Corporation in Longmont, CO for replication and distribution to the VLBI community.

References

[1] The Mark 5 web site at *http://web.haystack.mit.edu/mark5/Mark5.htm* contains much additional information about the Mark 5 system.

[2] "VLBI Standard Hardware Interface Specification - VSI-H", Revision 1.0, 7 August 2000, available at *http://dopey.haystack.edu/vsi/index.html.*

[3] "Mark 5B design specifications", available at *ftp://web.haystack.edu/pub/mark5/019.pdf.*

[4] "Data Input Module Mark 5B I/O Board Theory of Operation", available at *ftp://web.haystack.edu/pub/mark5/032.pdf.*

[5] "Phase Cal Extraction for the Mark 5B", available at *ftp://web.haystack.edu/pub/mark5/021.pdf.*

[6] "Mark 5B I/O Board Physical Description", available at *ftp://web.haystack.edu/pub/mark5/031.pdf*

Roger Cappallo: Integration of the Mark 5B Playback System into the Mark IV Correlator, IVS 2006 General Meeting Proceedings, p.205–205
http://ivscc.gsfc.nasa.gov/publications/gm2006/cappallo

Integration of the Mark 5B Playback System into the Mark IV Correlator

Roger Cappallo

MIT Haystack Observatory

e-mail: rjc@haystack.mit.edu

Abstract

The Mark 5B I/O boards, along with a few supporting modules, will bring a number of new capabilities to the Mark IV correlator. With this upgrade we will also be able to eliminate many of the problems associated with the Mark IV station unit. We will discuss the Mark 5B features, update the status of implementation of both correlator hardware and software, and present a brief look into our future plans for maximizing the effective usage of the Mark 5B.

[Note from the Editors: The overheads of the oral presentation of this contribution can be downloaded from the IVS 2006 General Meeting web site. Please get the PowerPoint file of the presentation at the URL ftp://ivscc.gsfc.nasa.gov/pub/general-meeting/2006/presentations/gm2006_4-08_cappallo.ppt.]

Dan Smythe: VSI Interfaces for Legacy Systems, IVS 2006 General Meeting Proceedings, p.206–210
http://ivscc.gsfc.nasa.gov/publications/gm2006/smythe

VSI Interfaces for Legacy Systems

Dan Smythe

MIT Haystack Observatory
e-mail: dsmythe@haystack.mit.edu

Abstract

The upgrade of a Mark 5A Data Transport System (DTS) to Mark 5B requires more than simply upgrading the Mark 5A system to Mark 5B. Since the Mark 5A system was designed as a plug-in replacement for a Mark IV or VLBA tape recorder, the station or correlator interfaces to the tape recorder DTS must be converted to the VSI, the VLBI Standard Interface. To that end, a set of interface boards has been designed to interface Mark IV or VLBA samplers to the VSI input of a Mark 5B Data Input Module, and to interface the Mark 5B Data Output Module to to a Mark IV correlator. This paper describes the details of these interface devices.

1. Introduction

Recent legacy VLBI recording and playback systems are based on modified versions of the Honeywell Model 96 Tape Drive. These legacy systems, and the new modules that will replace them include

- VLBA Data Acquisition System:
  - VLBA Formatter replaced with
  - VSIC Universal Converter
- VLBA Correlator:
  - VLBA Station Unit
  - To be determined in the future
- Mark IV Data Acquisition System:
  - Mark IV Formatter replaced with
  - Mark 5B Sampler Module
- Mark IV Correlator:
  - Mark IV Station Unit replaced with
  - Mark 5B Correlator Interface Module

The purpose of all of these interface modules is to convert the ECL input and output levels of the legacy systems to the LVDS levels of the Mark 5B VSI interfaces. Most of the functions of the formatters and station units have been incorporated into the Mark 5B Data Input Module (DIM) and the Data Output Module (DOM). For more information on the Mark 5B DIM and DOM, see The Mark 5B VLBI Data System by Alan Whitney [3].

1.1. VLBA Data Acquisition Systems

For VLBA data acquisition systems, the formatter will be replaced by a VSIC universal converter board described elsewhere [1]. The VSIC board converts the balanced ECL output of the

VLBA sampler modules to VSI for input to the Mark 5B DIM. Since the total output data rate of the two VLBA sampler modules in a VLBA data acquisition rack is 1024 Mb/s, connecting the VLBA samplers to a Mark 5B system doubles the maximum data rate of a VLBA system from 512 Mb/s to 1024 Mb/s.

1.2. VLBA Correlator

For the near future, the VLBA correlator is planning to use Mark 5A+ systems to play back Mark 5 B recordings, as described elsewhere in this volume by A. Whitney [3]. This arrangement requires playback through the VLBA station units, which limits the data rate to 512 Mb/s.

1.3. Mark IV Data Acquisition System

To convert a Mark IV data acquisition system to Mark 5B, the formatter is converted to a Mark 5B sampler module by replacing some of the circuit boards with a new VSI board. For a variety of reasons, the VSIC converter board described above for use with VLBA systems can not be used for this purpose.

1. The outputs of the Mark IV samplers are single-ended.
2. The total power integrators in the Mark IV video converters require a 1 Hz tick from the formatter.
3. An RS232 MAT interface is required to allow Field System control of the recording mode (geodetic, VLBA, or test vector) as described in reference [2]

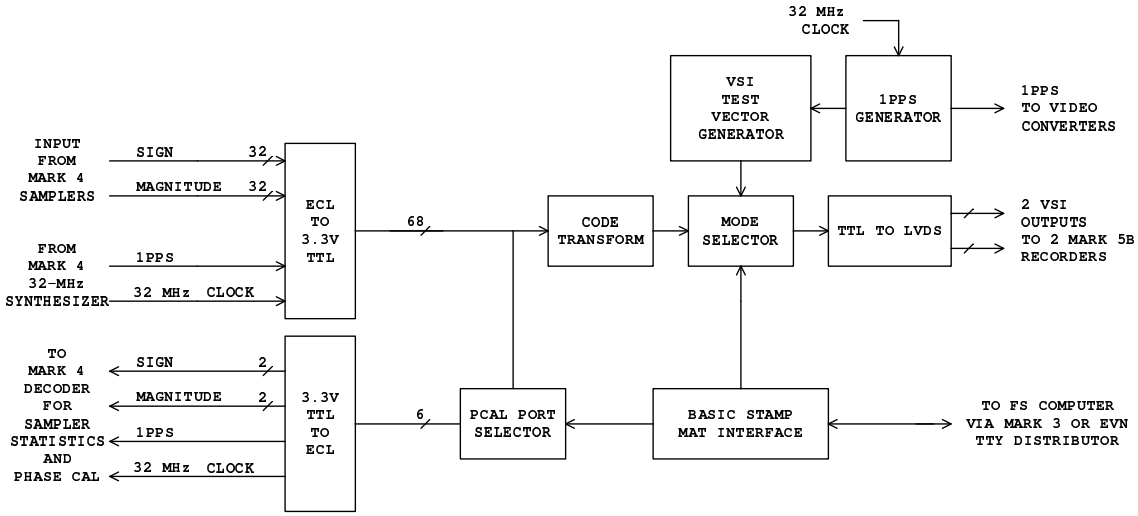

Figure 1. Block Diagram of the VSI Interface Board for the Mark 5B Sampler Module

A block diagram of the VSI interface board is shown in Figure 1. In addition to the three functions listed above, this board also encodes the sign and magnitude bit streams to make them compatible with the bit streams produced by the VLBA samplers. As an extra feature, sign and magnitude bit streams from any two video converters can be directed to the "X" and "Y" inputs

of a Mark IV Decoder to monitor sampler statistics and phase calibration tones. This feature has been used to verify proper operation of the prototype sampler module. Figure 2 is a photograph of the circuit board, and Figure 3 is a photograph of a Mark IV formatter that has been converted to a Mark 5B sampler module.

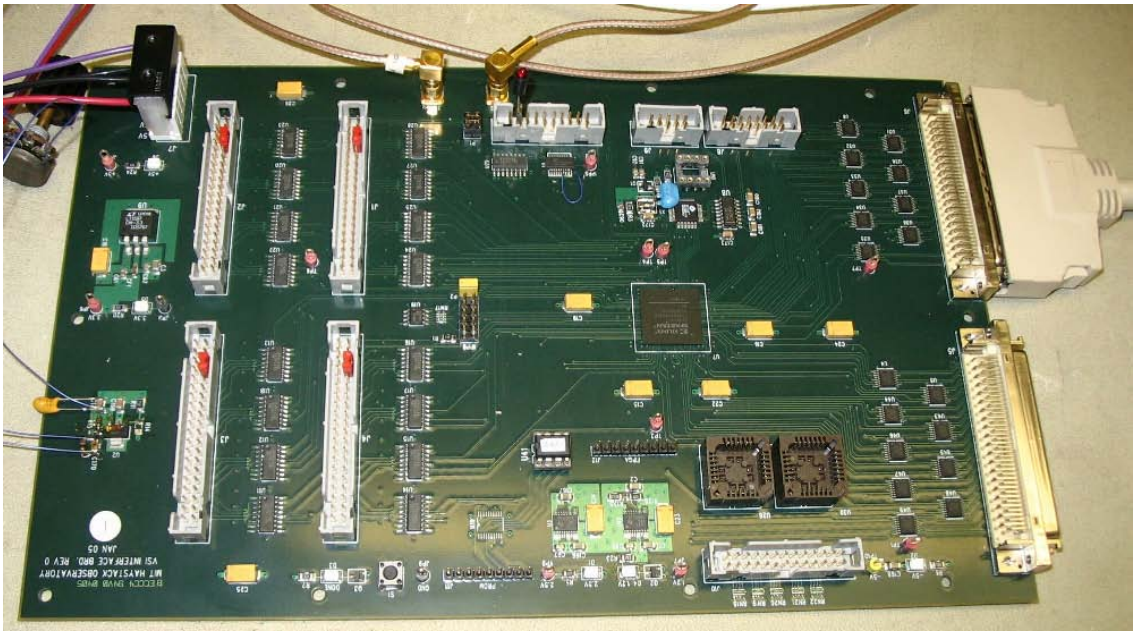

Figure 2. Photograph of the VSI Interface Board for the Mark 5B Sampler Module

Figure 3. Photograph of a Mark IV Formatter converted to a Mark 5B Sampler Module

1.4. Mark IV Correlator

A block diagram of the correlator interface board (CIB) is shown in Figure 4. It converts the LVDS levels from the VSI output of the Mark 5B DOM to the coaxial serial link outputs required for the input boards on the Mark IV correlator. It also performs some logical functions to convert the 32 sign and magnitude VSI bit streams from the DOM to the 48 encoded sign, encoded magnitude, and validity bits streams required by the Mark IV correlator. The correlator interface board also provides the DOM with the VSI clock and 1 Hz tick from the clock module on the Mark IV correlator (via the "TSPU"). A photograph of the CIB is shown in Figure 5; and a photograph of a correlator interface module, with power supplies and a CIB is shown in Figure 6.

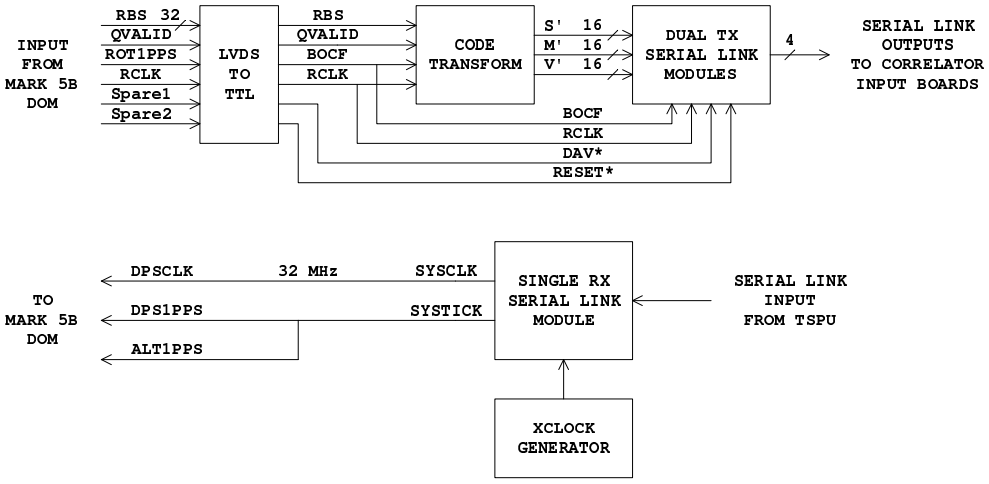

Figure 4. Block Diagram of the Correlator Interface Board

2. Summary

After upgrading to Mark 5B, all tape recorder ECL (RS422) interfaces are replaced with VSI LVDS interfaces. The functionality of the VLBA and Mark IV formatters is included in the Mark 5B DIM, and the functionality of the Mark IV station unit is included in the Mark 5B DOM. The recording data rate is doubled to 1024 Mb/s with VLBA samplers and to 2048 Mb/s with Mark IV samplers. Sixteen Video Converters or Base-band Converters (or a digital back end) and 2 Mark 5B recorders are required to achieve the full 2048 Mb/s data rate.

3. Acknowledgements

This work could not have been done without the help of Pete Bolis, Dave Fields, and Ken Wilson, who skillfully converted my designs into real hardware.

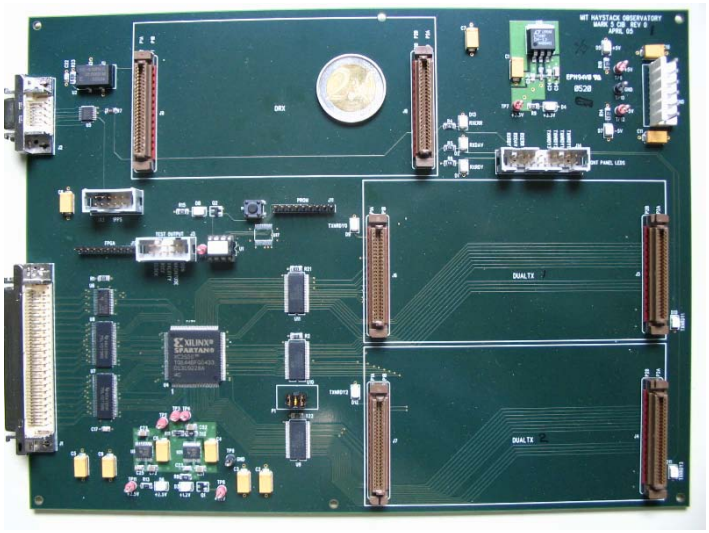

Figure 5. Photograph of a Correlator Interface Board

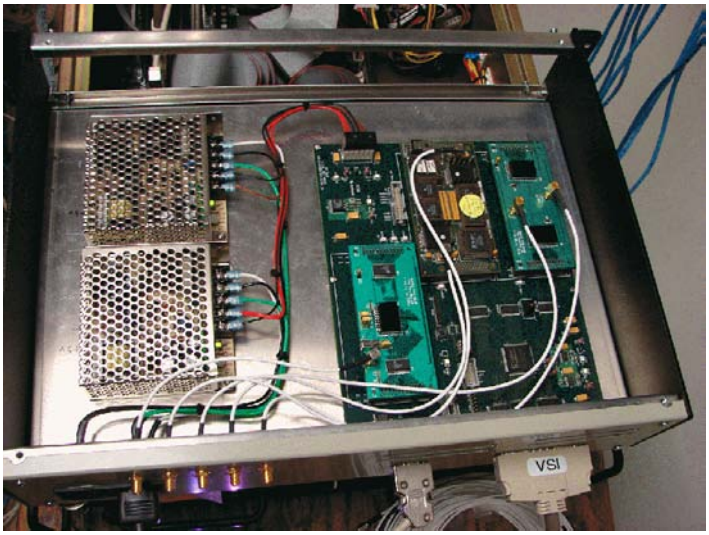

Figure 6. Photograph of a Correlator Interface Module

References

[1] Ritakari, J., A. Mujunen, Gbit/s VLBI and eVLBI with Off-The-Shelf Components, In: IVS 2004 General Meeting Proceedings, NASA/CP–2004-210002, N. R. Vandenberg and K. D. Baver (eds.), 182–185, 2004.

[2] Smythe, D., VSI Interface Board for the Mark IV Formatter, Mark 5 Memo #16, ftp://web.haystack.mit.edu/pub/mark5/016.pdf, 7 January, 2004.

[3] Whitney, A., The Mark 5B VLBI Data System, this volume, 2006.

Alan R. Whitney et al.: e-VLBI Development at Haystack Observatory, IVS 2006 General Meeting Proceedings, p.211–215
http://ivscc.gsfc.nasa.gov/publications/gm2006/Whitney3

e-VLBI Development at Haystack Observatory

Alan R. Whitney, Chester A. Ruszczyk

MIT Haystack Observatory
Contact author: Alan R. Whitney, e-mail: arw@haystack.mit.edu

Abstract

Haystack Observatory is engaged in a multi-faceted e-VLBI development program. Real-time intercontinental experiments using Mark 5A data systems and the Mark IV correlator at Haystack have been performed at sustained data rates up to 512 Mbps/station. Specialized algorithms and protocols for e-VLBI are being developed to take advantage of the unique characteristics of e-VLBI. Network performance monitoring tools have been developed. And research is being conducted using dynamically switched optical paths to provide wide dedicated pipes for e-VLBI data transmission. The biggest obstacles to widespread e-VLBI are limited connectivity of telescopes and time-varying end-to-end network performance.

1. Introduction

e-VLBI development has expanded rapidly over the past several years. At Haystack Observatory, a broad program of e-VLBI development is underway [1], including network strategy and protocol development, optically-switched network development, as well as both experimental and production e-VLBI data transfers. In this paper, we will briefly describe these areas of activity.

2. Advantages of e-VLBI

e-VLBI confers three strong advantages to VLBI measurements:

1. Bandwidth growth potential for higher sensitivity: Traditional record-and-ship VLBI is limited to a few Gbps, e-VLBI has the potential to increase data rates to 10-100 Gbps, dramatically improving sensitivity and higher-precision delay measurements.
2. Rapid processing turnaround: Processing of VLBI data can be reduced from weeks/months to hours, which is important for Earth-orientation measurements, particularly UT1, which support precision navigation.
3. Confidence in equipment and setup: e-VLBI allows test data to be correlated in advance of observing sessions to verify proper equipment setup and operation.

3. History of e-VLBI Experimental Developments

A brief accounting of e-VLBI milestones at Haystack Observatory may be instructive to understand the rate of progress in e-VLBI:

- 2002:
  - Near real-time VLBI data transferred at ~800 Mbps from Westford and GGAO

  - First intercontinental e-VLBI: Westford-Kashima at ~20 Mbps
  - Real-time e-VLBI data transfer from GGAO to Haystack observatory at 288 Mbps
- 2003:
  - First e-VLBI 'Intensive' UT1 result in under 24 hours - Westford-Kashima
- 2004:
  - Begin routine daily UT1 Intensive e-VLBI transfers from Wettzell
  - Real-time e-VLBI between Westford and GGAO at 32 Mbps
  - First intercontinental real-time e-VLBI experiment: Westford-Onsala at 32 Mbps
  - Real-time fringes at 128 Mbps between Westford and GGAO
  - Real-time fringes at 512 Mbps between Westford and GGAO
  - Begin regular transfers of K5 data from Kashima to Haystack
- 2005
  - Real-time fringes Westford-Onsala at 256 Mbps
  - Transmission of all CONT05 data from Tsukuba to Haystack (15 days at 256 Mbps); routine e-VLBI transmission of all data from Tsukuba and Kashima
  - Real-time e-VLBI demonstration at Super Computer 2005 conference: Three-station (Westford-GGAO-Onsala) real-time e-VLBI at 512 Mbps/station. Correlation results transmitted to Seattle showroom floor in real-time. See Figure 1.
- Early 2006
  - Begin commissioning of 100 Mbps e-VLBI link to Ny-Ålesund; expect to begin routine e-VLBI transmissions soon

This succession of events shows the evolution of e-VLBI from short one-time experiments to actual production transfers over a period of 3 years. Though this progress may seem impressive, there are still many problems to overcome before e-VLBI can become routine on a global basis.

Figure 1. Real-time e-VLBI demo at Super Computer 2005 conference, Nov 2005

3.1. Challenges of e-VLBI

The list of challenges confronting routine widespread global e-VLBI is significant:

- 'Last-mile' connectivity to telescopes
  - Most telescopes are deliberately placed in remote areas
  - Major initiatives in place in Europe, Japan and Australia to connect telescopes; U.S. is lagging
- End-to-end network performance is often well below advertised rates
- Performance of transport protocols
  - Untuned TCP stacks; fundamental limits of regular TCP
- Throughput limitations of COTS hardware
  - Disk to/from Network
  - Real-time VLBI data to/from network
- Complexity of e-VLBI experiments
  - e-VLBI experiments currently require significant network expertise to conduct
- Time-varying nature of network
  - R&E networks tend to be unstable, particularly towards end points

4. Antenna Connectivity

The following list shows the IP network connectivity of many of the worlds VLBI antennas and correlators (geodetic sites are underlined):

- $\geq$2 Gbps: JIVE Correlator (6 $\times$ 1 Gbps); Haystack (2.5 Gbps); Westford, MA (10 Gbps to Haystack; 1 Gbps to outside world); Kashima, Japan (2.5 Gbps); Usuda, Japan (2.5 Gbps); Nobeyama, Japan (2.5 Gbps); Koganei, Japan (2.5 Gbps); Tsukuba, Japan (2.5 Gbps)
- $\geq$1 Gbps: GGAO, MD (1 Gbps); Onsala, Sweden (1 Gbps); Torun, Poland (1 Gbps); Westerbork, The Netherlands (1 Gbps); Medicina (1 Gbps); Jodrell Bank (1 Gbps)
- Others: Arecibo, PR (155 Mbps); Wettzell, Germany ($\sim$30 Mbps); Kokee Park, HI (nominally $\sim$30 Mbps, but currently disconnected); TIGO ($\sim$2 Mbps); Svetloe (speed unknown)

In progress:

- Hobart - agreement reached to install high-speed fiber; details not known
- Ny-Ålesund - work in progress to provide 100 Mbps link for e-VLBI data to Haystack Observatory
- Fortaleza - funds secured for fiber connection at 2.5 Gbps; early 2006
- Metsahovi - 1 Gbps in 2006
- Zelenchukskaya, Russia - details unknown

- Badary, Russia - details unknown

Considerable effort is now being expended to connect most of the remaining antennas and correlators, but connections can be quite expensive and are often limited by budgetary resources. One major unconnected resource is the VLBA array of ten 25 m antennas.

5. e-VLBI Standardization (VSI-E)

A reference implementation of the proposed VSI-E (VLBI Standard Interface - e-VLBI) [2] is now being tested in transfers between Kashima and Haystack. This implementation is intended to act as a demonstration model for VSI-E and is available to all interested parties. The VSI-E framework provides signaling, control, framing and statistics support and is an extension to the internet RTP standard. It also provides flexibility in that it allows users to choose the transport protocol that best suits the network environment (e.g. UDP, TCP or other variants). Once the reference implementation is fully checked out and any needed changes are made, attention will be turned to optimizing the code for high-speed operation.

6. Throughput Limitation of COTS Hardware

Though the Mark 5 data system [3] can record and playback data at 1 Gbps, it is surprisingly difficult to manage those same data rates to/from network connections. Routine e-VLBI operation at 512 Mbps is readily achievable with today's systems, but operation at 1024 Mbps is difficult. In laboratory tests at Haystack Observatory using high-end PC motherboards with dual bonded Gigabit Ethernet links, data transfer rates of up to ~1280 Mbps have been achieved. To date, however, these rates have not yet been achieved in any practical e-VLBI experiments.

A new generation of PC motherboards is now appearing which replace the PCI bus with the PCIExpress bus. This high-speed serial bus promises much higher speed operation and should allow routine operation of e-VLBI at rates exceeding 1 Gbps.

7. Intelligent e-VLBI Applications

Based on observed usage statistics of a typical R&E backbone, such as the NSF 10 Gbps Abilene backbone network in the U.S., it is clear that there is much unused capacity. e-VLBI data has some unique qualities that may allow e-VLBI to effectively use some or much of this unused 'secondary' network capacity. Special characteristics of e-VLBI that might be taken advantage of include:

- Ability to tolerate some loss of data (up to ~5% or so) in many cases
- Ability to tolerate delay and jitter in data transmission, which can normally be accommodated by large buffers at both transmitting and receiving end

With support from the National Science Foundation, Haystack Observatory is developing an 'Experiment Guided Adaptive Endpoint' (EGAE) strategy designed to meet this challenge. EGAE performs dynamic adaptation based on simple high-level description of experiment requirements and its surrounding environment, expressed in language appropriate to the scientific end-user. These requirements are then translated by an application-specific translator into specific network requirements. EGAE controllers at both the network data and control planes gather information

and react to network conditions by altering the data flow between the DIM and DOM so as to be a 'friendly' user on the network, specifically lowering data rates quickly when higher priority 'primary' users demand network bandwidth. A prototype EGAE implementation is now in use in production e-VLBI transfers at Haystack.

8. Dynamically Optically-Switched Light Paths

Haystack Observatory is collaborating with the University of Maryland and others in the DRAGON (Dynamic Resource Allocation via GMPLS Optical Networks) project [4], under sponsorship of the National Science Foundation. The objective of the DRAGON Project is to create dynamic and deterministic end-to-end network transport services for high-end e-Science applications, and is concentrating on on-demand creation and teardown of optically-switched light paths. This type of network conditioning is made possible by two fairly recent technological breakthroughs:

1. Dense wave-division multiplex (DWDM) technology, which allows many (more than 100) individual wavelengths to be placed on a single fiber, each capable of carrying at least 10 Gbps of data.
2. Optical switches capable of switching individual wavelengths among an array of fibers.

These two capabilities, working together, allow the dynamic creation and teardown of all-optical high-bandwidth paths on user demand. Because the switching is all-optical, expensive routers and switches, which must convert from optical-to-electrical-to-optical, can be eliminated or minimized.

Haystack Observatory is working with the DRAGON project to develop software application interfaces applicable to e-VLBI and other applications that might benefit from this technique. Ultimately, the DRAGON project may allow e-VLBI data to/from Haystack Observatory to be routed entirely (or at least mostly) optically to/from the Abilene backbone network in the U.S. This work will be fully integrated with the EGAE project described above.

9. Summary

Though e-VLBI has been developing rapidly over the past few years, much more work needs to be done before it can become truly operational. This includes not only some of the areas we have described here, but must include others as well. For example, as more high-bandwidth applications compete for limited network bandwidth, bandwidth-reservation systems and direct optically-switched paths become attractive. Many groups in several countries are working on these problems, and e-VLBI will be truly successful only with the close international collaboration of the VLBI and global networking communities.

References

[1] Haystack e-VLBI program information available at *http://web.haystack.mit/e-vlbi/evlbi.html*

[2] VSI information available at "VLBI Standard Interface Specification - VSI-H," August 2000, Revision 1.0, available at *http://web.haystack.edu/vsi/index.html.*

[3] Mark 5 information available at *http://web.haystack.edu/mark5/Mark5.htm.*

[4] DRAGON project details at *http://dragon.maxgigapop.net/twiki/bin/view/DRAGON/webHome*

Yasuhiro Koyama et al.: e-VLBI Developments with the K5 VLBI System, IVS 2006 General Meeting Proceedings, p.216–220
http://ivscc.gsfc.nasa.gov/publications/gm2006/koyama

e-VLBI Developments with the K5 VLBI System

Yasuhiro Koyama [1], *Tetsuro Kondo* [1], *Moritaka Kimura* [1], *Hiroshi Takeuchi* [1], *Masaki Hirabaru* [2]

[1)] *Kashima Space Research Center, National Institute of Information and Communications Technology*
[2)] *National Institute of Information and Communications Technology*

Contact author: Yasuhiro Koyama, e-mail: koyama@nict.go.jp

Abstract

The K5 VLBI system has been developed at the Kashima Space Research Center of the National Institute of Information and Communications Technology (NICT). The concept of the K5 VLBI system is to realize real-time VLBI observations and correlation processing under the various observing modes by combining multiple components in a flexible manner. The system is also intended to be VSI-H compliant by using the VSI-H PCI interface card and VSI-E compliant by developing a set of software programs that work with the vtp (VLBI Transfer Protocol) libraries developed at Haystack Observatory. The current status of the K5 VLBI system's developments and the recent achievements for e-VLBI by using the K5 VLBI system will be reported.

1. Introduction

Recent research and developments in network technology have resulted in an environment in which the network data transmission rate far exceeds the data recording rate of magnetic tape recorders (typically 1024Mbps) and recent disk based VLBI recording systems. Therefore, a significant improvement in the sensitivity of VLBI observations can be expected if real-time correlation processing of observation data can be performed without the data recording procedure at observing sites. In addition, with the near-real-time processing of VLBI observation data enabled by e-VLBI, a high-precision estimation of the irregular variations of Earth orientation parameters becomes theoretically possible, which in turn can lead to improved precision in tracking deep-space probes and more precise determination of the satellite orbital information required for high-precision GPS measurements. These developments are expected to make a significant overall contribution to the fields of space exploration and geodesy.

Nevertheless, technical problems remain in the high-speed transmission of massive volumes of data over the Internet. Some of these problems form interesting themes for research and developments in network technology, with topics including maximizing use of available data transmission capacity in the presence of other types of traffic or effective congestion control under the situation of significant network transmission delay. Accordingly, numerous researchers are currently focusing concerted efforts on these and similar challenges.

In the past, the Tokyo Metropolitan Wide Area Crustal Deformation Monitoring Project (also known as the Keystone Project, or KSP) launched by the Communications Research Laboratory (CRL, now NICT) represented the first efforts to introduce the e-VLBI concept into the daily VLBI operations. System development for the project had as its goal the high-precision, high-frequency measurements of the relative positions of four VLBI stations, and was structured to override the existing framework of VLBI observation systems at several points [3]. One such innovation involved

the realization of real-time VLBI observation data processing for the four-station, six-baseline array via an ATM (Asynchronous Transfer Mode) network. This system, developed under the auspices of a collaboration between CRL and NTT Communications, Inc., dramatically reduced the time required for data processing relative to existing systems, which relied on magnetic tape recording. Further, this was the first system of its kind to be completely automated from observation to data processing and analysis with the results of the analysis of nearly non-stop VLBI observations automatically available to the public on the Internet [1]. The development of this system proved that e-VLBI technology could enable near-real-time data processing with virtually no delay between observation and processing.

However, this observation and processing system was tailored to an ATM network. As such, the system could not be used to connect multiple VLBI stations throughout the world since it was not feasible to construct an international dedicated ATM network just for e-VLBI. To increase the versatility of this system, the development of the K5 observation and processing system was begun in 2000, eventually resolving earlier problems by enabling data transmission via IP (Internet Protocol), under Internet network conditions involving the presence of other types of traffic.

2. Developments of the K5 System

The K5 VLBI system is designed to perform real-time or near-real-time VLBI observations and correlation processing using IP over commonly used shared network lines. Various components are being developed to realize the target goal in various sampling modes and speeds. The entire system will cover various combinations of sampling rates, number of channels, and number of sampling bits. All of the conventional geodetic VLBI observation modes will be supported as well as other applications like single-dish spectroscopic measurements or pulsar timing observations. Table 1 shows comparisons of the K3, K4 and K5 systems in various aspects to identify the characteristics of the K5 system. As shown in Table 1, the K5 system is characterized by the use of a disk based recording method and by the use of the IP protocol for e-VLBI. The data correlation processing is performed by using software correlator programs running on multiple PC systems in the K5 system. Similarly, the K4 system can be characterized by the use of rotary-head, cassette type magnetic tape recorders, and the K3 system can be characterized by the use of open-reel magnetic tape recorders.

In contrast to the real-time correlation processing unit developed for the KSP, which realized high-speed digital data processing through the use of the FPGA, a software correlator has been developed for the K5 system to perform distributed processing using a PC running on a versatile operating system. While a hardware correlator lacks flexibility due to the extended development time required, a software correlator may be modified easily to add new functions or to revise processing modes. In addition, development is also underway for software required to enable distributed processing using available computer resources (consisting of multiple CPUs) to the maximum extent, in order to provide the needed processing capacity for data collected at numerous VLBI stations in the context of large-scale VLBI experiments.

The concept of the K5 system is shown in Figure 1. ADS1000, ADS2000, and ADS3000 are high speed A/D samplers. Output digital signals from these A/D samplers are interfaced to the PCI bus of the PC by using the PC-VSI board according to the VSI-H (VLBI Standard Interface Hardware specifications) compliant signaling. Whereas the ADS1000 is designed as a single channel high speed sampler unit, the ADS2000 is designed for geodetic VLBI observations by supporting

Table 1. Comparisons of the K3, K4, and K5 systems.

	K3	K4	K5
Data Recorders	Magnetic Tapes Longitudinal Recorders	Magnetic Tapes Rotary Head Recorders	Hard Disks
e-VLBI	Telephone Line	ATM	IP
Correlators	Hardware	Hardware	Software
Years in use	1983-	1990-	2002-
Systems	M96 Recorder, K3 Formatter, K3 VC, K3 Correlator	DIR-1000, -L -M, DFC1100, DFC2100, K4 VC (Type-1, 2), TDS784, ADS1000, GBR1000, GBR2000D, K4 Correlator, KSP Correlators, GICO, GICO2	K5/VSSP, K5/VSSP32, K5/VSI, ADS1000, ADS2000, ADS3000, Software Correlatos (cor, fx_cor, GICO3)

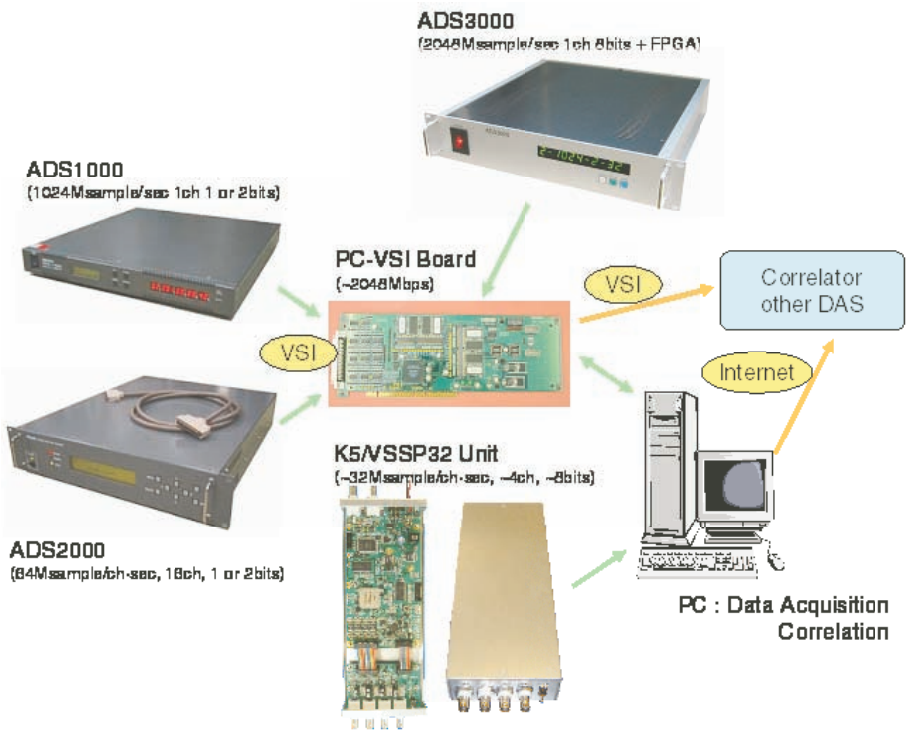

Figure 1. Concept of the entire K5 system.

16 channels with sampling rates up to 32Msps for each channel. The ADS3000 A/D sampler unit is currently under development and it will support various observing modes by using FPGA (Field Programmable Gate Array) and a 4Gsps high speed A/D sampler chip. The prototype unit of the ADS3000 has been completed and the first fringe was detected between the 34-m and 11-m stations at Kashima using single channel observations with 2048Msps, 2bits-per-sample sampling mode. When relatively low sampling rates are required, PC systems with the IP-VLBI units are

used as shown at the bottom of Figure 1. Originally, specially designed PCI boards called IP-VLBI boards were used in the K5/VSSP system. The boards are installed on the PCI expansion bus slots to support 4 input channels sampling at up to 16Msps. Recently, the external K5/VSSP32 units have been developed. The K5/VSSP32 units are connected with the PC system by using USB 2.0 interface cables. The new units support 32Msps and 64Msps sampling speeds which were not supported by the PCI type IP-VLBI boards. By using four units of the K5/VSSP32, 16 channel geodetic VLBI observations can be performed. VSSP is an acronym for Versatile Scientific Sampling Processor. This name is used because the system is designed to be used for general scientific measurements. The system has the capability to sample analog data streams by using the external frequency standard signal and the precise information of the sampled timing. The system is also used to process the sampled data. For geodetic VLBI observations, a software correlation program runs on the K5/VSSP system. Therefore, it can be said that the functions of the formatter, the data recorder, and the correlator are combined into a single system. It consists of four UNIX PC systems. In Table 2, the characteristics of these A/D sampling components developed for the K5 system are shown.

Table 2. Comparisons of A/D sampling systems in the K5 system.

	K5/VSSP	K5/VSSP32	ADS1000	ADS2000	ADS3000
Sampling Speed	40, 100, 200, 500kHz, 1, 2, 4, 8, 16MHz	40, 100, 200, 500kHz, 1, 2, 4, 8, 16, 32, 64MHz	1024MHz	64MHz	2048Msps
Sampling Bits	1, 2, 4, 8	1, 2, 4, 8	1, 2	1, 2	6
No. Channels	1, 4, 16 (with 4PCs)	1, 4, 16 (with 4PCs)	1	16	Programmable with FPGA
Max. Data Rate	512Mbps (with 4PCs)	2048Mbps (with 4PCs)	2048Mbps	2048Mbps	4096Mbps

3. e-VLBI Data Transfer Using VSI-E

By using the developed K5 system, we have started efforts to transfer the observed data over the network using the VSI-E protocol. VSI-E is under discussion to standardize the protocol of massive real-time data transfer for e-VLBI [2]. Based on the current draft proposal of the VSI-E, vtp (VLBI Transport Protocol) libraries have been developed by David Lapsley and his colleagues at Haystack Observatory. The library interfaces data stream from the transmitting sites to the receiving sites over the Internet network using either TCP/IP or UDP/IP. An interface program for the K5 data stream at the transmitting site has been developed by us and the program was used with the vtp libraries. By using these programs, a file format conversion demonstration was performed in July 2005 as shown in Figure 2. Recently, we are continuing our efforts to use these programs for real-time correlation by using the Mark IV correlator at the Haystack Observatory after converting the K5 format data stream at the transmitting site and sending the converted data stream over the network using the VSI-E protocol as shown in Figure 2. In the next step, we are planning to develop an interface for the receiving side to be converted into the K5 data stream format. When the program is completed, it will become possible to correlate the transmitted data with the K5 software correlator in real-time by using the data stream signals transmitted using

the VSI-E protocol.

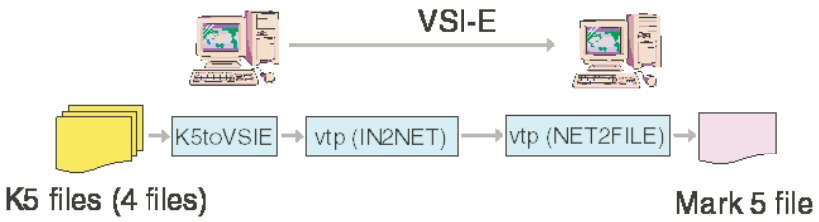

Figure 2. File format conversion by using VSI-E.

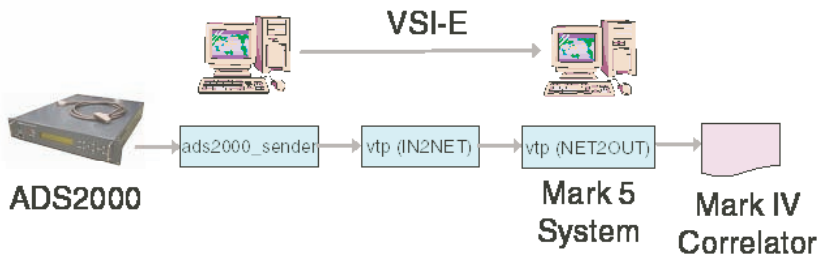

Figure 3. Real-time data transfer by using VSI-E.

Acknowledgement

The e-VLBI research and developments have been conducted jointly with a group of researchers from various institutes including the Haystack Observatory of the Massachusetts Institute of Technology. In Japan, the NICT is collaborating with the National Astronomical Observatory of Japan, the Geographical Survey Institute, the Japan Aerospace Exploration Agency, Gifu University, and Yamaguchi University. We are deeply grateful for the support of the NTT Laboratories, KDDI R&D Laboratories, NTT Communications, Inc. for using the research-dedicated high-speed network, and to the staff members managing the research networks of the JGNII, TransPAC2, Internet2, and Super SINET.

References

[1] Koyama, Y., N. Kurihara, T. Kondo, M. Sekido, Y. Takahashi, H. Kiuchi, and K. Heki, Automated geodetic very long baseline interferometry observation and data analysis system, Earth Planets Space, **50**, pp. 709-722, 1998.

[2] Draft Proposal for VSI-E - Rev 2.7, available at ftp://web.haystack.mit.edu/pub/e-vlbi/, Jan. 2004.

[3] Yoshino, T., Overview of the Key Stone Project, Special Issue of the J. Comm. Res. Lab., **46**, pp.3-6, 1999.

Hiroshi Takeuchi et al.: A VSI-compliant 2-Gsps DAS for Spacecraft Differential VLBI, IVS 2006 General Meeting Proceedings, p.221–225
http://ivscc.gsfc.nasa.gov/publications/gm2006/takeuchi

A VSI-compliant 2-Gsps DAS for Spacecraft Differential VLBI

Hiroshi Takeuchi, Moritaka Kimura, Junichi Nakajima, Ryuichi Ichikawa, Mamoru Sekido, Tetsuro Kondo, Yasuhiro Koyama

Kashima Space Research Center, National Institute of Information and Communications Technology (NICT), Japan

Contact author: Hiroshi Takeuchi, e-mail: ht@nict.go.jp

Abstract

A 2048-Msps (2048 Mega samples per second) data acquisition system (DAS) that complies with VLBI Standard Interface (VSI) has been developed. The new A/D sampler, named ADS-3000, is upward compatible with ADS-1000, current-generation 1-Gsps sampler used for wide-bandwidth astronomical observations. This new DAS has two VSI-H output ports and each operates at a clock frequency of 32 MHz or 64 MHz. Thus the maximum output rate reaches 4096 Mbps. The first-ever 4-Gbps (2048 Msps/2 bits) VLBI experimental observations were successfully performed between Kashima 34m and Kashima 11m antennas on November 25,2005 by using these samplers. Both the data sampling rate (2 Gsps) and the total data rate (4 Gbps) recorded the highest rate ever used for VLBI.

1. Introduction

High speed data acquisition is one of the key technologies for sensitive radio continuum observations in VLBI. To detect fainter radio sources with a shorter integration time, NICT has developed high-speed Gigabit A/D samplers, named K5/VSI series, that support the VSI-H specifications [1]. ADS-1000 [2] is a VSI-compliant, single-channel, 2-bit A/D sampler whose sampling rate is 1 GHz. It is widely used at Japanese domestic VLBI stations especially for wideband astronomical observations. ADS-2000 is a VSI-compliant, 2-bit A/D sampler equipped with 16-channel analog input ports, which is dedicated to geodetic VLBI observations. Sampling rate is selectable from 2,4,8,16,32 or 64 MHz and thus total data rate is up to 2 Gbps. As a successor of these samplers, we developed a new A/D sampler named ADS-3000 having the following features:

- Data sampling rate is increased to 2 GHz, providing $\sqrt{2}$ times improved sensitivity for astronomical purposes than using ADS-1000. The frequency difference between the lowest and the highest frequency channels at X-band exceeds 500 MHz in some recent IVS sessions. This data sampling rate is high enough for such geodetic sessions.
- The number of quantization bits is increased to 8 bits. While 2-bits quantization is enough for normal radio sources in conventional VLBI sessions, it is not enough for high SNR signals such as satellite downlink signals or for single-dish power-measurement experiments such as pulsar timing observations. This wide quantization bit depth allows it to be used not only for VLBI but also for a variety of general applications.

We describe the specifications of the ADS-3000 and report on the first VLBI experiments with the DAS.

2. System Overview

The main specifications of the sampler are summarized as follows:

- Reference signal: 1 pps signal, reference 10-MHz clock (0 dbm± 3dbm, 50Ω)
- A/D input: 0V±250mVp-p(50Ω), Sampling rate: 2048 MHz (fixed), 3.3 GHz full power input bandwidth(-3dB)
- Gain flatness: ±0.2dB(from DC up to 1.5 GHz)
- Low input VSWR: 1.2 Max From DC to 2.5 GHz
- SFDR = -54dBc, 6.5 Effective Bits for 2 GHz input [-1 dBFS]
- Bit error rate: 10e-12 at 2Gsps
- PLO phase noise: 100 Hz-up to 70 dBM/Hz, 1 kHz-up to 80 dBm/Hz, 10 kHz-up to 90 dBm/Hz, 100 kHz- up to 110 dBm/Hz
- Dimension: 88.1mm(H) x 482.6mm(W) x 430mm(D)
- Power supply voltage: AC100V-230V

In the sampler, 8-bit digitalized data with a 2-Gsps,10-bit A/D converter (Atmel Corporation, TS83102G0B) are sent to Field Programmable Gate Array (FPGA) device (Xilinx, XC2VP40) to be processed (Fig.3). This 16-Gbps input data can be decimated with the FPGA to limit the total output rate within 4Gbps, the highest output rate realized with two VSI-H ports. Selectable output modes are listed in Table 1. Because the used A/D converter chip has a sensitivity up to 3.3 GHz, the higher order sampling method, in which band-limited signals which have the higher frequency components compared to the Nyquist frequency of the sampler (1 GHz), is also available. FPGA code is easily programmable by inserting a CompactFlash (CF) memory card, on which FPGA program is written, into the CF slot (Fig.2) of the ADS-3000 so that it can be used for multiple independent applications.

Table 1. Selectable output modes of ADS-3000. There is a trade-off between sampling rate and number of quantization bits.

Total rate	**Sampling rate**	**# of bits**	**Clock rate**	**Output VSI-H ports**
1Gbps	128 Msps	8	32 MHz	Port1
2Gbps	1024 Msps	2	32 MHz	Port1(MSB) + Port2(LSB)
2Gbps	512 Msps	4	32 MHz	Port1(Upper 2bits) + Port2(Lower 2bits)
2Gbps	256 Msps	8	32 MHz	Port1(Upper 4bits) + Port2(Lower 4bits)
2Gbps	256 Msps	8	64 MHz	Port1
4Gbps	2048 Msps	2	64 MHz	Port1(MSB) + Port2(LSB)
4Gbps	1024 Msps	4	64 MHz	Port1(Upper 2bits) + Port2(Lower 2bits)
4Gbps	512 Msps	8	64 MHz	Port1(Upper 4bits) + Port2(Lower 4bits)

Figure 1. Front view of ADS-3000.

Figure 2. Rear view of ADS-3000. FPGA logic is easily programmable with a CompactFlash card, or an Ethernet port which will be equipped after the next upgrade. 2048-MHz PLL-output port and 2048-MHz input port are directly connected in most cases. 2048-MHz reference signal can be distributed to other units by using these ports.

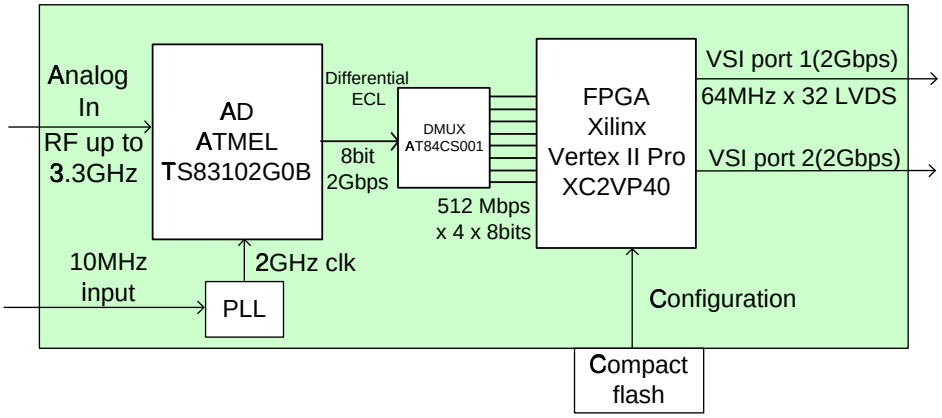

Figure 3. Schematic diagram of ADS-3000.

3. Applications

By configuring the FPGA device, a wide range of applications will be possible such as digital baseband converter for multi-channel geodetic VLBI, software demodulator for spacecraft downlink signal in spacecraft VLBI or satellite communications, or spectrometer for broadband astronomical observations (see Table 2). Some applications can be realized with free IP (Intellectual Property) cores distributed by FPGA vendors. Digital baseband converter (DBBC) is one of the expected applications, which substitutes the conventional multi-channel analog baseband converters. If the input IF signals are band-limited and 128Msps mode is available, general-purpose IP-core product [3] can be used for it. To utilize the full 1 GHz band, the input signal to the DBBC should be multiplexed and the dedicated parallel-processing digital mixer circuit, in which the number of bits is lower than general-purpose ones, should be used. Such FPGA-based DBBC systems dedicated to the backend system of radio telescopes have already been developed and used in several projects (See [4],[5],[6]). DBBC is also useful in differential VLBI observations for spacecraft navigations. In the observations, the target source is switched between spacecraft and phase-reference quasars in order to cancel out phase variations. To ensure a sufficient number of phase-reference quasars near the spacecraft, wide-bandwidth IF sampling is effective. On the other hand, DBBC is useful

for spacecraft observations because the bandwidth of the spacecraft signals is very narrow. Using the digital BBC system, the total data size can be reduced and the signal-to-noise ratio of the data can be improved for the narrowband spacecraft signals. Moreover, it is easy to compensate for the Doppler shift of the spacecraft signals by real-time tuning with direct digital synthesizer. Because the phase relationship is preserved through the baseband conversion processes, we can use wideband quasar signals as phase reference for narrowband spacecraft signals.

Table 2. Expected applications realized by FPGA IP cores.

Applications	**Available IP-cores**
DC-cut,RFI mitigation	Substractor,FIR filter
DBBC	DBBC, FIR filter, DDS
Spectrometer, Wideband P-cal detector	FFT, Integrator
Format converter (K5,Mark 5,PC-EVN...)	CRC, Look-up table
Dispersion compensator for pulsar observations	FFT, Complex multiplier
Software receiver for satellite communications	FIR filter, DBBC

4. Observations

The first-ever 4-Gbps VLBI fringe was successfully detected (Fig.5) in the HAYABUSA spacecraft navigation differential VLBI experiments performed between Kashima 34m and Kashima 11m antennas on November 25-26, 2005. Two-sets of PC-VSI recorders [7] were used at each

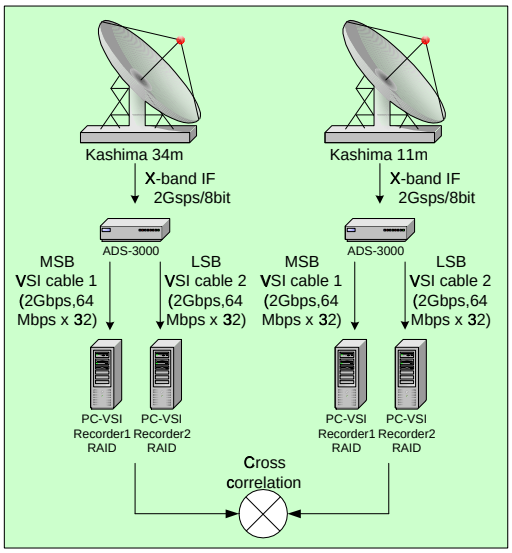

Figure 4. Schematic diagram of recording system for the 4-Gbps VLBI experiments.

station (Fig. 4). While 4-Gbps (2Gsps/2bit) of wide-bandwidth sampling mode was used for the scans for reference quasars, 512-Mbps/8bit mode was used to capture the high-SNR signals from HAYABUSA spacecraft.

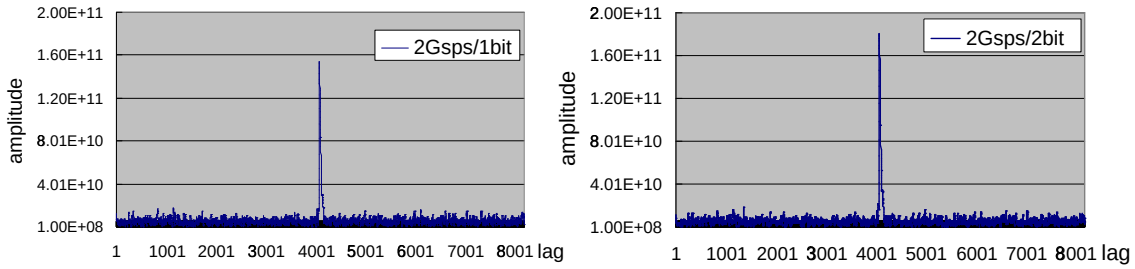

Figure 5. The first-ever 4-Gbps fringes between Kashima 34m and Kashima 11m antennas at X-band observation toward 3C273B on November 25,2005. Integration time is 4s. The over-sampling factor is 2, because the current IF bandwidth at Kashima 11m station is limited to 500 MHz. A correlation amplitude with 2-bit correlation was 123% of that with 1-bit correlation (using only the MSB data). This is consistent with the theoretical value of 124%(= 0.935/0.744).

5. Conclusion and Future Plan

We have developed a VSI-compliant 2048-Msps A/D sampler named ADS-3000, which is upward compatible with ADS-1000. The first-ever 4-Gbps (2 Gsps/2 bits) VLBI experiments were successfully carried out using the samplers. This sampler has an FPGA-based extensibility to enable it to be used for a wide range of applications. We expect that it will be used for not only a VLBI observation but also a general-purpose experiment which requires precise time label. We will install an FPGA-based DBBC system to perform spacecraft-navigation differential VLBI experiments, in which wideband IF signals are directly recorded in the scans for reference quasars and digitally extracted baseband signals are recorded for the narrow-band signals from spacecrafts to measure phase delays.

References

[1] Whitney, A.R., "VLBI Standard Hardware Interface Specification - VSI-H", 2000, Revision 1.0, Available from http://web.haystack.edu/vsi/

[2] Nakajima, J., Y. Koyama, M. Sekido, N. Kurihara, T. Kondo, M. Kimura, N. Kawaguchi, "1-Gbps VLBI, The First Detection of Fringes", Experimental Astronomy No.11, 57–69, 2001

[3] "GateFlow Wideband Ultra High-Speed DDC IP Core", Available from http://www.pentek.com/gateflow/gateflow_ipcore.cfm

[4] Tuccari, G., "DBBC - a Wide Band Digital Base Band Converter", In: IVS 2004 General Meeting Proceedings, NASA/CP–2004-212255, N. R. Vandenberg and K. D. Baver (eds.), 234–237, 2004

[5] Xiang, Y., G. Tuccari, W. Wei, "FPGA Implementation in DBBC", In: IVS 2006 General Meeting Proceedings, D. Behrend and K. D. Baver (eds.), 2006 (this volume)

[6] Comoretto, G.,"A Digital BBC for the ALMA Interferometer", ALMA Memo No.305, 2000

[7] Kimura, M., J. Nakajima, "The implementation of the PC based Giga bit VLBI system", IVS CRL Technology Development Center News, No.21, 31–33, 2002.

Ryuichi Ichikawa et al.: An Evaluation of Atmospheric Path Delay Correction in Differential VLBI Experiments for Spacecraft Tracking, IVS 2006 General Meeting Proceedings, p.226–230
http://ivscc.gsfc.nasa.gov/publications/gm2006/ichikawa

An Evaluation of Atmospheric Path Delay Correction in Differential VLBI Experiments for Spacecraft Tracking

Ryuichi Ichikawa, Mamoru Sekido, Yasuhiro Koyama, Tetsuro Kondo

Kashima Space Research Center, National Institute of Information and Communications Technology
Contact author: Ryuichi Ichikawa, e-mail: richi@nict.go.jp

Abstract

We evaluate an effect of cancelling out atmospheric path delay errors on the HAYABUSA differential VLBI measurements based on the delays derived from geodetic GPS analysis. The experiments were carried out on October 16 and 18, 2004. A large difference value of up to 10 cm of the differential path delay for the Kashima-Uchinoura baseline was estimated based on the analysis. It is considered that this large value is caused by the high water vapor content due to the typhoon approaching Uchinoura, the constellation of the baseline vector and the difference in elevation angle at the two stations.

1. Introduction

We perform differential VLBI ($\Delta VLBI$) experiments for tracking of interplanetary spacecraft. Our main goal is to obtain a precise and quasi-realtime navigation technique of the spacecraft using VLBI. With VLBI time delay measurements, we difference observations between the spacecraft and angularly nearby quasars to cancel out common measurement errors such as the propagation delays due to the ionosphere and the neutral atmosphere. However, we can not always observe desirable quasars. It is possible that they do not have enough intensity of the source flux to detect fringes. Unfortunately, sometimes we have no choice but to use quasars which are angularly far from the spacecraft. Then, we tried to evaluate the effects of cancelling errors by subtracting the group delays of the reference radio source from those of the spacecraft. In this short report, we focus on the issue of the path delay due to the neutral atmosphere estimated by geodetic GPS measurements.

2. VLBI and GPS Measurements

Table 1. Geodetic GPS stations nearby VLBI stations

VLBI station name	corresponding GPS station ID	Agency
Kashima 34-m and 11-m	KSMV (IGS)	KSRC, NICT
Koganei 11-m	KGNI (IGS)	NICT
Tsukuba 32-m	TSKB (IGS)	GSI
Usuda 64m	USUD (IGS)	ISAS/JAXA
Uchinoura 34-m	940099 (GEONET of GSI)	ISAS/JAXA

Two HAYABUSA $\Delta VLBI$ experiments were carried out, in October, 2004, in order to evaluate the reduction of propagation delays due to the ionosphere and neutral atmosphere using $\Delta VLBI$ technique . The experiment IDs of October 16 and 18 are "hy4290" and "hy4292", respectively. We used Kashima 34-m, Kashima 11-m and Koganei-11m of NICT, Usuda 64-m and Uchinoura 34-m of ISAS/JAXA, and Tsukuba 32-m of GSI antennas for the experiments at X-band. The VLBI stations in this study are shown in Figure 1. We acquired the VLBI data using both K5/VSSP system.

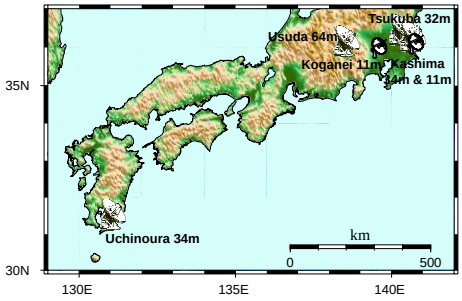

Figure 1. VLBI stations participated HAYABUSA DVLBI experiments

The observing time for each day was 7 hours from 0700 to 1400UT. The HAYABUSA spacecraft and an angularly nearby quasar "2126-158" were observed sequentially, not simultaneously, during each period with various time intervals of data acquisition (i.e. 50 seconds, 110 seconds, and 170 seconds). These switching intervals were chosen in order to investigate an effect on the phase delay analysis. A result of the investigation will be described in the another report. Two quasars, "NRAO530" and "3C454.3", were also observed at the beginning and the end of the experiment period as a reference source for determining a clock offset. For example, the maximum angular separations of the spacecraft from the quasar "2126-158" are less than 3 degrees on 18 October 2004 at Uchinoura.

In addition, we also acquired the data sets of the corresponding GPS stations near each VLBI station (Table 1). The GPS station "940099" is part of the GPS Earth Observation Network (GEONET), Geographical Survey Institute (GSI) in Japan and it is located about 1 km northeast from Uchinoura 34-m antenna. Other GPS stations are registered with the International GNSS Service (IGS) and all of them are adjacent to a VLBI antenna.

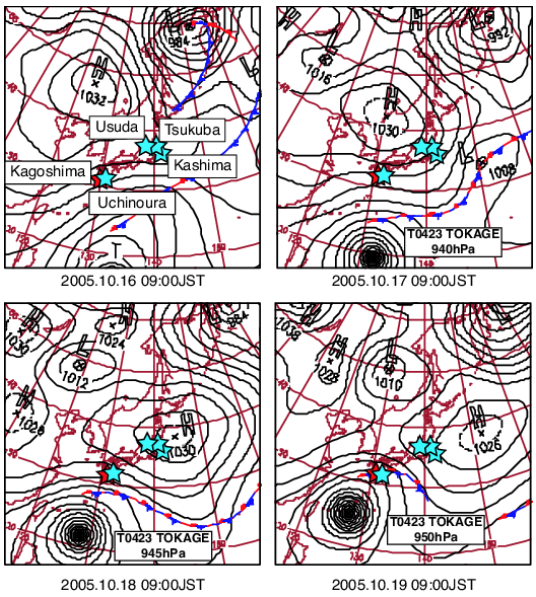

Figure 2. Synoptic weather charts around Japan from 0000UTC of 16th to 0000UTC of 19th October, 2004. Dark gray star and bright gray stars indicate the location of Kagoshima meteorological observatory, Japan Meteorological Agency (JMA) and the VLBI stations, respectively.

3. Meteorological Condition

Figure 2 shows synoptic weather charts around Japan from 0000UTC of 16th to 0000UTC of 19th October 2004. During the first experiment (hy4290), the weather was calm and sunny around the Japanese islands. After the 17th October, the strong typhoon 0423 (TOKAGE) was approaching south of Kyushu island, where Uchinoura station is located. The significant pressure depression at Kagoshima meteorological observatory of Japan Meteorological Agency (JMA), which is located

about 100 km west of Uchinoura, is indicated in Figure 2 (lower panel). So, we unfortunately had to interrupt the hy4292 experiment around 0600UTC. The center of the typhoon passed about 100 km east of Uchinoura on 20th October and it hit central Japan with severe damage caused by heavy rainfall and strong wind.

4. Estimation of Atmospheric Delay by GPS Measurements

4.1. Zenith Wet Delay

First, we estimate the path delay due to the neutral atmosphere at zenith direction (ZTD: Zenith Total Delay) for each station through the double-difference procedure using the Bernese GPS software version 4.2[1]. Next, we calculate the zenith path delay due to the water vapor (ZWD: Zenith Wet Delay) by subtracting the zenith hydrostatic delay (ZHD: Zenith Hydrostatic Delay) from the ZTD. The ZHD which is mainly caused by the dry components of the atmosphere is determined by surface pressure measurements[2]. Time series of ZWD values at Kashima, Tsukuba, Usuda, and Uchinoura during 15 to 19 October 2004 are shown in Figure 3. On October 16th, which is the day of the hy4290 experiment, the ZWD values at all stations are less than 10 cm and it is consistent with the calm weather shown in Figure 2.

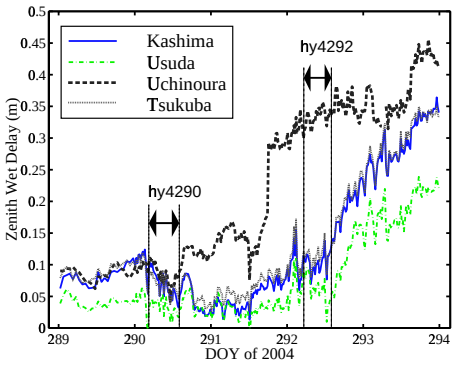

Figure 3. ZWD time series derived from GPS data sets at Kashima, Tsukuba, Usuda, and Uchinoura.

The ZWD value at Uchinoura dramatically increased from 15 cm to 27 cm within one hour on October 17th with the approach of typhoon TOKAGE. The ZWD values at Kashima and Tsukuba gradually increased up to 35 cm after October 18. At Usuda, where station altitude is above 1500 m, the ZWD value is relatively small compared with the values at other stations because of a low water vapor content at high altitude. However, even at Usuda the ZWD value was up to 25 cm until the end of October 19th. As shown in Figures 2 and 3, since meteorological conditions were significantly different between the two experiment periods, we consider that those experiments are very suitable for our study.

4.2. Slant Delay and Differential Delay

Conventionally, the slant-path wet delay ΔSLW_i at i_{th} epoch can be computed from the ZWD via

$$\Delta SLW_i = NMF(\theta_i) \times ZWD_i \tag{1}$$

where $NMF(\theta_i)$ is the Niell mapping function[3] and θ_i is an elevation angle of the HAYABUSA spacecraft or nearby quasar at i_{th} epoch. Next, we calculate resampled slant-path wet delay values $\Delta SLW'$ over the whole experiment period at all stations using piecewise cubic spline interpolation. A principle observable feature of VLBI is the difference in arrival times of radio signals between two stations. Then, we calculate differences between the values $\Delta SLW'$ at each station. We define this "differential wet delay".

The differential wet delays for the HAYABUSA spacecraft ($D\Delta SLW^H_{AB}\prime$) and for the quasar ($D\Delta SLW^Q_{AB}\prime$) are shown by:

$$D\Delta SLW^H_{AB}\prime = \Delta SLW^H_A\prime - \Delta SLW^H_B\prime \quad (2)$$

$$D\Delta SLW^Q_{AB}\prime = \Delta SLW^Q_A\prime - \Delta SLW^Q_B\prime \quad (3)$$

where the A and B denote stations at both the ends of the baseline.

Finally we calculate differences between both differential wet delays of the HAYABUSA spacecraft and those of the quasar:

$$D\Delta SLW^{QH}_{AB}\prime = D\Delta SLW^Q_{AB}\prime - D\Delta SLW^H_{AB}\prime \quad (4)$$

where $D\Delta SLW^{QH}_{AB}\prime$ denotes the difference between two differential delays.

If the angular separation is sufficiently small, the differential wet delays for both radio sources are almost equal. Then, these are canceled out by the difference procedures written in the equation (4). However, if these are different, the differences between them are added directly to the observables as an error source.

5. Results

Figure 4 shows time series of difference values, mentioned in the previous section (equation (4)), between two differential delays during the hy4290 experiment (a) and the hy4292 experiment (b).

The ZWD time series at all stations as shown in Figure 3 are consistent with each other in both amplitude and phase through the first experiment period. Thus, the difference values are almost equal to zero. This suggests that the difference procedure is efficient to correct the errors due to the atmospheric path delay under calm weather conditions. On the other hand, the characteristics of the time series for the Kashima-Uchinoura baseline as shown in the upper and lower panels are very different from each other. The maximum value of differences is less than 1.5 cm over the first experiment period (upper panel), whereas the maximum value of differences is up to more than 10 cm during the second experiment period (lower panel).

The primary cause of the large difference value is a significant difference in water vapor content during the second experiment at Uchinoura and Kashima. We can infer from the experiment schedule and the baseline azimuth that the effect is enhanced by the difference in elevation angle of the radio source at both stations.

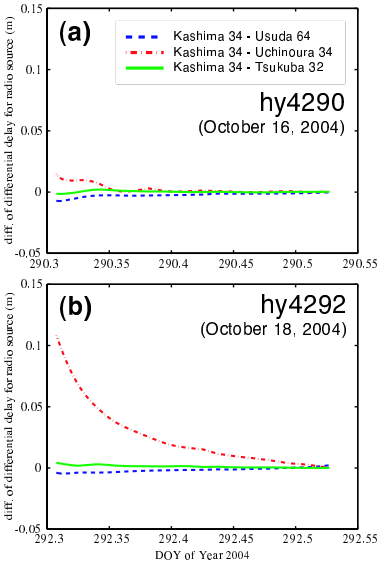

Figure 4. (a) Difference between the differential delays during the first experiment hy4290. (b) Same plot but for the second experiment hy4292.

Since the baseline vector between both stations is toward the west and the radio sources were in the southeastward direction, the elevation angle at Uchinoura is about four degrees smaller as compared to Kashima at the beginning of the second experiment period.

In general, we can estimate an atmospheric path delay as the one of unknown parameters from the VLBI observables only. However, it is very difficult to perform the same way in the $\Delta VLBI$ measurement analysis. Because the elevation and azimuth angles of the radio sources are not homogeneously distributed in the sky, a least square estimation becomes unstable due to the mutual distinguishability among the parameters.

In this report we mention the use of GPS-based ZWD estimates to evaluate the effects of atmospheric correction on the $\Delta VLBI$ measurements. At present, these estimates for each station have enough precision to improve the numerical weather prediction (NWP) models[4], [5]. The recent studies indicate that the GPS-based ZWD estimates agree well with those obtained by radiosonde data sets or a water vapor radiometer (WVR) at a few millimeter rms level (e.g. [7], [8]). Therefore, we are going to develop a new correction method based on the estimates in order to remove the atmospheric path delay error from the VLBI observables.

6. Summary

We performed two $\Delta VLBI$ experiments for the HAYABUSA spacecraft on October 16th and 18th, 2004. In these experiments we acquired the geodetic GPS data sets from the IGS stations and one GEONET GPS station of the GSI, Japan. These GPS stations are adjacent to the VLBI stations that participated in the experiments. We evaluate an effect of cancelling out atmospheric path delay errors on the $\Delta VLBI$ measurements based on the delays derived from geodetic GPS analysis. According to our analysis, a large difference value of up to 10 cm of the differential path delay for the Kashima-Uchinoura baseline was estimated in spite of a small separation angle of less than 3 degrees between the HAYABUSA spacecraft and quasar. Such a large value was mainly caused by the humid condition around Uchinoura due to an approaching typhoon. Moreover, the east-west direction of the baseline vector and the large difference in elevation angle of the radio source between both stations helped to enlarge the difference value.

References

[1] Rothacher. M., Orbits of Satellite Systems in Space Geodesy. *Geodaetisch.geophysikalische Arbeiten in der Schweiz*, 46, 1992.

[2] Davis et al., Geodesy by radio interferometry: effects of atmospheric modeling errors on estimates of baseline length, *Radio Science*, **Vol. 20**, No. 6, pp. 1593-1607, 1985.

[3] Niell, A., Global mapping functions for the atmosphere delay at radio wavelength, *J. Geophys. Res.*, **101(B2)**, 3227-3246, 1996.

[4] Reigber et al., Near real-time water vapor monitoring for weather forecast, *GPS World*, **13**, 18-27, 2002.

[5] Gendt G et al., Near real time GPS water vapor monitoring for numerical weather prediction in Germany. *J. Meteor. Soc. Japan*, **82(1B)**, 361-370, 2004.

[6] http://www.jma.go.jp/JMA_HP/jma/index.html

[7] Behrend et al., An inter-comparison study to estimate zenith wet delays using VLBI, GPS, and NWP models, *Earth Planets Space*, 52, 691-694, 2000.

[8] Haefele et al., Impact of radiometric water vapor measurements on troposphere and height estimates by GPS, *Proceedings of the 17th International Technical Meeting of the Satellite Division of The Institute of Navigation (ION GNSS 2004)*, Sept. 21-24, 2004.

Wang Guangli: Post-Correlation Processing of VLBI Satellite Observations at SHAO, IVS 2006 General Meeting Proceedings, p.231–235
http://ivscc.gsfc.nasa.gov/publications/gm2006/wang

Post-Correlation Processing of VLBI Satellite Observations at SHAO

Wang Guangli

Shanghai Astronomical Observatory, CAS
e-mail: wgl@shao.ac.cn

Abstract

VLBI technology has been chosen for the first Chinese lunar project "Chang-E", in conjunction with USB technology, to measure the angular position of the spacecraft and to determine its orbit during the approach to the moon and while orbiting the moon. Several experiments have been carried out to investigate the effectivity of the concept and the flexibility of its implementation. In this paper we will give an introduction to the post-correlation processing stage, including how to process the quasar observations and satellite observations and how to apply the quasar observation results for calibrating the satellite observables.

1. Background

The VLBI technology has been chosen for the first Chinese lunar project "Chang-E", in conjunction with USB technology, to measure the angular position of the spacecraft (S/C) and to determine its orbit during the approach to the moon and while orbiting the moon. Several experiments have been carried out to investigate the effectivity of the concept and the flexibility of its implementation. In this paper we will give an introduction to the post-correlation processing done at SHAO.

2. The Processing Scheme

Observation data from four domestic VLBI stations are sent to the correlation center via Internet (quasi real-time mode) or on disks via air freight (batch mode). The correlation is done by a hardware correlator and a software correlator. Both correlators are designed in FX mode, their output being visibility data in the same format and split into files by time. The time unit varies from tens of seconds to several minutes according to the data size and the request. The data are put onto an NFS hard disk server for post-correlation use.

In an accessories directory, quasar coordinates, station positions, EOP, and satellite orbit data are kept as a prioris. The station logs and pcal data are also maintained.

The correlation output is read and checked in the post-correlation, and the VLBI delay and delay rates of the quasars and the S/C are obtained. We will discuss the post-correlation process later.

The propagation medium modeling encompasses the ionospheric and tropospheric corrections to the observations using meteorological data and/or co-located GPS real-time data.

The S/C angular position and orbit are solved for in corresponding solution steps (Figure 1).

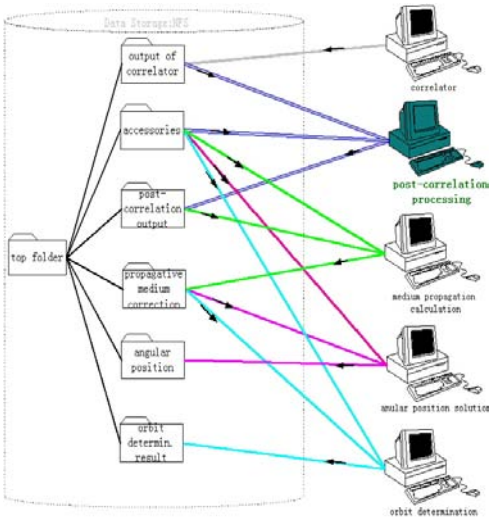

Figure 1. Diagram of the post-correlation processing for the Chang-E project. Arrows indicate the direction of the data flow.

3. The Post-Correlation Strategy

Alternating observations to quasars and the S/C is used to calibrate the S/C result with quasar observations. Generally, about 15 minutes quasar observations are used to correct several minutes to several tens of minutes of S/C observations depending on the required precision. In quasi real-time mode, ten degrees away from the S/C in the sky can be allowed for quasar observation. This mode is used during the approach stage of the S/C and the precision values for the delay and the delay rate for the S/C are at the 0.1 ns and ps/s level, respectively. Observations are taken at two IFs on the S/X band with 1-MHz bandwidth for quasars and S/C. In batch mode, the arc distance between quasars and S/C is limited to a few degrees, and the phase reference is used for high-precision positioning and orbit determination. The delays and delay rates are at less than 100 ps and less than 0.1 ps/s, when phase reference is used. The recording bandwidth for quasars is 8 MHz.

The processing flow is as follows. Firstly, residual delays and delay rates of the quasars are obtained. Single band delay fitting furnishes delays and phases at reference frequencies for two IFs. Using single band phases, multiband delays and delay rates are calculated. Then the atmospheric propagation correction for the quasars is calculated using the propagation medium calculation module and applied to the observations. The atmospheric delay is extrapolated (for quasi real-time mode) or interpolated (for batch mode) to the S/C observation epochs and applied as corrections to the S/C observations. Finally, the propagation corrections are applied to the S/C observations, where the corrections are again determined using the propagation medium calculation module.

4. The Post-Correlation Processing of Real Data

In March 2005, a three-day observation campaign (with about 10 hours of observations per day) was conducted. The satellite observed was TC-1, which is one of two satellites in the Sino-

European joint venture "Earth Space Double Stars Exploration Project". Three stations in China participated: Seshan, Urumqi, and Kunming. Kunming operates a 3-meter antenna. The quasars were observed the first 15 minutes of every hour, and the satellite was observed the remaining 45 minutes. The quasars were observed at S/X band on two frequencies in each band. The satellite was observed at S band and on a single frequency. The bandwidth was all 8 MHz in all cases. Here we show the single band results. The multiband data are still being processed.

The residual delays for the quasars are shown in Figure 2. "S" denotes Seshan station, "U" Urumqi, and "K" Kunming. Thus SU denotes the baseline Seshan-Urumqi. Every point represents a 15-minute average. The delay error is about 1 ns for baseline SU, and 10 ns for SK and UK using one minute integration. Because of the small antenna at Kunming, the baselines with Kunming are by a factor of ten worse than SU. The results are ionosphere-corrected. The ionospheric correction and tropospheric correction are taken from a GPS estimation.

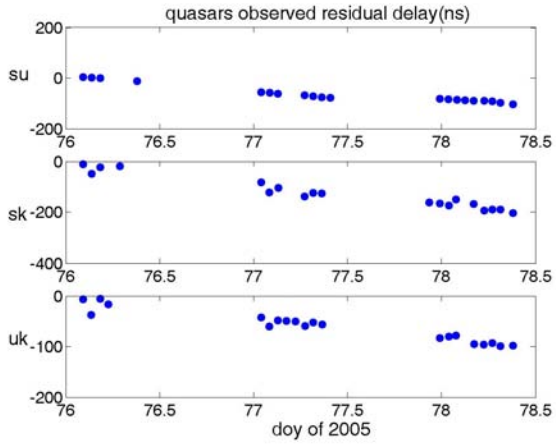

Figure 2. Observed residual delays for the quasars.

Then, 15-minute averages of the quasar delays are interpolated to the satellite observation epochs (see Figure 3). The black dots are the residual delays for the quasars, the green (gray) line are delays interpolated to the satellite epochs.

Finally, the corrections are applied to satellite residual delays (see Figure 4). The red (dark gray) dots are observed satellite residual delays (raw data), the green dots (light gray) are the delays after the quasar calibration has been applied, the blue (black) dots are the resulting residual satellite delays—including quasar calibration and satellite ionospheric/tropospheric delay corrections.

5. Conclusions

The three-day VLBI satellite observation campaign served as a proof-of-concept test. Results are preliminary, and we will continue to work on it. Using this kind of VLBI processing, the orbit determination wrms residual error is at the ns level, and a systematic error at the 10 ns level can be expected when compared to USB results (investigations are ongoing). It must be pointed out that, when combining the VLBI observations with USB data, the orbit determination is quite helpful, especially in orbit prediction. The VLBI results presented here stem from single band estimation.

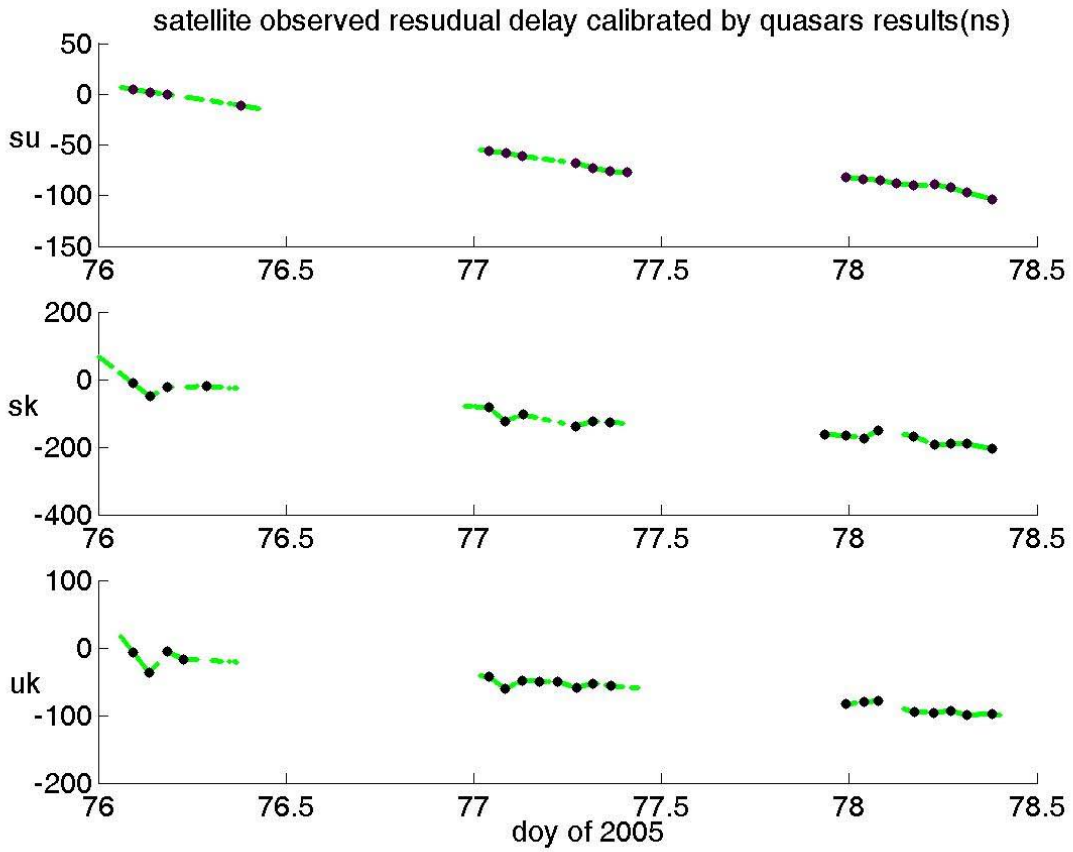

Figure 3. Interpolation of the residual quasar delays to the epochs of the satellite observations (explanation see text).

Preliminary band-synthesized results using two frequencies indicate that the delay errors are better by at least a factor of two.

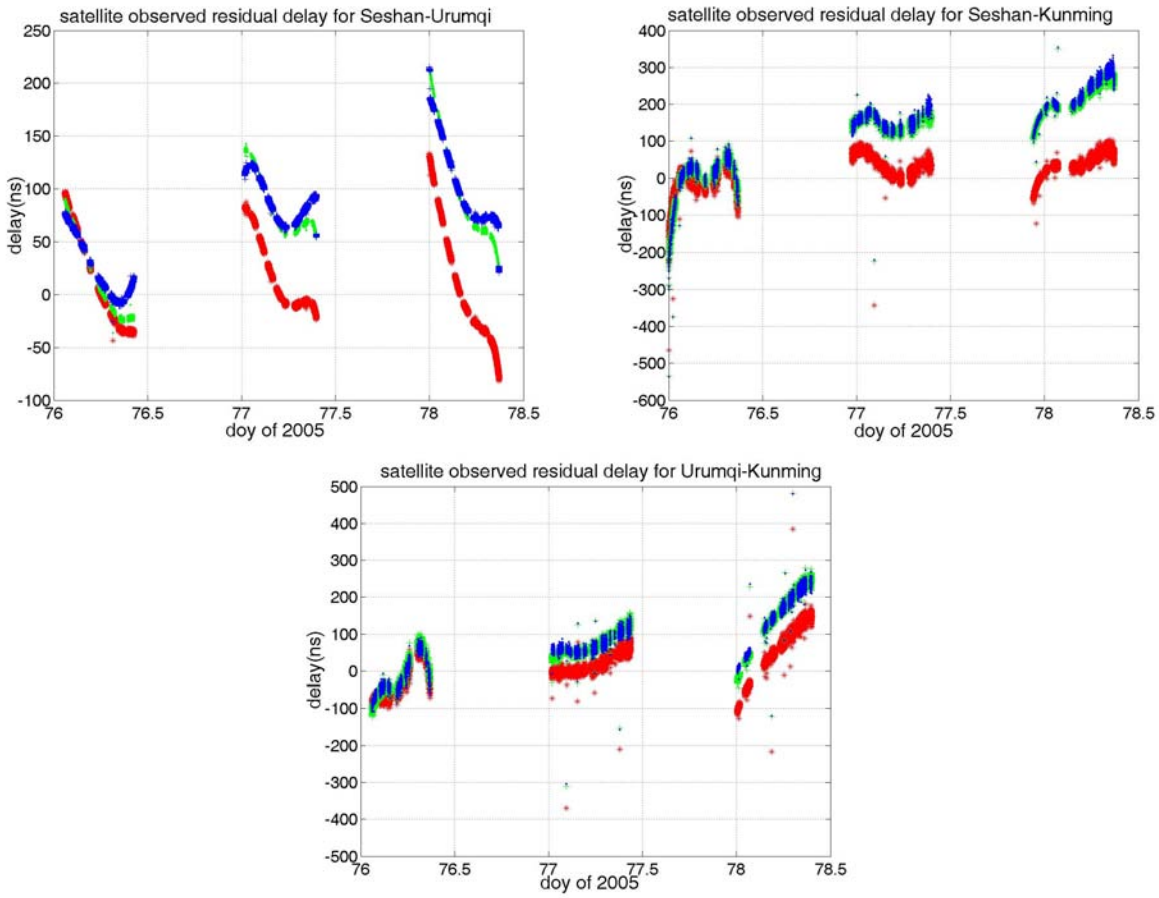

Figure 4. Quasar-calibrated satellite residual delays (explanation see text).

Gino Tuccari et al.: e-NRTV – Radar VLBI Network LFVN, IVS 2006 General Meeting Proceedings, p.236–240
http://ivscc.gsfc.nasa.gov/publications/gm2006/tuccari2

e-NRTV – Radar VLBI Network LFVN

Gino Tuccari [1], *Igor Molotov* [2], *Alexander Volvach* [3], *Alexander Konovalenko* [4], *Alexander Dementiev* [5], *Liu Xiang* [6], *Yuri Gorshenkov* [7], *Maria Nechaeva* [5], *Igor Falkovich* [4], *Alexander Pushkarev* [2], *Vladmir Samodurov* [8], *Alexander Antipenko* [5], *Nikolay Dugin* [5], *Salvatore Buttaccio* [1], *Gaetano Nicotra* [1], *Ivan Strepka* [3], *Vladimir Titenko* [2], *Vladimir Jazykov* [2]

[1] *INAF, Istituto di Radioastronomia*
[2] *Central Astronomical Observatory at Pulkovo, RAS*
[3] *Lab. Radio Astronomy of Crimean Astrophysical Observatory*
[4] *Institute of Radio Astronomy, NASU*
[5] *Radiophysical Research Institute*
[6] *Urumqi Astronomical Observatory*
[7] *Special Research Bureau of Moscow Power Engineering Institute*
[8] *Puschino Radio Astronomy Observatory of Lebedev Physical Institute, RAS*

Contact author: Gino Tuccari, e-mail: g.tuccari@ira.inaf.it

Abstract

The Near Real Time Radar VLBI Network LFVN is progressively increasing its performance and processing structures. Dedicated acquisition and recording NRTV terminals are placed at Bear Lakes (Russia), Noto (Italy), Simeiz (Ukraine), Evpatoria (Ukraine), Urumqi (China). A new, entirely digital terminal has been developed for this network, and two units will be placed at two radiotelescopes in 2006. A collaboration program is under development with the European Space Operations Center and the Ballistic Center of the Keldysh Institute of Applied Mathematics, and two VLBI sessions were carried out in 2005. The first experiment was in September for VLBI radar research of the small space debris fragments, the second experiment was in October for differential VLBI measurements of the Mars-Express interplanetary spacecraft position. A new dedicated software correlator is under development for a distributed correlation process. The more recent scientific results are reported. The VLBI fringes were received and fringe rates were measured for radar echo-signals of Moon, Venus and space debris objects on baselines involving the stations at Noto, Bear Lakes, Simeiz, and Urumqi.

1. Introduction

LFVN was initiated in 1996 under INTAS project 96-0183 to involve Russian and Indian radio telescopes in VLBI activities [1]. First observations were carried out with the help of Mk-2 terminals and the JPL/Caltech Block II correlator. Then it continued with a series of solar wind radio wave experiments arranged jointly with DSN. The Canadian S2 system and DRAO, Penticton, S2 correlator were used during the next stage of the project that allowed receiving the first LFVN images of AGN. The NRTV Internet based acquisition, transfer and correlation system has been used since 2003 in investigating the Solar system bodies with new VLBI radar techniques. In 2005, the first LFVN delta-VLBI run for Mars-Express interplanetary mission continued the series of the earlier spacecraft navigation experiments that were processed with NIRFI correlator in N. Novgorod. After the beginning of limited operations of the NIRFI-3 correlator and the NRTV correlator in Noto, the LFVN completed the last necessary part of a VLBI network, having

already available a set of radio telescopes collaborating for observations, scheduling and post-processing groups, and a technology development team. Today a new, entirely digital back-end system has been elaborated and a new dedicated NRTV software correlator is under development for a distributed correlation process.

2. e-NRTV and rDBBC

The e-NRTV Internet based acquisition, transfer and correlation system provides a maximum recorded signal bandwidth of 48 MHz, flexibly scalable up to few kilohertz. The system is based on 1 or 2 bit sampling at base band level, with further data packing and recording to PC-disk as files through a dedicated board, and has a possibility to transfer the full amount or portion of VLBI data in near real time to a correlator, using a standard Internet connection [2]. NRTV-terminals are currently installed at Noto, Bear Lakes, Urumqi, Simeiz, and Evpatoria. Other terminals will be installed in Puschino or Staraya Pustyn (Russia). During 2005 a GPS receiver was integrated to NRTV-terminals in order to simplify the synchronization of the recorded VLBI data.

A new backend system has been defined for the Radar VLBI network operating with an improved e-NRTV recording terminal. Such processor, named rDBBC is able to translate the RF or IF portion of band, where the radar echo is expected, to the recorder. 1 narrow band is used most of the time, but the terminal is able to handle portions of bands from 125 KHz up to 16 MHz. The terminal is integrated with the recorder and managed even remotely, so that the frequency settings, output modes, and the recording can be operated from a central point for the entire network. Input band is 128 MHz, spanning from 0.1 MHz up to 2.4 GHz, so that S band is directly down converted. Any other higher observing bansd need then to be converted in any portion of this wide interval. A very compact VLBI terminal is so obtained in a 'single box', having as input the sky RF (below 2.4 GHz) and as output the network connection, for both managing the system and data transfer. When the net connection is not fast enough, the disk recording acts as an elementary buffer.

The three main elements are then connected to from a single system, a digital data processor, a digital disk recorder, an industrial PC. External elements are: a NMEA GPS receiver with serial connection, H-Maser clock and 1PPS, RF coming from the antenna.

A new dedicated software correlator is under development, sharing more processes among different PC platforms and being baseline dependent. A simplification and correlation time reduction will come from the introduction of an initial preprocessing in the acquisition station before sending data to the correlator. The preprocessing step is performed within the acquisition computer taking into account an input file containing the a-priory expected frequency of the echo signals. A complex FFT is performed with high frequency resolution (0.015 Hz) and only data around the useful signal are kept to be transferred for correlation. The total data reduction can achieve a factor of 1000:1 depending on the echo frequency spread.

3. Solar Wind VLBI - Radio Sounding of Circumsolar Plasma

A series of experiments on VLBI radio probing of solar wind plasma was carried out at C, L and P bands from 1998-2005. A VLBI array received the radio emission of extragalactic sources located at different angular distances from the Sun (3-130°) after propagation through the turbulent circumsolar plasma. Correlation of recorded data was carried out in Penticton with NIRFI-3

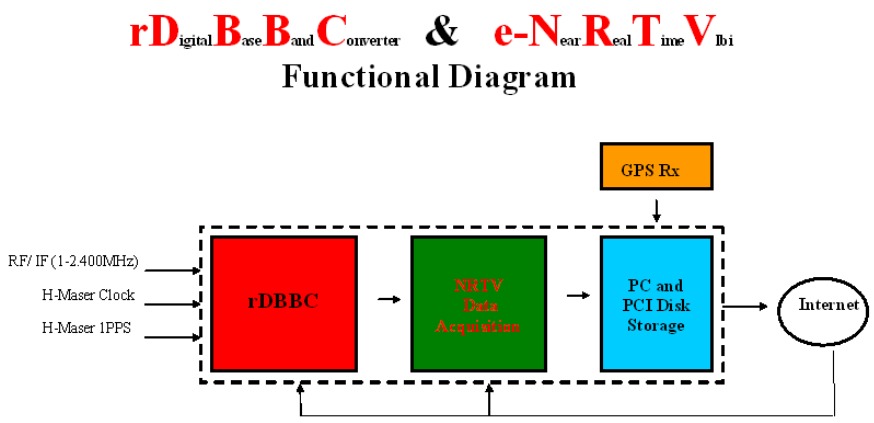

Figure 1. Data acquisition flow. IF coming from the receiver is down-converted using the rDBBC converter operating in the range 0.1-2.400 MHz, where two data channels of variable bandwidth are selected to be transferred to the Data Acquisition module. One or two bit data are stored on disk and sent through the Internet. Time synchronization is assured by a dedicated GPS receiver. The terminal is set through the Internet connection for fully remote operations.

processors. Value of solar wind velocity V and an index of spatial spectrum of electron density fluctuations p could be obtained by a spectral analysis of the correlated signals [1]. Distribution of large-scale intensive irregularities of electron density is derived from the variations of spectrum's width, and distribution of the weak small-scale irregularities may be understood from the spectrum "wings" shapes. The L-band INTAS00.3 experiment (Bear Lakes RT-64, Noto RT-32, GMRT-45, HartRAO RT-26, Shanghai RT-25, Puschino RT-22) allowed to measure the values of V and p from observations of 6 sources on 3 baselines: Bear Lakes–HartRAO, Bear Lakes–Noto, Noto–HartRAO. Figure 2 demonstrates the samples of power spectrums of the interferometry response on the $1514-241$ source emission located at angular distance of 14 degrees from the Sun. Velocity of solar wind was determined by frequency f of spectrum break points according to the expression $f = V/\rho$ (ρ - baseline projection on wave-front). The average value of solar wind was estimated as $V = 342 \pm 17$ Km/s. Evaluations of the spectral index p were carried out according to the slope of the interferometer signal spectrum. The average value of the spectral index p is equal to $p = 357 \pm 0.006$. It is the first time that the parameters V and p were evaluated independently of irregularities scales, comparable with baseline lengths from 2000 to 9000 km. The obtained results confirmed the adaptability of the "freezing-in hypothesis" and Kolmogorov power spectrum for the description of spatio-temporal variations in solar wind on large distances from the Sun $R > 40R\odot$ ($R\odot$ - solar radius).

4. AGN Results of INTAS00.3 Experiment

The INTAS00.3 experiment lasted about 50 hours in period 28.11.99 - 01.12.99 at left-circular polarization. Each source was observed in 5–6 scans of 30 minutes. The VLBI data of 8 MHz bandwidth with 1-bit sampling was recorded using the Canadian S2 system and then correlated in Penticton at 256 spectral channels, each 31.25 kHz with 2 s integration time for AGNs and 0.1 s

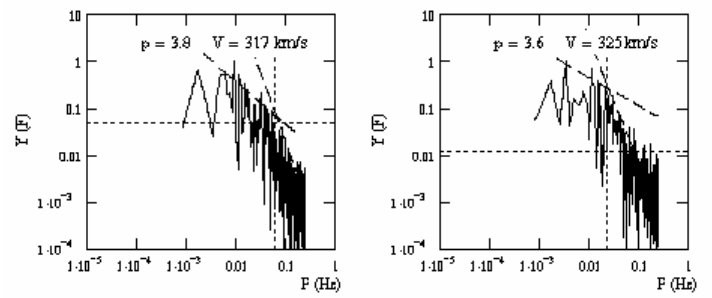

Figure 2. 1514-241 source interferometry signal power spectrums on Bear Lakes-Noto (left side) and Bear Lakes-HartRAO (right side) baselines

for solar wind sources. The data analysis, editing, and calibration were done using standard AIPS procedures. Gain curves and system temperatures measured for each participating antenna were used for amplitude calibration of the VLBI data. The primary phase calibration was done using the AIPS task FRING with 120 s coherent integration time, with subsequent phase corrections for the residual delays for the entire time of the experiment using Bear Lakes as the reference antenna. The imaging was performed in DIFMAP. A point source at the phase center was applied for the initial models in the hybrid mapping. Figure 3 presents constructed VLBI LL-images of BL Lac object 1418+546 ($z = 0.152$) and a quasar CTA 102 ($z = 1.037$). Both sources revealed one-sided core-jet structure (because of Doppler boosting) with a position angle of 120° and 145°, and with estimated brightness temperatures of $1.3 \cdot 10^{12} K$ and $5.9 \cdot 10^{12} K$ for 1418+546 and CTA 102, respectively.

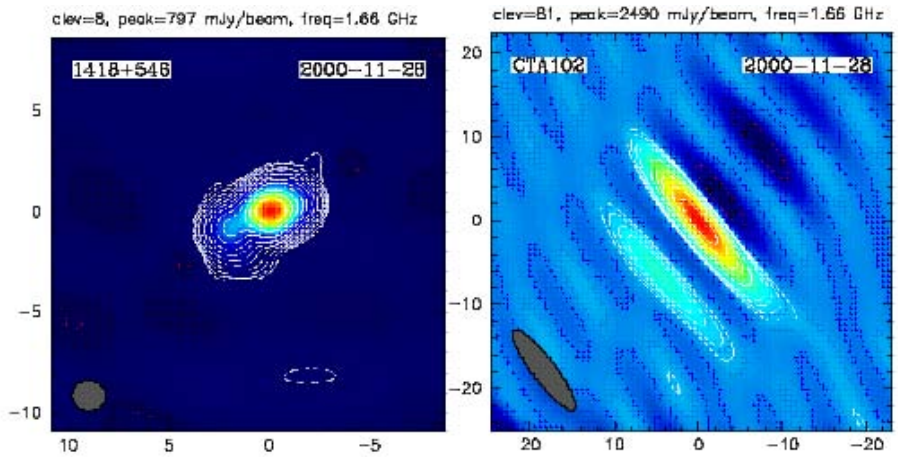

Figure 3. 1.66 GHz LFVN maps of 1418+546 and CTA 102. The lowest contours are drawn at levels of 1% of the peak value of 797 mJy/beam and 3.25% of the peak value of 2490 mJy/beam for 1418+546 and CTA 102, respectively. Axes are given in mas.

5. VLBR05.1 and MEX_053 deltaVLBI Experiments

The delta-VLBI technique allows to link the sky position of a measured object with the position of a close ICRF quasar on the celestial sphere to reconstruct the orbit of an object in the Radio Reference Frame. The series of delta-VLBI runs were carried out from 1984 to 1993 for the Venus-15, Vega-1, 2 and Phobos-1, 2 interplanetary stations, Astron and Granat high-apogee spacecrafts. Since 1999 the differential VLBI radar (VLBR) method is under development using a C-band transmitter at Evpatoria to radio-sound space objects. VLBR05.1 run, which was conducted out at C-band in period 10.09.05-16.09.05 with participation of Evpatoria, Bear Lakes, Simeiz, Urumqi and Puschino, continued the row of the trial VLBR observations of space debris objects, Moon, Venus and Mars to adjust the procedure of VLBI fringes obtained for radar echo signals. The received Doppler and fringe rate measurements are used at the Keldysh Institute of Applied Mathematics, RAS (see examples of VLBR measurements in Figures 4). The beginning of collaboration with the European Space Operations Center allowed to renew the experience of the classic delta-VLBI with Mars-Express interplanetary spacecraft. The first results of the MEX_053 experiment that was carried out at S/X-band in 09.10.05-11.09.05 with participating stations Evpatoria, Bear Lakes, Simeiz and Urumqi are presented in Figure 5.

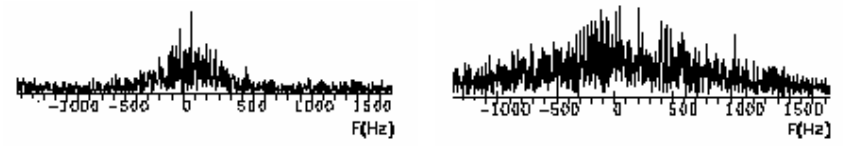

Figure 4. The VLBI fringes for C-band (5010.024 MHz) echo-signals reflected by the Moon on baselines Bear Lakes–Noto (left side) and Noto–Simeiz (right side), 2004, September, 9, 23:10:56 and 23:11:50, measured fringe rates respectively: 2160.001 Hz and -1999.249 Hz, VLBR04.3.

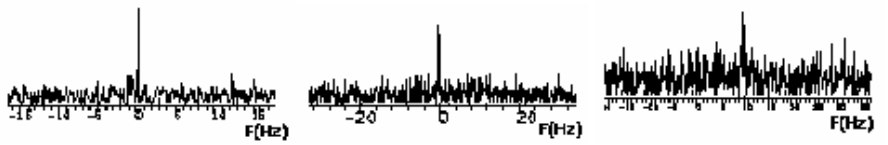

Figure 5. The VLBI fringes for Mars-Express S-band (2296.482 MHz) signal on baselines (from left to right) Bear Lakes–Evpatoria, Evpatoria–Urumqi, Urumqi–Bear Lakes, 2005, October, 10, 19:30:20, measured fringe rates respectively: 523.812 Hz, 1693.110 Hz, 1693.1797 Hz, MEX_053.

References

[1] Molotov I.E. et al., Low Frequency VLBI Project. The Universe at Low Radio Frequencies In: Proceedings of IAU Symposium 199, held 30 Nov - 4 Dec 1999, Pune, India, 492–493, 2002.

[2] G. Tuccari et al., E-LFVN - An Internet Based VLBI Network In: Proceedings of the 7th European VLBI Network Symposium, eds. R. Bachiller et al., October 12-15, Toledo, Spain, 331–332, 2004.

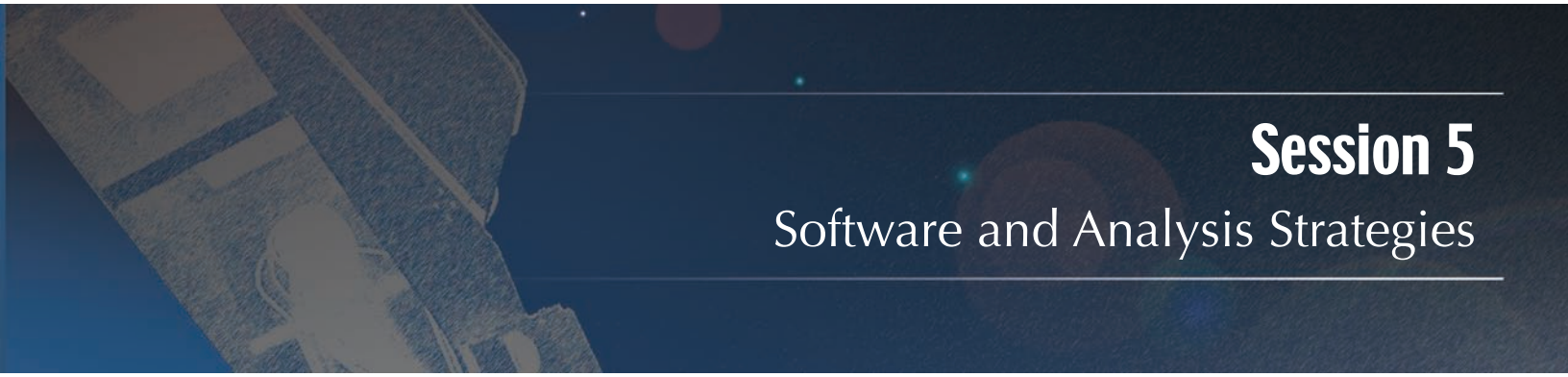

Session 5

Software and Analysis Strategies

Volker Tesmer et al.: Impact of Analysis Options on the TRF, CRF and Position Time Series Estimated from VLBI, IVS 2006 General Meeting Proceedings, p.243–251
http://ivscc.gsfc.nasa.gov/publications/gm2006/tesmer

Impact of Analysis Options on the TRF, CRF and Position Time Series Estimated from VLBI

Volker Tesmer [1], *Johannes Boehm* [2], *Robert Heinkelmann* [2], *Harald Schuh* [2]

[1)] *Deutsches Geodätisches Forschungsinstitut (DGFI)*
[2)] *Institute of Geodesy and Geophysics (IGG), TU Vienna*
Contact author: Volker Tesmer, e-mail: tesmer@dgfi.badw.de

Abstract

This paper compares estimated TRF, CRF and position time series of different solutions in terms of systematic differences, scale, annual signals and station position repeatabilities. Several analysis options are investigated: various tropospheric parameterisations, atmospheric loading, thermal deformation and a refined stochastic model of VLBI observations, which mainly consists of elevation dependent re-weighting. All solutions were computed at DGFI using OCCAM 6.1 and the DOGS-CS software with VLBI data from 1984 till 2005.

1. Introduction

When computing geodetic solutions, an analyst has to choose between many options to set up the solution. Some of these options are obviously preferable to others and/or subject to conventions, like the IERS Conventions ([15]), or technique dependent conventions proposed by the technique services (e.g. see [16]). But, neither can all options be judged objectively right or wrong, nor are the effects of all options on geodetic target parameters known in detail.

2. Solution Setup

All solutions compared in this investigation used the VLBI observations of 2699 daily sessions between 1984 and 2005 with 49 radio telescopes observing 1954 sources. In a first step the data were processed with the VLBI software OCCAM 6.1 ([14]), setting up normal equations for each single session using the least-squares adjustment algorithm of OCCAM. Unknown parameters are station positions and velocities, source positions, the EOP (polar motion and rates, UT1 and LOD, nutation), tropospheric zenith delays (ZD) mapped with the VMF1 (Vienna Mapping Function 1, [4]), horizontal gradients and station clocks.

In a second step, the tropospheric and clock parameters, and all EOP were (pre-)reduced in all 2699 datum free single session normal equations, using the software DOGS-CS ([2]). All normal equations were then accumulated (stacked) to one big equation system, solely containing the parameters of the reference frames (station positions and velocities, and source positions). To remove the datum deficiencies of VLBI solutions, no-net-translation (NNT) and no-net-rotation (NNR) condition equations were added to the coordinates and velocities of 25 radio telescopes w.r.t. ITRF2000 ([1]), as well as NNR conditions for 199 stable sources ([5]) wrt ICRF-Ext1 ([7]). Inverting such an equation system yields a completely undeformed and fully consistent terrestrial (TRF) and celestial (CRF) reference frames (see also [12]) .

As step three, station position time series were derived by session-wise solutions with NNR and NNT conditions w.r.t. the TRF that was computed with exactly the same solution setup. This strategy guarantees station position time series as homogeneous and least noisy as possible, because position time series will get noisier the less similar the TRF (used as basis for the daily NNR+NNT conditions) is to the TRF implied by the solution setups. This approach is comparable to carrying out a 6-parameter similarity transformation, which theoretically requires normal distribution of the residual station positions w.r.t. the TRF used as basis for the transformation. The similarity is especially critical in case of single VLBI sessions, because networks with few (4-8) stations are not robust in that respect.

3. Comparison I: Solution Approaches "Tropospheric Parameterisation Options"

In this section, results from a solution **"usual"** (estimating hourly tropospheric ZD, no a priori values for the horizontal gradients, using surface met data to derive the a priori hydrostatic ZD), are compared with three solutions, each changing only one option w.r.t. the **"usual"** setup:

- **"2hour"**: estimating ZD every two hours,
- **"aprgr"**: using constant a priori tropospheric gradients (courtesy of GSFC, DAO 90-95),
- **"zdcon"**: using constant a priori ZDs (in this investigation, most of them were computed at the height of nearby GPS antennas following [3] and [10]).

3.1. CRF Differences

Figure 1 shows the differences between CRF (declination, DE) from the solution setup **"usual"** as reference and the **"2hour"**, **"aprgr"** and **"zdcon"** solutions. While **"usual"−"2hour"** seems to be more or less scattered around zero, **"usual"−"aprgr"** is a very distinct function. This function has a similar form and sign as the one described in [6], where the authors compare CRF solutions with and without estimating tropospheric horizontal gradients. However, the maximum value found by [6] was much larger (0.5 mas compared to 0.055 mas for **"usual"−"aprgr"**). This behaviour of DE is likely due to the pseudo-observations (constraints), which are added to the observation equations with an empirically derived formal error (here 0.5 mm). These constraints stabilize the gradient estimates towards their a priori values. The differences **"usual"−"zdcon"** also show a similar behavior but smaller in size (-0.02 mas).

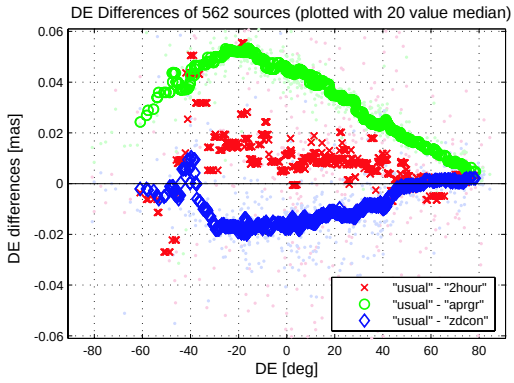

Figure 1. CRF declination differences: approach **"usual"** vs. **"2hour"**, **"aprgr"** and **"zdcon"**.

3.2. TRF Differences

Comparable to the CRF estimates, the TRF differences **"usual"−"2hour"** consist of random scatter only (see Figure 2). The differences **"usual"−"zdcon"** are of systematic nature, especially in the height component with a maximum value of −38 mm. This can be explained by the fact that a part of the hydrostatic zenith delay is mapped down with the wrong (wet) mapping function (as an example, +10 hPa error in the pressure used to compute the a priori hydrostatic ZD evokes about +2 cm error in the a priori hydrostatic ZD, resulting in a −0.4 cm error in the height estimate: for details please see [4]). As a consequence, the global scale for **"zdcon"** in this investigation differs by 0.2 ppb from the **"usual"** solution. The differences in the horizontal components for **"zdcon"** have a small shift of about +0.5 mm in north-south direction, which cannot be explained at the moment. The TRF differences **"usual"−"aprgr"** differ mostly in the horizontal components, where the a priori gradients evoke a clear north-south tilt up to −2 mm, probably because the a priori values for the gradients are constrained.

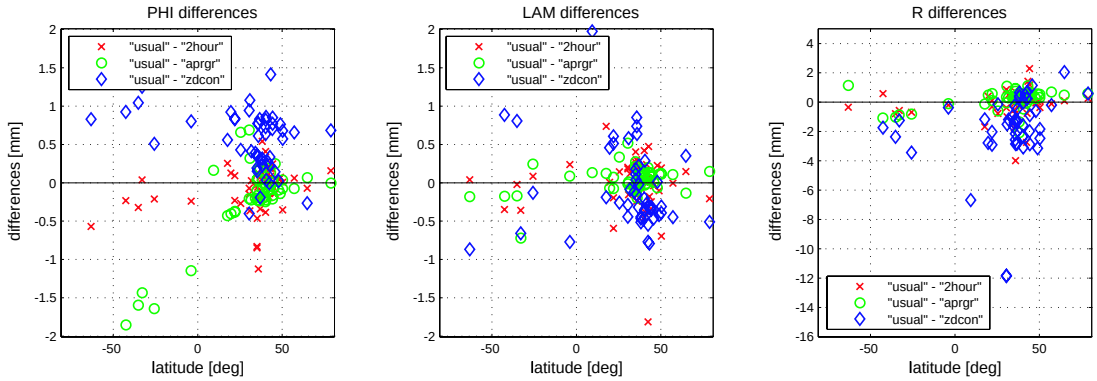

Figure 2. TRF position differences: approach **"usual"** vs. **"2hour"**, **"aprgr"** and **"zdcon"** (for reasons of clarity, the plots are zoomed—there are single values outside the visible boundaries, reaching up to −38 mm for R).

3.3. Station Position Time Series

Figure 3 illustrates the differences between station position time series of various solution approaches w.r.t. the **"usual"** solution. They show the differences for each single session w.r.t. the corresponding TRF (in light colored dots), as well as 70-day medians of these differences, computed every 7 days to better visualise periodic and annual parts of the differences.

NYALES20 (see Figure 3) is an extreme example for the strong influence of using **"zdcon"** on estimated height time series: there are very clear episodic signatures in the differences, superimposed by an annual part, altogether amounting to 4-5 mm.

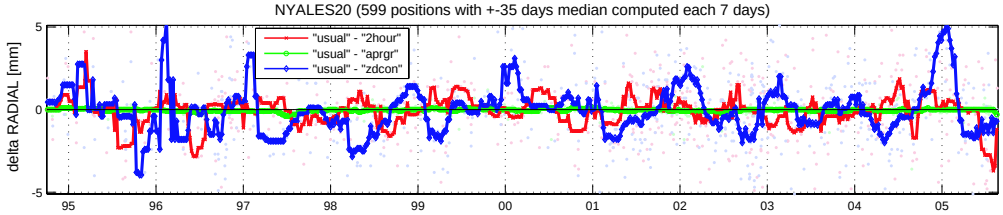

Figure 3. NYALES20 height time series differences: approach **"usual"** vs. **"2hour"**, **"aprgr"** and **"zdcon"**.

3.4. Station Position Repeatability

The station position repeatabilities were computed from the single session position estimates w.r.t. the corresponding TRF, with annual signals removed before computing the RMS and WRMS values. The RMS determined from all 2699 sessions between 1984 and 2005 for the **"usual"** solution setup were (PHI, LAM, R, all in [cm]) 0.50, 0.47, 1.09, the weighted RMS (WRMS) 0.27, 0.26, 0.49, respectively.

Generally, decreasing the temporal resolution of the estimated ZD from 1 hour to 2 hours leads to a degradation of station position repeatabilities by 2 to 3%. Using non-zero a priori gradients does not affect the station position repeatabilities. An amazing fact is that using constant a priori ZD instead of ZD derived from the measured surface met data leads to 2% better repeatabilities (up to 10% in WRMS for GILCREEK). This is probably due to errors in the surface pressure data taken for the solution, because other investigations with shorter time series show a clear advantage when using pressure data recorded at the sites ([4]).

4. Comparison II: Solution Approaches Using Atmospheric Loading, Thermal Deformation and a Refined Stochastic Model

In this section, results derived from a solution, in the following named **"usual"** (computed without atmospheric loading, without thermal deformation corrections and without using a refined stochastic model), were compared to the following solutions:

- **"atmos"**: with atmospheric loading correction ([8]),
- **"therm"**: with thermal deformation correction (see [9] and [16]),
- **"refst"**: using a refined stochastic model (elevation dependent re-weighting, see [11], [13]).

4.1. CRF Differences

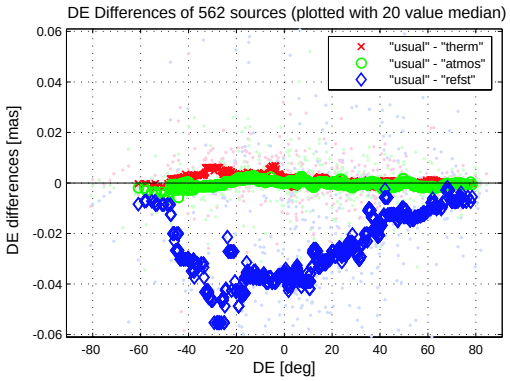

Figure 4. CRF declination differences: approach **"usual"** vs. **"atmos"**, **"therm"** and **"refst"**.

The only significant differences between CRF estimates occurred for the **"usual"−"refst"** comparisons (see Figure 4). The function that shows declination differences is very similar to the one that is evoked by using a priori non-zero horizontal tropospheric gradients (see Section 3.1) but having opposite sign: while for **"usual"−"aprgr"**, the maximum differences were 0.055 mas, the maximum for **"usual"−"refst"** is −0.050 mas. This is due to the fact that the gradient estimates were constrained to the a priori values. With the refined stochastic model, gradients have a smaller

influence on the solution because observations at low elevations, which mainly define the gradient estimates, are slightly weighted down. Thus, the **"usual"−"aprgr"** differences are to a certain extent comparable to the ones of **"usual"−"refst"**.

4.2. TRF Differences

A comparable phenomenon also occurs for the TRF estimates: while the **"usual"−"aprgr"** TRF differences are tilted in north-south direction up to −2 mm (see Figure 2), the **"usual"−"refst"** ones are tilted in north-south direction up to +1.5 mm (see Figure 5). Differences in estimated heights using **"atmos"** or **"therm"**, which vanish in this investigation, could arbitrarily be evoked by the chosen reference temperature and pressure. The solution using the refined stochastic model has a scale that is larger by 0.1 ppb than the **"usual"** TRF.

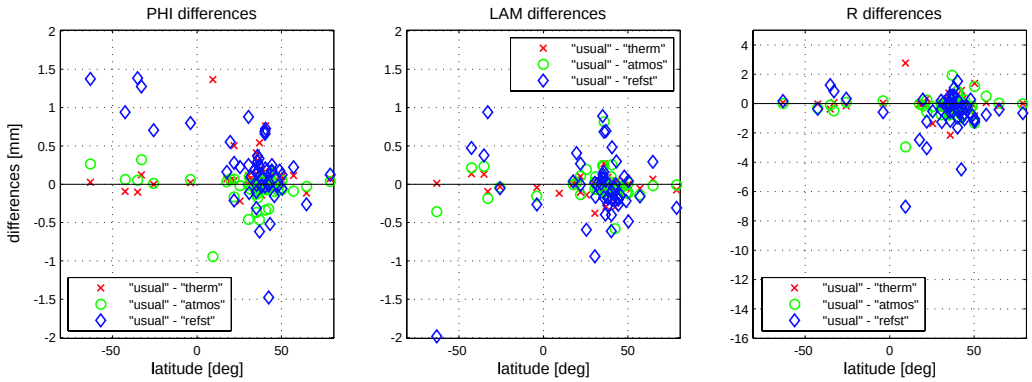

Figure 5. TRF coordinate differences: approach **"usual"** vs. **"atmos"**, **"therm"** and **"refst"** (for reasons of clarity, the plots are zoomed—there are single values outside the visible boundaries).

4.3. Station Position Time Series

The station position time series differences of the station GILCREEK are a good example to illustrate the influence of atmospheric loading corrections: Figure 6 shows the corresponding height differences due to atmospheric loading corrections, which obviously have an annual signal imposed with 5 mm amplitude. For GILCREEK, the thermal deformation correction is exactly out of phase compared to atmospheric loading, and has a smaller amplitude (2 mm). In the horizontal components (not shown here), both effects have annual signals with magnitude of about 0.7 mm.

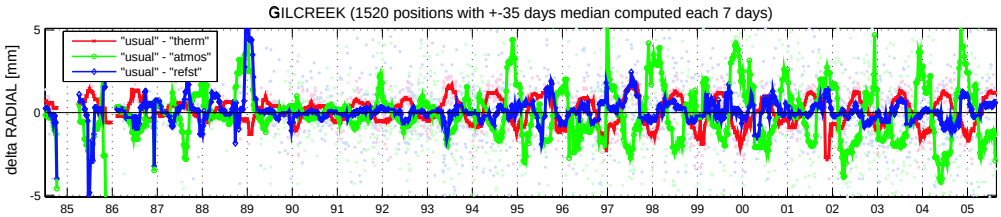

Figure 6. GILCREEK height time series differences: approach **"usual"** vs. **"atmos"**, **"therm"** and **"refst"**.

Another explicit example is the 46 m antenna ALGOPARK with a quite distinct annual thermal deformation signal in the height position time series of about 3 to 4 mm amplitude (Figure 7).

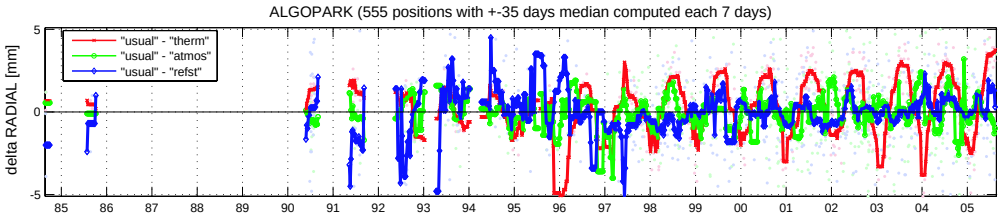

Figure 7. ALGOPARK height time series differences: approach **"usual"** vs. **"atmos"**, **"therm"** and **"refst"**.

4.4. Annual Signals in Station Position Time Series

Generally, the amplitudes of annual signals in station height time series are smaller than 5 mm (as illustrated in Figure 8) and smaller than 3 mm in the horizontal components (not shown here).

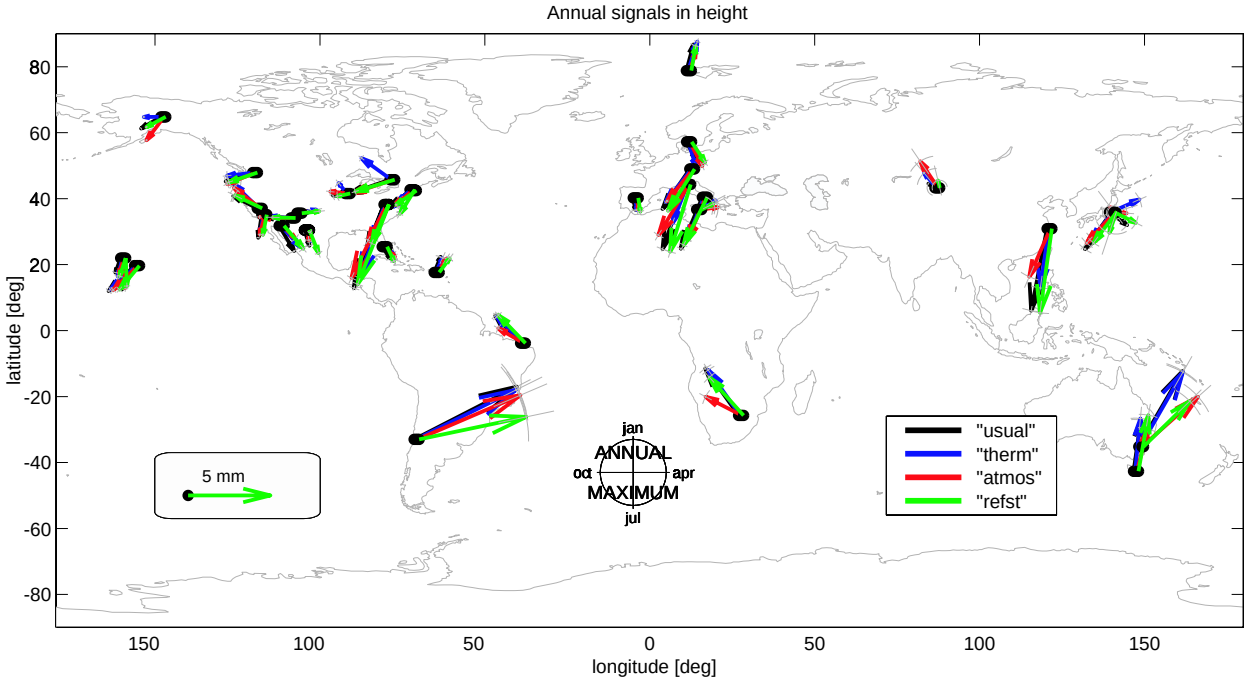

Figure 8. Annual signals in height time series: approach **"usual"**, **"atmos"**, **"therm"** and **"refst"**.

Figure 9 shows the differences between the amplitudes of the annual signals in the horizontal and height components, comparing the **"usual"** solution approach to **"atmos"**, **"therm"** and **"refst"**. The biggest influence is obviously evoked by applying thermal deformation: the annual amplitudes are reduced by up to 0.7 mm in height and 0.4 mm in the horizontal components. Using the atmospheric loading correction ([8]) also reduces the amplitudes of annual signals in height by up to 0.7 mm, but not in the horizontal components. The refined stochastic model does not significantly affect the annual signals.

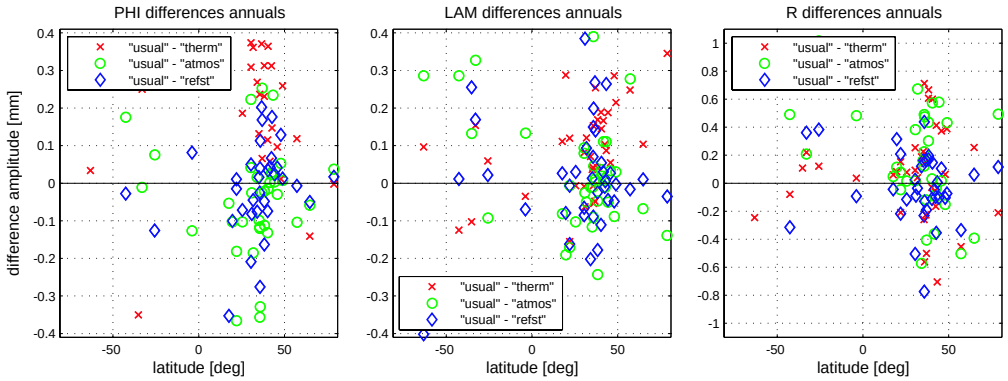

Figure 9. Differences of annual amplitudes in position time series: approach **"usual"** vs. **"atmos"**, **"therm"** and **"refst"** (for reasons of clarity, the plots are zoomed—there are single values outside the visible boundaries).

4.5. Station Position Repeatability

The effect of the solution options **"atmos"**, **"therm"** and **"refst"** on station position repeatabilities is as follows (please note that annual signals were removed from the position time series before computing the repeatabilities): As the thermal deformation correction does not improve the station position repeatabilities (less than 1% gain overall), one can assume that the present models are appropriate to describe the dominant annual part of this effect (see section 4.4). Atmospheric loading corrections improve the overall station height repeatability by 2% RMS and 4% WRMS, for some stations even between 5 and 10%. But, the repeatability of the horizontal components does not improve significantly. The biggest improvements concerning station position repeatabilities can be achieved using the refined stochastic model (mainly elevation dependent re-weighting), which yields an overall gain of about 3% RMS and 4% WRMS, for some stations even between 10 and 15%.

5. Summary

The results of VLBI solutions significantly depend on the solution setup, which can cause systematic effects. For all applications, like for geophysical studies or combination issues, these systematics must be considered thoroughly. The biggest influences due to the solution setups tested in this paper can be summarised as follows:

- The approach using (realistic) non-zero a priori values for the horizontal tropospheric gradients is sensible from a theoretical point of view and should yield more realistic results. But, compared to solutions where zero values are used, this approach influences the estimated declinations of radio sources by up to almost 0.055 mas. TRF estimates are mainly affected by a small tilt in north-south direction by up to -2 mm. These systematic effects are due to the common practice to stabilize gradient estimates towards their a priori values, because the gradients are sometimes weakly defined by the VLBI observations themselves.
- Using constant a priori ZD instead of ZD derived from surface met data can change the station heights of an estimated TRF to almost arbitrary values, because of the correlations between the estimated ZD and station height components. With the ZD data used in this

investigation, the station heights generally change less than 1 cm (the maximum is 38 mm), the overall scale is shifted by about 0.2 ppb. Periodic and annual signals in height position time series differences were found to reach up to ±4 mm.

- Decreasing the temporal resolution of the estimated ZD from 1 hour to 2 hours does not influence systematically any type of parameter investigated. It leads to episodic signals and noise in station position time series and degrades their repeatabilities by about 3%.
- Applying thermal deformation corrections reduces the annual amplitudes in station position time series by up to 0.7 mm in height and 0.4 mm in the horizontal components. Episodic signals reach up to ±3 mm in height and ±1 mm in the horizontal components. But this correction can only be used in VLBI solutions, computed for combination issues of the IVS or the IERS, if a clear and reasonable definition of the reference temperature exists. In the future, even local tie measurements from VLBI reference points to those of other techniques should comprise calibrated temperature measurements.
- The atmospheric loading corrections as proposed/provided by [8] generally reduce the amplitudes of the annual signals in height by up to 0.7 mm, but not in the horizontal components. Implied episodic differences in station position time series reach up to ±5 mm in height and ±1 mm in the horizontal components. Using this correction improves the overall station height repeatability by 2% RMS and 4% WRMS, for some stations even between 5 and 10%, whereas the repeatabilities of horizontal components do not change. Comparable to thermal deformation, a reasonable application to geodetic data analysis requires a well founded definition of the reference pressure.
- The last solution option under investigation was the refined stochastic model (mainly elevation dependent re-weighting as proposed by [13]). The effects on CRF and TRF are comparable to those evoked by using a priori non-zero horizontal tropospheric gradients, but with different sign: declination estimates are systematically changed by up to −0.050 mas, TRF estimates are tilted in north-south direction by up to 1.5 mm, the scale gets bigger by about 0.1 ppb. This is due to the fact that the "real" observations under low elevations (which mainly define the gradient estimates) are slightly weighted down using the refined stochastic model, and the gradient a priori values are constrained in VLBI solutions. Applying the refined stochastic model, the station position repeatabilities overall improve by 3% RMS and 4% WRMS in height and the horizontal components (which is the best improvement of the solution setup options analysed in this investigation). For some stations the gain is even between 10 and 15%.

Acknowledgement

This study made extensive use of VLBI-data provided by the International VLBI Service for Geodesy & Astrometry (IVS). Thanks to all IVS components.

References

[1] Altamimi, Z.: ITRF2000: A new Release of the International Terrestrial Reference Frame for Earth Science Applications. Journal of Geophysical Research, Vol. 107, B10, 2214, 10.1029/2001JN000561, 2002

[2] Angermann, D., H. Drewes, M. Krügel, B. Meisel, M. Gerstl, R. Kelm, H. Müller, W. Seemüller, V. Tesmer: ITRS Combination Center at DGFI - A Terrestrial Reference Frame Realisation 2003. Deutsche Geodätische Kommission, Reihe B, Nr. 313, München, 2004

[3] Berg, H.: Allgemeine Meteorologie. Dümmler-Verlag, Bonn, 1948

[4] Boehm, J., B. Werl, H. Schuh: Troposphere mapping functions for GPS and very long baseline interferometry from European Centre for Medium-Range Weather Forecasts operational analysis data. Journal of Geophysical Research, 111, B02406, doi:10.1029/2005JB003629, 2006

[5] Feissel-Vernier, M.: Selecting Stable Extragalactic Compact Radio Sources from the Permanent Astrogeodetic VLBI Program. A & A 403, 105-110, 2003

[6] MacMillan, D., C. Ma: Atmospheric Gradients and the VLBI Terrestrial and Celestial References Frames. Geophysical Research Letters, Vol. 24, No. 4, 453-456, 1997

[7] Ma, C., F. Arias, M. Eubanks, L. Fey, A.-M. Gontier, C. Jacobs, O.J. Sovers, B. Archinal, P. Charlot: The International Celestial Reference Frame as Realised by Very Long Baseline Interferometry. The Astronomical Journal 166, 516-546, 1998

[8] Petrov, L., J.P. Boy: Study of the atmospheric pressure loading signals in very long baseline interferometry observations. Journal of Geophysical Research, Vol. 109, B03405, doi:10.1029/2003JB002500, 2004

[9] Nothnagel, A., M. Pilhatsch, R. Haas: Investigations of Thermal Height Changes of Geodetic VLBI Telescopes. Lanotte, R., G. Nianco (Eds.): Proceedings of the 10^{th} Working Meeting on European VLBI for Geodesy and Astrometry, Matera, Italy, Agenzia Spatiale Italiana, 121-133, 1995

[10] Saastamoinen, J.: Contribution to the theory of atmospheric refraction. Bulletin Géodésique 105-107, 279-298, 383-397, 13-34, 1973

[11] Tesmer, V.: Refinement of the Stochastic VLBI Model: First Results. In: W. Schwegmann, V. Thorandt (Eds.): Proceedings of the 16^{th} Working Meeting on European VLBI for Geodesy and Astrometry, Bundesamt für Kartographie und Geodäsie, Frankfurt/Leipzig, 207-218, 2003

[12] Tesmer, V., H. Kutterer, H. Drewes: Simultaneous estimation of a TRF, the EOP and a CRF. In: Vandenberg, N., K. Baver (Eds.): IVS 2004 General Meeting Proceedings, NASA/CP-2004-212255, 311-314, 2004

[13] Tesmer, V., H. Kutterer: An advanced stochastic model for VLBI observations and its application to VLBI data analysis. In: Vandenberg, N., K. Baver (Eds.): IVS 2004 General Meeting Proceedings, NASA/CP-2004-212255, 296-300, 2004

[14] Titov, O., V. Tesmer, J. Boehm: OCCAM v.6.0 software for VLBI data analysis. In: Vandenberg, N., K. Baver (Eds.): IVS 2004 General Meeting Proceedings, NASA/CP-2004-212255, 267-271, 2004

[15] http://www.iers.org/MainDisp.csl?pid=46-25776

[16] http://vlbi.geod.uni-bonn.de/IVS-AC/thermal-info.html

Arthur Niell: Interaction of Atmosphere Modeling and VLBI Analysis Strategy, IVS 2006 General Meeting Proceedings, p.252–256
http://ivscc.gsfc.nasa.gov/publications/gm2006/niell

Interaction of Atmosphere Modeling and VLBI Analysis Strategy

Arthur Niell

MIT Haystack Observatory
e-mail: aniell@haystack.mit.edu

Abstract

Estimates of the height component of station position are sensitive to the minimum elevation of observations included in the analysis, which is usually a global parameter that applies to all antennas. Two effects are strongly elevation dependent and compete in determining what minimum elevation should be adopted: the formal uncertainty of the height estimate from each 24-hour session, and the additional uncertainty not included in the session formal uncertainties that is due to errors in the atmosphere delay mapping functions. The parameter estimate uncertainties for a session depend on many things, but, in general, the lower the elevation that can be observed, the smaller the uncertainty in the height component. On the other hand, the error due to the inadequacy of the atmosphere mapping function increases as the minimum elevation is reduced.

The dependence of the combined height uncertainty on minimum elevation has been calculated for the antennas of the CONT94 continuous observing campaign and for four different atmosphere delay mapping functions. For best height estimation with current antenna sensitivities the VMF1 mapping functions should be used, and observations down to 5° elevation should be observed.

1. Introduction

In geodetic applications of VLBI and GPS both the value and the uncertainty of the estimate of the height of an antenna are sensitive to the minimum elevation of the observations. Two choices made during the planning and analysis stages of a VLBI session, typically composed of 24-hours of data, compete in determining what minimum elevation should be adopted. In planning the observations better height precision can be obtained by including observations at lower elevations, thus improving the geometric strength. However, the standard deviation of the session values about some long term value or trend, due to errors in the atmosphere model, will be increased as data are included at lower elevations.

In this paper the magnitudes and dependence on minimum elevation of these competing effects are illustrated, and a quantitative basis for choosing among available atmosphere models and deciding what minimum elevation to use is given. In Section 2, the errors due to atmosphere models and to geometry are described. The available mapping functions and trade-offs among them are provided in Section 3. The uncertainties in height due to the combined effect of geometry and atmosphere model are illustrated in Section 4. Finally, some choices are recommended in Section 5.

2. Height Uncertainties

The height uncertainty is dominated by the geometry of the observations and by the accuracy of the atmosphere model. The lower in elevation to which observations are made at a site, the smaller will be the formal uncertainties for the UP coordinate. The uncertainties for seven stations for one day of the CONT94 campaign are shown in Figure 1. Although this is referred to as "geometric"

uncertainty, the improvement in height uncertainty is in general less than anticipated because of the lower signal to noise ratio (SNR) for observations at low elevations due to increased system temperature and other effects.

Acting in the opposite direction is the increase in height uncertainty due to errors in the mapping functions. While the mapping function errors are also a function of latitude, the dependence on minimum elevation in a fractional sense is similar at all latitudes. This dependence has been investigated by calculating the atmosphere delay at three elevations, 15°, 7.5°, and 5°, using the IMF hydrostatic mapping function [5] for one year of data every six hours then finding the RMS deviation about these values using the NMF hydrostatic mapping function [4]. The data used were for 1992 from the National Center for Environmental Prediction (NCEP). The hydrostatic zenith delays were calculated from the NCEP data for use with both mapping functions. The delay differences were scaled to height error using a coefficient of 0.056*minimum elevation, which was determined from simulations using GPS geometry. This gives errors about 20% larger than the dependence found by MacMillan and Ma [3]. From Figure 2 it can be seen that, relative to the value at 5°, the error decreases to about 60% at 7.5°, and to about 20% at 15°. The implication of using a different scaling factor will be addressed in Section 4.

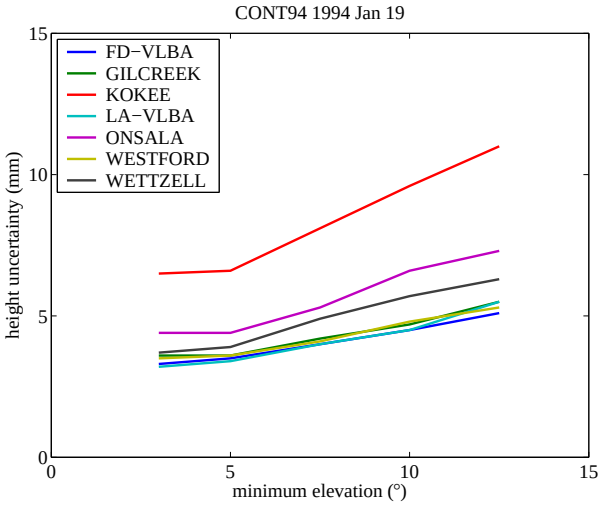

Figure 1. The per session height uncertainty for the antennas of CONT94 as a function of minimum elevation. From top down, the upper three lines are for Kokee, Onsala, and Wettzell.

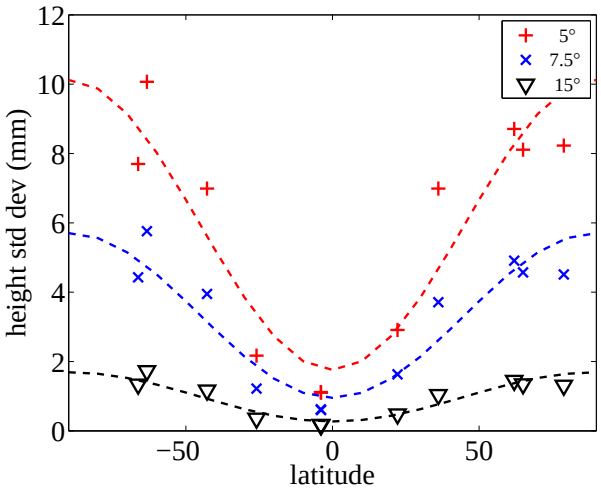

Figure 2. The expected height standard deviation as a function of latitude, and for minimum elevations of 5°, 7.5°, and 15°, from using the NMF hydrostatic mapping function. See text for significance.

3. Trade-Offs Among Atmosphere Mapping Functions

There are four mapping functions available in the current generation, with varying attributes for ease of use and accuracy. NMF [4] is widely used for both VLBI and GPS because it is independent of external data, depending only on station latitude and height and on day of year. The new GMF [1] uses the same input plus station longitude and reduces the largest errors in NMF. Two other mapping functions utilize data from a Numerical Weather Model. They are IMF [5] and VMF1 [2]. These have the advantage over NMF and GMF of reflecting actual sub-daily

changes in the properties of the atmosphere at the locations of interest.

The accuracies of these mapping functions can be evaluated by comparison with mapping functions calculated from radiosonde profiles. Both the mean difference and the standard deviation are important. Aside from NMF, which has larger errors for the hydrostatic component in the far southern latitudes and around Japan, the mapping functions agree well in the mean with the radiosondes and with each other. The equivalent scatters in height, calculated for 5° minimum elevation as described above, are shown in Figure 3 for the hydrostatic and wet components as a function of latitude.

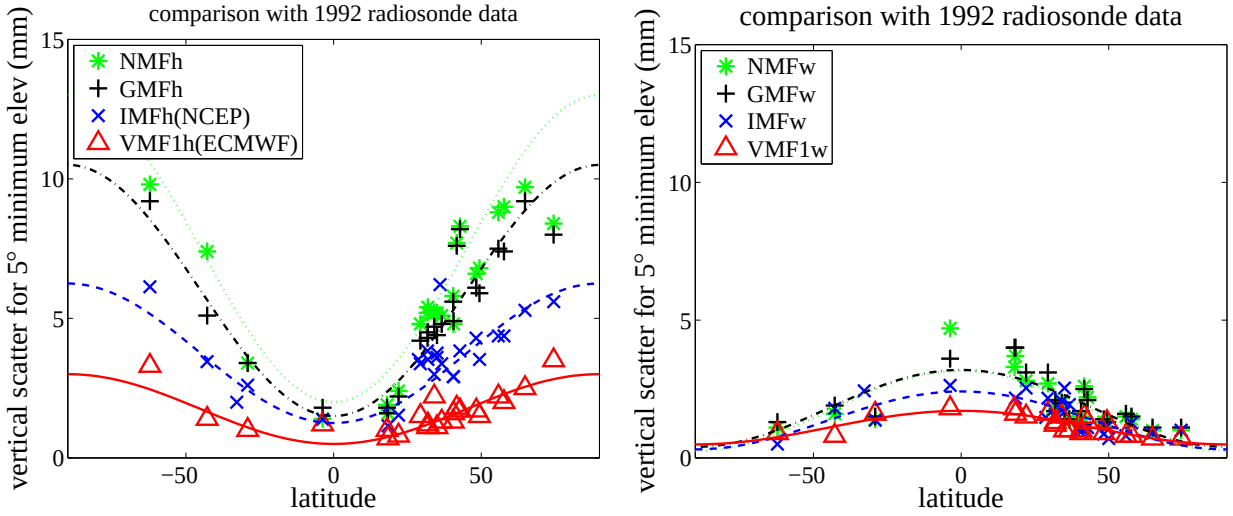

Figure 3. Height-equivalent scatter for 5° minimum elevation due to hydrostatic (left) and wet (right) components of the mapping functions.

An important improvement in the NWM-based mapping functions, compared to those based only on day of year, is clearly the reduced error in the high latitude regions. This is easily understood since the atmosphere has significant variations on a time scale of several days that cannot be reproduced by a seasonal model, and these variations are larger in the higher latitudes. Similarly, hydrostatic VMF1 (VMF1h) is more representative of the atmosphere as measured by radiosondes than is IMF since VMF1h makes use of all levels of the atmosphere provided by the NWM while IMFh uses only a single level.

The primary difference between IMF and VMF1 is the availability. IMF is produced on a global grid and is thus calculable for any location on the surface of the Earth, while VMF1 requires a separate calculation of the parameters for each individual location. For VLBI this has not been a problem because of the small number of sites, so the VMF1 parameters have been calculated for all VLBI sites from the earliest possible use.

On the other hand, the number of GPS sites is very large so the amount of calculation for VMF1 is inhibiting. As a consequence VMF1 is available only for a subset of GPS sites and as of this writing only for data taken since 2005 Jan 1. In contrast IMF may be calculated for any site for any epoch since 1979 Jan 1. The possible consequence of using the lower accuracy IMF will be seen in Section 4.

4. Combination of Atmosphere and Geometric Uncertainties

The errors due to the two competing choices are uncorrelated, so the total effect will be close to the quadratic sum. An example is shown in Figure 4, for Gilcreek. An important result can be seen from this figure: as the average geometric error over all elevations decreases, i.e. as an antenna becomes more sensitive, the optimum minimum elevation increases.

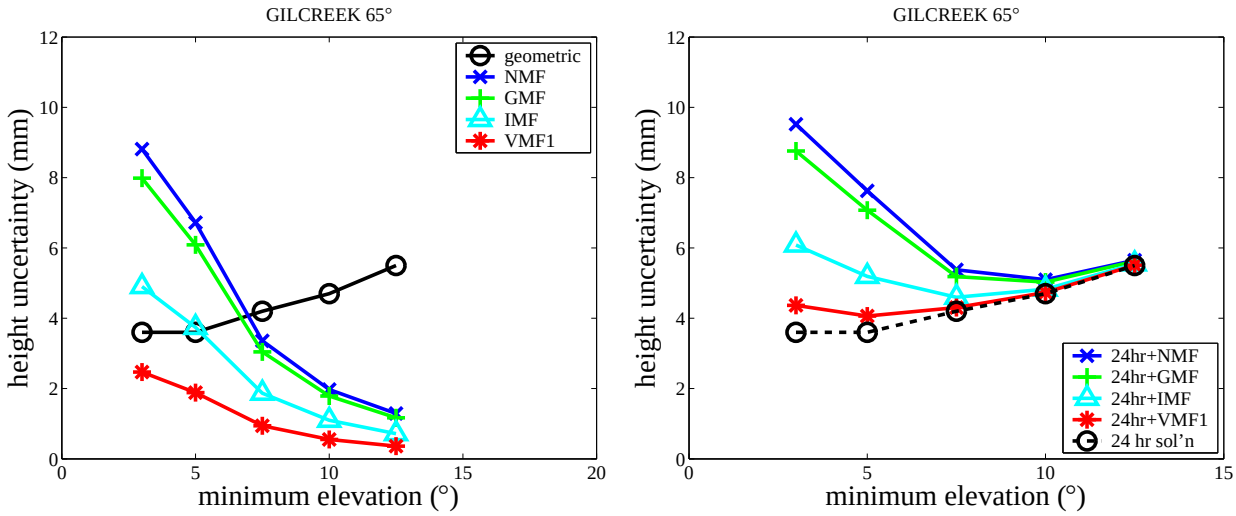

Figure 4. Height uncertainty for Gilcreek as a function of minimum observed elevation when combining the effects of the 24-hour session formal uncertainty and the mapping function error. On the left the effects are shown for each total mapping function and for the geometric uncertainty. On the right the effects are combined quadratically; the 24-hour uncertainty is included for reference as the lowest (dashed) line.

The total combined uncertainties are shown in Figure 5 for two antennas that have relatively low and high sensitivities for each of the four mapping functions. The 24-hour session height uncertainty (the "geometric" uncertainty) is also shown. It is apparent that making use of the NWM-based mapping functions should result in smaller height uncertainties for all but the weakest antenna (Kokee). Furthermore using VMF1 provides better precision than IMF for the more sensitive antennas. Finally, if VMF1 is used, data down to 5° elevation should be scheduled and included in the solution.

As indicated above in Section 2, the conversion from delay error at the lowest elevation to height uncertainty is in itself uncertain, perhaps by as much as 25%. Since the effects are added quadratically and the minimum of the resultant spans several degrees in elevation, and since there are likely to be other errors that have not been included, this lack of precision should not have a significant impact on the choice of minimum elevation.

It is important to note that the only way to reduce the combined height uncertainty is by reducing the per-session uncertainty. This will permit raising the minimum elevation and reducing the relative contribution of the atmosphere modeling error. This may already be the case for recent sessions such as CONT05 or for the RDV series, and this analysis should be applied to the antennas for each type of session if the per-session height uncertainties are different. (Ideally the analysis would be made for each session, but that is probably not justified because of the uncertainties in the method.)

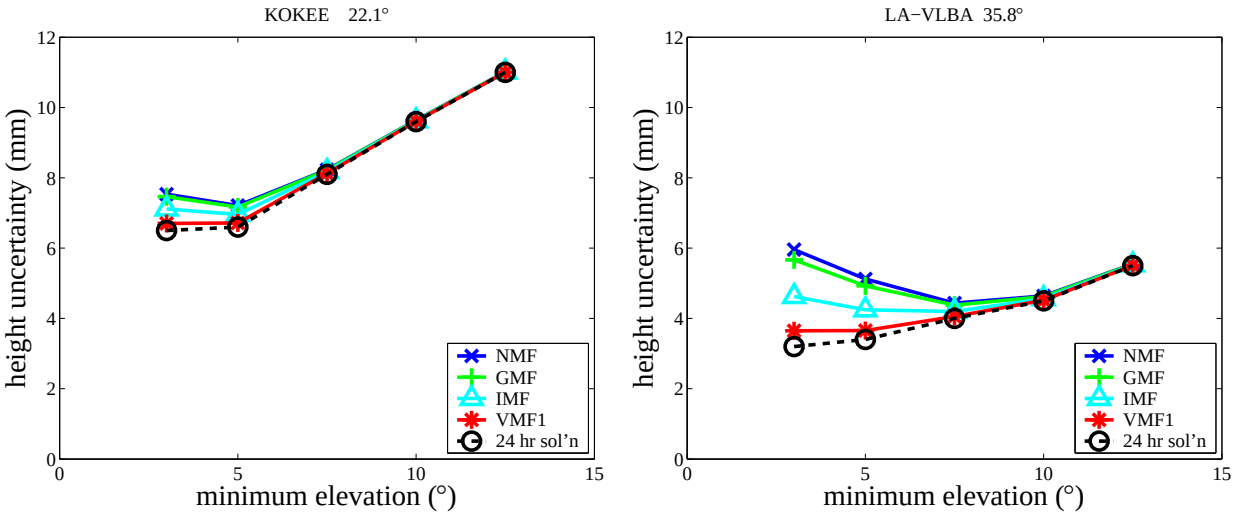

Figure 5. Height uncertainty for the low latitude sites Kokee (22°) and LA-VLBA (35°) as a function of minimum observed elevation for the combined effects of the 24-hour session formal height uncertainty and the mapping function error.

5. Recommendations

- The VMF1 mapping functions should be used for geodetic VLBI analysis.
- With the height uncertainties attained by the current antennas, observations should be scheduled for elevations down to 5° when using VMF1.
- The IMF mapping function can be used with little loss of accuracy at most sites, although the minimum elevation should be tailored to the sensitivity and location of the antenna.

References

[1] J. Boehm, A. Niell, P. Tregoning, H. Schuh, The Global Mapping Function (GMF): A new empirical mapping function based on numerical weather model data, Geophysical Research Letters, in press 2006. (accepted version)

[2] Boehm, J., B. Werl, and H. Schuh (2006), Troposphere mapping functions for GPS and very long baseline interferometry from European Centre for Medium-Range Weather Forecasts operational analysis data, J. Geophys. Res., 111, B02406, doi:10.1029/2005JB003629.

[3] MacMillan, D. S., and C. Ma, (1994). Evaluation of very long baseline interferometry atmospheric modeling improvements, *J. Geophys. Res.*, 99(B1), p. 637-651.

[4] Niell, A.E., Global mapping functions for the atmosphere delay at radio wavelengths, J. Geophys. Res., 101, B2, 3227-3246, 1996.

[5] Niell, A.E.: Improved atmospheric mapping functions for VLBI and GPS, Earth, Planets, and Space, 52, 699-702, 2000.

Wolfgang Schlüter et al.: Comparison of Wet Path Delays Observed with Water Vapour Radiometers, Solar Spectrometer, Radiosondes, GPS and VLBI at the Fundamental Station Wettzell, IVS 2006 General Meeting Proceedings, p.257–260
http://ivscc.gsfc.nasa.gov/publications/gm2006/schlueter2

Comparison of Wet Path Delays Observed with Water Vapour Radiometers, Solar Spectrometer, Radiosondes, GPS and VLBI at the Fundamental Station Wettzell

Wolfgang Schlüter [1], *Walter Schwarz* [1], *Beat Bürki* [2], *Alexander Somieski* [2], *Petra Häfele* [3], *Jungho Cho* [4]

[1)] *Bundesamt für Kartographie und Geodäsie, Fundamentalstation Wettzell*
[2)] *Eidgenössische Technische Hochschule (ETH)*
[3)] *Universität der Bundeswehr, Univ. FAF*
[4)] *Astronomy and Space Science Institute, Korea*
Contact author: Wolfgang Schlüter, e-mail: wolfgang.schlueter@bkg.bund.de

Abstract

Water vapour in the atmosphere contributes significantly to tropospheric refraction. Geodetic observations, in particular observations in the microwave domain as GPS and VLBI, are suffering from the inhomogeneous distribution of such water vapour. Even if the analysis models take into account the water vapor's influence, it is of interest to observe independently, with Water Vapour Radiometers, the water vapour and its influence on the observations.

In April 2005, five water vapour radiometers (WVR) and one solar spectrometer were co-located at the Fundamental Station Wettzell in order to investigate the resolution of the zenith wet delay (ZWD) observed with radiometers in terms of precision and systematic effects. A solar spectrometer allowed us to determine the zenith wet path delays only during day time, in particular when the sun was out. Such observations provide independently precise results that can be used to calibrate radiometers. In addition, during a period of 10 days, balloons radiosondes were launched, at noon and midnight every day, measuring temperature, pressure, and humidity profiles up to 25 km in height. This allowed us to estimate the zenith path delay for the launch times. As the zenith path delays were also derived from GPS and VLBI observations, a set of interesting ZWD data is available for comparisons.

1. Co-location of Various Water Vapour Radiometers (WVR) and a Solar Spectrometer at Wettzell

In the period from April 4 to 22, 2005 parallel observations with

- 2 Water Vapour Radiometers , type Radiometrics (Figure 1(a)), R42 and R43
- 3 Water Vapour Radiometers, type ETH (Figure 1(b)), ETH WA, - WC and - ZA, and
- 1 Solar Spectrometer GEMOSS (Geodetic Mobile Solar Spectrometer), built by ETH Zürich, in collaboration with the Institute for Analytical Sciences (ISAS) in Berlin (Figure 2)

were organised by Bundesamt für Kartographie und Geodäsie (BKG), Fundamental Station Wettzell, in collaboration with the

- Eidgenössische Hochschule (ETH) in Zürich, Switzerland and
- Universität der Bundeswehr in München, Germany

The goal was to compare the observed results with the results derived from the GPS- and VLBI observations, performed routinely at the FS Wettzell, in order to investigate systematic offsets and the precision of the various techniques.

During the period from April 11 to 20, 2005, in addition, 19 radiosondes were launched at 0:00 and 12:00 UTC (Figure 3). Figure 4 shows the location where the WVR were installed and balloons were launched. GPS- and VLBI- observations were carried out routinely at the

Figure 1. Water Vapour Radiometer built (a) by Radiometrics and (b) by ETH-Zürich.

Figure 2. Solar Spectrometer GEMOSS from ETH-Zürich.

Fundamental Station Wettzell. The Zenith Wet Path Delays are regular products, made available by the services IGS and IVS.

2. Comparison of the Results

Due to several technical problems during the observation period, only the WVR R43 (Radiometrics) and ETH ZA ran without failures. The observations show a repeatability of approximately 3 mm for the Radiometrics system and 6 mm for the ETH system. Figure 5(a) shows good agreement between both the ZWD derived from WVR R43 and from GPS. WVR shows a much higher time resolution (5-min compared to 1-h by GPS). This explains the obviously higher scatter of the

Figure 3. Preparation of a radiosonde launch.

Figure 4. Water Vapour radiometers in front of the 20m-Radiotelescope Wettzell.

R43 time series. The Radiometrics system R42 had an azimuth drive failure. The WVR ETH-ZA showed comparable results, but an offset of 1 to 2 cm, compared to GPS results, occurred. The ETH WA and ETH WC had hardware problems, resulting in unreliable data.

Figure 5(b) shows the comparisons of the radiosondes and solar spectrometer (GEMOSS) versus the GPS and VLBI derived ZWD. Balloon radiosondes provide temperature, pressure and humidity profiles, which allow for the evaluation of independent information about the ZWD. Some profiles were observed continuously, while during some launches the data transmission failed due to disturbances and interruptions of the data link. The function of the solar spectrometer GEMOSS (GEodetic MObile Solar Spectrometer), developed by the ETH and the Institute of Analytical Sciences (ISAS), Berlin [1], is based on differential optical spectroscopy. It makes use of simultaneous observations at numerous selected H_2O absorption lines between 728nm and 915nm. Information about the wet zenith path delays can be derived only during sunshine. Nevertheless, as it is a completely independent technique, GEMOSS provides valuable observations which can be used for calibration of WVR-results. Between the various methods offsets in the order of a few mm up to 2 cm occur, apart from the different resolutions in the time of the various techniques.

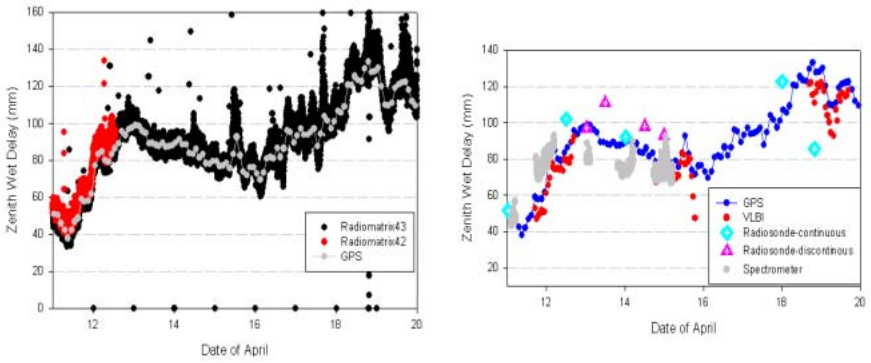

Figure 5. Comparison of the ZWD (a) WVR R42 and 43 versus GPS and (b) radiosondes and GEMOSS versus GPS and VLBI.

3. WVR Observations during CONT05

Based on the comparison, it was decided which of the available WVR should be placed in co-location with the radio telescopes in Kokee Park (USA-Hawaii), Wettzell (Germany) and Hartebeesthoeck (South Africa) during CONT05. For Wettzell, the Radiometrics system R43 was selected. In addition the GEMOSS instrument was made available by ETH and radiosondes were launched as well. For Kokee Park, the Radiometrics R42 system was employed after the repair of the azimuth drive. For Hartebeesthoeck, the best ETH system (ETH-ZA) was made available. Figure 6 shows the data obtained at Wettzell with the Radiometer R42, GEMOSS and radiosondes.

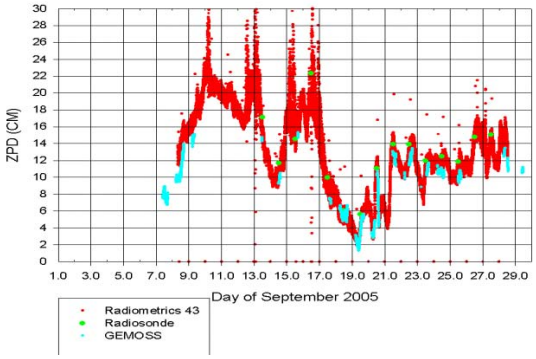

Figure 6. Zenith Weth Path Delay (ZPD) observed in Wettzell during CONT05 with WVR R43, GEMOSS and radiosondes.

References

[1] Somieski, A., Geodetic Mobile Solar Spectrometer, In: Geodätisch-geophysikalische Arbeiten in der Schweiz, Schweizerische Geodätische Kommission, Volume 68, 2005

Johannes Boehm et al.: Linear Horizontal Gradients vs. 3D Raytracing, IVS 2006 General Meeting Proceedings, p.261–263
http://ivscc.gsfc.nasa.gov/publications/gm2006/boehm1

Linear Horizontal Gradients vs. 3D Raytracing

Johannes Boehm, Harald Schuh

Institute of Geodesy and Geophysics / Vienna University of Technology
Contact author: Johannes Boehm, e-mail: johannes.boehm@tuwien.ac.at

Abstract

A simple way of determining linear horizontal gradients for VLBI and GPS analysis from numerical weather models is shown. Although downloading and computational efforts are small, it agrees very well with more sophisticated methods, what makes it applicable for a large number of geodetic sites on a routine basis. First VLBI results for CONT02 are very promising.

1. Introduction

In VLBI and GPS analysis it is important to take into account azimuthal asymmetries of the neutral atmosphere delays at the stations. State of the art is the estimation of total (hydrostatic plus wet) north and east gradients G_n and G_e for a certain time interval (e.g. 24 hours) within the least-squares adjustment. Equation 1 shows the total delay ΔL as the sum of a symmetric part (zenith delay L^z times mapping function m) and a gradient term that is dependent on the azimuth α of the observation (MacMillan, 1995 [4]).

$$\Delta L\,(\epsilon,\alpha) = L^z \cdot m(\epsilon) + m(\epsilon) \cdot \cot(\epsilon) \cdot (G_n \cdot \cos\alpha + G_e \cdot \sin\alpha) \tag{1}$$

The Vienna Mapping Function 1 (VMF1, Boehm et al., 2006 [2]) is the most accurate mapping function for the elevation-dependence of the delays that is currently available. The accuracy at 5° elevation is below $1cm$, which corresponds to station height errors of less than $2mm$. On the other hand, $1cm$ at 5° elevation corresponds to a gradient of $0.1mm$. Thus, it would be desirable to get a priori gradients from numerical weather models with an accuracy of $0.1mm$.

If no local measurements from water vapour radiometers (WVR) are available, 3D-raytracing through numerical weather models of highest resolution and accuracy is the best way to extract delays in the neutral atmosphere for observations at arbitrary elevations and azimuths. However, since these delays are not yet accurate enough to serve as fixed values in GPS and VLBI analysis, we again use the concept of (azimuth-dependent) mapping functions as rigorous reference of exploiting numerical weather models. For CONT02, a two-weeks continuous VLBI campaign in October 2002, the Vienna Mapping Function was determined not just once per site every six hours but also every 30° in azimuth (VMF2). This huge effort covers the download and the processing of hundreds of refractivity profiles at each station (Boehm et al., 2005 [1]).

By definition, the linear horizontal gradients (LGH) as introduced by Davis et al. (1993 [3]) only depend on the gradients of refractivity above the site (equation 2).

$$G_n = \int_{z=H}^{\infty} dN_{ns} \cdot z \cdot dz \tag{2}$$

Thus, only two more profiles of refractivity – one towards north and one towards east – are needed to derive the profiles of north-south (dN_{ns}) and east-west (dN_{ew}) refractivity gradients and to determine the north and east gradients G_n and G_e. Figure 1 shows the north gradients of refractivity (weighted with height) at the site Algonquin Park (Canada) on 15 October 2002 at 0:00 UT. The LHG can be derived by vertical integration and the application of a reduction factor that accounts for the curvature of the Earth (and the troposphere).

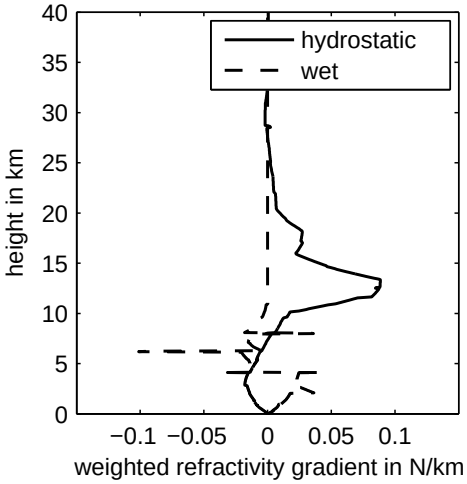

Figure 1. Hydrostatic (solid) and wet (dashed) refractivity weighted with height in Neper/km.

The maximum contribution to hydrostatic LHG can be attributed to heights between 10 and 15 km, whereas the maximum contribution to wet LHG is due to variations in the first few kilometers above the site.
Some outliers in the wet gradients of refractivity can be neglected because the LHG result from vertical integration, i.e. they correspond to the area w.r.t. zero gradients.

2. Results for CONT02

Figure 2 shows the total east gradients at the site Algonquin Park (Canada) during CONT02 as derived from vertical integration (equation 2), from VMF2 (Boehm et al., 2005 [1]), and as estimated in VLBI analysis as 24-hour offsets. Typically, the RMS delay differences at 5° elevation are at the 1 to 3cm level between VMF2 and LHG and at the 2 to 6cm level between VMF2 and the gradients estimated with VLBI.

Although the agreement between VMF2 and LHG is significantly better, this does not necessarily mean that the LHG are more accurate than the gradients estimated with VLBI. To assess the quality of the different types of gradients, baseline length repeatabilities are determined for CONT02 with (1) LHG fixed (no estimation of additional gradients), and (2) estimation of total gradients as 24-hour offsets. Approach (1) yielded slightly better repeatabilies (by $1mm^2$ median and $7mm^2$ mean improvement), what seems to be an indication that the application of LHG from high-accuracy numerical weather models is superior to the estimation of gradients.

3. Outlook

The application of LHG as derived by equation 2 improves baseline length repeatabilities for CONT02 w.r.t. standard solutions, i.e. with estimation of gradients. Compared to VMF2, the

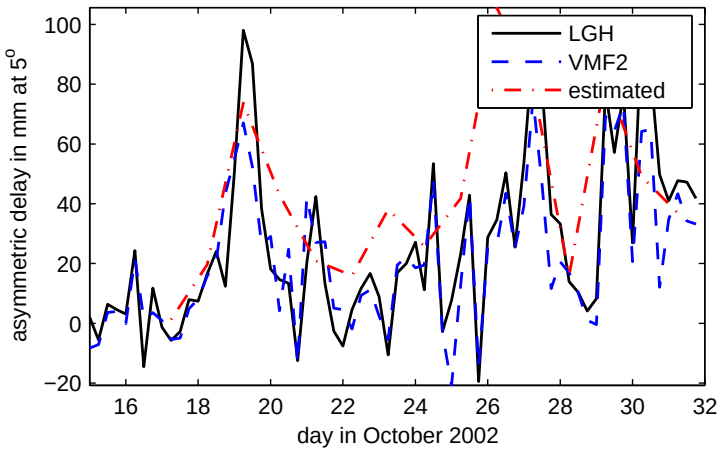

Figure 2. Total east gradients at Algonquin Park during CONT02 expressed as asymmetric delay in mm at 5° elevation.

downloading and computational efforts for these gradients are significantly reduced, allowing the provision of these parameters for a large number of stations on a routine basis. However, further investigations need to be done, e.g. on the use of LHG as a priori gradients plus the estimation of residual gradients with strong constraints.

4. Acknowledgements

We would like to thank the Austrian Science Fund (FWF) for supporting this work (P18404-N10) and the Zentralanstalt für Meteorologie und Geodynamik (ZAMG) for providing us access to the data of the European Centre for Medium-Range Weather Forecasts (ECMWF).

References

[1] Boehm, J., M. Ess, and H. Schuh, Asymmetric Mapping Functions for CONT02 from ECMWF, in: Proceedings of the 17th Working Meeting on European VLBI for Geodesy and Astrometry, edited by M. Vennebusch and A. Nothnagel, April 22-23 2005, 64-68, 2005.

[2] Boehm, J., B. Werl, and H. Schuh, Troposphere Mapping Functions for GPS and VLBI from ECMWF operational analysis data, Journal of Geophysical Research, in press, 2006.

[3] Davis, J.L., G. Elgered, A.E. Niell, and C.E. Kuehn, Ground-based measurement of gradients in the 'wet' radio refractivity of air, Radio Science, Vol. 28, No. 6, 1003-1018, 1993.

[4] MacMillan, D.S., Atmospheric gradients from very long baseline interferometry observations, Geophys. Res. Letters, Vol. 22, No. 9, 1041-1044, 1995.

Sebastien B. Lambert et al.: A Comparison of R1 and R4 IVS Networks, IVS 2006 General Meeting Proceedings, p.264–268
http://ivscc.gsfc.nasa.gov/publications/gm2006/lambert1

A Comparison of R1 and R4 IVS Networks

Sebastien B. Lambert [1], *Anne-Marie Gontier* [2]

[1)] *Royal Observatory of Belgium (formerly at NVI, Inc./US Naval Observatory)*
[2)] *Paris Observatory, SYRTE, CNRS/UMR8630*
Contact author: Sebastien B. Lambert, e-mail: s.lambert@oma.be

Abstract

This study compares the two parallel 24-hour R1 and R4 networks run by the IVS since 2002. We investigate the possible influence of the network geometry as well as the consistencies between Earth orientation parameters solutions and terrestrial reference frame realized separately through R1 or R4 experiments. We point out finally that the effects of using two different networks with different geometries and observational strategies show up in the operational series. Such consequences should be carefully examined in the future.

1. Overview of the Networks

The 24-hour rapid R1 and R4 experiments are conducted on Mondays and Thursdays, respectively, since January 2002. They are the cornerstone in the production of Earth orientation parameters (EOP) through very long baseline interferometry (VLBI) on a regular basis. It has been shown that the network geometry can produce inconsistencies at the level of accuracy of the actual VLBI measurements (see e.g., [1]). Therefore, it is essential to assess the consistency of the current networks, with two main goals: to correct the errors and to orient the future VLBI network towards a more perfect scheme.

R1 and R4 parallel networks used a total of 15 stations between 2002 and 2005.5. The stations are not the same for the two networks and their rate of use is also different. Figure 1 displays the most representative sites of the R1 and R4 networks over 2002-2005.5. A strong difference appears in the geometry, especially in the spatial extension of the networks. The R1 network allows very long East-West baselines (America-Europe and Europe-Japan) and large polyhedral areas sensitive to all 3 Earth orientation parameters (x_p, y_p and $UT1 - UTC$) thanks to sites in the southern hemisphere and across the five continents. The R4 network is significantly smaller, covering about a third of the Earth's surface. Sites in the southern hemisphere are poorly used, except FORTLEZA. TIGOCONC becomes sparsely used in 2003.

Figure 2 shows the number of sessions in which each station is participating over the 2002-2005.5 observing program. It appears that R4 uses quite systematically a subset of stations (WETTZELL, NYALES20, KOKEE, FORTLEZA, ALGOPARK for which the number of sessions is larger than 100) while the other sites are poorly used (number of sessions decreasing rapidly well below 20). In the R1, WESTFORD, WETTZELL and GILCREEK are systematically used, followed by TIGOCONC and HARTRAO. The number of sessions for the rest of the sites remains well above 20 excepted for 4 of them. This implies that, unlike the R4's, the R1 geometry is changing from one session to another, involving a lot of different baselines, and therefore the network geometry can be very different from one session to another.

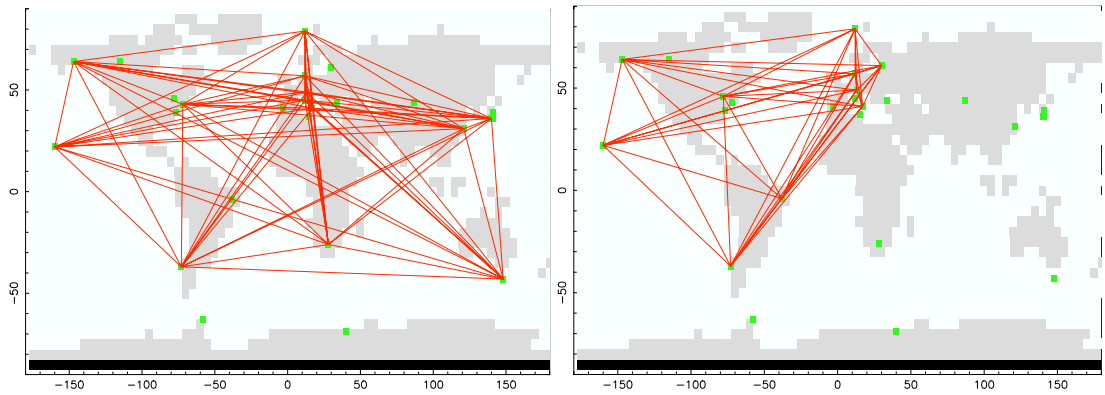

Figure 1. R1 (left) and R4 (right) networks represented with the most representative stations participating in the 2002-2005.5 observing program.

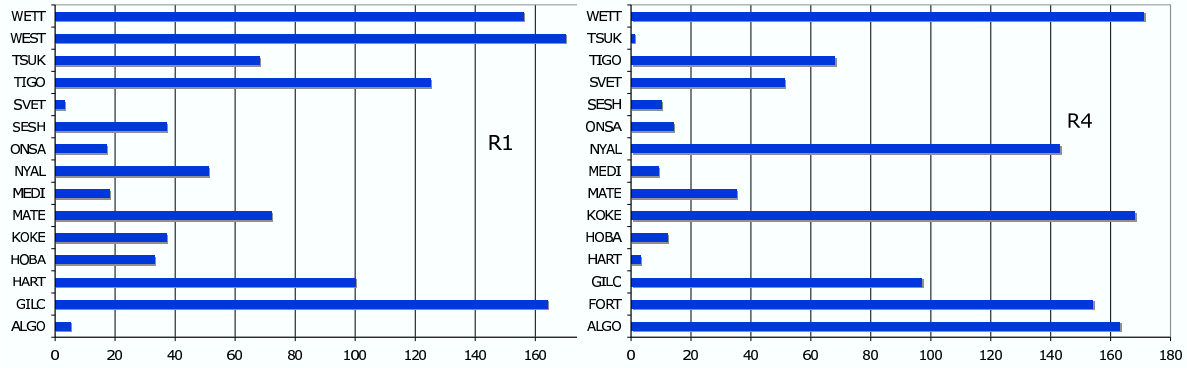

Figure 2. Number of sessions per stations in R1 (left) and R4 (right) networks over 2002-2005.5 observing program.

2. Comparison of EOP and TRF Realizations

Global solutions are run, carrying stations positions and velocities, antennas axes and sources positions as global parameters. The no-net-rotation and no-net-translation constraints on positions and velocities with respect to VTRF 2005 (Nothnagel 2005) are applied to all stations, excluding sites having known episodic motions (GILCREEK's position has been corrected in November 2002 after the Denali fault earthquake 100 miles south of Fairbanks). A no-net-rotation constraint is also applied to all the 212 ICRF defining sources. Other observed sources are estimated as global parameters. EOPs are estimated as arc parameters and compared against IERS Bulletin A ([3]). The following solutions are obtained with the CALC/SOLVE geodetic VLBI data reduction package developed at NASA/GSFC:

- EOP1, realized through the R1 experiments from experiment number 1 to 172,
- EOP4, realized through the R4 experiments from experiment number 1 to 176, and
- EOPA, realized through all the R1 and R4 experiments (348 sessions).

The CONT02 campaign is not included (note that its effect remains marginal). The EOP series are displayed in Figure 3. It appears that the current R1 experiments have residuals against Bulletin A with standard deviation similar to R4. However, EOP1 and EOP4 have different

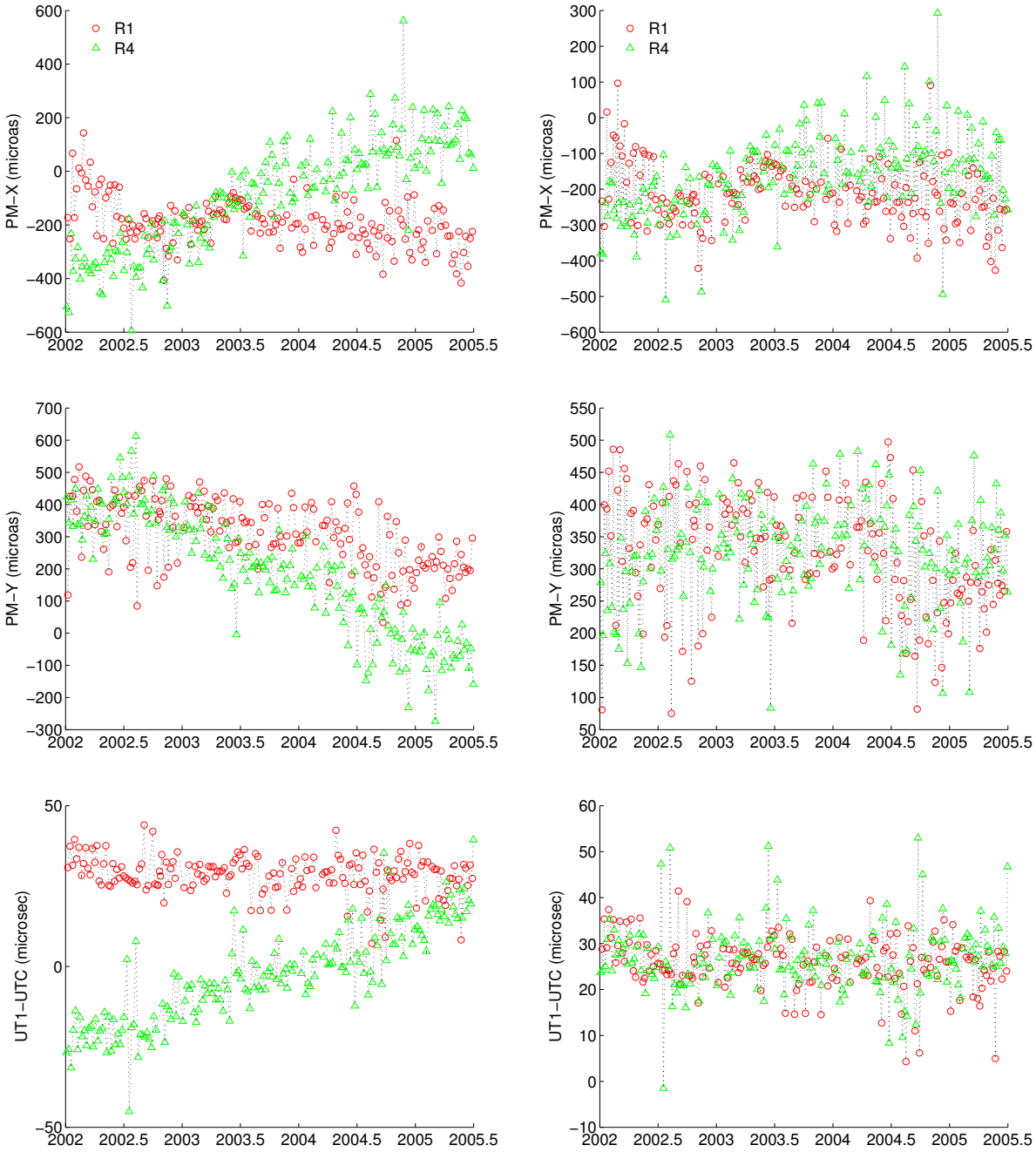

Figure 3. Differences between solutions EOP1 (left column, circles), EOP4 (left column, triangles), EOPA (right column with different markers for R1 (circles) and R4 sessions (triangles)) and IERS Bulletin A for the terrestrial pole coordinates x_p (top), y_p (middle) and UT1 − UTC (bottom) over 2002-2005.

biases and rates. The lower rates yielded by the R1-derived solution make EOP1 closer to the

Bulletin A. The differences in bias and rate between EOP1 and EOP4 can reach several hundreds of microarcseconds over a year, which is significant compared to the formal errors obtained on the EOP estimates (typically 100 μas). One must keep in mind that the two solutions EOP1 and EOP4 are obtained using the same assumptions and constraints. The only difference is the subset of stations used in the network (location of the antennas within the continents, geometry of the array, capabilities of the receivers, system failures, plate motions and faults, episodic events, etc.). It is obvious that the network and its geometry are the key parameters in the accuracy of EOP determined by VLBI among other sources of error. This raises very challenging questions and concerns which must be addressed before scheduling observations. This section seems to show that R1 experiments are "better" (in the sense that they give EOP realizations that match better the Bulletin A).

In the solution EOPA (combining both R1 and R4 sessions), it appears that the R1 and R4 x_p-components are evolving separately with a different rate. Before 2003, R4 is below R1 and this is reversed after 2003. The same phenomenon is visible also on the other components with a lower magnitude. It does reflect the differences in rate between EOP1 and EOP4.

The Helmert's parameters between individual TRF realized through solutions EOP1 and EOP4 and VTRF 2005 are reported in Table 1.

Table 1. The Helmert transformation parameters in mm for ΔX, ΔY and ΔZ, in ppm for s and in μas for α_1 and α_2, and μs for α_3, between R1 and R4-derived TRF and VTRF 2005. Formal errors are in italics.

	ΔX		ΔY		ΔZ		s		α_1		α_2		α_3	
EOP1	-1.0	*0.5*	0.7	*0.6*	-0.3	*0.5*	0.001	*0.001*	33	*305*	370	*242*	-10	*20*
EOP4	-0.6	*0.6*	0.2	*0.6*	-0.1	*0.6*	-0.004	*0.001*	-246	*208*	150	*166*	62	*31*

The determination of α_1 and α_2 for the R1 network shows significantly larger errors than for the R4's while the errors are comparable on α_3. If one remembers that the formal error is inversely proportional to the number of observations, one can explain these differences between R1 and R4 by crossing the results of Table 1 with the information of Figure 2. It has been pointed out in the previous section that a large part of the R1 sites are not used in all sessions but sparsely, and their respective number of observations is decreased. In the R4 network, a subset of sites are used regularly so that the network is almost the same in each session. A consequence is that the efficiency of R1 for the TRF determination is degraded compared to the R4. These remarks do not allow to conclude that the current R4 network is better than the R1 but they indicate:

- that a large number of sites is clearly an advantage in constraining and estimating the TRF,
- but that a changing network significantly degrades the TRF estimates.

3. Concluding Remarks

To conclude, consider a recent USNO analysis center 24-hour VLBI EOP solution ([4]) in which the other experiments are dropped (see Figure 4). The discrepancy between R1 and R4 noticed for EOPA is still present in component x_p with a weaker effect: the R4 experiments appear to be above the R1. The discrepancy is not significant for the other components.

Next, we would like to address the arguments that could be made that a limited study, such as

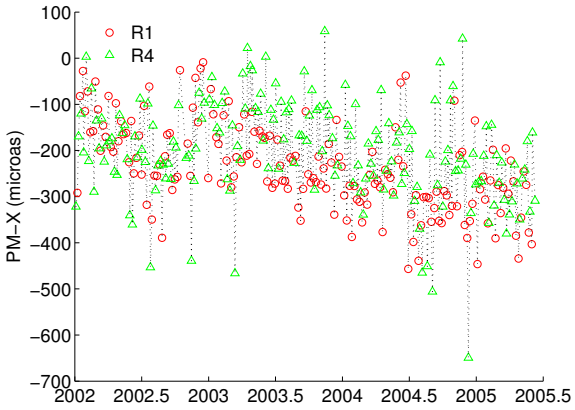

Figure 4. VLBI operational solutions USNO 2005b (x_p) represented with different markers for R1 (circles) and R4 sessions (triangles) against IERS Bulletin A.

this one, using only a small subset of VLBI sessions, is not truly representative of the long-term VLBI solutions. The argument that the long-term VLBI solutions consider many older sessions and that these additional sessions partly cancel out the effects of the inconsistencies observed here due to imperfect network is not completely valid. Many of these older experiments use similar networks (e.g., NEOS) and have their own sources of error that are not fully understood. Furthermore, this study clearly shows that the effects of these inconsistencies do show up in the operational data. Since the IVS is continuing to run these two networks in parallel and new stations will be needed to replace older ones that go out of service, the sources of errors affecting operational data must be investigated.

References

[1] Feissel-Vernier, M., Ray, J., Altamimi, Z., Dehant, V., & de Viron, O. 2004, VLBI and Earth rotation: geophysical and geodetic challenges, In: N. R. Vandenberg and K. D. Baver (Eds.): International VLBI Service for Geodesy and Astrometry 2004 General Meeting Proceedings, NASA/CP-2004-212255.

[2] Nothnagel, A. 2005, VTRF 2005 - A combined VLBI Terrestrial Reference Frame, In: M. Vennebusch and A. Nothnagel (Eds.): Proceedings of the 17th Working Meeting on European VLBI for Geodesy and Astrometry, Noto, Italy.

[3] IERS 2005, Bulletins maintained by the IERS Rapid Service/Prediction Center at USNO. Available on SOLVE erp format at http://gemini.gsfc.nasa.gov/apriori_files/usno_finals.erp.

[4] USNO 2005, maintained by the USNO Radio and Optical Reference Frame group. Available at http://rorf.usno.navy.mil/solutions/.

Daniel MacMillan et al.: First Results from CONT05, IVS 2006 General Meeting Proceedings, p.269–273
http://ivscc.gsfc.nasa.gov/publications/gm2006/macmillan1

First Results from CONT05

Daniel MacMillan [1], *Dirk Behrend* [1], *David Gordon* [2], *Chopo Ma* [3]

[1)] *NVI, Inc./NASA Goddard Space Flight Center*
[2)] *Raytheon ITSS/NASA Goddard Space Flight Center*
[3)] *NASA Goddard Space Flight Center*

Contact author: Daniel MacMillan, e-mail: dsm@leo.gsfc.nasa.gov

Abstract

CONT05 was a 15-day campaign of continuous VLBI sessions with a network of eleven globally distributed stations in September 2005. One of the main design goals for CONT05 was to obtain the highest accuracy that VLBI is capable, with some practical limitations, over the continuous two-week period. We discuss the scheduling and geometrical design for CONT05 and present preliminary analysis results on EOP precision, baseline length precision, and the observed subdaily EOP estimates compared with a tidal model. Daily EOP values determined by CONT05 have a precision matched only by the larger RDV sessions. Formal errors are in the range of ∼35–40 μasec for X and Y pole, ∼1.4–1.5 μs for UT1, and ∼75 and ∼30 μasec for nutation in longitude and obliquity.

1. Introduction

During the period September 12–27, 2005 the IVS conducted a campaign of continuous observing using a network of 11 antennas. The plan for CONT05 was to obtain the highest accuracy that VLBI is capable, with practical limitations, over the continuous two-week period. Goals of CONT05 were to address several scientific questions including the origin of discrepancies between high frequency (subdaily) Earth Orientation Parameters (EOP) tidal models and observed subdaily EOP, to study technique improvement, to study reference frame accuracy day to day, and to compare measurements made by co-located geodetic systems.

Figure 1. CONT05 Observing Network.

The CONT05 campaign was the latest in a series of continuous campaigns beginning with CONT94. Figure 1 shows the station locations of the CONT05 network, which has more stations

and generally better global distribution than the previous campaigns. Nevertheless, it would have been desirable to have more southern latitude stations or at least more stations at latitudes less than 20°N. We discuss the scheduling and geometrical design for CONT05 and present preliminary analysis results from the campaign.

2. Network Selection and Session Scheduling

In order to determine which stations were to participate in the CONT05 campaign, a pool of 14 candidate stations was selected. The selection was based on the high quality performance of the stations, on the experience from previous CONTs, and on the results of simulation studies. A call for participation was sent to the candidate stations. All stations agreed on becoming a CONT05 station except for Seshan (due to a scheduled hardware upgrade) and Hobart (lack of observing time). Fortaleza's participation was dependent on a timely upgrade to the Mark 5 system which unfortunately was not possible. The final network consisted of 11 stations as depicted in Figure 1.

The schedules were created using NASA's sked software. The observing mode corresponded to the IVS-R1 sessions with an observation rate of 256 Mbit/s. With the network fixed, several different schedules with varying scheduling parameters were made and the best schedule was chosen based on the expected EOP formal uncertainties.

Special care was taken for the selection of the radio sources. The sources for the schedules were based on the best 80 sources of the good geodetic source catalog. One source was taken out due to known source structure. Five other sources were taken out using a scoring scheme derived from the number of non-detections of the most recent (six months) R1 and R4 sessions. Only sources that had non-detection rates of less than 15% were retained. The number of sources being used for the scheduling was 74.

3. Quality Assessment

An obvious measure for the quality of the CONT05 data set are the formal uncertainties of the parameters solved for in the adjustment process. Table 1 compares the EOP formal uncertainties from CONT05 and from the R1, R4, and RDV series in 2005. Intra-scan observations on baselines from the same station are correlated due to unmodeled noise (such as station-inherent instrumental errors and atmospheric delays). Not accounting for this correlation has the formal uncertainties decrease too rapidly with the number of stations. Scaling up the formal uncertainties of an N-station network by a factor of $\sqrt{\frac{(N-1)}{2}}$ yields a more realistic measure of the observed uncertainty. Table 1 shows that the uncertainties (not scaled up) were significantly better for CONT05 than for the operational R1 and R4 series. Also the larger 2005 RDV sessions did not attain the high precision of the CONT sessions. Only a comparison to earlier RDV sessions (e.g., 2003-2004) shows a similar precision. Another way of assessing the precision of a series of experiments is to compute the baseline length repeatability. This measure has the advantage that it is independent of translation or rotation that can be absorbed into station topocentric coordinate time series. Figure 2 shows that the baseline length repeatabilities over all CONT05 baselines are at the 1 ppb level. All of the TIGOCONC baselines are longer than 8000 km and have the largest repeatabilities. With non-TIGOCONC baselines, the precision is 0.7–0.9 ppb.

To assess the EOP accuracy of the CONT05 data set, we compared the EOP results with values derived from GPS. For that we computed the differences VLBI–GPS for CONT05 as well as

Table 1. Average EOP formal uncertainties for selected sessions of the observing year 2005.

Series	Number	X-pole	Y-pole	UT1	Psi	Eps
		μas	μas	μs	μas	μas
CONT05	15	37	37	1.5	76	28
R1	50	73	72	3.0	157	62
R4	49	68	65	2.5	149	60
RDV	5	44	51	2.6	89	35

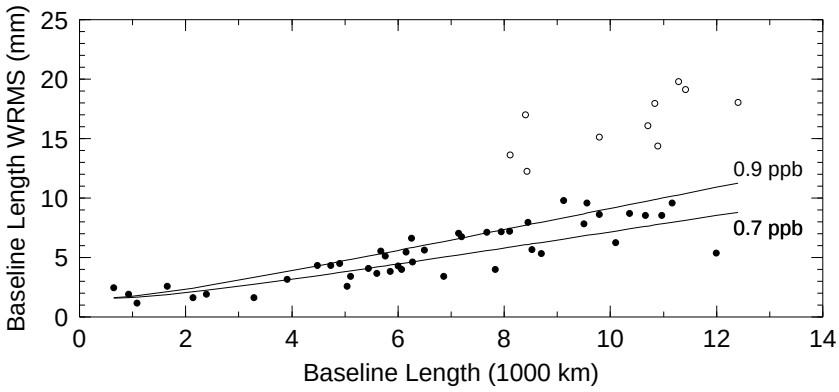

Figure 2. CONT05 baseline length repeatability where TIGOCONC baselines are denoted by open circles

for the R1 and R4 series during 2005. To do this we interpolated (cubic spline) the International GNSS Service (IGS) EOP series [2] to the VLBI epochs. Figure 3 shows the corresponding polar motion differences. The CONT05 EOP series are significantly closer to the IGS series (by about 50–60%) than either the R1 or R4 series. The statistics of the differences are given in Table 2.

Table 2. WRMS and χ^2/dof after removing offsets and biases for the polar motion and length of day differences between VLBI and GPS for CONT02 and CONT05 and the 2005 R1 and R4 series

Parameter	CONT02		CONT05		R1		R4	
	WRMS	χ2/dof	WRMS	χ2/dof	WRMS	χ2/dof	WRMS	χ2/dof
X-pole (μas)	99	3.1	55	2.1	92	2.4	96	2.2
Y-pole (μas)	65	1.9	36	0.9	91	2.5	106	2.9
X-pole rate (μas/d)	202	1.1	198	3.3	275	2.2	328	2.1
Y-pole rate (μas/d)	264	3.9	158	2.1	286	2.2	284	1.7
LOD (μs/d)	12.1	2.2	16.7	6.0	17	3.9	18.5	3.7

Possible reasons for the improved EOP agreement for CONT05 include (1) that the R1 and R4 networks only had 7–8 stations whereas CONT05 had 11 stations—in fact, a few R1 networks were subsets of the CONT05 network—and (2) that the global distribution of sites was generally

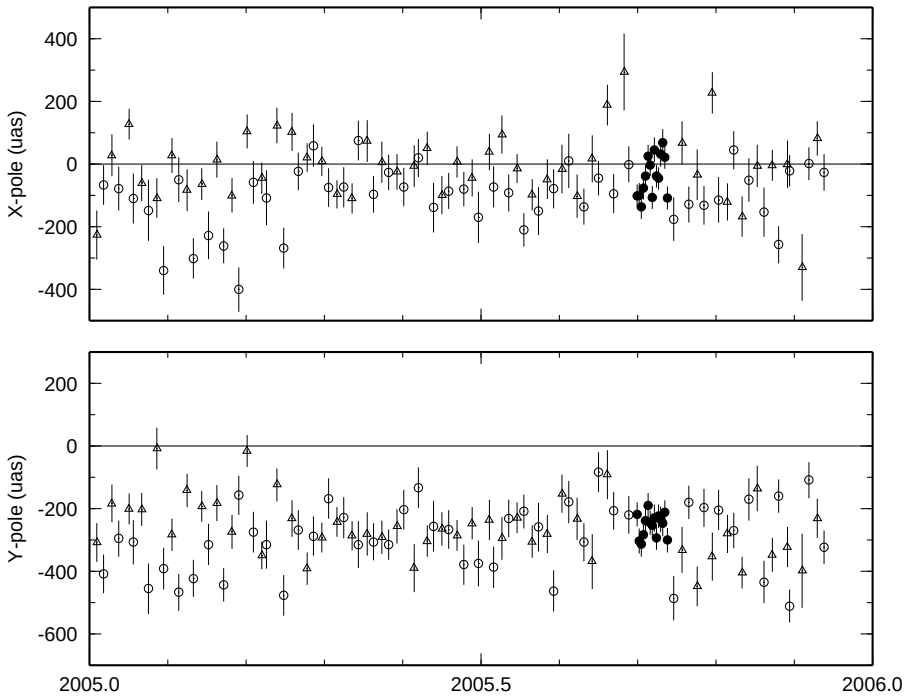

Figure 3. Polar motion differences between VLBI and GPS for the CONT05 series (solid circles), the R1 series (open triangles), and R4 series (open circles).

better for CONT05 than for the R1 and R4 experiments. In order to test this hypothesis, several test runs were made using subsets of the full CONT05 network. The agreement between EOP values from IGS and from VLBI subnets degraded significantly. Using these subsets, the EOP RMS differences were about twice as large as for the full CONT05 network.

4. Subdaily Earth Orientation Parameters

One of the principal motivations for doing the CONT series is to study the subdaily Earth orientation. We performed a solution to estimate EOP at 1-hour intervals using constraints of 10 mas/day for polar motion and 1 ms/day for UT1. The estimated subdaily UT1 series relative to the slowly-varying daily a priori series is shown in Figure 4. Superimposed is the high frequency tidal model of Gipson [1996] in which polar motion and UT1 tidal terms were estimated from all the VLBI data from 1980-1997.

Table 3 provides a summary of several statistics regarding daily and subdaily estimates of EOP from the CONT campaigns. It can be seen that the formal EOP precision for CONT05 is significantly better than the previous campaigns. Subdaily residuals have been computed after removing a high frequency tidal model from Gipson [1996; updated model in 1999 with more data]. These residuals have an RMS of about 180 μas, which is somewhat greater than the formal uncertainties. It is likely that these residuals are due mainly to atmospheric and oceanic angular momentum variation.

Table 3. Formal EOP uncertainties (precision) and subdaily residuals from continuous campaigns.

	Daily Precision			Hourly Precision			Subdaily Residual RMS		
Network	X (μas)	Y (μas)	UT1 (μs)	X (μas)	Y (μas)	UT1 (μs)	X (μas)	Y (μas)	UT1 (μs)
CONT94	46	43	1.9	185	228	7.8	185	176	10.4
CONT96	69	65	2.5	208	196	8.6	238	207	10.2
CONT02	50	40	1.7	196	157	8.0	201	183	11.4
CONT05	32	33	1.2	120	117	5.2	170	167	10.2

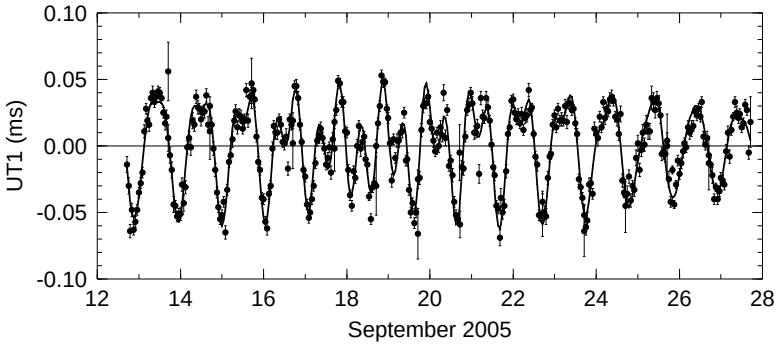

Figure 4. Subdaily estimates of UT1 at hourly intervals (dots) compared to Gipson's updated tidal model (solid line).

5. Conclusions

Daily EOP values determined by CONT05 have a precision matched only by the larger RDV sessions. Formal errors are in the range of ~35–40 μasec for X and Y pole, ~1.4–1.5 μs for UT1, and ~75 and ~30 μasec for nutation in longitude and obliquity. The CONT05 data set appears to be highly suitable for inter-technique comparisons, investigation of geophysical signals, and technique improvement studies.

6. Acknowledgements

We wish to thank everyone from the stations and the correlators as well as many others who contributed to making CONT05 a success.

References

[1] J. Gipson, "Very long baseline interferometry determination of neglected tidal terms in high-frequency Earth orientation variation," J. Geophys. Res., Vol. 101, B12, 28051-28064, 1996.

[2] G. Beutler, M. Rothacher, S. Schaer, T.A. Springer, J. Kouba, and R.E. Neilan, "The International GPS Service (IGS): An Interdisciplinary Service in Support of Earth Sciences," Adv. Space Res. Vol. 23, No. 4, pp. 631-635, 1999.

Daniel MacMillan: Radio Source Instability in the Analysis of VLBI Data, IVS 2006 General Meeting Proceedings, p.274–278
http://ivscc.gsfc.nasa.gov/publications/gm2006/macmillan2

Radio Source Instability in the Analysis of VLBI Data

Daniel MacMillan

NVI, Inc./NASA Goddard Space Flight Center
e-mail: dsm@gemini.gsfc.nasa.gov

Abstract

The source position time series for many of our frequently observed sources show systematic variation of as much as 0.5-1.0 mas due mainly to source structure changes and observing network changes. In our standard geodetic solutions, we only estimate global source position from data from all observing sessions. If these effects are not modeled, they produce corresponding systematic variations in estimated Earth orientation parameters (EOP) at the level of 0.02-0.04 mas in nutation and 0.01-0.02 mas in polar motion. We discuss two strategies for handling source instabilities: 1) estimate the positions of all unstable sources for each session they are observed and 2) estimate spline parameters chosen to fit the specific variation seen in the position time series. The second strategy improves VLBI EOP and nutation accuracy by reducing the biases and wrms differences between independent measurements from the simultaneous CORE-A and NEOS-A networks.

1. Introduction

In our standard geodetic solutions, we have generally ignored source structure effects and only estimate a single global source position for each source using its entire observing history. However, estimation of source position time series shows that many sources have significant systematic position variation that can be as much as 0.5-1.0 mas. This position variation is due to source structure changes and to the effect of observing sources with structure with networks consisting of different baselines. If these variations are not modeled, their effects will propagate into systematic effects on Earth orientation and nutation estimates. In this paper, we consider two ways of handling sources with significant position instabilities: 1) estimate the position of such sources for each session in which they were observed or 2) estimate global spline parameters chosen to fit the observed systematic variations of the position time series.

2. Source Position Time Series

We generated source position time series for 653 sources that were observed in 4017 experiment sessions from August 1979 until October 2005. For this paper, we concentrated on sources that were classified as unstable by Feissel-Vernier [2003]. Of the set of 107 geodetic sources, which includes the most frequently observed sources in the geodetic VLBI observing program, 23 sources were classified as unstable. Several of these sources show clear systematic linear or nonlinear variation. To illustrate how large the apparent source position variation of sources can be, we show the time series for 4C39.25 and 2145+067 in Figures 1 and 2. Fey et al. [1997] studied 4C39.25 and found consistency between the astrometric position time series and the evolution of the position of source components in VLBA and Mark III images. They observed that the apparent motion in right ascension was decreasing quadratically and that the motion should stop around

1997.7. However, one can see from Figure 1 that the astrometric position has continued to change.

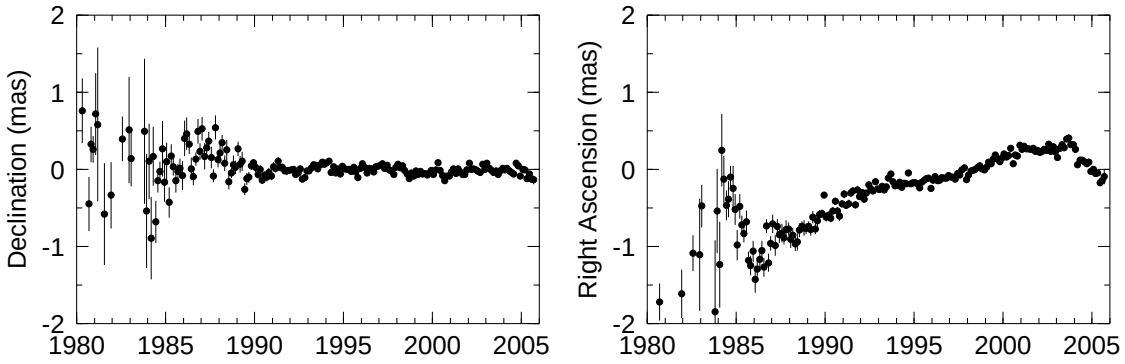

Figure 1. Radio source position time series in right ascension and declination for 4C39.25. Positions shown are 1.5 month averages

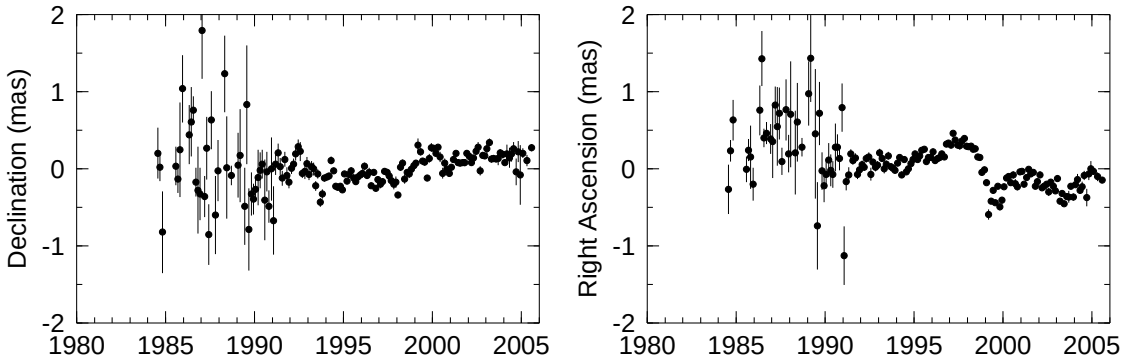

Figure 2. Radio source position time series in right ascension and declination for 2145+067. Positions shown are 1.5 month averages

3. Strategies for Modeling Source Position Instabilities

Ideally, one would derive source structure corrections from radio source images of an unstable source and then apply the corrections in the geodetic analysis. However, source image histories are generally not complete and it is a significant effort to correctly register the image of a quasar and to identify its stationary core. For this paper, we have used a more practical approach. We have identified unstable sources from position time series and then modified the estimation strategy to correct the effect of the instabilities. Here, we considered 3 estimation strategies:

A. Estimate all source positions as global parameters based on observations of all sources over all epochs of observation (conventional strategy).

B. Estimate positions for all 105 sources classified as unstable by Feissel-Vernier [2003].

C. Estimate spline parameters to fit nonlinear variations of 8 geodetic sources (0014+813, 0528+134, 1739+522, 2145+067, 2234+282, 2243-123, 4C39.25, and 3C446) among the 23 unstable geodetic sources identified by Feissel-Vernier [2003] and estimate only an offset and rate for 3 other sources (OK290, 0955+476, and 2126-158) with rates greater than 30 μas/yr. For the remainder of the 23 sources, positions were estimated as global parameters.

4. Effect of Source Position Variations

If source position instabilities are not modeled, the residual apparent source motion will be absorbed in estimates of other parameters. Figures 3 and 4 show the effect on nutation in obliquity using estimation strategies B and C rather than the conventional strategy A. These difference plots have a similar systematic variation, although the weighted root mean square (WRMS) scatter for the B-A differences (60 μas) is significantly greater than for the C-A differences (26 μas) since so many source positions (105) are being estimated as arc parameters. The differences $\delta\epsilon$(t) in both plots appear to have a variation with an amplitude of about 25 μsec at a period that is close to the 18.7 year nutation period.

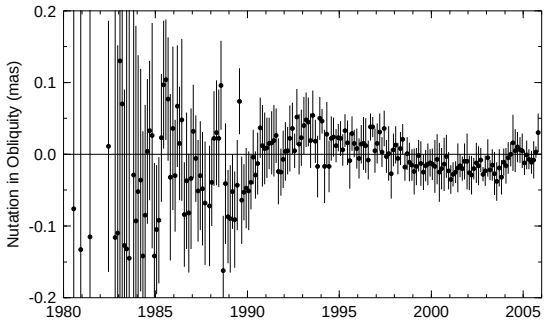

Figure 3. Effect on nutation in obliquity estimates when strategy B is used instead of A. For clarity, 1.5 month averages of the A-B differences are plotted

5. Determining the Best Estimation Strategy

One way of evaluating different stategies of parameter estimation is to look at baseline length repeatabilities. In Figure 5 and 6, we compared the repeatabilities from site position solutions using the three estimation strategies discussed in this paper. The repeatabilities using strategy B were worse than the conventional approach A and slightly better using stategy C, but only by at most 0.5 mm. These tests appear to show that the terrestrial reference frame is not very sensitive to these choices of estimation approach.

To assess the EOP accuracy of the different estimation strategies, we compared the EOP and nutation estimates from simultaneous independent VLBI networks. We used the set of 80 simultaneous CORE-A and NEOS-A experiments during the period 1997-2000. Table 1 summarizes the statistics of these differences. The strategy B of estimating for each session the positions of all

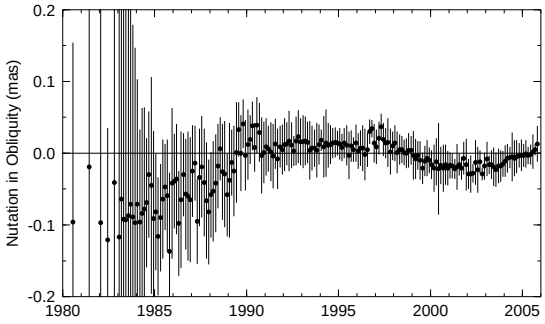

Figure 4. Effect on nutation in obliquity estimates when strategy C is used instead of A. For clarity, 1.5 month averages of the A-C differences are plotted

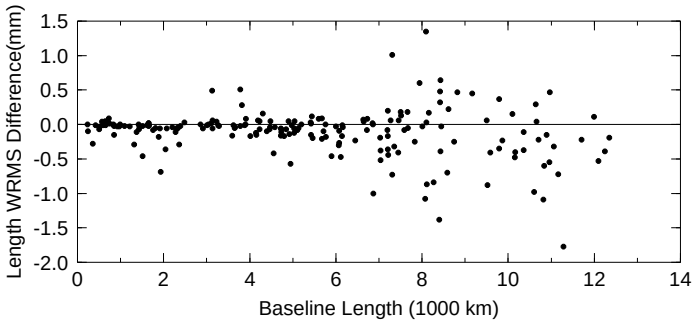

Figure 5. Improvement in baseline length wrms repeatability with strategy C compared with A in the sense wrms(A)-wrms(C)

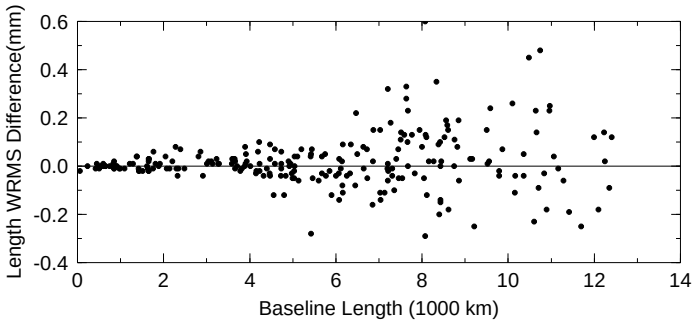

Figure 6. Improvement in baseline length wrms repeatability with strategy B compared with A in the sense wrms(A)-wrms(C)

sources classified as unstable by Feissel-Vernier [2003] leads to WRMS and bias differences that are mostly larger than the standard strategy A (except for X-pole). Strategy C yields smaller biases and WRMS differences for most components than the conventional approach A.

Table 1. NEOS-A minus CORE-A simultaneous session differences

Parameter	A		B		C	
	WRMS	Bias	WRMS	Bias	WRMS	Bias
X-pole (μas)	221	55±15	203	31±15	207	32±15
X-pole rate (μas/d)	523	25±49	556	54±51	511	30±49
Y-pole (μas)	154	12±12	153	28±13	152	18±12
Y-pole rate (μas/d)	556	-78±45	558	-79±47	542	-70±45
UT1 (μs)	8.9	1.1±0.6	9.3	2.4±0.6	9.1	2.2±0.6
UT1 rate (μs/d)	19.2	-4.4±1.8	19.3	-3.8±1.9	18.6	-4.1±1.8
Psi (μas)	376	152±29	374	143±32	375	153±29
Eps (μas)	142	39±11	159	50±12	138	30±11

6. Conclusions

The position time series of many of the radio sources observed by geodetic networks have significant systematic variations. These variations can be nonlinear and can have large linear rates. We found that estimation of additional position parameters for unstable sources improves the internal accuracy of EOP and nutation estimates. Estimation of spline parameters for a subset of 11 of the 105 sources identified by Feissel-Vernier [2003] yields better accuracy than estimation of all 105 unstable source positions as arc parameters (estimated for each experiment session). Not modeling the instability of these sources appears to lead to a cyclic variation in estimates of nutation in obliquity that has a period close to the 18.7 year nutation period. In this paper, we mainly considered the effect of the most frequently observed sources, which are the 107 sources in the geodetic observing catalog. In the future, we will examine the stability of sources not currently in the geodetic catalog. In weekly R1 sessions over the last two years, we have been monitoring the positions of candidate sources not in the current catalog. We plan to use this information combined with previous source position histories to add new stable sources to the geodetic catalog and remove unstable sources.

7. Acknowledgements

The author thanks Karen Baver for running a series of solutions to determine the source position time series analyzed in this paper.

References

[1] A. L. Fey, "The Proper Motion of 4C39.25," Astron. J., Vol. 114, No. 6, 2284-2291, 1997.

[2] M. Feissel-Vernier, "Selecting Stable Extragalactic Compact Radio Sources from the Permanent Astrogeodetic VLBI Program," Astron. Astrophys.,Vol. 403, 105-110, 2003.

Oleg Titov: Effect of Reference Radio Source Instabilities on the TRF Solution, IVS 2006 General Meeting Proceedings, p.279–280
http://ivscc.gsfc.nasa.gov/publications/gm2006/titov

Effect of Reference Radio Source Instabilities on the TRF Solution

Oleg Titov

Geoscience Australia
e-mail: oleg.titov@ga.gov.au

Abstract

The goal of this paper is to evaluate the effect of reference radio source instabilities on daily estimates of station positions and, finally, on VLBI site coordinate estimates. It was shown that geodetic positions of Southern Hemisphere VLBI sites are more strongly due to the scarcity of the reference radio source positions.

1. Introduction

The radio source positions for the ICRF are obtained with VLBI technique and referred to a fixed time epoch J2000. The first catalogue consisted of 608 objects, 212 of them were 'defining' sources forming the core of the ICRF [1]. In addition 294 'candidate' sources having fewer observations and, finally, 102 'other' sources were added to densify the ICRF.

Many radio sources, presumably considered pointlike, show an extended structure [2]. The structure instability causes temporal variations of the radio source astrometric position. Gontier et al. [3] noted a variability of the differential rotation angles from year to year of several hundred sources over 1987-1999, mostly before 1990. Feissel-Vernier [4] developed a detailed scheme for the selection of stable radio sources using time series of the position estimates during 1979-2002 produced by the US Naval Observatory. The yearly values from 1990.0 to 2002.0 of the right ascension and declination averaged from their original daily positions were analysed to derive several statistical parameters for 362 preselected radio sources. Finally, 199 radio sources were recommended for further improvement of the ICRF, as being 'stable'. It was found that the new selection scheme improved the stability of the ICRF [5] in comparison with the 'defining' ICRF radio source list.

Unfortunately, there are only 77 common objects in the lists of 212 'defining' and 199 'stable' radio sources. Therefore, the daily station position estimates differ, depending on the reference radio source list that is used.

2. VLBI Data Analysis and Geodetic Results

The geodetic time-series were obtained from two global VLBI solutions from about 3 million group delays between 1979 and 2005. All data were processed using the OCCAM software [6] with the least squares collocation method [7]. The strategy and observational data set of both solutions differ only by the list of radio sources treated as global parameters. The first solution (designated as aus2005b1) uses the 207 ICRF-Ext.2 objects [8] as global radio sources with the NNR-constraints, whereas the second solution (aus2005b2) uses the list of 199 'stable' radio sources [4]. 107 radio

sources (102 'other' and 5 'defining') are treated as 'arc' parameters for the aus2005b1 solution, and 163 'unstable' radio sources for the aus2005b2. All other radio sources were considered as global parameters without the NNR-constraints.

Both solutions were done in two steps. The first step the positions of the radio sources, treated as global parameters, were only estimated. The second step all 'arc' parameters (including daily estimates of the VLBI site coordinates) were estimated with respect to the reference radio source positions, improved in the previous step.

From daily coordinates of all the VLBI sites we estimate the initial position (for epoch 1997.0) and linear drift of each site. Then, the time-series of differences between the aus2005b1 and aus2005b2 solutions for each component were generated. The mean offset and weighted RMS statistic were used to evaluate the ICRF uncertainty effect on the resulting geodetic parameters.

There is no evidence of a geodetic position bias due to radio source instabilities for VLBI sites in the Northern Hemisphere at the level larger than 3 mm.

However, in the Southern Hemisphere the mean offset of geodetic positions for VLBI sites can be larger. For example, Hobart has a statistically significant offset (10.6 +/- 1.4 mm) in its vertical component.

References

[1] Ma, C., E.-F., Arias, T. Eubanks, A. Fey, A.-M., Gontier, C. Jacobs, O. Sovers, B. Archinal, P. Charlot The International Celestial Reference Frame as realised by Very Long Baseline Interferometry, Astron. J., 116, 516–546, 1998.

[2] Fey, A., P. Charlot VLBA observations of radio reference frame sources. III Astrometric suitability of an additional 225 sources, Astroph. J. Suppl. Ser., 128, 17–83, 2000.

[3] Gontier,A.-M., K. Le Bail, M. Feissel, T. Eubanks, Stability of the extragalactic VLBI reference frame, Astron. Astroph., 375, 105–110, 2001.

[4] Feissel-Vernier, M., Selecting stable extragalactic compact radio sources from the permanent astro-geodetic VLBI program, Astron. Astroph., 403, 105–110, 2003

[5] Feissel-Vernier, M., Stability of the VLBI-Derived Celestial Reference Frame, In: General International VLBI Service for Geodesy and Astrometry Proceedings, NASA/CP–2004-212255, N. R. Vandenberg and K. D. Baver (eds.), 346–350, 2004.

[6] Titov, O., V. Tesmer, J. Boehm, OCCAM 5.0 User Guide, AUSLIG Technical Note, 7, AUSLIG, Canberra

[7] Titov, O, Estimation of subdiurnal tidal terms in UT1-UTC from VLBI data analysis In: IERS Technical Notes, 28, Observatoire de Paris B. Kolaczek, H. Schuh, and D. Gambis (eds.), Paris, 2000.

[8] Fey, A., C. Ma, E. F. Arias, P. Charlot, M. Feissel-Vernier, A-M. Gontier, C. Jacobs, J. Li, D. MacMillan, The second extension of the international celestial reference frame: ICRF-Ext.1, Astron. J., 127, 3587–3608, 2004.

Gerald Engelhardt et al.: First Steps to Investigate Long-Term Stability of Radio Sources in VLBI Analysis, IVS 2006 General Meeting Proceedings, p.281–285
http://ivscc.gsfc.nasa.gov/publications/gm2006/engelhardt

First Steps to Investigate Long-Term Stability of Radio Sources in VLBI Analysis

Gerald Engelhardt, Volkmar Thorandt

Bundesamt für Kartographie und Geodäsie

Contact author: Gerald Engelhardt, e-mail: gerald.engelhardt@bkg.bund.de

Abstract

Presently, the observation period of several radio sources observed by geodetic VLBI covers more than 20 years. So, the estimation of global source parameters with the modelling of only one source position for the complete length of VLBI data should only be applied to stable compact radio sources. One important tool to handle this aspect consists of analyzing time series for radio source coordinates. The main features regarding the estimation of time series of radio source positions in global VLBI solutions are explained. On the basis of these time series a weighted mean was estimated for each radio source component. The residuals to the weighted mean were tested for normal distribution for the purpose of uncovering systematic errors. First results are discussed.

1. General Information

Presently global complete geodetic VLBI solutions with more than 20 years of data are possible. Stable compact radio sources can be modelled with only one source position for the whole length of time. Unstable radio source, with, e.g., a known high-level source structure, are not suitable for this. This would cause a modelling error. So the question arises; which radio sources are stable? Currently support is given by the list of the ICRF defining sources (ref. [3]), the list of stable compact radio sources determined by MARTINE FEISSEL-VERNIER (ref. [2]), and the list of structure indices of radio sources set up by PATRICK CHARLOT (ref. [1]). But, also, the estimation and analsis of time series for radio source positions constitute a possibility to answer this question.

2. Time Series for Radio Source Positions

The basis to derive time series for radio source positions is a global complete VLBI solution with 24 hours VLBI sessions from January 1984 to February 2005. The main parameter types are globally estimated station coordinates and their velocities and 199 stable radio source positions detected by MARTINE FEISSEL-VERNIER (ref. [2]). Minimal constraints for the datum definition are applied to get zero net rotation and zero net translation for 26 selected station positions and velocities with respect to VTRF2003 (ref. [4]) and to get zero net rotation for 199 stable sources (ref. [2]) with respect to ICRF (ref. [3]). All other source positions are estimated in a local mode in each session for generating the time series. This solution is called basis solution 1. But there is a problem. This solution does not produce time series for the 199 stable radio sources. One possibility to solve this is to reduce the set of stable radio sources for the datum definition by one source. A separate solution with no other changes with regard to the basis solution 1 gets the estimations of local source positions for this selected stable radio source in the respective sessions.

The advantage of this procedure is that there is nearly no change in datum definition for generating time series for all radio source positions. But the disadvantage is the separate calculation for each stable radio source. After these additional computations time series for all radio sources are available.

3. Weighted Mean for Each Radio Source

The following step is based on the assumption that all radio sources are considered stable. So it is possible to use the time series with locally determined source positions L and their standard deviations s to estimate a weighted mean x for each radio source component. If the weights p are given by

$$p_i = (s_i)^{-2} \qquad \text{and}$$

$i = 1, 2, \ldots, n$ (n number of values in the time series of the source component) then the weighted mean x can be estimated by

$$x = \frac{[pL]}{[p]} \qquad \text{and the residuals are}$$

$$v_i = x - L_i.$$

This procedure results in a weighted mean and the corresponding residuals for all radio sources in both components (declination and right ascension).

4. Outlier Detection

The purpose of outlier detection is to increase the reliability of the used data. The basis applied here is the outlier test by GRUBBS (e.g. ref. [7]) with the test of the maximum amount of the residual v_{max}. The test statistic g is computed by

$$g = \frac{|v|_{max}}{\sqrt{\frac{[vv]}{n}}}.$$

The confidence level g_s is listed in a table with the number of data points and the significance level of 1 percent. The decision rule says, if $g \leq g_s$ than no outlier is detected and no action is necessary. But if $g > g_s$ than an outlier is detected and the corresponding data point is not used for the new estimation of the weighted mean.

5. Test for Normal Distribution

Based on time series of radio source position residuals to the weighted mean of a radio source component can be tested for normal distribution. At least 25 sessions should be available for a radio source. Time series with less than 25 sessions are not considered for the test. The purpose of the test is the uncovering of systematic phenomena in the time series of radio source positions. The basis is a smooth test between the empirically determined distribution and the theoretical normal distribution (e.g. ref. [5]). The parameters of the normal distribution are the mean value and the variance computed from the sample (residuals). The mean value is given by $v_{mean} = [v]/n$

and the variance can be estimated by $s^2 = [(v - v_{mean})^2]/n - 1$. The test statistic χ^2 is computed by

$$\chi^2 = \sum_{m=1}^{r} \frac{(h_m - np_m)^2}{np_m} \qquad \text{and}$$

r number of classes ($r = 10$), class width $= s/2$
m current number of classes
h_m empirical absolute frequency of class m
p_m theoretical probability of class m.

The confidence level χ_s^2 is listed in a table of the chi-square distribution with the significance level of 1 percent. The decision rule says here, if $\chi^2 < \chi_s^2$ than the distribution of the sample (residuals) is in no contradiction with the assumption that it comes from a normal population. So systematic phenomena could not be proven. But if $\chi^2 > \chi_s^2$ than the distribution of the sample (residuals) is in contradiction with the assumption that it comes from a normal population. So systematic phenomena could be proven, e.g. instabilities of radio source components exist.

6. First Results and Comparisons

Altogether 938 radio sources with position time series are available. 223 radio sources with at least 25 sessions could be investigated. The normal distribution was not rejected ($\chi^2 < \chi_s^2$) for 121 radio sources in both components, declination and right ascension, and for 62 radio sources in only one component, declination or right ascension. If the ICRF stability criterion is applied for the 121 radio sources than the following equation can be set up:

$$121 = 37d + 49c + 29o + 6n,$$

where d defining source, c candidate source, o other source, n new source.
Figure 1 is an example for the time series of radio source 0215+015 in declination and right ascension. For this defining source the test for normal distribution was not rejected in both components.

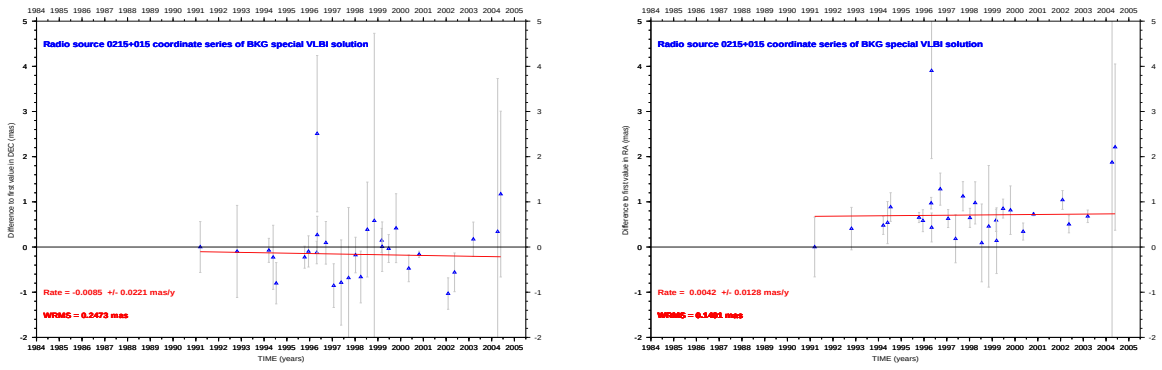

Figure 1. Time series of radio source 0215+015 (DEC on the left, RA on the right)

Figure 2 shows the corresponding histogram with the normal curve for both components.

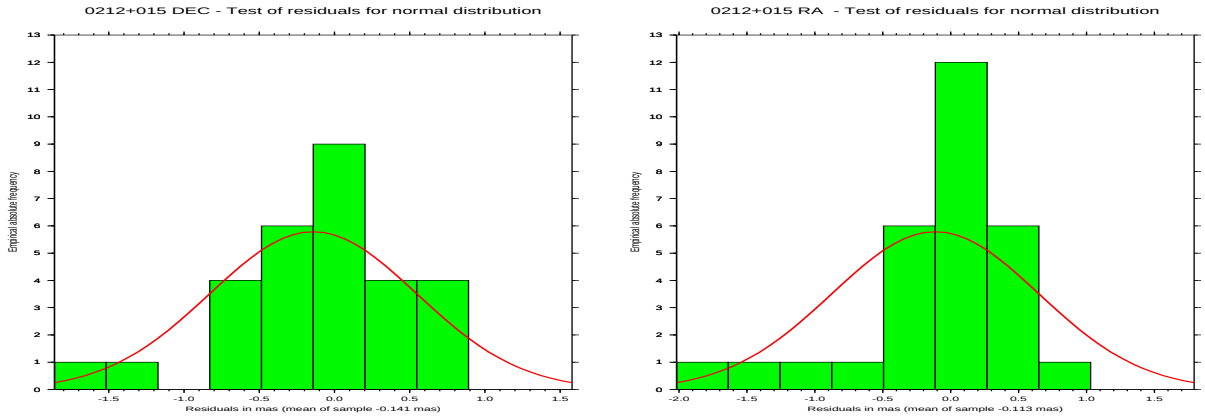

Figure 2. Histogram and normal curve of radio source 0215+015 (DEC on the left, RA on the right)

A comparison with the stability criterion derived by MARTINE FEISSEL-VERNIER (ref. [2]) shows the values 1 and 2 (stable) for 61 radio sources, 3 and 4 (unstable) for 51 sources. 9 sources were not determined. Another comparison with the source structure index for X band, the level of position disturbance (1 least disturbed, 4 most disturbed), derived by PATRICK CHARLOT (ref. [1]) amounts to the values 1 and 2 for 56 radio sources, value 3 for 29 sources, 4 for 8 sources. 28 sources were not determined. A complete list of 183 radio sources with their stability criteria, each one positively tested in one or both components, islisted in 1 (ref [6]); Table 1 shows an excerpt.

Table 1. Stability criteria for 183 radio sources, I = stability criterion ICRF, II = source structure index for X band / S band by P. Charlot, level of position disturbance expected as a result of the source structure, 1=least disturbed, 4=most disturbed, III = stability criterion by M. Feissel-Vernier, 1 and 2=stable sources, 3=unstable, 4=highly unstable, IV = result of statistical test for normal distribution of residuals to the weighted mean on the basis of time series of radio source positions, N2=normally distributed in both radio source components, N1_DEC=normally distributed in declination, N1_RA=normally distributed in right ascension, Number of data points A=all data, M1=one-month average coordinates (smoothed data set)

No.	Source name IVS/IERS or IVS	I	II	III	VI	Number of data points	A/M1	Length of time
1	0003-066	c	3/1	2	N2	114	M1	1988.04 2005.11
2	0013-005	c	2/1	4	N2	37	A	1990.83 1999.86
3	0016+731	o	2/1	2	N1_RA	74	M1	1988.01 2004.23
4	0104-408	o	-	1	N2	147	M1	1988.96 2005.12
5	0111+021	c	3/1	1	N1_RA	83	M1	1987.62 2004.70
6	0119+041	c	2/1	2	N1_RA	186	M1	1987.50 2005.08
7	0119+115	c	2/1	2	N2	116	M1	1990.11 2005.11
8	0146+056	c	3/1	4	N2	40	A	1989.07 2000.32
9	0202+149	c	2/2	2	N1_DEC	183	M1	1987.49 2005.11
10	0212+735	o	2/2	3	N1_RA	189	M1	1984.05 2004.90
11	0215+015	d	1/1	1	N2	29	A	1991.19 2004.40

No.	Source name IVS/IERS or IVS	I	II	III	VI	Number of data points	A/M1	Length of time
12	0229+131	c	2/1	2	N1_DEC	245	M1	1984.07 2005.11
13	0234+285	c	3/2	2	N1_DEC	173	M1	1984.05 2005.12
14	0238-084 NGC1052	o	4/2	4	N1_DEC	107	M1	1988.04 2004.17
15	0239+108	d	2/2	4	N2	47	A	1988.96 2004.82
16	0256+075	d	2/1	1	N2	43	A	1987.59 2004.65
17	0300+470	o	2/1	2	N2	98	M1	1984.07 2004.86
18	0306+102	d	3/1	2	N2	35	A	1993.73 2005.11
19	0308-611	d	-	2	N2	57	A	1991.89 2003.84
20	0316+413 3C84	o	-	-	N2	53	A	1985.35 2004.65
⋮	⋮	⋮	⋮	⋮	⋮	⋮	⋮	⋮
182	2355-106	c	1/1	2	N2	68	M1	1989.26 2005.03
183	2356+385	c	-	4	N2	90	M1	1994.46 2005.11

7. Conclusions and Outlook

Generating and statistically analyzing time series for radio source positions are useful to get more information about long-term stability of radio sources. After the successful test for normal distribution of residuals to the weighted mean of both radio source components also an inspection of WRMS, rate estimation, and distribution of the data points (sessions) in the time scale are necessary to answer the question for stable sources. Another helpful way for answering this question is also the planned development of a procedure for checking the stability of the axes of the CRF materialized by a set of selected radio sources.

The investigations about stable radio sources are not finished yet. So be careful with the use of the "N2" stable sources from Table 1.

References

[1] Charlot Patrick (2005): Radio source structures, web reference (http://www.obs.u-bordeaux1.fr/m2a/charlot/structure.html).

[2] Feissel-Vernier Martine (2003): Selecting stable extragalactic compact radio sources from the permanent astrogeodetic VLBI program, In: Astronomy and Astrophysics manuscript no. MS3523, March 10, 2003.

[3] ICRF with defining sources (1998), web reference (http://hpiers.obspm.fr/icrs-pc).

[4] Nothnagel Axel(2003): VTRF2003: A Conventional VLBI Terrestrial Reference Frame, In: Proceedings of the 16th Working Meeting on European VLBI for Geodesy and Astrometry, held at Leipzig, May 09-10, 2003, edited by W. Schwegmann and V. Thorandt, Bundesamt für Kartographie und Geodäsie, Frankfurt/Leipzig, 2003.

[5] Reißmann Günter (1976): Die Ausgleichungsrechnung, Grundlagen und Anwendungen in der Geodäsie, Verlag für Bauwesen, Berlin, 1976.

[6] Web reference (ftp://ftp.leipzig.ifag.de/pub/analysis/sources_stability_criteria/table1.txt).

[7] Wolf Helmut (1975): Ausgleichungsrechnung, Formeln zur praktischen Anwendung, Ferd. Dümmlers Verlag, Bonn, Dümmlerbuch 7835, 1975.

John M. Gipson: Correlation Due to Station Dependent Noise in VLBI, IVS 2006 General Meeting Proceedings, p.286–290
http://ivscc.gsfc.nasa.gov/publications/gm2006/gipson

Correlation Due to Station Dependent Noise in VLBI

John M. Gipson

NVI, Inc./NASA Goddard Space Flight Center
e-mail: jmg@leo.gsfc.nasa.gov

Abstract

I study the effects of including station dependent delay noise in the analysis of geodetic VLBI. Such terms increase the observational noise, as well as introducing correlation between observations. I demonstrate by looking at CONT05 and the R1 & R4 sessions from 2005 that introducing such noise terms reduces baseline scatter and gives more realistic formal errors.

1. Introduction

The VLBI observable, colloquially called the "delay", is the difference in arrival time of a signal at two different stations. The delay is measured by correlating the signals received at the stations. This process has a uncertainty associated with it which, for clarity, I call *measurement noise* and denote by σ_{meas}. One can show, assuming SNRs commonly used in VLBI, that the measurement noise on different baselines is uncorrelated. The standard assumption in VLBI processing is that the *observational noise* in VLBI is just the measurement noise. This has the corrolary that the VLBI observations are independent.

There are several indications that this assumption is false. First, χ^2 from individual session solutions is much larger than it should be. Second, the scatter of baseline lengths is larger than it should be based on the formal errors. Third, comparison of EOP measurements from simultaneous VLBI sessions are inconsistent with the formal errors. All of these are indicative of incorrect modeling and/or unmodeled error sources.

There are many other error sources besides measurement noise. For example: 1) phase cal errors; 2) RF interference in the signals; 3) other correlator related errors; 4) source structure; 5) source position errors; 6) errors in geophysical models; 7) mismodeling clocks and/or atmospheres; 8) underparametrizing the time variation of clocks and/or atmospheres; etc. All of these increase the noise of individual observations. Many also introduce correlation between observations.

In this paper I look at the special case of error sources which manifest themselves as station dependent delay, e.g., mismodeling atmosphere delay. These cause changes in the measured delay. This will show up as excess delay noise. Since this delay error is common for all baselines involving a station, these observations are no longer independent, and the covariance matrix is no longer diagonal.

Other scientists have studied the stochastic model used in VLBI. Schuh and Wilkin [1] derived empirical correlation coefficients from 19 VLBI sessions, but did not take the next step of modifying the normal equations. Schuh and Tesmer [2] derived empirical correlation coefficients, and, together with the a priori variance, σ^2_{meas}, constructed the covariance matrix. They demonstrated that this improved repeatability on 36 IRIS-S sessions from December 1994 through December 1998. Tesmer [3] and Tesmer and Kutterer [5] modified the covariance matrix by inflating the diagonal terms

with additional contributions due to sources, stations, and elevations. They found a reduction in the scatter of station position of a few percent.

In the next section, I present the least squares equations for VLBI. In Section 3, I discuss how station dependent delay modifies the covariance matrix. In Section 4, I study the effect of including "clock-like" errors and errors due to mismodeling the atmosphere. Using two data sets, CONT05, and the R1s & R4s during 2005, I demonstrate that including these terms increase the formal error of our baseline estimates, making them more realistic, and decreases baseline scatter, indicating that the estimates are actually better. I conclude with a discussion of future work.

2. Least Squares Equations in VLBI

The VLBI observable is the time delay $\tau_{ij}(t)$ between two stations i, j at some epoch t. The delay is a function of various parameters A_a. In the linear approximation the observed delay is:

$$\tau_{ij}(t) = \tau_{0,ij}(t) + \sum_a A_a \frac{\partial \tau_{ij}(t)}{\partial A_a} + \varepsilon_{ij,obs}(t) = \tau_{0,ij}(t) + \sum_a A_a F_{a,ij}(t) + \varepsilon_{ij,obs}(t) \tag{1}$$

$\tau_{0,ij}(t)$ is the a priori delay and $\varepsilon_{ij,obs}(t)$ is the noise associated with the observation, and $F_{a,ij}(t)$ the partial derivative of the delay. Let Ω be the covariance matrix of the observations:

$$\Omega_{ijt,klt'} = < \varepsilon_{ij,obs}(t)\varepsilon_{kl,obs}(t') > \tag{2}$$

The least squares equations are given by:

$$\sum_a \left(\sum_{ijt} \sum_{klt'} F_{b,ij}(t) F_{a,kl}(t') \Omega^{-1}_{ijt,klt'} \right) A_a = \sum_{ij} \sum_t F_{b,ij}(t) \Omega^{-1}_{ijt,klt'} \left(\tau_{kl}(t') - \tau_{0,kl}(t') \right) \tag{3}$$

These equations can be formally inverted to solve for the A_a:

$$A = \left(F^T \Omega^{-1} F \right)^{-1} F^T \Omega^{-1} \tau_{o-c} \tag{4}$$

3. Effect of Station Dependent Delay Noise on Covariance Matrix

Let the delay $\tau_{i,obs}$ at a station i be given by:

$$\tau_{i,obs} = \tau_{i,geom} + \tau_{i,mod} + \varepsilon_{i,A} + \varepsilon_{i,B} + \varepsilon_{i,C} + ... \tag{5}$$

$\tau_{i,geom}$ is the geometric delay. $\tau_{i,mod}$ incorporates both calibration and modeling terms. The $\varepsilon_{i,A}$ are station dependent delay error terms. The observational noise $\varepsilon_{ij,obs}(t)$ for baseline ij is:

$$\varepsilon_{ij,obs}(t) = \varepsilon_{ij,meas}(t) + \varepsilon_{ij,A}(t) + \varepsilon_{ij,B}(t) + \varepsilon_{ij,C}(t) + ... \tag{6}$$

where $\varepsilon_{ij,meas}(t)$ is the measurement noise due to the correlation process, and the remaining terms are due to different kinds of station dependent delay error: $\varepsilon_{ij,A}(t) = \varepsilon_{i,A}(t) - \varepsilon_{j,A}(t)$.

The following assumptions simplify the evaluation of the covariance matrix:

1. Different kinds of delay error are uncorrelated: $< \varepsilon_A \varepsilon_B >= 0$ for $A \neq B$.
2. Delay errors at different times are uncorrelated: $< \varepsilon_{ij,A}(t)\varepsilon_{kl,A}(t') >= 0$ for $t \neq t'$.

3. Delay errors at different stations are uncorrelated.

The covariance matrix is $\Omega =< \varepsilon_{obs}^2 >$. By assumption 1, the cross terms vanish, and the covariance matrix is just a sum of terms:

$$\begin{aligned}\Omega &= < \varepsilon_{meas}^2 > + < \varepsilon_A^2 > + < \varepsilon_B^2 > + < \varepsilon_C^2 > ... \\ &= \Omega_{meas} + \Omega_A + \Omega_B + \Omega_C ....\end{aligned}$$

The first term Ω_{meas} is the (diagonal) covariance matrix associated with the measurement process, and the remaining terms are the covariance matrices associated with each type of noise.

Assumption 2 implies that the covariance matrix is block diagonal, with each block being the covariance matrix for a single scan. By assumption 3, cross-terms involving different stations vanish. The diagonal elements for baseline ij are:

$$\Omega_{A,ij,ij}(scan) =< (\varepsilon_{i,A} - \varepsilon_{j,A})^2 >=< \varepsilon_{i,A}^2 + \varepsilon_{j,A}^2 >= \sigma_{i,A}^2 + \sigma_{j,A}^2 \tag{7}$$

i.e., just the sum of the noise terms for each station. The off-diagonal terms of the covariance matrix are non-zero *if, and only if* the baselines have a station in common. In this case we have:

$$\Omega_{A,ij,il}(scan) = -\Omega_{A,ij,li} =< (\varepsilon_{i,A} - \varepsilon_{j,A})(\varepsilon_{i,A} - \varepsilon_{l,A}) >=< \varepsilon_{i,A}^2 >= \sigma_{i,A}^2 \tag{8}$$

Note that both the diagonal and off-diagonal terms depend *only* on the variance of the noise. Hence station dependent delay noise has two effects: 1) The noise level of the observations is increased; and 2) Observations involving a common station at a given time are correlated.

Since the covariance matrix is block diagonal, building up the normal equations given in Eq. (3) is straightforward. This is done on a scan by scan basis: 1) compute the covariance matrix for a given scan; 2) invert it; and 3) compute the contribution of this scan to the normal matrix.

4. Clock Noise and Azimuthal Asymmetry Mismodeling in VLBI

In this section I look at the efffect of incorporating station dependent delay error using two VLBI data sets: 1) CONT05 is close to the current state of the art in geodetic VLBI, and all of the sessions are contiguous in time; 2) The R1 & R4 sessions during 2005 are a relatively good operational network with sessions over a prolonged period of time.

I modified the GSFC *solve* analysis software to take into account the effects of clock-like error and atmospheric azimuthal mismodeling. Clock like delay error can be caused by underparametrizing the clock variation, by errors in the cable calibration, and other sources. I assume that the variance is uniform and time independent:

$$\sigma_{clk}^2 = a_{clk}^2 \tag{9}$$

One source of atmosphere mismodeling is to neglect the effect of turbulence. Assuming a 2/3 power law for spatial fluctuations, the unmodeled azimuthal variance is:

$$\sigma_{az}^2 = \left(a_{az} \times \cot^{2/3}(el)\right)^2 \tag{10}$$

Figure 1 plots the difference in baseline repeatability, as a function of baseline length, between the standard solution and a solution assuming that $a_{az} = 15$ ps at each station. Points above (below) the x-axis are baselines where the scatter in the standard solution is larger (smaller) than in the new solution. For 46 out of 54 baselines, the new solution reduces the scatter and *improves* the VLBI solution. The average improvement is 0.81 mm, or 11.1%. The average χ^2 of the baseline scatter from the standard solution is 2.16, indicating that the formal errors are too optimistic by $\sqrt{2.16} \simeq 1.47$. The average χ^2 from the new solution is 1.08, indicating that the formal errors are too optimistic by a factor of 1.04.

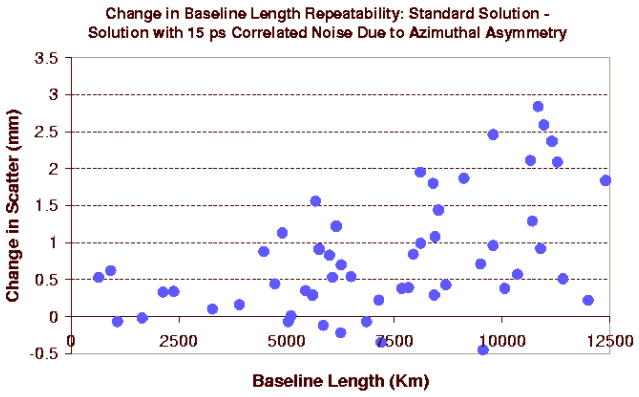

Figure 1. Difference in baseline repeatability for the CONT05 data set between the standard solution and one incorporating 15 ps of noise due to azimuthal asymmetry. Points above (below) the x-axis are baselines where the scatter is reduced for the new (standard) solution.

I ran a series of solutions using different values for a_{clk} and a_{az}. For each solution I considered all baselines with more than 10 observations, found the best fit line through the baseline lengths, and calculated χ^2 per degree of freedom and the WRMS about the best fit line. Table 1 summarizes these results. For each solution, Table 1 displays the WRMS and χ^2 averaged over all baselines. Also displayed is the average change in scatter compared to the standard solution, expressed in millimeters and in per cent, and the number of baselines where the scatter is reduced. Incorporating the effect of clock-like noise makes χ^2 more realistic, i.e., closer to 1, but does not reduce baseline scatter very much. In contrast, including the effect of azimuthal assymetry reduces χ^2 and reduces the baseline scatter: The formal errors are more realistic, and the solution is better. The optimal value for a_{az} is about 15 ps.

Table 1. Effect of clock and atmosphere station dependent delay.

		CONT05					R1s & R4s for 2005				
a_{clk}	a_{az}	Avg	WRMS	Avg. Imp.		#BL	Avg.	WRMS	Avg. Imp.		#BL
ps	ps	χ^2	mm	mm	%	Imp.		mm	mm	%	Imp.
0	0	2.16	7.56	-	-	-	1.94	12.27	-	-	
5	0	1.96	7.52	.04	0.6%	34/54	1.83	12.25	0.02	0.1%	24/51
10	0	1.4	7.51	.05	1.0%	31/54	1.64	12.24	0.02	0.0%	24/51
15	0	1.21	7.54	.02	0.6%	28/54	1.46	12.30	-0.03	-0.6%	23/51
0	5	1.75	7.17	0.39	5.2%	49/54	1.73	12.11	0.16	1.7%	37/51
0	10	1.34	6.87	0.69	9.8%	48/54	1.46	11.99	0.28	2.9%	35/51
0	15	1.08	6.75	0.81	11.1%	46/54	1.25	12.00	0.27	2.8%	32/51
0	20	0.91	6.73	0.72	11.0%	45/54	1.10	12.11	0.17	2.0%	29/51
10	10	1.20	6.99	0.57	8.4%	49/54	1.35	12.06	0.21	2.0%	34/51

One possibility is that the improvement in baseline scatter is due entirely to inflating of the diagonal components of the covariance matrix, i.e., the only important effect of station-dependent noise is to increase the noise of the observations, and the correlation between observations can be ignored. To test this theory I reran some of the above solutions, setting the off-diagonal terms of the covariance matrix to 0. The results are displayed in Table 2. Although the baseline scatter is reduced, the amount of reduction is only half that of using the full covariance matrix, indicating that the correlations are important, and including them improves the solution.

Table 2. Effect of clock and atmosphere station dependent delay (diagonal components only).

		CONT05					R1s&R4s for 2005				
a_{clk}	a_{az}	Avg.	WRMS	Avg. Imp.		#BL	Avg.	WRMS	Avg. Imp.		#BL
ps	ps	χ^2	mm	mm	%	Imp.	χ^2	mm	mm	%	Imp.
0	0	2.16	7.56	-	-	-	1.94	12.27	-	-	
0	5	1.94	7.42	0.14	2.5%	44/54	1.79	12.20	0.08	0.9%	34/51
0	10	1.61	7.28	0.28	5.0%	42/54	1.57	12.15	0.15	1.6%	34/51
0	15	1.36	7.23	0..33	6.2%	40/54	1.38	12.18	0.13	1.5%	32/51

5. Conclusion and Future Work

Including station dependent delay noise has the potential to reduce baseline scatter estimates and result in more realistic formal errors. The effect of including clock-like errors is relatively small. In contrast, including the effect of atmospheric asymmetry results in a dramatic decrease in baseline scatter. This improvement is not due simply to inflating the observational errors, but depends as well on the correlations introduced in the measurement.

Under current investigation are extensions to this work such as: 1) Include other sources of station dependent delay, such as mapping function error. 2) The present work assumed that the variance was station independent. It seems plausible that this would vary from station-to-station. 3) The tests done in the present paper showed impovement based on internal consistency. Another test is to compare VLBI results with those from other techniques, e.g., GPS.

References

[1] Schuh, H., Wilkin, A., Determination of Correlation Coefficients between VLBI-Observables, Proc. of the 7th Working Meeting on European VLBI, Madrid, Spain, CSIC, A.Ruis (ed), p. 79-91, 1989.

[2] Schuh, H., Tesmer V., Considering A Priori Correlations in VLBI Data Analysis, 2000 IVS General Meeting Proceedings, Kotzting, Germany, N. Vandenberg and K. Baver, (ed), p. 237-242, 2001

[3] Tesmer, V., Refinement of the Stochastic VLBI Model: First Results, Proceedings of the 16th Working Meeting on European VLBI, p. 207-218. p. 79-91, 1989.

[4] Tesmer, V., Das stochastische Modell bei der VLBI-Auswertung, PhD thesis, University of Munich, Munich, Germany, 2003.

[5] Tesmer, V., Kutterer, H., An Advanced Stochastic Model for VLBI Observations and its Application to VLBI Data Analysis, 2004 IVS General Meeting Proceedings, Ottawa, Canada, N. Vandenberg and K. Baver, (ed), p. 296-300, 2005

David Gordon et al.: Calc 10 Implementation, IVS 2006 General Meeting Proceedings, p.291–295
http://ivscc.gsfc.nasa.gov/publications/gm2006/gordon

Calc 10 Implementation

David Gordon [1], *Dan MacMillan* [2], *Karen Baver* [1]

[1)] *Raytheon/NASA Goddard Space Flight Center*
[2)] *NVI, Inc./NASA Goddard Space Flight Center*
Contact author: David Gordon, e-mail: dgg@leo.gsfc.nasa.gov

Abstract

Calc 10 has been updated to comply with the IAU 2000 Resolutions and the IERS Conventions (2003). Comparisons with Calc 9 of the solved-for EOP parameters and the TRF are discussed.

1. Introduction

Calc version 10 has been updated to comply with the IAU 2000 Resolutions and the IERS Conventions (2003). Among other changes, Calc now uses the "non-rotating origin", or CIO-based (Celestial Intermediate Origin) method to compute the transformation from the terrestrial reference frame to the celestial reference frame (TRF-to-CRF). Much of the new code was taken from the IERS Conventions web site and modified to include time derivatives and various partial derivatives. [These are SOFA-based routines (the IAU's 'Standards of Fundamental Astronomy' software). See http://www.iau-sofa.rl.ac.uk.]

2. Summary of Changes in Calc 10

2.1. Nutation/Precession

Calc 10 makes two nutation/precession computations. First, X and Y (coordinates of the Celestial Intermediate Pole (CIP) in the Geocentric Celestial Reference System (GCRS)), and s (which locates the CIO on the equator of the CIP) are computed (using a modified version of subroutine XYS2000A). Second, classical nutation offsets ($\Delta\psi$, $\Delta\epsilon$) are computed based on the IAU2000A nutation model (using a modified version of subroutine NU2000A). Partial derivatives of the delays and rates with respect to X and Y are computed from the CIO-based formulation, and with respect to the classical nutation offsets $\Delta\psi$ and $\Delta\epsilon$ from the classical formulation. This allows solving for either observed corrections to X and Y or classical nutation corrections with respect to IAU2000A.

2.2. Polar Motion

The polar motion rotation matrix now has a small rotation about the Z-axis through the angle -s', where s' locates the Terrestrial Ephemeris Origin (TEO) on the equator of the CIP. Angle s' is approximated as linear with time (-47*Cent μarcsec, where Cent is the epoch in fractional centuries from 2000.0).

Short period ocean tide and nutation contributions to polar motion are now computed, as directed by the 2003 Conventions. Short period nutation contributions are computed using the

terms of Table 5.1, and short period ocean tide contributions are computed using Richard Eanes' Ortho_EOP subroutine. They should be added after interpolation of the X-pole and Y-pole tabular points. They will be optional in Calc/Solve (not included in the default delays and rates), available via the Lcodes 'WOBNUTAT' and 'WOBORTHO', which can be applied using the Solve CORFXX file. If used, the current Solve high frequency EOP model, jmg96.hf, should be turned off.

2.3. UT1

UT1 is now used to compute an Earth rotation angle for the CIO-based transformations. And the computation of Greenwich Sidereal Time for the classical transformations was modified. The complementary terms in the equation of the equinoxes are more complicated and are computed using a modified form of subroutine EECT2000. Also, some structural changes were made in the UT1 interpolation. Smoothing of the tabular UT1 points is no longer done, and a 1.0 day interval EOP series must be used (5 day intervals no longer accepted). Subroutine Ortho_EOP also computes short period UT1 corrections for ocean tide effects. They are stored as Lcode 'UT1ORTHO' and can be applied using the Solve CORFXX file.

2.4. Fundamental Arguments

The fundamental arguments were modified to match the IERS Conventions (2003) and expanded to include the 9 planetary terms, for the CIO-based computations. Calc 10 has two other sets of fundamental arguments - for the IAU2000A nutation model and for the IAU1980 (Wahr) nutation model, each with small differences in some of the components. As a further complication, it seems there have been two different sets of fundamental arguments used in the past for computing Wahr nutations. One is the original set used with the 1976/1980 IAU Precession/Nutation models (used in Calc 8 and earlier). The second is a set specified in the IERS Conventions (1996) for use with both the IERS 1996 Nutation model (Herring code) and the 1976/1980 IAU Precession/Nutation (Wahr) model (used in Calc 9). It is not clear which set should really be used, but after some discussions here and with other colleagues, we decided to return to the original set.

2.5. Planetary Ephemeris

The JPL DE/LE405 ephemeris is now used. Two binary versions will be distributed with Calc 10. One is a 100-year file (1950-2050, 9.3 Mbytes) for use on Unix (Big Endian) systems. The other is an 80-year file (1960-2040, 7.5 Mbytes) for PC Linux (Little Endian) systems.

2.6. Solid Earth Tide

Some small changes were made to match the new Conventions, as described in Chapter 7. Step 1 is unchanged from Calc 9, except there is now no elastic/anelastic option. Step 2 uses different tables and additional terms. Also, the partial derivatives defined by John Gipson for Calc 9 were never used, so they were removed.

2.7. Pole Tide

Mean (secular) pole offsets (linear with time) are subtracted from the polar motion values, then these modified X-pole and Y-pole values are used to compute the pole tide corrections. The same

was done in Calc 9, but with slightly different linear formulas. Also as in Calc 9, we compute a delay and rate contribution ('PTOLDCON') that will remove this step. Adding the 'PTOLDCON' values to the delays and rates will be the same as computing the pole tide with X-pole and Y-pole values uncorrected for secular polar motion.

2.8. Antenna Fixed Axis Tilts and Axis Offsets

Calc 10 was updated to read an antenna fixed-axis tilt file. This file has a large set of tilts (E-W and N-S) for Pietown (1989-2004), and single tilts for the other 9 VLBA antennas (only SC-VLBA's is significant though). If anyone knows of other antennas that should be included here, please let me know. Calc 10 uses these tilts in the axis offset computations. For Pietown, the current tilt ($\sim$4 arc-minutes) can make a delay difference of $\pm$8 psec maximum.

A small error was found in the axis offset computations. Apparently it was never quite correct. A small atmosphere term was incorrectly modified several versions ago, when it should have been replaced with a small relativity correction. It has finally been corrected. Very little change should be expected though, except at a few stations with large axis offsets.

3. Comparison of Calc 10 and Calc 9

The TRF-to-CRF transformation in Calc has changed for the first time in its $\sim$30 year history, so a detailed study of its effect on the data solutions was made. We made matching Calc 9 and 10 Solve/Globl solutions for 3785 VLBI sessions from 1979.6 through 2005.8, to compare differences in the solved-for parameters. To limit the differences as much as possible, the same apriori's (site positions, source positions, EOP's, and ocean loading coefficients) were used. Figures 1-3 and 5-6 show the unmodified differences (Calc 10 minus Calc 9) between the solved-for X-pole, Y-pole, UT1, and IAU1980 nutation. The data before 1984 is considerably noisier and has been excluded.

3.1. X-pole, Y-pole Differences

The polar motion differences of Figures 1 and 2 are small compared to their formal errors (typically $\sim$35-100 μas), but some systematic effects are seen. X-pole has an $\sim$13 μas offset. The reason has not yet been determined, but may be related to a reversal in the order of rotations in the polar motion matrix, or in the application of the pole tide correction.

3.2. UT1 Differences

The UT1 differences of Figure 3 show a semi-annual cycling, modulated in amplitude with a period of approximately half the lunar cycle. This is due to the effect of the quantity s in the CIO-based transformations. It can be seen more clearly in the equation of the equinoxes complementary terms in the equivalent equinox-based transformations. If we compute and remove the differences between the complementary terms used in Calc 10 and Calc 9, we get the 'corrected' differences shown in Figure 4. Most of the systematic effects are gone, but a small slope of $\sim$-3.1 μsec/century, or $\sim$-47 μarcsec/century remains. This slope is apparently due to the Z-axis rotation in the polar motion matrix of *-s'*, or +47*Cent μarcsec.

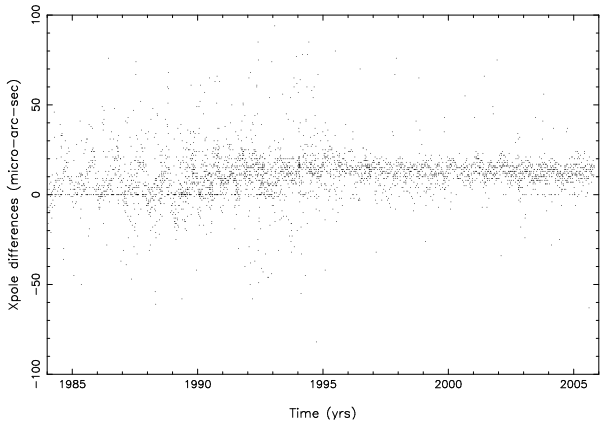

Figure 1. X-pole differences (μasec).

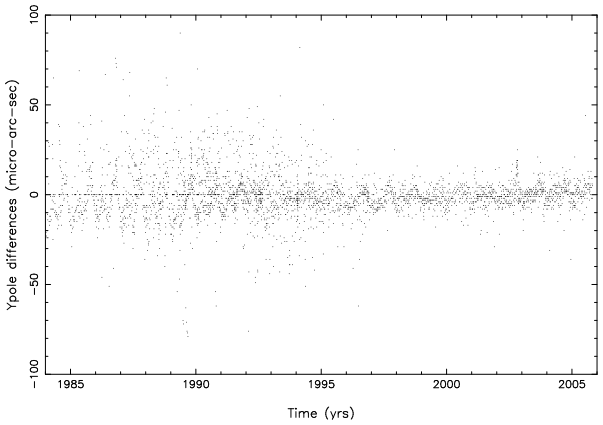

Figure 2. Y-pole differences (μasec).

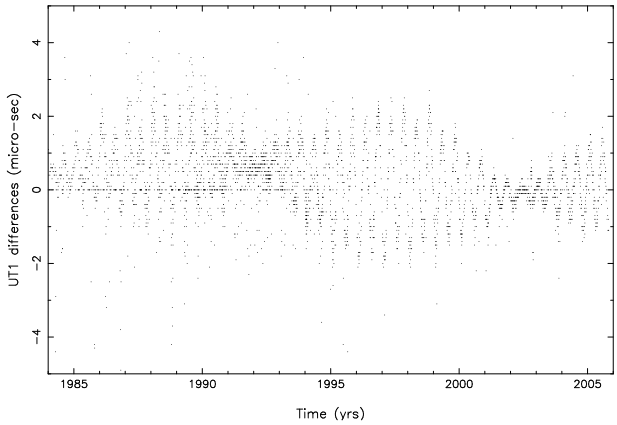

Figure 3. UT1 differences (μsec).

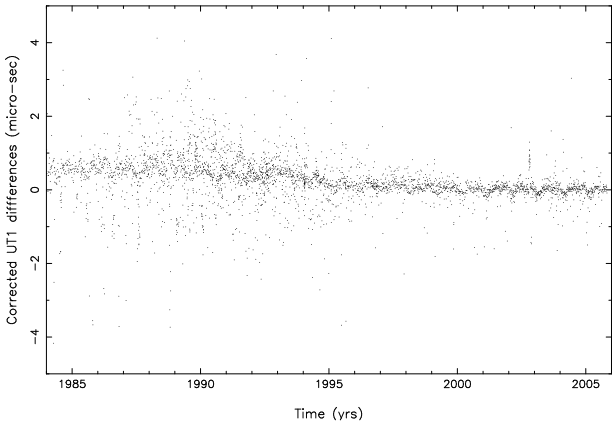

Figure 4. 'Corrected' UT1 differences (μsec).

3.3. Nutation Differences

The IAU1980 (Wahr) nutation differences in Figures 5 and 6 also show semi-annual cycles, with somewhat non-linear long term drifts. As mentioned earlier, the fundamental arguments are slightly different for Calc 9 and 10. If we compute and remove the effect of different fundamental arguments, we get Figures 7 and 8. The cycling is gone, but nearly linear drifts remain, with slopes of $\sim$-.45 and $\sim$+.50 m-arc-sec/century (1984-2005.8) for $\Delta\psi$ and $\Delta\epsilon$. In Solve, the IUA2000A adjustments were converted to the IAU1976/1980 precession/nutation (Wahr) frame by adding the following terms for the frame offset and the difference in precession constants:

$\Delta\psi$: -299.65*Cent - 41.775 (m-arc-sec)
$\Delta\epsilon$: -25.24*Cent - 6.8192 (m-arc-sec)

N. Capitaine (private communication) has pointed out that some small slopes should remain, due to differences in the reference frame treatment of bias and precession, and to the inclusion of a R.A. bias in the new transformations. Theoretically, these should produce slopes of -.418 and +.514 m-arc-sec/century, which is close to what we see. Eventually Solve will directly estimate ΔX and ΔY for reporting to the IERS, so this conversion should not be necessary.

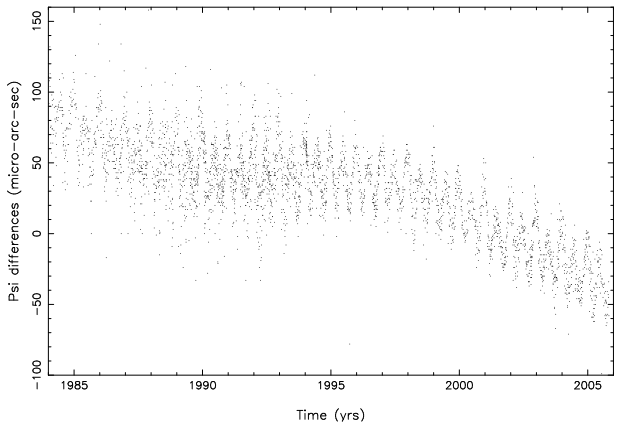

Figure 5. $\Delta\psi$ differences (μasec).

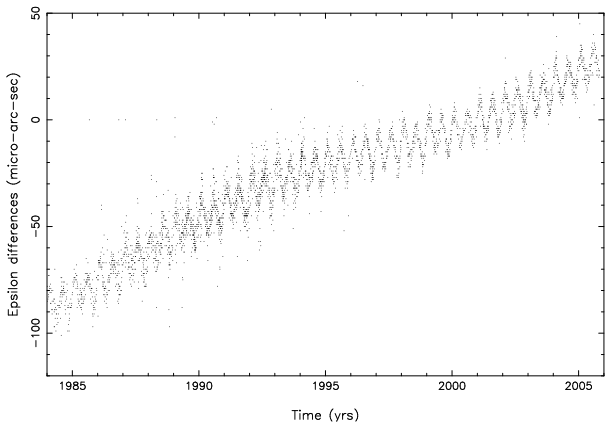

Figure 6. $\Delta\epsilon$ differences (μasec).

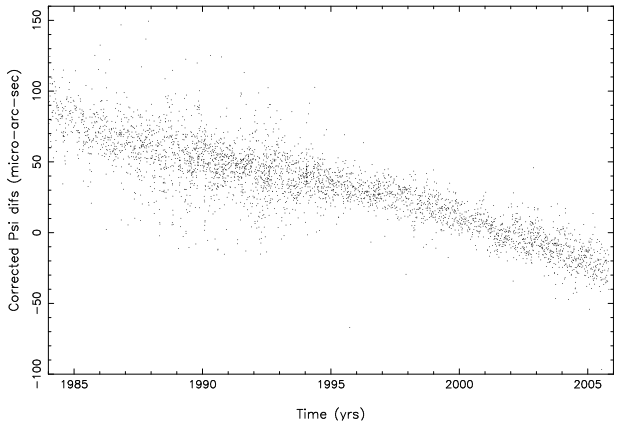

Figure 7. 'Corrected' $\Delta\psi$ differences (μasec).

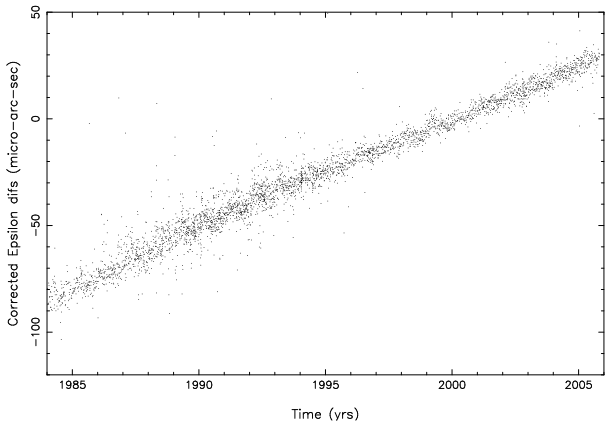

Figure 8. 'Corrected' $\Delta\epsilon$ differences (μasec).

3.4. Terrestrial Reference Frame and Axis Offset Differences

We solved for a simple translation/rotation between the terrestrial reference frames of the Calc 10 and Calc 9 solutions. We get a rotation of -3.2, -2.3, and +1.5 μasec; and a translation of 0.041, 0.075, and -0.036 mm in X, Y, and Z, respectively, with no significant scale factor (-0.0166 $\pm$.0152 ppb). Velocity differences show a rotation of -.13, -.31, and -.15 μasec/yr. These differences are essentially insignificant. The Calc 10 vs. Calc 9 solved-for axis offsets were also compared. In all cases the formal errors were the same or slightly smaller in the Calc 10 solution. Differences of $\sim$.1% or less are seen for the larger axis offsets.

References

[1] McCarthy, D. D. (ed.), IERS Technical Note 21, IERS Conventions (1996), 1996.

[2] McCarthy, D. D., Petit, G. (ed.), IERS Technical Note 32, IERS Conventions (2003), 2003.

Sebastien B. Lambert: Baseline and Site Repeatability in the IVS Rapid Network, IVS 2006 General Meeting Proceedings, p.296–299
http://ivscc.gsfc.nasa.gov/publications/gm2006/lambert2

Baseline and Site Repeatability in the IVS Rapid Network

Sebastien B. Lambert

Royal Observatory of Belgium (formerly at NVI, Inc./US Naval Observatory)
e-mail: s.lambert@oma.be

Abstract

Lengths of 88 baselines ranging from 1,000 to 12,400 km and coordinates of 15 sites participating in the IVS rapid 24-hour networks R1 and R4 are studied. The wrms of the baseline lengths increases by 1.57 mm per thousand kilometers, which can be interpreted as a loss of accuracy when the VLBI networks uses longer baselines. Two baselines, linking the TIGO antenna at Concepción (Chile) to Fortaleza (Brazil) and to Algonquin Park (Ontario), have wrms values significantly above this level. An analysis of the sensitivity to the tropospheric gradients reveals that their determination degrades the determination of baseline lengths below 8,000 km by about 5 mm but may improve the determination of longer baseline lengths by up to 1 cm. Considering the site coordinates, the estimation of the gradients improves the determination, except for TIGO whose Up and North components are significantly degraded.

1. Description of the Solution

Local site positions and baseline components are derived from R1 and R4 experiments between January 1st, 2002 and June 30th, 2005 (358 experiments including the CONT02 campaign which has an R1-like geometry). Algonquin Park (Ontario) is adopted as a priori station with fixed coordinates and velocity in ITRF2000. Polar motion and UT1 − UTC are not estimated; instead a priori values are taken from IERS Bulletin A ([1]). The no-net-rotation is applied to the 212 ICRF defining sources. Other radio sources positions are estimated as arc parameters along with site coordinates, nutation offsets and length-of-day. Ocean tidal and atmospheric pressure loading are not applied. Niell's mapping functions ([3]) are used for the atmospheric dry and wet components. The computation was done at USNO using the CALC/SOLVE geodetic VLBI analysis software package developed at NASA/GSFC. To eliminate edge effects caused by the arbitrary beginning of the two rapid turnaround session series and the influence of the coseismic displacement due to the 2002 Denali fault earthquake near Fairbanks ([2]), which affected significantly the position of the GILCREEK antenna, the time series analysis of the baseline lengths and site positions is started in January 2003.

2. Baseline Lengths

Figure 1 plots the baseline length repeatability (weighted root mean square after having removed a trend and an annual signal) versus the baseline length. The wrms points are contained in a cone centered at the origin with an aperture of about 20 degrees. A linear regression line can be fit to model the wrms as a function of baseline length. The slope is 1.57 ± 0.03 mm per thousand kilometers. This value can be interpreted as the degradation of the accuracy of the VLBI network when long baselines are used instead of short ones. The equivalent geometric time delay

is 5.26 ± 0.10 ps per thousand kilometers. Note that this value has to be compared to the mean postfit residual rms of the solution of 20.37 ps.

Two baselines linking TIGOCONC (Concepción, Chile) to FORTALEZA (Brazil) and to ALGOPARK (Canada) appear significantly above the linear regression line. Their lengths are about 5,000 km and 8,000 km respectively. Seven other baselines involving TIGOCONC in this study do not present such a significant departure, even for baselines longer than these two. I would like to point out that (i) the two baselines cited above are used in more that 60 sessions and are therefore not affected by a lack of data, and (ii) that Figure 1 reflects the effect of the current network and analysis strategy for the baseline length determination. Therefore, the results concerning a site or a set of sites cannot be related only to the site or to the set of sites, but should be considered with great care as they potentially include other sources of error due to observational and/or analysis strategies.

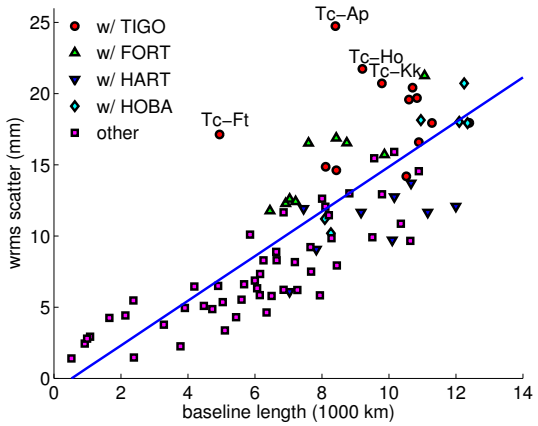

Figure 1. Baseline length repeatability versus baseline length. Ap: ALGOPARK, Ft: FORTLEZA, Ho: HOBART, Kk: KOKEE, Tc: TIGOCONC.

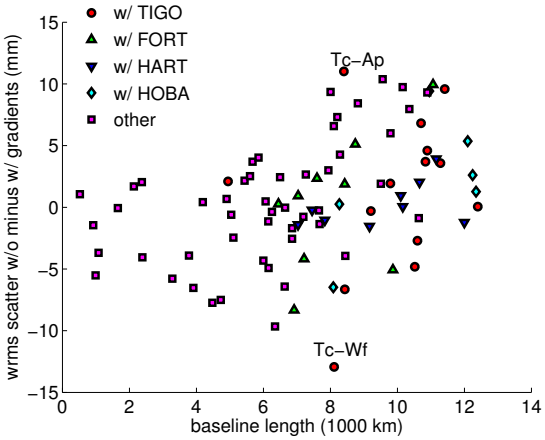

Figure 2. Difference of baseline length repeatability between unmodeled and modeled troposphere gradient solutions. Ap: ALGOPARK, Ft: FORTLEZA, Ho: HOBART, Kk: KOKEE, Tc: TIGOCONC, Wf: WESTFORD.

Figure 2 displays the variation of the wrms when the tropospheric gradients are or are not estimated as a function of baseline length. A positive value indicates that estimating the gradients improves the results. The mean effect of the tropospheric gradients appears to stay around zero with a deviation of ± 1 cm, implying that omitting the gradients causes an underestimation or overestimation of the baseline length by less than 1 cm (4.8 ps). For baseline lengths below 8,000 km, the mean variation is negative: the gradients degrade the estimates of the length. In this range, there appears to be no clear link between the variation and the baseline length, showing that the sensitivity to the atmosphere is site-dependent (as opposed to baseline-dependent such as the wrms itself, as noted above). However, for longer baselines, it appears that estimating the gradients can improve the baseline length determination by up to 1 cm. Note that the baseline TIGOCONC-ALGOPARK is significantly improved, whereas TIGOCONC-WESTFORD (MA, USA) is significantly degraded, although they are very close.

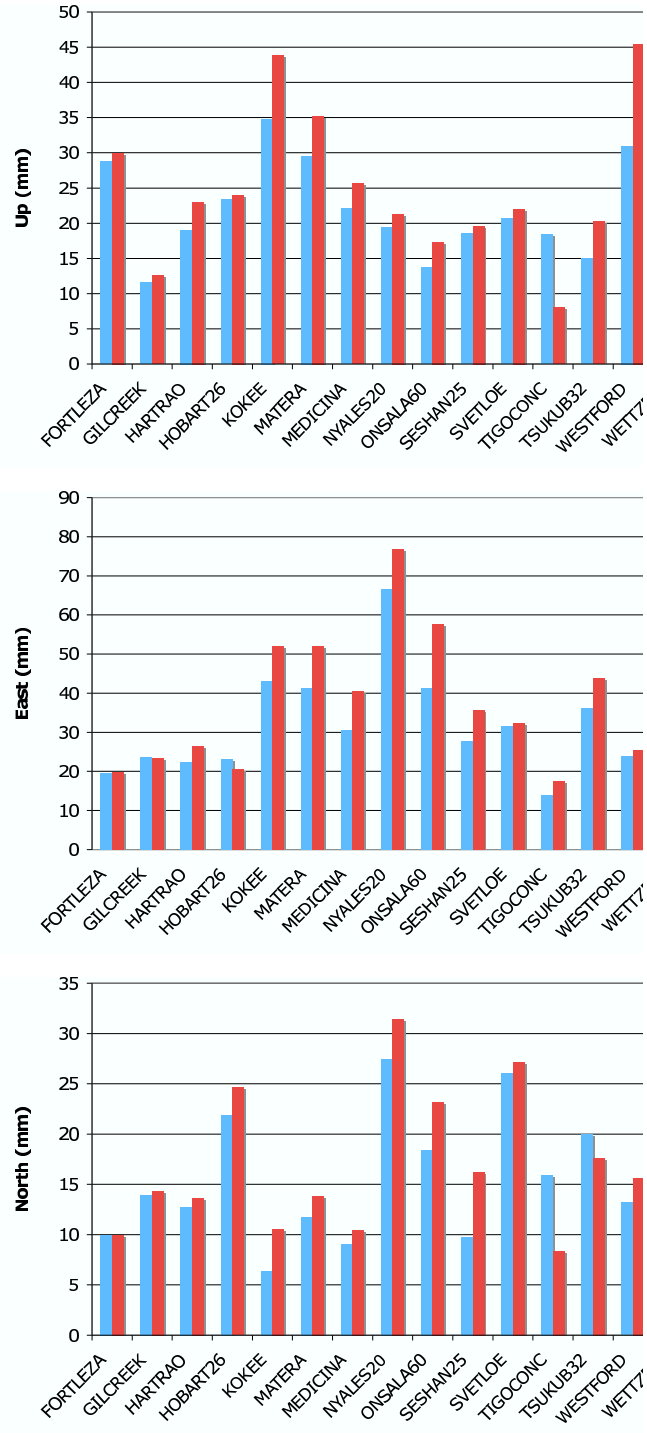

Figure 3. Wrms scatter of the Up, East and North components of all sites involved in the R1 and R4 networks between 2002 and 2005.5. Left bar: wrms when the gradients are estimated. Right bar: wrms when the gradients are not estimated.

3. Site Positions

Figure 3 shows the wrms scatter of the site components with and without estimating the troposphere gradients. The wrms is generally improved (sometimes insignificantly) by estimating the gradients (see for instance KOKEE, ONSALA, WESTFORD, WETTZELL). The case of TIGOCONC is interesting because the wrms is significantly degraded on vertical (Up) and North components when the gradients are estimated. However, the East component is not very sensitive. As can be seen in meteorological datasets (e.g., NCEP/NCAR Reanalysis project) the coastal site of TIGO presents a strong departure from azimuthal symmetry in air temperature and water vapor quantity in the atmosphere, mainly due to local geography (between Pacific coast and Andes mountains), strongly perturbing the refractivity. It results that the East component of the troposphere gradients (combination of temperature and humidity contributions) is much stronger than the North component. A difficulty in estimating the gradients with the current models could partly explain these results.

References

[1] IERS 2005, Bulletins maintained by the IERS Rapid Service/Prediction Center at USNO. Available on SOLVE erp format at http://gemini.gsfc.nasa.gov/apriori_files/usno_finals.erp.

[2] MacMillan, D.S., & Cohen, S. 2004, Postseismic transient after the 2002 Denali fault earthquake from VLBI measurement at Fairbanks, In: N. R. Vandenberg and K. D. Baver (Eds.): International VLBI Service for Geodesy and Astrometry 2004 General Meeting Proceedings, NASA/CP-2004-212255.

[3] Niell, A.E. 1996, Global mapping functions for the atmosphere delay at radio wavelengths, J. Geophys. Res., 101, 3227.

Joerg Wresnik et al.: Thermal Deformation of Radio Telescopes Onsala and Wettzell, IVS 2006 General Meeting Proceedings, p.300–303
http://ivscc.gsfc.nasa.gov/publications/gm2006/wresnik2

Thermal Deformation of Radio Telescopes Onsala and Wettzell

Joerg Wresnik [1], *Johannes Boehm* [1], *Rüdiger Haas* [2], *Harald Schuh* [1]

[1)] *Institute of Geodesy and Geophysics (IGG), Vienna University of Technology, Austria*
[2)] *Onsala Space Observatory (OSO), Chalmers University of Technology, Sweden*
Contact author: Joerg Wresnik, e-mail: wresnik@mars.hg.tuwien.ac.at

Abstract

Geodetic VLBI is one of the major space geodetic techniques that contributes to the International Terrestrial Reference Frame (ITRF). Errors due to atmospheric propagation effects, loading phenomena and technical reasons have been minimized during the last years. Today the accuracy of geodetic VLBI results is at the sub-cm level. For further improvements the thermal deformations of the radio telescopes have to be taken into account in the analysis of geodetic VLBI data. Thermal deformation effects typically contain seasonal and daily signatures. The annual amplitudes can reach several millimeters in particular for the vertical position of the antenna reference point. The magnitude depends on the design of the antenna structure, the material, and on environmental influences. Two radio telescopes, Onsala (Sweden) and Wettzell (Germany), are equipped with measurement systems that are based on invar rods or invar wires and provide direct observations of the vertical variation of the telescope reference points. Based on these measurements we developed models that can be used to account for thermal deformations as a function of environmental temperature. Direct observations of thermal deformation of the radio telescopes at Onsala and Wettzell are presented and the corresponding models for thermal deformation are discussed.

1. Measurement Facilities of the Onsala Antenna

The measuring system of the 20 m telescope at Onsala station has been installed in 1996 and was documented under the project title "The Pisa Project" (Johansson et al., 1996 [1]). It is equipped with 16 temperature sensors in the construction of the tower, two temperature sensors recording the air temperature inside the radome and two temperature sensors recording the air temperature inside the tower. The vertical deformation is measured with an invar rod and an inductive position sensor. Figure 1 (left) shows the high correlation (ρ=0.999) between the mean concrete temperature of the telescope tower and the measured vertical deformation.

2. Measurement Facilities of the Wettzell Antenna

In Wettzell, temperature is recorded at three locations inside the telescope tower. One of the sensors gives the concrete temperature, and an invar wire measurement system provides the vertical deformation. The invar measurement system uses an invar wire that is attached to a 1 kg weight. The weight of the anchor was doubled on February 28, 2000. The sampling rate for recording the data is 15 minutes (Zernecke, 1999 [4]). Figure 1 (right) shows the correlation (ρ=0.973) between the measured temperature of the antenna tower and the measured vertical deformation which is almost as high as for Onsala.

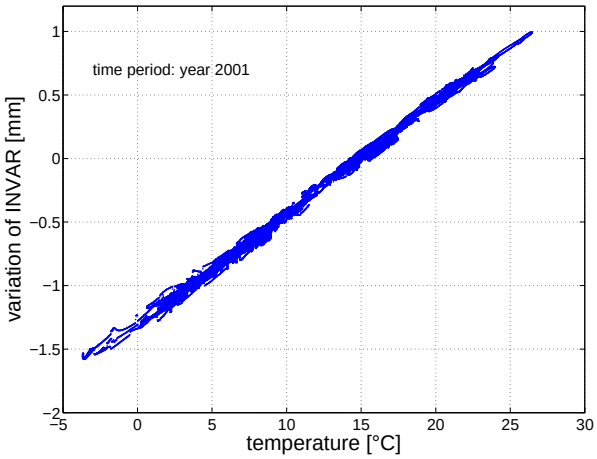

ONSALA

Measured vertical height changes of the tower of the Onsala 20 m telescope versus mean temperature of all 16 temperature sensors in the antenna tower for 2001.

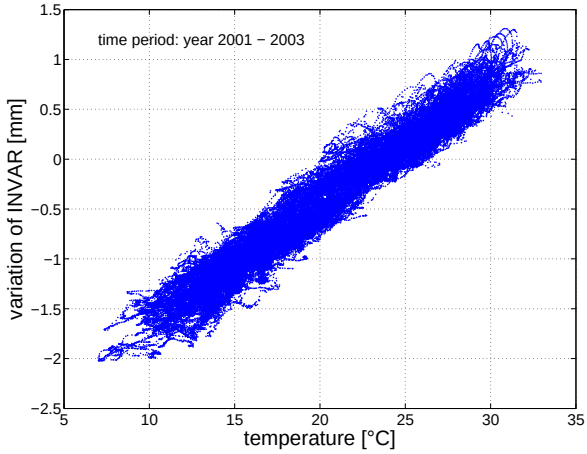

WETTZELL

Measured vertical height changes of the Wettzell 20 m telescope versus temperature values of the sensor T2 for the period 2001 to 2003.

Figure 1. Correlation between measured mean antenna tower temperature and hight deformation for Onsala (left) and Wettzell (right).

3. Model for Correction

Figure 1 shows a very high correlation between the temperature of the antenna structure and its vertical deformation. Thus, if we know the temperature of the construction we can easily compute a correction, *corr* [mm], due to vertical thermal deformation by taking the expansion coefficient of the material and the dimensions of the antenna (Equation 1), where γ_f and γ_a are the expansion coefficients of concrete ($1.0{\cdot}10^{-5}$ 1/°C) and steel ($1.2{\cdot}10^{-5}$ 1/°C), h_f [m] is the height of tower, h_p [m] the height of the antenna part, T_i [°C] the tower temperature, and T_0 [°C] the reference temperature.

$$corr = [\gamma_f \cdot (T_i - T_0) \cdot h_f + \gamma_a \cdot (T_i - T_0) \cdot h_p] \cdot 1000 \qquad (1)$$

Since at most VLBI stations there are no temperature data available for the antenna structures, but sensors exist that record the air temperature, the idea of modeling the antenna temperatures as a function of the air temperatures is rather obvious. The model must take into account that the deformation caused by variation of the air temperature has a time lag, and that the antenna material stores temperature for a certain period of time. The time lag amounts to about 6 hours with concrete and to about 2 hours with steel constructions (Nothnagel et al., 1995 [2]). The model should contain annual and diurnal temperature variations.

The model for the Onsala antenna was realized by a digital filter technique. The model temperature T_m at a time i is calculated as weighted sum of the recent air temperatures, with temperatures from earlier time periods getting lower weights than temperatures close to time epoch i. This weighting is done exponentially. The sum is normalized by dividing it by the sum of the weights. This is done for a short and a long period term. To get the very short period temperature

variation, too, the short period term uses a temperature interval of 12 hours and the long period term uses an interval of three days before epoch i. The weighting factors q which are different for short and long period effects are adjusted empirically. The factors f and the *offset* are calculated by least-squares adjustment.

$$T_{mi} = f_{short} \cdot \frac{\sum_{j=i-z_{short}}^{i} T_{Aj} \cdot q_{short}^{(z_{short}-(i-j)\cdot d)}}{\sum_{j=i-z_{short}}^{i} q_{short}^{(z_{short}-(i-j)\cdot d)}} + f_{long} \cdot \frac{\sum_{j=i-z_{long}}^{i} T_{Aj} \cdot q_{long}^{(z_{long}-(i-j)\cdot d)}}{\sum_{j=i-z_{long}}^{i} q_{long}^{(z_{long}-(i-j)\cdot d)}} + offset \tag{2}$$

The parameters of the model are T_{mi}, and T_{Aj} which represent the modeled telescope temperature at epoch i and the observed air temperature at epoch j, the sampling rate d (e.g. 5 min), the coefficients q_{short} and q_{long} for long period and short period variations of the outside temperature, the weight factors f_{short} and f_{long} for the short and long period terms, and finally z_{short} and z_{long} which express memory effect for 12 hours and 3 days, respectively (Equation 2). The parameters of this model were determined for the Onsala telescope by least-squares adjustment based on the time series of outside air temperature and temperature of the telescope structure. All details of this modeling approach are described in Wresnik et al. (2005)[3].

Table 1. Parameters for the filter model and standard deviations

Parameter	Onsala	Wettzell
q_{short}	0.999	0.99999
q_{long}	0.99999999	0.9999999
f_{short}	0.19316	0.28161
f_{long}	0.72798	0.44132
$offset$	4.42°C	13.62°C
rms temperature	0.82°C	1.42°C
rms deformation	0.10 mm	0.13 mm

4. Conclusions

The use of highly precise terrestrial measurement facilities for the vertical deformation (invar rod or invar wire) shows a very high correlation between the measured temperature of the antenna structure and the vertical deformation. Thus, the vertical thermal deformation of the VLBI antenna can be modeled very well if the antenna temperature is precisely known and added to the logfile. The presented model contains the tower temperature which can be approximated by the air temperature that is available at most VLBI stations. For the Onsala antenna we are able to model the tower temperature with an rms of 0.82°C and for the calculated vertical deformation we achieve an rms of 0.10 mm. The same strategy was used to design a model for the Wettzell antenna. The results for this antenna during the years 2001 to 2003 give an rms of 1.42°C for the

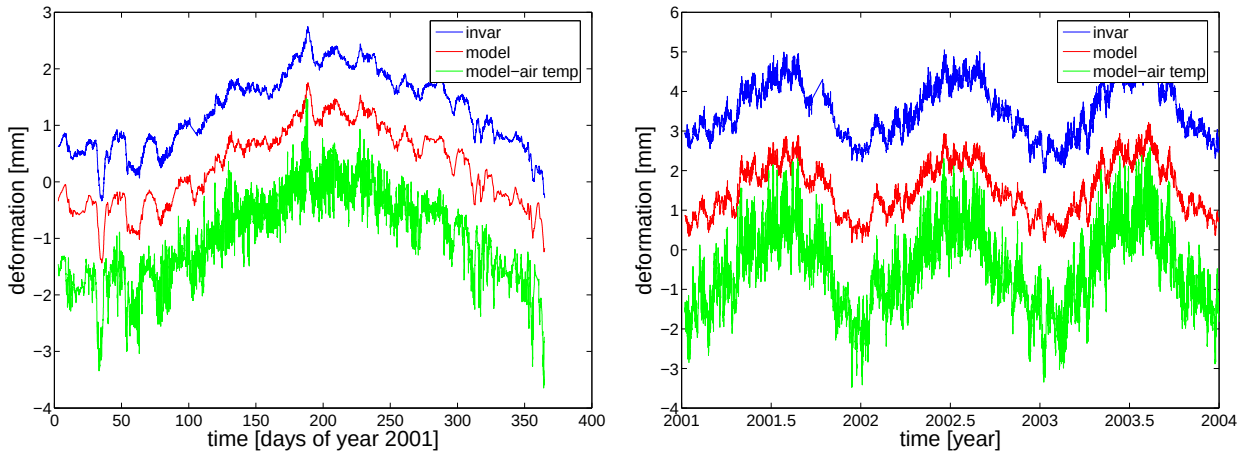

Figure 2. Measured vertical deformation (upper curve) and the calculated antenna deformation using the modeled temperature (central curve) and finally using the measured air temperature (lower curve), which is stored in the VLBI logfiles (left for the Onsala antenna and right for the Wettzell antenna). The curves are plotted with an offset of 1 mm for Onsala and 2 mm for Wettzell for better illustration.

temperature and an rms of 0.13 mm for the vertical deformation.

References

[1] Johansson, L.A., F. Stodne and S. Wolf, The Pisa Project, Variations in the height of the foundation of the 20 meter radio telescope, Research Report No 178, 1996.

[2] Nothnagel, A., M. Pilhatsch and R. Haas, Investigations of Thermal Height Changes of Geodetic VLBI Radio Telescopes, Proceedings of the 10th Working Meeting on European VLBI for Geodesy and Astrometry, 121-133, edited by R. Lanotte and G. Bianco, Matera, 1995.

[3] Wresnik, J., R. Haas, J. Boehm and H. Schuh, Thermal deformation of VLBI antennas, Proceedings of the 17th Working Meeting on European VLBI for Geodesy and Astrometry, 45-50, edited by M. Vennebusch and A. Nothnagel, April 21-23, Noto, 2005.

[4] Zernecke, R., Seasonal Variations in Height demonstrated at the Radiotelescope Reference Point, 13th Working Meeting on European VLBI for Geodesy and Astronomy, 15-18, edited by W. Schlueter and H. Hase, Viechtach, 1999.

Session 6

Results and Geodetic/Geophysical/Astrometric Interpretation

Edward Fomalont: VLBA Phase Referencing for Astrometric Use, IVS 2006 General Meeting Proceedings, p.307–315
http://ivscc.gsfc.nasa.gov/publications/gm2006/fomalont

VLBA Phase Referencing for Astrometric Use

Edward Fomalont

National Radio Astronomy Observatory
e-mail: efomalon@nrao.edu

Abstract

The differences in the type of VLBI observations used by radio astronomers to study the structure and motion of radio sources and that associated with IVS and ICRF-based observations, are discussed. An example of a VLBA phase reference observation to determine the gravitional deflection of the sun demonstrates that relative astrometric precision of 0.02 mas can be obtained. The changing structure of virtually all radio sources is now affecting the accuracy of both types of observations and a method to alleviate this problem is demonstrated by determining the position of the radio core very accurately. A scheme is outlined for which the accurate relative positions from phase referencing might be extended to the entire sky.

1. Introduction

The observational technique of phase referencing alternates short scans of a calibrator, a compact radio source, with a target in order to determine the *relative* position between the calibrator and target, and to determine the angular structure of the target [1]. These results are obtained with Fourier-transform techniques of the phase delay, and it is a coherent process, meaning that the target can be extremely faint, but signal-to-noise (SNR) can be built up with observing time. The image fidelity is about 50:1 (this does not include strong sources for which self-calibration techniques give $> 1000:1$ SNR) and the relative positional accuracy is often 0.05 mas or better at 8 GHz with an array like the VLBA.

In contrast, the IVS takes a more global view of astrometry. Since quasars are extremely distant, they define a quasi-inertial reference frame much more accurately than stars. But, in order to determine a catalog of quasar positions, the location and space motion of the radio telescopes must also be obtained; hence, this requires the measurement of the earth orientation and rotation, the dynamics of many solar system objects, and the crustal perturbations of the earth's surface. This requires observations over 24-hours of many radio sources and relatively fast cycling around the sky to determine the variable tropospheric refraction [2]. Another major difference with phase referencing is that the main observable is not the phase, but the change of phase with frequency, or the group delay, since the residual (observed - model) phase delay is often in error by more than one revolution. Hence IVS observations span wide-bandwidths in order to measure accurate group delays. This difference in observing technique has perhaps separated the two communities more than is necessary, even though there are some common problems that each need to address to increase the position accuracies.

After an example of a phase-reference experiment using the VLBA in §2, the problems associated with quasar structure and changes are illustrated in §3. This 'jitter' of the quasar emission is becoming one of the sources of errors in obtaining both accurate relative positions and absolute positions. A phase-reference observing scheme that can bridge the high accuracy in obtaining

relative positions to encompass the whole sky, is outlined in §4. Observations are underway with the VLBA to determine if this approach is a feasible method for increasing the accuracy of the ICRF.

2. A Phase Referencing Example

About half of the present VLBA proposals use phase referencing, and some examples of the impressive astrometric and astrophysical results are: the determination of the motion of the galactic center [3]; the determination of the Hubble constant by measuring the relative motion of two mega-masers in M33 [4]; the gravitational deflection of radio waves by Jupiter [5]; the complex evolution of x-ray binaries [6]; the space motion and parallax of pulsars [7].

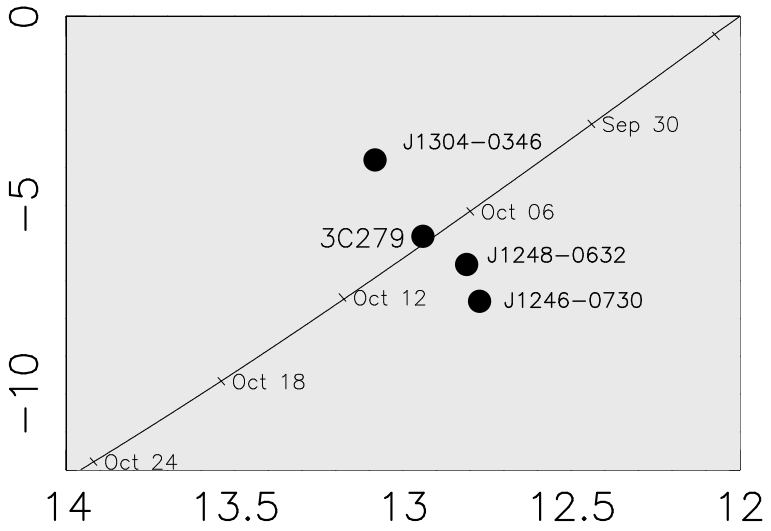

Figure 1. **The Sun-Source Configuration for the October 2005 Solar Bending:** The location of the four radio sources and the motion of the sun during the experiment are shown. Observations were made on October 1, 5, 6, 7, 9, 10, 11 and 18 between UT 17h and 23h. The expected deflection is 1.75″ at the solar limb (16′ from the center of the sun) and decreases inversely proportional to the sun-source angular distance. At a sun-source separation of 2°, the deflection is 230 mas and can be measured to an accuracy of less than 1 part in 1000.

We will illustrate VLBA relative astrometry using a classic deflection experiment in October 2005 when the radio source 3C279 passed near and behind the sun [8]. The configuration of 3C279 and three calibrator sources and the sun during October 2005 are shown in Fig. 1. In order to measure the changing relative positions among the sources, the experimental procedure cycled one-min scans among the four radio sources for six hours on each day, and on eight observing days between October 1 and October 18 to measure the relative positions among the sources. The General Relativistic bending parameter γ is 1.0 and predicts a deflection of a radio source at the limb of the sun of 1.75″. Deviations from $\gamma = 1.0$ are possible with non-Einstein theories and from some large-scale cosmological anisotropies [9]. Because the solar coronal produces a frequency-

dependent deflection of the radio waves (the gravitational deflection is frequency independent), the experiment alternated every twenty minutes among three frequencies, 14, 23 and 43 GHz, in order to remove this frequency-dependent ionospheric component.

The general reduction steps are: First, the most accurate apriori astrometric and geodetic parameters are used during the correlation process for the determination of the model delays using a recent Calc version [10], and updates to the measured earth-orientation and rotation are added off-line. Next, from measurements of the group delay using two 30-min bursts of observations of calibrators over the sky, in an identical manner to IVS observations, a better tropospheric zenith-path delay is determined at the beginning and at the end of the observations for each day [11]. The resultant phase delays among the sources then are sufficiently stable for additional analysis.

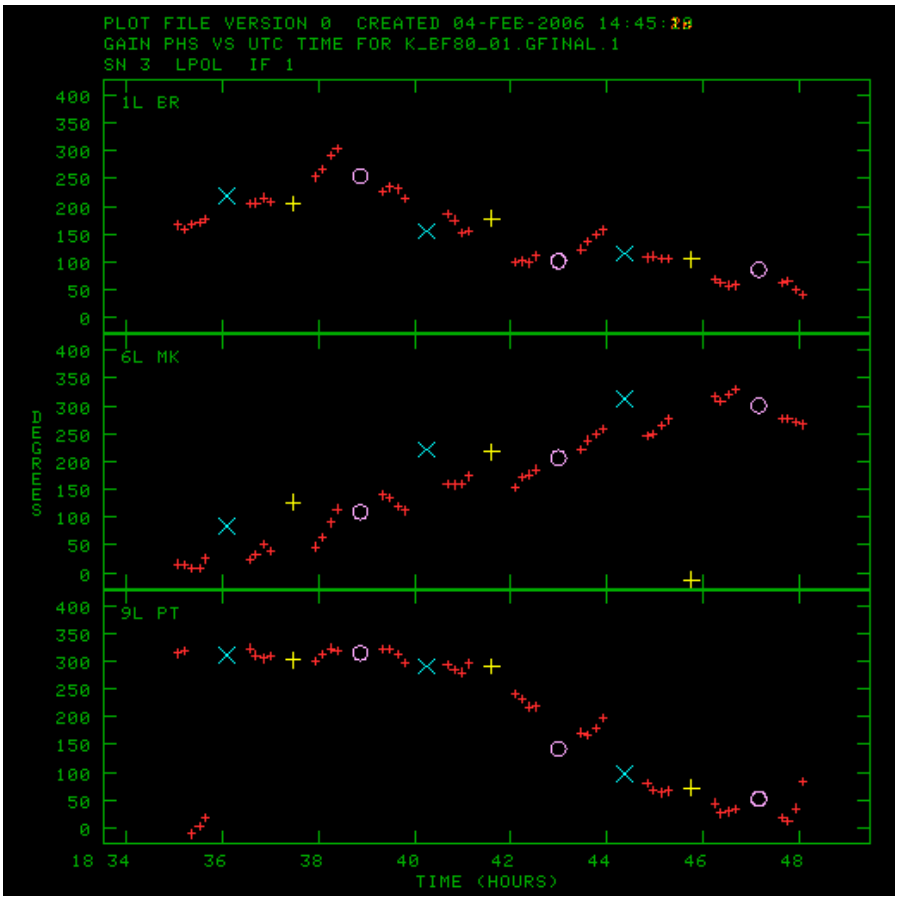

Figure 2. **The Observed Phases of the Four Sources at 23 GHz on October 1:** The three panels show the observed phase versus time over a 13-minute period for the LA-BR (1760 km), LA-MK (4970 km) and LA-PT (236 km) baselines, respectively, after correction for the best-fit residual source positions and the linear phase gradient in the sky. A phase of 100° corresponds to a delay of 12 psec. Each scan was 40-sec in length and the small (red) crosses are for 3C279 every 10-sec during the scan. The other sources, with one average phase per scan are for J1248 cross (white), J1246 circle (blue) and J1304 plus (yellow).

The phases are then analyzed to determine a temporal variable clock correction, plus a constant

position offset for each source on each day, plus a variable phase gradient in the sky in the region of the sources [12, 13]. This phase gradient direction is primary in the elevation direction and is associated with changes in the tropospheric refraction and other remaining astrometric errors. The result of this analysis is shown in Fig. 2 for a 15-min period at 23 GHz on October 1. With the improved relative positions of the sources and removal of the local phase-gradient in the sky, all of the source phases are consistent with the temporal clock term. A rough estimate of the position accuracy can be obtained as follows: The rms phase scatter for a scan is 15° (about 2 psec) for the LA-BR baseline, and this corresponds to a position scatter of about 0.1 mas. This positional accuracy is somewhat independent of baseline-length. When averaged over each scan and over the day, a relative accuracy among the sources is about 0.02 mas.

The reductions are still in progress, but the changes in source position among the three frequencies are consistent with ionospheric refraction, and the ionosphere-corrected positional accuracy is 0.03 mas except when the sources are within 2° of the sun where coronal turbulance decreases the positional accuracy. The preliminary estimated accuracy of γ from this experiment is about 2×10^{-4}, a factor of four better than previous experiments of the gravitational deflection of 3C279.

3. The Effect of Source Structure

The effect of source structure has been discussed in previous IVS meetings and it is of concern since the implicit assumption in phase referencing and IVS observations is that the radio sources are stable with time [14]. This variability causes two effects: First, the sources are not point-like and introduce unmodeled changes in the phase and group delays. Since the structure of the radio sources can often be determined using self-calibration techniques of the relevant observations, this correction can be included in the analysis. A more serious and insidious problem is that the *apparent* location of the source may change. In fact, the definition of the source position is arbitrarily defined by the initial detection of the data (fringe-fitting) that defines the location very close to the brightest emission peak. This location is resolution dependent and may not be the stationary point of the radio source (the black hole or the base of the jet) since a variable moving jet component may, in fact, dominate the emission from a central region of the source. This correction requires the knowledge of the evolution of the source and its various components and needs multi-epoch and multi-frequency observations to determine.

An example of the improved position stability obtained with careful modeling of the structure of a radio source is demonstrated by the parallax measurement of G127 [15]. This source is located near the middle of a super-nova remnant (SNR) about 8 kpc away, but it is unclear if it is really associated with the SNR or merely a background extra-galactic radio source, much more distant. Thus, VLBA observations at 8 GHz were made at six-month intervals between May 2002 and April 2004. The phase referencing observations alternated between G127 and an 0.08-Jy calibrator only 1.5° away. Because G127 was much stronger than the calibrator, we used G127 as the primary reference source and measured (via images) the position of the calibrator that was unresolved. Thus, any parallax motion determined for the calibrator would be the reflexive parallax of G127.

The structure of G127 is given in Fig. 3, left contour plot. It is about 6 mas across and aligned nearly east-west. G127 shows the usual structure properties of nearly all compact radio sources, and the radio visibility data has been fit by four Gaussian components using the Caltech Difmap package [16]. It is composed of a point source with about 0.07 Jy, a strong small-scale elliptical component (jet) emanating to the west with about 0.24 Jy, more extended emission with 0.025 Jy

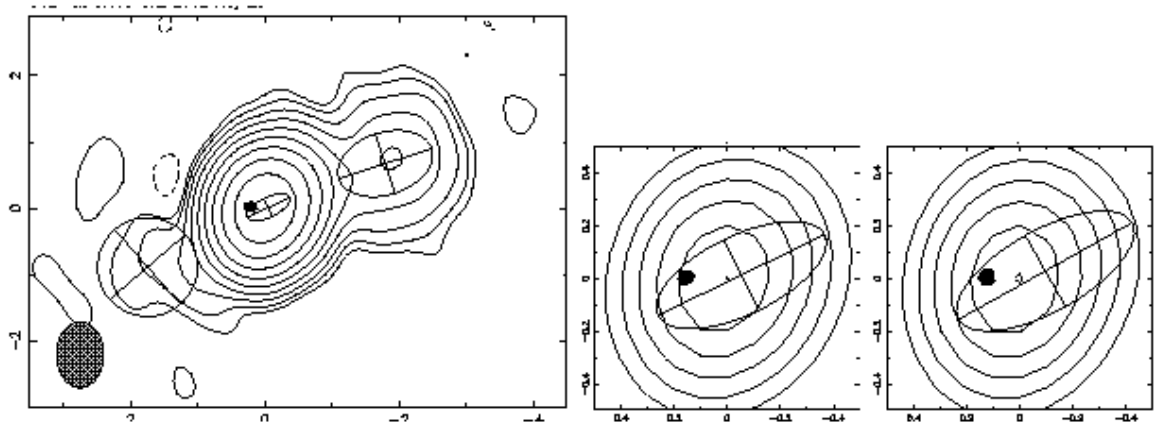

Figure 3. **The Structure Change of G127:** The left-most contour plot shows the structure of G127 for the May 20, 2002 observations. The lowest contour level is 0.2 mJy with levels at multiples of -1,2,4,8,16,32,64,128 and the source extends 6 mas, mostly in the east-west direction. The structure can be fit accurately to the four indicated elliptical components (full-width, half-power levels shown), with the dot as the location of a point component. The two contour plots to the right show the inner-most part of the structure for the May 20, 2002 and Sep 21, 2003 observations, with peak brightness of 0.251 and 0.226 Jy, respectively. The contour levels are at 50,60,70,80,90,98% of the peak. The black dot shows the location of the point component and the ellipse shows the fit to the western jet. The fringe-fit position is at the center of the image, coincident with the brightness peak of this central component. The resolution of all images is 1.0×0.7 mas, and the angular scales in mas are labeled.

further to the west, and a faint extended component, east of the point source, with 0.005 Jy. The fitting of the bright central component with a point component and an extended component may appear somewhat arbitrary, but this model is supported by the high resolution studies that show the central emission regions of most quasars contain a point component plus extended emission which generally points in the direction of the more extended emission. The relative location of these two components was obtained naturally from the model fit, and was not assumed during the fit. The location of the point component is generally assumed to be near the compact object in the center of the galaxy or star and is, thus, probably a better approximation to the stationary part of the radio emission than the peak brightness of the central component which is the default source position obtained from the fringe algorithm.

The radio emission and approximate angular size of the central region varied somewhat over the observation period, so that slight structure changes were occurring. A blow-up of the central region of G127 for the May 2002 and September 2003 central regions are shown in Fig. 3, the right two contour plots. Since the positional accuracy of components in relatively simple sources can be obtained to an accuracy of the resolution divided by the signal to noise of the components, which is > 100, it is, thus, possible to determine their positions to an accuracy 0.01 mas. This modeling shows that the point component is about 0.10 mas east of the brightness peak of the central component, and that its position is 0.04 mas further to the east for the May 2002 observation. The effect of these small changes can be seen in the visibility data of the MK-SC baselines which is 0.08 Jy for the May 2002 data and 0.12 Jy for the Sep 2003 data. This is consistent with the

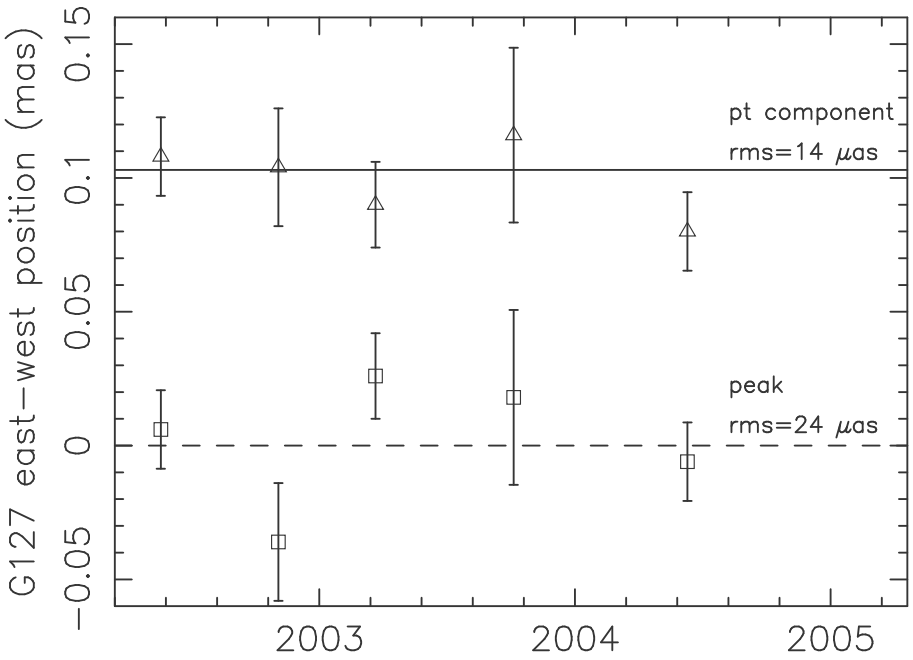

Figure 4. **The Parallax Fit for G127:** The observed east-west relative positions of G127 with respect to the calibrator for the five sessions are shown. The square boxes are the positions with respect to the location of the maximum brightness of the central component in G127, the fringe location. The triangles show the position with respect to the point component determined from the detailed modeling of this bright component. The solid and dashed lines show the best-fit average separation over the five sessions. There is no significant parallax, the rms scatter from the fit decreases when the point component is assumed to be the stationary location of G127.

slightly larger separation of the point component from the nominal center of the source.

Whether the peak of the bright component or the location of the point component is more likely the stationary point in the source can be tested by the quality of the parallax/proper motion fit for the two cases, and these fits is shown in Fig. 4. The top plot shows the fit of the parallax to the location of the point component. Although there is an 0.10 mas offset from the apriori position of G127, the rms fit to the parallax from the mean offset is 14 μas over the five observing sessions. In the bottom plot however, the parallax fit to the peak of the location of the bright component has a significantly larger rms of 24 μJy. Thus, the point component to the east of the brightness peak has the more stable position when compared with the calibrator source that is nearly unresolved. The formal parallax limit is < 0.04 mas (two-sigma result); hence G127 is more then 25 kpc from the sun and is almost certainly a background galaxy and not associated with the SNR.

The above example demonstrates that for quasars which are about 0.5 Jy (and most ICRF sources are this strong), the location of the point component that is associated with a stable location of the quasar can be determined to an accuracy of about 0.02 mas.

4. The ICRF and Phase Referencing

Can the accurate measurement of the relative position of close sources using phase referencing be extended around the sky to determine more accurate ICRF positions than are now available? Two extensions of phase referencing are needed: First, the area of sky for which sources can be successfully phase-connected must be increased from the maximum radius of 5° now used to at least a radius of 20°. Otherwise, building up a global set of source positions would take the combination of too many small fields. Since there is usually a calibrator within about 4° of any target source, the area for which phase referencing is successful has not been pushed in angular scale. However, the use of several calibrations has been demonstrated to determine the parameters of the variable phase screen over each telescope over large areas to increase the position accuracy and the phase-referencing field of view.

Secondly, the accurate positions obtained in one phase referenced field must be transferred from field to field in order to build up a precise global ICRF. The use of overlapping sources in adjacent fields is the most straight-forward method for this position transfer, but the transferal accuracy and the propagation of zonal errors must be well understood.

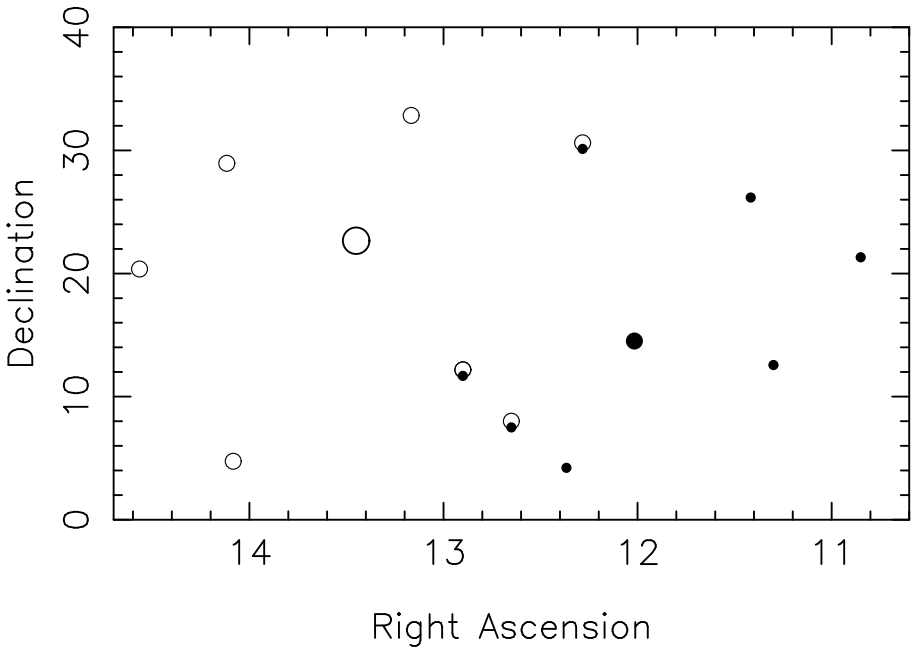

Figure 5. **Source Configuration for Test Observations:** The filled circles show the location of the sources in the phase referencing field 1. The larger circle is that of the primary phase calibrator. The open circles show the sources in the phase referencing field 2, with the larger open circle as the primary phase calibrator. Three sources are in both fields. The location of the field is arbitrary, but was taken near the equator to provide a more challenging test.

Test observations for the VLBA have recently been proposed in order to try to answer the above questions. The observations will consist of phase referencing observations in two adjacent fields, and the proposed configuration of sources is shown in Fig. 5. Each observation will be at S/X band using the identical frequency configuration for IVS observations. Each scan will

be one minute in length and the observations will cycle among eight sources, around a central main phase primary calibrator that will be observed more often. With the use of eight calibrators we hope to determine a phase screen model that is more complicated than a linear drift, and estimate the ultimate size of that multi-source phase referencing. The relatively large number of calibrators is also needed to uncouple the small source position errors (the ICRF accuracy of 0.3 mas is greater than the expected phase-reference position accuracy of < 0.05 mas) from the phase gradient terms. Each field will be observed for three hours. Just before and after the above phase-referencing observations, a 30-min burst of ICRF calibrators over the sky will permit an approximate determination of the global zenith-path delay and other astrometric parameters to lessen somewhat the phase gradients over each field.

We will overlap three sources between the two adjacent fields that will be observed. We know that there must be a registration offset between the two fields because the internal positions will be referenced to different primary calibrators in each field, with an expected position offset of ≈ 0.2 mas. However, the offset position of the sources observed in the two fields should be identical. Hence, three overlapping sources seems reasonable. Since one of the overlapping sources is 20° from the other two, some feeling for the size of the zonal errors may be obtained by the difference in the offset among the three sources. This stitching method from small-scale to large-scale areas of sky is similar to the one proposed for Space Interferometry Mission [18].

This data should be easily analyzed in Calc/Solve in the standard manner. The initial AIPS reduction will determine the structure of each source and its contribution to the phase and group delay will be removed [17]. The registration of each structure at the location of the central point component, as in the G127 example, will be attempted. The subsequent reduction in Solve will first use the group delays to determine the approximate solutions and ionosopheric refraction, and it is expected that the resultant phase delays will not have any ambiguities. Since the Solve package does not formally fit for a phase-gradient in the sky, it is likely that a few of the astrometric parameters will be solved for in order to simulate a variable phase gradient; eġ; troposphere and one nutation term, in addition to the variable clock. Because we are determining the relatively small scale properties of the troposphere and cycling around the 40° region in less than ten minutes, the determination of the troposphere and clock changes over this period of time will be made. This is the main reason why more accurate positions can be obtained compared with the global IVS type observations that determine the approximate all-sky tropospheric properties and clock variations from 30-min to 60-min time scales.

Depending on the accuracy of the above initial observations, further testing and more extended observations of ICRF sources around the sky will be proposed. Extension of this method to higher frequencies, say 23 and 43 GHz, may be difficult because the size of the phase referencing field will decrease too much for effective stitching of positions around the sky [19].

5. Acknowledgements

The National Radio Astronomy Observatory is a facility of the National Science Foundation operated under cooperative agreement by Associated Universities, Inc. I thank G. Lanyi and A. Fey for useful discussions about the test observations.

References

[1] Beasley, A. J. & Conway, J. E. 1995, ASP Conf. Ser. 82, Very Long Baseline Interferometry and the VLBA, ed. J.A. Zensus, P.J. Diamond & P.J.Napier (San Francisco: ASP), 328

[2] Ma, C., Arias, E. F., Eubanks, T. M., Fey, A. L., Gontier, A.-M., Jacobs, C. S., Sovers, O. J., Archinall, B. A., Charlot, P. 1998, AJ, 116, 516

[3] Reid, M. J. & Brunthaler, A, 2005 ASP Conf. Ser. 340, The 10th Anniversary of the VLBA, ed. J. Romney and M. Reid (San Francisco: ASP), 253

[4] Brunthaler, A., Reid, M. J., Falcke, H., Greenhill, L. J. & Henken, C. 2005, Science, 307, 1440

[5] Fomalont, E. B. & Kopeikin, S.M. 2003, ApJ, 598, 704

[6] Fomalont, E. B, Geldzahler, B. J. & Bradshaw, C. W., 2001, ApJ, 558, 283

[7] Briskin, W.F., Thorsett, S.E., Golden, A. & Goss, W.M. 2003, ApJ 593

[8] Lebach, D. E., Corey, B. E., Shapiro. I. I., Ratner, M. I., Webber, J. C., Rogers, A. E. E., Davis, J. L.& Herring, T. A. 1995, Phys. Rev. Lett. 75, 1439

[9] Bertotti, B., Less, L. & Tortora, P., Nature, 2003, 425, 374

[10] Ryan, J.W., Clark, T.A., Ma, C., Gordon, D., Capretee, D. & Himwich, W.E. 1993, in Contributions of Space Geodesy to Geodynamics: Earth Dynamics, ed D.E. Smith & D. L. Turcotte (Washington:Am.Geophys. Unions), 37

[11] Mioduszewski, A. 2004, AIPS memo #110, http://www.aoc.nrao.edu/aips/aipsmemo.html

[12] Fomalont, E .B. & Kogan, L. 2005, AIPS memo #111, http://www.aoc.nrao.edu/aips/aipsmemo.html

[13] Fomalont, E. B. 2005 ASP Conf. Ser. 340, The 10th Anniversary of the VLBA, ed. J. Romney and M. Reid (San Francisco: ASP), 340

[14] Charlot, P. 2002, in IVS 2002 General Meeting Proceedings, edited by R. Vandenberg and K. D. Baver, NASA/CP-2002-210002, 233-242.

[15] Geldzahler, B. G. & Shaffer, D. B. 1982, ApJ 260, L69

[16] Shepherd, M. C. 1997 in ASP Conf. Series. 125, Astronomical Data Analysis Software and Systems VI, ed. by G. Hunt & H. E. Payne (San Francisco: ASP), 77

[17] Greisen, E. W. 1988 in Acquisition, Processing and Archiving of Astronomical Images, ed. G. Longo & G. Sedmak (Napoli: Osservatorio Astronomico di Capodimonte), 125

[18] Unwin, S. C. 2005 in ASP Conf. Series. 338, 37, ed. P. K. Seidelmann and A. K. B. Monet (San Francisco:ASP), 37

[19] Jacobs, C. S. et al. 2006 in IVS 2006 General Meeting Proceedings, edited by D. Behrend and K. D. Baver, this volume

Rüdiger Haas: Investigating High-Frequency Earth Orientation Variations with Continuous Geodetic VLBI Campaigns, IVS 2006 General Meeting Proceedings, p.316–319
http://ivscc.gsfc.nasa.gov/publications/gm2006/haas

Investigating High-Frequency Earth Orientation Variations with Continuous Geodetic VLBI Campaigns

Rüdiger Haas

Onsala Space Observatory, Department of Radio and Space Science, Chalmers University of Technology
e-mail: haas@oso.chalmers.se

Abstract

The analysis of geodetic VLBI data allows to investigate high-frequency variations in earth orientation and rotation. Results from the three continuous VLBI campaigns CONT94, CONT02 and CONT05 are presented and compared to corresponding model predictions. The remaining residuals do show significant signal strength in the diurnal and semi-diurnal frequency bands. However, these residual signals are not identical for the different CONT campaigns.

1. Introduction

Geodetic VLBI is one of the most important space geodetic techniques for the observation of earth rotation and orientation. The analysis of geodetic VLBI data provides the complete set of earth rotation and orientation parameters. It also allows to investigate high-frequency polar motion and UT1 variations which are caused by geophysical processes. Therefore it promises to contribute to a better understanding of these processes.

2. Theoretical Background

High-frequency variations of earth orientation and rotation are caused by exchange of angular momentum between ocean, atmosphere and solid earth. The theoretical basis for these geophysical variations of earth orientation and rotation is described for example in [1], [2], [3].

During the last decades, a number of models for ocean tidal influences on polar motion and UT1 in the diurnal and sub-diurnal frequency band have been developed, e.g. [4], [5], [6], [7], [8], [9], [10]. The use of an hydrodynamical ocean model [11] allowed to model even ter-diurnal ocean tidal influences on polar motion [12]. Exchange of non-tidal ocean angular momentum is predicted to cause diurnal polar motion and UT1 variations [3]. The influence of atmospheric tides, thermal and gravitational, on polar motion and UT1 is described by [13] [14]. Furthermore, sub-diurnal effects on polar motion due to external luni-solar torques acting on the tri-axial figure of the earth are predicted [15], [16], [17].

3. Observational Results

The data archive of the International VLBI Service for Geodesy and Astrometry (IVS) includes geodetic VLBI observations since the early 80ies of the last century. Most of the sessions are individual 24 hour long sessions that were observed in different global VLBI networks. However, there are also a number of continuous campaigns that were observed during several days with the same global VLBI networks. Examples are the campaigns CONT94, CONT02 and CONT05 that

were observed in 1994, 2002 and 2005, respectively. Due to their continuous and consistent data, these campaigns are of particular interest for the investigation of high-frequency earth orientation and rotation variations [18].

VLBI data analysis with the CALC/SOLVE analysis software [19] allows to estimate polar motion and UT1 as piece-wise linear functions with hourly updates. Figure 1 shows for example the time series of hourly polar motion and UT1 observations determined from the continuous VLBI campaign CONT05. The circles with error bars are hourly values for polar motion and UT1, while the continuous line shows the model predictions according to the Ray-model [6], [7].

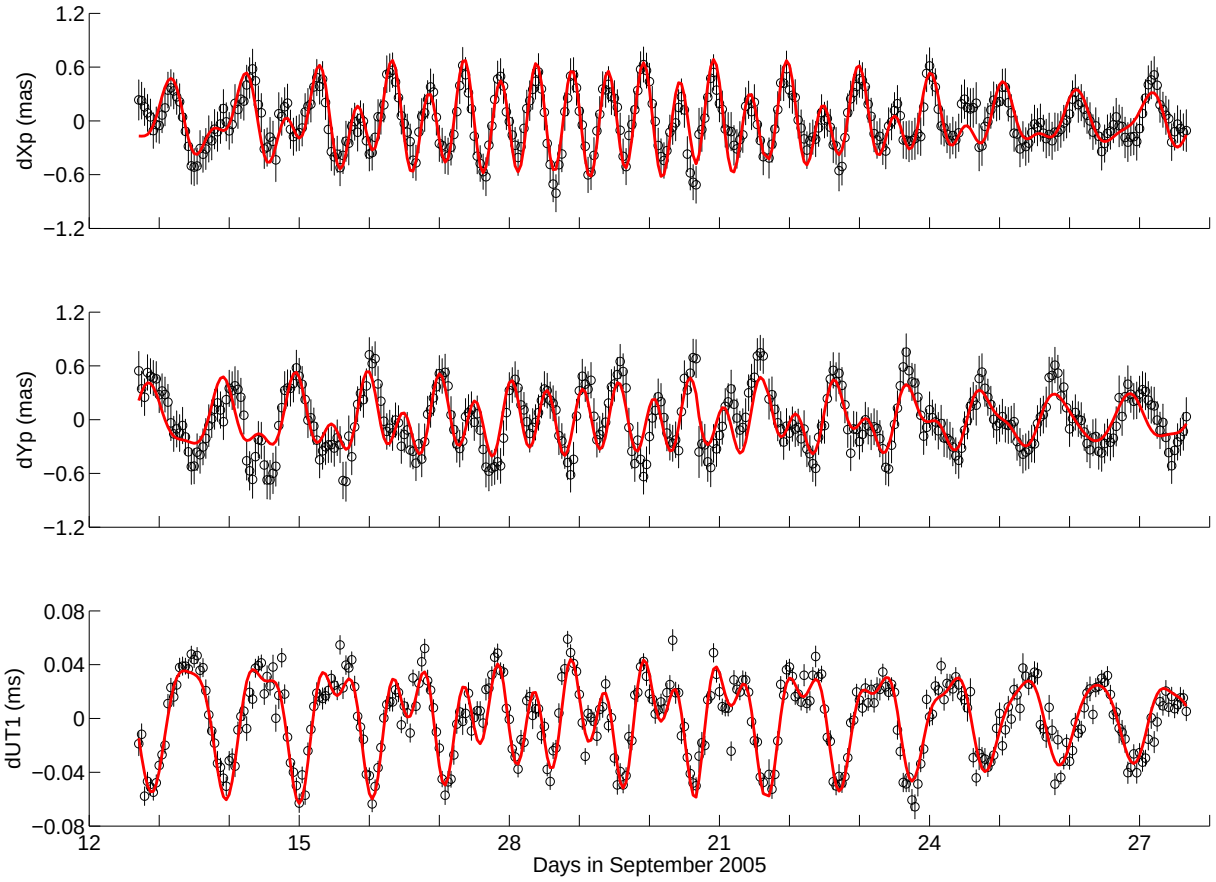

Figure 1. Hourly estimates of polar motion and UT1 from CONT05 VLBI shown as circles with errorbars that indicate the formal errors of the analysis. The continuous thin line shows the corresponding predictions based on the extended version of the Ray-model [6], [7].

Figure 2 shows the amplitude spectra of the residual hourly polar motion and UT1 estimates from CONT94, CONT02 and CONT05 after subtracting the extended Ray-model [6], [7]. Significant residual signals in the diurnal and sub-diurnal frequency bands are clearly visible. However, the amplitude spectra of the three different VLBI campaigns are not identical. In particular the strong signal with 8 hour period in the CONT02 residuals cannot be seen in the CONT94 and CONT05 results. Also the signals in the diurnal and semi-diurnal frequency band do not agree.

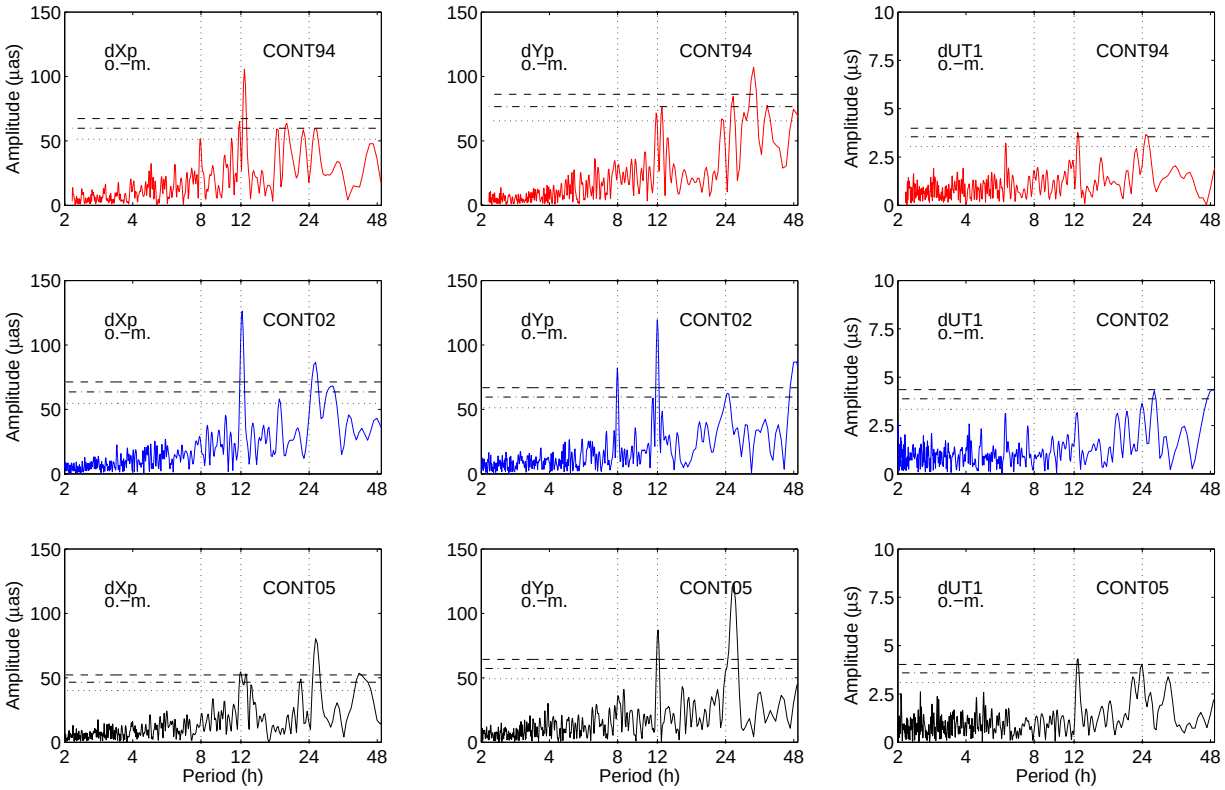

Figure 2. Amplitude spectra of residual hourly polar motion and UT1 estimates for CONT94, CONT02 and CONT05 after subtracting the extended Ray-model [6], [7]. The vertical dotted lines indicate periods of 8, 12 and 24 hours. The horizontal lines indicate the significance levels of 99.5% (dashed), 95% (dashed-dotted) and 50% (dotted).

4. Discussion and Outlook

The continuous VLBI campaigns can be used to investigate high-frequency earth orientation and rotation variations. To a large extent the empirical results can be explained by ocean tidal influences. However, the remaining residual signals after subtracting the model predictions do not show the same results for the three different continuous campaigns. In particular a polar motion signal with 8 hour period that was reported from the CONT02 data set [20] cannot be confirmed from the analysis of the CONT94 and CONT05 data. The remaining signals in the diurnal and semi-diurnal frequency range do not agree either among the three continuous campaigns. The reason for these discrepancies is so far not understood. More effort is needed to investigate this problem and future continous VLBI campaigns will support this work.

References

[1] Barnes R.T.H., Hide R., White A.A., Wilson C.A.: Atmospheric angular momentum fluctuations, length-of-day changes and polar motion. *Proc. R. Soc. London, Ser. A*, **387**, 31–73, 1983.

[2] Brzezinski A.: Polar motion excitation by variations of the effective angular momentum function II: Extended model. *Manuscr. Geod.* **19**, 151–171, 1994.

[3] Brzezinski A., Ponte R.M., Ali, A.H.: Nontidal oceanic excitation of nutation and diurnal/semidiurnal polar motion revisited. *J. Geophys. Res.*, **109**, B11407, doi:10.1029/2004JB003054, 2004.

[4] Brosche P., Seiler U., Sündermann J., Wünsch J.: Periodic changes in earth's rotation due to oceanic tides. *Astron. Astrophys.*, **220**, 318–320, 1989.

[5] Brosche P., Wünsch J.: On the "rotational angular momentum" of the oceans and the corresponding polar motion. *Astron. Nachr.*, **315(2)**, 181–188, 1994.

[6] Ray R.D., Steinberg D.J., Chao B.F., Cartwright D.E.: Diurnal and semidiurnal variations in the earth's rotation rate induced by oceanic tides. *Science*, **264**, 830–832, 1994.

[7] IERS: *IERS Technical Note*, **32**, 2003.

[8] Seiler U., Wünsch J.: A refined model for the influence of ocean tides on UT1 and polar motion. *Astron. Nachr.*, **316**, 419–423, 1995.

[9] Chao B.F., Ray R., Egbert G.D.: Diurnal/semidiurnal oceanic tidal angular momentum: Topex/Poseidon models in comparison with Earth's rotation rate. *Geophys. Res. Letters*, **22(15)**, 1993–1996, 1995.

[10] Chao B.F., Ray R.D., Gipson J.M., Egbert G.D., Ma C.: Diurnal/semidiurnal polar motion excited by oceanic angular momentum. *J. Geophys. Res.*, **101(B9)**, 20151–20163, 1996.

[11] Seiler U.: Periodic changes of the angular momentum budget due to the tides of the world ocean. *J. Geophys. Res.*, **96(B6)**, 10287–10300, 1991.

[12] Wünsch J., unpublished, 2001.

[13] Brzezinski A., Bizouard C., Petrov S.D.: Influence of the atmosphere on earth rotation: what new can be learnt from the recent atmospheric angular momentum estimates? *Surv. Geophys.*, **23(1)**, 33–39, 2002.

[14] de Viron O., Schwarzbaum G., Lott F., Dehant V.: Diurnal and subdiurnal effetcs of the atmosphere on the Earth rotation and geocenter motion. *J. Geophys. Res.*, **110**, B11404, doi:10.1029/2005JB003761, 2005.

[15] Chao B.F., Dong D.N., Liu H.S., Herring T.A.: Libration in the Earth's rotation. *Geophys. Res. Lett.*, **18**, 2007–2010, 1991.

[16] Wünsch J.: Small waves in UT1 caused by the inequality of the equatorial moments of inertia A and B of the earth. *Astron. Nachr.*, **312(5)**, 321–325, 1991.

[17] Brzezinski A., Capitaine, N.: Lunisolar perturbations in earth rotation due to the triaxial figure of the earth: geophysical aspects. In: N. Capitaine (ed.), *Proc. Journées Systemes de Reference Spatio-Temporels 2001*, Paris Observatory, 51–58, 2002.

[18] Clark T.A., Ma C., Ryan W., Chao B.F., Gipson J.M., MacMillan D.S., Vandenberg N.R., Eubanks T.M., Niell A.E.: Earth rotation measurement yields valuable information about the dynamics of the Earth system. *EOS Trans. AGU*, **79(17)**, 205, 209, 1998.

[19] Ma C., Sauber J.M., Bell L.J., Clark T.A., Gordon D., Himwich W.E., Ryan J.W.: Measurement of horizontal motions in Alaska using very long baseline interferometry. *J. Geophys. Res.*, **95(2)**, 21991–22011, 1990.

[20] Haas R., Wünsch J.: Sub-diurnal earth rotation variations from the VLBI CONT02 campaign. *J. Geodyn.*, **41**, 94–99, 2006.

C. S. Jacobs et al.: Extending the ICRF to Higher Radio Frequencies: Global Astrometric Results at 24 GHz, IVS 2006 General Meeting Proceedings, p.320–320
http://ivscc.gsfc.nasa.gov/publications/gm2006/jacobs1

Extending the ICRF to Higher Radio Frequencies: Global Astrometric Results at 24 GHz

C. S. Jacobs [1], *G. E. Lanyi* [1], *C. J. Naudet* [1], *O. J. Sovers* [1], *L. D. Zhang* [1], *P. Charlot* [2], *E. B. Fomalont* [3], *D. Gordon* [4], *C. Ma* [4], *KQ VLBI Collaboration* [5]

[1)] *NASA/Caltech's JPL*
[2)] *Bordeaux Observatory*
[3)] *NRAO*
[4)] *NASA's GSFC*
[5)] *multiple affiliations*

Contact author: C. S. Jacobs, e-mail: Chris.Jacobs@jpl.nasa.gov

Abstract

A celestial reference frame at K-band (24 GHz) has been constructed using eight 24-hour VLBA sessions which covered the full 24 hours of right ascension and declinations down to -40 deg. The resulting catalog contains 259 sources with median formal position uncertainties of 100 micro-arcsec in RA cos(dec) and 200 microarcsec in declination. In order to constrain the long arcs of the K-band catalog to those obtained with the S/X-band ICRF, four K-band high quality source positions well-separated in the sky were set to the S/X-band positions. After this registration, comparison of the K-band frame to an S/X-band ICRF-like frame shows agreement of 200 micro-arcsec in RA cos(dec) and 300 micro-arcsec in declination. The motivations for extending the ICRF to frequencies above 8 GHz are to use more compact sources less susceptible to structure changes in order to construct a more stable frame, to provide calibrators for phase referencing, and to support spacecraft navigation at higher frequencies.

[Note from the Editors: The overheads of the oral presentation of this contribution can be downloaded from the IVS 2006 General Meeting web site. Please get the PowerPoint file of the presentation at the URL ftp://ivscc.gsfc.nasa.gov/pub/general-meeting/2006/presentations/gm2006_6-03_jacobs.ppt.]

Patrick Charlot et al.: Astrometric Suitability of ICRF Sources Based on Intrinsic VLBI Structure, IVS 2006 General Meeting Proceedings, p.321–325
http://ivscc.gsfc.nasa.gov/publications/gm2006/charlot

Astrometric Suitability of ICRF Sources Based on Intrinsic VLBI Structure

Patrick Charlot [1], *Alan Fey* [2], *Roopesh Ojha* [2], *Dave Boboltz* [2]

[1)] *Observatoire de Bordeaux*
[2)] *US Naval Observatory*
Contact author: Patrick Charlot, e-mail: charlot@obs.u-bordeaux1.fr

Abstract

The intrinsic radio structure of the extragalactic sources is one of the limiting errors in the analysis of astrometric and geodetic VLBI observations. Based on VLBI images obtained with the VLBA and other VLBI telescopes around the world, we evaluate this effect for 557 sources (78% of the ICRF) and calculate a so-called "structure index" to define the astrometric source quality. The structure index ranges from 1 for the most compact sources to 4 for the most extended sources. The most recent addition to our data base is for a hundred southern hemisphere sources. We discuss the overall distribution of structure index in the ICRF and the structure index variability with time for those sources that have VLBI images available at multiple epochs. Based on these data, we identify a set of 239 sources that have good or excellent astrometric suitability. We also suggest that the structure index indicator be used as a primary criterion to select defining sources for the next ICRF realization.

1. Introduction

Extensive VLBI imaging surveys reveal that many of the extragalactic radio-emitting sources used to define the International Celestial Reference Frame (ICRF) show extended emission structures on milliarcsecond scales and hence are only imperfect fiducial points in the sky [1, 2, 3, 4, 5]. This extended emission and its frequency and time dependence can introduce significant structural contributions in the measured VLBI group delays, which deteriorate the source position accuracy and the overall quality of the VLBI analysis if not accounted for [6]. It is especially important to quantify these structural effects when realizing the celestial frame so that the most suitable sources, i.e. those that produce the smallest such effects, may be used for defining the frame.

The expected effects of intrinsic source structure on bandwidth synthesis delay observations depend on the exact form of the spatial brightness distribution of the extended radio source relative to the coordinates of the VLBI baseline vector projected onto the plane of the sky [6]. The "structure index", introduced in [2], defines the astrometric source quality according to the median value of the structure delay corrections, $\tau_{\rm median}$, calculated for all projected VLBI baselines that could be possibly observed with Earth–bound VLBI, separating the sources into four classes as follows:

$$\text{Structure Index} = \begin{cases} 1, & \text{if } 0 \text{ ps} \le \tau_{\rm median} < 3 \text{ ps}, \\ 2, & \text{if } 3 \text{ ps} \le \tau_{\rm median} < 10 \text{ ps}, \\ 3, & \text{if } 10 \text{ ps} \le \tau_{\rm median} < 30 \text{ ps}, \\ 4, & \text{if } 30 \text{ ps} \le \tau_{\rm median} < \infty. \end{cases}$$

Structure index values of 1 and 2 point to excellent and good astrometric suitability, respectively, while values of 3 and 4 point to poor suitability. A given source may have differing structure indices at 8 GHz (X band) and 2 GHz (S band) depending on the source structure at each frequency band.

Initial studies focused on estimating structure indices for as many ICRF sources as possible, based on dedicated imaging observations with the Very Long Baseline Array (VLBA). From these data, structure indices were derived for a total of 389 sources, representing approximately 90% of the ICRF sources north of $-20°$ declination [2, 3]. In addition, structure indices have recently been obtained for 111 southern ICRF sources, most of which at declinations below $-20°$, which were mapped using a southern hemisphere VLBI network [5]. In this paper, we extend further our calculation by using additional VLBI imaging data, which include those from a dozen Research & Development VLBA (RDV) experiments. This brings the total number of ICRF sources with available structure indices to 557. We also devise a scheme to account for the temporal variability of the structure index for the sources that have been imaged at multiple epochs.

2. Observational Data and Multi-Epoch Structure Index

The VLBI maps used to derive the structure index data base discussed below are part of the Radio Reference Frame Image Data Base (available at http://rorf.usno.navy.mil/rrfid.shtml) and were produced from a total of 28 VLBI sessions conducted between 1994 and 2005. These comprise:

- 8 dedicated dual-frequency (S/X) VLBA imaging sessions conducted between July 1994 and January 1997 [1, 2, 3];
- 13 dual-frequency (S/X) RDV sessions conducted between January 1997 and July 2004; these sessions include the 10 VLBA stations and up to 10 additional geodetic telescopes;
- 5 dedicated southern hemisphere X-band imaging sessions conducted between July 2002 and April 2004 with the Australian Long Baseline Array, augmented by radio telescopes in South Africa, Hawaii, and Japan [4, 5];
- 2 VLBA sessions at S/X/K and X/K frequency bands, respectively, in February 2004 and August 2005, as part of a project to extend the ICRF to higher frequencies[1] [7].

Altogether, this represents a total of 1735 maps at X band from 557 sources and 1543 maps at S band from 459 sources. Less sources have been imaged at S band because the southern hemisphere sessions did not observe at this frequency. There are up to 19 VLBI epochs available for some intensively observed sources, whereas only one epoch is available for other less observed sources.

Figure 1 shows a series of maps and structure indices for two ICRF sources, one of which (0048-097) is very compact with a structure index value of 1 at all epochs, whereas the other one (the BL Lac object 1156+295) shows significant structure changes and variability of the structure index over the two-year span of the data. For 1156+295, there is first an increase in the structure index (from 2 to 3), at a time when the source weakened (peak of emission dropping from 0.8 to 0.3 Jy/beam). By superresolving the maps, it appears that the dominant component of the structure became also more resolved at these epochs, possibly because a secondary sub-component was ejected from the core. Following this event, the source quickly brightened (peak brightness rising from 0.3 to 2.0 Jy/beam within a year), with the sub-structure being dominated again by a single sub-component, while the structure index decreased from a value of 3 to a value of 1 at the same time (Fig. 1). This rapid flux and structure variability is typical of BL Lac objects.

The above example indicates that 1156+295 was a highly suitable reference source at epoch 1999.0, whereas this was not the case a year earlier. In this respect, it is important to account for

[1] Only the X band and S band structure indices are discussed in this paper. For results at K band, see [7, 8].

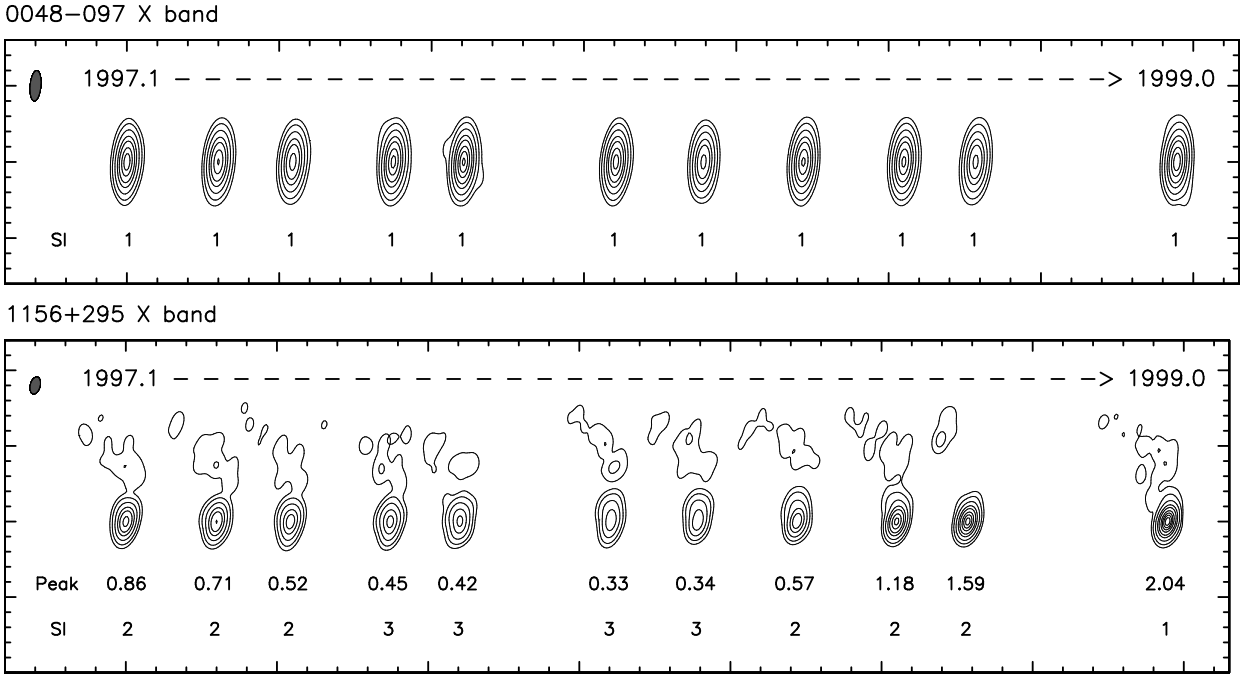

Figure 1. VLBI images of the ICRF sources 0048–097 and 1156+295 at X band for 11 successive epochs spanning the period 1997.1–1999.0. The maps are aligned horizontally according to the dominant structural component and are spaced linearly according to their observing epochs. The interval between minor tick marks (vertical scale) is 1 mas. The structure index (SI) is indicated below each map. For comparison, the peak brightness (Peak), expressed in Jy/beam, is also indicated below each map in the case of 1156+295. Contour levels are drawn at 0.0035, 0.014, 0.056, 0.175, 0.35, 0.70, 1.05, 1.40, and 1.75 Jy/beam.

the structure index variability when defining the astrometric suitability of a given source. Adopting a conservative approach, we chose the maximum value of the structure index as the source quality indicator when multi-epoch structure indices are available. As before, we suggest that only those sources that have values of the structure index of either 1 or 2 should be identified as high-quality sources. In other words, if a source shows a structure index value of 3 or 4 at one or more epochs, it should be regarded as unsuitable for highly accurate astrometry even though it has structure index values of 1 or 2 at some other epochs. Examples of sources excluded based on this multi-epoch criterion include 0014+813, 2145+067, and 2234+282. It is interesting that these sources also show significant position instability, as reported by several authors during this meeting [9, 10].

3. Discussion

As noted above, we have now obtained structure indices for 557 sources at X band and 459 sources at S band (representing 78% and 64% of the current 717 sources of the ICRF, respectively). The X-band structure index distribution (Fig. 2) shows that 242 sources (or equivalently a portion of 43% of the sources) are astrometrically suitable at this frequency according to our criterion (structure index value of either 1 or 2). This is less than the percentage of good sources

we reported before (57%, as quoted in [8]) because our new multi-epoch approach led us to downgrade some sources with variable structure that were found suitable in our previous single-epoch analyses. At S band, 88% of the sources have a structure index value of either 1 or 2 (Fig. 2). This indicates that the contribution of the S-band structure to the dual-frequency calibrated delay is usually smaller compared to the X-band structure contribution (as already noted in [2]). Comparing the X- and S-band structures indices individually for each source shows that, with three exceptions, all sources that have an S-band structure index of either 3 or 4 have also an X-band structure index of 3 or 4. Based on the S-band structure index, we thus exclude only 3 additional sources, which leaves a total of 239 ICRF sources astrometrically suitable at both frequencies.

In Fig. 3, the X-band structure index distribution is compared for each ICRF source category (defining, candidate, "other", "new") [11, 12]. As expected, the distribution is somewhat better for the defining sources than for the candidate and "other" sources. However, only about half of the ICRF defining sources have a structure index value of either 1 or 2. The portion of suitable sources drops down to 40% for the candidate sources and 37% for the "other" sources, while it is 54% for the "new" sources. Overall, these results confirm that revision of source categories will be mandatory when a new realization of the ICRF is made.

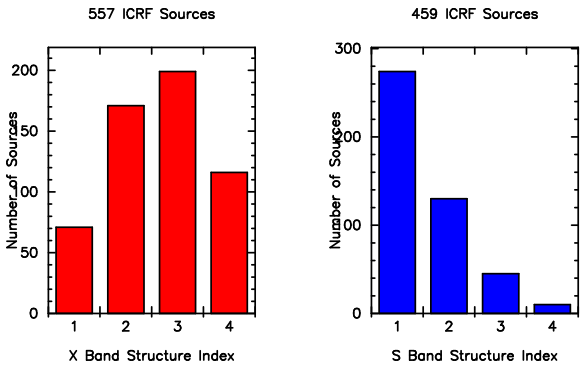

Figure 2. The structure index distribution at X band and S band for all ICRF sources that have a structure index available at these frequencies.

Additionally, we also studied the structure index distribution for the sample of 199 sources identified as stable in [13]. Of the 193 such sources that have a structure index available at X band, 41% were found to have a structure index value of 3, while 11% have a structure index value of 4. We recommend that these sources, which have extended or very extended structures, be excluded from the potential list of defining sources when building the next ICRF. In fact, some of these sources (e.g., 2200+420) have long been known for showing correlated structure and position variations [14]. We also point out that the comparison between the structure index and stability criterion presented in [13] is inappropriate because it is based on the S-band structure which contributes only a small part to the overall structure effect, as originally reported in [3].

4. Conclusion

We have evaluated the astrometric suitability of roughly 80% of the sources in the ICRF based on multi-epoch VLBI maps of their structures. It is anticipated that the remaining 20% of ICRF sources for which this astrometric suitability has not been assessed (mostly in the southern sky) will be imaged in the near future through further VLBI observing programs in the southern hemisphere. Based on this analysis, we have identified a sample of 239 astrometrically suitable ICRF sources which have compact or very compact structures according to our "structure index" indicator. We suggest that this indicator be used as a primary criterion to select defining sources for the next ICRF realization. It is possible that this sample of suitable sources be reduced in the future in the case that some sources are downgraded as new maps are being made for additional VLBI epochs.

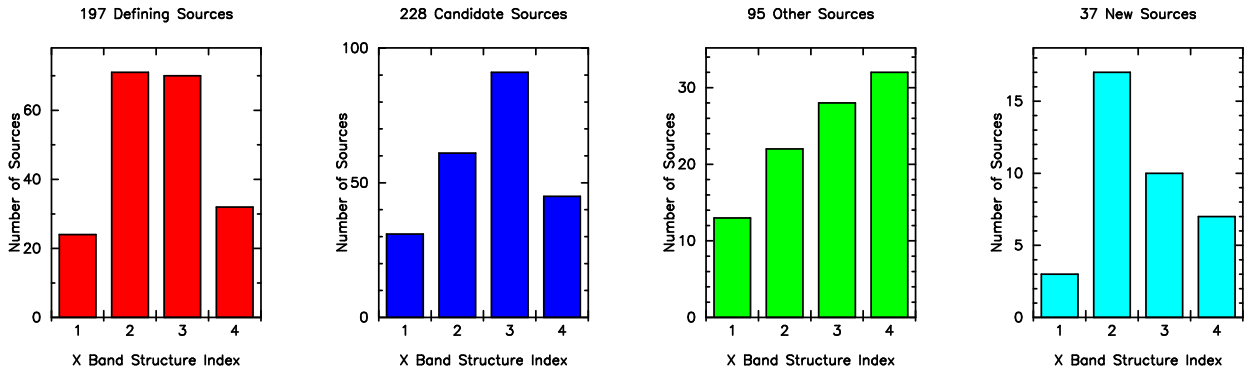

Figure 3. Distribution of the X-band structure indices in each ICRF source category (defining, candidate, "other", "new"). The 557 ICRF sources with currently available structure indices are included in this figure.

References

[1] Fey, A. L., A. W. Clegg, E. B. Fomalont, VLBA Observations of Radio Reference Frame Sources. I., ApJS, 105, 299–330, 1996.

[2] Fey, A. L., P. Charlot, VLBA Observations of Radio Reference Frame Sources. II. Astrometric Suitability Based on Observed Structure, ApJS, 111, 95–142, 1997.

[3] Fey, A. L., P. Charlot, VLBA Observations of Radio Reference Frame Sources. III. Astrometric Suitability of an Additional 225 Sources, ApJS, 128, 17–83, 2000.

[4] Ojha, R., A. L. Fey, K. J. Johnston, et al., VLBI Observations of Southern Hemisphere ICRF Sources. I., AJ, 127, 3609–3621, 2004.

[5] Ojha, R., A. L. Fey, P. Charlot, et al., VLBI Observations of Southern Hemisphere ICRF Sources. II. Astrometric Suitability Based on Intrinsic Structure, AJ, 130, 2529–2540, 2005.

[6] Charlot, P., Radio-Source Structure in Astrometric and Geodetic Very Long Baseline Interferometry, AJ, 99, 1309–1326, 1990.

[7] Boboltz, D. A., A. L. Fey, P. Charlot, et al., Extending the ICRF to Higher Radio Frequencies – Imaging and Source Structure, In: IVS 2004 General Meeting Proceedings, N. R. Vandenberg and K. D. Baver (eds.), NASA/CP-2004-212255, 361–365, 2004.

[8] Charlot, P., The ICRF: 2010 and Beyond, In: IVS 2004 General Meeting Proceedings, N. R. Vandenberg and K. D. Baver (eds.), NASA/CP-2004-212255, 12–21, 2004.

[9] MacMillan, D. S., Radio Source Instability in the Analysis of VLBI Data, these Proceedings, 2006.

[10] Titov, O., Effect of the Radio Source Instability on the TRF solution, these Proceedings, 2006.

[11] Ma, C., E. F. Arias, T. M. Eubanks, et al., The International Celestial Reference Frame as Realized by Very Long Baseline Interferometry, AJ, 116, 516–546, 1998.

[12] Fey, A. L., C. Ma, E. F. Arias, et al., The Second Extension of the International Celestial Reference Frame. ICRF-Ext.2, AJ, 127, 3587–3608, 2004.

[13] Feissel-Vernier, M., Selecting Stable Extragalactic Compact Radio Sources from the Permanent Astro-geodetic VLBI Program, A&A, 403, 105–110, 2003.

[14] Charlot, P., Modeling Radio Source Structure for Improved VLBI Data Analysis, In: IVS 2002 General Meeting Proceedings, N. R. Vandenberg and K.D. Baver (eds.), NASA/CP-2002-210002, 233–242, 2002.

Richard Porcas et al.: How Compact Are Faint Radio Sources?, IVS 2006 General Meeting Proceedings, p.326–329
http://ivscc.gsfc.nasa.gov/publications/gm2006/porcas

How Compact Are Faint Radio Sources?

Richard Porcas [1], *Walter Alef* [1], *Chris Salter* [2], *Tapasi Ghosh* [2], *Simon Garrington* [3]

[1)] *Max-Planck-Institut für Radioastronomie*

[2)] *Arecibo Observatory*

[3)] *Jodrell Bank Observatory*

Contact author: Richard Porcas, e-mail: porcas@mpifr-bonn.mpg.de

Abstract

We present preliminary results from a statistical survey of compact structure in faint radio sources. Around 1000 sources from the VLA FIRST survey (flux densities $\geq$ 1 mJy at 1.4 GHz) have been observed with the single-baseline interferometer Effelsberg-Arecibo. We observed each source, selected from a narrow strip of sky at declination 28°, for just one minute. The baseline sensitivity at 1.4 GHz, using 512 Mb/s recording, is such that *any* FIRST source, selected at random, would be detected if most of its flux density is in compact structure. We discuss the detection-rate statistics from one epoch of these observations.

1. Introduction

We have been investigating the existence of compact structure in the faint radio source population using a single, but highly sensitive, long-baseline interferometer between the 305-m Arecibo and 100-m Effelsberg radio telescopes. Preston et al. (1985) showed the value of such observations by surveying 1398 known radio sources at 2.29 GHz between 1974 and 1983, using single baselines between the (then) 64-m DSN antennas, in order to select candidate sources for use in establishing the celestial reference frame. Sparse u,v-coverage VLBI observations were also used by Lawrence et al. (1985) at 22 GHz to investigate highly compact structure in radio sources, as a preliminary to future space-VLBI projects.

In the same spirit as these previous surveys, we decided to investigate the prevalence of compact structure in a sample of sources chosen from the 1.4 GHz FIRST survey (Becker et al., 1995). This survey, made using the VLA with a resolution of 5.4″, contains 138,665 sources down to 1 mJy in the first instalment (White et al., 1997), with a sensitivity of 0.15 mJy. Garrington et al. (1999) have made global 5-GHz observations of a small sample of 35 FIRST sources, with flux densities $\geq$ 10 mJy and preselected using MERLIN to have compact structure. They detected 27 sources, using the phase-referencing technique.

In our investigation we have used a highly sensitive long-baseline interferometer, between Arecibo and Effelsberg, using the FIRST survey frequency of 1.4 GHz and recording using 512 Mb/s. For a given integration time this baseline is 42 times more sensitive than a single VLBA baseline, 6.2 times more sensitive than the full (phase-referenced) VLBA, and 12.5 times more sensitive than the full VLBA at its sustainable recording rate of 128 Mb/s. We believe this is the most sensitive VLBI baseline ever used.

2. Observations and Source Selection

We made VLBI observations between Arecibo and Effelsberg using Mark IV recording at 512 Mb/s. We observed the 64-MHz band from 1.366-1.430 GHz in both LHC and RHC polarization, using 2-bit sampling, and subdivided into 4 upper and 4 lower sideband channels, each of 8 MHz, for each polarization. At Effelsberg the signal was recorded using a Mark 5A system. At Arecibo the data was recorded on a VLBA4 recorder using 2 heads. We configured this so that the LHC signal was recorded by one head, and RHC by the other, thus making it convenient to make a preliminary analysis of the polarizations separately from the results of the necessary 2-pass correlation (see Section 3).

Since the Arecibo telescope has a limited hour-angle range, we decided to make "single-shot" observations of FIRST sources at a fixed hour-angle. We observed sources in a 1°-wide declination strip between declinations 28° and 29° at ∼30 mins before Arecibo transit, in order to minimize Arecibo drive times between sources whilst being at a reasonable elevation (∼34°) at Effelsberg. The projected baseline results in a resolution of ∼6 mas in PA ∼20°. We planned an on-source integration time of 60 s, for which the estimated rms noise is 0.1 mJy. This permits us to detect *any* FIRST source if it is sufficiently compact. We allowed 30 s for telescope drive-time between sources, resulting in observation of 15 target sources for every 22 min tape pass. We initially planned four 6-hour observing periods, separated by a few weeks; in the end we had 4 observing epochs in October 2003, March and June 2004, providing a total of 27.5 hours of observing. At our first observing epoch we were also able to add the 76-m Jodrell Bank Lovell Telescope and the phased Westerbork Array, for the purpose of investigating short-baseline flux densities for some of the stronger FIRST sources.

From the outset we decided to make an un-biased selection from the FIRST catalogue, without regard to flux density, size or radio spectrum. Our motivation is not to identify "compact radio sources" but, rather, to make a *statistical* survey of the existence of compact structure in *all* source types. We thus calculated a notional right ascension for each 60 s observation and selected the first source in the FIRST catalogue with an RA greater than this within our declination strip, provided it had not been observed in a previous epoch. We also identified 11 VLBA calibrator sources within the strip. At each epoch these were substituted for the closest target sources selected.

There are 11,699 sources listed in White et al. (1997) within our declination strip. Excluding the calibrator sources, we scheduled 992 target sources (215+259+259+259) for our 4 observing epochs. However, there is often more than one FIRST source within the Arecibo beam (FWHM = 210″) and we are able to investigate a further ∼400 FIRST sources using multi-pass correlation.

3. Correlation and Fringe Detection

We are correlating these observations using the Mark IV correlator at the MPIfR in Bonn. As the tape-drives are equipped with only a single playback head it is necessary to make at least 2 correlation passes, one for each head (polarization). Further passes are needed to correlate other FIRST sources which are known to be within the same Arecibo beam of the target sources. Their response is necessarily attenuated by up to 0.7; note that as the Effelsberg FWHM beam width is much larger it is the Arecibo amplitude beam which is relevent. We use a correlator mode providing a pre-average time of 1 s and 128 delay steps per 8 MHz sideband (equivalent to 62.5 kHz frequency resolution). Correlation is inhibited under control of Effelsberg and Arecibo off-source flags. For

most sources, between 60 and 70 s of correlated data are recovered.

We use the Haystack HOPS package fringe-fitting program FOURFIT to search for a source response in the correlator output for each source. Source positions from the FIRST catalogue have accuracies of $\sim 1''$ or better. The delay and fringe-rate resolution of our observations are typically 170 mas in PA 20° and $2''$ in PA –50°, respectively. We can search using a range of delay and rate windows to optimise our detection threshold whilst taking into account possible instrumental and FIRST source position errors.

4. Preliminary Statistical Analysis

We present here a very preliminary analysis of results from our second epoch, observed on 22 March 2004 between UT 02h00 and 09h11. It represents only about a quarter of our sample, and uses a separate search in the LHC and RHC data, using conservative (wide) search windows and uncalibrated data. Some 7 of our 259 targets were lost due to a recording malfunction, resulting in a sub-sample of 252 sources.

A total of 71 (28%) of the 252 target sources were detected in either LHC or RHC correlations above a conservative threshold of 8-sigma, and at the expected residual fringe-rate and delay. Of these, 63 were detected in both polarizations. Note that the addition of the polarizations would result in detections above 11-sigma for these sources. For the sources detected in a single polarization the response in the other polarization was above 6.8-sigma in all cases. Analysis of the distribution of S/N-ratio for the detected sources suggests that at least a further 14 sources may be detected above 8-sigma in polarization-added data, bringing the detection rate to 33%.

We have also searched data from 86 other FIRST sources located within the target source beams. Some 11 sources were detected, in both polarizations. This lower fraction (13%) reflects signal attenuation away from the centre of the Arecibo beam.

We have investigated the detection rate as a function of the (peak) flux density listed in the FIRST catalogue. The parent distribution of flux densities in the FIRST catalogue (derived from our subsample of 1392 target or in-beam sources) has quartiles of 1.35, 2.24 and 5.42 mJy, and for the subsample of 252 sources observed here the values are similar: 1.41, 2.24 and 4.86 mJy. The numbers of sources detected in these ranges are 8, 19, 22 and 22. The median FIRST catalogue peak flux density of our detected sources is 3.37 mJy. 11 sources are in the range 1.0 to 1.5 mJy. Fringe detection plots for the 5 detections with lowest listed flux densities are presented in Figure 1.

5. Conclusions

It is, of course, premature to draw any definitive conclusions, but our preliminary analysis suggests that up to a third of all FIRST sources contain detectable compact structure at the mJy level. Note that long, thin structures—e.g. jets—may be missed in our observations if the structure is oriented along our resolution direction. Interestingly, the detection rate for sources $\geq$4.9 mJy is not significantly higher than that for weaker sources. Our 8-sigma single-polarization detection threshold corresponds to $\sim$1.1 mJy. For sources with true flux densities in the 1-2 mJy range, a detection implies that at least half of the total flux must reside in compact components. The fall-off in detection rate between 1.41 and 1.00 mJy may represent this fraction falling below our detection threshold, or may reflect source variability or increasingly large errors in the FIRST flux densities at the bottom of the survey. Once the data have been calibrated, a detailed investigation

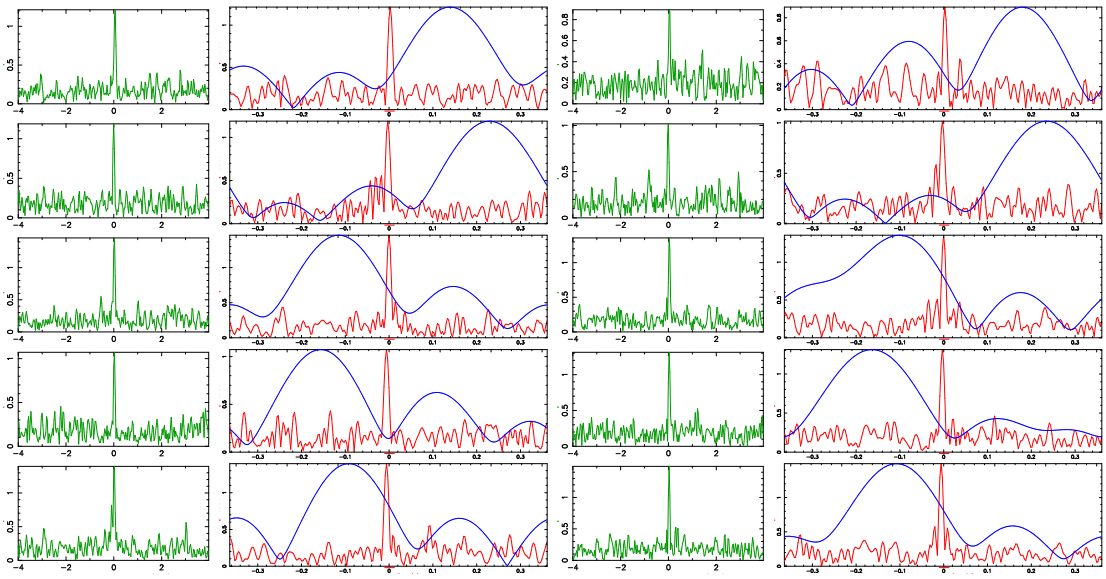

Figure 1. Residual single-band delay and fringe-rate functions for RHC polarization (left) and LHC polarization (right) for the 5 detected sources with the lowest listed flux densities in the FIRST catalogue (1.03, 1.11, 1.21, 1.27 and 1.28 mJy).

of the distribution of source visibilities will allow these effects to be investigated further.

6. Acknowledgements

We thank Dave Graham for assistance with observing at Effelsberg, Emmanuel Momjian for assistance at Arecibo, and 2 generations of Effelsberg and Arecibo schedulers, Rolf Schwartz, Alex Kraus, John Harmon and Hector Hernandez, for their patience in supporting this project.

References

[1] Becker, RH, White, R.L. & Helfand, D.J. 1995, Ap.J. 450, 559

[2] Garrington, S. T., Garrett, M. A. & Polatidis, A. 1999, New A.R. 43, 629

[3] Lawrence, C. R., Readhead, A. C. S., Linfield, R. P., Payne, D. G., Preston, R. A., Schilizzi, R. T., Porcas, R. W., Booth, R. S. & Burke, B. F. 1985, Ap.J. 296, 458

[4] Preston, R.A., Morabito, D. D., Williams, J.G., Faulkner, J., Jauncey, D. L. & Nicolson, G. 1985, A.J. 90, 1599

[5] White, R.L., Becker, R.H., Helfand, D. J. & Gregg, M.D. 1997, Ap.J. 475, 479

Anthony Searle: E3 Network Results, IVS 2006 General Meeting Proceedings, p.330–334
http://ivscc.gsfc.nasa.gov/publications/gm2006/searle1

E3 Network Results

Anthony Searle

Geodetic Survey Division/Natural Resources Canada
e-mail: asearle@nrcan.gc.ca

Abstract

For the past four years the Canadian Technology Development Center has been coordinating and analyzing the IVS-E3 network. The E3 network uses the S2 VLBI system at 6 stations worldwide and its sessions are correlated at the Dominion Radio Astronomical Observatory. Analysis of the E3 observations for EOP and TRF are presented. Experience with the network has allowed for the use of new approaches to operations. The future of the network is discussed with an eye towards VLBI2010.

1. IVS-E3 Network History

The IVS-E3 network is an international VLBI network designed to provide additional EOP data to the IVS time series, and add unique points to the VLBI determined TRF. The monthly sessions are observed with the S2 VLBI system. The S2, developed by the Canadian Technology Development Center, also offers a check for bias between other VLBI systems. The E3 network has been operating since March of 2002.

1.1. E3 Network and Observations

Because Earth orientation determination at the level of the R4 series is one of the goals of the E3 network, and the S2 correlator can handle six stations without repeat passes, the network has expanded to six stations. Algonquin Park, Kokee, Svetloe, TIGO-Concepcion, and the Canadian Transportable VLBI Antenna (CTVA) located in St. John's, Newfoundland participate in E3 sessions year round. In the North American summer, Yellowknife observes while the winter sessions were handled by Gilmore Creek. With the recent mothballing of the Gilmore Creek antenna the E3 sessions will be concentrated between June and September to maximize the EOP determination and the Yellowknife position. Table 1 summarizes the participation of each station in E3 sessions.

Table 1. E3 observations by station.

IVS Station	Number of E3 Sessions (Jan. 06)
ALOGPARK	44
CTVASTJ	31
GILCREEK	5
KOKEE	32
SVETLOE	18
TIGOCONC	35
YLOW7296	10

The stations provide good extent in North-South and East-West baselines; however half the stations used are intended to be mobile, so limited sensitivity is an obstacle to the E3 network. The S2-DAS operates at 128 Mbps, observing 18 channels with 16-MHz bandwidth using 2-bit sampling, but recording only 2 channels at any given time. To compensate for the smaller antennas the E3 network is heavily dependent on the larger dishes: Svetloe and Algonquin. Scheduling is modified to maximize the small dish inclusion with one of the two larger dishes, and maximizes the integration times for scans by recording all "on source" time, guaranteeing maximum integration times and SNR. Recording is done using a modified set of 8 VHS video cassette recorders.

2. E3 Analysis

To ensure the utility of the E3 data, regular global solutions are run at NRCan using CALC/SOLVE. Solutions for EOP, site and baseline repeatability, and terrestrial reference frame are determined.

2.1. Station Positions

Two types of solutions are run to examine the station positions as determined by the E3 network. The first computes a single station position and rate at a given epoch. To evaluate the effect of the E3 data, a solution is run with and without the E3 sessions, and position and velocity differences are compared. As would be expected the additional E3 data modestly reduces the uncertainty of E3 stations. The IVS TRF is aided by E3 observations, which make up all of the observing in St. John's and the majority of observations in Yellowknife. The second type of solution is to examine the station and baseline repeatabilities by solving station positions at every session. In these solutions a subset of stations is used to constrain the solutions to No-Net Rotation with regard to ITRF2000. The NNR constraint tends to reduce the scatter of some stations in small networks. Baseline lengths, however, are independent of rotation, and offer the method of comparison of position determination. Baseline repeatabilities of the E3 network results are compared to a small set of R1 and R4 baseline lengths involving similar stations in Figure 1.

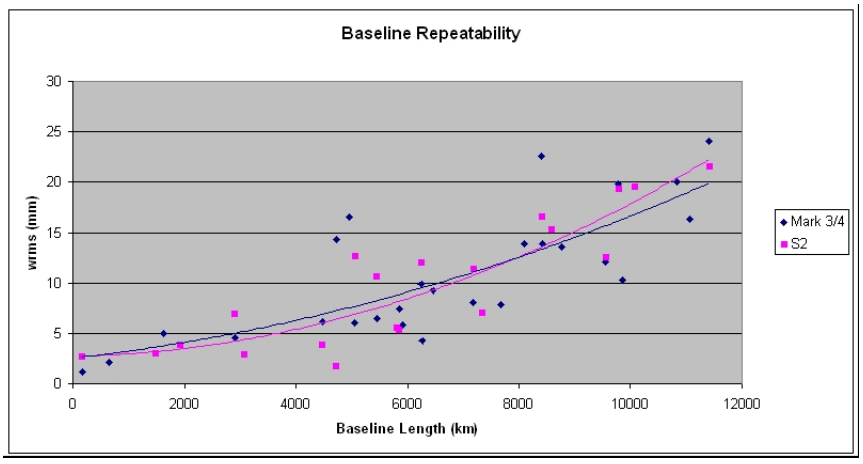

Figure 1. Baseline repeatabilities for E3 and R1/4 sessions

E3 baselines repeatability compares well with the standard IVS Rapid series, though the baseline repeatability tends to grow faster on longer baselines in the E3. This is due to having many mobile antennas throughout the network, which tends to increase scatter, especially on longer baselines. Similarly, repeatabilities for the E3 stations are regularly monitored against positions determined by the R1 and R4 sessions. E3 data shows slightly larger sigma values, but no bias compared to the more standard sessions.

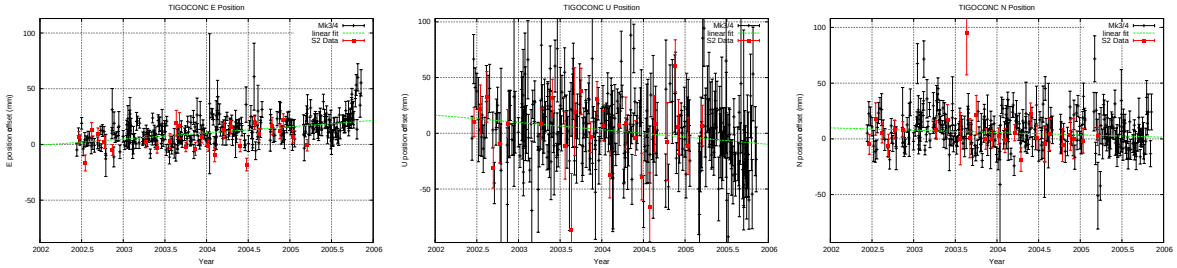

Tigo North Offset Tigo Up Offset Tigo East Offset

Figure 2. TIGOCONC position repeatability.

In Figure 2 there is no significant difference between the site positions determined with the S2 or Mark IV/5. This is typical of the E3 stations.

2.2. Earth Orientation Parameters

The goal of the E3 series is to provide additional EOP determinations to the IVS product. Though the network is small and sensitive to antenna loss, Earth orientation can be determined from most sessions. Following global solutions, the EOP determined from the IVS Rapid sessions and the E3 sessions are compared to the IERS C04 EOPs.

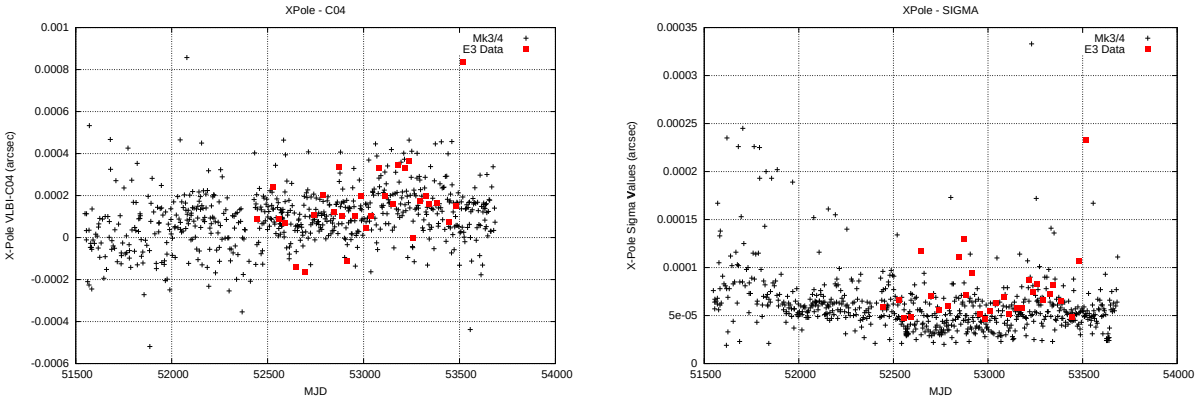

Compared to C04 Sigma Values

Figure 3. X-Pole Comparison

It can be seen that when all stations of the E3 network are operating, sigma levels are compara-

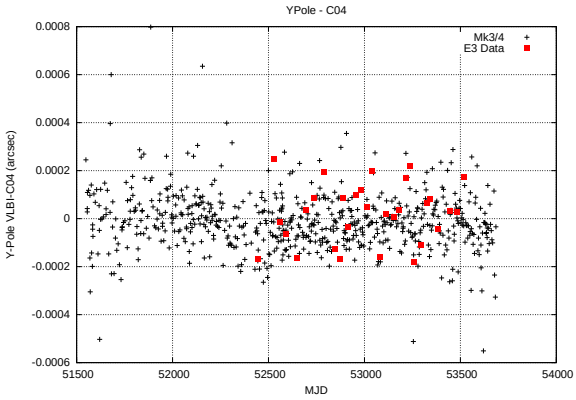

Compared to C04

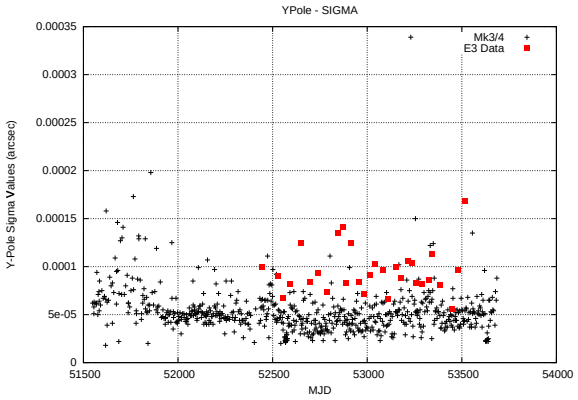

Sigma Values

Figure 4. Y-Pole Comparison

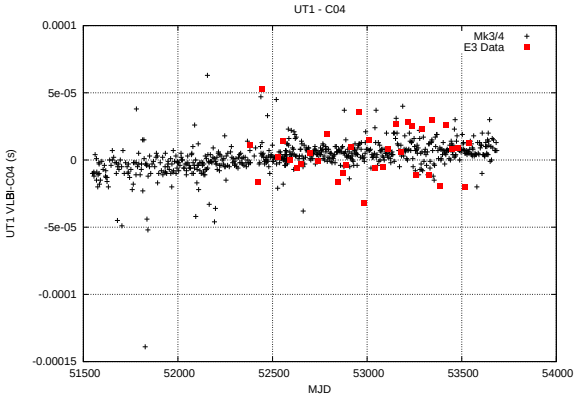

Compared to C04

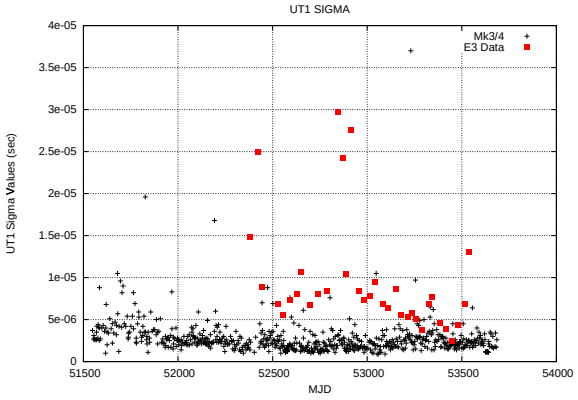

Sigma Values

Figure 5. UT comparison.

ble with the R4 series; however the E3 network is very sensitive to station failures. On average EOP uncertainties are 10-30 percent greater for the E3 network, but in sessions with 5 or 6 participating stations there is less than a 10 percent difference.

3. Future Plans

Recently, an XM terrestrial repeater was activated in St. John's and saturated the S-Band front end of the CTVA. As a result, it is hoped that the antenna will be relocated in 2006. As the S2 recorders age, both the correlator and stations have begun experiencing problems with the tape recorders. Preliminary development work has begun on a disk based replacement for the recording system. At the same time, NRCan has been granted a license for the NICT Software Correlator package which may provide support to our small correlator staff. Work continues to make observations as automated as possible, reducing the demand for observers. It is hoped that

some of the experiences in automation and equipment development are useful in the realization of the VLBI2010 vision.

4. Conclusions

The results of the E3 VLBI sessions have been presented and compared against routine IVS operations. It has been shown that when the network is fully operational it performs at a level comparable to the standard sessions. Inclusion of E3 data to VLBI determined TRF solutions will maintain the Yellowknife point and add a point at St. John's, Newfoundland. There are currently many obstacles facing the E3 network. Aging equipment, RFI, and human resources all pose challenges which will require innovative solutions which may aid in the realization of VLBI2010.

J. Cho et al.: A Generalized Scheme to Retrieve Wet Path Delays from WVR Measurements Applied to the European Geodetic VLBI Network, IVS 2006 General Meeting Proceedings, p.335–335
http://ivscc.gsfc.nasa.gov/publications/gm2006/cho

A Generalized Scheme to Retrieve Wet Path Delays from WVR Measurements Applied to the European Geodetic VLBI Network

J. Cho [1], *A. Nothnagel* [2], *A. L. Roy* [3], *R. Haas* [4]

[1)] *Korea Astronomy & Space Science Institute and Geodetic Institute, University of Bonn*

[2)] *Geodetic Institute, University of Bonn*

[3)] *Max-Plank Institute for Radio Astronomy*

[4)] *Onsala Space Observatory, Chalmers University of Technology*

Contact author: J. Cho, e-mail: jojh@kasi.re.kr

Abstract

A fluctuation in the water vapor in the atmosphere is one of the largest sources of error of ground-based space geodetic techniques using radio frequencies such as VLBI and GPS. A number of different water vapor radiometer (WVR) instruments are currently deployed for the determination of wet path delays (WPD) to be used as corrections for space geodetic techniques. Although a WVR is an ideal instrument for monitoring the water vapor content in the atmosphere, its benefits for geodetic VLBI have not been demonstrated yet. Site-dependent and frequency-dependent WPD retrieval problems still inhibit the routine use of these corrections. In this study we focused on whether one can find a reliable WPD retrieval scheme that can be applied to the several different microwave radiometers operated at four sites of the European geodetic VLBI network. To validate the WVR measured WPD, which is necessary before introducing the WPD into VLBI data processing, we have used several different WPD inversion methods and compared the resulting WPDs for each site. Finally we discussed a generalized scheme to extract valid WPDs from WVR data for most geodetic stations as a step towards the proposal in the VLBI2010 plan.

[Note from the Editors: The overheads of the oral presentation of this contribution can be downloaded from the IVS 2006 General Meeting web site. Please get the PDF file of the presentation at the URL ftp://ivscc.gsfc.nasa.gov/pub/general-meeting/2006/presentations/gm2006_6-07_cho.pdf.]

Christopher S. Jacobs et al.: Improving Astrometric VLBI by Using Water Vapor Radiometer Calibrations, IVS 2006 General Meeting Proceedings, p.336–340
http://ivscc.gsfc.nasa.gov/publications/gm2006/jacobs2

Improving Astrometric VLBI by Using Water Vapor Radiometer Calibrations

Christopher S. Jacobs, Stephen J. Keihm, Gabor E. Lanyi, Charles J. Naudet, Lance Riley, Alan B. Tanner

Jet Propulsion Laboratory

Contact author: Christopher S. Jacobs, e-mail: Christopher.S.Jacobs@jpl.nasa.gov

Abstract

Astrometric observations of distant active galactic nuclei (AGN) using the VLBI technique have been used to construct quasi-inertial global reference frames, most notably the International Celestial Reference Frame (ICRF) which now forms the basis for all astrometry including deep space navigation.

The accuracy of VLBI global astrometry has long been limited by systematic errors–notably path delay variations induced by stochastic spatial and temporal fluctuations in the distribution of atmospheric water vapor. In order to calibrate the water vapor induced path delay fluctuations, a pair of advanced design water vapor radiometers (A-WVR) have been built and deployed. We present intercontinental VLBI results calibrated with the A-WVRs showing a factor of 2.5 to 3 decrease in phase delay residuals over time scales of 10 to 1000 seconds. These results suggest that it may be possible to develop the next generation ICRF (at X/Ka-band) much more rapidly than previously estimated and that spacecraft navigation may be possible at sub-nanoradian levels of accuracy.

1. Introduction

Many studies have shown that astrometric applications of Very Long Baseline Interferometry (VLBI) often have their accuracy limited by systematic errors arising from tropospheric water vapor (e.g. Truehaft & Lanyi, 1987). One approach to this problem that has been pursued over the last several decades has been to calibrate the spatial and temporal fluctuations of atmospheric water vapor by measuring emissions from the 22 GHz rotational line of water.

2. The VLBI Observations

The results presented here are from two observing sessions done during the summer of 2004 using NASA's Deep Space Station (DSS) 26 in Goldstone, California and DSS 55 near Madrid, Spain to form an 8400 km interferometer baseline.

The first session was on Day-of-Year (DOY) 200 (18 July 2004) and the second session was on DOY 217 (4 August 2004). We recorded VLBI data simultaneously at X (8.4 GHz) and Ka-band (32 GHz) sampling each band at a rate of 64 Mbps. The data were sampled, digitally filtered and recorded to hard disk using the JPL designed VLBI Science Receivers (VSRs). The data were then played back over a network connection and correlated with the SOFTC software correlator (Lowe, 2006). Fringe fitting was done with the FIT fringe fitting software (Lowe, 1992). This procedure resulted in a phase delay measurement for each second of an hour-long scan. The observed elevations were moderate ranging from roughly 30 to 50 degrees. The table below indicates elevations at the start and stop of the scan on each of the two days for each of the two stations.

Table 1. Observations

Time	DSS 26	DSS 55
DOY/hh:mm	El (deg)	El (deg)
200/10:00	31.7	53.5
200/11:00	43.7	41.9
217/09:00	33.0	52.0
217/10:00	45.1	40.6

3. The Advanced WVR

The Advanced Water Vapor Radiometer (A-WVR), as shown in Figure 1, is a JPL designed and built microwave radiometer with observing bands at 22.2 GHz, 23.8 GHz and 31.4 GHz. Design highlights include a 1.5-meter offset parabolic antenna which provides a highly efficient 1 degree beam, and very high radiometric stability. Drifts in the radiometric calibrations are well below 0.01 Kelvin of brightness temperature on time scales of 10,000 seconds. Key to this stability is the non-cryogenic instrument enclosure which uses thermo-electric coolers to maintain an internal temperature of 35 $\pm$ 0.005 Celsius in all weather. In addition to the A-WVR, our atmospheric measurement suite also includes a Microwave Temperature Profiler (MTP) and surface metrology package which are used to better constrain the water vapor retrievals of the A-WVR. These are to the left of the A-WVR in Figure 1. A detailed description of the A-WVR system is given in Tanner & Riley (2003).

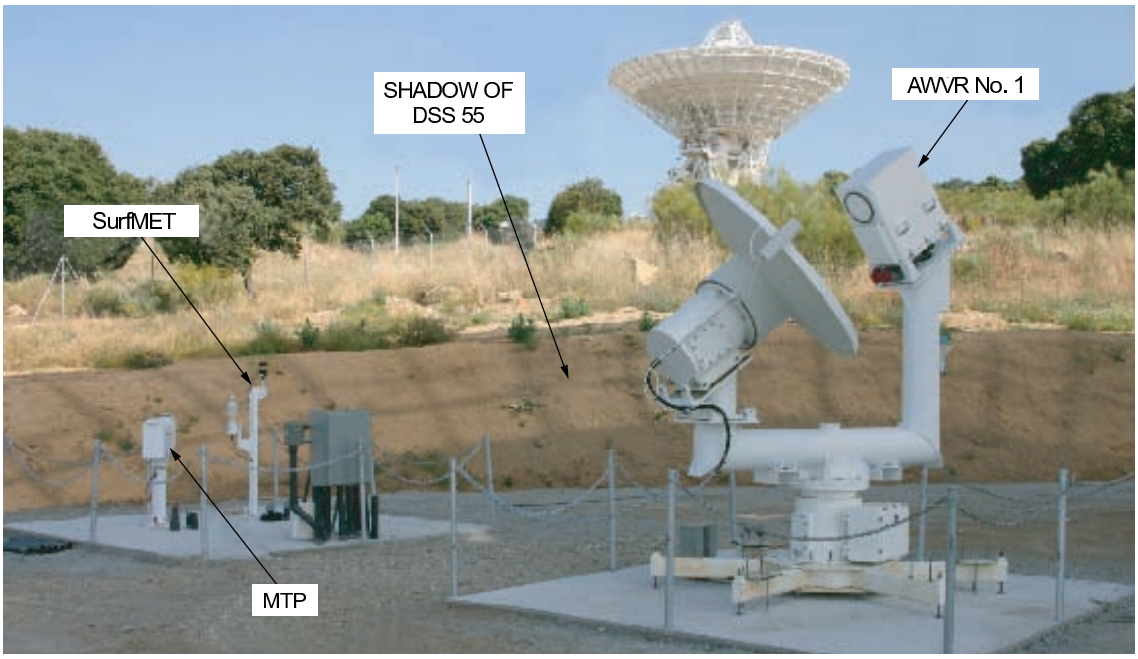

Figure 1. The Advanced Water Vapor Radiometer (A-WVR) instrument package deployed in Spain.

The Advanced WVR design improves several items relative to our previous generation of WVRs.

First, previous designs simple feedhorn was improved upon by adding the 1.5 meter clear aperture dish antenna. This narrowed the beam to about 1 degree from the feedhorns 7 deg beam. In parallel, the radiometer pointing knowledge was improved by an order of magnitude to +-0.05 deg. This resulted in an instrument that more nearly sampled the same spatial scales and direction as the VLBI antenna. Also, one may now observe much closer to the horizon before ground pickup through sidelobes becomes a problem. Second, as previously mentioned, the gain stability of the radiometer was improved. Third, the addition of a Microwave Temperature Profiler (MTP) allows empirical determination of the atmospheric temperature vs. altitude above the site during the measurements.

4. Results

The plots in Figure 2 show the VLBI phase residuals in black and the A-WVR wet troposphere delay in blue (dark gray). A quadratic term was estimated from the VLBI-AWVR differences in order to remove slowly changing systematic effects such as station location and nutation mismodeling. These plots clearly show a high correlation between the VLBI phase and the A-WVR troposphere calibrations. The improvement in residuals is a bit less than a factor of three. For example, the DOY 200 VLBI phase residuals improved from 3.4 mm down to 1.2 mm—a factor of 2.8 improvement. For scale, an 8.4 mm rotation of our 8400 km long interferometer represents 1 nano-radian or about 200 μasec.

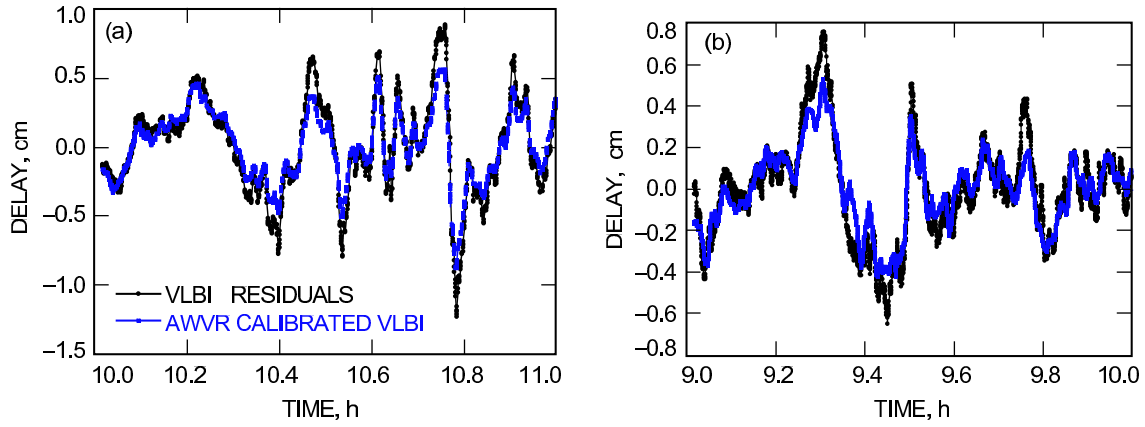

Figure 2. VLBI phase delay residuals (black) vs. A-WVR Calibrations (blue, dark gray).

In order to examine the range of time scales over which the VLBI residuals are being improved, we calculated the Allan standard deviation of the VLBI phases. Figure 3 shows the VLBI data before (red) and after the A-WVR calibration (green). The result shows a strong improvement on time scales of 10 to 1000 seconds. For times scales shorter than 10 seconds, we note that SNR considerations for the A-WVR measurement forced its shortest measurement integrations to be 10 seconds—thus the lack of significant improvement on times scales less than 10 seconds. The DOY 200 and 217 experiments only lasted 3600 seconds thus limiting our ability to examine the quality of calibrations on time scales much longer than 1000 seconds. Longer data arcs will have to be acquired before we can evaluate the quality of calibrations on time scales of 10,000 seconds to a day which are also of interest to global VLBI astrometry.

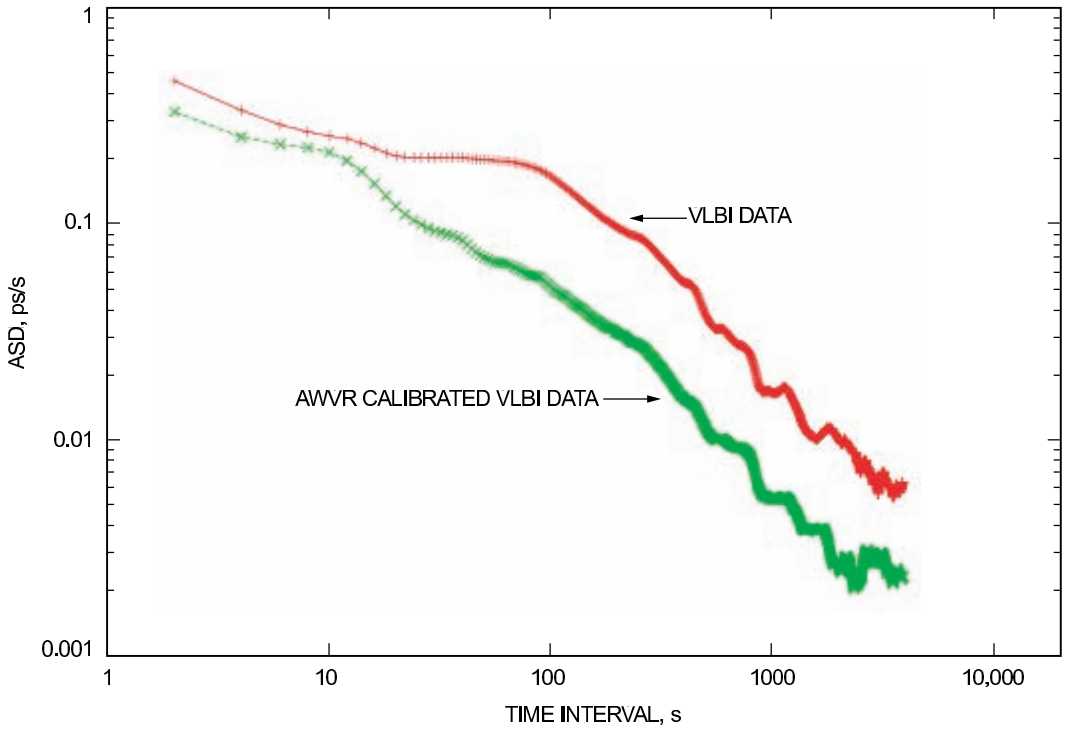

Figure 3. Allan Deviation of VLBI phase with and without A-WVR calibrations.

5. Areas for Further Study and Conclusions

The results shown represent a work in progress. There is a suggestion in the data that the A-WVR does not track some sharp peaks in the VLBI phase. This has not yet been carefully studied. The wider beam of the A-WVR (1 deg) relative to the VLBI antenna (0.02 deg at Ka-band, 32 GHz) and the spatial offset of the two instruments (of order 100 meters) are potential contributors to this effect.

We also note that these tests probed only time scales on the order of 10 to 1000 seconds. Because global VLBI experiments often last for 24 hours, one would like to demonstrate that the A-WVR calibrations reduce VLBI residuals on time scales as long as a day (~100,000 sec). Furthermore, these measurements represent one continuous track of a single natural radio source as it moves slowly across the sky. We have not yet demonstrated that the dramatic improvements seen in our data can be sustained in a typical global astrometry scenario in which the target radio source is changed every few minutes to a different part of the sky.

However, if the improvements that our limited data show can be sustained in more challenging global astrometry scenarios then the benefit would be dramatic. A threefold improvement in residuals would mean that A-WVR calibrated data would carry almost ten times the weight of un-calibrated data in a least squares fit. This could dramatically reduce the amount of time needed to develop an X/Ka-band (8.4/32 GHz) celestial reference frame for applications such as spacecraft tracking. For actual spacecraft tracking sessions, the application of A-WVR calibrations has the potential to help enable a factor of 2-3 improvement in spacecraft tracking accuracy.

Acknowledgements

The research described in this paper was performed at the Jet Propulsion Laboratory of the California Institute of Technology, under a contract with the National Aeronautics and Space Administration.

References

[1] Lowe, S. T., 'Theory of Post-BlockII VLBI Observable Extraction', JPL Publication 92-7, JPL, Pasadena, CA, 15 Jul 1992.

[2] Lowe, S. T., 'SOFTC: A Software VLBI Correlator', JPL, Pasadena, CA, in preparation, 2006.

[3] Tanner, A. B., and A. L. Riley (2003), 'Design and performance of a high-stability water vapor radiometer', Radio Science, 38(3), 8050, doi:10.1029/2002RS002673.

[4] Treuhaft, R. N., and G. E. Lanyi, 'The Effect of the Dynamic Wet Troposphere on Radio Interferometer Measurements', Radio Science, vol 22, pp. 251-265, March-April 1987.

Robert Heinkelmann et al.: Combination of Long-term Time Series of Tropospheric Parameters Observed by VLBI, IVS 2006 General Meeting Proceedings, p.341–343
http://ivscc.gsfc.nasa.gov/publications/gm2006/heinkelmann1

Combination of Long-term Time Series of Tropospheric Parameters Observed by VLBI

Robert Heinkelmann, Johannes Boehm, Harald Schuh

Institute of Geodesy and Geophysics/University of Technology, Vienna
Contact author: Robert Heinkelmann, e-mail: rob@mars.hg.tuwien.ac.at

Abstract

The long-term time series of wet zenith delays from five IVS Analysis Centers (AC) are combined on the level of results. Outliers are eliminated by robust outlier detection and weights are determined by variance component estimation. That is done for each AC series of each station. In this paper the method of combination is described briefly.

1. Combination Method

Within the IVS (International VLBI Service for Geodesy and Astrometry) five IVS Analysis Centers (AC) (see Table 1) send their long-term time series of tropospheric parameters including formal errors to the Institute of Geodesy and Geophysics (IGG), Vienna for comparison and combination. The requirements for the individual parameters are minimal: zenith delays and gradients have to be provided at integer hours and the time resolution of the zenith delays has to be one hour. For the combination the solutions are considered being independent, i.e. correlations between them are assumed to be zero. The long-term time series are combined by a three step procedure.

Table 1. ACs contributing to the IVS combined long-term time series of tropospheric parameters

BKG	Bundesamt fuer Kartographie und Geodaesie, Frankfurt a.M., Germany
GSF	Goddard Space Flight Center, Greenbelt, USA
IAA	Institute of Applied Astronomy, St. Petersburg, Russia
IGG	Institute of Geodesy and Geophysics, Vienna, Austria
MAO	Main Astronomical Observatory, National Academy of Sciences, Kiev, Ukraina

1.1. Data Editing

At first, basic checks are performed and outliers are eliminated. Then, each time series of zenith delays is modeled by a trend and seasonal components. The amplitudes and phases of the annual and semi-annual variations are determined by least-squares estimation. The outlier detection is achieved by the BIBER algorithm (Wicki, 1999, [5]). In each step of this iterative algorithm one observation, the observation with the biggest standardized residuum, is considered to be an outlier. If its standardized residuum exceeds an empirically determined treshold[1] the observation will be

[1] The treshold is set to 3.

downweighted in such a way that it just fulfills the criteria to be not an outlier any more. After this procedure the residuals fit the assumption of the normal distribution, a requirement for the variance component estimation.

1.2. Determination of Weights

A common observation vector is built up from the observations of the ACs with the mean values shifted to the common mean value. The formal errors reported by the ACs are considered, too, after their mean values were brought on a common level. They form a common diagonal covariance matrix. The variance components, additional unknowns in the linear Gauss-Markov model, are iteratively estimated with the method of Foerstner (1979, [1]) as described in Koch (1999, [3]).

1.3. Computation of the Combined Series

For each station the combined series is obtained by the sum of the weighted observations of the individual ACs. More details can be found on the web site of this IVS product [4].

2. Conclusions and Outlook

The combined tropospheric parameter series are more reliable than a single solution and can be used as a reference for any kind of comparisons, e.g. with other techniques, and for climate studies. There is a discrepancy between the formal errors of the combined solution and the deviations between contributing individual solutions, what shows that the formal errors of the combined series are too optimistic. Before a rigorous combination of the tropospheric parameters, i.e. on the level of normal equations, stricter requirements for the parameter model, the epochs, and the formal errors have to be followed. In addition, the various constraints on the tropospheric parameters should be avoided or reported together with the parameters in the SINEX file, to enable their removal before the combination process.

3. Acknowledgements

Thanks to the IVS and its member institutions. In particular we are grateful to the analysis groups mentioned in Table 1 for providing their results for the combination done at IGG, Vienna. Project P16992-N10, VLBI for climate studies, is funded by the Austrian Science Fund (FWF).

References

[1] Foerstner W.: Ein Verfahren zur Schaetzung von Varianz- und Kovarianzkomponenten. AVN 11-12, 446-453, 1979

[2] Heinkelmann R., J. Boehm, H. Schuh: IVS long-term series of Tropospheric Parameters. In: Vennebusch M., Nothnagel A. (Eds.): Proceedings of the 17^{th} Working Meeting on European VLBI for Geodesy and Astrometry, held at Noto, Italy, 69-73, 2005

[3] Koch K. R.: Parameter Estimation and Hypothesis Testing in Linear Models. Springer Berlin, New York, 1999

[4] http://mars.hg.tuwien.ac.at/~ivstrop/longtimeseries.html

[5] Wicki F.: Robuste Schaetzverfahren fuer die Parameterschaetzung in geodaetischen Netzen. Mitteilungen des Instituts fuer Geodaesie und Photogrammetrie an der ETH Zuerich, Nr. 67, Zuerich, 1999

Thomas Hobiger et al.: VLBI as a Tool to Probe the Ionosphere, IVS 2006 General Meeting Proceedings, p.344–348
http://ivscc.gsfc.nasa.gov/publications/gm2006/hobiger1

VLBI as a Tool to Probe the Ionosphere

Thomas Hobiger [1], *Tetsuro Kondo* [2], *Harald Schuh* [1]

[1)] *Institute of Geodesy and Geophysics, Vienna University of Technology*

[2)] *Kashima Space Research Center, National Institute of Information and Communications Technology*

Contact author: Thomas Hobiger, e-mail: thobiger@mars.hg.tuwien.ac.at

Abstract

By a method, developed within project VLBIonos[1] at the IGG, Vienna it is possible to estimate ionospheric parameters in terms of vertical total electron content from VLBI data without any external information (Hobiger et al., 2006, [2]). This paper deals with the results from this approach and cross-validates them against GPS, satellite altimetry data and measurements of solar flux. As geodetic VLBI observations cover more than two complete solar cycles, longer than all other space geodetic techniques using radio signals, the relation to space weather indices on long time-scales can be shown. It can be stated that the overall agreement between VLBI and GPS is within the formal error of each technique and that both systems detect the same periods of ionospheric variations.

1. Ionospheric Parameters from VLBI

It is possible to derive absolute values of vertical total electron content (VTEC) for each station from VLBI data. A description of the estimation strategy can be found in Hobiger (2005, [1]) and Hobiger et al. (2006, [2]). Applying such a method to the whole database of geodetic VLBI observations enables us to study long-term trends of the ionosphere such as the solar cycle of about 10.5 years.

2. Comparison to GPS

Figure 1 shows the results of the estimated vertical total electron content values for station Wettzell (Germany) using all available 24 hours VLBI experiments. As for the analysis only sessions with a duration of 24 hours or more were selected, daily mean VTEC values can be computed (Figure 2), which clearly reveal the annual variation of the ionosphere. For a cross-technique validation of our results with GPS, the VTEC values for station Wettzell were computed from global ionosphere models, provided by the Astronomical Institute of the Univ. Berne[2]. Figure 3 shows a histogram of the differences (GPS minus VLBI) for station Wettzell, with a mean bias of +0.5 TECU and a standard deviation of 4 TECU. Small biases between the techniques can be explained by contributions from the plasmasphere and by mapping function mis-modelling (Hobiger, 2005, [1]). In order to reveal the spectral characteristics wavelet scalograms were computed for each technique and compared against each other. The upper plot of Figure 4 presents the wavelet scalogram of the VLBI time-series for station Wettzell and the lower plot shows the corresponding one from the (shorter) GPS series. Annual and semi-annual signals are detected by both techniques, and the good overall agreement is confirmed by the cross-scalogram (Figure 5). Normalized wavelet

[1] http://iono1.hg.tuwien.ac.at/

[2] Center for Orbit Determination in Europe (CODE), AIUB, http://www.aiub.unibe.ch/ionosphere.html

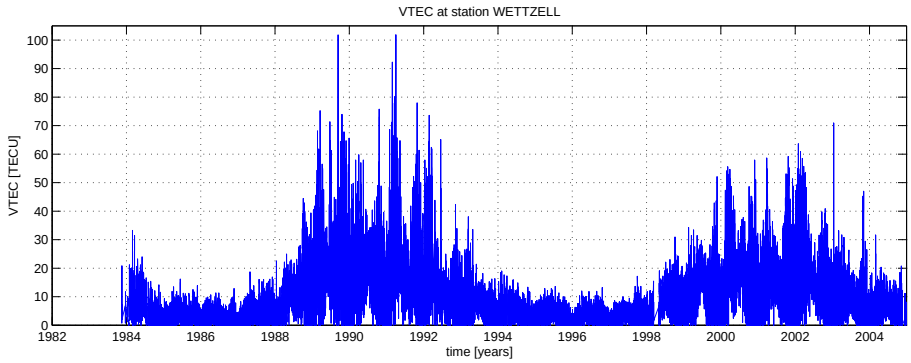

Figure 1. VTEC at station Wettzell (Germany) from VLBI

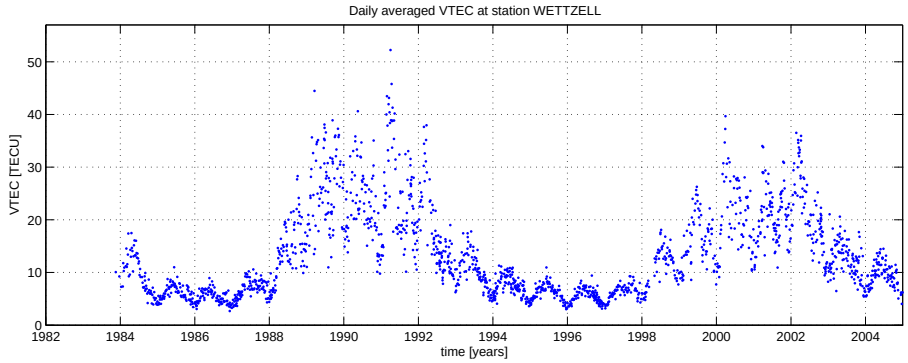

Figure 2. Daily mean values of VTEC at station Wettzell (Germany) from VLBI

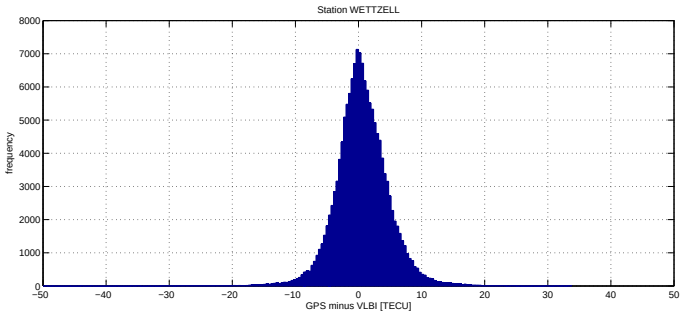

Figure 3. Differences of VTEC at station Wettzell (Germany) between GPS and VLBI

coherency (left part of Figure 5) is close to one for periods longer than 100 days, and always bigger than 0.7, which demonstrates that both techniques are able to detect the same periods in the range of 10 days to 2 years.

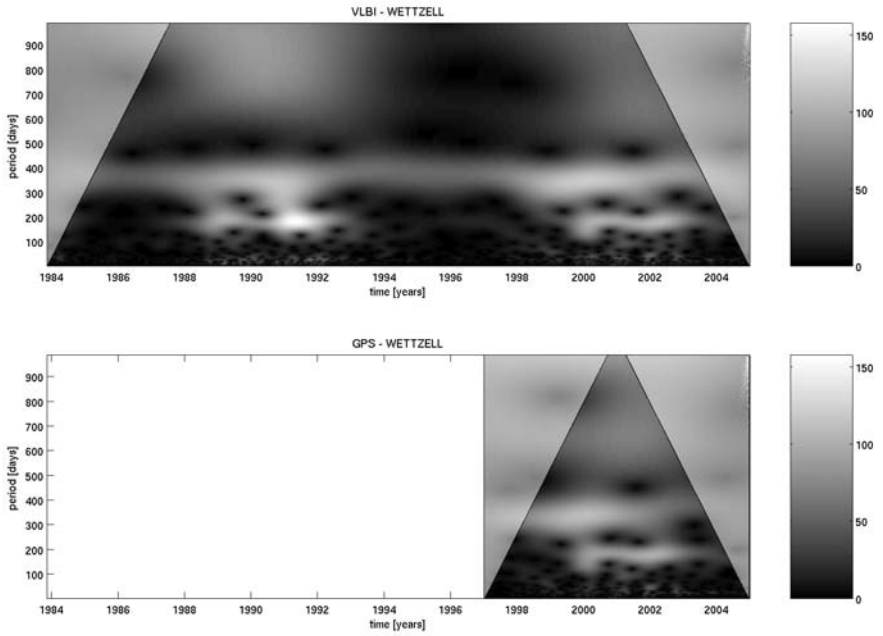

Figure 4. Wavelet spectra of VLBI and GPS (both Wettzell)

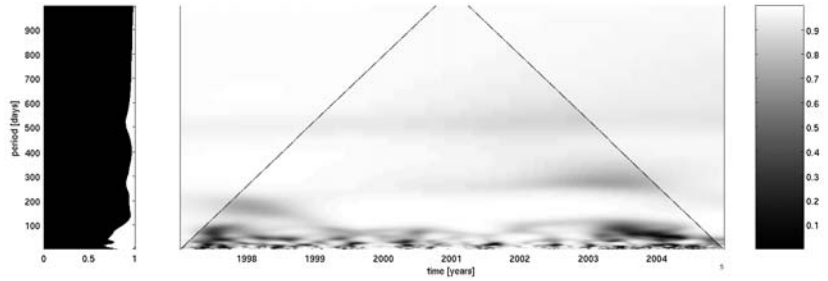

Figure 5. Quadratic cross-scalogram (right) and normalized Wavelet coherency (left) at station Wettzell

3. Correlations with Solar Flux

Solar flux at 10.7 cm^3 was compared with the VTEC time-series of VLBI and GPS at station Wettzell. The Fourier spectra of each series were computed using the CLEAN algorithm (Baisch and Bokelmann, 1999, [3]) and the results are displayed in Figure 6. The diurnal, semi-annual and annual signals can be seen from the results of VLBI and GPS. But only VLBI is able to exactly reveal the signal of the solar cycle with a period length of 10.5 years. Additionally, correlation coefficients between solar flux and a reduced (i.e. annual and semi-annual signals removed) mean

[3]Space Physics Interactive Data Resource, National Oceanic & Atmospheric Administration (NOAA), http://spidr.ngdc.noaa.gov/spidr/

VLBI VTEC time series were computed for time lags between -10 and 10 days (Figure 7). Maximum correlation is found for a time lag of 2-3 days, which is equal to the travelling time caused by a coronal mass ejection with a speed of 500-600 km/s (Lara et al., 2003, [4]).

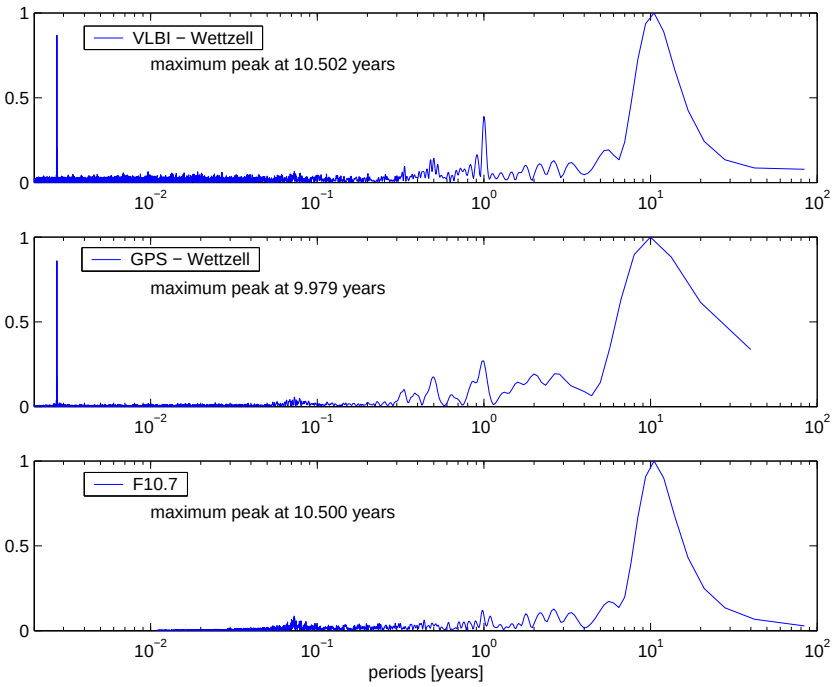

Figure 6. CLEANed spectra of VLBI and GPS (both Wettzell) and F10.7

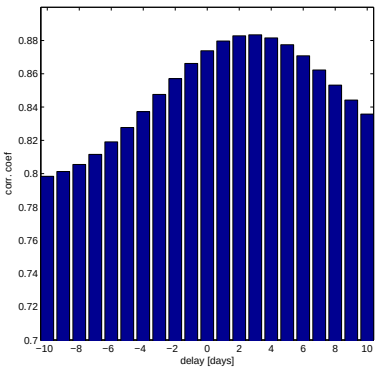

Figure 7. Correlation coefficient between reduced mean VTEC and solar flux (F10.7) for several time lags

4. Comparison with Satellite Altimetry Data

VLBI station Kokee Park located on Hawaii was selected for a comparison with VTEC values, which were obtained from satellite altimetry data. Data were taken for comparison, when the

footprints of JASON-1 and TOPEX/POSEIDON satellites were within a radius of 0.5 degree from Kokee Park. The measured VTEC values from each satellite were compared to the VLBI results (Figures 8 and 9), revealing a small overall bias of +1.2 TECU in the differences (JASON-1 or TOPEX/POSEIDON minus VLBI) and a standard deviation of about 9.0 TECU.

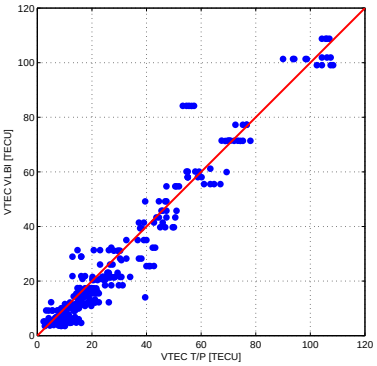

Figure 8. VTEC values of TOPEX/POSEIDON vs. VLBI

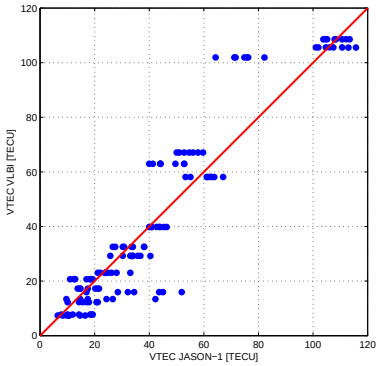

Figure 9. VTEC values of JASON-1 vs. VLBI

5. Summary and Outlook

It was shown that ionospheric parameters computed from VLBI data agree well with results from GPS and satellite altimetry missions. The relation to solar activity was verified and it was pointed out that VLBI is still the only space geodetic technique which can contribute to precise long term studies of the ionosphere as it covers two complete solar cycles, i.e. more than 20 years. VTEC values from VLBI can be used for validation purposes of existing ionosphere models or can be incorporated into global models representing the ionosphere in space and time.

6. Acknowledgements

The authors want to thank the Austrian Science Fund (FWF, project P16136-N06) and the Japanese Society for the Promotion of Science, JSPS (project PE 04023) for supporting this work.

References

[1] Hobiger, T., VLBI as a tool to probe the ionosphere, PhD thesis, Vienna Univ. of Technology, 2005

[2] Hobiger, T., T. Kondo, H. Schuh (2006), Very long baseline interferometry as a tool to probe the ionosphere, Radio Sci., 41, doi:10.1029/2005RS003297.

[3] Baisch, S., G.H.R. Bokelmann, Spectral analysis with incomplete time series: an example from seismology, Computers & Geosciences, Vol. 25, 1999

[4] Lara, A., N. Gopalswamy, S. Nunes, G. Munoz, S. Yashiro, A statistical study of CMEs associated with metric type II bursts, Geophysical Research Letters, Vol. 30, Nr. 12, 2003

Thomas Hobiger et al.: Detection of Short Period Ionosphere Variations from VLBI Fringe Phases, IVS 2006 General Meeting Proceedings, p.349–350
http://ivscc.gsfc.nasa.gov/publications/gm2006/hobiger2

Detection of Short Period Ionosphere Variations from VLBI Fringe Phases

Thomas Hobiger [1], *Tetsuro Kondo* [2], *Kazuhiro Takashima* [3], *Harald Schuh* [1]

[1)] *Institute of Geodesy and Geophysics, Vienna University of Technology*
[2)] *Kashima Space Research Center, National Institute of Information and Communications Technology*
[3)] *Geographical Survey Institute*

Contact author: Thomas Hobiger, e-mail: thobiger@mars.hg.tuwien.ac.at

Abstract

The usage of fringe phase information from VLBI measurements is a new and challenging field of research, which can be utilized for the detection of short period variations (scintillations) of the ionosphere. A method for the extraction of such disturbances has been developed and it is discussed how dispersive influences can be separated from intra-scan delay variations. It is shown that a short period variation can be detected very precisely, if the SNR is high enough. Physical origins of such disturbances are discussed and fields of application will be mentioned. This paper is an extended abstract of the paper Hobiger et al. (2006, [1]).

1. Introduction

The correlator integrates the observation data, utilizing a-priori values of delay and delay rate, and splits the data into time blocks of a few seconds duration. Usually, post-correlation analyses corrects discrepancies between a-priori values and actual delay and delay rate. But the correlator output (i.e. fringe phase and correlation amplitude for each accumulation period) can be taken directly for studies of delay changes if phases can be connected within each channel. Thus, dispersive delay effects (assigned to ionosphere variations) can be separated from delay changes, when fringe phase information from several channels is used.

2. Functional and Stochastic Model

The fringe phase $\phi_i(t)$ of channel i can be split up into

- a residual delay $\Delta\tau(t)$, i.e. the difference between the theoretical delay, computed from a polynomial of higher order, and the measured delay from single-band delay search,
- an ionospheric contribution, proportional to the difference of the ionosphere conditions between both stations, expressed by $\Delta STEC(t)$,
- a phase offset $\hat{\phi}_i$, which is aligned within bandwidth synthesis by applying the phase-cal signals,
- a random error ϵ caused by the electronics of the receiving system.

Therefore,

$$\phi_i(t) = 2\pi f_i \Delta\tau(t) - 2\pi \frac{40.28}{f_i} \Delta STEC(t) + \hat{\phi}_i + \epsilon \qquad (1)$$

where f_i is the RF frequency of channel i. When only using single channel data it is impossible to separate ionosphere contributions from delay changes. But, if fringe phases can be computed for individual channels, it will become possible to distinguish the effects as they are scaled by the corresponding channel frequency. The phase offset $\hat{\phi}_i$ can be determined together with the other unknowns (i.e. parameters describing $\Delta\tau(t)$ and $\Delta STEC(t)$) in the adjustment process. The standard deviation of phase measurements is inversely proportional to their signal to noise ratio (SNR). Therefore the weight matrix used within the adjustment process is given by

$$P_{nm} = \begin{cases} SNR_{nm}^2 & (n = m) \\ \\ 0 & (n \neq n) \end{cases} . \tag{2}$$

3. Possible Fields of Application and Requisites

VLBI is able to detect even smallest variations of the ionosphere with a high time resolution as the sampling rate of fringe phases is equal to the parameter period length (here two seconds). Strong radio sources are necessary to ensure high signal to noise ratio in order to enable phase connection and/or phase unwrapping. If this is guaranteed and if the scan is long enough it should be principally possible to detect all TEC variations of the ionosphere. Therefore one can think of the following application fields:

- Detection of traveling ionospheric disturbances (TIDs).
- Detection of plasma bubbles.
- Monitoring diurnal TEC variations with high precision by special experiments.
- Detection of ionospheric disturbances caused by earthquakes, tsunamis or rocket launches.
- Demonstrating the different reactions of the ionosphere to solar excitations and geomagnetic disturbances.

Besides ionospheric tasks the proposed method gives also a basis for handling intra-scan delay variations and providing phase delay information for geodetic/astrometric purposes or for navigation of spacecrafts.

References

[1] Hobiger, T., T. Kondo, K. Takashima, H. Schuh (2006), Utilizing VLBI fringe phase information for ionospheric studies, submitted to Journal of Geodesy, 2006

Bong Won Sohn et al.: Simultaneous Dual Frequency VLBI Observation Using VERA, IVS 2006 General Meeting Proceedings, p.351–355
http://ivscc.gsfc.nasa.gov/publications/gm2006/sohn

Simultaneous Dual Frequency VLBI Observation Using VERA

Bong Won Sohn [1], *Tae Hyun Jung* [1], *Hideyuki Kobayashi* [2], *Tetsuo Sasao* [1], *Tomoya Hirota* [2], *Osamu Kameya* [2], *Yoon Kyung Choi* [2], *Hyun Soo Chung* [1], *Hyun Goo Kim* [1]

[1)] *Korea Astronomy & Space Science Institute*

[2)] *National Astronomical Observatory of Japan*

Contact author: Bong Won Sohn, e-mail: bwsohn@kasi.re.kr

Abstract

We report the first simultaneous dual beam, dual frequency VLBI experiment using VLBI Exploration Radio Astronomy (VERA). The aim of this experiment is to demonstrate the feasibility of the simultaneous multi-frequency phase referencing using VERA and the upcoming Korean VLBI Network (KVN). This multi-frequency phase referencing is based on the idea that the differential atmospheric phase delay is mainly caused by the differential water-vapor-induced excess path length in the troposphere. The technique takes advantage of the non-dispersive nature of the water-vapor-induced phase delay. Our VERA observation was conducted on 15th April 2005 between 14:15 and 21:30 (UT). At 22GHz (Beam A), NRAO512 and at 43GHz (Beam B), a bright quasar 3C345, which is only 0.5 degree apart from NRAO512, were observed simultaneously. Different from the conventional frequency switching phase referencing observation, radio signals from two quasars were recorded simultaneously. This simultaneous observation ensures that the phase delay solution interval problem, which could be severe in the conventinal method, does not exist in our case.

1. Introduction

In the high radio frequency VLBI observation, it is well known that the long-term phase noise, typically of time scales longer than several seconds, is dominated by the tropospheric fluctuation, more precisely of water-vapor content(Rogers et al. 1984; Asaki et al. 1996; Sasao 2003). Since this fluctuation has non-dispersive nature, i.e. $\propto \nu$, it is a serious hindrance of the high frequency VLBI observation. In order to get rid of this hindrance, various phase referencing techniques are suggested. The basic idea behind the various phase referencing techniques is literally to refer to the phase of another (stronger) source(s). At mm wavelength, the phase variation due to the fluctuation is often so extreme that the phase changes more than π radian in a few tens of seconds (e.g. in Fig. 1). That means the target source and the phase reference source should be observed at the same time for effective phase referencing. VLBI Exploration Radio Astronomy (VERA) is the VLBI facility dedicated to high accuracy astrometry ($\sim 10\mu$arcsec) adopting the simultaneous phase referencing (Kobayashi et al. 2003). VERA has a unique dual beam system for simultaneous phase referencing (Kawaguchi et al. 2000). The phase referencing feasibility of VERA is well demonstrated by Honma et al. (2003) at 22GHz.

The aim of this experiment is to test and to demonstrate the feasiblilty of the simultaenous multi-frequency phase referencing using VERA. The experiment is designed to demonstrate that VERA could do 'phase reference', not only between two sources at the same frequencies, e.g. at 22GHz ('single-dual'), but that it is also feasible between two sources at two different frequency such as 22GHz and 43GHz ('double-dual'). At higher frequency, in general, the receiver performance

becomes worse, the aforementioned atmospheric fluctuation increases with $\propto \nu$, and the source flux decreases. These altogether lead to a rapidly decreasing number of the possible phase reference sources at mm wavelength. Therefore phase referencing to a lower frequency is of general interest for mm VLBI research. For that reason, the frequency switching phase referencing is tested (e.g. Middelberg et al. 2005). However, considering the rapid phase change at mm wavelength, the simultaneous observation, such as this 'double-dual', is favorable.

2. Korean VLBI Network

KVN is the first VLBI facility in Korea and is the first dedicated mm VLBI facility in the world. KVN is designed for simultaneous multi-frequency observation (Minh et al. 2003; Kim et al. 2004). Using the simultaneous, multi-frequency phase referencing, KVN is expected to provide precise astrometric information at wide radio frequency range, from 22GHz up to 129GHz (Minh et al. 2003; Kim et al. 2004). The precise positional information of celestial objects at wide range of radio frequency is invaluable in various astrophysical and also in interdisciplinary contexts (e.g. Lobanov 1998; Philips et al. 2003; Schlueter & Vandenberg 2003; Middelberg et al. 2005). This and another important goal, sensitive multi-band VLBI imaging through long integration time, will be done by simultaneous multi-frequency observation. At mm wavelength, due to the known limitations (Section 1), the multi-frequency phase referencing (i.e. self-phase referencing) seems to be more promising than the other methods (Sasao 2003). The KVN beam transporting system employs frequency selective surface lowpass filters (LPFs) (Kim et al. 2004 and reference therein). KVN is under construction and plans to begin its test observation in 2007/08.

3. Observation

The VERA observation was done on 15th April 2005 [UT 14:15-21:30]. The 'double-dual' mode was configured as below. With the beam A we observed NRAO512 at 22GHz, a bright BL Lac object. With the beam B at 43GHz, an even brighter quasar 3C345, which is only 0.5 degree apart from NRAO512, was observed simultaneously. 128MHz broadband mode with 250KHz channel width (512 channels) was taken and single LL circular polarization mode was used. At each station, data was recorded on tapes and delivered to Mitaka correlation center of National Astronomical Observatory, Japan.

4. Data Reduction

After the instrumental phase calibration, the residual phase delay solutions were obtained. At the shortest baseline, Mizusawa-Iriki baseline, the solutions are most stable (Fig. 1). At the longer baselines, e.g. Miz.-Ogasawara, Miz.-Ishigaki, the phases change more rapidly. In order to test the feasibility of the phase transfer between two frequencies, the correlation coefficients were estimated. It was done at the time range where the phase changes are rather moderate. The correlation coefficients with various solution intervals, i.e. 20/30/60 seconds, are compared. High positive values are obtained from Miz.-Iri. & Miz.-Oga. baselines (> 0.9). At the longest baseline, Miz-Ish., weak anti-correlation is seen. This is due to n*pi ambiguity in the phase solutions. It increases with baseline length and with water vapor in the atmosphere. It is clearly shown that , n*pi ambiguity should be removed for successful phase transfer and for long integration time.

Fig. 2 and Fig. 3 show the trial n*pi ambiguity free phase soluion at 22 & 43GHz. Long-term, $\gg$ atmospheric coherence time, phase residual which is proportional to frequency is seen. It could be due to the error in the tracking-center psotions or the error in the station position (Honma et al. 2003). The analysis to remove this residual is being done. Together with the final phase referencing result, it will be presented elsewhere.

5. Atmospheric Phase Delay

The tropospheric excess path delay is largely non-dispersive over a wide range of radio frequencies. Asaki et al. (1998) demonstrate mm (146GHz) phase delay compensation through cm (19.5GHz) phase reference source with Pair-Antenna-Method; they observe two sources simultaneously at two frequencies. The Middelberg et al.(2005) experiment shows the feasibility of the 'fast frequency switching' method (14.5GHz & 86GHz); a source is observed at two frequencies in sequence. Though their methods could be argued to deliver spatially or timely incoherent phase compensation solutions, they could prove the non-dispersive nature of the path length delay and prove that sensitive mm VLBI imaging is achievable with multi-frequency phase referencing method (Asaki 1998; Middelberg et al. 2005). For astrometric purposes, however, the ionospheric phase delay which has dispersive nature, should be corrected (Middelberg et al. 2005), too. This correction has been done through GPS measured Total Electron Content (TEC), so far. Since the GPS signals do not come from the target source direction and GPS data are spatially very sparsely sampled, the modeled ionosphere is often not accurate enough for astrometric purposes. A more precise determination of the ionospheric influence can be obtained, if the group delay is obtained from the source direction at lower radio frequency. Further experiments including this idea will be made.

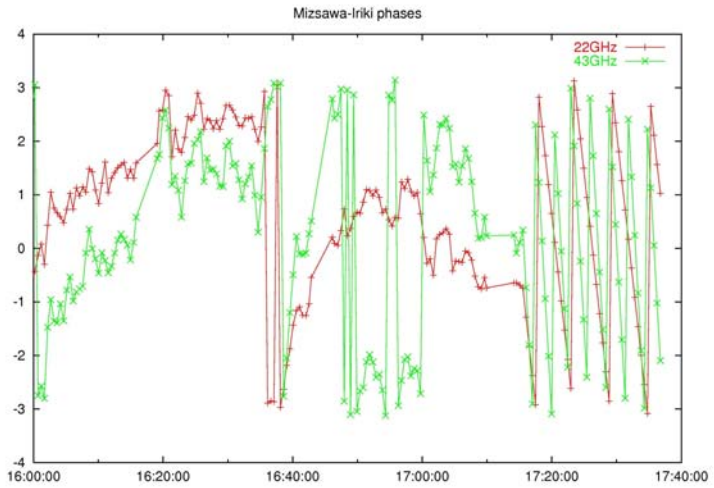

Figure 1. Phase solution of the first half of the observation after the instrumental calibration. Faster phase at 43GHz is visible. The faster phase rotation brings 2π ambiguity of 43GHz in the given time range. The phase rotation of the last 20 minutes is an artifact.

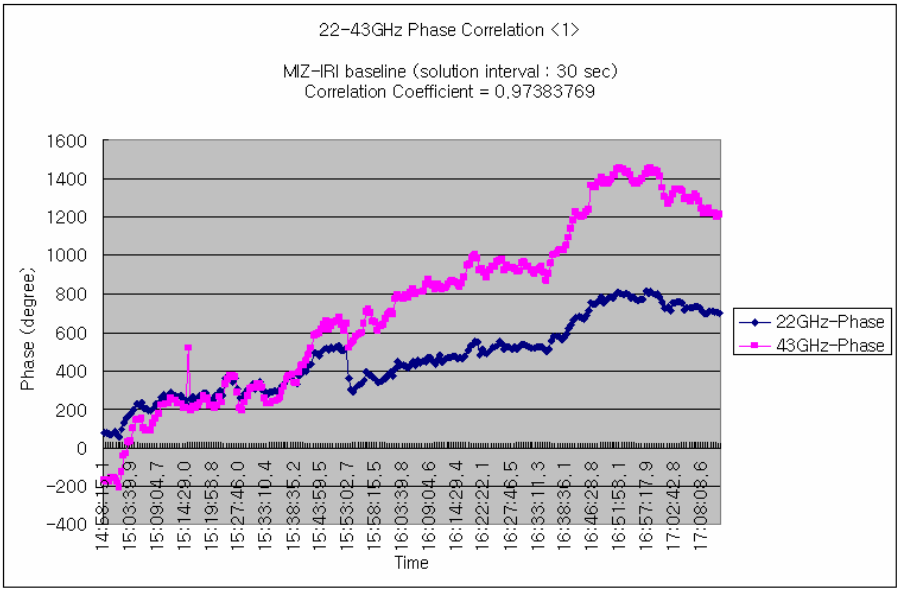

Figure 2. The phase solution of the first half of the observation after 2π ambiguity removal. Long-term increase of the phases which is obviously not from the atmosphere is seen.

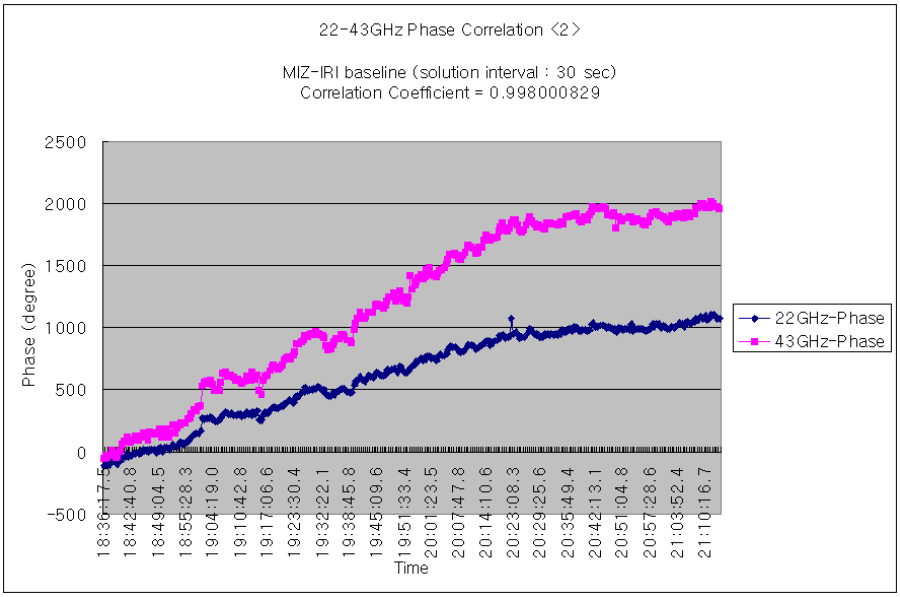

Figure 3. The phase solution of the second half of the observation after 2π ambiguity removal. The long-term non-atmospheric, but frequency-proportional increase of the phases is more clearly noticeable.

References

[1] Asaki, Y. et al., Radio Science, 31, 1615, 1996.

[2] Asaki, Y. et al., Radio Science, 33, 1297, 1998.

[3] Honma, M. et al., Publication of Astronomical Society of Japan, 55, L57, 2003.

[4] Kawaguchi, N. et al., In: Proceedings of SPIE 4015, Radio Telescope, H. R. Butcher(ed.), 544, 2000.

[5] Kim, H. G. et al., Construction of the Korean VLBI Network (revised version), In: Proceedings of the 7th Symposium of EVN, R. Bachiller, F. Colomer, J.-F. Desmurs, & P. de Vicente(eds.), 281, 2004.

[6] Kobayashi, Y. et al., VERA project, In: New technologies in VLBI, ASP Conference Series, Vol. 306 Y. C. Minh (ed.), 48, 2003.

[7] Lobanov, A. et al., Astronomy and Astrophysics, 330, 79, 1998.

[8] Middelberg, E. et al., Astronomy and Astrophysics, 433, 897, 2005.

[9] Minh, Y. C. et al., Construction of the Korean VLBI Network, In: New technologies in VLBI, ASP Conference Series, Vol. 306 Y. C. Minh (ed.), 373, 2003.

[10] Philips, R. B. et al., Astrophysical Journal, 588, 105, 2003.

[11] Sasao, T., Technologies for mm and Sub-mm VLBI: Multi-frequency Feed as a Tool for mm-Wave VLBI, In: New technologies in VLBI, ASP Conference Series, Vol. 306 Y. C. Minh (ed.), 53, 2003.

[12] Schlüter, W. & Vandenberg, N. R., Geodetic VLBI - Wishes and Limitations, In: New technologies in VLBI, ASP Conference Series, Vol. 306 Y. C. Minh (ed.), 21, 2003.

Annika Edh et al.: Crustal Deformation in South America from GPS and VLBI, IVS 2006 General Meeting Proceedings, p.356–360
http://ivscc.gsfc.nasa.gov/publications/gm2006/edh-haas

Crustal Deformation in South America from GPS and VLBI

Annika Edh, Rüdiger Haas

Onsala Space Observatory, Department of Radio and Space Science, Chalmers University of Technology
Contact author: Rüdiger Haas, e-mail: haas@oso.chalmers.se

Abstract

The western coast of South America is a tectonically active convergent margin, where the Nazca and Antarctic plates subside under the South American continent. We present contemporary crustal deformation obtained from GPS and VLBI data. A network of 20 permanent GPS stations, mainly on the west coast, was analyzed using the Precise Point Positioning (PPP) strategy with the GIPSY/Oasis II software. The movement of the stations during more than five years, starting in late 1999, was derived and the corresponding strain rate field was calculated. Station velocities were compared to corresponding results from VLBI analyses.

1. Introduction

The analysis of GPS and VLBI observational data provides important crustal deformation results for geophysical research. Crustal deformation in terms of station velocities and strain rate fields can be derived. Zones of deformation, where tectonic plates converge, are of special interest, due to the variety of geological processes that occur there.

2. Background - The Tectonic Setting in South America

The subsidence of the oceanic Nazca and Antarctic plates beneath the South American continental plate creates the Andean subduction zone (ASZ). It represents the longest convergent margin in the world, stretching for over 7500 km along the South American west coast from Colombia to the south of Chile. Due to the active plate margin, the Andes comprise high mountain peaks and volcanoes, and most parts of the area have been struck by earthquakes.

The relative convergence vector between the Nazca and South American plates is 65 mm/yr [1]. The total relative plate motion in the ASZ can be divided into different components controlling crustal deformation [2]. Roughly half of the motion accumulates in the locked parts of the plate interface, leading to transient elastic deformation, which is released in large thrust earthquakes. Some motion is expected to occur as stable sliding at the interface, since the slip rate of large subduction earthquakes is generally less than the convergence rate. The vertical crustal thickness of the Andes and its root implies that some of the motion also causes permanent crustal shortening and mountain building.

3. GPS and VLBI: Data, Analysis and Results

The area of investigation is enclosed by 16°S in the north and 54°S in the south and stations are located on both sides of the Andes. The majority of the 20 GPS stations chosen for this study are IGS sites. Additionally, GPS data from a station operated at the ALMA site at Chajnantor

in Northern Chile at about 5000 m height [4] are included. Five permanent GPS sites in eastern South America were added for reference. The station locations are listed in Table 1, together with the location of the few VLBI sites in South America.

GPS data from this network between late 1999 and mid 2005 were downloaded from SOPAC GPS data archive [3]. The data were analyzed using the GIPSY/Oasis II software [5] with the Precise Point Positioning strategy [6] and a non-fiducial approach. The daily coordinate results were transformed to ITRF2000 using transformation parameters provided by IGS and JPL, respectively.

VLBI data were not analyzed by ourselves; instead we used the velocity solution of the combined VLBI Terrestrial Reference Frame (VTRF2005) [7].

3.1. Station Velocities

GPS station velocities were derived by a least-squares fit to the time series of topocentric station positions. Examples for time series are shown in Fig. 1. Row one shows the west coast station SANT in Chile, row two shows the west coast station AREQ in southern Peru that was affected by a strong earthquake in 2001, the third row shows the station CHAJ in northern Chile on the altiplano at about 5000 m height, and the last row shows the station BRAZ in the eastern part of South America.

Outliers were removed in two steps, based on the formal standard deviations and simple outlier tests. Topocentric station velocities were determined by fitting offset, linear trends, and annual signals to the time series. For the station AREQ in southern Peru, which suffered from a M_w=8.4 earthquake in June 2001, parameters of a post-seismic relaxation model for the horizontal displacement were also determined. The best fit relaxation times were 0.26 and 1.04 years for the North and East component, respectively. Table 1 lists the results for topocentric GPS station velocities, as well as the velocities of the few VLBI stations in South America.

We find that the west coast stations move landward in a NE direction. This is due to coupling at the thrust interface during an inter-seismic phase. The velocities are highest at the coast, close to the trench, and decrease further away from it. Horizontal velocities for stations in the ASZ are on the order of 10-35 mm/yr and in the eastern part around 10 mm/yr. The horizontal VLBI velocities agree reasonably well with the GPS derived velocities. However, the vertical velocities do show significant discrepancies.

3.2. Strain Rate Field

Knowing the GPS station positions and velocities, the strain rate field was calculated for almost the entire South American continent. A Delauney triangulation was used to densify the network into a finite element structure. The velocity field of this finite element structure was calculated with a least-squares collocation method. Then, three dimensional strain rate tensors were determined for all finite elements [8]. Figure 2 shows the tangential part of the strain rate tensors. A band of extensive compressional deformation along the west coast between latitude 20°S and 40°S is clearly visible. The average compression is on the order of 5-15 nanostrain/yr with peak values of up to 100 nanostrain/yr, while extension directly east of the Andes is about 5-10 nanostrain/yr. The average compression and extension in the eastern part of South America are both on the order of 1 nanostrain/yr with peak values of up to 6 nanostrain/yr.

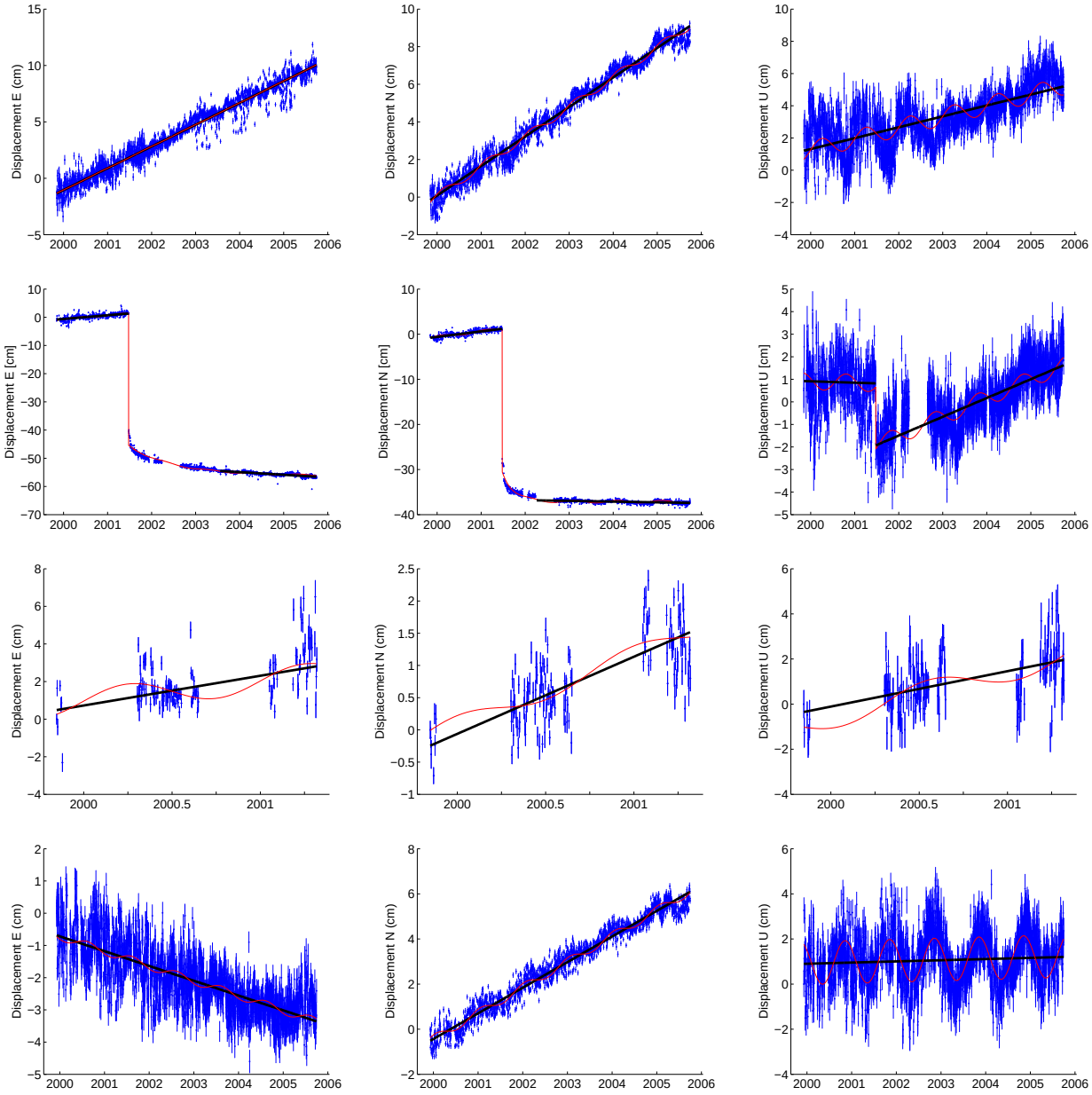

Figure 1. Examples of GPS derived time series of topocentric station positions in South America. Row 1–4 show the stations SANT, AREQ, CHAJ and BRAZ, and column 1–3 the East, North and Up components, respectively. The estimated linear station velocities are shown as straight lines whereas the sinusoidal curves represent seasonal components. For the horizontal motion of the station AREQ an exponential relaxation model was applied.

Table 1. Station names, geographic positions, and topocentric velocities of South American GPS stations. (1) Results only before the June 2001 earthquake. (2) Results only after the June 2001 earthquake. (3) Results only before June 2005. (4) Results only before May 2005.

Station	λ °E	ϕ °N	v_E (mm/yr)	σ_{v_E} (mm/yr)	v_N (mm/yr)	σ_{v_N} (mm/yr)	v_U (mm/yr)	σ_{v_U} (mm/yr)
AREQ[1]	−71.49	−16.47	13.13	0.17	12.14	0.05	−0.62	0.48
AREQ[2]	−71.49	−16.47	−9.34	0.76	−1.61	0.01	8.33	0.12
CFAG	−68.23	−31.60	5.19	0.01	11.40	0.01	0.30	0.11
CHAJ	−67.79	−22.90	10.70	0.78	10.82	0.20	20.67	1.40
CORD	−64.47	−31.53	−0.68	0.04	10.77	0.01	2.01	0.11
PARC	−70.88	−53.14	3.41	0.04	12.18	0.03	−0.82	0.12
RIOG	−67.75	−53.79	2.76	0.02	11.46	0.01	6.03	0.06
SANT	−70.67	−33.15	19.31	0.03	15.82	0.01	6.96	0.07
TUCU	−65.23	−26.84	0.20	0.05	9.89	0.02	3.92	0.14
IQQE[3]	−70.13	−20.27	22.86	0.04	13.79	0.02	7.86	0.17
COPO	−70.34	−27.38	17.41	0.05	13.46	0.02	11.97	0.15
UNSA	−65.41	−24.73	2.98	0.03	10.38	0.01	3.36	0.10
VALP	−71.63	−33.03	27.65	0.16	21.47	0.08	−1.27	0.52
CONZ[4]	−73.03	−36.84	28.91	0.04	19.50	0.02	8.40	0.18
ANTC	−71.53	−37.34	12.91	0.12	9.76	0.06	9.30	0.36
COYQ	−71.89	−45.51	−4.01	0.09	9.96	0.05	0.46	0.27
BRAZ	−47.88	−15.95	−4.60	0.04	11.40	0.01	0.55	0.08
FORT	−38.43	−3.88	−4.37	0.11	11.02	0.02	2.15	0.18
CHPI	−44.99	−22.69	−4.51	0.09	9.78	0.04	3.22	0.32
LPGS	−57.93	−34.91	−3.14	0.03	10.54	0.02	5.25	0.10
KOUR	−52.81	5.25	−6.07	0.03	12.23	0.01	3.88	0.09
VLBI station locations and topocentric velocities [7]								
FORT	−38.43	−3.88	−4.41	0.20	11.89	0.11	−0.24	0.09
TIGO	−73.03	−36.84	30.38	1.12	20.32	0.68	4.39	1.26
SANT	−70.67	−33.15	19.84	0.54	15.75	0.15	5.03	0.50

4. Discussion and Conclusions

The results of this study agree with previous investigations [9], [10]. During inter-seismic periods velocities in the ASZ are generally landward and greatest close to the trench, up to 35 mm/yr, induced by the motion of the incoming Nazca and Antarctic plates. On occasions of fault slip, like the one close to Arequipa, Peru, in 2001, the crust suddenly moves seawards and the post-seismic signal shows slow continued movement in the same direction.

The horizontal velocity of the GPS station at Chajnantor is comparable to other GPS station on the altiplano [2].

The few available VLBI velocities in general confirm the findings of this GPS study.

The strain rate field is, as expected, highly pronounced along the South American west coast. In this area it is dominated by compression with values from 10-100 nanostrain/yr. Some regions east of the Andes experience smaller extension of about 5-10 nanostrain/yr. The eastern part of South America is dominated by a strain rate field with values on the order of 1-6 nanostrain/yr.

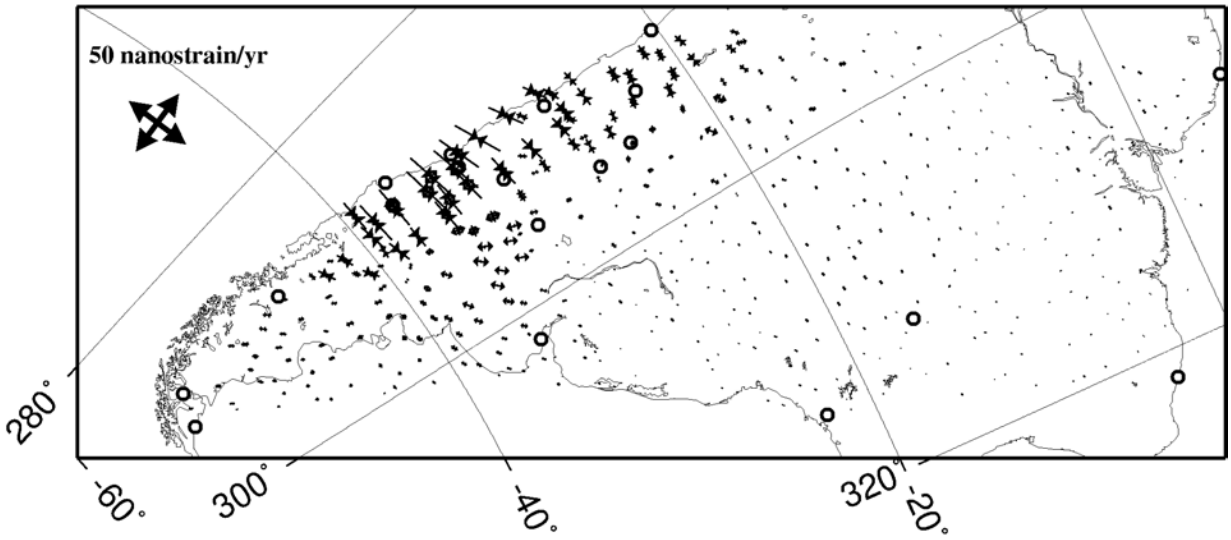

Figure 2. The GPS-derived strain rate field in South America. The circles mark GPS sites.

References

[1] Angermann, D., Klotz, J., and Reigber, C.: Space-geodetic estimation of the Nazca-South American Euler Vector. *Earth Planet. Sci. Lett.*, **171**, 329–334, 1999.

[2] Norabuena, E., Leffler-Griffin, L., Mao, A., Dixon, T., Stein, S., Sacks, S., Ocola, L., and Ellis, M.: Space-geodetic Observations of Nazca-South American Convergence Across the Central Andes. *Science*, **279**, 1998.

[3] `ftp://garner.ucsd.edu/pub/rinex`

[4] Gradinarsky, L. P., Johansson, J. M., Elgered. G., and Jarlemark, P.: GPS site testing in Chajnantor in Chile. *Phys. Chem. Earth*, **26(6–8)**, 421-426, 2001.

[5] F.H. Webb and J.F. Zumberge: An introduction to GIPSY/OASIS-II. *JPL Publication D-11088*, Jet Propulsion Laboratory, Pasadena, 1993.

[6] J.F. Zumberge, M.B. Hefflin, D.C. Jefferson, M.M. Watkins, and F.H. Webb: Precise point positioning for the efficient and robust analysis of GPS data from large networks. *J. Geophys. Res.*, vol. 102(B3), pp. 5005–5018, doi:10.1029/96JB03860, 1997.

[7] Nothnagel, A.: VTRF2005 A combined VLBI Terrestrial Reference Frame. In: *Proc. 17th Work. Meet. Euro. VLBI Geodesy and Astrometry*, 118-124, 2005.

[8] Haas, R., Scherneck, H.-G., Gueguen, E., Nothnagel, A., and Campbell, J.: Large-scale strain-rates in Europe derived from observations in the European geodetic VLBI network. *EGU Stephan Mueller Special Publication Series*, **2**, 139–152, 2002.

[9] Klotz, J., Khazaradze, G., Angermann, D., Reigber, C., Perdomo, R., and Ciuentes, O.: Earthquake cycle dominates contemporary crustal deformation in Central and Southern Andes. *Earth Planet. Sci. Lett.*, **193**, 437-446, 2001.

[10] Khazaradze, G., and Klotz, J.: Short and long-term effects of GPS measured crustal deformation rates along the South-Central Andes. *J. Geophys. Res.*, **108(B4)**, doi:10.1029/2002JB001879, 2003.

Younghee Kwak et al.: A Preliminary Study on Plate Motion Measurements on the Korean Peninsula with the New Korean VLBI Array, IVS 2006 General Meeting Proceedings, p.361–365
http://ivscc.gsfc.nasa.gov/publications/gm2006/kwak

A Preliminary Study on Plate Motion Measurements on the Korean Peninsula with the New Korean VLBI Array

Younghee Kwak [1], *Tetsuo Sasao* [1], *Tuhwan Kim* [2]

[1)] *Ajou University and Korea Astronomy and Space Science Institute*

[2)] *Ajou University*

Contact author: Younghee Kwak, e-mail: bgirl02@kasi.re.kr

Abstract

Although the officially adopted global plate motion model in ITRF, the NNR-NUVEL-1A, assumes that the Korean Peninsula is located on the Eurasian plate (EU), many researchers now postulate that it is on a separate plate, called the Amurian plate (AM). In the near future, we will have 4 VLBI stations in Korea: a geodetic VLBI station and 3 astronomical/geodetic VLBI stations (Korean VLBI Network, KVN). This compact Korean VLBI array is capable of achieving a good determination of the plate motion parameters, as shown in our simulation with small VLBI arrays arranged on stable sites on the North American plate (NA). We estimated the precision of AM motion parameters with the Korean VLBI array. The results showed that the Korean VLBI array would verify the existence of AM, provided an observation precision of 0.2–0.5 mm/yr for station velocities was achieved. Therefore, the new Korean geodetic VLBI array can contribute to crustal deformation studies in East Asia. Moreover, the Suwon site can be an important reference point for defining the ITRF, if it indeed turns out to be a stable mid-plate VLBI station in East Asia.

1. Introduction

1.1. VLBI in Korea

In Korea, within a few years, there will be 3 VLBI stations for astronomical/geodetic purposes, KVN which will be composed of three 21m antennas, to be located in Seoul, Ulsan and Jeju, with 2/8, 22, 43, 86, and 129GHz receivers [7]. The National Geographic Information Institute (NGII) is planning to construct a geodetic VLBI station in Suwon. We will be able to measure the movement of the Korean Peninsula more precisely using these four stations (Figure 1).

1.2. Amurian Plate

The existence of the Amurian plate (AM), which covers the region from the Baikal rift to the Nankai trench, including the Korean Peninsula, was proposed first by Zonenshain and Savostin (1981) [11]. They used seismic data of the Baikal rift zone in order to determine plate motion parameters of AM. Recent developments in high precision space-geodetic measurements imply that it is difficult to explain motions actually observed at various sites on the Earth using only 12 major plates that have been assumed in NNR-NUVEL-1A [1][4]. Many authors divide the major plates into new small plates and blocks (micro-plates). One of them is AM in East Asia. The assumed AM includes the Korean Peninsula as a part of its stable interior. Therefore, precise geodetic measurements on the Korean Peninsula are best suited to determine the motion of AM, and judge if it is in fact a separate micro-plate, and not part of EU as assumed in NNR-NUVEL-1A. Large earthquakes often occur in East Asia causing many disasters. It is suspected that the

Figure 1. Site locations of the KVN and Suwon antennas in Korea.

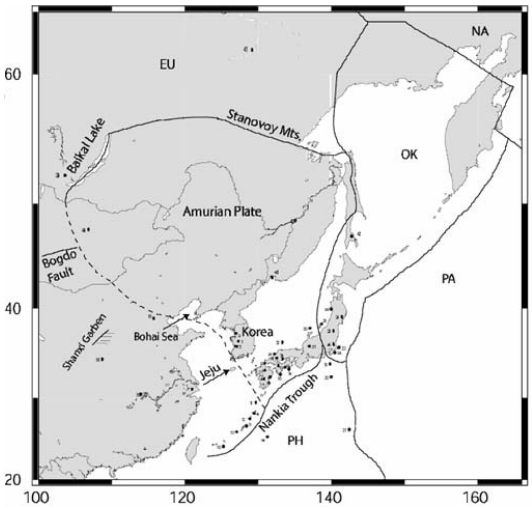

Figure 2. Amurian plate (Eastern Asia Joint Project, 2004).

majority of the recent large earthquakes in the East Sea and Japan Islands area are likely to have occurred along the eastern boundary of AM [6]. A more accurate plate motion model is needed in order to clarify mechanisms and recurrences of earthquakes in this region.

2. Previous Research on the Amurian Plate Using GPS

There were several GPS research projects on the AM. Figure 3 shows the pole positions of the estimated AM-EU relative plate angular velocities. For estimating the motion of the AM, all of the authors who used GPS data had only 3-5 stations located on the postulated AM [6][8][9][10]. This means that this area does not have enough data to estimate the plate motion, compared with other areas of the world. It is evident from Figure 3 that their results are inconsistent with each other, beyond estimated statistical errors, even though they usually used GPS data of the same stations. Hence it is difficult to draw a definite conclusion about the existence of the AM as a separate rigid plate in this region. At this point, we need another independent space geodetic technique in order to distinguish existing results on the Euler vector. In order to determine precise plate motion parameters in East Asia, geodetic VLBI, which has quite good accuracy [2], is desirable.

3. Future VLBI Array in Korea

3.1. Determination of Plate Motion Parameters with the Compact VLBI Array

In order to examine whether the compact VLBI array, such as the one expected in Korea, can determine plate motion parameters to the needed extent, we performed a simulation using existing VLBI stations on the North American plate (NA). We selected two small networks, each consisting of 3 stations, as shown in Figure 4. The positions and velocities of the stations are published in IERS Technical Notes No. 31 as VLBI ITRF2000 station positions at epoch 1997.0

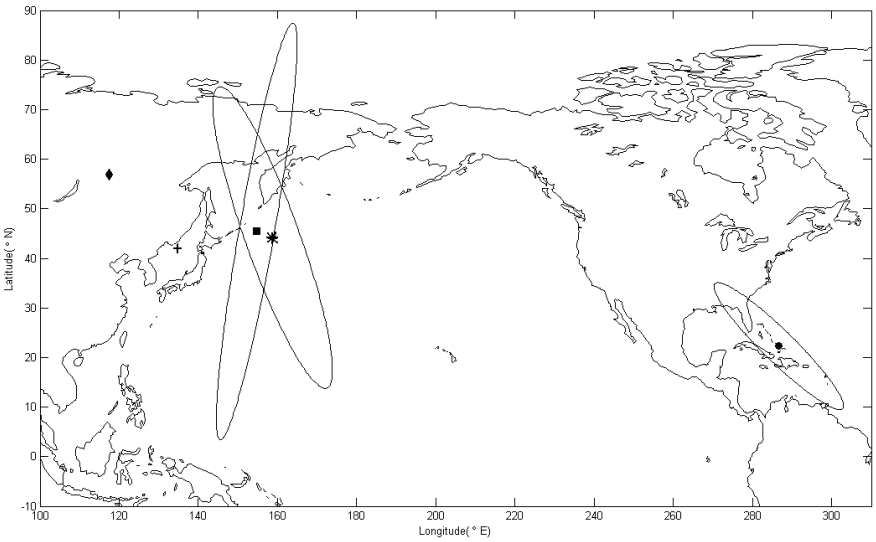

Figure 3. The pole positions and their error ellipses of the plate angular velocities of the AM with respect to the EU in previous research works. ◇ : Zonenshain & Savostin (1981), seismic data, o : Heki *et al.* (1999) GPS, ∗ : Sella *et al.* (2002) GPS, + : Steblov *et al.* (2003) GPS, □ : Prawirodirdjo & Bock (2004) GPS. The error ellipses of Zonenshain & Savostin (1981) and Steblov *et al.* (2003) are not available.

and velocities. From the data, we estimated the rotation vector of NA relative to ITRF2000 with the weighted least squares method. Table 1 shows that the rotation vector of the small array in the East Coast relative to ITRF2000 is almost the same as the Euler vector of the North American plate listed in the IERS Technical Notes No. 31 [3] on the basis of many space geodetic data for NA. The result is also very close to Prawirodirdjo and Bock's (2004) result derived from data of 22 GPS stations in NA. Differences in the estimated vectors are smaller than statistical errors in the present calculation. Hence, the statistical error estimation seems to be reasonable. In the case of the West Coast stations: Fort Davis, Pietown and Los Alamos, the agreement of the rotation vector obtained from these stations with the reference values is fairly good (20% in rotation rate). Accordingly, even a small VLBI network with a small number of stations is able to give a well determined rotation vector of a plate, if the stations are located in the stable interior of the plate. The Korean Peninsula is known to be away from plate boundaries, and seismic activity is quite low in Korea. We can expect that the Euler vector of the plate, which the VLBI stations of the Korean Peninsula form part of, will be well estimated and therefore will allow to verify the existence of AM as a separate plate.

3.2. Error Estimation for the Euler Vector of the AM Relative to ITRF

We estimated the errors of the plate motion parameters expected for the Korean VLBI array, assuming that the errors in the observed velocities are uniform and equal to 0.5 mm/yr for both the NS and EW components, which is typical in present day geodetic VLBI observations. Results are shown in Table 2. It does not seem to be too difficult to achieve a velocity precision of 0.2 mm/yr through geodetic VLBI observations over several years. Then, with several years of

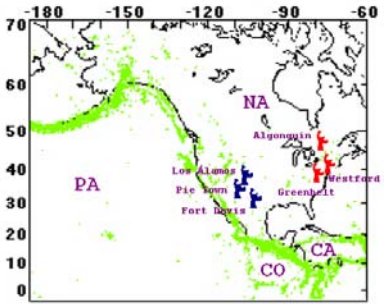

Figure 4. Seismic belts as the boundaries between NA and PA (Pacific plate), NA and CO (Cocos plate), and NA and CA (Caribbean plate), and two small VLBI arrays on NA for the determination of plate motion parameters.

Table 1. Comparison of plate angular vectors relative to ITRF2000 with small VLBI arrays

	Latitute °N	Longitude °E	ω deg/Myr	σ_ω deg/Myr	Error Ellipse, deg		
					σ_{maj}	σ_{min}	Azimuth[a]
IERS Technical Notes No. 31	-83.144	-5.036	0.194	0.003	–	–	–
Prawirodirdjo and Bock [2004]	-84.702	-3.583	0.200	0.003	0.87	0.25	101
East	-83.452	-4.606	0.192	0.010	3.46	0.44	81
West	-88.642	1.981	0.236	0.016	2.68	0.39	27

[a]Azimuth of the semi-major axis in degrees measured clockwise from north

VLBI observations, the value of the error will become remarkably smaller. Therefore, if the high precision of station velocities, 0.2-0.5mm/yr, is realized, any systematic movements of the Korean VLBI stations can contribute to determine the plate angular velocity of the AM and verify the existence of the AM as a separate rigid plate.

4. Conclusion

We compared results of previous research works, by Heki *et al.* (1999), Sella *et al.* (2002), Steblov *et al.* (2003) and Prawirodirdjo and Bock (2004) for the plate motion of East Asia, reducing them to a common platform. The results of the comparison showed that movements derived by the above authors are inconsistent with each other, even though they applied the same technology (GPS) for the same area (East Asia).

We performed a simulation study for plate parameter determination, using measured velocities of several VLBI stations in North America. The results of the simulation showed that even small VLBI arrays are able to well determine the plate motion parameters, if the arrays are located in a stable area (e.g., Westford–Greenbelt–Algonquin array in NA).

We estimated the accuracy of the plate motion parameter to be determined with the new VLBI stations in Korea (KVN and Suwon sites). The results showed that the Korean VLBI array will

Table 2. Error estimation for the plate angular velocity of the AM relative to ITRF.

	σ_ω	Error Ellipse, deg		
	deg/Myr	σ_{maj}	σ_{min}	θ_{maj}[a]
0.5 mm/yr[b]				
Seoul–Ulsan–Jeju–Suwon	0.0240	12.21	0.44	-52.17
0.2 mm/yr[c]				
Seoul–Ulsan–Jeju–Suwon	0.0096	4.88	0.17	-52.17

[a]The azimuth of the semi-major ellipse axis in degrees clockwise from north
[b]The assumed velocity errors both in NS and EW directions typical for modern VLBI stations.
[c]The assumed velocity errors after several years of regular geodetic VLBI observations.

be able to provide accurate plate motion parameters, and verify the existence of AM as a separate rigid plate, if the observation accuracy of 0.2-0.5 mm/yr for station velocities is realized.

References

[1] Argus, Donald F., and Gordon, Richard G., "No-net-rotation model of current plate velocities incorporating plate motion model NUVEL-1," *Geophys. Res. Lett.*, **18**, 2039-2042, 1990.

[2] Altamimi, Z., P. Sillard, and C. Boucher, "ITRF2000: A new release of the International Terrestrial Reference Frame for earth science applications," *J. Geophys. Res.*, **107**(B10), ETG 2-1 - ETG 2-19, 2002.

[3] Boucher, C., Z. Altamimi, P. Sillard, and M. Feissel-Vernier, The ITRF2000(IERS Technical Note No. 31), IERS ITRS Centre, 2004.

[4] DeMets, C., R. G. Gordon, D. F. Argus, and S. Stein, "Effect of recent revisions to the geomagnetic reversal time scale on estimates of current plate motions," *Geophys. Res. Lett.*, **21**(20), 2191-2194, 1994.

[5] Hamdy, M., Park, P., Lim, H., Park, K., " Present-day relative displacements between the Jeju Island and the Korean peninsula as seen from GPS," *Earth Planets and Space,* **56***(9), 927-931, 2004*

[6] Heki, K., S. Miyazaki, H. Takahashi, M. Kasahara, F. Kimata, S. Miura, N. F. Vasilenko, A. Ivashenko, and K. D. An, "The Amurian plate motion and current plate kinematics," *J. Geophys. Res.*, **104**(B12), 29,147-29,155, 1999.

[7] Minh Y. C., Roh, D. G., Han, S. T., and Kim, H. G., "Construction of the Korean VLBI Network(KVN)," *ASP Conference Series*, **306**, 2003.

[8] Prawirodirdjo and Bock, "Global plate motion model from CGPS," *J. Geophys. Res.*, **109**, B08405, doi:10.1029/2003JB002944, 2004.

[9] Sella, G. F., T. H. Dixon, and A. L. Mao, "REVEL: A model for recent plate velocities from space geodesy," *J. Geophys. Res.*, **107**(B4), 2081, doi:10.1029/2000JB000033, 2002.

[10] Steblov, G. M., M. G. Kogan, R. W. King, C. H. Scholz, R. Burgmann, and D. I. Frolov, "Imprint of the North American plate in Siberia revealed by GPS," *Geophys. Res. Lett.*, **30**(18), 1924, doi:10.1029/2003GL017805, 2003.

[11] Zonenshain, L. P., and L. S. Savostin, "Geodynamics of the Baikal rift zone and plate tectonics of Asia," *Tectonophysics*, **76**, 1-45, 1981.

Yoshimitsu Masaki et al.: Local Tie Survey at VERA Ogasawara Station at Site Chichijima, IVS 2006 General Meeting Proceedings, p.366–370
http://ivscc.gsfc.nasa.gov/publications/gm2006/masaki

Local Tie Survey at VERA Ogasawara Station at Site Chichijima

Yoshimitsu Masaki [1], *Shigeru Matsuzaka* [1], *Yoshiaki Tamura* [2]

[1)] *Geographical Survey Institute*

[2)] *National Astronomical Observatory of Japan*

Contact author: Yoshimitsu Masaki, e-mail: ymasaki@gsi.go.jp

Abstract

We made a local tie survey between the VERA-Ogasawara VLBI station of the National Astronomical Observatory of Japan (DOMES number 21732S005), and the GPS station CCJM at Chichijima (DOMES number 21732S003). Chichijima is one of the Bonin (Ogasawara) Islands on the Philippine Sea plate. Since there is no other suitable site for geodetic observations nearby, the local ties at Chichijima play an important role for the maintenance of the terrestrial reference frame. This is the first local tie at this site, not counting the one classified as 'a dubious tie'.

Our result shows that the relative position between these two stations is determined with uncertainties of (X, Y, Z) = (2.0mm, 1.4mm, 1.5mm). We show error budgets in our analysis process and found that the GPS accuracy has a key role to obtain precise local ties.

1. Introduction

Local ties play an important role for construction and maintenance of a terrestrial reference frame (TRF) because local ties are the only techniques that can combine geodetic solutions obtained by different space geodetic techniques (VLBI, GPS, SLR, etc.) into a unique one. The current accuracy required for local ties is about 1 cm, but mm-level accuracy should be achieved in the next decade (Altamimi et al. [2]). On the other hand, non-uniformly distributed local ties over the world may cause serious problems for the global consistency of a TRF. Filling observation gaps is a key issue to solve the problem.

In this paper, we report our local tie survey made on the island of Chichijima (site number 21732, approximate location: 27°05′N, 142°10′E). This site is classified as an important site for the construction of a TRF (see Altamimi (2001) [1]). The island is located on the Philippine Sea plate, where no other sites are available near by. In spite of the importance of local ties at the site, no survey has been made until the current survey, not counting one classified as a dubious tie.

The VERA project, promoted by the National Astronomical Observatory of Japan, is aiming at precise radio astrometry observation with 10 μas accuracy and precise geodetic observation. Four stations were constructed, the Ogasawara station is one of them. The current status of the VERA project was presented by Jike et al. (2006) [3] and Kobayashi et al. (2006) [4] at this meeting.

2. Survey and Analysis

We made an in-situ survey on the island during December 10-20, 2003. We tried to make a tie between the GPS station S003 and the VERA VLBI station S005. Our local survey network is shown in Figure 1.

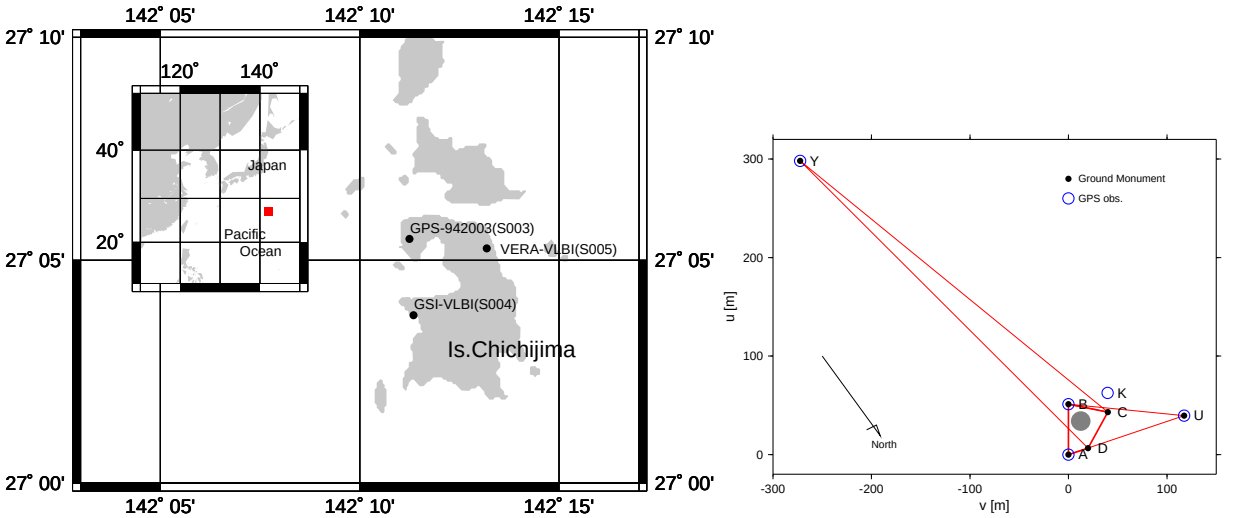

Figure 1. (a) Island Chichijima (site number 21732). The island is located on the Philippine Sea plate. The baseline length between the GPS station S003 and the VERA-Ogasawara station S005 is about 3,200 meters. (b) Our survey network. The VLBI antenna is located in the quadrangle formed by ABCD.

Our analysis process is composed of four steps. First, we determined the positions of six ground monuments (designated as A to D, U and Y in Figure 1). Second, we measured the relative positions of a CATEYE reflector attached to the rigid support of the VLBI antenna with respect to the four ground monuments, A to D. (Matsuzaka et al. [5] describe details on the reflector.) Because a target reflector moves on a spherical shell centered at the VLBI reference point during Az-El driving, we can determine the spherical center by using a least squares method (Step 3).

We also made GPS observations at the four ground monuments A, B, U and Y, in order to relate the local coordinates (U, V, W) to the global Cartesian coordinates (X, Y, Z) using a Helmert transformation. In Step 4, we transform the local coordinates of the antenna reference position into the global coordinates by a Helmert transformation.

3. Results

Our results on the relative baseline vector from the GPS S003 to the VLBI S005 are:

$$\begin{aligned} dX &= -2143.0748 \pm 0.0020 \ \text{[m]} \\ dY &= -2358.3014 \pm 0.0014 \ \text{[m]} \\ dZ &= -343.6853 \pm 0.0015 \ \text{[m]}, \end{aligned} \tag{1}$$

or (the coordinates (N, E, U) are tangent to the reference ellipsoid at the GPS station S003)

$$\begin{aligned} dN &= -418.5073 \pm 0.0007 \ \text{[m]} \\ dE &= 3176.9961 \pm 0.0008 \ \text{[m]} \\ dU &= 63.4282 \pm 0.0026 \ \text{[m]}. \end{aligned} \tag{2}$$

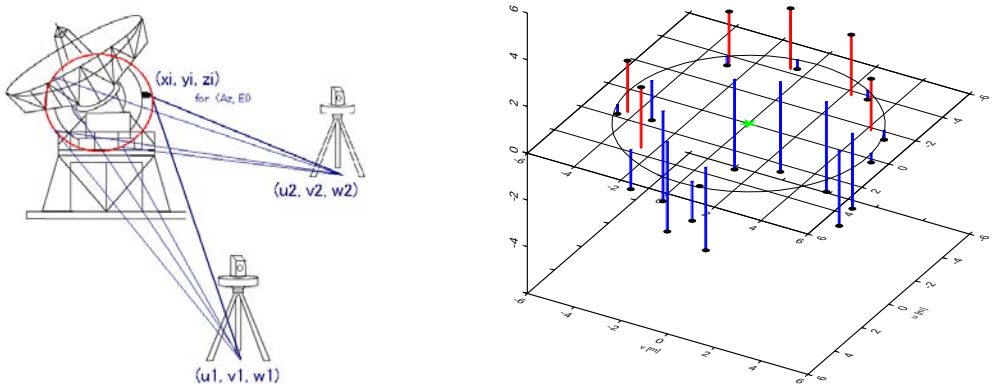

(a) (b)

Figure 2. (a) Explanatory illustration how to determine the positions of a CATEYE reflector from two ground monuments. (b) The 3-D distribution of the measured CATEYE positions (black dots) for the estimation of the VLBI reference point. The reference point of the antenna (equivalent to the spherical center of CATEYE positions) is determined with errors $(\sigma_U, \sigma_V, \sigma_W) = (0.28, 0.31, 0.44)$ [mm] in the local coordinates. The RMS fitting error of a spherical shell in the radial direction is 0.19 mm.

The baseline vector from the GPS station K to the VLBI S005 (tangent to the reference ellipsoid at K) is:

$$\begin{aligned} dN &= 7.1660 \pm 0.0007 \ \text{[m]} \\ dE &= 38.9515 \pm 0.0009 \ \text{[m]} \\ dU &= 7.5730 \pm 0.0031 \ \text{[m]}. \end{aligned} \tag{3}$$

For the sake of accuracy check, we compare this result to another one obtained independently for the baseline vector from the GPS antenna K to the VLBI S005. These two horizontal positions show good agreement.

4. Future Improvements

As summarized in Table 1 and 2, GPS positions determined from a 24-hour session degrade uncertainties to a sub-mm level, despite smaller uncertainties of $(\sigma_U, \sigma_V, \sigma_W) = (0.28, 0.31, 0.44)$ [mm] achieved in the determination of the antenna reference point through our ground survey.

When we collect GPS data for much longer sessions, the uncertainties of GPS positioning are supposed to be decreased by an inverse square-root law with time. In theory, GPS data for more than two weeks is necessary to achieve the uncertainties within 1mm.

5. Acknowledgements

The authors acknowledge to Y. Sasaki, M. Shibahara, T. Tsutsumi and J. Miyamoto (Geographical Survey Institute) for this successful in-situ survey with us, and K. Horiai and O. Kameya (National Astronomical Observatory of Japan) for their sincere supports for using the VERA facility.

Table 1. Errors of our local tie analysis. Units are [mm]. We fix the position of A during a net adjustment. The VLBI reference point in the local coordinates (U, V, W) is obtained through Step 3. GPS uncertainties are given for baseline measurements relative to the GPS station S003. The last three columns are expected uncertainties after a Helmert transformation. GPS data at Y is excluded from the determination of transformation parameters due to its large misfits.

Monument	ground survey (Steps 1 and 3)			GPS obs.			after Helmert trans. (Step 4)		
	σ_U	σ_V	σ_W	σ_N	σ_E	σ_U	σ_N	σ_E	σ_U
A	-	-	-	0.64	0.66	3.00	0.65	0.69	3.23
B	0.59	0.15	0.14	0.83	0.86	3.97	0.79	0.99	4.24
C	0.53	0.48	0.15	-	-	-	1.28	0.65	3.23
D	0.13	0.25	0.10	-	-	-	0.66	0.76	2.96
U	0.65	1.31	1.46	0.58	0.60	2.62	1.29	1.25	4.15
Y	1.71	1.79	2.47	0.57	0.61	2.61	..	..	..
VLBI ref. point	0.28	0.31	0.44	-	-	-	0.73	0.90	3.12

Table 2. Summary of the error budgets of our local-tie analysis.

Steps	Position(s) to be determined [Uncertainties quatified by]	Position uncertainties
Step 1	Ground monements [Standard deviations of a net adjustment]	a few mm
Step 2	Cateye reflector [RMS discrepancies in CATEYE positions between two measurements]	a few mm
Step 3	VLBI antenna reference point in local coordinates (U, V, W) [RMS spherical shell fitting errors by least squares method]	sub-mm
Step 4	VLBI antenna reference point in global coordinates (X, Y, Z) [Formal errors propagated through a Helmert transformation with GPS observation data]	several mm (sub-cm)

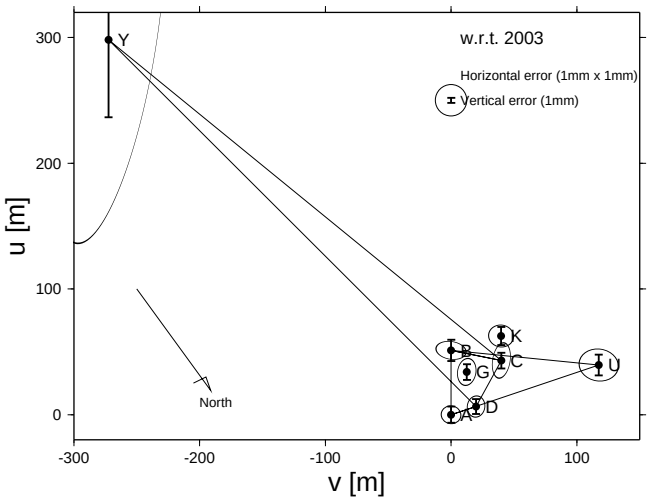

Figure 3. Expected uncertainties of the relative positions to the GPS station S003 after a Helmert transformation into the (N, E, U) coordinates. See also Table 1. We discard GPS data at Y due to its quality.

References

[1] Altamimi, Z., 2001, Report on Local Tie Problems in Colocation Sites as Result from ITRF2000 Analysis, in *ITRF Report 4 on Local Ties*, `http://lareg.ensg.ign.fr/ITRF/ITRF2000/ITRF2000.TIE-prob`

[2] Altamimi, Z., Sillard, P. and Boucher, C., 2002, ITRF2000: A new release of the International Terrestrial Reference Frame for earth science applications, Journal of Geophysical Research, 107(B10), 2214, ETG2 1-19, doi:10.1029/2001JB000561

[3] Jike, T., Tamura, Y., Manabe, S. and NAOJ VERA Group, 2006, The First Year of VERA Geodetic Experiments, in this volume

[4] Kobayashi, H., Manabe, S., Kawaguchi, N., Shibata, K.-M., Tamura, Y., Kameya, O., Honma, M., Hirota, T., Imai, H. and Omodaka, T., 2006, VERA System and Recent Results, in this volume

[5] Matsuzaka, S., Hatanaka, Y., Nemoto, K., Fukuzaki, Y., Kobayashi, K., Abe, K. and Akiyama, T., 2002, VLBI-GPS Collocation Method at Geographical Survey Institute, IVS 2002 General Meeting Proceedings (eds. Vandenberg, N. R. and Baver, K. D.), 96-100

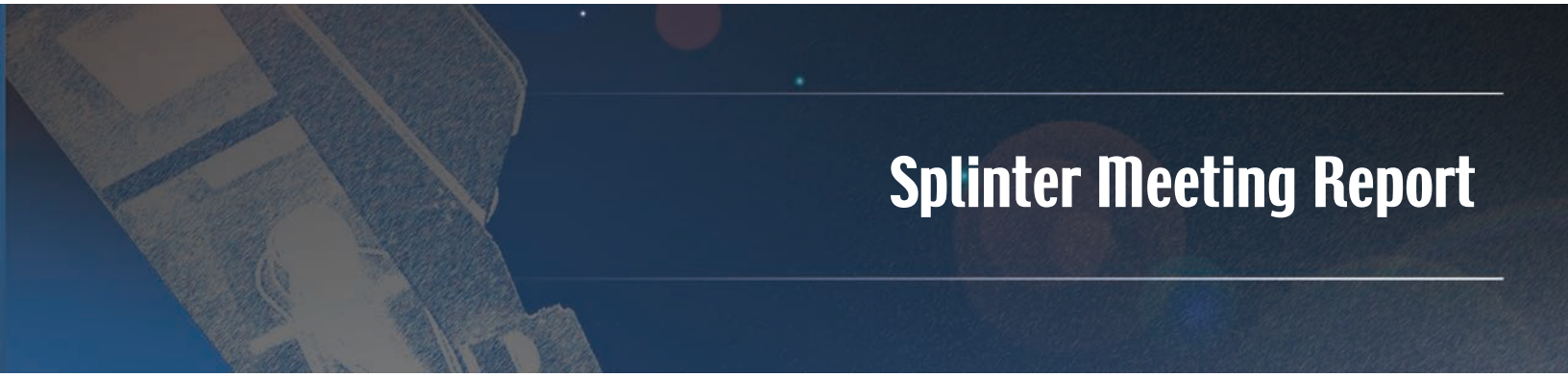

Splinter Meeting Report

Axel Nothnagel: Summary of the 7th IVS Analysis Workshop, IVS 2006 General Meeting Proceedings, p.373–376
http://ivscc.gsfc.nasa.gov/publications/gm2006/nothnagel

Summary of the 7th IVS Analysis Workshop

Axel Nothnagel

Geodetic Institute, University of Bonn
e-mail: nothnagel@uni-bonn.de

Abstract

On January 12, 2006, the 7th IVS Analysis Workshop was held in Concepción, Chile, in connection with the Fourth IVS General Meeting. This summary briefly describes the most important discussions and decisions.

1. Introduction and General Information

As has been good practice at previous IVS General Meetings, the gathering at Concepción offered a good opportunity to call for an IVS Analysis Workshop. On invitation of Hayo Hase, BKG, and the Universidad de Concepción, the 7th IVS Analysis Workshop was, thus, held in Concepción on January 12, 2006. Close to 40 participants attended the one-day workshop in the building of the Facultad de Inginería with many fruitful discussions and decisions on procedures of IVS data analysis. This summary will address the most important ones.

2. Calc 10

Very recently, implementation and testing of the Calc 10 routines with their improved modelling have been completed by the Goddard VLBI group (GSFC). The plans for the transition from Calc 9 to Calc 10 will have an immediate effect also on the general way of IVS analysis procedures and are, therefore, outlined here.

Around March 1, 2006, the GSFC group will release new versions of Calc/Solve based on Calc 10. They incorporate the changes within Solve which are necessary to accommodate also the Calc 10 LCODES. At the same time the group will start re-calcing all databases available at IVS Data Centers and re-submit them as Calc 10 databases. In order to be able to use these new databases the IVS Analysis Centers using Calc/Solve as their standard software are required to update their software as well. As soon as the existing databases have been converted to Calc 10, only Calc 10 databases should be submitted to the IVS Data Centers in order to avoid confusion. VLBI observation data in NGS format will not be affected by this transition. The whole process should be completed by the end of March 2006.

3. Combination Issues

The combination of VLBI products of different IVS Analysis Centers and with those of other techniques has become an important issue within the IAG and its services. This has been demonstrated by the enormous endeavours which have been invested in the GGOS project (Global Geodetic Observing System). We have been very glad that Markus Rothacher, the IERS Analysis Coor-

dinator and Chairman of the GGOS Project, was able to attend the IVS Analysis Workshop and to give direct input and advice on a number of topics.

3.1. Precession and Nutation

The imminent completion of implementation and testing of the Calc 10 routines offers a good opportunity to realize the change-over from the old equinox-based precession and nutation models to the new ones which refer to the non-rotating origin and the celestial intermediate pole (CIP). In order to maintain consistency with the IAU 2000 resolutions the position of the CIP should be described in X and Y components

After some discussion it was decided that IVS and its analysis centers will publish offsets with respect to X and Y only (ΔX and ΔY) in units of milliarcseconds (mas). In order to avoid inconsistencies from the fact that free core nutation (FCN) in the MHB2000/IAU2000a model [1] is modelled properly only until the year 2000, FCN should not be modelled at all in standard VLBI data analysis for submissions of Earth orientation parameters (EOP).

In the describing text of EOP time series and in the SINEX files it should be clearly stated which apriori precession and nutation model was used and that FCN was switched off. The precession model is also of importance since the IAU will adopt a new model (P03) later this year. Although the latest SINEX file format description foresees nutation rates also, it is possible that these may be reported as a standard parameter only at a later stage.

3.2. EOP Epochs

For the combination process with other space techniques, especially SLR and GPS, the VLBI EOP results always have to be transformed to the 1200 UTC epoch. Although this transformation/interpolation adds an extra amount of noise to the uncertainties of the VLBI results, the satellite techniques dominate this process and interpolation of the VLBI results cannot be avoided. There are two options to accommodate this:

- The IVS Analysis Centers continue to submit EOP at their epoch of choice (mainly middle of session but may depend on weighting and outlier elimination) and the IVS Analysis Coordinator's office does the interpolation. This can be done either by a scheme which takes into account the behaviour of the EOP within a frame of five days with the deterministics coming from the IERS C04 series (Feissel-Vernier, priv. comm.) or by using the rates reported by the analysis centers. The EOP rates reported by the analysis centers heavily depend on the particular way of doing the analysis and show quite a large scatter between analysis centers.
- The second option is that the IVS Analysis Centers report EOP at 12.00h UTC. This option bears the advantage that the interpolation to a common reference epoch stays in the hands of the analyst and any peculiarities of modelling the intra-day behaviour of the EOP is contained in the VLBI analysis.

We, therefore, suggest that all IVS Analysis Centers modify their EOP reference epoch to 1200 UTC changing to this epoch as soon as possible but not later than June 30, 2006.

3.3. SINEX Combination

It is well known that EOP determinations are heavily dependent on the apriori TRF and that the discrepancies between EOP results of different analysis centers, to a certain extent, are a consequence of the use of different realisations of the TRF. In order to apply a common TRF to all solutions the IVS Analysis Coordinator plans to change the general reporting procedure of the IVS Analysis Centers from submissions of EOP time series to datum-free normal equations in SINEX format. The date of the transition is set to January 1, 2007. From this time onwards only combinations on the basis of datum-free normal equations in SINEX files will be used for the official IVS EOP products.

Within the topic of the SINEX submissions it was also discussed how to handle the different levels of modelling details in VLBI data analysis. For the ITRF2005 initiative a special GSFC solution has been generated on the basis of the smallest common denominator, e.g. without applying atmospheric loading corrections. The SINEX files of this and the standard solution are stored in separate directories in the IVS Data Centers. This situation should not be maintained beyond the process of generating the input for ITRF2005. The IVS Analysis Coordinator proposes that SINEX files are generated by all analysis centers on a best effort basis and that each analysis center maintains only one directory in the IVS Data Centers. The argument for this is that differences in the results of the individual analyses are still larger than discrepancies which originate from different geophysical models alone.

In a further step of combination, the VLBI zenith delay estimates will be combined with results from GPS. In order to make this work it is necessary that the epochs of the atmosphere parameters are not arbitrary but will match full hour epochs. When fractions of days like 15, 20, or 30 minute intervals are chosen, they should also be set to fit the full hour intervals. Analysts and program developers should start preparing their code for an easy implementation of this scheme. The implications of this process will be discussed again at the next IVS Analysis Workshop.

4. Surface Meteorological Data

At present, standard procedures read meteorological data from the sensors at the observatories and store them in the current log file. The log files normally do not contain any information about calibrations of the sensors or any other meta data. In order to overcome this deficit a new scheme has been proposed. It calls for the introduction of separate files for the meteorological sensor readings which should then also contain adequate meta data. A small analysis working group headed by Arthur Niell was formed to prepare a full proposal for a transition to this new scheme.

5. Miscellaneous

- The IERS Analysis Coordinator, Markus Rothacher, will contact the IERS Sub-Bureau for Loading for a decision on a generalized treatment of reference pressure values for space geodetic observing sites. At the same time the IERS will devise a plan for official reference temperatures.
- On the IVS Analysis Coordinator Web site (http://vlbi.geod.uni-bonn.de/IVS-AC) a page

has been set up which is meant to be filled with helpful information about problems which have been solved by colleagues already. The Analysis Coordinator will maintain this web page and is eagerly awaiting your input. The more information that is made available, the better we can spread the experience.

- The IVS Pilot Project "Baseline Lengths" is progressing well (see http://vlbi.geod.uni-bonn.de/baseline-project/index.php). Contributing analysis centers should see that all geodetic VLBI sessions since 1984.0 have been processed. Otherwise the combined results are distorted.
- Estimated EOP rates show large discrepancies between results of individual analysis centers. However, the formal errors indicate already that the quality of the EOP rates is similar to the level of the discrepancies. In this context, possible differences of the software packages in the modelling of sub-daily variations was briefly addressed but not discussed any further. Here, it would be helpful if analysts could check their programs and models how the EOP rates are handled and how they may be affected by sub-daily variations.
- The next IVS Analysis Workshop will take place in Vienna, Austria, at the Institute for Geodesy and Geophysics of the Vienna University of Technology on Saturday, April 14, 2007 just prior to the General Assembly of the European Geosciences Union.

References

[1] Mathews P.M., T.A. Herring, B.A. Buffet (2002): Modeling of nutation-precession: New nutation series for the non-rigid Earth, and insights into the Earth's Interior; J. Geophys. Res., 107, B4, 10.1029/2001JB000390

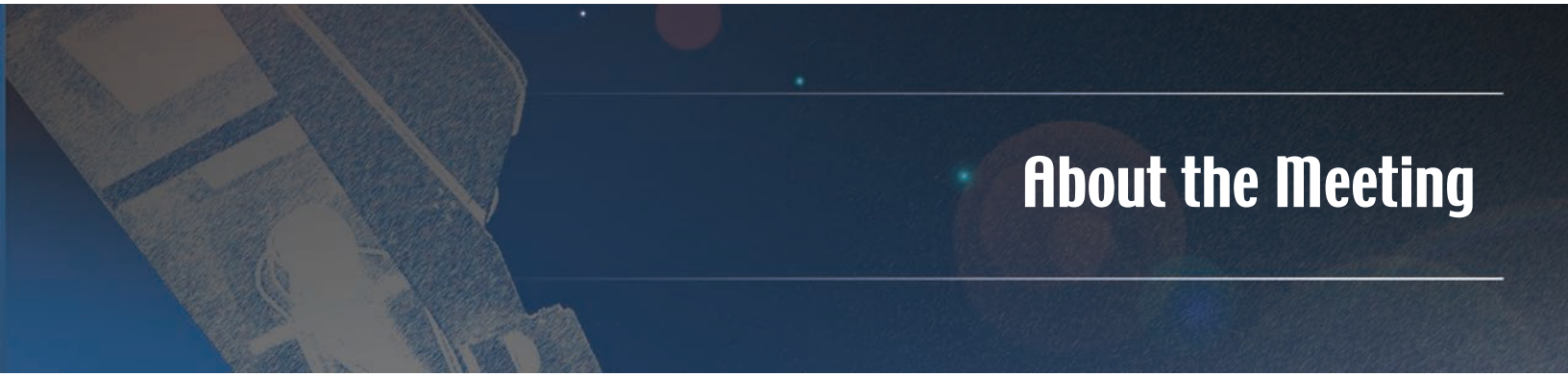
About the Meeting

Registered Participants

Name	Institution	Country	E-mail
Aedo, Roberto	Universidad del Bío-Bío	Chile	roberto.aedo@tigo.cl
Andrei, Alexandre Humberto	Observatorio Nacional/MCT and Observatorio do Valongo/UFRJ	Brazil	oat1@on.br
Barache, Christophe	Paris Observatory	France	Christophe.Barache@obspm.fr
Behrend, Dirk	NVI, Inc./GSFC	USA	dbb@ivscc.gsfc.nasa.gov
Böckmann, Sarah	Geodetic Institute of the University of Bonn	Germany	boeckmann@uni-bonn.de
Böhm, Johannes	Vienna University of Technology	Austria	johannes.boehm@tuwien.ac.at
Boer, Armin	BKG	Chile	aboer@udec.cl
Brzezinski, Aleksander	Space Research Centre, Polish Academy of Sciences	Poland	alek@cbk.waw.pl
Cappallo, Roger	MIT Haystack Observatory	USA	rjc@haystack.mit.edu
Charlot, Patrick	Bordeaux Observatory	France	charlot@obs.u-bordeaux1.fr
Cho, Jungho	Korea Astronomy and Space Science Institute	South Korea	jojh@kasi.re.kr
Colomer, Francisco	Observatorio Astronómico Nacional, Instituto Geográfico Nacional	Spain	f.colomer@oan.es
Corey, Brian	MIT Haystack Observatory	USA	bcorey@haystack.mit.edu
Costa, Alexandre	FUNCEME, UECE	Brazil	alex@funceme.br
Engelhardt, Gerald	BKG, Leipzig	Germany	gerald.engelhardt@bkg.bund.de
Fomalont, Ed	NRAO	USA	efomalon@nrao.edu
Fukuzaki, Yoshihiro	Geographical Survey Institute	Japan	fukuzaki@gsi.go.jp
Gipson, John	NVI, Inc./NASA GSFC	USA	jmg@leo.gsfc.nasa.gov
Gomez-Gonzalez, Jesus	Instituto Geográfico Nacional	Spain	jggonzalez@mfom.es
Gontier, Anne-Marie	Paris Observatory	France	Anne-Marie.Gontier@obspm.fr
Gulyaev, Sergei	Auckland University of Technology	New Zealand	sergei.gulyaev@aut.ac.nz
Haas, Rüdiger	Onsala Space Observatory, Chalmers University of Technology	Sweden	haas@oso.chalmers.se
Hase, Hayo	BKG	Chile	hayo.hase@tigo.cl

Name	Institution	Country	E-mail
Heinkelmann, Robert	Vienna University of Technology	Austria	rob@mars.hg.tuwien.ac.at
Himwich, Ed	NVI, Inc./NASA GSFC	USA	weh@ivscc.gsfc.nasa.gov
Ichikawa, Ryuichi	Kashima Space Research Center, NICT	Japan	richi@nict.go.jp
Jacobs, Christopher	Jet Propulsion Laboratory NASA/Caltech	USA	Chris.Jacobs@jpl.nasa.gov
Jara, Cristobal	TIGO	Chile	cristobal.jara@tigo.cl
Jike, Takaaki	National Astronomical Observatory of Japan	Japan	jike@miz.nao.ac.jp
Kaufmann, Pierre	CRAAM, Mackenzie Presbyterian University	Brazil	kaufmann@craam.mackenzie.br
Kawano, Nobuyuki	National Astronomical Observatory of Japan	Japan	kawano@miz.nao.ac.jp
Kim, Tuhwan	Ajou University	South Korea	thkim@ajou.ac.kr
Kingham, Kerry	U.S. Naval Observatory	USA	kak@cygx3.usno.navy.mil
Kobayashi, Hideyuki	VERA Observatory, National Astronomical Observatory of Japan	Japan	hideyuki.kobayashi@nao.ac.jp
Kondo, Tetsuro	Kashima Space Research Center, NICT	Japan	kondo@nict.go.jp
Koyama, Yasuhiro	Kashima Space Research Center, NICT	Japan	koyama@nict.go.jp
Kwak, Younghee	Ajou University	South Korea	bgirl02@kasi.re.kr
Lambert, Sebastien	Royal Observatory of Belgium	Belgium	s.lambert@oma.be
Li, Jinling	Shanghai Astronomical Observatory	China	jll@shao.ac.cn
Ma, Chopo	Goddard Space Flight Center	USA	cma@gemini.gsfc.nasa.gov
Machida, Morito	Geographical Survey Institute	Japan	machida@gsi.go.jp
MacMillan, Daniel	NVI, Inc./NASA GSFC	USA	dsm@leo.gsfc.nasa.gov
Manabe, Seiji	National Astronomical Observatory of Japan	Japan	manabe@miz.nao.ac.jp
Masaki, Yoshimitsu	Geographical Survey Institute	Japan	ymasaki@gsi.go.jp
Matsuzaka, Shigeru	Geographical Survey Institute	Japan	shigeru@gsi.go.jp
Müskens, Arno	Geodetic Institute of the University of Bonn	Germany	mueskens@mpifr-bonn.mpg.de

Name	Institution	Country	E-mail
Negusini, Monia	Istituto di Radioastronomia, National Institute for Astrophysics (INAF)	Italy	negusini@ira.inaf.it
Nicotra, Gaetano	Istituto di Radioastronomia, National Institute for Astrophysics (INAF)	Italy	g.nicotra@ira.inaf.it
Niell, Arthur	MIT Haystack Observatory	USA	aniell@haystack.mit.edu
Nothnagel, Axel	Geodetic Institute of the University of Bonn	Germany	nothnagel@uni-bonn.de
Petrachenko, Bill	Natural Resources Canada (NRCan)	Canada	wtpetra@yahoo.ca
Porcas, Richard	Max-Planck-Institut für Radioastronomie, Bonn	Germany	porcas@mpifr-bonn.mpg.de
Remedi, Gonzalo	TIGO	Chile	gonzalo.remedi@tigo.cl
Schlüter, Wolfgang	BKG, FS Wettzell	Germany	wolfgang.schlueter@bkg.bund.de
Schuh, Harald	Vienna University of Technology	Austria	harald.schuh@tuwien.ac.at
Searle, Anthony	Natural Resources Canada (NRCan)	Canada	asearle@nrcan.gc.ca
Shield, Peter	Patriot Antenna Systems/InterTronic Solutions	Canada	pshield@intertronicsolutions.com
Sierk, Bernd	BKG, Observatorio TIGO	Chile	sierk@tigo.cl
Smythe, Dan	MIT Haystack Observatory	USA	dsmythe@haystack.mit.edu
Sobarzo, Sergio	TIGO	Chile	ssobarzo@tigo.cl
Takahashi, Fujinobu	Yokohama National University (YNU)	Japan	fjtaka@ynu.ac.jp
Takeuchi, Hiroshi	NICT	Japan	ht@nict.go.jp
Tesmer, Volker	DGFI	Germany	tesmer@dgfi.badw.de
Thorandt, Volkmar	BKG, Leipzig	Germany	volkmar.thorandt@bkg.bund.de
Thornton, Bruce	NVI, Inc./USNO	USA	thornton.bruce@usno.navy.mil
Titov, Oleg	Geoscience Australia	Australia	oleg.titov@ga.gov.au
Tornatore, Vincenza	Politecnico di Milano—Diiar	Italy	vincenza.tornatore@polimi.it
Tuccari, Gino	Istituto di Radioastronomia, National Institute for Astrophysics (INAF)	Italy	g.tuccari@ira.inaf.it
Vennebusch, Markus	Geodetic Institute of the University of Bonn	Germany	Vennebusch@uni-bonn.de
Verdugo, Carlos	TIGO	Chile	carlos.verdugo@tigo.cl
Wang, Guangli	Shanghai Astronomical Observatory	China	wgl@shao.ac.cn

Name	Institution	Country	E-mail
Whitney, Alan	MIT Haystack Observatory	USA	awhitney@haystack.mit.edu
Wresnik, Joerg	Vienna University of Technology	Austria	wresnik@mars.hg.tuwien.ac.at
Xu, Zhi-jun	Shanghai Astronomical Observatory	China	xuthus@shao.ac.cn
Ye, Shuhua	Shanghai Astronomical Observatory	China	ysh@shao.ac.cn
Ying, Xiang	Shanghai Astronomical Observatory	China	yxiang@shao.ac.cn
Zhang, Xiuzhong	Shanghai Astronomical Observatory	China	xzhang@shao.ac.cn

Fourth IVS General Meeting
Concepción, Chile

PROGRAM

Sunday, January 8, 2006

13:30 Registration
Hotel Diego de Almagro, Sala Llanquihue

20:00 Icebreaker Reception
Hotel Diego de Almagro, Sala Llanquihue

Monday, January 9, 2006

Opening Ceremony *(Casa del Arte)*

08:30 Bus from Hotel Diego de Almagro to Casa del Arte, UdeC

09:00 Welcome Addresses and Folkloristic Show
(1) Sergio Lavanchy, Rector Universidad de Concepción; (2) Wolfgang Schlüter, IVS Chair; (3) Ballet of UdeC

10:00 Official Conference Photo

Session 1: VLBI in Science and Application *(Facultad de Ingeniería)*
Chair: Harald Schuh

10:05 Break

10:35 1-01 Chair's Report
Wolfgang Schlüter, Bundesamt für Kartographie und Geodäsie (BKG)

10:45 1-02 Coordinating Center Report
Dirk Behrend, NVI, Inc./GSFC

10:55 1-03 GGOS *(invited)*
Markus Rothacher, GeoForschungsZentrum Potsdam (GFZ)

11:20 1-04 GAIA and a New Optical Reference Frame *(invited)*
Alexandre H. Andrei, Observatorio Nacional/MCT & Observatorio do Valongo/UFRJ

11:45 1-05 Role of VLBI for Investigating Earth Rotation *(invited)*
Aleksander Brzezinski, Space Research Center, Polish Academy of Sciences

12:10 1-06 The ALMA Project *(invited)*
Massimo Tarenghi, ALMA Consortium

12:35 1-07 IVS' Contribution to the IERS Combination Pilot Project and to the ITRF2004: Status and Results
Markus Vennebusch, Geodetic Institute of the University of Bonn

12:50 1-08 Ionosphere Delay Corrections in Satellite VLBI Observations
Jinling Li, Shanghai Astronomical Observatory, Chinese Academy of Sciences

13:05 Lunch

Session 1: VLBI in Science and Application (cont.)
Chair: Jinling Li

14:45 1-09 GPS Meteorology over Northeast Brazil: Perspectives
A. Costa (1,2), A. M. Pereira de Lucena (3), P. Kaufmann (4), F. Sales Ávila Cavalcante (2), F. Geraldo de Melo Pinheiro (2), F. de Assis Travares Ferreira da Silva (3), J. Bosco Verçosa Leal Jr. (2), V. de Paula Silva Filho (1,3); (1) FUNCEME, (2) UECE, (3) INPE, (4) Mackenzie University

15:00 1-10 Global VLBI Solution IGG05R01
Robert Heinkelmann (1), Johannes Böhm (1), Harald Schuh (1), Volker Tesmer (2), (1) Institute of Geodesy and Geophysics, Vienna University of Technology, (2) Deutsches Geodätisches Forschungsinstitut

15:15 1-11 International VLBI Tracking of SELENE
Nobuyuki Kawano, National Astronomical Observatory of Japan

15:30 1-12 Spacecraft Tracking with the Chinese VLBI Network
Xiuzhong Zhang and the Chinese VLBI Network Team, Shanghai Astronomical Observatory, Chinese Academy of Sciences

15:45 1-13 The First Year of VERA Geodetic Experiments
Takaaki Jike, Yoshiaki Tamura, Seiji Manabe, NAOJ VERA Group; VERA Observatory, National Astronomical Observatory of Japan

16:00 1-14 VERA System and Recent Results
H. Kobayashi (1), S. Manabe (1), N. Kawaguchi (1), K-M. Shibata (1), Y. Tamura (1), O. Kameya (1), M. Honma (1),T. Hirota (1), H. Imai (2), T. Omodaka (2); (1) VERA Observatory, National Astronomical Observatory of Japan; (2) Department of Science, Kagoshima University

Session 2: Next Generation VLBI
Chair: Arthur Niell

16:15 2-01 Achieving a Quantum Leap in Observation Density
Bill Petrachenko, Natural Resources Canada (NRCan)

16:30 2-02 A Wide-Band VLBI Digital Backend System
Alan Whitney, Shep Doeleman, Brian Fanous, Hans Hinteregger, MIT Haystack Observatory

16:45 Break

17:15 2-03 A New Lower Cost 12m Full Motion Antenna *(invited)*
Peter Shield, Mark Godwin, InterTronic Solutions, Patriot Antenna Systems Inc.

17:40 2-04 Uses of the ICRF and Implications for Future VLBI
Chopo Ma, Goddard Space Flight Center

Session 2: Next Generation VLBI (cont.)
Chair: Bill Petrachenko

17:55 2-05 Softc + Beowulf – JPL's Newest Correlator
Stephen Lowe, Jet Propulsion Laboratory

18:10 2-06 Real Time Correlator in FPGA
Zhijun Xu, Xiuzhong Zhang, Shanghai Astronomical Observatory, Chinese Academy of Sciences

18:25 2-07 Simulations for VLBI 2010
Jörg Wresnik, Johannes Böhm, Harald Schuh, Institute of Geodesy and Geophysics, Vienna University of Technology

18:40 2-08 Singular Value Decomposition – A Tool for VLBI Simulations
Markus Vennebusch, Geodetic Institute of the University of Bonn

19:00 Bus to hotel

Tuesday, January 10, 2006

Session 3: Network Stations, Operation Centers, Correlators
Chair: Ed Himwich

08:30 Bus from Hotel Diego de Almagro to Facultad de Ingeniería, UdeC

09:00 3-01 A New 40-m Radio Telescope in Yebes (Spain) for Geodetic VLBI Studies by IGN *(invited)*
Jesús Gómez-González, Francisco Colomer, Alberto Barcia, José Antonio López-Fernández, Instituto Geográfico Nacional (IGN) of Spain

09:25 3-02 K5/VSSP Data Processing System of Small Cluster Computing at Tsukuba VLBI Correlator *(invited)*
Morito Machida, Masayoshi Ishimoto, Kazuhiro Takashima, Tetsuro Kondo, Yasuhiro Koyama, Geographical Survey Institute, National Institute of Information and Communications Technology (NICT)

09:50 3-03 Remote Control of VLBI Operations
Gonzalo Remedi, Sergio Sobarzo, Cristobal Jara, Roberto Aedo, Carlos Verdugo, Hayo Hase, UBB, UdeC, BKG

10:05 3-04 National Geodetic VLBI Plan in Korea
Tuhwan Kim (1), Tetsuo Sasao (1,2), Younghee Kwak (1), Kidok An (3), Wonkuk Lee (3), Jongwan Kim (3); (1) Ajou University, (2) Korea Astronomy & Space Science Institute, (3) National Geographic Information Institute

10:20 3-05 Radio Astronomy and VLBI Developments in Brazil
Pierre Kaufmann, Mackenzie Presbyterian University

10:35 3-06 Footprint Observations at the Fundamental Station Wettzell
Wolfgang Schlüter, Thomas Klügel, Christian Schade, Bundesamt für Kartographie und Geodäsie (BKG)

10:50 Break

Session 3: Network Stations, Operation Centers, Correlators (cont.)
Chair: Yasuhiro Koyama

11:20 3-07 Bonn Correlator Report for Astronomy and Geodesy
Arno Müskens, Walter Alef, Dave Graham, Geodetic Institute of the University of Bonn, Max-Planck-Institute for Radioastronomy

11:35 3-08 Washington Correlator Report
Kerry Kingham, U.S. Naval Observatory

11:50 3-09 Network Coordinator Report
Ed Himwich, NVI Inc./GSFC

12:05 3-10 First Fringes to New Zealand
Sergei Gulyaev, Auckland University of Technology

Session 4: New Technology Developments in VLBI
Chair: Alan Whitney

12:20 4-01 DBBC – A Flexible Platform for VLBI Data Processing
Gino Tuccari (1), Salvatore Buttaccio (1), Gaetano Nicotra (1), Ying Xiang (2), Michael Wunderlich (3); (1) IRA/INAF, (2) SHAO/CAS, (3) MPI-Bonn

12:35 4-02 FPGA Implementation in DBBC
Ying Xiang (1), Gino Tuccari (2), Wenren Wei (1); (1) Shanghai Astronomical Observatory (CAS), (2) National Astrophysical Institute (IRA)

12:50 4-03 e-VLBI Developments with the K5 VLBI System
Yasuhiro Koyama, Tetsuro Kondo, Moritaka Kimura, Hiroshi Takeuchi, Masaki Hirabaru, National Institute of Information and Communications Technology (NICT)

13:05 Lunch

15:00 4-04 The Development of the Streamlined Correlation Software Using Bitset Class Library
Fujinobu Takahashi (1), Kazuki Yanashima (1), Yuji Yoshida (1), Tetsuro Kondo (2); (1) Yokohama National University (YNU), (2) National Institute of Information and Communications Technology

15:15 4-05 Development of a New VLBI Sampler Unit (K5/VSSP32) Equipped with a USB 2.0 Interface
Tetsuro Kondo, Yasuhiro Koyama, Hiroshi Takeuchi, Moritaka Kimura; Kashima Space Research Center/NICT

Session 4: New Technology Developments in VLBI (cont.)
Chair: Gino Tuccari

15:30 4-06 VSI Interfaces for Legacy Systems
Dan Smythe, MIT Haystack Observatory

15:45 4-07 Integration of the Mk5B Playback System into the Mk4 Correlator
Roger Cappallo, MIT Haystack Observatory

16:00 4-08 The Mark 5B VLBI Data System
Alan Whitney, MIT Haystack Observatory

16:15 4-09 e-VLBI Development Program at Haystack Observatory
Alan Whitney, Chet Rusczcyk, MIT Haystack Observatory

16:40 Bus to TIGO

17:00 TIGO Visit and Cocktail

19:00 Bus to hotel

Wednesday, January 11, 2006

Session 5: Software and Analysis Strategies
Chair: Oleg Titov

08:30 Bus from Hotel Diego de Almagro to Facultad de Ingeniería, UdeC

09:00 5-01 Impact of Different Tropospheric Mapping Functions on the TRF, CRF, and Position Time Series Estimated from VLBI *(invited)*
Volker Tesmer (1), Johannes Böhm (2), Robert Heinkelmann (2), Harald Schuh (2); (1) Deutsches Geodätisches Forschungsinstitut (DGFI), (2) Institute of Geodesy and Geophysics, Vienna University of Technology

09:25 5-02 Interaction of Atmosphere Modeling and Analysis Strategy
Arthur Niell, MIT Haystack Observatory

09:40 5-03 Comparison of Wet Path Delays Observed with WVR, Sun Spectrometer, Radiosondes, GPS and VLBI at Wettzell
Wolfgang Schlüter (1); Walter Schwarz (1); Beat Bürki (2); Alexander Somieski (2); Petra Häfele (3); (1) Fundamentalstation Wettzell, (2) Eidgenössische Technische Hochschule Zürich/CH, (3) Universität der Bundeswehr, München

09:55 5-04 Linear Horizontal Gradients of Refractivity vs. 3D Raytracing
Johannes Böhm, Harald Schuh, Institute of Geodesy and Geophysics, Vienna University of Technology

10:10 5-05 A Comparison of R1 and R4 IVS Networks
Sebastien Lambert (1), Anne-Marie Gontier (2); (1) Royal Observatory of Belgium, (2) Paris Observatory

10:25 5-06 First Results from CONT05
Dan MacMillan, David Gordon, Dirk Behrend, Chopo Ma, Goddard Space Flight Center

10:40 Break

Session 5: Software and Analysis Strategies (cont.)
Chair: Johannes Böhm

11:10 5-07 Radiosource Instability in the Analysis of VLBI Data *(invited)*
Daniel MacMillan, NVI, Inc./GSFC

11:25 5-08 The Effect of Reference Radiosource Instabilities on the TRF Solution
Oleg Titov, Geoscience Australia

11:40 5-09 First Steps to Investigate Long-term Stability of Radio Sources in VLBI Analysis
Gerald Engelhardt, Volkmar Thorandt, Bundesamt für Kartographie und Geodäsie

11:55 5-10 Correlation in VLBI Observations
John M. Gipson, NVI, Inc./GSFC

Session 6: Results and Geodetic/Geophysical/Astrometric Interpretation
Chair: Seiji Manabe

12:10 6-01 VLBA Phase Referencing for Astrometric Use *(invited)*
Edward Fomalont, National Radio Astronomy Observatory

12:35 6-02 High-frequency Earth Orientation Variations and Geodetic VLBI *(invited)*
Rüdiger Haas, Chalmers University of Technology, Onsala Space Observatory

13:00 Lunch

15:00 6-03 Extending the ICRF to Higher Radio Frequencies: Global Astrometric Results at 24 GHz
C.S. Jacobs, G.E. Lanyi, C.J. Naudet, O.J. Sovers, L.D. Zhang (1); P. Charlot (2); E.B. Fomalont (3) D. Gordon, C. Ma (4); and the KQ VLBI Collaboration; (1) NASA/Caltech's JPL, (2) Bordeaux Observatory, (3) NRAO, (4) NASA/GSFC

15:15 6-04 Astrometric Suitability of ICRF Sources Based on Intrinsic VLBI Structure
Patrick Charlot (1); Alan Fey (2); Roopesh Ojha (3); David Boboltz (2); (1) Bordeaux Observatory, (2) U. S. Naval Observatory, (3) Australia Telescope National Facility

15:30 6-05 How Compact Are Faint Radio Sources?
Richard Porcas, MPIfR Bonn

Session 6: Results and Geodetic/Geophysical/Astrometric Interpretation (cont.)
Chair: Dan MacMillan

15:45 6-06 E3 Network Results
Anthony Searle, Mario Bérubé, Bill Petrachenko, Natural Resources Canada (NRCan)

16:00 6-07 A Generalized Scheme to Retrieve Wet Path Delays from WVR Measurements Applied to the European Geodetic VLBI Network
J. Cho (1,2), A. Nothnagel (2), A. L. Roy (3), R. Haas (4); (1) Korea Astronomy & Space Science Institute, (2) Geodetic Institute, University of Bonn, (3) Max-Plank Institute for Radio Astronomy, (4) Onsala Space Observatory, Chalmers University of Technology

16:15 6-08 Combination of Long Time Series of Tropospheric Parameters
Robert Heinkelmann, Johannes Böhm, Harald Schuh; Institute of Geodesy and Geophysics, Vienna University of Technology

Poster Sessions and Closing

16:30 Closing Remarks
Wolfgang Schlüter, Bundesamt für Kartographie und Geodäsie (BKG)

16:45 Poster Sessions and Refreshments

18:45 Bus to hotel

19:30 Bus from Hotel Diego de Almagro to Golf Club House "La Posada"

20:00 Conference Dinner

23:30 Bus to hotel

Posters

Session 1P: VLBI in Science and Application

1-01P VLBI Delay Model for Radio Sources at Finite Distance
Mamoru Sekido (1), Toshio Fukushima (2); (1) National Institute of Information and Communications Technology, (2) National Astronomical Observatory Japan

Session 2P: Next Generation VLBI

2-01P Carbon Fibre Antennas for Geodetic VLBI
Peter Dewdney (1), Gordon Lacey (1), Bill Petrachenko (2); (1) National Research Council of Canada (NRC), (2) Natural Resources Canada (NRCan)

2-02P Network Size Simulations
Anthony Searle, Mario Berube, Bill Petrachenko; Geodetic Survey Division, Natural Resources Canada

Session 3P: Network Stations, Operation Centers, Correlators

3-01P Antenna Cross-Polarization Characteristics at Geodetic VLBI Stations
Brian Corey, Michael Titus; MIT Haystack Observatory

3-02P An Investigation on a GPS-based Approach to Local Tie Computation
Claudio Abbondanza (1), Monia Negusini (2), Pierguido Sarti (2), Luca Vittuari (1); (1) DISTART - Università di Bologna, Italy (2) Istituto di Radioastronomia - INAF - Bologna, Italy

3-03P GPS Measurements on the VLBI Telescopes at Onsala and Ny-Ålesund
Daniel Hernandez, Rüdiger Haas; Chalmers University of Technology, Onsala Space Observatory

3-04P Photogrammetry, Laser Scanning, Holography and Terrestrial Surveying of the Noto VLBI Dish
Pietro Bolli (1), Simonetta Montaguti (1), Monia Negusini (1), Pierguido Sarti (1), Luca Vittuari (2), Gianluigi Deiana (3); (1) Istituto di Radioastronomia - INAF - Bologna, Italy (2) DISTART - Università di Bologna, Italy (3) Osservatorio Astronomico di Cagliari - INAF, Italy

3-05P Observation Activities at the Tsukuba Station
Junichi Fujisaku, Kensuke Kokado, Masayoshi Ishimoto, Kazuhiro Takashima and Yoshihiro Fukuzaki; Geographical Survey Institute

3-06P Status and Results of JARE Syowa Station, Antarctica
Yoshihiro Fukuzaki (1), Kazuo Shibuya (2), Koichiro Doi (2); (1) Geographical Survey Institute, (2) National Institute of Polar Research

3-07P Onsala Space Observatory - Station Report
Rüdiger Haas, Chalmers University of Technology, Onsala Space Observatory

3-08P Noto Station Status Report
Gaetano Nicotra, Gino Tuccari, Salvatore Buttaccio, Pietro Cassaro, Corrado Contavalle, Leonardo Nicotra, Carlo Nocita, Luigi Papaleo, Mario Paternò, Francesco Schillirò; Istituto di Radioastronomia - INAF (Italy)

Session 4P: New Technology Developments in VLBI

4-01P e-VLBI Demonstrates Real-time Correlation Using Both K5 and Mark 5 End Systems
Chester Ruszczyk (1), Yasuhiro Koyama (2), Alan Whitney (1); (1) MIT Haystack Observatory, (2) Kashima Space Research Center/NICT

4-02P e-NRTV - Radar VLBI Network
Gino Tuccari (1), Igor Molotov (2), Alexander Volvach (3); (1) Istituto di Radioastronomia INAF (Italy), (2) Central Pulkovo Astronomical Observatory (Russia), (3) Institute of Radio Astronomy (Ukraine)

4-03P An Evaluation of Atmospheric Path Delay Correction in Differential VLBI Experiments for Spacecraft Tracking
Ryuichi Ichikawa, Mamoru Sekido, Yasuhiro Koyama, Tetsuro Kondo; Kashima Space Research Center, NICT

4-04P A 2 Gbps DAS for Spacecraft VLBI
Hiroshi Takeuchi, Moritaka Kimura, Junichi Nakajima; NICT

4-05P The Post-Correlation Processing of VLBI Satellite Observations at SHAO
Guangli Wang, Shanghai Astronomical Observatory, Chinese Academy of Sciences

Session 5P: Software and Analysis Strategies

5-01P Calc 10 Implementation
David Gordon (1), Dan MacMillan (2), Karen Baver (1); (1) Raytheon/NASA GSFC; (2) NVI Inc./NASA GSFC

5-02P Baseline and Site Repeatability in the IVS Rapid Network
Sebastien Lambert; Royal Observatory of Belgium (formerly at NVI, Inc./U.S. Naval Observatory)

5-03P Thermal Deformation of Radio Telescopes Onsala and Wettzell
Jörg Wresnik (1), Rüdiger Haas (2), Johannes Böhm (1), Harald Schuh (1); (1) Institute of Geodesy and Geophysics, Vienna University of Technology, (2) Chalmers University of Technology, Onsala Space Observatory

Session 6P: Results and Geodetic/Geophysical/Astrometric Interpretation

6-01P Improving Astrometric VLBI by Using Water Vapor Radiometer Calibrations
C.S. Jacobs, S.J. Keihm, G.E. Lanyi, C.J. Naudet, L. Riley, A.B. Tanner; Jet Propulsion Laboratory NASA/Caltech

6-02P Tropospheric Parameters Long Time Series Analysis
Sergey Kurdubov, Elena Skurikhina, Julia Sokolova; Institute of Applied Astronomy RAS

6-03P VLBI as a Tool to Probe the Ionosphere
T. Hobiger (1), T. Kondo (2), H. Schuh (1); (1) IGG, Vienna University of Technology; (2) NICT

6-04P Detection of Short Period Ionospheric Variations from VLBI Fringe Phases
T. Hobiger (1), T. Kondo (2), K. Takashima (3), H. Schuh (1); (1) IGG, Vienna University of Technology; (2) NICT; (3) Geographical Survey Institute

6-05P The First Dual Frequency VLBI Observation Using VERA
Bong Won Sohn (1), Hideyuki Kobayashi (2) Tetsuo Sasao (1), Tomoya Hirota (2), Osamu Kameya (2), Yoon Kyung Choi (2); (1) KASI, Korea Astronomy & Space Science Institute; (2) NAOJ, National Astronomical Observatory of Japan

6-06P Crustal Deformation in South America from GPS and VLBI
Annika Edh, Rüdiger Haas; Chalmers University of Technology, Onsala Space Observatory

6-07P Preliminary Study on Plate Motion Measurements in Korean Peninsula by New Korean VLBI
Younghee Kwak (1), Tetsuo Sasao (1,2), Tuhwan Kim (1); (1) Ajou University, (2) Korea Astronomy & Space Science Institute

6-08P Modeling of the Earth Free Core Nutation
V.S. Gubanov, S.L. Kurdubov; Institute of Applied Astronomy of RAS, St. Petersburg, Russia

6-09P Local Tie Survey at VERA Ogasawara Station at Site Chichijima
Yoshimitsu Masaki (1), Shigeru Matsuzaka (1), Yoshiaki Tamura (2); (1) Geographical Survey Institute, (2) National Astronomical Observatory of Japan

Author Index

(First authors are designated by (1) at the end of the title.)

National Aeronautics and Space Administration

International VLBI Service for Geodesy and Astrometry

International VLBI Service for Geodesy and Astrometry

IVS Coordinating Center
NASA Goddard Space Flight Center
Code 698
Greenbelt, MD 20771

http://ivscc.gsfc.nasa.gov
ivscc@ivscc.gsfc.nasa.gov

phone: 301-614-5939
fax: 301-614-6522